Synthèse et Auto-assemblage de Copolymères Fluorés Amphiphiles

Marc Guerre

THÈSE

Pour obtenir le grade de

Docteur

Délivré par **L'Ecole Nationale Supérieure de Chimie de Montpellier**

Préparée au sein de l'école doctorale
Sciences Chimiques Balard (ED459)
de l'unité de recherche
ICGM (UMR 5253)
Et de l'équipe
IAM

Spécialité : **Chimie et Physicochimie des Matériaux**

Présentée par **Marc Guerre**

Synthèse et Auto-Assemblage de Copolymères Fluorés Amphiphiles

Soutenanu prévue le Mercredi 10 Mai 2017 devant le jury composé de

M. D. Taton, Professeur, LCPO Bordeaux	Président
M. A. Laschewsky, Professeur, APC Potsdam	Examinateur
M. F. D'Agosto, Directeur de Recherche, LCPP Lyon	Rapporteur
M. M. Destarac, Professeur, IMRCP Toulouse	Rapporteur
M. V. Ladmiral, Chargé de Recherche, ICGM-IAM Montpellier	Directeur de Thèse
M. B. Améduri, Directeur de Recherche, ICGM-IAM Montpellier	Directeur de Thèse
M. G. Silly, Professeur, ICGM-ChV Montpellier	Invité
M. R. Poli, Professeur, LCC Toulouse	Invité

Préface

Remerciements

« Soyons reconnaissants aux personnes qui nous donnent du bonheur;
elles sont les charmants jardiniers par qui nos âmes sont fleuries »
Marcel Proust

Ces travaux de thèse ont été réalisés au sein de l'équipe Ingénierie et Architectures Macromoléculaires (IAM) de l'Institut Charles Gerhardt (UMR 5253) et ont été financés par le Ministère de l'Education Nationale de l'Enseignement Supérieur et de la Recherche.

Je tiens tout d'abord à remercier M. Patrick Lacroix-Desmazes pour m'avoir accueilli au sein de l'équipe IAM et de m'avoir permis de conduire ces travaux de thèse.

Je remercie particulièrement M. Franck d'Agosto, et M. Mathias Destarac pour avoir accepté d'être rapporteur de ma thèse.

Je remercie également M. Daniel Taton ainsi que M. André Laschewsky qui me font l'honneur de juger ces travaux en qualité d'examinateur.

Je tiens à remercier M. Gilles Silly et M. Rinaldo Poli d'avoir accepté de participer à ce jury de thèse et d'avoir pris le temps de lire ce mémoire.

Je tiens à exprimer mes plus vifs et sincères remerciements à M. Vincent Ladmiral et M. Bruno Améduri qui ont dirigé ces travaux de thèse. Je tiens particulèrement à remercier M. Vincent Ladmiral pour son soutien, sa grande disponibilité, son aide ainsi que pour tout ce qu'il m'a apporté au cours de cette thèse.

Je remercie particulièrement Mme Mona Semsarilar pour le temps qu'elle m'a accordé à la préparation d'échantillons et les prises d'images MET.

J'associe à mes remerciements M. Gérald Lopez, M. Thibaut Soulestin, M. Sanjib Banerjee, M. Cédric Totée, M. Gilles Silly, M. Vincent Lapinte, Mme Olinda Gimello, M. Wahidur Rahaman, M. Rinaldo Poli, Mme Judith Schmidt, M. Yeshayahu Talmon, M. Enrique Folgado, Mme. Armelle Ouali, M. Mineto Uchiyama, M. Kotaro Satoh et M. Masami Kamigaito avec qui j'ai eu le plaisir de collaborer et sans qui, certains travaux n'auraient pu être menés à terme.

Je remercie les membres de l'équipe IAM, permanents comme non-permanents, nouveaux et anciens, pour leur aide et l'agréable environnement de travail dans lequel j'ai évolué. Je tiens à remercier personellement Mme. Claire Negrell pour ses precieux conseils en CES et M. Ghislain David pour sa confiance, l'opportunité qu'il m'a offerte et toute l'aide qu'il m'a apporté dans la partie enseignement de ma thèse.

Mes plus profonds remerciements s'adressent à mes parents, qui m'ont toujours soutenu, aidé, encouragé. Ils m'ont inculqué les valeurs fondamentales de la vie et m'ont donné toutes les chances pour réussir. Leur amour me porte et me guide chaque jour. Je remercie également mes frères et soeur, Alexandre, Gregory, Sirina et tout particulièrement ma grande sœur Aurore. Une petite pensée à mes neveux et nièces qui de part leurs joie de vivre ont su me redonner le sourire et me faire oublier un tant soit peu la thèse. J'associe également à ces remerciements toute ma famille et belle famille ainsi que mes amis.

Enfin, je tiens à remercier ma fiancée Mélina, pour son aide, sa patience, son écoute et son amour quotidien, qui m'ont été d'un énorme soutien durant ces années.

A mes parents

Abréviations

A

ATRP	Atom-transfer radical-polymerization
AA	Acrylic acid

B

BA	Butyl acrylate
BPFCBPMA	p-(2-(4-biphenyl)perfluorocyclobutoxy)phenyl methacrylate
BTFVBP	4,4'-bis(1,2,2-trifluorovinyloxy)-biphenyl)
BzA	Benzyl acrylate
BzMA	Benzyl methacrylate
BMA	Butyl methacrylate

C

$CHCl_3$	Chloroform
CL	ε-Caprolactone
COEMA	2-Cinnamoyloxylethyl methacrylate
CROP	Cationic ring-opening polymerization
Cryo-TEM	Cryogenic transmission electronic microscopy
CuAAC	Copper(I)-catalyzed alkyne-azide cycloaddition
CyAFPEMA	2-(cyclohexylamino)-2-oxo-1-(perfluorophenyl) ethyl methacrylate

D

Da	Dalton
DEAEMA	2-(Diethylamino)ethyl methacrylate
DHFOMA	1H,1H,-Perfluorooctyl methacrylate
DI	Deionized
DLS	Dynamic light scattering
DMAEMA	2-(Dimethylamino)ethyl methacrylate
DMS	Dimethylsiloxane
DMF	Dimethyl formamide
DMPP	Dimethylphenylphosphine

E

EAFPEMA	2-((2-ethoxy-2-oxoethyl)amino)-2-oxo-1-(perfluorophenyl)ethyl methacrylate
EtOAc	Ethyl acetate
EtOH	Ethanol

F

2-FEMA	2-Fluoroethyl methacrylate
FDA	1H,1H,2H,2H-Perfluorodecyl acrylate
FDMA	1H,1H,2H,2H-Perfluorodecyl methacrylate
FDPMA	Dodecafluoroheptyl methacrylate
FEMA	Perfluoroalkyl ethyl methylacrylate
FPOVE	2-(2,2,3,3,3-Penfluoropropoxy)ethyl vinyl ether

G

GMA	Glycidyl methacrylate

H

HEA	2-Hydroxy ethyl acrylate
HepFBA	2,2,3,3,4,4,4-Heptafluorobutyl acrylate
HepFBMA	2,2,3,3,4,4,4-Heptafluorobutyl methacrylate
HexFBA	2,2,3,4,4,4-Hexafluorobutyl acrylate
HexFBMA	2,2,3,4,4,4-Hexafluorobutyl methacrylate
HFP	Hexafluoropropylene
HOVE	2-Hydroxyethyl vinyl ether
HPFP	2H,3H-Perfluoropentane
HFBOVE	2,2,3,3,4,4,4-Hepta-fluorobutoxy)ethyl vinyl ether

I

IB	Isobutylene
IFPMA	Iodotetrafluorophenoxy methacrylate
iPOH	Isopropyl alcohol

L

LA	Lactic acid

M

MAA	Methacrylic acid
MANa	Sodium methacrylate
MBTFVB	2-methyl-1,4-bistrifluorovinyloxybenzene
MCM	Multi-compartment micelle
MEK	Methyl ethyl ketone
MeOH	Methanol
MMA	Methyl methacrylate
MOMA	Methoxymethyl acrylate
MPP	Methyl phenyl phophazene
MPS	3-(trimethoxysilyl) propyl methacrylate
MRI	Magnetic resonance imaging

N

NB	Norbornene
NFHMA	3,3,4,4,5,5,6,6,6-Nonafluorohexyl methacrylate
NIPAM	N-Isopropylacrylamide
NMR	Nuclear magnetic resonance

O

OEGA	Oligo(ethylene glycol)methyl ether acrylate
OEGMA	Oligo(ethylene glycol)methyl ether methacrylate
OEGSt	Oligo(ethylene glycol)methyl ether styrene
OFPMA	2,2,3,3,4,4,5,5-Octafluoropentyl methacrylate

P

BLG	γ-Benzyl L-glutamate
PEE	Poly ethylethylene
PEG	Polyethylene glycol
PEO	Polyethylene oxyde
PFCB	Perfluorcyclobutyl
PFPE	Perfluoropolyether
PFPMA	Pentafluorophenyl methacrylate
PFPO	Perfluoropropylene oxide

PFS	Pentafluorostyrene
PISA	Polymerization-induced self-assembly
POSS	Polyhedral oligomeric silsesquioxanes-tethered
PGA	Propylene glycol Acrylate
PPMA	3-phenylpropyl methacrylate
PSPEG	Poly styrene polyethylene glycol
PUMI	Polyurethane macro initerfer

R

RAFT	Reversible addition-fragmentation chain-transfer
ROMP	Ring-opening methathesis polymerization
ROP	Ring-opening polymerization

S

S	Styrene
SANS	Small angle neutron Scattering
SAXS	Small angle X-ray Scattering
SEM	Scanning electron microscopy
SLS	Static light scattering

T

tBAFPEMA	2-(tert-butylamino)-2-oxo-1-(perfluorophenyl) ethyl methacrylate
tBMA	*tert*-Butyl methacrylate
TEM	Transmission electron microscopy
TFEP	bis(Trifluoroethoxy)phosphazene
TFEOVE	2,2,2-Trifluoroethoxy)ethyl vinyl ether
TFMA	α-Trifluoromethacrylic acid
TFT	Trifluorotoluene
THF	Tetrahydrofuran
THFOA	1H,1H,2H,2H-Perfluorooctyl acrylate
THFOMA	1H,1H,2H,2H-Perfluorooctyl methacrylate
TPFCBBMA	4-(4'-ptolyloxyperfluorocyclobutoxy)benzyl methacrylate
TriFEMA	2,2,2-Trifluoroethyl methacrylate

V

2VP	2-Vinylpyridine
VBM	4-methyl-4-(4- vinylbenzyl)morpholin-4-ium chloride
VBFP	pentafluorophenyl 4-vinylbenzyl ether
VDF	Vinylidene fluoride

W

WLM	Worm like micelles

Table des Matières

Table des Matières

Introduction Générale

Introduction Générale

Les polymères fluorés (polymères contenant au moins un atome de fluor sur la chaîne principale) constituent une classe de polymères à part. En effet, les propriétés de ces polymères, mais aussi la réactivité particulière des monomères fluorés qui les composent les distinguent des autres classes de polymères. Ces polymères fluorés sont très versatiles : ils peuvent être thermoplastiques, élastomères, plastomères ou élastomères-thermoplastiques. Selon leur composition et les procédés utilisés pour leur synthèse, ces polymères ont une structure semi-cristalline ou bien totalement amorphe. La présence de fluor, élément peu polarisable, mais fortement électronégatif et responsable des liaisons carbone-fluor très stables confère à ces polymères leurs remarquables propriétés. Les propriétés les plus intéressantes sont 1) une résistance aux attaques chimiques, biologiques et thermiques quasiment sans rivaux, 2) de faibles constantes diélectriques, une faible inflammabilité, un faible indice de réfraction, et une faible perméabilité au gaz. Les propriétés de surface des polymères fluorés sont également singulières, ils sont à la fois hydrophobes et lipophobes. De plus, certains d'entre eux comme le PVDF, par exemple, sont électroactifs (ferroélectriques ou piézoélectriques). En revanche, les polymères fluorés présentent un certain nombre d'inconvénients. Ils sont souvent très cristallins et donc peu solubles dans la plupart des solvants usuels et difficiles à mettre en forme en raison de leur haute température de fusion. Enfin, l'absence de groupements réactifs les rend difficiles à réticuler.

Grâce à cette versatilité et à ces propriétés originales, les polymères fluorés ont trouvé de nombreuses applications dans les peintures et vernis, l'électronique (revêtement de câbles, super condensateurs,…), les industries chimiques et pétrolières, l'aéronautique (joint d'étanchéité et élastomères haute performance), l'automobile et l'espace. Dans le domaine de l'énergie, ces polymères font aussi l'objet d'intenses recherches pour la fabrication de membranes de piles à combustibles, de cellules photovoltaïques et de batteries lithium-ion. Pour de nombreuses applications, les polymères fluorés représentent indéniablement la solution la plus performante. Ces polymères de niche sont incontournables dans de nombreuses applications industrielles de haute valeur ajoutée. (Figure 0-1)

Figure 0-1: Exemples d'applications des polymères fluorés

Toutefois, en dépit de leurs propriétés singulières et des applications industrielles que celles-ci permettent, les polymères fluorés n'ont pas encore attiré tout l'intérêt qui leur est dû de la part de la communauté scientifique. Ainsi, jusqu'à présent et dans leur grande majorité, les polymères fluorés sont préparés par polymérisation radicalaire. Les exemples de polymères fluorés à architectures bien contrôlées sont rares. A notre connaissance, la télomérisation des monomères fluorés et l'ITP (Iodine Transfer Polymerization) sont les seuls procédés bien étudiés. Ces techniques permettent, certes la synthèse d'architectures polymères intéressantes, mais elles souffrent de deux inconvénients majeurs : 1) Elles ne permettent pas d'accéder à des polymères de hautes masses molaires, et 2) les indices de polymolécularité sont rarement inférieurs à 1,5-1,8. En conséquence, les études physiques de ségrégation de phases en films ou en masse, ou bien celles qui portent sur l'autoassemblage des polymères fluorés en solution ont été très peu signalés. Il demeure donc un vaste champ de recherche pratiquement vierge.

L'objectif de cette thèse vise à saisir cette opportunité scientifique *via* le développement de nouvelles voies de synthèses dédiées à la préparation de nouvelles architectures bien définies à base de PVDF. Le comportement de ces copolymères semi-cristallins sera ensuite étudié par différents auto-assemblage en solution

Nous avons focalisé notre attention sur deux axes principaux:

1er axe : L'établissement d'une méthode permettant d'obtenir des PVDFs architecturés fonctionnels bien définis (Chapitres II – IV)

2eme axe : l'étude de la nanostructuration de copolymères de PVDF *via* l'auto-assemblage en solution. (Chapitres V-VI)

Cette thèse a été réalisée au sein de l'équipe IAM de l'Institut Charles Gerhardt de Montpellier (ICGM) qui possède une grande expertise dans le domaine des polymères fluorés ainsi que dans les méthodes de polymérisations radicalaires contrôlées. Des collaborations ont également été menées avec le Professeur Rinaldo Poli du Laboratoire de Chimie de Coordination (Toulouse), le Professeur Masami Kamigaito de l'Université de Nagoya et le Professeur Gilles Silly de l'Université de Montpellier.

Ce mémoire de thèse est divisé en six parties. Le premier chapitre propose par l'intermédiaire d'une revue exhaustive, un état de l'art des copolymères fluorés ((méth)acrylates, styrènes, perfluoropolyéthers…) utilisés en auto-assemblage en solution, ainsi que les différentes méthodes de synthèse utilisées. Cette première partie permet de faire le bilan sur les différentes morphologies observées en auto-assemblage de copolymères fluorés et met en avant le clair décalage entre les polymères fluorés de type acrylate et les polymères issus d'oléfines fluorées.

Le deuxième chapitre de ce mémoire est consacré à l'étude de la polymérisation radicalaire contrôlée du VDF par la méthode RAFT. Ce chapitre est subdivisé en trois parties distinctes : *(i)* une première partie démontre le potentiel des agents de transferts de type xanthate pour contrôler de manière convenable la polymérisation du VDF *(ii)* dans la deuxième partie, une caractérisation profonde par RMN a été effectuée sur un PVDF synthétisé par RAFT pour analyser de manière optimale la microstructure et conforter les suggestions émises dans le première partie du chapitre *(iii)* la dernière partie fait le point sur les limites de la polymérisation du VDF par RAFT et examine en details le contrôle, la fonctionnalité et le mécanisme de la polymérisation RAFT du VDF.

Le troisième chapitre de ce mémoire est dédié à la préparation de macromonomères à base de PVDF par l'utilisation de la chimie des thiols, accessible *via* les extrémités de chaînes RAFT. Cette étude a permis d'établir un protocole en une étape, facile et efficace, pour préparer des macromonomères de PVDF de type méthacrylate.

Le quatrième chapitre traite de la synthèse et de la caractérisation de copolymères diblocs à base de PVDF. Dans un premier temps, la synthèse par RAFT séquentielle du VDF et VAc donnant un copolymère dibloc de type PVDF-*b*-PVAc est présentée. Puis, dans un deuxième temps, une partie est consacrée à la préparation de dibloc PEVE-*b*-PVDF aliant RAFT cationique des éthers vinyliques et RAFT radicalaire du VDF.

Dans le cinquième chapitre de ce mémoire, les unités acétates de vinyle du copolymère dibloc PVDF-*b*-PVAc susmentionné ont été saponifiées en milieu basique pour conduire à un copolymère amphiphile de type PVDF-*b*-PVA, comportant un segment PVA hydrosoluble. Ce copolymère a ensuité été caractérisé et auto-assemblé dans l'eau.

Enfin, dans l'ultime partie de ce mémoire, nous nous sommes consacrés à la polymérisation en dispersion RAFT du VDF en présence de macro agents RAFT de type PVAc. Cette polymérisation a induit un autoassemblage de copolymères diblocs PVAc-*b*-PDVF en structures cristallines de type rose des sables et anis étoilé.

Chapitre I. Etat de l'art sur la Synthèse et l'Auto-Assemblage de Copolymères Fluorés

Table des Matières

Introduction Chapitre I

A l'instar des tensioactifs, les diblocs amphiphiles, lorsqu'ils sont dispersés dans un solvant sélectif pour l'un des blocs, s'auto-assemblent de façon à minimiser les interactions du bloc insoluble avec le solvant. Généralement, les morphologies que les diblocs adoptent en solution dépendent de trois principales contributions à l'énergie libre du système: 1) l'élongation des chaînes non solubles au sein du noyau des structures, 2) l'énergie interfaciale, et 3) la répulsion entre les chaînes solubles qui composent la couronne solvatée. Ces interactions se traduisent par une courbure à l'échelle moléculaire qui détermine la morphologie de l'auto-assemblage. Les micelles sphériques, cylindriques et vésicules ne sont que quelques exemples parmi les nombreuses morphologies possibles pour les diblocs amphiphiles (micelles sphériques de Janus, micelles « hamburger » à compartiments, micelles cylindriques à branches, bicouche en forme de pieuvre, toroïdes,…). Cette diversité morphologique résulte de la grande variété architecturale des copolymères à blocs amphiphiles ainsi que des nombreuses interactions potentielles supplémentaires entre les groupements fonctionnels portés par les différents blocs. Il existe en outre une différence majeure entre les systèmes de tensioactifs et les systèmes constitués de copolymères à blocs amphiphiles : ces derniers ne sont pas ergodiques. Dans le cas des polymères à blocs et contrairement aux tensioactifs, il n'y a aucun échange de constituants entre les structures formées. Les chaînes polymères constitutives d'une micelle A ne sont pas transférées à une autre micelle B à l'échelle de temps expérimental. Ces structures polymères sont donc des structures figées par la cinétique plutôt que des produits thermodynamiques. Ceci implique que les structures obtenues dépendent non seulement de la nature des polymères constitutifs mais aussi de la méthode utilisée pour les obtenir. En définitive, il est possible d'obtenir des morphologies différentes à partir d'un même copolymère selon la méthode de préparation choisie

Ce chapitre relate sous la forme d'une revue, l'ensemble des auto-assemblages de copolymères fluorés qui a pu être rapporté dans la littérature au cours des 20 dernières années. Une majeure partie de ce chapitre rapporte l'utilisation de copolymères de méthacrylate, de styrène et de perfluoropolyéther (pour n'en nommer que quelques uns), qui ont suscité un intérêt tout particulier. Les auto-assemblages fournissant des morphologies originales telles que des micelles multicompartiments ou des micelles stimulables ont été spécialement appronfondies.

Synthesis and Self-Assembly of amphiphilic fluorinated copolymers

Marc Guerre,[a] Gerald Lopez,[a] Bruno Ameduri,[a] Vincent Ladmiral[a*]

[a]Institut Charles Gerhardt, Ingénierie et Architectures Macromoléculaires, UMR 5253 – CNRS, UM, ENSCM - Ecole Nationale Supérieure de Chimie de Montpellier, 8 rue de l'Ecole Normale, 34296 Montpellier, France
*Corresponding author: vincent.ladmiral@enscm.fr

I. Introduction

Recent years have seen a continuous increase of interest in the development of nanoscale technologies dedicated to the production and control of the self-assembly of nano-objects into organized patterns.[1-4] The self-association of copolymers, was particularly investigated through solution-based processes,[5,6] which under particular conditions, can form sophisticated morphologies such as spheres, cylinders, bilayer sheets and vesicles (polymersomes)[7-9] for example. The morphologies of self-assembled structures depends mainly on the molecular and structural characteristics of the polymeric building blocks, such as composition, number of segments, segment lengths, block sequence, interactions between the blocks, or architecture. The self-assembled morphologies are also largely affected by the solution self-assembly conditions[10,11] (assembly methods, solvent mixtures): external stimuli (e.g., , pH, salt concentration, temperature, light irradiation), or other polymer characteristics such as crystallinity,[12-13] donor-acceptor interactions,[14,15] H-bonds…). The resulting assemblies are often kinetically trapped and stable because of the inability of the system to thermodynamically equilibrate. This implies that one polymer can potentially produce different (meta)stable morphologies of various topological complexity depending on the path taken to effect the self-assembly. Multicompartment micelles are a representative example of complex morphologies that can be formed by self-assembly of block copolymers. The concept of multicompartment micelles which originated from blood proteins such as serum albumin (which provides circulatory transport for diverse and often sparingly soluble compounds) has attracted much interest in the last two decades. Multicompartiment micelles comprise water-soluble stabilizing shells and subdivided hydrophobic cores which can potentially simultaneously accommodate two or more incompatible drugs. This kind of nanoparticle possesses potential applications in biomedicine, pharmacy, and biotechnology.[16,17] Multicompartment micelles can be obtained by self-assembly of a wide variety of macromolecular architectures such as linear multiblock terpolymers,[18] multiarmed or

miktoarm star copolymers,[19] or hyperbranched copolymers. The first multicompartment micelles reported were formed from assemblies of statistical and block copolymers based on hydrogenated and fluorinated monomers.[20] Fluorous materials and specifically fluorinated copolymers have recently attracted intense interest in solution self-assembly. The incompatibility between the fluorinated and nonfluorinated segments promotes a strong phase segregation in these systems. In turn, this phase segregation leads to an impressive morphological varietis and facilitate the formation of separate hydrophobic, fluorophilic and hydrophilic compartments. Stimuli-responsive polymer assemblies (or so called smart polymers) are another category of very interesting polymeric objects promised to a wide range of potential applications.[21,22] In response to a suitable stimulus (often temperature, pH or light), polymer nanoobjects can can undergo different changes, including (i) disassembly into individual polymer chains (ii) expansion/shrinking caused by swelling/ deswelling of the solvophobic core polymer, or extension/collapse of the stabilizing corona, or (iii) transformation into other morphologies, such as spherical and worm-like micelles for example in the case of polymersomes. Recently, several groups used the synthetic block copolymers to prepare CO_2- and O_2- responsive vesicles.[23-24] CO_2 can reversibly react with amine, amidine or carboxyl groups and fluorinated copolymers are known for their high affinity for oxygen.[26] Such CO_2- and O_2- responsive nanoobjects changes may find applications in biology and biomedicine.

This review sorted by monomer and polymer class, presents a comprehensive report of the self-assembly in solution of fluorinated copolymers. Specific attention has been paid to multicompartment morphologies and stimuli responsive morphologies.

II. Self-Assembly Methods

The self-assembled morphologies of amphiphilic copolymers are strongly affected by the experimental conditions used for their preparation. For the sake of clarity, the most usual preparation methods are briefly described below and will be called by their number in the subsequent sections of the review.

Method 1: Direct dissolution

The polymer is slowly added into a solvent specific to one of the block (such as water for instance) under vigorous stirring.

Method 2: Addition to a bad solvent

A solution of the polymer in a good solvent is added to a bad solvent for one of the component of the polymer under vigorous stirring and studied as is without modification.

Method 3: Addition to a bad solvent and removal of the good solvent by evaporation /distillation

Identical as Method 2, but the good solvent is eliminated by evaporation/distillation.

Method 4: Addition to a bad solvent and removal of the good solvent by dialysis

Identical as Method 2, but the good solvent is eliminated by dialysis.

Method 5: Bad solvent addition + removal of the good solvent by evaporation/distillation

Bad solvent is added to a solution of the polymer under vigorous stirring and the good solvent is removed by evaporation/distillation.

Method 6: Bad solvent addition + removal of the good solvent by dialysis

Identical as Method 5, but the good solvent is eliminated by dialysis.

Method 7: Dialysis

A solution of the polymer in a good solvent is dialyzed against a bad solvent.

III. Self-Assemblies of Poly (Fluorinated (meth)acrylate)-based Copolymers

III.1 Conventional Self-Assembly

Poly(fluorinated (meth)acrylate) copolymers possess unique properties such as low surface energies, low friction coefficients, and high insolubility in conventional solvents. Since reversible-deactivation radical polymerization (RDRP) is among the most rapidly developing areas of chemistry and polymer science, a large number of well-defined block copolymers (BCPs) based on fluorinated (meth)acrylates have been synthesized. However, the self-assemblies of fluorinated poly(meth)acrylate BCPs have been relatively understudied compared to their fully hydrogenated analogs. At the beginning of the century, fluorinated block copolymers and especially triphlic copolymers (amphiphilic copolymers comprising of a hydrophilic segment and two hydrophobic yet mutually incompatible segments which generate a local microphase-separation.) have have attracted much interest. These copolymers possess the exceptional ability to form multicompartment micelles with hydrophobic, fluorophilic and hydrophilic separated domains. These unusual morphologies, which favor the independent uptake and release of different (and potentially incompatible) compounds, are thought to be promising for drug delivery and controlled release strategies.

This section deals with the self-assembly of fluorinated methacrylates-based diblock and hyperbranched copolymers. It is organized by families of fluorinated methacrylates with increasing number of fluorine atoms (Scheme I-1). One should bear in mind that poly(fluorinated (meth)acrylates) can be amorphous or crystalline depending on the length of their fluoroalkyl side chains. This charateristic can impact the structure of the self-assemblies (*e.g.* polyfluoroalkyl acrylates bearing perfluorinated side chains longer than 6 carbons are usually semi-crystalline and are very hydrophobicity).[27-29]

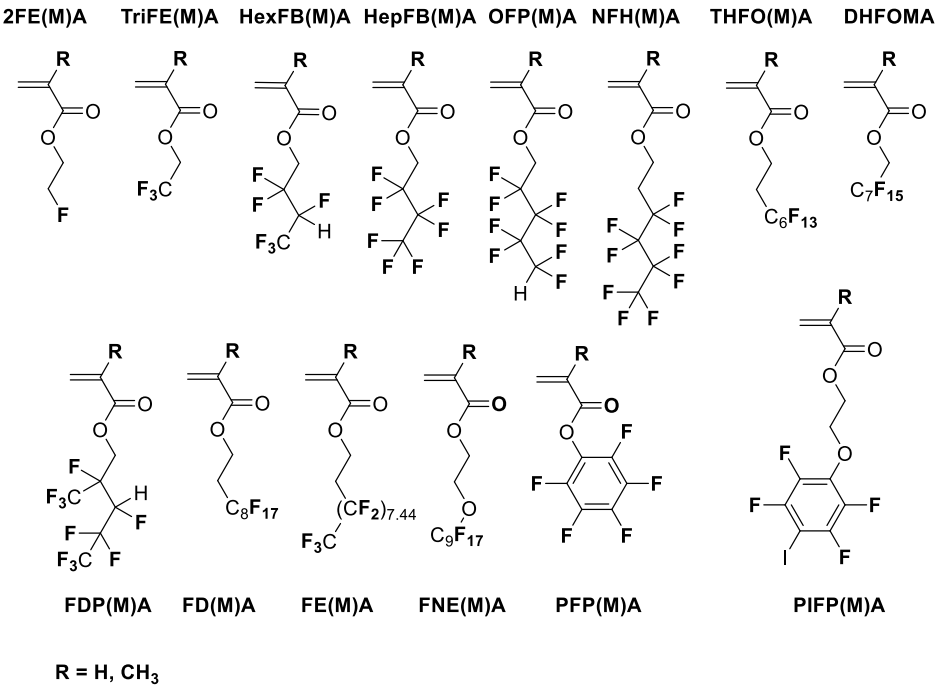

Scheme I-1: Structure of self-assembled fluorinated (meth)acrylates

III.1.1 2-Fluoroethyl methacrylate (2FEMA)

In 2011, Hong *et al.*[30] reported the self-assembly of linear triblock terpolymers PnBMA-*b*-PMMA-*b*-P2FEMA synthesized by RAFT polymerization. The copolymers were self-assembled using Method 2 in a 1:3 v:v mixture of THF (good solvent) and methanol (bad solvent). The $PnBMA_{162}$-*b*-$PMMA_{189}$-*b*-$P2FEMA_{250}$ triblock formed well-defined and uniform spherical aggregates, as observed by SEM (Figure I-1).

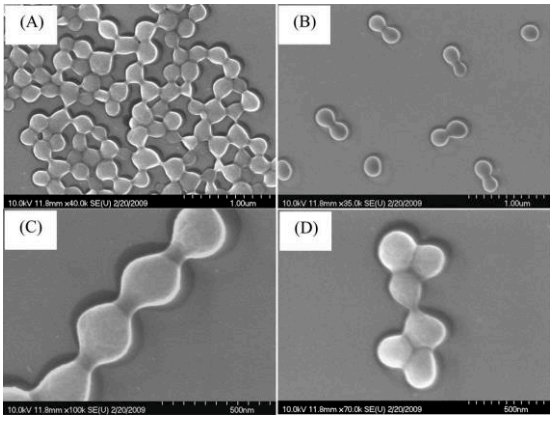

Figure I-1: SEM images of micellar aggregates formed by self-assembly of $PnBMA_{162}$-b-$PMMA_{189}$-b-$P2FEMA_{250}$ in THF/methanol (1:3 v:v) mixture. Reproduced with the permission from ref.[30]. Copyright 2011 Wiley.

III.1.2 2,2,2-Trifluoroethyl methacrylate (TriFEMA)

III.1.2.1 Diblock copolymers

In 2014, Zhang *et al.*[31] reported the self-assembly of PMMA-*b*-PTriFEMA diblock copolymer synthesized by RAFT polymerization. To induce the self-assembly, the block copolymer was dissolved in THF (good solvent for both PMMA and PTriFEMA) and 20 wt. % of water (bad solvent for both blocks) was slowly added. This strategy led to the precipitation of the copolymer into large aggregates (> µm).

The same year, Giacomelli *et al.*[32] reported the one-pot sequential RAFT polymerization synthesis of block copolymers consisting of TriFEMA and OEG(M)A. These copolymers chains undergo self-assembly into well-defined sub-100 nm spherical particles using Method 1 or Method 6.

Zhu *et al.*[26] prepared CO_2- and O_2-responsive polymer nanoaggregates consisting of a hydrophilic PEG block, a CO_2-responsive hydrophobic PDMAEMA and O_2-responsive PTriFEMA block copolymers. The PEG_{45}-*b*-$PDMAEMA_{88}$-*b*-$TriFEMA_{43}$ triblock copolymer was synthesized by ATRP in 2 steps and self-assembled in water into vesicular nanoaggregates using Method 4 (Figure I-2). When treated with CO_2, the vesicular morphology transformed into objects of smaller size, to accommodate the increased interfacial free energy. When treated with O_2, the vesicular morphology was preserved, but its volume expanded. This phenomenon was attributed to the intermolecular interaction between O_2 and PTriFEMA that slightly improved water solubility of the hydrophobic block.

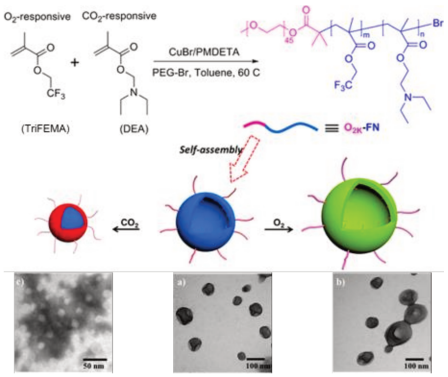

Figure I-2: Figure X. Synthetic routes of CO_2- and O_2-sensitive copolymers. Schematic representations and TEM pictures of CO_2- and O_2-driven self-assemblies in water of PEG_{45}-b-$PDMAEMA_{88}$-b-$TriFEMA_{43}$ triblock copolymers. Adapted with the permission from ref. [26]. Copyright 2014 ACS.

III.1.2.2 Triblock copolymers

In 2012, Whittaker *et al.*[33] reported the effect of solvent on the self-assembly of PAA_{50}-*b*-P(nBA_{39}-*co*-$TriFEA_{115}$) and PAA_{52}-*b*-P(nBA_{39}-*co*-$TriFEMA_{103}$). The triblock copolymers were initially dissolved in acetone or DMF and subsequently analyzed by TEM. Then, the copolymers solutions were dialyzed against DI water and characterized by TEM. In pure DMF, large and diffuse aggregates were observed, while in acetone, cylindrical structures were formed, consistent with predictions based on the relative polymer-solvent interaction parameters. Upon addition of water, both systems formed cylindrical micelles. The same group[34] also reported multifunctional hyperbranched polymers containing iodine and fluorine atoms for applications as MRI contrast agents and bimodal imaging agents.

III.1.2.3 Gradient copolymers

In 2013, Wang *et al.*[35] reported the RAFT synthesis and self-assembly of PAA-*grad*-PTriFEMA gradient copolymers. The copolymers were self-assembled in different THF:water and dioxane:water solvent mixtures. The authors claimed that the copolymers self-assembled in selective solvents to form crew-cut micelles with different ordered structures and that the micellar morphology was significantly affected by the types of solvents and the water concentration in the solvent binary mixtures. These conclusions are solely supported by TEM pictures.

III.1.2.4 Graft copolymers

Xu et al.[36] reported the self-assembly of bottlebrush polymers with PTriFEMA side chains and polynorbornene (PNB) backbones, synthesized *via* sequential ARTP and ROMP. PNB_{21}-*g*-$PTFEMA_{22}$ graft copolymer was self-assembled in EtOAc using method 1 and formed near-spherical particles with a diameter of ca. 10 nm, corresponding to the morphology of a single unimer. When the L/D ratio increased to 2.5 (with L standing for the backbone length and D the side chain diameter), the bottlebrush polymer adopted an elongated shape. Upon further increasing of the L/D ratio to 10, large “spherical” particles with a diameter of *ca.* 25 nm were observed by TEM suggesting that the backbone was partly coiled.

III.1.2.5 Hyperbranched copolymers

Wooley *et al.*[37] synthesized hyperbranched-star amphiphilic fluoropolymers with a core-shell morphology. The hyperbranched core was synthesized in 2 steps. Then poly(TriFEMA-co-*tert*-BA) of various compositions were "grafted" from the core affording 120-140 kDa amphiphilic fluorinated hyperbranched-star polymers. These hyperbranched structures were self-assembled into 20 nm polymer micelles, which presented interesting properties for applications in ^{19}F MRI.

III.1.3 2,2,3,4,4,4-Hexafluorobutyl methacrylate (HexFBMA)

III.1.3.1 Diblock copolymers

Mya *et al.*[38] reported the synthesis and self-assembly in water of PHexFBMA-based block copolymers prepared by sequential RAFT polymerization of HexFBMA and PPGA. $PHexFBMA_{145}$-*b*-$PPGA_{33}$ diblock copolymer was self-assembled in water *via* Method 3. DLS and SLS analyses revealed the presence of large micellar aggregates (50 nm of diameter) with an aggregation number of 40, in good agreement with TEM images (Figure I-3).

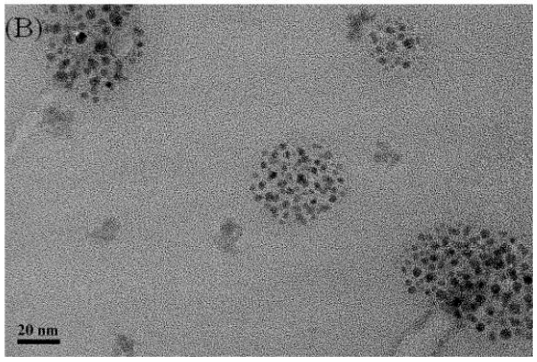

Figure I-3: TEM micrographs of packed structure of $PHexFBMA_{145}$-b-$PPGA_{33}$ diblock copolymer self-assembled in water. Reproduced with the permission from ref. [38]. Copyright 2010 ACS.

III.1.3.2 Triblock copolymers

Zhao *et al.*[39]. reported the synthesis and self-assembly behavior of PHexFBMA-*b*-PMMA-*b*-PMPS triblock copolymer prepared by sequential ATRP of HexFBMA, MMA, and MPS. Upon direct dissolution (Method 1), $PHexFBMA_{15.8}$-*b*-$PMMA_{328}$-*b*-$PMPS_{24.8}$ triblock copolymer self-assembled into spherical micelles in THF, into half-spherical layered micelles in $CHCl_3$, and into multicore micelles in MEK.

In 2014, Feng *et al.*[40] pioneered the synthesis and self-assembly of CO_2-switchable multi-compartment micelles (MCMs) prepared from a linear ABC triblock copolymer synthesized by RAFT polymerization and composed of a PHexFBMA block, a hydrophilic block of PEO and a CO_2-responsive block of PDMAEMA. The (PEG_{113}-*b*-$PHexFBMA_{110}$-*b*-$PDMAEMA_{212}$) triblock copolymer was self-assembled using method 7 and analyzed by TEM. Before CO_2 treatment, the assemblies appeared as spherical aggregates composed of a light core and a dark outer shell, with only little phase segregation in the core. After treatment with CO_2, the aggregates showed clear segregated microdomains typical of MCMs. Different phase-segregated morphologies such as "hamburgers" (1 in Figure I-4b), "reverse hamburgers" (2 in Figure I-4b), "clovers" (3 in Figure I-4b), "soccer ball" (4 in Figure I-4b) and more complicated structures (5 in Figure I-4b) were formed. These phase-segregated morphologies could be switched "on" and "off" by treatment with CO_2 and N_2, via protonation and deprotonation of the tertiary amine groups of the PDMAEMA block.

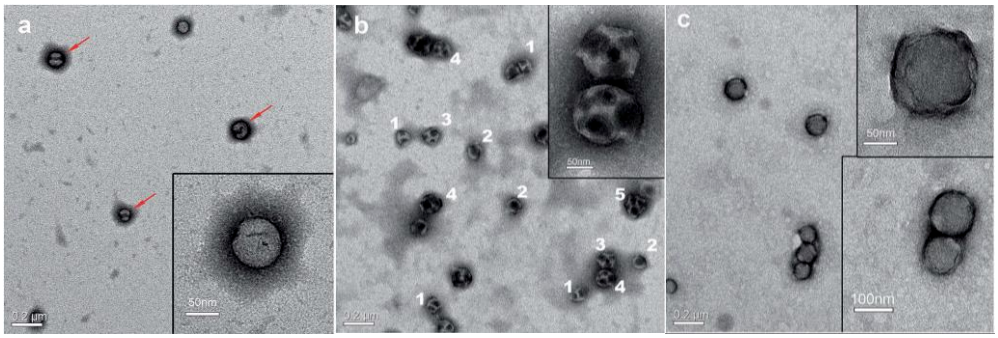

Figure I-4:TEM images of PEG_{113}-b-$PHexFBMA_{110}$-b-$PDMAEMA_{212}$ triblock copolymer self-assemblies in water. (a) before bubbling CO_2, (b) after bubbling CO_2, and (c) after CO_2 removal by N_2 bubbling. Reproduced with the permission from ref. [40]. Copyright 2014 RSC.

The same authors reported[41] the preparation of worm-like micelles (WLMs) from the same PEG-*b*-PHexFBMA-*b*-PDMAEMA triblock copolymer employing method 1. An evolution from spherical micelles to short rods, then cylinders, and finally worm-like micelles was observed when the water volume ratio increased from 0 to 50% in a water/ethanol binary solvent mixture (Figure I-5). It was shown that higher polymer concentrations favored the formation of WLMs, while the length of PDMAEMA block has less impact. The gradually tighter packed arrangement of fluorinated block driven by accumulated interfacial energy may account for the morphological transformation and for the stabilization of the WLMs under CO_2 stimulus even under ultrasonic treatment.

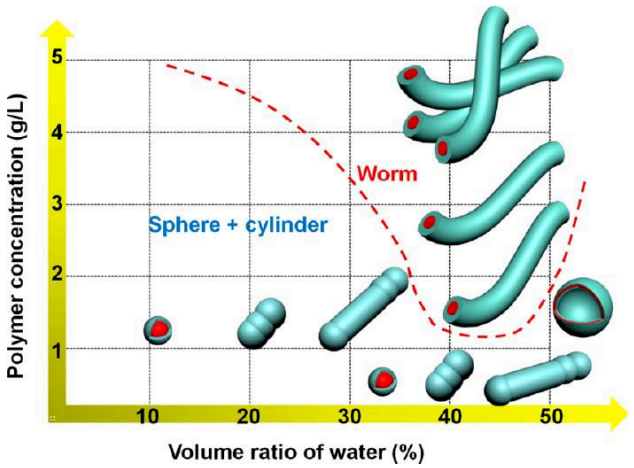

Figure I-5: Phase diagram of the PEG_{113}-b-$PHexFBMA_{110}$-b-$PDMAEMA_{212}$ triblock copolymer in water/ethanol mixed solvent as a function of volume ratio of water and polymer concentration. Reproduced with the permission from ref. [41]. Copyright 2015 ACS.

In 2016, the same group group reported the synthesis and self-assembly of a series of PEG-*b*-PHexFBMA-*b*-PDMAEMA triblock copolymers.[42] The resulting morphologies were spherical for most polymers even under treatment with CO_2. Only nanostructures formed from triblock copolymers of specific and narrow HexFBMA content range ($0.34 \leq f_{HexFBMA} \leq 0.38$) were able to transition from spherical micelles to MCMs after action of CO_2 (Figure I-6).

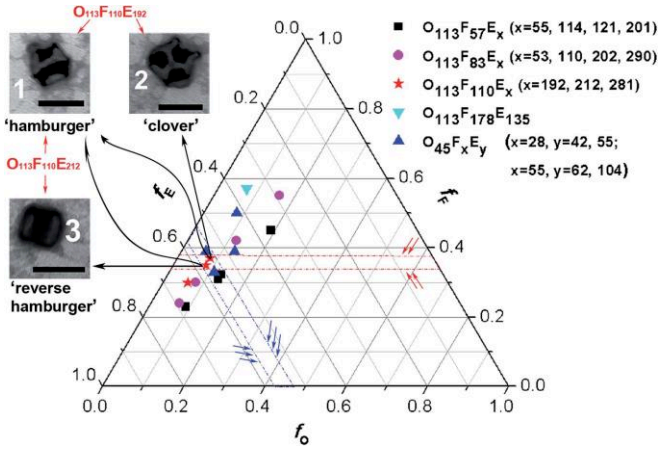

Figure I-6: Ternary phase diagram for PEG-b-PHexFBMA-b-PDMAEMA triblock copolymers in an aqueous solution as a function of composition. f_O, f_F and f_E are the volume fractions of the O (PEG), F (PHexFBMA) and E (PDMAEMA) blocks. Reproduced with the permission from ref. [42]. Copyright 2016 RSC.

III.1.3.3 Graft copolymers

In 2009, Xu *et al.*[43] described the synthesis, self-assembly and encapsulation properties of a series of amphiphilic graft copolymers PHexFBMA-*g*-PSPEG comprising PHexFBMA backbones and PEG side chains. Three solutions of self-assembled nanostructures (c= 0.18 g/L, 0.24 g/L, and 0.3 g/L) were prepared by Method 1. TEM micrographs showed spherical

micellar morphologies in all cases. After bovine serum albumine solution addition, the morphologies evolved from spherical to worm-like (0.18 g/L), vesicle-like (0.24, 0.30 g/L) structures.

In 2016, Pang *et al.*[44] reported the preparation of well-defined thermoresponsive block-graft copolymers PHexFBMA-*b*-(PGMA-*g*-PNIPAM) by ATRP and CuAAC click chemistry. The copolymers were self-assembled using Method 5 and TEM images showed stable spherical nanoparticles with a diameter of about 30–40 nm at 20 °C. Larger and more irregular particles appeared at higher temperatures due to the phase transition of the thermo-sensitive PNIPAM segments.

III.1.4 2,2,3,3,4,4,4-Heptafluorobutyl (meth)acrylate (HepFBMA)

III.1.4.1 Diblock copolymers

Luo *et al.*[45] reported the synthesis and self-assembly of PS-*b*-PHeptFBMA diblock copolymers synthesized by ATRP. The block copolymers were self-assembled in THF/EtOAc binary mixture using Method 2. TEM images suggested transitions from spheres to vesicles with increasing fraction of EtOAc in the solvent mixture.

In 2015, Singha *et al.*[46] reported the synthesis of $PPEGMA_{100}$-*b*-$PHepFBA_{39}$ diblock copolymer and their self-assembly in water using method 1. TEM pictures revealed spherical micelles morphologies. This diblock copolymer was successfully used as surf-RAFT agent (*i.e.* surfactant and macro-RAFT agent) for the miniemulsion polymerization of styrene. The same authors reported the synthesis and self-assembly of $PMMA_{185}$-*b*-$PHepFBA_{152}$ block copolymers.[47] These diblock copolymers were self-assembled *via* Method 2 in MEK:THF binary mixtures. The authors claimed that the self-assembled morphologies evolved depending on the THF:MEK volume ratio from stacked lamellar-like morphologies (THF:MEK = 5:0), to individual lamella rolled-up into nanotubes (THF:MEK = 3:2), worm-like morphologies (THF:MEK = 1:4), and finally spherical micelles (THF:MEK = 0:5).

III.1.4.2 Triblock copolymers

In 2011, Laschewsky and Berlepsch *et al.*[48] studied the self-organization of an amphiphilic ABC triblock copolymer synthesized by sequential RAFT polymerizations of hydrophilic oligo(ethylene oxide) monomethyl ether acrylate (A), lipophilic benzyl acrylate (B), and fluorophilic HepFBA (C). ABC, ACB, and BAC triblock were prepared. These triphlic

copolymers were self-assembled in water using method 5 and characterized by DLS and cryo-TEM. Multiple morphologies were identified: core-shell-corona micelles, spherical micelles with "sickle" fluorocarbon domains at the external interface of the core, bispherical micelles, "soccer ball" morphologies, micelles with "capsule" of fluorocarbon domains inside the core, micelles with "cell" morphologies, and vesicles (Figure I-7).

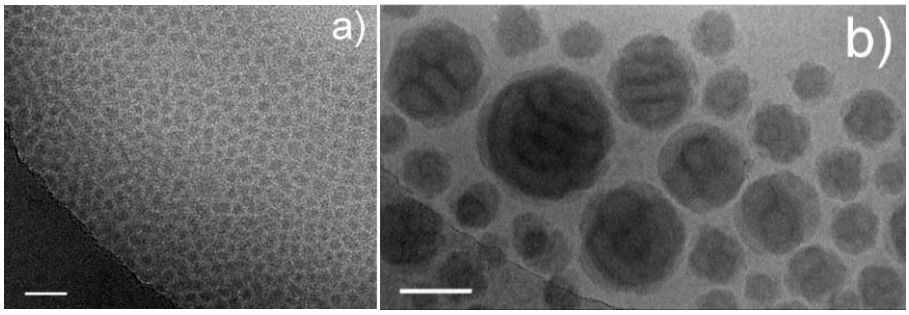

Figure I-7: "Soccer ball" morphologies observed by cryo-TEM images of a 0.5 wt.% solution of $PBzA_{45}$-b-$POEGA_{40}$-b-$PHepFBA_{30}$ in water: (a) as prepared at ambient temperature, and (b) after annealing for 2 weeks at 75 °C (scale bars: 50 nm). Reproduced with the permission from ref. [48]. Copyright 2011 ACS.

The authors showed that the lengths of the individual blocks in the copolymers as well as the block sequences strongly influenced the self-assembled morphologies. Moreover, annealing also had a significant effect. Selective solubilization of substantial quantities of hydrocarbon and fluorocarbon low molar mass compounds by the lipophilic and fluorophilic block, respectively, was demonstrated.

In 2013, Luo *et al.*[49] reported the preparation of spherical aggregates of a non-amphiphilic fluoro-silicone triblock copolymers (PDMS-*b*-PMMA-*b*-PHepFBMA) which was used to stabilize gold nanoparticles.

III.1.4.3 Gradient copolymers

The same year, Luo *et al.*[50] also synthesized a fluorinated amphiphilic gradient copolymers poly(AA-*grad*-HepFBMA) by semi-batch ATRP followed by acid hydrolysis. The copolymer was self-assembled in THF:water binary mixture using Method 2. TEM pictures showed a rich variety of morphologies including crew-cut micelles, pearl chain, dimple-shaped structures, flute-shaped structures, and layered structures depending on the water content in the solvent mixture. Unusual morphologies such as cubic or circle particles were also observed upon varying the polymer concentration.

III.1.5 2,2,3,3,4,4,5,5-Octafluoropentyl methacrylate (OFPMA)

III.1.5.1 Triblock copolymers

Ni *et al.*[51] studied the self-assembly behavior of fluorinated and double-hydrophilic $MePEG_{16}$-*b*-PDMAEMA-*b*-POFPMA triblock copolymers synthesized *via* oxyanion-initiated polymerization. Triblock copolymers were self-assembled using Method 1 at pH =7. Spherical morphologies were mainly observed, but a transition from sphere to rod morphologies occurred upon decreasing the lengths of the MePEG and PDMAEMA blocks. In 2016, Ni and He *et al.*[52] also studied the self-assembly behavior of PIB-*b*-PDMAEMA-*b*-POFPMA and PS-*b*-PDMAEMA-*b*-POFPMA triblock copolymers. It was demonstrated that the flexible PIB block strongly influenced the nature of the self-assembled morphologies, which evolved from spherical multicompartment micelles to fiber-like aggregates, to nanotubules, and finally to rod-like aggregates upon increase of the polymer concentration. Conversely, the rigid PS-based system self-assembled into multicompartment micelles, hamburger-like structures and flowerlike nanoparticles (Figure I-8).

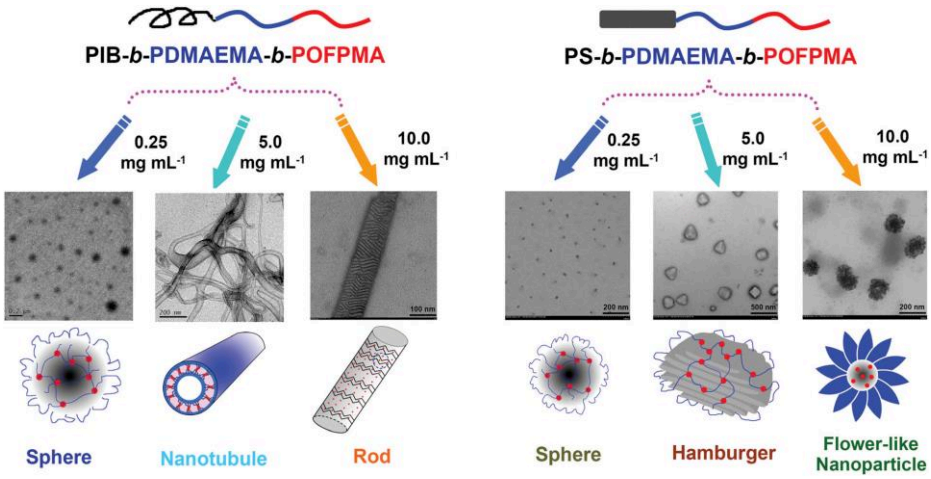

Figure I-8: Schematic illustration and TEM images of the numerous hierarchical assemblies formed from PIB-b-PDMAEMA-b-POFPMA and PS-b-PDMAEMA-b-POFPMA triblock terpolymers. Reproduced with the permission from ref. [52]. Copyright 2016 RSC.

III.1.5.2 Pentablock copolymers

Ni *et al.*[53] also reported the synthesis and self-assembly of fluorinated amphiphilic pentablock copolymers POFPMA-*b*-PEO_{100}-*b*-PPO_{65}-*b*-PEO_{100}-POFPMA using Methods 1 and 3. Method 1 led to well-ordered frozen micelles. As expected, Method 3 resulted in more sophisticated morphologies such as multicompartment micelles or vesicles depending on the length of the fluorinated block.

III.1.5.3 Hyperbranched copolymers

In 2007, Ni *et al.*[54] pioneered the synthesis (via oxyanion-initiated polymerization) and self-assembly of fluorinated hyperbranched star-block copolymers composed of hyperbranched poly[3-ethyl-3-(hydroxymethyl)oxetane] as a core, and PDMAEMA and POFPMA as the constituting blocks of the arms. Using Method 1 in acidic aqueous solution, all the copolymers self-organized into simple multicompartment micelles. In a (1:2, v:v) DMF:water binary mixture at pH 3, HP-DMAEMA$_{30}$-*b*-POFPMA$_{10}$ copolymer self-assembled into well-dispersed multicompartment micelles, while surprisingly, HP-DMAEMA$_{60}$-*b*-POFPMA$_{10}$ copolymer formed nanofibers with thread-like morphologies.

III.1.6 3,3,4,4,5,5,6,6,6-Nonafluorohexyl methacrylate (NFHMA)

III.1.6.1 Diblock copolymer

In 2004, Matsumoto *et al.*[55] reported the synthesis and self-assembly of well-defined PMANa-*b*-PNFHMA amphiphilic diblock copolymers. Using Method 1, these copolymers formed micelles in aqueous solution. DLS, SAXS and SANS analyses revealed that PMANa-*b*-PNFHMA diblock copolymers formed larger micelles than their nonfluorinated analogs. The authors also demonstrated the fluorophilicity of PMANa-*b*-PNFHMA diblock copolymers by selective solubilization of fluorinated low molar mass compounds.

III.1.6.2 Graft copolymer

In 2014, Wang *et al.*[56] reported the aqueous self-assembly using Method 3 of mPEG-*b*-PCL-*g*-PNFHMA terpolymers synthesized by ROP and ATRP. Due to the incompatibility of PCL and PNFHMA, well-segregated Janus-cores were formed. These findings demonstrate that the architecture of each hydrophobic segment can play a significant role in the formation of specific compartmentalized structures.

III.1.7 1H,1H,2H,2H-Perfluorooctyl methacrylate (THFOMA)

In 2003, Busse *et al.*[57] described the self-association properties of di- and triblock copolymers synthesized by ATRP, containing PEO as the hydrophilic blocks and PTHFOMA as the hydrophobic blocks. The block copolymers were self-assembled in water using Method 1 and were analyzed by DLS and TEM. DLS revealed the existence of different types of aggregates in solution, including single chains, micelles, and large clusters. Surprisingly, only large clusters were detected in the case of the triblock copolymers. In addition, depending on

the initial concentration, single micelles, fibrous networks, and irregular morphologies were revealed by TEM.

In 2004, Lim *et al.*[58] reported the synthesis of diblock and statistical copolymers from OEGMA and THFOMA prepared by ATRP and their self-assembly using Method 1 in water and chloroform. In water, micelles were observed by DLS and TEM. In chloroform, $POEGMA_{6.5k}$-*b*-$PTHFOMA_{20k}$ formed worm-like micelles while $POEGMA_{3.4k}$-*b*-$PTHFOMA_{28k}$ self-assembled into large aggregates.

Sawamoto *et al.*[59] reported multipode self-folding copolymers *via* the thermoresponsive intramolecular self-assembly of PEG–methacrylate and THFOMA random copolymers in water, DMF, and 2HPFP. The random copolymers were efficiently obtained by ruthenium-catalyzed living radical copolymerization. They displayed various self-folding structures and local association.

III.1.8 1H,1H,-Perfluorooctyl methacrylate (DHFOMA)

In 2008, Lim *et al.*[60] reported the self-assembly of diblock copolymers consisting of a hydrophilic PEO block and a hydrophobic PDHFOMA block. After direct dissolution in chloroform, PDHFOMA-*b*-PEO diblock copolymers solutions were spin-cast at room temperature. This procedure resulted in the formation of well-ordered spherical morphologies with average diameter of 12-26 nm observed by TEM.

III.1.9 Dodecafluoroheptyl methacrylate (FDPMA)

III.1.9.1 Diblock copolymer

In 2008, Liu *et al.*[61] reported the synthesis and self-assembly of PAA-*b*-PFDPMA diblock copolymers synthesized by RAFT polymerization. These amphiphilic block copolymers were self-assembled using Method 6 with 2-butanone as the good solvent, water:methanol as binary mixtures as bad solvent (then 2-butanone and methanol was remove by dialysis versus water). As revealed by TEM, the morphologies varied from spheres, rods, and vesicles depending on the intitial water fraction of the water/methanol binary mixtures (Figure I-9). The addition of fluorinated hydrophobic homopolymers turned the spheres, rods, and vesicles into larger spheres.

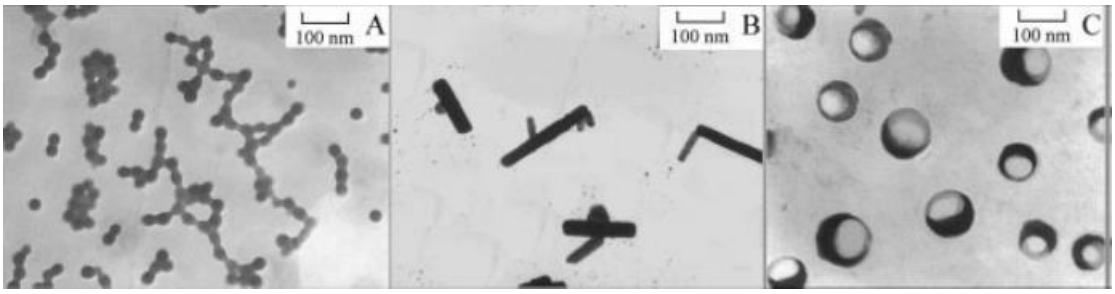

Figure I-9: TEM pictures of the PAA-b-PFDPMA diblock copolymers: Weight fraction before dialysis against water, (A) 84 wt.% 2-butanone and 16 wt.% water/methanol, (B) 62 wt.% 2-butanone and 38 wt.% water/methanol, (C) 50 wt.% 2-butanone and 50 wt.% water/methanol. Reproduced with the permission from ref. [61]. Copyright 2008 Wiley.

In 2012, He and Zhao *et al.*[62] studied the self-assembly of PMMA-*b*-PFDPMA diblock copolymers synthesized by ATRP. These diblock copolymers were self-assembled using method 1 in $CHCl_3$, THF and trifluorotoluene (TFT). In $CHCl_3$, acom-shape particles were observed with a bright and dark color arising from the PMMA and the PFDPMA blocks, respectively. In THF, the TEM pictures showed spherical particles with dark centers and lighter edges. In TFT, the aggregates were constituted of homogeneous unimers due to the good solubility of both PMMA and PFDPMA in this solvent (Figure I-10).

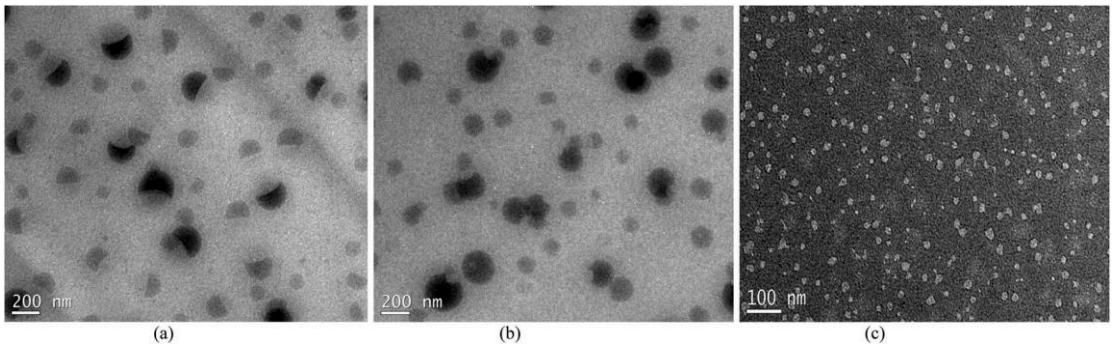

Figure I-10: TEM pictures of PMMA-b-PDPMA diblock copolymers in $CHCl_3$ (a), THF (b), and TFT (c) solutions. Reproduced with the permission from ref. [62]. Copyright 2012 RSC.

III.1.9.2 Hybrid copolymer

In 2015, He *et al.*[63] described the synthesis and self-assembly of polyhedral oligomeric silsesquioxanes-tethered (POSS) fluorinated linear-shaped (ap-POSS‑PMMA-*b*-PFDPMA) and star-shaped (s-POSS‑PMMA-*b*-PFDPMA) diblock copolymers. The two topological diblock copolymers were self-assembled in THF *via* Method 1 and characterized by TEM. Both s-POSS‑PMMA-*b*-PFDPMA and ap-POSS‑PMMA-*b*-PFDPMA self-organized into 200 nm core/shell micelles with a 70‑80 nm shell thickness. The specific morphology of the

micelles was confirmed by elemental mapping and element distribution of the core/shell structures of s-POSS‑PMMA-*b*-PFDPMA.

III.1.9.3 Multiblock copolymer

In 2013, Tuo *et al.*[64] demonstrated that a multiblock structure, synthesized using tetraphenylethane-based polyurethane (PUMI) as macroiniferter for the free-radical polymerization of FDPMA, can self-assemble into various nanostructures during the course of the polymerization. The incompatibility of FDPMA and PUMI leads to the significant decrease of the solubility of PUMI in DMF with the addition of FDPMA monomer, and drives the formation of multicore particles. This morphology can evolve into disk-like structure and form a perfect array, while the tiny particles can reassemble into nanofibers.

III.1.10 1H,1H,2H,2H-Perfluorodecyl (meth)acrylate (FD(M)A)

III.1.10.1 Diblock copolymers

Imae *et al.*[65] investigated the direct self-organization of PMMA-*b*-PFDMA diblock copolymers in acetonitrile and chloroform.Spherical aggregates were observed by cryo-TEM in both solvents. The same authors also investigated the self-organization of PMAA-*b*-PFDMA and PtBMA-*b*-PFDMA diblock copolymers in solution. The size of the polymer micelles increases, as the degree of dissociation of the PMAA blocks increases. Since the charged PMAA block adopts a more stretched structure, PMAA-*b*-PFDMA can easily form large micelles due to the low steric hindrance of PMAA blocks. Addition of NaCl screened electrostatic repulsions in the PMAA chains and induced the formation of smaller micelles. The micelles of PMAA-*b*-PFDMA in ethanol were larger than those of PtBMA-b-PFDMA in the same solvent. The micelle of PMAA-*b*-PFDMA in water possessed a rather thick shell and a large volume per molecule, consistent with the extended hydrated PMAA chain. In contrast, the shell of the PtBMA-*b*-PFDMA micelle in ethanol is thin but has a large surface area (Figure I-11).

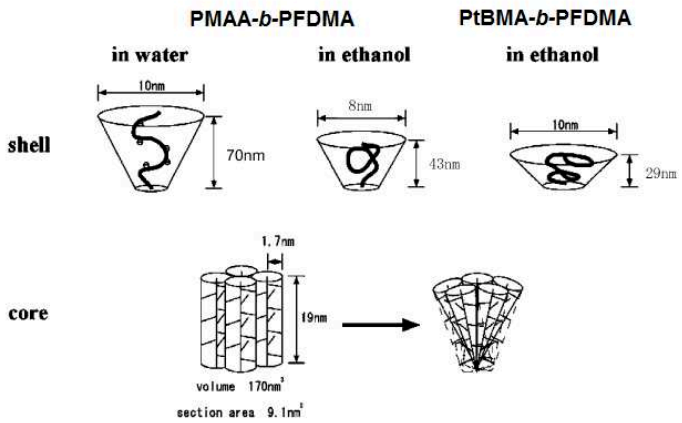

Figure I-11: Schematic representations of PMAA-b-PFDMA and PtBMA-b-PFDMA self-assembled aggregates. Adapted with the permission from ref. [65]. Copyright 2004 Elsevier.

III.1.10.2 Triblock copolymers

In 2009, Laschewsky's and Berlepsch's group[66] reported the RAFT polymerization synthesis of linear amphiphilic diblock and triblock copolymers, from a PEO macromolecular chain transfer agent, butyl- or 2-ethylhexyl acrylate, and FDMA. The self-assembly was performed using Method 5 at room temperature and at 70 °C. In both cases, the polymers tended to form micellar aggregates, which appeared stable over a long period of time. However, fluorinated nanodomains in the cores of the micelles were not observed.The authors suggested the formation of domains that were too small to be resolved. The same authors[67] reported the synthesis and aqueous self-assembly of $PEHA_{120}$-*b*-$POEGA_{50}$-*b*-FDA_{40} triblock copolymer. The self-assembly protocol followed method 5. This triblock copolymer self-assembled into multicompartment micelles both at room temperature andat 70 °C. At 70°C, the micelles were less polydisperse. Such triblock copolymer with two incompatible hydrophobic blocks (POEGA and PFDA) readily form multicompartment micellar aggregates that were characterized in details with powerful imaging techniques (Figure I-12).

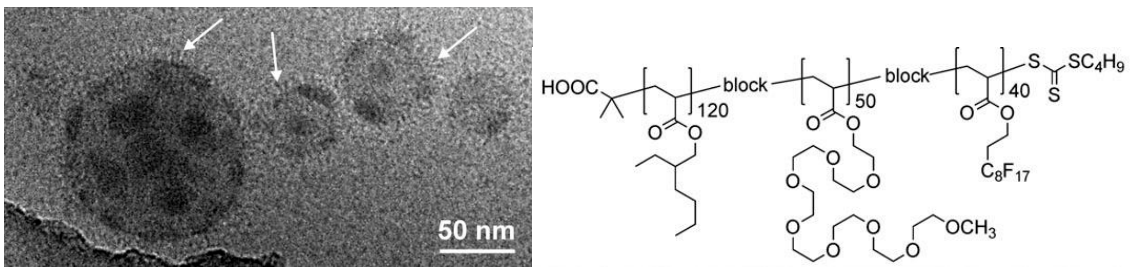

Figure I-12: Cryo-TEM micrographs of $PEHA_{120}$-b-$POEGA_{50}$-b-FDA_{40} triblock copolymer self-assembled in water. Reproduced with the permission from ref. [67]. Copyright RSC 2009.

In 2010, the same authors[68] explored the self-assembled morphologies of a series of POEGA-*b*-PFDA, POEGA-*b*-PBA-*b*-PFDA and PEHA-*b*-POEGA-*b*-PFDA block copolymers. The blocks copolymers were self-assembled in water using Method 3 and Method 6. Whereas only spherical aggregates without phase segregation were observed for the POEGA-*b*-PFDA diblock copolymer, unprecedented multicompartment morphologies, such as "patched double micelle" and larger "soccer ball" structures were identified for POEGA-*b*-PBA-*b*-PFDA and PEHA-*b*-POEGA-*b*-PFDA triblock copolymers.

In 2012, Liu *et al.*[69] reported four triblock copolymers PAA_{65}-*b*-$PCOEMA_{54}$-*b*-$PFDMA_{16}$, PAA_{120}-*b*-$PCOEMA_{100}$-*b*-$PFDMA_{22}$, $PtBA_{65}$-*b*-$PCOEMA_{54}$-*b*-$PFDMA_{16}$, $PtBA_{120}$-*b*-$PCOEMA_{100}$-*b*-$PFDMA_{22}$., and their self-assemblies. Using Method 1, PAA_{65}-*b*-$PCOEMA_{54}$-*b*-$PFDMA_{16}$, PAA_{20}-*b*-$PCOEMA_{100}$-*b*-$PFDMA_{22}$, and $PtBA_{65}$-*b*-$PCOEMA_{54}$-*b*-$PFDMA_{16}$ triblock copolymers formed cylindrical micelles at room temperature in TFT/MeOH binary mixtures with f_{TFT} = 44%, 30%, and 10 vol %. PAA_{65}-*b*-$PCOEMA_{54}$-*b*-$PFDMA_{16}$, PAA_{20}-*b*-$PCOEMA_{100}$-*b*-$PFDMA_{22}$ also self-assembled into cylindrical micelles in either TFT/EtOH or TFT/iPOH at f_{TFT} = 44 vol %. The only exception was $PtBA_{120}$-*b*-$PCOEMA_{100}$-*b*-$PFDMA_{22}$, which had the lowest FDMA weight fraction and the highest soluble block weight fraction among the four triblock copolymers studied. $PtBA_{120}$-*b*-$PCOEMA_{100}$-*b*-$PFDMA_{22}$ formed cylindrical micelles in TFT/MeOH at f_{TFT} = 10 vol %, but a mixture of cylindrical and spherical micelles at f_{TFT} = 30% and 44 vol %. The micelles all possessed an PFDMA core, a PCOEMA shell, and a PAA or PtBA corona. TEM images indicated that the PFDMA chains in the core-forming block were almost fully stretched and that the PCOEMA shell chains in the PAA/PCOEMA/PFDMA cylindrical micelles were radially compressed relatively to their undisturbed dimensions. The authors suggested that it probably arise from the fluorinated-block-driven micellization, which yielded cylinders with abnormal shell thicknesses.

The same authors[70] also reported the preparation of a triblock terpolymer PEO-*ONB*-PFDMA-*b*-PCOEMA for application in coatings. PEO is water-soluble, PCOEMA is photo-cross-linkable, PFDMA has low surface tension, and *ONB* denotes a photocleavable *o*-nitrobenzyl unit at the junction of the PEO and PFDMA blocks. The copolymer was self-assembled in water *via* Method 2. The resulting dispersions were aero-sprayed, and the coating was analyzed by TEM and AFM. TEM images of the aerosprayed micelles seemed to exhibit a bimodal distribution of spherical aggregates. The smaller particles had average AFM and TEM diameters of 31 ± 5 and 18 ± 4 nm, respectively, while the larger particles had AFM and TEM diameters of 47 ± 7 and 33 ± 6 nm, respectively.

Finally, they reported[71] the preparation of micellar aggregates with shapes resembling quadrilaterals, triangles, and eyes morphologies from an ABC triblock terpolymer containing PAA, PCOEMA, and PFDMA blocks. The polygonal micelle aggregates were produced via recrystallization in TFT/MeOH mixture with f_{TFT} = 10 vol % (Figure I-13).

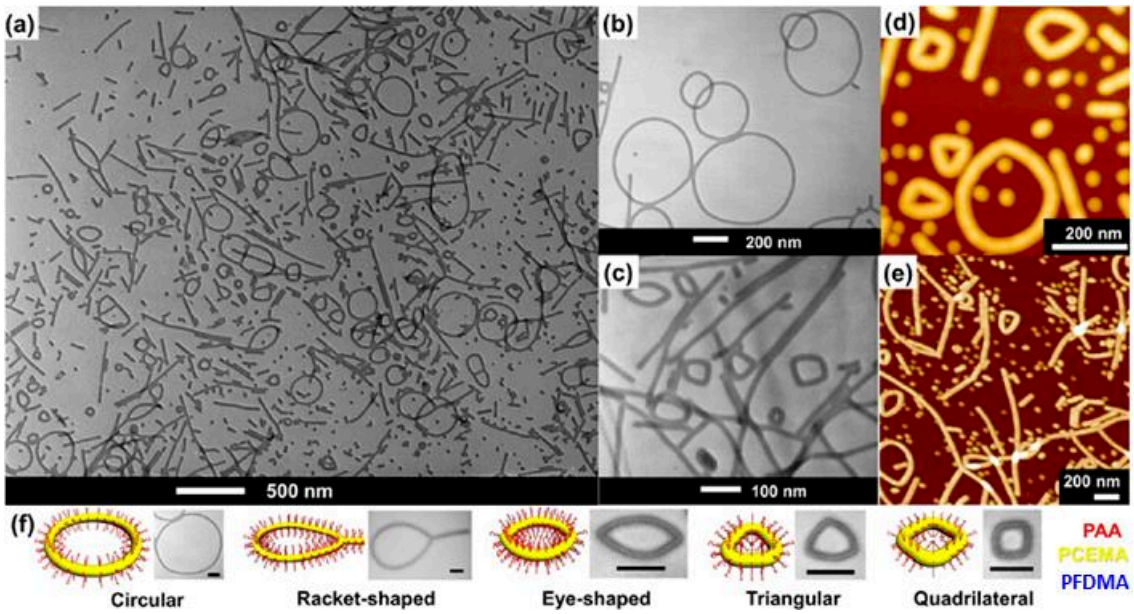

Figure I-13: (a-c) TEM images and (d-e) AFM images of PAA_{65}-b-$PCEMA_{54}$-b-$PFDMA_{16}$ micellar aggregates prepared at 1.0 mg/mL in TFT/MeOH at f_{TFT} = 10 vol %. (f) Schematic structures and representative TEM images for toroid, racket-shaped, and some polygonal micellar aggregates. Reproduced with the permission from ref. [71]. Copyright 2013 ACS.

III.1.11 Perfluoroalkyl ethyl methylacrylate (FEMA)

III.1.11.1 Diblock copolymers

In 2014, Li *et al.*[72] reported P(MMA-*co*-MAA)-*b*-PFEMA diblock copolymers synthesized by RAFT polymerization and self-assembled in water *via* method 3. The triphilic copolymers (hydrophilic, lipophilic, and fluorophilic due to MAA, MMA, and FEMA units, respectively) displayed nanostructures, which changed from spheres and short worms to wormlike structures, to tapered worms, and finally to nail-shaped structures, as the water content increased from 10, 20, 40 to 80 vol %. The micelle morphologies evolved upon the addition of water due to the increase of the interfacial tension between the core-forming block and the solvent (Figure I-14).

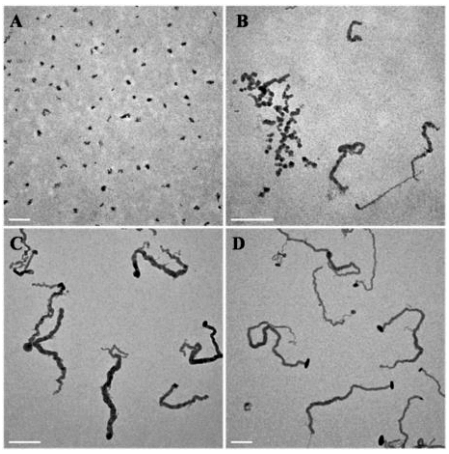

Figure I-14: TEM pictures of P(MMA-co-MAA)-b-PFMA micelles evolution with the addition of water: (A) WC-10%; (B) WC-20%; (C) WC-40% and (D) WC-80 vol % (WC stands for water content). Reproduced with the permission from ref. [72]. Copyright 2014 RSC.

III.1.12 Iodotetrafluorophenoxy methacrylate (IFPMA)

In 2015, Taylor *et al.*[73] described an attractive method based on non-covalent halogen bonding interactions as the driving force for the solution self-assembly of fluorinated copolymers. First, a PEG-*b*-PDMAEMA acceptor diblock copolymer was synthesized by ATRP, then PEG-*b*-PIFPMA diblock copolymers donors were prepared by RAFT (PIFPMA stands for poly(iodotetrafluorophenoxy methacrylate)). When a block copolymer donor was combined with a block copolymer bearing halogen-bond-accepting amine groups, higher-order structures were obtained in both organic solvents and water. TEM, DLS, and NMR data are consistent with structures having cores composed of the interacting halogen-bond-donor and acceptor segments.

III.1.13 Mixture of Monomers

Lim *et al.*[74] reported the preparation of amphiphilic semifluorinated block copolymers composed of PDMAEMA as the hydrophilic block and PDHFOMA or PTHFOMA block as the fluorophilic block. After direct dissolution in water and chloroform, the micellar characteristics of the copolymers were investigated by quasi-elastic light scattering and TEM. The size and morphologies of the micelles were greatly influenced by the copolymer composition, the pH, and the temperature. In addition, the formation of water-in-carbon dioxide (W/C) microemulsions were studied and the block copolymer showed an excellent ability to stabilize W/C microemulsions.

In 2014, Niu *et al.*[75] studied the self-assembly and surface behavior of a linear fluorosilicone pentablocks synthesized *via* two-step ATRP using a bifunctional poly(dimethylsiloxane)

macro-initiator, followed by a chain extension with PMMA and polymers of various fluorinated methacrylates such as TriFEMA, HexFBMA, OFPMA, and FDMA. Due to the excellent surface properties of PFDMA-*b*-PMMA-b-PDMS-*b*-PMMA-*b*-PFDMA pentablock copolymer, the effect of $CHCl_3$, THF, TFT and $CHCl_3$–TFT solvents on the self-assembly and surface properties were investigated by DLS and TEM. The analyses showed that this pentablock copolymer self-assembled into pure micelles in TFT solution, in a mixture of micelles and unimers in $CHCl_3$ and $CHCl_3$–TFT solution, while it was completely dissolved in THF.

Rodionov *et al.*[76] briefly studied a number of fluorinated amphiphilic star block-copolymers starting from a tris(benzyltriazolylmethyl)amine, and composed of diblocks of polypentafluorostyrene (PPFS), PHepFBA, or PTHFOA and hydrophilic POEGSt or POEGMA. Spherical aggregates with diameters ranging between 20 and 50 nm were the main type of assemblies for PFS-, HepFBA- and THFOA-based copolymers. However, increasing the weight fraction of the PHepFBA fluorinated block in the copolymer led to more complex morphologies. For instance, $(PHepFBA_{20}$-*b*-$POEGSt_4)_3$ star block copolymer, which contains 67 wt.% of the fluorinated monomer, self-assembled into well-defined vesicles (unilamellar and multilamellar) (Figure I-15).

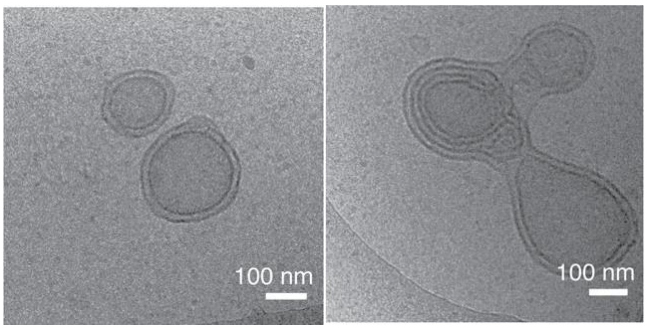

Figure I-15: Cryo-TEM images of $(PHepFBA_{20}$-b-$POEGSt_4)_3$ vesicular structures (unilamellar and multilamellar). Reproduced with the permission from ref. [76]. Copyright 2014 RSC.

III.2 Polymerization-Induced Self-Assembly

Polymerization-Induced Self-Assembly (PISA) strategy has emerged as a very powerful technique to prepare self-assembled polymer aggregates with controlled and defined morphologies at high solids contents and with high reproducibility.[77,78] Typically, under PISA process, a solvophilic polymer precursor dissolved in a solvent is extended with a solvophobic polymer. As the polymerization proceeds, the chain extension leads to an

"amphiphilic" block copolymer that self-assembles into self-stabilized nano-objects. When combined to RAFT techniques (to name the most commonly used RDRP techniques in PISA), it allows the formation of sophisticated morphologies such as worm-like micelles and vesicles, and so one. So far, most PISA protocols have used RAFT polymerization in dispersion or in emulsion .

III.2.1 Alkyl Perfluorinated (meth)acrylate

In 2008, Thurecht and Howdle[79] pioneered the use of fluorinated macro-RAFT agent to the surfactant-free for the polymerization of MMA in $ScCO_2$. A PDHFOMA macro-CTA was synthesized by RAFT and chain extended with PMMA. The polymerization exhibited exceptionally good control in dispersion polymerization conditions and resulted in well-defined core-shell spherical 1-5 μm particles.

A few years later, Armes[80] and coworkers reported the morphological transition of PMAA-*b*-PBzMA block copolymers self-assembled nanostructures upon chain extension of the diblock with poly(TriFEMA) in alcoholic dispersion. (Figure I-16)

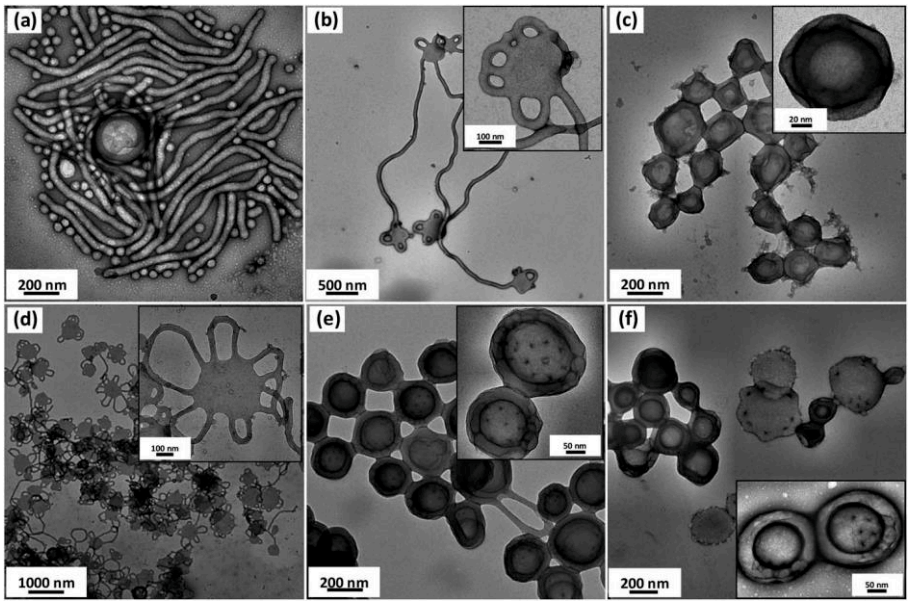

Figure I-16: Representative TEM images obtained for a) $PMAA_{70}$-b-$PBzMA_{100}$-b-$PTFEMA_{100}$; (b) $PMAA_{70}$-b-$PBzMA_{200}$-b-$PTFEMA_{200}$; (c) $PMAA_{70}$-b-$PBzMA_{70}$-b-$PTFEMA_{223}$; (d) $PMAA_{70}$-b-$PBzMA_{191}$-b-$PTFEMA_{60}$; (e) $PMAA_{70}$-b-$PBzMA_{243}$-b-$PTFEMA_{60}$; (f) $PMAA_{70}$-b-$PBzMA_{273}$-b-$PTFEMA_{60}$. Reproduced with the permission from ref. [80]. Copyright 2014 RSC.

A series of PMAA−*b*−PBzMA diblock copolymer nanoparticles formed by RAFT alcoholic dispersion polymerization of BzMA using a PMAA macro-CTA were synthesized. Chain extension reactions were then carried out in the presence of TriFEMA. These seeded PISA protocols resulted in remarkable morphological transitions. For example, as the TriFEMA polymerization proceeded, the copolymer self-assembled nanostructures evolved from worm-like micelles to spheres to worms again and ultimately to vesicles. When $PMAA_{70}$-*b*-$PBzMA_x$-*b*-$PTriFEMA_y$ triblock of various compositions were prepared, surprising morphologies like bilayer-type flat patches (Figure I-16b) or flat bilayer patches with multiple worm loops were observed (Figure I-16d).

The same group[81] achieved the first polymerization induced self-assembly of TriFEMA in ethanol. First a range of PMMA and PDMAEMA macro-CTAs were synthesized by RAFT and extended with PTriFEMA. TEM images indicated that well-defined spherical nanoparticles were obtained when using either the $PMAA_{70}$ or the $PDMAEMA_{94}$ macro-CTAs. In contrast, using a shorter $PDMAEMA_{43}$ macro-CTA led to the formation of spheres which evolved into worms and polydisperse vesicles with TriFEMA conversion. This evolution of the self-assembled morphologies is caused by the gradual reduction in the molecular curvature of the growing copolymer chains. In addition, spherical nanoparticles were also prepared using anionic $PMAA_{70}$ and cationic $PDMAEMA_{43}$ macro-CTAs and targeting somewhat shorter DPs for the core-forming PTriFEMA block.

The same year, Li 's group[82] reported a similar PISA process using a PMAA macro-CTA and PTriFEMA as the core-forming fluorinated polymer. They observed the same evolution from spheres, to worms and vesicles as the polymerization of TriFEMA proceeds.

Recently, Detrembleur's group[83] used the PISA process in water for the preparation of transparent superhydrophobic coatings. Hydrophilic PMAA macro-CTA was synthesized, and chain-extendedwith poly(n-butyl acrylate). In a third step, FDMA and n-butyl acrylate were successfully copolymerized in the presence of the PMAA-*b*-PBA macroCTA to produce stable fluorinated particles. The synthesis of PMAA-*b*-PFDMA diblock copolymer by PISA without intermediate PBuA block was also attempted. This led to a mixture of PMAA-*b*-PBA and PFDMA. The PMAA-*b*-PBA-*b*-P(BA-*co*-FDMA) micelles (33 nm in diameter revealed by DLS and TEM) solutions were successfully spin-coated onto several substrates and produced after further treatment superhydrophobic transparent coatings.

In 2015, Ma's group[84,85] reported the *ab initio* emulsifier-free emulsion copolymerization of a mixture of monomers (2-(Acryloyloxy)ethyl)trimethylammonium chloride, Styrene, Butyl Acrylate, HexFBMA, Stearyl Acrylate) using a quaternized PDMAEMA-*b*-PHexFBA as macro-CTA. The authors claimed with little evidence the successful copolymerization of the monomer mixture and the efficient chain extension of the PDMAEMA-*b*-PHexFBA macro-CTA. The same group[86] reported the formation in ethanol of stabilized spherical particles synthesized by PISA using PAA as the hydrophilic block and PHexFBMA as the fluorophilic/hydrophobic block. TEM and DLS investigations showed spherical core-shell latex particles composed of PAA-*b*-PHexFBA block copolymers. The size of these latex particles tended to increase with increasing pH.

In a another study, Armes and coworkers[87] investigated by SAXS, the effective particle density, steric stabilizer layer thickness as well as the volume-average number of a series of $PGMA_x$-*b*-$PTFEMA_y$ nanoparticles synthesized by PISA.

III.2.2 Pentafluorophenyl (meth)acrylates

Perfluorinated alkyl methacrylates have been the most studied fluorinated monomer in PISA process to date. The Lowe group reported two articles dealing with the PISA of pentafluorophenyl methacrylates.

In 2014, they reported[88] the preparation of fluorinated polymethacrylate copolymer via RAFT dispersion polymerization in ethanol of 3-phenylpropyl methacrylate (PPMA) in presence of 3 fluorinated macro-CTAs: (Scheme I-2). All PISA yielded soft matter aggregates presenting the usual morphologies: spherical micelles, worms and vesicles. The pentafluorophenyl segment was further chemically modified by a thiosugar in the presence of an organobase. In the case of the poly[($DMAEMA_{31}$-*co*-$tBAFPEMA_2$)-*b*-$PPMA_{48}$] with TEM indicated no change in the morphology after reaction with the thiosugar while worm-like nanoparticles formed from poly[(DMAEMA31-*co*-$tBAFPEMA_2$)-*b*-$PPMA_{95}$] resulted into a mixed phase of spheres and worms after glycosylation.

Following a similar methodology, the same group also reported[89] the preparation of other fluorinated soft matter nanoparticles with various morphologies via RAFT-PISA. Starting from a stearyl methacrylate (SMA) and pentafluorophenyl methacrylate (PFPMA) (up to 12 mol % PFPMA) copolymer macro-CTA of synthesized in toluene, they performed the RAFT dispersion polymerization of 3-phenylpropyl methacrylate (PPMA) in n-octane or n-

tetradecane. TEM images showed typical PISA morphologies such as spheres, worms and vesicles. The reactive pentafluoro methacrylate units were then modified into acrylamide via acyl substitution reaction with primary amine.

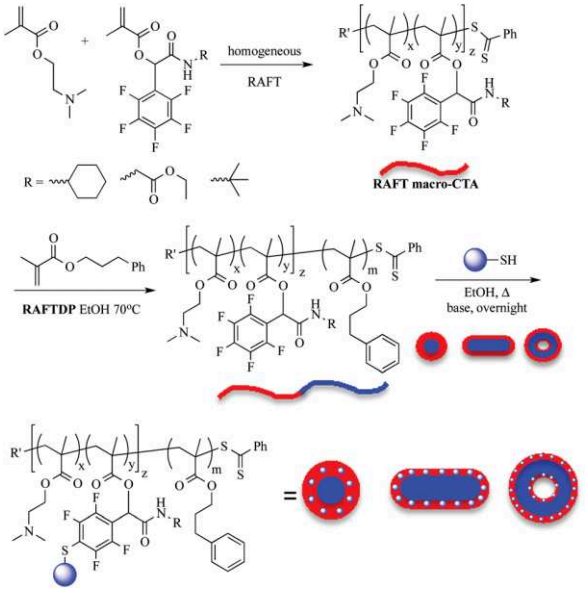

Scheme I-2: PISA of pentafluorophenyl methacrylate via a combination of homogeneous RAFT with Passerini-synthesized methacrylates (CyAFPEMA, EAFPEMA or tBAFPEMA), RAFT dispersion polymerization and nucleophilic aromatic substitution with thiols. Reproduced with the permission from ref. [88]. Copyright 2015 RSC.

IV. Self-Assemblies of amphiphilic fluorinated styrene-based copolymers

In 2005, the aqueous self-assembly of an ABC linear triblock copolymer, poly(4-methyl-4-(4-vinylbenzyl)morpholin-4-ium chloride)-*b*-polystyrene-*b*-poly(pentafluorophenyl 4-vinylbenzyl ether) (PVBM-*b*-PS-*b*-PVBFP) was reported by Laschewsky *et al.*[90] (Figure I-17). The copolymer building blocks consist of a long cationic hydrophilic block, PVBM, and two short consecutive hydrophobic blocks: a hydrocarbon block (PS) and a mixed hydrocarbon/fluorocarbon block (PVBFP). PVBM-*b*-PS-*b*-PVBFP triblock copolymer was obtained by reaction of *N*-methylmorpholine with poly(vinylbenzyl chloride)-*b*-PS-*b*-PVBFP precursor. This triblock precursor was prepared by a three-step RAFT process using benzyl dithiobenzoate as the CTA. The triblock copolymer was dispersed in a dioxane/water binary mixture and self-assembled using Method 7. Cryo-TEM images revealed the presence of 20–30 nm multicompartment micelles. Their core was segregated into nanometer-sized

compartments in which many small, fluorocarbon-rich domains coexisted with a continuous hydrocarbon-rich region (Figure I-17).

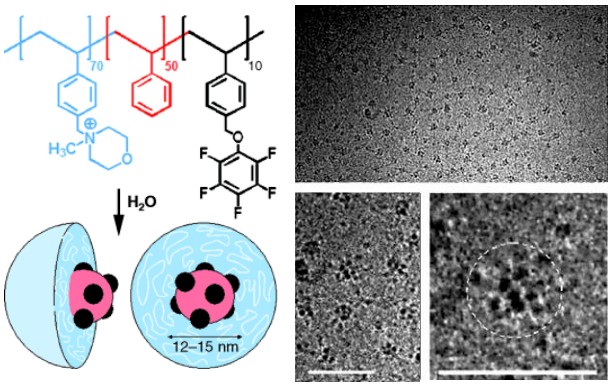

Figure I-17: Structure of PVBM-b-PS-b-PVBFP triblock copolymer, cryo-TEM images, and schematic representation of multicompartment micelles arising from the self-assembly of PVBM-b-PS-b-PVBFP triblock copolymer in water. The corona of the micelles is not visible. The scale bars correspond to 50 nm. Adapted with the permission from ref. [90]. Copyright 2005 Wiley Interscience.

Taking advantage of the slow kinetics of block copolymer chains in solution and of the complexation of charged blocks with multivalent counterions, Pochan *et al.*[91] obtained complex micelles containing multiple hydrophobic blocks within the same micelle core that can undergo local, intramicellar phase separation. The key point for choosing the different chemistries of the two hydrophobic blocks is that the two blocks are highlyimmiscible. Polystyrene (PS) and poly(2,3,4,5,6-pentafluorostyrene) (PPFS) were employed as the different, third hydrophobic blocks in the two triblock copolymers PAA_{94}-*b*-PMA_{103}-*b*-PS_{117} and PAA_{93}-*b*-PMA_{99}-*b*-$PPFS_{100}$, synthesized by ATRP. Equal molar amounts of these two triblock copolymers were dissolved in pure THF. Then, 2,2'-(ethylenedioxy)diethylamine (EDDA) was added to reach a final 1:1 molar ratio of amine and acid functional groups. The diamines underwent complexation with the PAA blocks, thereby forming aggregates with PAA-diamine cores. Notably, these aggregates contained both triblock copolymers. Next, introduction of water into the THF solution up to a final ratio of THF:water = 1:2 triggered the formation of cylindrical micelles. However, the presence of immiscible PS and PPFS in the triblock copolymer aggregates, resulting from thePAA-diamine complexation, forced the local co-assembly of unlike third hydrophobic blocks into the micelle cores. In addition, the lack of chain exchange in solution that disallows global chain migration and maintains nonequilibrated micelle structures, combined with the fact that the PAA chains in the corona of the newly formed micelles were still complexed with diamines and were not freely mobile within the micelle, guaranteed the stability of the mixed-core micelle. The immiscibility of the two different hydrophobic blocks, PS and PPFS, eventually resulted in internal phase

separation at the nanoscale, producing multicompartment micelles. Internal phase separation is clearly indicated by the strong undulations along the cylinder surfaces and the TEM contrast variation along the cylinders (Figure I-18).

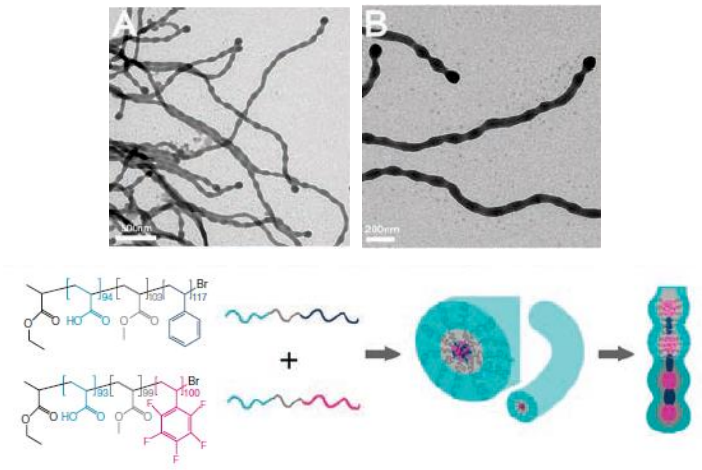

Figure I-18: Nanostructured multicompartment cylinders. (A and B) Bright-field TEM images. Dark regions present polypentafluorostyrene-chain rich area (G) Schematic illustration of formation of multicompartment cylinders. Adapted with the permission from ref. [91] Copyright 2007 Science.

In 2009, Davis *et al.*[92] reported the synthesis of a pH-responsive amphiphilic block copolymer poly(2-dimethylaminoethyl methacrylate)-*b*-poly(pentafluorostyrene) (PDMAEMA-*b*-PPFS) using RAFT polymerization. Copolymer micelle formation, in aqueous solution using method 1, was investigated by fluorescence spectroscopy, SLS, DLS, and TEM. DLS and SLS measurements revealed that the diblock copolymers formed spherical micelles with large aggregation numbers ($N_{agg} \approx 30$) where the dense PPFS core is surrounded by dangling PDMAEMA chains as the micelle corona. The hydrodynamic radii, R_h of these micelles was large, at pH 2–5 as the protonated PDMAEMA segments swelled the micelle corona. Above pH 5, the PDMAEMA segments were gradually deprotonated, resulting in a lower osmotic pressure and enhanced hydrophobicity within the micelle, thus decreasing the R_h. However, the radius of gyration (R_g) remained independent of pH as the dense PPFS cores predominated.

In 2010, Davis *et al.*[93] synthesized well-defined fluorinated brush-like amphiphilic diblock copolymers of poly[poly(ethylene glycol)methyl ether methacrylate] (PPEGMA) and PPFS by ATRP. The self-assembly behavior of these polymers in aqueous solutions using method 1 was studied by ^{1}H NMR, fluorescence spectrometry, SLS, DLS, and TEM. The micellar structure comprised of PPFS as the core and comb-like polymers as the coronae. The hydrodynamic radius (R_h) of the micelles in aqueous solution was in the nanometer range,

independent of the polymer concentration, consistent with a closed association model. Diblock copolymers with a longer PPEGMA block formed micelles with smaller R_h and lower aggregation numbers consistent with an improved solubilization of the core. The micelles possessed a thick hydration layer as verified by the R_g/R_h ratio. The aggregation number and R_g/R_h ratio were observed to increase with temperature (20-50 °C), while the R_h of the micelle decreased slightly over the same temperature range. An increase in temperature induced the comb-like PEG segments in the corona to dehydrate and shrink. This LCST behavior led to theformation of micelles with larger aggregation numbers.

The same authors also reported the synthesis, micelle formation, and bulk properties of semifluorinated amphiphilic PEG-*b*-PPFS-*g*-POSS (POSS stands for polyhedral oligomeric silsesquioxane).[94] The synthesis of PEG-*b*-PPFS diblock copolymer was achieved *via* ATRP using a modified poly(ethylene glycol) as the macroinitiator. Subsequently, a portion of the reactive fluorine atome on the *para* position of the PPFS units was replaced with aminopropylisobutyl POSS through aromatic nucleophilic substitution reactions. The products, PEG-*b*-PPFS and PEG-*b*-PPFS-*g*-POSS, were subsequently self-assembled in aqueous solutions using method 3 to form micellar structures. The CMC of these polymer family was found to decrease concomitantly with the number of POSS particles grafted per copolymer chain. The R_h of the micelles, calculated from DLS data, increase as the number of POSS molecules grafted per copolymer chain increases. For instance, R_h increased from *ca.* 60 nm for PEG-*b*-PPFS to *ca.* 80 nm for PEG-*b*-PPFS-*g*-$POSS_{25}$. The R_g/R_h values were consistent with a spherical particle model having a core-shell structure.

In 2010, Wooley *et al.*[95] synthesized complex amphiphilic polymers *via* core-first polymerization followed by alkylation-based grafting of poly(ethylene oxide) (PEO). 1-(40-(bromomethyl)-benzyloxy)-2,3,5,6-tetrafluoro-4-vinylbenzene was synthesized and subjected to atom transfer radical self-condensing vinyl polymerization to afford hyperbranched fluoropolymer (HBFP) as the hydrophobic core component with a number-average molar mass of 29 kDa and a dispersity of 2.1. The alkyl halide chain ends on the HBFP were allowed to undergo reaction with monomethoxy-terminated poly(ethylene oxide) amine (PEO_x-NH_2) to produce PEO-functionalized HBFPs of different grafting densities with different PEO chain lengths. The amphiphilic grafted block copolymers were found to aggregate in aqueous solution using method 6 to give 12–28 nm micelles. An increase of the PEO:HBFP ratio, by increase in either the grafting densities or in the PEO chain lengths, led to smaller micelle. These complex, amphiphilic $(PEO_x)_y$-HBFPs were expected to find

potential applications as nanoscopic biomedical devices, such as drug delivery vehicles and ^{19}F magnetic resonance imaging agents.

Tan *et al.*[96] synthesized a series of amphiphilic copolymers by radical copolymerization of sodium 2-acryamido-2-methylpropanesulfonate and styrene derivatives with a fluorocarbon side chain. The aggregation behavior of the copolymer in aqueous solution using Method 1 was studied by surface tension, electrical conductivity, DLS, TEM, and fluorescence measurements in different conditions. The results indicated that the surface activity was dependent on the fluorocarbon groups content in the copolymer structure. The surface tension and the CMC concentration decreased with increasing sodium chloride concentration. The copolymers formed micelle-like aggregates and the fluorocarbon groups exhibited a strong tendency for intermolecular association.

V. Self-Assemblies of PFPE-based Copolymers

V.1 PFPE-based miktoarm triblock copolymers

In the early 90's, Ringsdorf stated: "polymer science is able to contribute to the simulation of cellular processes".[97] The concept of multicompartment micelles is an important step toward achieving this goal since it draws inspiration from naturally occurring phenomena. For instance, biological systems such as eukaryotic cells possess subdivided domains, which fulfill numerous different cellular functions. Similarly, multicompartment micelles may enable the concurrent transport of incompatible molecules within their subdivided compartments.[98] The ABC miktoarm (μ-ABC) star terpolymer architecture provides a versatile and powerful route toward multicompartment micelles. Indeed, due to the mandatory convergence of three blocks at a common point, the miktoarm star architecture effectively suppresses the formation of the default core/shell/corona "onion-like" arrangement often adopted by linear ABC triblock terpolymers. This leads to segregation of all three mutually immiscible polymer chains at their point of contact. In 2004, Lodge *et al.*[19] observed the formation in dilute aqueous solution of a previously unknown class of multicompartment micelles from a miktoarm star polymer comprisinga water-soluble poly(ethylene oxide) (PEO)arm and two hydrophobic immiscible components, poly(ethylethylene) (PEE) and poly(perfluoropropylene oxide) (PFPO) (Scheme I-3).

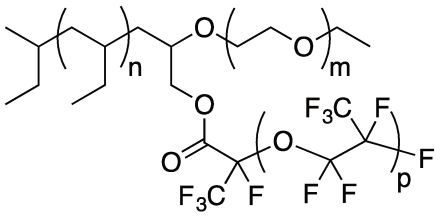

Scheme I-3: Structure of miktoarm μ-(PEE)(PEO)(PFPO) triblock copolymers synthesized by Lodge et al.[19]

These μ-(PEE)(PEO)(PFPO) star triblock copolymers, abbreviated μ-EOF, were prepared using two successive anionic polymerization steps and one polymer-polymer coupling reaction.[99] First, polybutadienyllithium was end-capped by 2-methoxymethoxymethyloxirane (MOM), resulting in the formation of a polymeric hydrocarbon containing one free hydroxyl group and one MOM-protected hydroxyl group at the same chain-end. The corresponding polyethylethylene (PEE-OH) was then obtained by subsequent catalytic hydrogenation. The PEO-PEE diblock copolymer was prepared by polymerization of ethylene oxide from the corresponding alkoxide macroinitiator (PEE-O^-). After removal of the MOM protecting group located at the junction of the PEO and PEE blocks, acid chloride end-functional PFPO was reacted with the free hydroxyl group to form well-defined μ-EOF star triblock copolymers. Different type of multicompartment micellar structures were identified in dilute aqueous solution depending on the composition of the μ-EOF star triblock copolymers, as revealed by cryogenic transmission electron microscopy (cryo-TEM) (Figure I-19).[100]

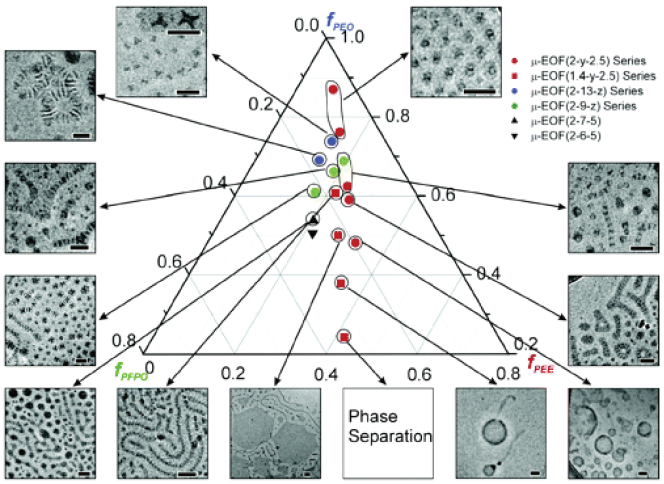

Figure I-19: Multicompartment micelle morphology diagram for μ-EOF miktoarm star terpolymers in dilute aqueous solution as a function of composition. f_{PEE}, f_{PEO}, *and* f_{PFPO} *are the volume fractions of the PEE, PEO, and PFPO blocks, respectively. They are designated μ-EOF(x-y-z), where x, y, and z represent the E, O, and F block molar masses, respectively, in kD. Reproduced with permission from ref [100]. Copyright 2006 American Chemical Society.*

The observed micellar structures were generally correlated with the O corona size and the relative length of the E and F blocks. The strong incompatibility of the three polymeric components drove the formation of segregated micelle cores even at modest molar mass. The extreme hydrophobicity of the F block placed the system in the superstrong segregation regime (SSSR),[101] within which the interfacial tension is so large that the minority core-forming block is essentially fully extended and the interfacial area per chain is minimized. Upon decreasing the length of the O block, the resulting micelles evolved from "hamburger" micelles to segmented worms and ultimately to nanostructured bilayers and vesicles. When the F block was the minority component, segmented ribbons, Y -junctions, and networks were preferred. When the F block became longer than the E block, a double frustration in the self-assembly resulted in another set of novel multicompartment micelles such as raspberry-like micelles and multicompartmentalized worms.[102]

Solvent selectivity has also been shown to be an efficient way to reach various micellar morphologies with miktoarm star μ-EOF micellar systems. By incorporating tetrahydrofuran (THF), a good solvent for the E block, into aqueous dispersions of a μ-EOF block, the micellar structure evolved from multi-compartment disks to core shell corona worms and spheres and finally to mixed corona (E + O) oblate ellipsoidal micelles with increasing THF content.[103] Nevertheless, the THF/water system is not particularly suitable for biomedical applications.

Using a μ-ABC/AB blending strategy, the same authors have reported that relatively narrowly distributed "hamburger" micelles were formed from a binary mixture of spherical micelles, formed from EO diblock copolymers, and segmented worm-like micelles, formed from μ-EOF miktoarm star terpolymers.[104] The morphological evolution was proposed to occur via a collision/fusion/fission mechanism whereby the long μ-EOF segmented worm-like micelles first fused with EO spherical micelles, followed by fission, giving progressively shorter micelles, which finally evolved into more stable hamburger-like micelles.

To date, the use of multicompartment micelles for nanotechnology applications that utilize their inherent storage and release capacities remain limited. To this end, Lodge *et al.*[105] also demonstrated the possibility to use μ-EOF-based multicompartment micelles to solubilize two distinct hydrophobic dye molecules within two separate nanosized compartments. Crucially, these findings indicate that there is little relationship between the distinct solubilization

efficiencies and therefore that the storage and release of two different hydrophobic payloads simultaneously or sequentially could be realized.

V.2 PFPE-based miktobrush terpolymers

In 2016, Hillmyer *et al.*[106] reported the aqueous self-assembly of μ-A(BC)$_n$ miktobrush terpolymers. In this system, the A block is hydrophilic poly(ethylene oxide), "O", the B block is hydrophobic poly(methylcaprolactone), "C", and the C block is hydrophobic and oleophobic poly(perfluoropropylene oxide), "F" (Scheme I-4).

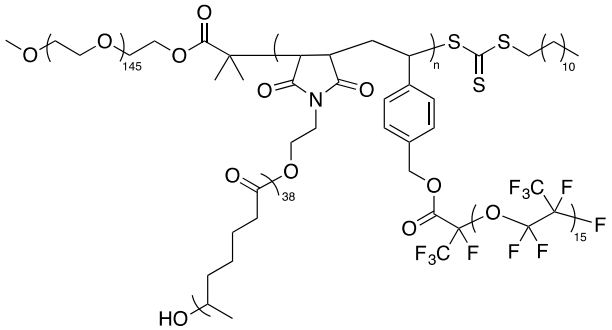

Scheme I-4: Structure of miktobrush μ-O(CF)$_n$ terpolymers synthesized by Hillmyer et al.[106]

Briefly, three end-functionalized polymers were synthesized and combined by RAFT copolymerizations to produce μ-O(CF)$_n$ miktobrush terpolymers: poly(ethylene oxide) (PEO), "O" block (21 kDa) with a RAFT chain transfer agent (CTA) end-group; poly-(methylcaprolactone) (PMCL), "C" macromonomer block (5.3 kDa) with a maleimide end-group; and poly-(perfluoropropylene oxide) (PFPO), "F" macromonomer block (2.6 kDa) with a styrene end-group. The authors examined the aqueous self-assembly of μ-O(CF)$_n$ miktobrush terpolymers using DLS and cryo-TEM. The first terpolymer investigated, μ-O(C_2F_2) (f_{PEO} = 0.63, f_{PMCL} = 0.28, f_{PFPO} = 0.09), at long incubation times formed hamburger and then raspberry-like micelles, likely owing to the larger volume fraction of PEO. Within the hamburger micelles, the PMCL chains formed "buns" around an oblate PFPO disk core, thereby decreasing the interfacial penalty between the PFPO domain and the solvated PEO blocks. Over time, this morphology evolved towards raspberry-like micelles with more dispersed F domains shielded from solvated PEO by PMCL chains. These findings are broadly consistent with previous research on μ-EOF and μ-EOC miktoarm star terpolymer systems. The solution structures adopted by the μ-O(C_3F_2) terpolymer (f_{PEO} = 0.57, f_{PMCL} = 0.35, f_{PFPO} = 0.08) were multilamellar vesicles or polymersomes with nanoscopic periodicity within the bilayer, attributed to dispersed domains of PFPO within a matrix of PMCL.

V.3 PFPE-based linear block copolymers

Thüneman *et al.*[107] synthesized a symmetric linear ABCBA pentablock copolymer consisting of: (A) PEO, (B) poly(*γ*-benzyl L-glutamate) (PBLG), and (C) a PFPE (Fluorolink® C) (Scheme I-5).

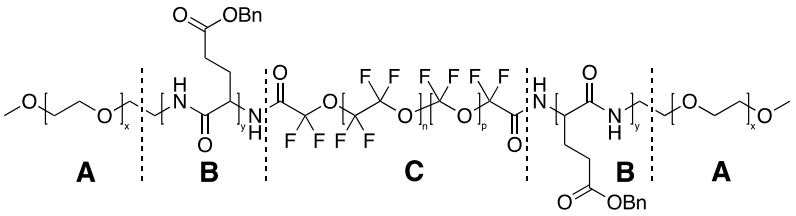

Scheme I-5: Structure of the PEO-b-PBLG-b-PFPE-b-PBLG-b-PEO ABCBA pentablock copolymer synthesized by Thüneman et al.[107]

The diblock copolymer PEO-*b*-PBLG (Mn = 6000 g mol^{-1}) was synthesized by ring-opening polymerization of the *N*-carboxy anhydride of *γ*-benzyl-L-glutamate using an ammonium chloride-functionalized PEO as the macroinitiator. In a second step, the PEO-*b*-PBLG diblock was covalently coupled to a α,ω-dicarboxyl-PFPE (DP = 30) *via* a carboxyl-amine reaction. The different blocks were highly immiscible and formed two-compartment micelles of mainly cylindrical shape in aqueous solution with lengths in the range of 100 to 200 nm and diameters of about 24 nm. The morphology of these structures was most likely a core-shell-corona micelle with two immiscible compartments (PFPE and oligopeptide). The PFPE blocks formed the core of the micelles (*d* = 6 nm), surrounded by a *ca.* 2 nm thick first shell of consisting of β-sheets of PBLG and a second 7 nm shell of PEO.

In 2006, Lodge *et al.*[108] reported the first example of a coil-coil nonionic diblock copolymer adopting a flat disk morphology (Figure I-20). The diblock copolymer was synthesized through the coupling reaction of hydroxy-terminated 1,2-polybutadiene (M_n = 6000 g mol^{-1}) and acid-chloride-end-functionalized PFPE (Krytox 157-FSH, Mn = 5700 g mol^{-1}). Both blocks were atactic, noncrystalline, and flexible (low *T*g). The micellization was examined in the polybutadiene glass forming selective solvent bis(2-ethylhexyl) phthalate. The copolymer self-assembled into thin disk micelles, with radii ranging from 20 to 150 nm, as observed by cryo-TEM. Small-angle X-ray scattering (SANS) measurements were effectively modeled by a thin disk form factor and gave a core thickness of approximately 10 nm. Dynamic light scattering (DLS) measurements gave a distribution of hydrodynamic radii that was fully consistent with the dimensions inferred from microscopy and X-ray scattering. The adopted morphology was clearly the result of an unusually large interfacial tension between the

fluoropolymer and the solvated polybutadiene. The observation of flat disk micelles was at least qualitatively consistent with expectation based on the SSSR theory.

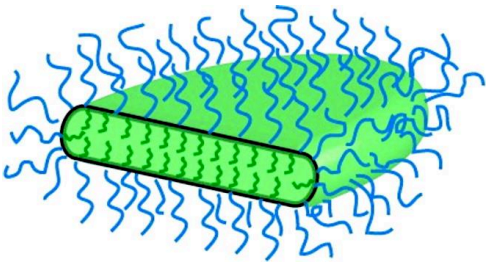

Figure I-20: An illustration of a thin disk micelle. Reproduced with permission from ref [108]. Copyright 2006 American Chemical Society.

Lodge *et al.*[109,110] studied the self-assemblies of two PFPE-based triblock copolymers, BOF and FOF (Scheme I-6). First, a hydroxy-terminated poly(1,2-butadiene)-*b*-poly(ethylene oxide) (BO) diblock copolymer was synthesized by two successive living anionic polymerizations. Carboxylic acid end-capped poly(perfluoropropylene oxide) (PFPO-COOH) was converted to the acid chloride derivative by reaction with oxalyl chloride. The BOF (1.9-26-2.3) triblock was obtained by coupling the hydroxy end-functional PB-PEO with the acid chloride end-functional PFPO (the numbers in brackets denote the molar masses of the three blocks in kg mol^{-1}). FOF (2.3-23-2.3) was synthesized by reacting α,ω-dihydroxy-PEO with acid chloride end-functional PFPO.

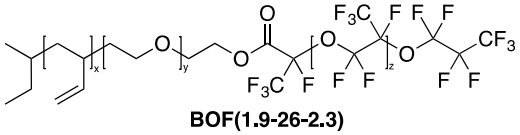

BOF(1.9-26-2.3)

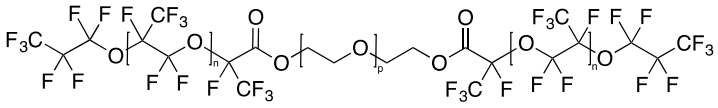

FOF(2.3-23-2.3)

Scheme I-6: Structures of the PFPE-based triblock copolymers synthesized by Lodge et al.[109,110] The numbers in brackets denote the molar masses of the three blocks in kg mol^{-1}.

Aqueous gels formed from this polymers at concentrations ranging from 10 to 50 wt.% were investigated using cryogenic scanning electron microscopy (cryo-SEM) and SANS. The cryo-SEM micrographs revealed significant differences among the morphologies of the gels obtained, depending on the end-blocks used (Figure I-21). The FOF copolymers formed networks by aggregation of the end-blocks, but the PFPO blocks tended to adopt disklike or even sheetlike structures. This was attributed to the extremely high interfacial tension of PFPO with water, consistent with the SSSR behavior. The heterotelechelic BOF terpolymers

adopted a quite different structure, namely an intricate bicontinuous open-cell foam, with cell sizes of the order of 500 nm and cell walls composed of PFPO disks embedded in PB sheets. These different network structures illustrate the potential of using end-block chemistry to manipulate both the morphology and the physical properties of polymer gels.

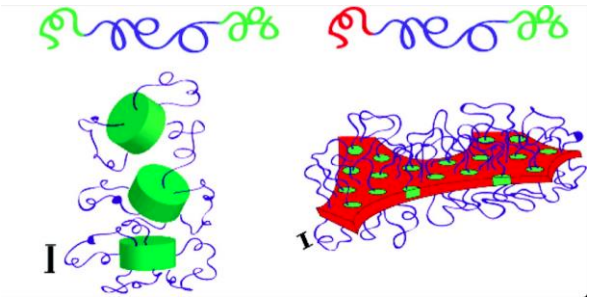

Figure I-21: Schematic representations showing the dependence of network morphology on the end-blocks. 1,2-Polybutadiene, poly(ethylene oxide), and poly(perfluoropropylene oxide) are shown in red, blue, and green, respectively. The scale bars represent 5 nm. Adapted with permission from ref. [110]. Copyright 2010 American Chemical Society.

Qiao *et al.*[111] reported the synthesis of a perfluoropolyether-*b*-poly(*t*-butyl acrylate) ($PFPE_{1800}$-*b*-P*t*BA_{8400}) diblock copolymer in two steps (Scheme I-7).

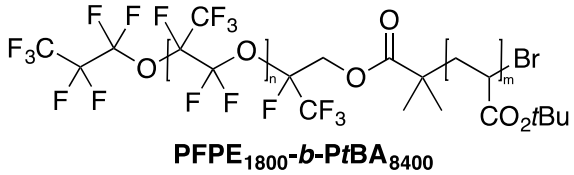

$PFPE_{1800}$-*b*-P*t*BA_{8400}

Scheme I-7: Structure of the $PFPE_{1800}$-b-PtBA_{8400} diblock copolymer synthesized by Qiao et al.[111]

Briefly, a mono-hydroxy PFPE was reacted with 2-bromo*iso*butyryl bromide to form a macroinitiator containing a terminal bromine moiety. This ATRP macroinitiator was then used to polymerise *t*-butyl acrylate (*t*BA) to form the expected diblock copolymer. Self-assembly of the $PFPE_{1800}$-*b*-P*t*BA_{8400} diblock copolymer was conducted in benzene (goodsolvent of P*t*BA and bad solvent of PFPE). The copolymer was be expected to self-assemble in such a way that the PFPE block would be shielded from the solvent by the P*t*BA block. DLS analyses revealed the successful formation of 400 nm micelles with polydispersities of ca. 0.2 -0.3. The diblock copolymer was also used to prepare honeycomb patterned films on both planar and non-planar surfaces via the 'Breath' technique using a static casting system.

Lopez et al. reported[112] the synthesis of a PEG_{2000}-based amphiphilic triblock copolymer containing a $PFPE_{1200}$ central core that was synthesized by copper(I)-catalyzed alkyne–azide cycloaddition (CuAAC) between a telechelic alkyne PFPE and a PEG-azide (Scheme I-8).

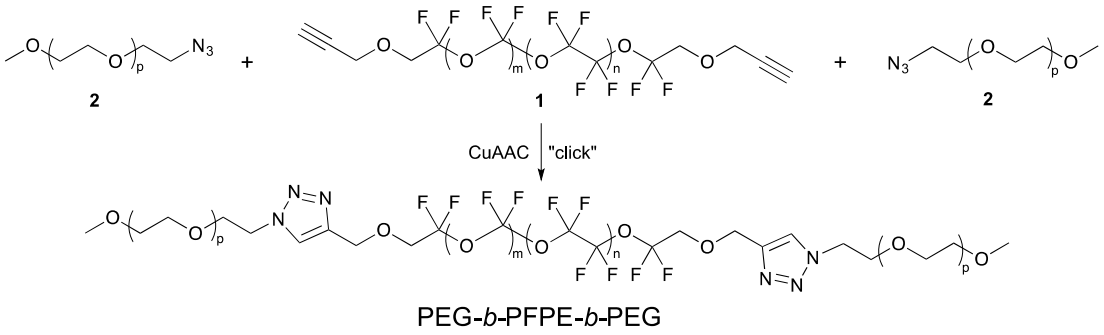

Scheme I-8: Synthesis of an amphiphilic PEG_{2000}-b-$PFPE_{1200}$-b-PEG_{2000} triblock copolymer by copper(I)-catalyzed alkyne–azide cycloaddition (CuAAC) between PFPE-diyne 1 and PEG-azide 2, as reported by Lopez et al.[112]

The PEG_{2000}-*b*-$PFPE_{1200}$-*b*-PEG_{2000} triblock copolymer self-assembled into micelles in aqueous solution as confirmed by DLS, DOSY-NMR, and cryo-TEM, which all unambiguously validated the formation of 10–20 nm spherical nanoassemblies. Fluorimetry measurements were performed, and indicated a critical micelle concentration (CMC) of 0.1 mg mL^{-1}.

In 2007, Lodge *et al.*[113] synthesized two polylactide-*b*-poly(perfluoropropylene oxide) (PLA_{5000}-*b*-$PFPO_{4000}$ and PLA_{4000}-*b*-$PFPO_{6000}$) diblock copolymers *via* coupling of acid chloride end-functionalized PFPOs and hydroxy-terminated PLAs. The solubility of these materials in $ScCO_2$ was measured using a variable-volume high-pressure cell. At a concentration of 1 wt %, the diblock copolymers were found to be soluble at modest pressures (<500 bar) over the temperature range of 30−65 °C. The size of the resulting micelles in $ScCO_2$ solution was characterized by high-pressure-DLS. These measurements indicated the formation of predominantly small, spherical micelles for PLA_{4000}-*b*-$PFPO_{6000}$ and large aggregates with hydrodynamic radii of 100 nm for PLA_{5000}-*b*-$PFPO_{4000}$. By kinetically trapping the aggregates in CO_2 through vitrification of the PLA cores, redispersing them in an analogous PFPO selective solvent, and imaging them using TEM, the authors confirmed the formation of block copolymer vesicles in liquid CO_2.

Drops of water-in-fluorocarbon emulsions created in a drop-based microfluidic device are employed as 3D scaffolds for in vitro translation, encapsulation, and incubation of cells.[114]

Nonionic fluorosurfactants made of PFPEs provide long-term stability to the drops by preventing coalescence while PEG moieties serve as a biocompatible, inert interior surface of the water drops. The flexible design of the microfluidic device allows for the creation of drops with easily varied diameters ranging upward from 10 μm. Therefore, the change in droplet diameter and consequent change in the curvature, together with the soft nature of this system, increase its potential to confer the key physical functions of native antigen-presenting cells (APCs). Spatz *et al.*[115] developed a novel approach to form gold-nanostructured and specifically biofunctionalized droplets of water-in-oil emulsions with the potential to serve as 3D APC surrogates (Figure I-22).

The PFPE-*b*-PEG-*b*-PFPE triblock copolymer B (Figure I-22) was obtained using a one-step condensation reaction between PEG_{600}-diol and $PFPE_{2500}$-dicarboxylic acid. PFPE-*b*-PEG-Gold diblock surfactant C (Figure I-22) was synthesized using a one-step condensation reaction between $PFPE_{7000}$-carboxylic acid and (11-mercaptoundecyl)-tetra(ethylene glycol)-functionalized gold nanoparticles. Two different approaches were used to test how efficiently the gold nanoparticles inside the droplets could serve as anchoring points and provide the required chemical and biological key functions of APCs. The first approach was based on the functionalization of the nanostructured droplets with His_6-tagged green fluorescent protein *via* a nitrilotriacetic acid-thiol linker. Remarkably, more than 90% of encapsulated T cells were found to be in contact with the inner periphery of the droplets. The second approach involved two steps: the synthesis of gold-linked surfactants coupled to bioactive molecules and the subsequent creation of bioactive droplets. The cells in the functionalized droplets exhibited induced proliferation and remained viable for up to 5 days of incubation without any external nutrition.

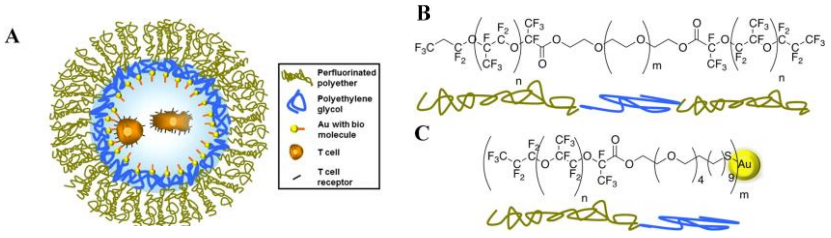

Figure I-22: (A) Schematic representation of a nanostructured and specifically biofunctionalized drop of a water-in-oil emulsion as a 3D APC analogue. Two T cells encapsulated inside the drop are shown schematically. This schematic representation is not to scale. (B, C) Structures of the PFPE-b-PEG-b-PFPE triblock copolymers and PFPE-b-PEG-Gold diblock surfactants, respectively. Reproduced with permission from ref [115]. Copyright 2013 American Chemical Society.

VI. Self-Assemblies of Amphiphilic Perfluorocyclobutyl(PFCB)-based Copolymers

The chemistry of perfluorocyclobutyl polymers (PFCB) was developed by the Dow Chemical Company in the early 1990s.[116] David Babb pioneered the study of of 1,2-bisaryloxy-substituted perfluorocyclobutane (PFCB) ring containing polymers. PFCB ring-containing polymers with various macromolecular architectures such as linear, branched, and cross-linked are prepared by [2+2] cycloaddition of single molecules containing multiple aryl trifluorovinyl ether groups.[117] Typically, thermoplastic or thermosetting PFCB polymers can be obtained by simply heating aryl trifluorovinyl ether monomers in the bulk or in solution above 150 °C. The PFCB backbone contains equal numbers of randomly distributed *cis*- and *trans*-1,2-disubstituted hexafluorocyclobutanes. Initially developed for aerospace and microelectronics applications at Dow Chemical, PFCB polymers find uses as materials for microphotonics, coatings, nanocomposite dispersing matrix, hole transport layers for light-emitting diodes, cross-linking groups in electro-optic chromophores, and proton exchange membrane materials for hydrogen fuel cells.[118]

Self-Assemblies of amphiphilic PFCB-based copolymers were solely investigated by the group of Huang. In 2009, they reported for the first time the synthesis and the self-assembly behavior of a PFCB-based block copolymer. A new PFCB-based methacrylate monomer (TPFCBBMA) was prepared in 5 steps from 4-methylphenol (Scheme I-9).[119] Well-defined PTPFCBBMA-*b*-PEO-*b*-PTPFCBBMA amphiphilic triblock copolymers were synthesized by ATRP of TPFCBBMA from telechelic PEG-based macroinitiators (Scheme I-9).

The critical micelle concentrations (CMC) of these amphiphilic ABA triblock copolymers in aqueous media were determined by *N*-Phenyl-1-naphthylamine fluorescence probe technique. The CMC were in the range of 10^{-6} g L^{-1} but decreased upon increasing the length of the hydrophobic PTPFCBBMA blocks. PTPFCBBMA-*b*-PEG-*b*-PTPFCBBMA triblock copolymers are difficult to dissolve in water due to the relative high content of hydrophobic TPFCBBMA moieties. Therefore, method 6 was employed to prepare micelles. Micellar morphologies were analyzed by TEM and the authors argued that spherical micelles were formed with shorter hydrophobic block then turned into cylindrical micelles when the content of the TPFCBBMA block length increased. Nevertheless, this statement was not supported by the TEM images provided.

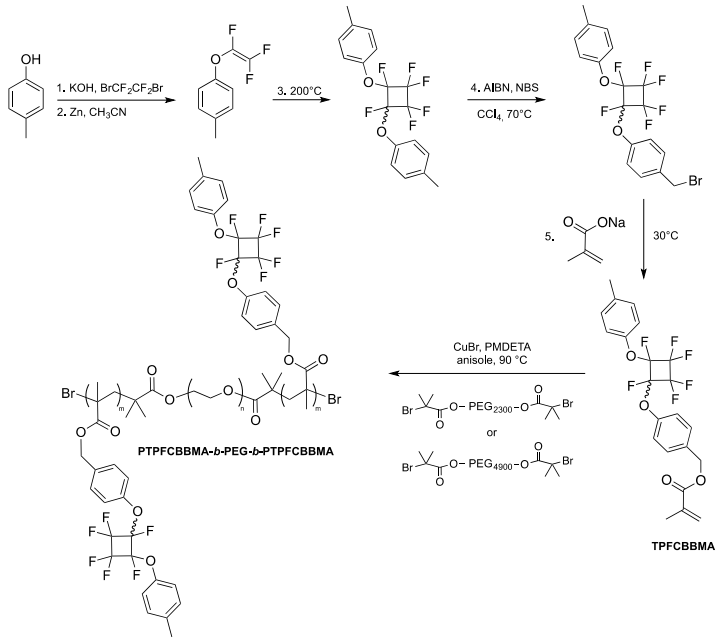

Scheme I-9: Synthesis of PTPFCBBMA-b-PEG-b-PTPFCBBMA amphiphilic triblock copolymers as reported by Hu and Huang et al.[119]

In 2010, they reported[120] the synthesis (Scheme I-10) and the self-assembly of a series of well-defined semi-fluorinated amphiphilic diblock copolymers with hydrophilic PAA and fluorophilic PTPFCBBMA segments. ATRP of MOMA afforded well-defined PMOMA homopolymers. PMOMA-*b*-PTPFCBBMA diblock copolymers were then synthesized by ATRP of TPFCBBMA from the PMOMA-Br macroinitiators. Finally, PAA-*b*-PTPFCBBMA amphiphilic diblock copolymers were obtained *via* the selective acid hydrolysis of the PMOMA block. The critical micelle concentrations (CMC) of PAA-*b*-PTPFCBBMA diblock copolymers in aqueous media were determined by fluorescence spectroscopy using pyrene as the probe. The CMC values for PAA-*b*-PTPFCBBMA diblock copolymers were all around 10^{-7} g mL^{-1}. CMC values decreased with increasing length of fluorophilic PTPFCBBMA segment (keeping the hydrophilic PAA block length constant).

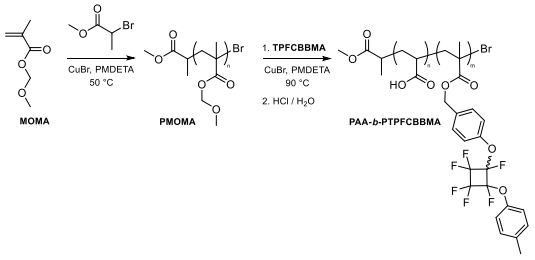

Scheme I-10: Synthesis of PAA-b-PTPFCBBMA amphiphilic diblock copolymers as reported by Hu and Huang et al.[120]

Method 3 was employed to trigger the self-assembly. Micellar morphologies were visualized by TEM. Diblock copolymers with short fluorophilic PTPFCBBMA blocks aggregated into spherical micelles and longer PTPFCBBMA blocks led to pearl-necklace-like aggregates.

The same group reported again the synthesis and the self-assembly of PAA-*b*-PTPFCBBMA amphiphilic diblock copolymers the same year.[121] The synthetic part was slightly modified and it was found that the size of the micelles increased with the length of the PTPFCBBMA segment.

In 2011, they reported the synthesis and the self-assembly of a series of well-defined semi-fluorinated amphiphilic diblock copolymers with hydrophilic PDEAEMA and fluorophilic PTPFCBBMA segments.[122] First, RAFT homopolymerization of TPFCBBMA was initiated by AIBN using cumyl dithiobenzoate as the chain transfer agent. Then, PTPFCBBMA homopolymer was used as macro-RAFT agent to mediate the RAFT polymerization of DEAEMA. *N*-phenyl-1-naphthylamine was used as fluorescence probe to measure the CMC (*ca.* 10^{-6} g L^{-1}) of the resulting PTPFCBBMA-*b*-PDEAEMA diblock copolymers. Method 6 was employed to prepare micelles. The copolymers mainly aggregated into well-ordered large spherical compound micelles (LCMs) with diameters of 400–600 nm, as shown by TEM and DLS.

In 2014, these authors reported the synthesis and the self-assembly in organic solvents of a series of well-defined ABA triblock copolymers constituted of PIB (A) and PBPFCBPMA (B) segments (Scheme I-11).[123]

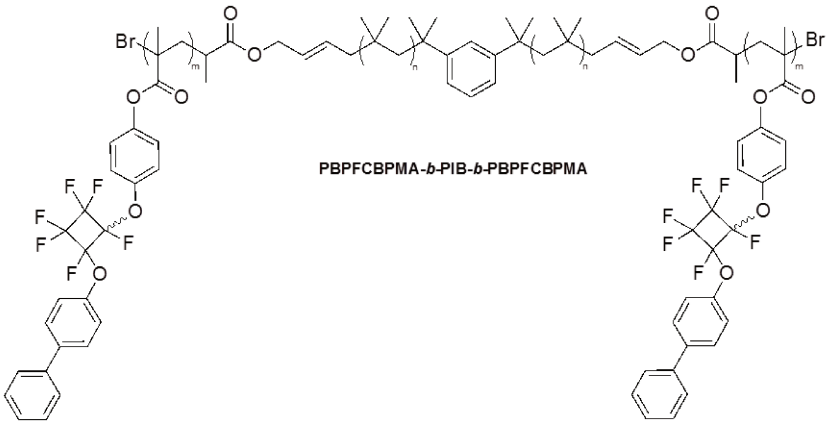

Scheme I-11: Structure of PBPFCBPMA-b-PIB-b-PBPFCBPMA triblock copolymers as reported by Feng and Huang et al.[122]

First, living cationic polymerization of isobutylene was performed, followed by end-capping with 1,3-butadiene to provide a well-defined diallyl-Cl-terminated PIB. This PIB was further

transformed into an ATRP macroinitiator Br-PIB-Br. PBPFCBPMA-*b*-PIB-*b*-PBPFCBPMA triblock copolymers were obtained *via* ATRP of BPFCBPMA initiated by the difunctional Br-PIB-Br.

The self-assembly behavior of these triblock copolymers in *n*-hexane, acetone, and 1,1,1-trifluoroacetone was investigated by TEM. The results indicated that spherical LCMs with PIB chain coronae were formed in *n*-hexane, whereas LCMs and bowl-shaped micelles with PBPFCBPMA block coronae were formed in acetone and 1,1,1-trifluoroacetone, respectively (Figure I-23).

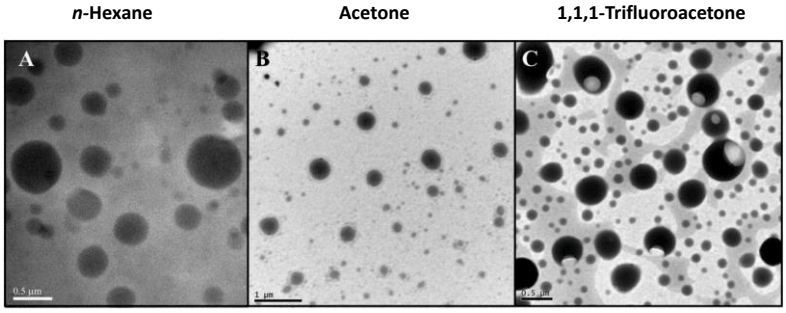

Figure I-23 : TEM images of micelles formed by PBPFCBPMA-b-PIB-b-PBPFCBPMA triblock copolymers self-assembled in n-hexane (left), acetone (middle), and 1,1,1-trifluoroacetone (right). Adapted with permission from ref.[123]. Copyright 2014 RSC.

They also reported[124] the preparation of "sun-shaped" amphiphilic copolymers with PFCB aryl ether-based backbone and PAA lateral side chains as depicted in Figure I-24.

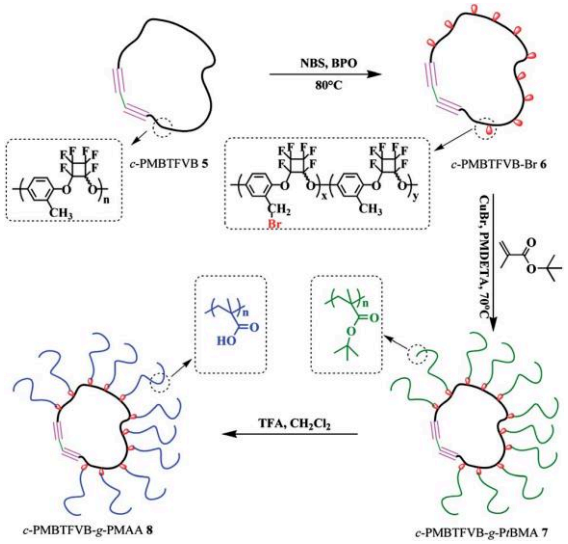

Figure I-24: Schematic representation of c-PMBTFVB-g-PMAA synthesis. Reproduced with permission from ref. [124]. Copyright 2014 RSC.

The self-assembly in water of these polymers was achieved using method 6 and the resulting morphologies were characterized by TEM and DLS. In both analyses, only solid 100-120 nm spherical micelles were observed.

In 2015, they synthesized a series of amphiphilic PFCB-based ABA triblock copolymers PDEAEMA-*b*-PBTFVBP-*b*-PDEAEMA. A BTFVBP trifluorovinyl aryl ether monomer was first polymerized to form a semi-fluorinated perfluorocyclobutyl aryl ether-based segment, and end-functionalized to afford a Br-PBTFVBP-Br macroinitiator. Then, ATRP of DEAEMA was initiated by Br-PBTFVBP-Br to lead to PDEAEMA-*b*-PBTFVBP-*b*-PDEAEMA triblock copolymers (Scheme I-12).[125]

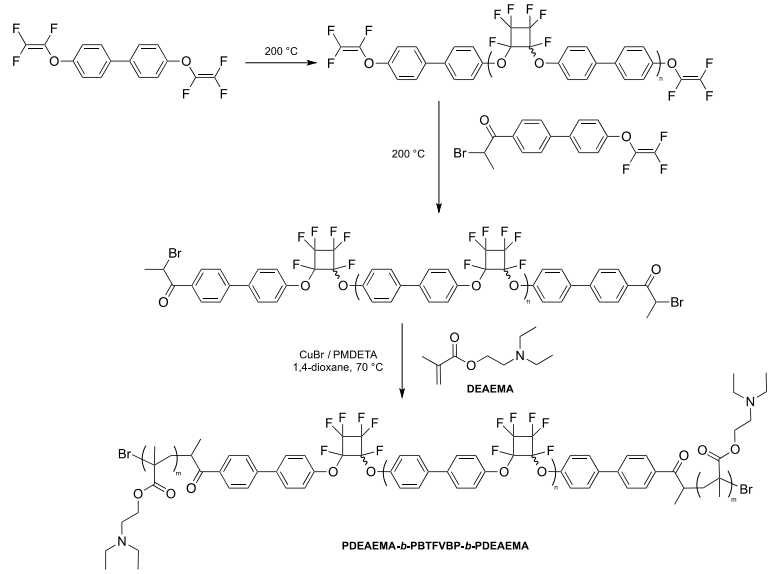

Scheme I-12: Synthesis of PDEAEMA-b-PBTFVBP-b-PDEAEMA amphiphilic triblock copolymers as reported by Lu and Huang et al.[125]

As above, the CMC of the obtained amphiphilic triblock copolymers was evaluated to be around 10^{-6} g L^{-1} and increased with increasing hydrophilic PDEAEMA segment length.

Method 6 was used to prepare micelles. Spheres were formed for $PDEAEMA_{21}$-*b*-$PBTFVBP_{15}$-*b*-$PDEAEMA_{21}$, $PDEAEMA_{26}$-*b*-$PBTFVBP_{15}$-*b*-$PDEAEMA_{26}$, and $PDEAEMA_{43}$-*b*-$PBTFVBP_{15}$-*b*-$PDEAEMA_{43}$ copolymers, with average diameters of 169 nm, 190 nm, and 246 nm, respectively. Since the diameters of the spheres were much higher than the lengths of the triblock copolymers, LCMs were supposed to be formed. The authors speculated that the PBTFVBP segment formed the corona of micelles and that the core consisted of numerous reverse micelles with islands of PBTFVBP in a continuous phase of PDEAEMA. $PDEAEMA_{36}$-*b*-$PBTFVBP_{27}$-*b*-$PDEAEMA_{36}$ and $PDEAEMA_{49}$-*b*-$PBTFVBP_{27}$-

b-PDEAEMA$_{49}$ with longer PBTFVBP segments also formed LCMs with diameters ranging from 100 nm to 250 nm (Figure I-25 B and C). Conversely, PDEAEMA$_{22}$-*b*-PBTFVBP$_{27}$-*b*-PDEAEMA$_{22}$, which possesses the lowest PDEAEMA/PBTFVBP ratio, self-assembled into vesicles of 300 nm in diameter (Figure I-25A).

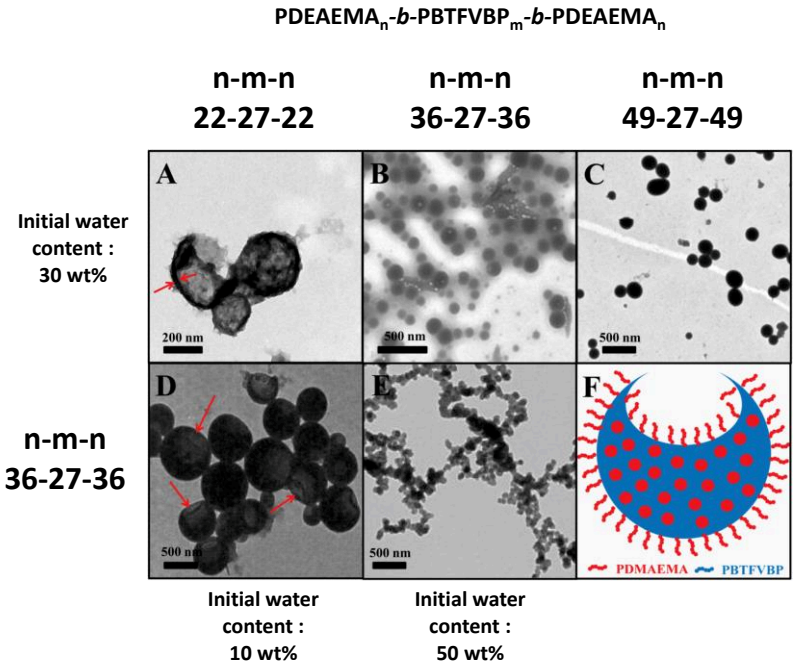

Figure I-25: TEM images of morphologies formed by three different PDEAEMA-b-PBTFVBP-b-PDEAEMA triblock copolymers self-assembled in water when varying the initial water content. Adapted with permission from ref. [125]. Copyright 2015 RSC.

On the basis of previous results, the authors argued that a lower repulsion between the corona chains facilitated the formation of micelles with smaller interfacial areas.

As the initial water content was decreased from 30 wt.% to 10 wt.%, bowl shaped micelles with a diameter of about 500 nm were formed for PDEAEMA$_{36}$-*b*-PBTFVBP$_{27}$-*b*-PDEAEMA$_{36}$ (Figure I-25D). As the initial water content was increased to 50 wt.% this copolymer self-assembled into 100 nm spherical micelles (Figure I-25E). A higher initial content of the selective solvent for the core-forming block generally results in a shorter time for the core-formed segment to reach its thermodynamic state by adjusting its conformation. Hence, micelles with a larger interfacial area form in a higher initial content of water. Thus, the diameter of micelles decreases with an increase of the initial water content.

The same year, they synthesized amphiphilic graft copolymers bearing a hydrophobic poly(2-methyl-1,4-bistrifluorovinyloxybenzene) (PMBTFVB) backbone and hydrophilic poly(ethylene glycol) (PEG) side chains (Scheme I-13).[126] The PMBTFVB was prepared by

thermal step-growth cycloaddition polymerization of MBTFVB and sequential end-capping with 4-methoxy-trifluorovinyloxybenzene. The subsequent bromination of PMBTFVB with *N*-bromosuccinimide using benzoyl peroxide as the free radical initiator at 80 °C yielded PMBTFVB-Br precursors. Then, PMBTFVB-*g*-PEG copolymers were synthesized through the Williamson reaction between the hydroxyl end-group of PEG and the pendant benzyl bromide functionality of PMBTFVB-Br.

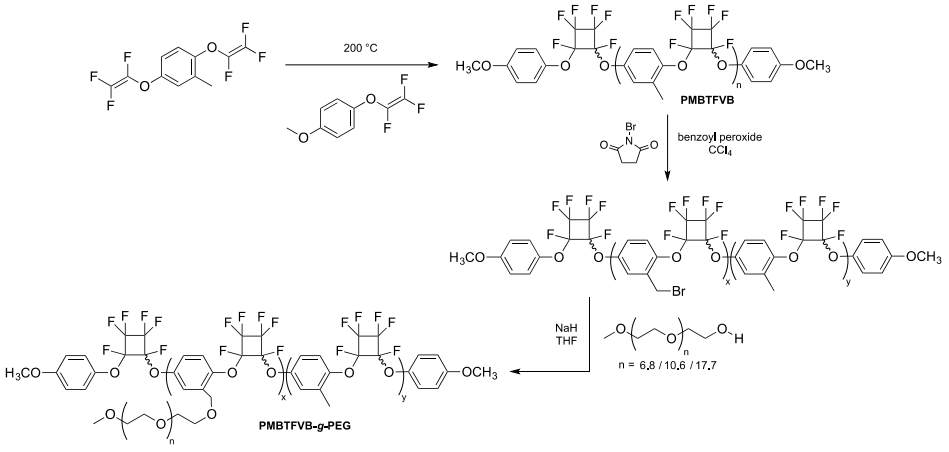

Scheme I-13: Synthesis of PMBTFVB-g-PEG amphiphilic graft copolymers as reported by Gao, Feng, and Huang et al.[126]

Method 3 and 5 were employed to self-assemble this graft-copolymer. TEM images showed diverse morphologies such as spherical micelles, spindle micelles, and large compound vesicles depending on the solvent mixture water content, copolymer concentration, and preparation method.

The same year, they reported the synthesis of amphiphilic graft copolymers bearing a hydrophobic poly(2-methyl-1,4-bistrifluorovinyloxybenzene) (PMBTFVB) backbone and (PAA) side chains.[127] PMBTFVB-*g*-PAA graft copolymers were synthesized by ATRP of *tert*-butyl acrylate initiated by the PMBTFVB-Br macroinitiator followed by the acidolysis of the hydrophobic poly(*tert*-butyl acrylate) side chains into hydrophilic PAA segments.

Method 6 was employed to trigger the self-assembly of the graft-copolymers. Again, diverse micellar morphologies including vesicular, worm-like, and bowl-shaped nanostructures were obtained depending on the water content (from 25 to 70 wt.%) and the length of the PAA side chains. The copolymer aggregated to form vesicles (*ca.* 400–1100 nm) in water/THF (25:75 wt.%) binary mixture at a concentration of 1 g L^{-1} (Figure I-26 A_1). The authors noted a 120 nm black dot at the center of each vesicle and speculated that this might result from the contraction of the shell of vesicles during the TEM sample preparation. In water/THF (50/:50

wt.%) binary mixture, 250–500 nm bowl-shaped aggregates were formed (Figure I-26 B_1). In water/THF (25:75 wt.%) binary mixture, and forcopolymer initial concentration of 0.2 mg mL^{-1}, several micrometer long worm-like micelles with a 200 nm diameter were formed (Figure I-26 A_2). When more water was added before dialysis (50 wt.% at 2 mg mL^{-1}), a network of worm-like micelles was formed (Figure I-26B_2). As the polymer concentration decreased, less polymer chains could get into the micelles in the metastable state when polymer chains of micelle cores were not completely frozen. Hence, a lower polymer concentration leads to a decrease in the aggregation number of micelles, which facilitated the morphology transformation from bilayers (vesicles) to worm-like micelles.

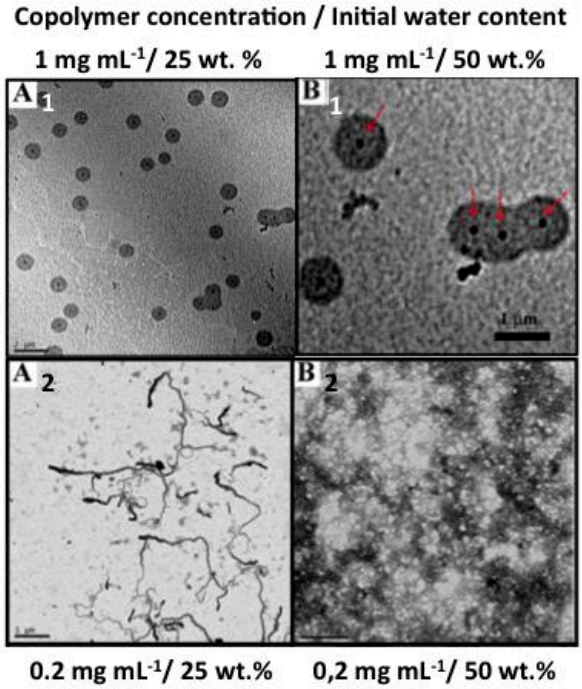

Figure I-26: TEM images of morphologies formed by PMBTFVB-g-PAA amphiphilic graft copolymers self-assembled in water when varying the initial water content and the concentration. Adapted with permission from ref. [127]. Copyright 2015 RSC.

VII. Self-Assemblies of amphiphilic fluorinated poly(2-oxazoline)-based copolymers

Poly(oxazolines) have been the subject of a considerable amount of research since the 1960s, with a significant number of papers focusing on the polymerization of 2-substituted oxazolines.[128-131] Polymerizations are usually carried out *via* a living cationic ring-opening mechanism (CROP), which yields well-defined polymers of narrow average molar mass distributions. The CROP of 2-oxazolines was first reported in 1966 by four independent

research groups. The initiation step by an electrophile such as methyl tosylate, methyl triflate, methyl iodide, or benzyl bromide, formsan oxazolinium species possessing a weakened CO-bond prone to nucleophilic attack by the nitrogen of another monomer. The resulting cationic oxazolinium propagating species is growing by further additions of monomers. The addition of a nucleophile to the reaction mixture causes the termination of the polymerization and can be exploited for the introduction of a functional end group. Poly(2-oxazolines) have found applications in adhesive and coating formulations, pigment dispersants in inks, and drug delivery. The living character of this polymerization technique allows the addition of further monomers, resulting in the sequential polymerization of different monomers, providing access to the formation of block copolymers. Poly(2-oxazolines) with different properties can be prepared by varying the substituent on the monomers. In contrast to short alkyl side groups, longer analogs and aromatic side chains lead to water-insoluble polymers. Amphiphilic systemsare easily accessible and can be applied, for example, as micellar catalysts, nonionic surfactants, compatibilizing agent, and for the formation of hydrogels. Nevertheless, the synthesis and self-assembly behavior of fluorinated poly(2-oxazolines)-based copolymers have been scarcely investigated.

In 2008, Papadakis *et al.*[132] pioneered the synthesis and self-assembly of amphiphilic fluorinated block poly(2-oxazolines) in water. Amphiphilic poly(2-alkyl-2-oxazoline) diblock copolymers of 2-methyl-2-oxazoline (MOx) as the hydrophilic block and 2-(1H,1H',2H,2H'-perfluorohexyl)-2-oxazoline (FOx) for the fluorophilic block were synthesized by sequential CROP. The synthesis of the $PMOx_{40}$-*b*-$PFOx_6$ diblock copolymer was performed in an acetonitrile/chlorobenzene mixture using methyl triflate as the initiator and a three-fold excess of piperidine for termination (Scheme I-14 and Figure I-27 up-left structure).

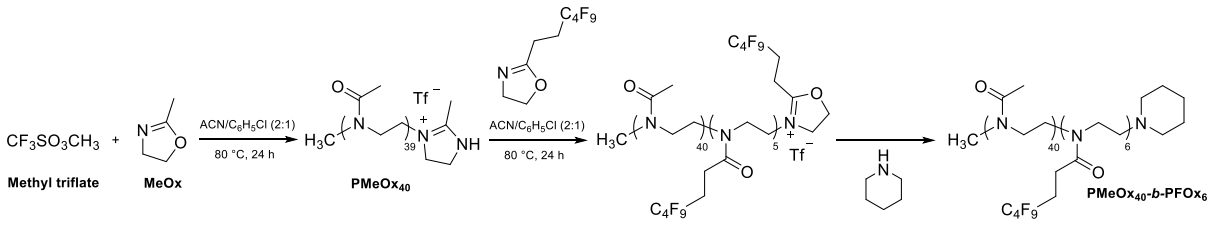

Scheme I-14: Synthesis of $PMeOx_{40}$-b-$PFOX_6$ amphiphilic diblock copolymer synthesized by Papadakis et al.[132]

Method 1 was employed to effect the micellization of the diblock copolymers in water. As evidenced by SANS and TEM, $PMOx_{40}$-*b*-$PFOx_6$ formed elongated core/shell micelles.

The same year Schubert *et al.*[133] showed for the first time that well-defined gradient copolymers of 2-ethyl-2-oxazoline (EtOx) and 2-(*m*-difluorophenyl)-2-oxazoline (F_2PhOx) can be prepared in one-pot under microwave irradiation (Figure I-27 top-right structure). Thesegradient copolymers featured an amphiphilic character resulting in the formation of self-assembled micelles in aqueous solution using method 2. AFM and DLS characterization of the micelles indicated that the copolymers formed spherical micelles with an average diameter of around 15 nm.

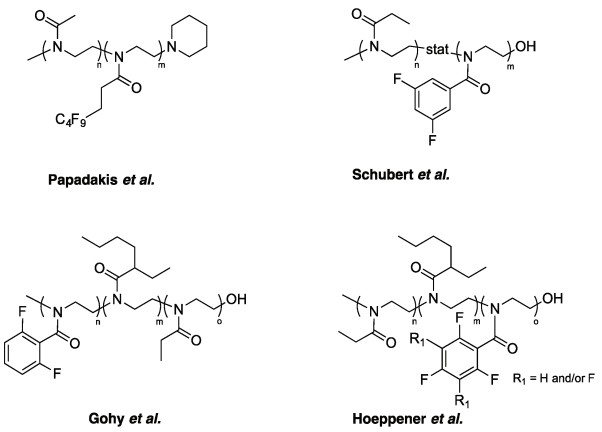

Figure I-27: Structures of fluorinated poly(2-oxazolines)-based copolymers

In 2010, Gohy *et al.*[134] reported the synthesis and self-assembly of a triblock copolymer containing fluorinated 2-(2,6-difluorophenyl)-2-oxazoline (ODFOx), lipophilic 2-(1-ethylheptyl)-2-oxazoline (EPOx), and hydrophilic EtOx blocks (Figure I-27 down-left structure). Aqueous solutions of the poly($ODFOx_{23}$-*b*-$EPOx_{28}$-*b*-$EtOx_{49}$) triblock copolymer obtained *via* method 1 were analyzed by DLS and cryo-TEM (Figure I-28).

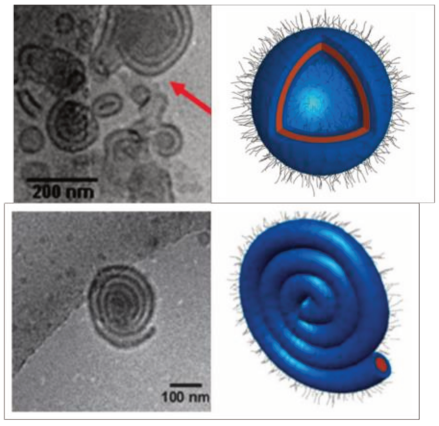

Figure I-28: Cryo-TEM pictures of micellar aggregates formed by the poly($ODFOx_{23}$-b-$EPOx_{28}$-b-$EtOx_{49}$) triblock copolymer self-assembled in water. Adapted with permission from ref. [134]. Copyright 2010 RSC.

Two main morphologies were observed to coexist in water, namely vesicles and flat aggregates of rolled-up cylindrical micelles. The authors hypothesized that the vesicles most probably consisted of a segregated hydrophobic domain based on the contrast in cryo-TEM and the demixing of a mixture of both hydrophobic ODFOx and EPOx homopolymers. The rolled-up spiral-like micellar aggregates were proposed to be metastable intermediates of the transition from cylindrical micelles to vesicles. The limited solubility of the EtOx blocks in water might induce further aggregation of the initially formed cylindrical micelles while the low T_g of the EPOx block provided sufficient flexibility for the cylindrical micelles to roll-up. These two structural parameters were believed to be the key factors driving the formation of the observed rolled-up hierarchical superstructures.

Based on the promising structural features of the aforementioned work, the same authors studied the influence of the fluorophilic character on the formation of triblock copolymers aggregates.[135] For this purpose, a series of (PEtOx-*b*-PEPOx-*b*-PXFPhOx) structure (X = tri, tetra, penta) triblock copolymers was synthesized (Figure I-27 bottom-right structure). Cryo-TEM pictures revealed rod- and sheet-like morphologies for the triflurophenyl-based triblock copolymers (Figure I-29 images a and b). The authors suggested a mechanism of formation based on the strong hydrophobicity of the PTriFPhOx block and the stacking of the fluorinated phenyl rings caused by C-F dipole-dipole interactions. An increaseg of the number of fluorine atoms from PTriFPhOx to PTetFPhOx block, resulted in better-defined overall shapes, with the presence of few separated sheet-like structures and entangled rod-like features (Figure I-29 images c and d). For PPentFPhOx blocks, well-defined supramolecular structures were observed with perfectly round-shaped aggregates (Figure I-29 images e and f). Further investigations revealed the presence of “onion-like” multilamellar vesicle structures with perfectly segregated concentric lamellar features. A large amount of rod-like micelles were also observed next to the well-defined “superaggregates”. The ultimate thermodynamically stable aggregate structure were also determined by temperature-induced equilibrium and showed large size distribution of simple and multilamellar vesicles, but no rod-like morphologies. Thus, the authors attributed the structure formation to the coexistence of bicontinuous and lamellar phases, which formed non-equilibrium superaggregates as transient structures towards the formation of vesicular structures.

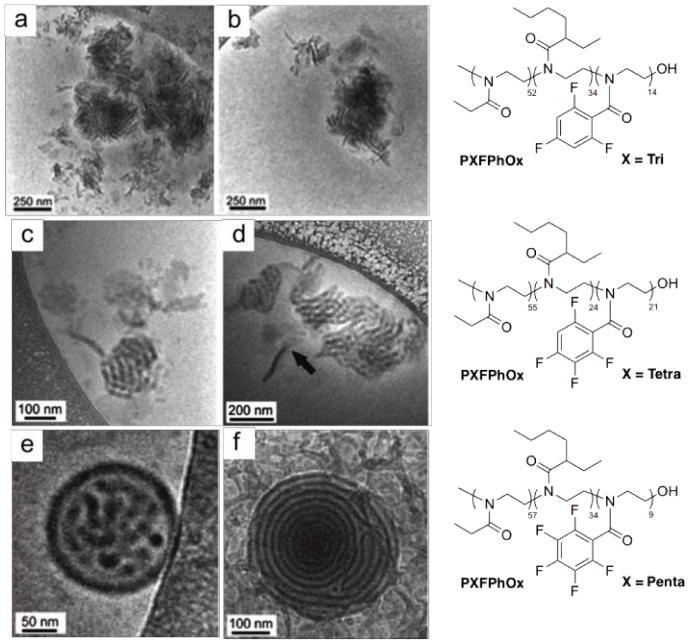

Figure I-29: Cryo-TEM pictures of micellar aggregates formed by PEtOx-b-PEPOx-b-PXPhFOx triblock copolymers self-assembled in water. Adapted with permission from ref.[135]. Copyright 2013 RSC.

VIII. Miscellaneous

VIII.1 Fluorinated acrylamide

In 2013, Lee *et al.*[136] reported fluorinated polyacrylamides, poly[*N*-(2,2-difluoroethyl)acrylamide], with thermoresponsive properties. The authors demonstrated that the thermosensitivity of fluorinated polyacrylamides is easily controlled by changing the number of fluorine atoms in the terminal alkyl group of the *N*-ethyl moiety. Mono- substituted poly[*N*-(2-fluoroethyl)acrylamide] (P1F) is water-soluble while tri- substituted poly[*N*-(2,2,2-trifuoro-ethyl)acrylamide] (P3F) is water-insoluble. Interestingly, di substituted poly[*N*-(2,2-difluoroethyl)acrylamide] (P2F) exhibits a LCST in water of around 26–28 °C, which is comparable to that of poly-(*N*-isopropylacrylamide) (PNIPAM). In continuation of this work, thermoresponsive double-hydrophilic fluorinated block copolymers were synthesized by RAFT.[137] First, poly[*N*-(2,2-difluoroethyl)acrylamide] (P2F) was synthesized *via* RAFT polymerization of *N*-(2,2-difluoroethyl)acrylamide (M2F) using 2-dodecylsulfanylthiocarbonylsulfanyl-2- methylpropionic acid as the CTA. The resulting P2F macroCTA was further chain extended with *N*-(2-fluoroethyl)acrylamide (M1F) to yield poly{[*N*-(2,2-difluoroethyl)acrylamide]-*b*-[*N*-(2-fluoroethyl)acrylamide]} (P2F-*b*-P1F) diblock copolymers with different lengths of the P1F block. Turbidimetry by UV-Visble (UV-Vis) spectroscopy, DLS, and in situ temperature-dependent ^{1}H NMR measurements

demonstrated that the P2F block underwent a thermal transition from hydrophilic to hydrophobic, which induced the self-assembly of the unimers into aggregates. TEM images demonstrated that polymeric aggregates formed from an aqueous solution of P2F-*b*-P1F at 60 °C were disrupted by cooling down to 20 °C and regenerated by heating to 60 °C. Temperature-triggered release of a model hydrophobic drug, coumarin 102, was also demonstrated.

In 2017, Huang *et al.*[138] synthesized the monomer 2,2,2-trifluoroethyl 3-(*N*-(2-(diethylamino)ethyl)acrylamido)propanoate (TF-DEAE-AM) from *N*,*N*-diethylethylenediamine, 2,2,2-trifluoroethyl acrylate, and acryloyl chloride (Scheme I-15). Interestingly, TF-DEAE-AM contains both O_2- and CO_2-responsive functionalities.

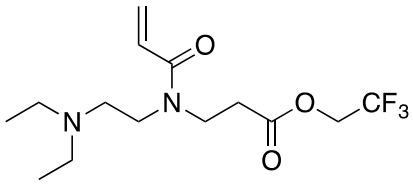

TF-DEAE-AM

Scheme I-15: Structure of TF-DEAE-AM monomer synthesized by Feng and Huang.[138]

Subsequently, a series of dual-gas responsive polymers poly(TF-DEAE-AM) and PEG-*b*-poly(TF-DEAE-AM) were synthesized by RAFT and self-assembled in water using method 5. Due to the reaction between CO_2 and the DEAE groups, and the specific van-der-Waals interactions between O_2 and C–F bonds, micelles consisting of poly(TF-DEAE-AM) or PEG-*b*-poly(TF-DEAE-AM) display distinct CO_2 and O_2 responsiveness in aqueous media. The authors demonstrated that pyrene (a model hydrophobic drug) can be encapsulated in the PEG-*b*-poly(TF-DEAE-AM)micelles . It was found that the release of pyrene sharply increased after bubbling CO_2 or O_2 compared to N_2, and the release rate of the solution treated with CO_2 is the fastest.

VIII.2 Fluorinated vinyl ether

In 1999, Yamaoka *et al.*[139] reported the synthesis of fluorine-containing block copolymers consisting of PHOVE and PTFEOVE. PHOVE-*b*-PTFEOVEs were synthesized by living cationic polymerization and subsequent hydrolysis. CMC of the block polymers were found to range between 10^{-4} and 10^{-5} mol L^{-1} by surface tension measurements. The formation of block polymers micelles in water using method 1 was confirmed by SAXS measurements. Analysis

of the SAXS profiles revealed that the micelle had a core-shell spherical morphology and that the aggregation number increased as the length of TFEOVE segment increased. Solubilization experiments revealed that PHOVE-*b*-PTFEOVE) had a higher sability to solubilize fluorinated compounds than non-fluorinated amphiphilic block copolymers. The same authors confirmed this teh following year when they[139] reported the synthesis and self-assembly of amphiphilic ABA triblock copolymers, (PHOVE-*b*-PFPOVE-*b*-PHOVE) (HFH), (PFPOVE-*b*-PHOVE-*b*-PFPOVE)] (FHF). SAXS measurements revealed that HFH formed core-shell spherical micelles in 1 wt.% aqueous solutions, whereas FHF formes more sophisticated morphologies. In 2004, the same group[141] reported the synthesis and self-assembly (PHOVE-*b*-PTFEOVE), (PHOVE-*b*-PFPOVE), and (PHOVE-*b*-HFBOVE). SANS, SAXS, and DLS analyses revealed that the block copolymers bearing larger fluorinated groups were more likely to form rod-like micelles although the cross-sectional radii of the micelles was not affected much. Scattering analysis of the copolymer micelle solutions with hydrophobic dyes suggested that the solubilization strongly affected the micelle structures.

VIII.3 Fluorinated isoprene

In 2011, Mays *et al.*[142] reported the synthesis and self-assembly of sulfonated polystyrene-*b*-fluorinated polyisoprene (sPS-*b*-fPI) (Scheme I-16). sPS-*b*-fPI block copolymers were synthesized by anionic polymerization, followed by fluorination and sulfonation.

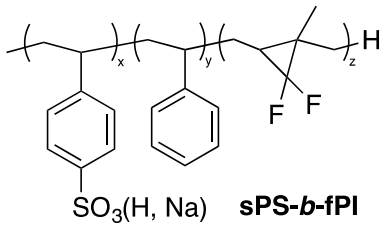

Scheme I-16: Structure of sPS-b-fPI diblock copolymers synthesized by Mays et al.[142]

Self-assembly was achieved in water employing method 6, and the resulting aggregates were examined by TEM. sPS-*b*-fPI with 38.8 % of sulfonation formed worm-like nanostructures, which changed from ribbon-shaped to tapered structures as the sample aged from one week to one month. The diblock copolymer with 29.6 % of sulfonation exhibited similar morphologies, although the micelles appeared to be stiffer. The authors suggested that the higher sulfonation degree soften the assembled structure due to an increased solubility of the corona chains in water. As seen in Figure I-30, the morphologies evolved from spheres (Figure I-30a) to tapered rod-like micelles (Figure I-30b) after aging 4 and 13 days,

respectively. At early times, mixed morphologies were observed: spheres, large compound micelles and rigid long fibers (Figure I-30a). As the sample aged, tapered rods developed (Figure I-30b and Figure I-30c) and further evolved into more complicated structures (aged for 60 days), which consisted in hairy worms, smooth rigid ‘‘fibers’’, and extended tapered rod morphology. However, this aging did not significantly affect the dimensions of the nanostructures.

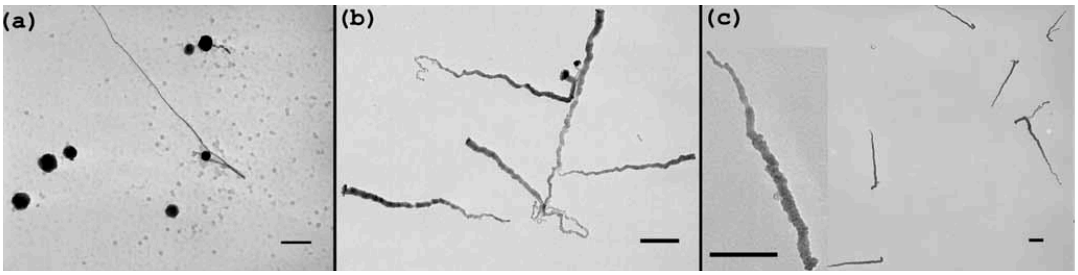

Figure I-30: TEM images for sPS-b-fPI diblock copolymer with 29.6 % sulfonation at (a) 4 days, (b) 13 days, and (c) 25 days. Adapted with the permission from ref. [142]. Copyright 2011 RSC.

VIII.4 Fluorinated Polyphosphazene

In 2016, Presa Soto *et al.*[143] reported the preparation of long-term-stable giant unilamellar vesicles (GUVs, diameter ≧ 1000 nm) and large vesicles (diameter ≧ 500 nm) by self-assembly in THF of the crystalline-*b*-coil polyphosphazene block copolymers $[N=P(OCH_2CF_3)_2]_n$-*b*-$[N=PMePh]_m$ (PTFEP-*b*-PMPP) (n=30/m=20, n=90/m=20, or n=200/m=85), which combined flexible crystalline PTFEP and amorphous PMPP blocks. SEM, TEM, and WAXS experiments demonstrated that the stability of these GUVs was induced by crystallization of the PTFEP blocks in walls of the GUVs. Higher degrees of crystallinity of the GUV walls were found in the bigger vesicles. This suggested that the crystallinity of the PTFEP block facilitated the formation of large vesicles. The GUVs were responsive to strong acids (HOTf) and, after selective protonation of the PMPP block, they underwent a morphological transition to smaller spherical micelles in which the core and corona were inverted. This morphological evolution was totally reversible upon neutralization with a base (NEt_3), which regenerated the original GUVs (Figure I-31:).

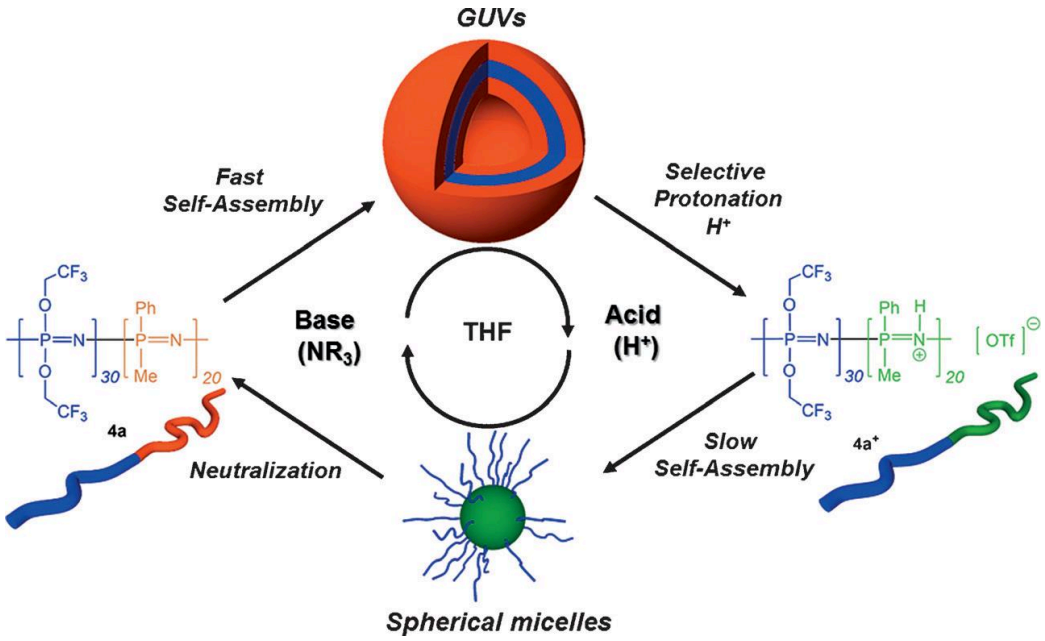

Figure I-31: Schematic representation of the reversible morphological evolution from GUVs to spherical vesicles, promoted by a selective acid–base reaction. Reproduced with the permission from ref. [143]. Copyright 2016 Wiley.

The same group also showed that bicontinuous nanospheres or toroidal micelles could be obtained by the self-assembly of a single crystalline-*b*-coil (PTFEP-*b*-PS) diblock copolymer in THF (without additives), by simply adjusting the block copolymer concentration.[144] Moreover, these two rare morphologies were reversibly transformed one into the other in THF by simple dilution (adding THF) or concentration (evaporating THF) of the block copolymer solution. WAXS analysis of dried films containing bicontinuous or toroidal aggregates showed that whereas the PTFEP blocks were essentially amorphous in the bicontinuous nanospheres, the crystallization of these polymer in the core of the toroidal micelles was crucial to the stability of these morphologies. Hence, the crystallinity of the core-forming PTFEP block appeared to be the main driving-force for the creation of bicontinuous nanospheres and toroidal micelles. The self-assembly of a single linear PTFEP-*b*-PS diblock copolymer to create bicontinuous or toroidal micelles can be controlled by modulating the crystallization of the PTFEP segments by simply changing the block copolymer concentration.

VIII.5 Fluorinated Siloxane

In 2012, Perahia *et al.*[145] reported the self-assembly of a poly(semi-fluorinated siloxane)-containing diblock copolymer, poly(trifluoro propyl methylsiloxane)-*b*-polystyrene (PSiF-*b*-PS) in toluene (a selective solvent for PS). The high incompatibility of the PSiF block drove

aggregation. For example, the symmetric triblock copolymer formed elliptical micelles with unique temperature stability compared to the aggregates formed by diblock copolymers in the lower segregation regime. The micelles formed hada relatively low aggregation number and contained high amounts of solvent in their core. As expected, the curvature of the core–corona interface was significantly affected by the volume fraction of the Si–F block.

In 2015, Manners *et al.*[146] investigated the self-assembly of diblock copolymers containing a crystalline poly(ferrocenyldimethylsilane) (PFS) block and a poly(fluorinated siloxane) coil block (PFMVS = poly(methylvinylsiloxane) with 1*H*,1*H*,2*H*,2*H*-perfluorooctane dangling chains). After direct dissolution of the block copolymer in trifluorotoluene (TFT), only a unimer film was observed by TEM after 24 h, suggesting that TFT may act as a good solvent for both blocks. After allowing the solution to stand for 1 week, the exclusive formation of cylindrical micelles was observed, indicating that TFT is actually a poor solvent for PFS segment (Figure I-32).

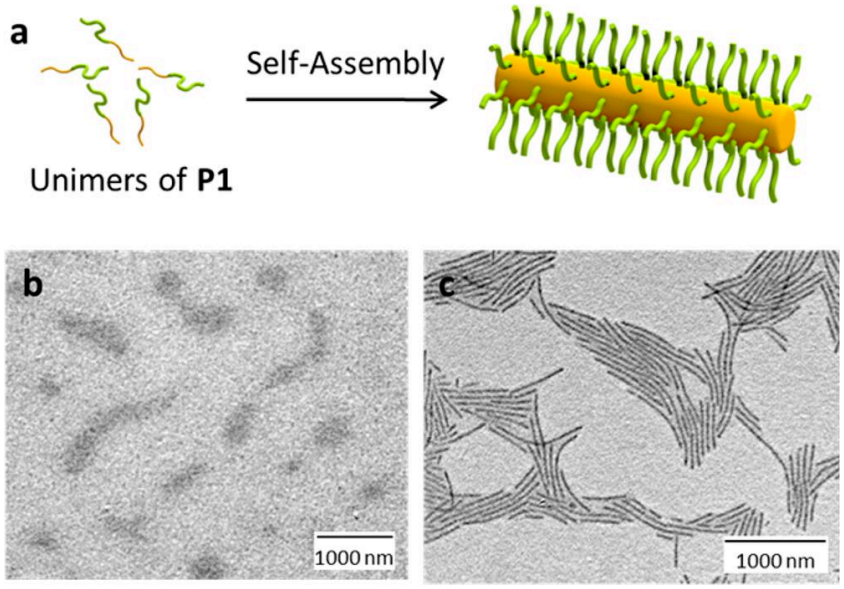

Figure I-32: Schematic representation of the self-assembly of PFS-b-PFMVS to form cylindrical micelles. PFS = yellow, PFMVS functionalized with perfluoroalkane = light green (a). TEM micrographs of a drop-cast sample in TFT (60 mg/mL) after 24 h (b), and 1 week (c). Reproduced with the permission from ref. [146]. Copyright 2015 ACS.

Self-seeding protocols were also successfully employed to prepare micelles with controlled lengths and structures with low polydispersities. Finally, by partial functionalization of the PFMVS block copolymers with fluorescent dye molecules, the authors showed that well-defined, functional nanomaterials could be obtained in the fluorous phase.

In 2015, Dong *et al.*[147] reported the solution self-assembly of an ABC block terpolymer consisting of a polystyrene-*b*-poly(ethylene oxide) (PS-*b*-PEO) diblock copolymer tail tethered to a fluorinated polyhedral oligomeric silsesquioxane (FPOSS) cage. This terpolymer was self-assembled in 1,4-dioxane/water binary mixture using method 2. At low water contents (10 wt %), spherical micelles with a uniform size distributions were observed. A sphere to worm-like micelles transition occured when the water content increased to 18 wt %. Other circular morphologies were observed at water contents ranging from 22 to 34 wt %, including toroids (Figure I-33a), tadpoles and dumbbells (Figure I-33b), interlocked toroids (Figure I-33c), etc. Toroid was the prevalent morphology. These toroidal structures had similar diameter and identical core-shell-corona molecular arrangement as the worm-like micelles. Hence, they were suspected to originate from closure of worm-like micelles as the water content increased (Figure I-33).

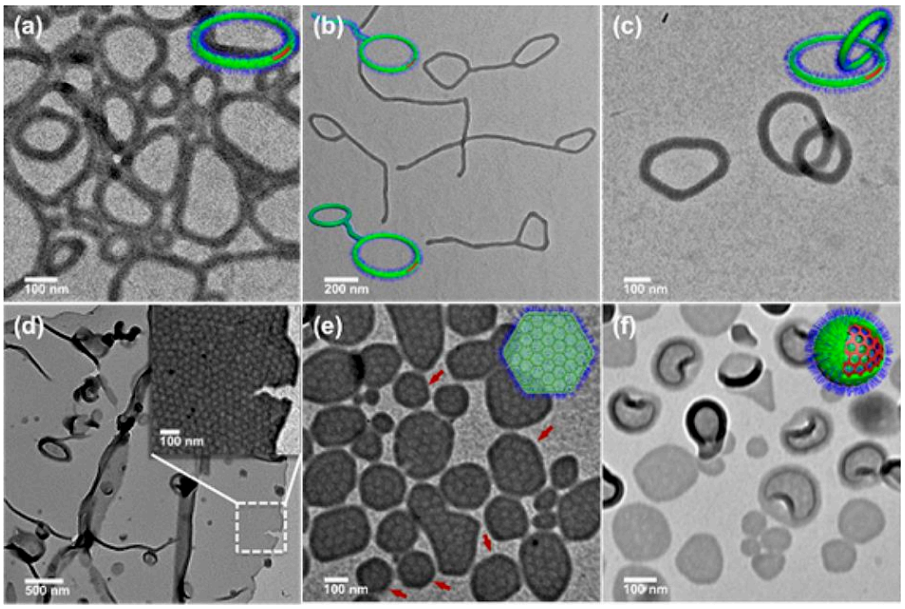

Figure I-33: TEM images of (a) toroids, (b) tadpoles and dumbbells, (c) interlocked toroids, (d, e) 2D nanosheets, and (f) laterally structured vesicles. FPOSS = red; PS = green; PEO = blue. Reproduced with the permission from ref. [147]. Copyright 2015 ACS.

Lateral aggregation and fusion of the worm-like micelles resulted also in primitive nanosheets stabilized by thicker rims to partially release the rim-cap energy. Rearrangement of the parallel-aligned FPOSS cylindrical cores generates hexagonally patterned nanosheets.

VIII.6 Poly(Vinylidene Fluoride)-based copolymers

In 2010, Gohy *et al.*[148] reported the self-assembly of blend of terpolymers: poly(VDF-*ter*-HFP-*ter*-TFMA) and PS-*b*-P2VP-*b*-PEO triblock terpolymer. The micellar solutions were

obtained by first dissolving one of the blend partners into DMF, followed by the addition of the second blend partner as a powder. Formation of hydrogen-bonded complexes between the TFMA and P2VP units was observed leading to the formation of insoluble micelles consisting of P2VP/poly(VDF-*ter*-HFP-*ter*-TFMA) terpolymer cores surrounded by a mixture of PS and PEO chains.

Asandei *et al.*[149] reported the self-assembly of PNaSS-*b*-PVDF-*b*-PNaSS triblock copolymers synthesized by NaN_3 deprotection of the neopentyl styrene sulfonate (NpSS) functions of PNpSS-*b*-PVDF-*b*-PNpSS triblock copolymers. Using method 1 and 3, all the PNaSS-*b*-PVDF-*b*-PNaSS triblock copolymers provided colloidally stable nanoparticles in aqueous solution, even under the high ionic strength of a phosphate buffered saline (PBS) solutions (pH=7.4, giving 0.01 M phosphate buffer, 0.0027 M potassium chloride and 0.137 M sodium chloride), modeling cell-isotonic conditions.

Our group[150] recently reported the preparation and self-assembly in water of PVDF-*b*-PVA diblock copolymers obtained by RAFT polymerization followed by basic hydrolysis. Using method 7, the self-assembly of the diblock copolymer in water, studied by DLS and cryo-TEM, led to the formation of a major population of spherical nanoobjects constituted of a PVDF core and a PVA shell with diameters centered around 147 nm. Protocols of VDF RAFT dispersion polymerization in the presence of PVAc macro-CTAs were also recently published.[151] This polymerization-induced self-assembly (PISA) of PVAc-*b*-PVDF block copolymers resulted into desert rose-like branched micrometer-long crystalline morphologies. Although the self-assembly was triggered by the PVDF growing block, the morphologies of these structures are thought to be governed by the crystallization of PVDF.

IX. Conclusion

Fluoropolymers constitute an attractive family of polymeric materials with remarkable properties (high resistance to chemicals and heat, ferroelectricity and piezoelectricity for semi-crystalline polymers, to name a few). The incorporation of fluorinated block can confer unique properties to block copolymers, and offer tremendous promise for advanced applications. The combination of exceptionnal properties, imparted by the fluorinated part, combined the self-assembly method is an appealing strategies for preparing fluorinated nanostructures. Nowadays, a large diversity of fluorinated monomers, and polymers, are availaible to premade fluorinated copolymers architectures. This current research focus on

fluorinated polymeric material employed in solution self-assembly nanostructuration. Metchacrylate, Perfluoropolyether and styrene based-copolymers was specially investigated and revealed unique multicomparment and stimuli responsive aggregates. However, a number of other fluorinated polymers were scarerly reported such as oxazoline, PVDF or siloxane, and represents a wide potential for the preparation of new flurorinated nanostructures.

X. Références

[1] J. Yan, M. Bloom, S. C. Bae, E. Luijten, S. Granick, *Nature*, 2012, **491**, 578–581.

[2] S. C. Glotzer, M. J. Solomon, *Nat. Mater*., 2007, **6**, 557–562.

[3] A. H. Gröschel, A. Walther, T. I. Löbling, F. H. Schacher, H. Schmalz, A. H. Muller. *Nature*, 2013, **503**, 247–251.

[4] L. Cademartiri, K. J. M., Bishop, *Nat. Mater*., 2015, **14**, 2–9.

[5] S. Jain, F. S. Bates, *Macromolecules*, 2004, **37**, 1511.

[6] H. G. Cui, Z. Y. Chen, K. L. Wooley, D. J. Pochan, *Macromolecules*, 2006, **39**, 6599.

[7] L. Zhang, A. Eisenberg, A., *Science,* 1995, **268**, 1728–1731

[8] S. Jain, F. S. Bates, *Science*, 2003, **300**, 460–464.

[9] B. M. Discher, Y. Y. Won, D. S. Ege, J. C. Lee, F. S. Bates, D. E. Disher, D. A. Hammer,

Science, 1999, **284**, 1143–1146.

[10] Y. Mai, A. Eisenberg, *Chem. Soc. Rev*., 2012, **41**, 5969-5985.

[11] L. Zhang, A. Eisenberg, *J. Am. Chem. Soc*., 1996, **118**, 3168-3181

[12] H. Qiu, Z. M. Hudson, M. A. Winnik, I. Manners, *Science,* 2015, **347**, 1329–1332.

[13] J. Schmelz, F. H. Schacher, H. Schmalz, *Soft Matter*, 2013, **9**, 2101-2107.

[14] L. Meazza, J. A. Foster, K. Fucke, P. Metrangolo, G. Resnati, J. W. Steed, *Nat. Chem*. 2013, **5**, 42−47.

[15] N. Houbenov, R. Milani, M. Poutanen, J. Haataja, V. Dichiarante, J. Sainio, J. Ruokolainen, G. Resnati, P. Metrangolo, O. Ikkala, *Nat. Commun*., 2014, **5**, 4043.

[16] K. Stähler, J. Selb and F. Candau, *Langmuir*, 1999, **15**, 7565‑7576.

[17] C. V. Synatschke, T. Nomoto, H. Cabral, M. Förtsch, K. Toh, Y. Matsumoto, K. Miyazaki, A. Hanisch, F. H. Schacher, A. Kishimura, N. Nishiyama, A. H. E. Müller and K. Kataoka, *ACS Nano*, 2014, **8**, 1161‑1172.

[18] J. S. Haataja, O. Ikkala, H. H. Gröschel, A. H. E. Müller, *Nature comm*., 10.1038/ncomms12097

[19] Z. Li, E. Kesselman, Y. Talmon, M. A. Hillmyer, T. P. Lodge, *Science*, 2004, **306**, 98-101

[20] H. Ringsdorf, In *3rd EURESCO Conference on Supramolecular Chemistry (Molecular Recognition and Drug-Receptor Interactions)*, Salamanca, Spain, August 29‑September 3, 1996.

[21] F. Xia, L. Jiang, *Adv. Mater,*. 2008, **20**, 2842−2858.

[22] C. LoPresti, H. Lomas, M. Massignani, T. Smart, G. Battaglia, *J. Mater. Chem*., 2009, **19**, 3576−3590.

[23] Q. Yan, Y. Zhao, *J. Am. Chem. Soc*. 2013, **135**, 16300−16303.

[24] Q. Yan, Y. Zhao, *Angew. Chem., Int. Ed*., 2013, **52**, 9948−9951.

[25] B. Yan, D. H. Han, O. Boissiere, P. Ayotte, Y. Zhao, *Soft Matter,* 2013, **9**, 2011−2016.

[26] Q. Zhang, S. Zhu, *ACS Macro Lett*., 2014, **3**, 743-746.

[27] W. R. Dreher, A. Singh and M. W. Urban, *Macromolecules*, 2005, **38**, 4666‑4672.

[28] M. J. Krupers, M. Möller, *J. Fluorine Chem*., 1997, **82**, 119‑ 124.

[29] Z. Qinghua, Z. Xiaoli, C. Fengqiu, S. Ying and W. Qiongyan, *J. Polym. Sci., Part A: Polym. Chem.*, 2007, **45,** 1585–1594.

[30] L. He, J. P. Hinestrosa, J. M. Pickel, S. Zhang, D. G. Bucknall, S. M. Kilbey II, J. W. Mays, K. Hong*, J. Polym. Sci. Part A: Polym. Chem*., 2011, **49**, 414-422.

[31] G. Li, A. Xu, B. Geng, S. Yang, G. Wu, S. Zhang, *J. Fluor. Chem*., 2014, **165**, 132-137.

[32] P. I. R. Muraro, A. G. O. de Freitas, S. G. Trindade, F. C. Giacomelli, J-J. Bonvent, V. Schmidt, F. P. dos Santos, C. Giacomelli, *J. Fluor. Chem*., 2014, **168**, 251-259.

[33] H. Peng, K. J. -Thurecht, I. Blakey, E. Taran, A. K. Whittaker, *Macromolecules*, 2012, **45**, 8681-8690

[34] K. Wang, H. Peng, K. J. Thurecht, S. Puttick, A. K. Whittaker, *Polym. Chem*., 2016, **7**, 1059-1069.

[35] Y. Chen, Y. Zhang, Y. Wang, C. Sun, C. Zhang, *J. Appl. Polym. Sci*., 2013, **127**, 1485-1492.

[36] Y. Xu, W. Wang, Y. Wang, J. Zhu, D. Uhrig, X. Lu, J. K. Keum, J. W. Mays, K. Hong, *Polym. Chem*., 2016, **7**, 680

[37] W. Du, A. M. Nyström, L. Zhang, K. T. Powell, Y. Li, C. Cheng, S. A. Wickline, K. L. Wooley, *Biomacromolecules*, 2008, **9,** 2826-2833

[39] K. Y. Mya, E. M. J. Lin, C. S. Gudipati, H. B A. S. Gose and C. He, *J. Phys. Chem. B*, 2010, **114**, 9128-9134.

[39] A. Pan, L. He, T. Zhang, X. Zhao, *Colloid Polym. Sci*., 2015, **293**, 2281-2290

[40] H. Liu, Y. Zhao, C. A. Dreiss, Y. Feng, *Soft Matter*, 2014, **10**, 6387-6391

[41] H. Liu, W. Wang, H. Yin, Y. Feng, *Langmuir,* 2015, **31**, 8756-8763

[42] H. Liu, Z. Guo, S. He, H. Yin, Y. Feng, *RSC Adv*., 2016, **6,** 86728-86735

[43] S-D. Xiong, L. Li, S-L. Wu, Z-S. Xu, P. K. Chu*, J. Polym. Sci.: Part A Polym. Chem*., 2009, **47**, 4895-4907.

[44] B. Jiang, H. Pang, *J. Polym. Sci. Part A: Polym. Chem*., 2016, **54**, 992-1002.

[45] Y-N. Zhou, H. Cheng, Z-H. Luo, *J. Polym Sci Part A: Polym Chem.*, 2011, **49**, 3647-3657.

[46] B. P. Koiry, A. Chakrabarty, N. K. Singha*, RSC Adv*., 2015, **5**, 15461-15468.

[47] B. Koiry, S. Ponnupandian, S. Choudhury, N. K. Singha, *J. Fluor. Chem*., 2016, **189**, 51-58.

[48] J-N. Marsat, M. Heydenreich, E. Kleinpeter, H. v. Berlepsch, C. Böttcher, A. Laschewsky, *Macromolecules*, 2011, **44**, 2092-2105.

[49] L. Yu, J-J. Qiu, H. Cheng, Z-Z. Luo, *Mat. Chem. And Phys*., 2013, **138**, 780-786.

[50] J. Chen, J-J. Li, Z-H. Luo, J. *Polym Sci Part A: Polym Chem*., 2013, **51**, 1107-1117.

[51] Y. Hao, M. Zhang, J. Xu, C. Liu, P. Ni, *J. Macromol. Sci. Part. A Appl. Chem.*, 2010, **47**, 941-95*1*.

[52] S. Li, J. He, M. Zhang, H. Wang, P. Ni, *Polym. Chem*., 2016**, 7**, 1773-1781.

[53] J. He, P. Ni, C. Liu, *J. Polym. Sci. Part A: Polym. Chem.,* 2008, **46**, 3029-3041.

[54] J. Mao, P. Ni, Y. Mai, D. Yan, *Langmuir,* 2007, **23,** 5127-5134

[55] K. Mastumoto, T. Ishizuka, T. Harada, H. Matsuoka, *Langmuir*, 2004, **20**, 7270-7282.

[56] W. Wang, J. Zhang, C. Li, P. Huang, S. Gao, S. Han, A. Dong, D. Kong, *Colloids Surf. B Biointerfaces*, 2014, **115**, 302-309

[57] H. Hussain, K. Busse, J. Kressler, *Macromol. Chem. Phys*., 2003, **204**, 936-946.

[58] H. S. Hwang, H. J. Kim, Y. T. Jeong, Y-S. Gal, K. T. Lim, *Macromolecules*, 2004, **37**, 9821-9825.

[59] Y. Koda, T. Terashima, M. Sawamoto, *Macromolecules*, 2016, **49**, 4534-4543.

[60] M. Y. Lee, S. H. Kim, J. T. Kim, S. W. Kim, K. T. Lim, *J. Nano. Tech*., 2008, **8**, 4864-4868.

[61] S. Xu, W. Liu, *J. Polym. Sci. Part B: Polym. Phys*., 2008, **46**, 1000-1006.

[62] X. Dong, L. He, N. Wang, J-Y. Liang, M-J. Niu, X. Zhao, *J. Mater. Chem*., 2012, **22**, 23078-23090

[63] A. Pan, S. Yang, L. He*, RSC Adv*., 2015, **5**, 55048-55058

[64] Y. Zhang, L. Wang, Z. Zhang, Y. Zhang, X. Tuo*, J. Polym Sci Part A: Polym Chem*., 2013, **51**, 2161-2170.

[65] T. Imae, H. Tabuchi, K. Funayama, A. Sato, T. Nakamura, N. Amaya, *Colloids and Surfaces A: Physicochem. Eng. Aspects*, 2000, **167**, 73-81

[66] K. Skrabania, A. Laschewsky, H. v. Berlepsch, C. Böttcher, *Langmuir*, 2009, **25**, 7594-7601.

[67] H. Berlepsch, C. Böttcher, K. Skrabania, A. Laschewsky, *Chem. Comm*., 2009, 2290-2292.

[68] K. Skrabania, H. v. Berlepsch, C. Böttcher, A. Laschewsky, *Macromolecules*, 2010, **43**, 271-281.

[69] Y. Gao, X. Li, L. Hong, G. Liu, *Macromolecules*, 2012, **45**, 1321-1330.

[70] M. Rabnawaz, G. Liu, *Macromolecules*, 2012, **45**, 5586-5595.

[71] X. Li, Y. Gao, X. Xi,g, G. Liu, *Macromolecules,* 2013, **46**, 7436-7442.

[72] S. Li, Y. Yang, G. Li, S. Lin, *Polym. Chem.,* 2014, **5**, 4553-4560

[73] A. Vanderkooy, M. S. Taylor, *J. Am. Chem. Soc*., 2015, **137**, 5080-5086

[74] H. S. Hwang, J. Y. Heo, Y. T. Jeong, S-H. Jin, D. Cho, T. Chang, K. T. Lim, *Polymer*, 2003, **44**, 5153-5158

[75] M. Niu, L. He, J. Liang, A. Pan, X. Zhao, *Progress in Org. Coat*., 2014, **77**, 1603-1612.

[76] C. Mugemana, B-T. Chen, K. V. Bukhryakov, V. Rodionov, *Chem. Commun*., 2014, **50**, 7862-7865.

[77] Charleux, G. Delaittre, J. Rieger, F. D'Agosto, *Macromolecules*, 2012, **45**, 6753-6765.

[78] S. L. Canning, G. N. Smith, S. P. Armes, *Macromolecules*, 2016, **49**, 1985-2001.

[79] M. Zong, K. J. Thurecht, S. M. Howdle, *Chem. Comm*., 2008, 5942-5944

[80] M. Semsarilar, V. Ladmiral, A. Blanazs, S. P. Armes, *Polym. Chem*., 2014, **5**, 3466-3475

[81] M. Semsarilar, E. R. Jones, S. P. Armes, *Polym. Chem*., 2014, **5,** 195-203

[82] L. Guo, Y. Jiang, T. Giu, Y. Meng, X. Li, *Polymer*, 2014, **55**, 4601-4610.

[83] F. Ouhib, A. Dirani, A. Aqil, K. Glinel, B. Nysten, A. M. Jonas, C. Jerôme, C. Detrembleur, *Polym. Chem*., 2016, **7**, 3998-4003

[84] X. Chen, J. Zhou, J. Ma, *RSC Adv*., 2015, **5**, 97231-97238.

[85] J. Zhou, X. Chen, J. Ma, Prog. *Org. Coat*., 2016, **100**, 86-93

[86] J. Zhou, R. He, J. Ma, *Polymers,* 2016, **8**, 207-220

[87] B. Akpinar, L. A. Fielding, V. J. Cunningham, Y. Ning, O. O. Mykhaylyk, P. P. Fowler, S. P. Armes, *Macromolecules*, 2016, **49**, 5160-5171

[88] Y. Pei, J-M. Noy, P. J. Roth, A. B. Lowe, *Polym. Chem*., 2015, **6,** 1928-1931

[89] Y. Pei, J-M. Noy, P. J. Roth, A. B. Lowe*, J. Polym. Sci. Part A: Polym. Chem*., 2015, **53**, 2326-2335.

[90] S. Kubowicz, J-F. Baussard, J-F. Lutz, A. F. Thünemann, H. v. Berlepsh, A. Laschewsky, *Angew. Chem. Int. Ed*., 2005, **44**, 5262 –5265

[91] H. Cui, Z. Chen, S. Zhong, K. L. Wooley, D. J. Pochan, *Science*, 2007, **317**, 647-650

[92] B. H. Tang, C. S. Gudipati, H. Hussain, C. He, Y. Liu, T. P. Davis, *Macromol. Rapid Commun*. 2009, **30**, 1002–1008.

[93] B. H. Tan, H. Hussain, Y. Liu, C. B. He, T. P. Davis, *Langmuir*, 2010, **26**, 2361–2368.

[94] H. Hussain, B. H. Tan, K. Y. Mya, Y. Liu, C. B. He, T. P. Davis, *J. Polym. Sci. Part A: Polym. Chem.*, 2010, **48**, 152-163.

[95] W. Du, A. M. Nyström, C. Cheng, K. L. Wooley, 2010, *J. of Polym. Sci.: Part A: Polym. Chem.*, 2010, **48**, 3487–3496.

[96] C. Sing, D. Ao, X. Wang, J. Zhang, Y. Tan, *Colloid Polym. Sci*., 2013, **291**, 2815-2823.

[97] H. Ringsdorf, B. Schlarb, J. Venzmer, *Angew. Chem. Int. Ed*., 1988, **27**, 113.

[98] A. O. Moughton, M. A. Hillmyer, T. P. Lodge, *Macromolecules*, 2012, **45**, 2.

[99] Z. Li, M. A. Hillmyer, T. P. Lodge, *Macromolecules*, 2004, **37**, 8933.

[100] Z. Li, M. A. Hillmyer, T. P. Lodge, *Langmuir,* 2006, **22**, 9409.

[101] A. N. Semenov, I. A. Nyrkova, A. R. Khokhlov, *Macromolecules,* 1995, **28**, 7491.

[102] Z. Li, M. A. Hillmyer, T. P. Lodge, *Nano Lett.,* 2006, **6**, 1245.

[103] C. Liu, M. A. Hillmyer, T. P. Lodge, *Langmuir* , 2008, **24**, 12001.

[104] Z. Li, M. A. Hillmyer, T. P. Lodge, *Macromolecules*, 2006, **39**, 765.

[105] T. P. Lodge, A. Rasdal, Z. Li, M. A. Hillmyer, *J. Am. Chem. Soc*., 2005, **127**, 17608.

[106] A. O. Moughton, T. Sagawa, L. Yin, T. P. Lodge, M. A. Hillmyer, *ACS Omega*, 2016, **1**, 1027.

[107] A. F. Thünemann, S. Kubowicz, H. von Berlepsch, H. Möhwald, *Langmuir,* 2006, **22**, 2506.

[108] W. F. Edmonds, Z. Li, M. A. Hillmyer, T. P. Lodge, *Macromolecules*, 2006, **39**, 4526.

[109] R. R. Taribagil, M. A. Hillmyer, T. P. Lodge, *Macromolecules*, 2009, **42,** 1796.

[110] Taribagil, R. R.; Hillmyer, M. A.; Lodge, T. P. *Macromolecules*, 2010, **43**, 5396.

[111] Z. Zhang, X. J. Hao, P. A. Gurr, A. Blencowe, T. C. Hughes, G. G. Qiao, *Aust. J. Chem.,* 2012, **65**, 1186.

[112]G. Lopez, M. Guerre, J. Schmidt, Y. Talmon, V. Ladmiral, J-P. Habas, B. Ameduri, *Polym. Chem.,* 2016, **7,** 402.

[113] W. F. Edmonds, M. A. Hillmyer, T. P. Lodge, *Macromolecules,* 2007, **40**, 4917.

[114] T. W. Hofmann, S. H. Hänselmann, J. W. Janiesch, A. Rademacher, C. H. Böhm, *J. Lab Chip,* 2012, **12**, 916.

[115] I. Platzman, J-W. Janiesch, J-P. Spatz, *J. Am. Chem. Soc*., 2013, **135**, 3339.

[116] D. A. Babb, B. R. Ezzell, K. S. Clement, W. F. Richey, A. P. Kennedy, *J. Polym. Sci. Part A: Polym. Chem.* **1993**, **31**, 3465–3477.

[117] D. W. Smith Jr., D. A. Babb, H. V. Shah, A. H. R. Traiphol, D. Perahia, H. W. Boone, C. Langhoff, M. Radler, *J. Fluorine Chem.*, **2009**, *130*, 354– 360.

[118] J. Jin, S. T. Iacono, D. W. Smith, In *Handbook of Fluoropolymer Science and Technology*; John Wiley & Sons, Inc.: Hoboken, NJ, 2014, 343-361.

[119] L. Tong, Z. Shen, D. Yang, S. Chen, Y. Li, J. Hu, G. Lu, X. Huang, *Polymer*, 2009, **50,** 2341-2348.

[120] D. Yang, L. Tong, Y. Li, J. Hu, S. Zhang, X. Huang, *Polymer*, 2010, **51**, 1752-1760.

[121] Y. Li, S. Zhang, H. Liu, Q. Li, W. Li, X. Huang, *J. Polym. Sci. Part A: Polym. Chem*. 2010, **48**, 5419.

[122] W. Yao, Y. Li, S. Zhang,, X. Huang, *J. Polym. Sci. Part A: Polym. Chem.* 2011, **49**, 4433-4440.

[123] W. Yao, Y. Li, C. Feng, G. Lu, X. Huang, *Polym. Chem*., 2014, **5**, 6334-6343

[124] W. Yao, Y. Li, C. Feng, G. Lu, X. Huang, *RSC Adv*., 2014, **4**, 52105-52116

[125] C. Feng, C. Zhu, W. Yao, G. Lu, Y. Li, X. Lv, M. Jia, X. Huang, *Polym Chem.,* 2015, **6**, 7881-7892.

[126] G. Lu, H. Liu, H. Gao, C. Feng, Y. Li, X. Huang, *RSC Adv*., 2015, **5**, 39668-39676

[127] H. Liu, S. Zhang, C. Feng, Y. Li, G. Lu, X. Huang, *Polym. Chem*., 2015, **6**, 4309-4318.

[128] R. Hoogenboom, *Angew. Chem. Int. Ed*.,2009, **48**, 7978-7994.

[129] C. Weber, R. Hoognboom, U. S. Schubert, *Prog. Polym. Sci*., 2012, **37**, 686-714.

[130] F. Wiesbrock, R. Hoogenboom, M. A. M. Meenen, M. A. R. Meier, U. S. Schubert, *Macromolecules*, 2005, **38**, 5025-5034.

[131] F. Wiesbrock, R. Hoogenboom, C. H. Abeln, U. S. Schubert, *Macromol. Rapid. Comm.*, 2004, **25**, 1895-1899.

[132] R. Ivanova, T. Komenda, T.B. Bonné, K. Lüdtke, K. Mortensen, P.K. Pranzas, R. Jordan, C.M. Papadakis, *Macromol. Chem. Phys.*, 2008, **209**, 2248–2258.

[133] M. Lobert, R. Hoogenboom, C.-A. Fustin, J.-F. Gohy, U.S. Schubert, *J. Polym. Sci. Part A: Polym. Chem.*, 2008, **46**, 5859–5868.

[134] K. Kempe, R. Hoogenboom, S. Hoeppener, C.-A. Fustin, J.-F. Gohy, U.S. Schubert, *Chem. Commun*., 2010, **46**, 6455–6457.

[135] U. Mansfeld, S. Hoeppener, K. Kempe, J.-M. Schumers, J.-F. Gohy, U.S. Schubert, *Soft Matter*, 2013, **9** ,5966–5974.

[136] J. M. Bak, K-B. Kim, J-E. Lee, Y. Park, S. S. Yoon, H. M. Jeong, H-I. Lee, *Polym. Chem.*, 2013,**4**, 2219-2223.

[137] J. M. Bak, H-I. Lee, *J. Polym. Sci.: Part A Polym*. Chem., 2013, **51**, 1976-1982.

[138] J. Xue, C. Feng, L. Guolin, X. Huang, *Polym. Chem*., 2017, DOI: 10.1039/c6py02004f

[139] K. Matsumoto, M. Kubota, H. Matsuoka, H. Yamaoka, *Macromolecules*, 1999, **32**, 7122-7127.

[140] K. Matsumoto, H. Mazaki, R. Nishimura, H. Mastuoka, H. Yamaoka, *Macromolecules*, 2000, **33**, 8295-8300.

[141] K. Matsumoto, H. Mazaki, H. Matsuoka, *Macromolecules*, 2004, **37**, 2256-2267.

[142] X. Wang, K. Hong, D. Baskaran, M. Goswami, B. Sumpter, J. Mays, *Soft Matter*, 2011, **7**, 7960-7964.

[143] S. Suàrez-Suàrez, G. A. Carriedo, A. Presa Soto, *Chem. Eur. J.,* 2016, **22**, 4483-4491.

[144] D. Presa-Soto, G. A. Carriedo, R. De la Campa, A. Presa Soto, *Angew. Chem. Int. Ed*., 2016, **55**, 10102-10107.

[145] D. R. Ratnaweera, U. M. Shrestha, N. Osti, C-M. Kuo, S. Clarson, K. Littrell, D. Perahia, *Soft Matter*, 2012, **8**, 2176-2184

[146] Z. M. Hudson, J. Qian, C. E. Boott, M. A. Winnik, I. Manners, *ACS Macro. Lett*., 2015, **4**, 187-191.

[147] B. Ni, M. Huang, Z. Chen, Y. Chen, C-H. Hsu, Y. Li, D. Pochan, W-B. Zhang, S. Z. D. Cheng, X-H. Dong, *J. Am. Chem. Soc.*, 2015, **137**, 1392-1395

[148] J-F. Gohy, N. Lefèvre, C. D'Haese, S. Hoeppener, U. S. Schubert, G. Kostov, B. Ameduri, *Polym. Chem.*, 2011, **2**, 328-332.

[149] P. Cernoch, Z. Cernochova, S. Petrova, D. Kankova, J-S. Kim, V. Vasu, A. D. Asandei, *RSC Adv*., 2016, **6,** 55374-55381.

[150] M. Guerre, J. Schmidt, Y. Talmon, B. Ameduri, V. Ladmiral, *Polym. Chem*., 2017, **8**, 1125-1128.

[151] M. Guerre, M. Semsarilar, F. Godiard, B. Ameduri; V. Ladmiral, *Polym. Chem*., 2017, **8**, 1477-1487.

Conclusion Chapitre I

Ce chapitre répertorie sous forme d'une revue, les copolymères fluorés employés dans la préparation d'auto-assemblages en solution. Il en ressort un fort intérêt pour les méthacrylates fluorés, les styrènes ainsi que sur les perfluoropolyéthers. Les morphologies telles que les micelles multicompartiments ou les micelles réagissant à un stimulus externe ont suscité un intérêt tout particulier. En effet, la ségrégation de phase observée dans les micelles multicompartiments, tout comme les évolutions de morphologies observées dans les micelles stimulables, ont généré des morphologies totalement inédites. De plus, les encapsulations sélectives possibles par les micelles multicompartiments ont apporté un réel intérêt applicatif, notamment dans la délivrance de médicaments. Il apparait également que la plupart des auto-assemblages ont été réalisés sur des copolymères fluorés très bien définis avec des dispersités pour la plupart, inférieures à 1,2. Néanmoins, les copolymères fluorés semi-cristallins ont été très peu étudiés, tout comme l'effet de la cristallisation sur les morphologies finales observées. Enfin, ce travail bibliographique a permis de mettre en lumière le peu d'articles signalant la structuration de copolymères issus d'oléfines fluorées. Ce décalage est très probablement dû aux peu de méthodes disponibles permettant de synthétiser de manière bien contrôlées des architectures des copolymères fluorés, et notamment des architectures PVDF.

Un rappel sur les méthodes de polymérisation radicalaire contrôlée disponibles dans la littérature, ainsi que le développement d'une nouvelle méthode, est décrite dans le chapitre suivant de ce mémoire.

Chapitre II. Polymérisation RAFT du VDF

Table des Matières

Introduction Chapitre II

Le chapitre précédent a mis en évidence le clair décalage entre les études d'auto-assemblage en solution des polymères fluorés de type poly(méthacrylate) et des polymères issus d'oléfines fluorées tel que le PVDF. Ce décalage est en grande partie dû à la rareté des méthodes de polymérisation radicalaire contrôlée efficaces, permettant la synthèse d'architectures bien définies et fonctionnelles. En effet, les oléfines fluorées possèdent une réactivité très particulière avec une double liaison vinylique pauvre en électron dû à la forte électronégativité des atomes de fluor. L'hexafluoropropène (HFP) par exemple n'homopolymérise pas, mais copolymérise avec le fluorure de vinylidène (VDF) et forme des copolymères alternés avec les éthers vinyliques. Le chlorotrifluoroéthylène (CTFE) et le tétrafluoroéthylène (TFE) forment aussi des copolymères alternés avec les éthers vinyliques et copolymérisent avec le VDF, mais homopolymérisent. De plus, leurs bas points d'ébullition à pression atmosphérique ($b.p._{(HFP)}$ = - 29 °C, $b.p._{(VDF)}$ = - 82 °C, $b.p._{(CTFE)}$ = - 28 °C, $b.p._{(TFE)}$ = - 75 °C) nécessitent des équipements peu communs et résistants à de hautes pressions (Autoclave). Ces caractéristiques très particulières font que la polymérisation contrôlée des oléfines fluorées et plus particulièrement du VDF, a été très peu étudiée à ce jour. (en comparaison des monomères plus usuels du type : acrylate, méthacrylate, styrène, acrylamide, etc.)

L'objectif de ce chapitre est donc de développer une nouvelle méthode de polymérisation radicalaire contrôlée efficace du VDF. La technique de polymérisation utilisée dans cette étude est bien connue pour les autres familles de monomères hydrocarbonés: la polymérisation par transfert de chaîne réversible par addition-fragmentation (Reversible-Addition Fragmentation Transfer, RAFT). Une étude approfondie sur la cinétique de polymérisation, sur le mécanisme de la RAFT, ainsi que sur les principales problématiques (réactions de transferts, additions inverses du VDF) sont détaillés dans ce chapitre.

Partie 1 –

En 1979, Tatemoto (de la société Daikin) a rapporté la première polymérisation radicalaire contrôlée d'oléfines fluorées en utilisant la polymérisation par transfert d'iode (iodine transfer polymérisation, ITP). Cette méthode a permis le développement d'une large gamme de copolymères fluorés commerciaux possédant diverses propriétés. Cependant des dispersités (Đ) supérieurs à 1,4 ont été rapportés, et tout particulièrement dans le cas des monomères fluorés dissymétriques tel que le VDF. En effet, la polymérisation du VDF conduit à des défauts d'enchaînements tête-tête (addition du radical CF_2 sur le CF_2 du VDF, générant un radical $CH_2^{\bullet}$ et un enchaînement -CH_2-CF_2-CF_2-CH_2-) et queue-queue (addition d'un radical $CH_2^{\bullet}$ sur le CH_2 du VDF, générant un radical $CF_2^{\bullet}$ et un enchaînement -CF_2-CH_2-CH_2-CF_2-) qui, dans le cas de l'ITP, provoquent une accumulation de bouts de chaînes –CH_2-I totalement irréactivable au contraire de son que son homologue -CF_2-I, et entraine ainsi un élargissement de la distribution de masses molaires. De plus, ces extrémités de chaînes –CH_2-I sont communément considérées comme « mortes » et non-réactivables en présence de monomères hydrogénés communs. Il est aussi couramment observé une perte de fonctionnalité ainsi qu'une coloration du polymère dû à la formation d'iode libre.

Les procédés de polymérisation de type RAFT (ou MADIX , Macromolecular Design via the Interchange of Xanthates, qui correspond à la partie de la RAFT utilisant des agents de transfert xanthates) ont récemment montré des résultats prometteurs. Cependant, les conditions d'expérimentation n'ont été que peu optimisées, les valeurs de Đ des copolymères obtenus étaient généralement supérieures à 1,4 et les mécanismes de la polymérisation ont été délaissés au profit des propriétés des copolymères.

Cette partie décrit donc dans un premier temps la synthèse de PVDF par RAFT, qui reste un sujet peu développé et qui nécessite une étude bien plus approfondie. Ce travail a fait l'objet d'un article scientifique publié dans *Macromolecules*.[1]

Deeper insight into the MADIX Polymerization of Vinylidene Fluoride

Marc Guerre,[a] Benjamin Campagne,[a] Olinda Gimello,[a] Karine Parra,[b] Bruno Ameduri,[a] Vincent Ladmiral[a*]

[a]Institut Charles Gerhardt, Ingénierie et Architectures Macromoléculaires, UMR 5253 – CNRS, UM, ENSCM - Ecole Nationale Supérieure de Chimie de Montpellier, 8 rue de l'Ecole Normale, 34296 Montpellier, France
[b]Institut des Biomolécules Max Mousseron, Laboratoire de Mesures Physiques, UMR 5247 CNRS, UM, ENSCM, 15, Avenue Charles Flahault, 34093 Montpellier, France.
*Corresponding author: vincent.ladmiral@enscm.fr

I. Abstract

Controlled radical polymerization protocols for Vinylidene Fluoride (VDF) are still very elusive. MADIX polymerization of VDF has been very rarely reported. The synthesis of PVDF using MADIX solution polymerization was thus investigated in details. More efficient protocols of solution polymerization were developed and afforded relatively well-defined PVDF. The careful polymer chain-end monitoring using MALDI-TOF as well as ^{1}H, ^{19}F, and HETCOR ^{1}H-^{19}F NMR nonetheless revealed that VDF reverse additions and transfer to solvent reactions severely affect the control of the polymerization. Indeed, these unwanted reactions are responsible for a non-negligible loss of CTA and for the accumulation of non-reactive polymer chains in the reaction medium. These reactions lead to the synthesis of PVDF with high chain-end functionality, but these chains cannot reinitiate the polymerization of VDF. This work is the first comprehensive study of the MADIX solution polymerization of VDF.

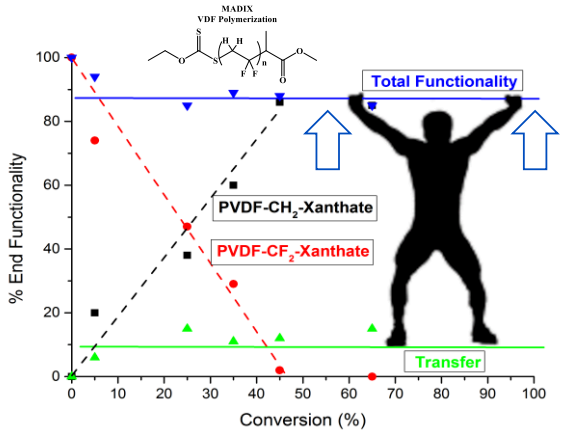

II. Introduction

Poly(vinylidene fluoride) (PVDF) is an interesting fluoropolymer endowed with remarkable properties such as thermal stability, chemical inertness to solvents, oils, and acids (but not to bases), and piezo-, pyro-, and ferroelectric properties.[1−7] PVDF, like most polyfluoroolefins, is synthesized by free radical polymerization under emulsion, suspension, or solution conditions using initiators such as persulfates or organic peroxides or percarbonates.[6,7]

The controlled radical polymerization of fluoroolefins, and of VDF in particular, is very challenging, and very few studies have been reported so far. Tatemoto from Daikin pioneered the iodine transfer polymerization[8] (ITP) of fluoroolefins in 1979 and published a few reports in the 80s and 90s.[9] Arcella et al.[10] also reported the use of ITP to polymerize fluoroolefins. ITP is a very simple technique, and it has been used industrially to produce high-value-added products. Indeed, thermoplastic elastomers based on hard−soft−hard triblock copolymers produced by ITP have been commercialized by Daikin (Daiel[11]), DuPont Performance Elastomers (Viton[12]), and Ausimont,[13,14] now Solvay Specialty Polymers (Tecnoflon[13]). In spite of its advantage (simplicity, low cost), ITP does not afford very good control. Indeed, the iodine transfer is not fast enough to allow very narrow polydispersity, and loss of the iodine atom on the chain-ends is also often a problem.

Moreover, in the case of VDF, head-to-head monomer additions are an additional source of molecular weight distribution broadening. This issue was carefully examined by the IAM team. In 2005, Boyer et al.[15] reported a detailed study on the ITP of VDF and showed that chain defects due VDF head-to-head (HH) addition have a dramatic effect on the control of the polymerization. Indeed, HH addition followed by transfer to an iodine-terminated dormant chain leads to the formation of a $-CF_2CH_2-I$ chain-end, which does not reactivate. As the polymerization proceeds, more and more HH additions occur, which leads to the accumulation in the reaction medium of unreactive $-CF_2CH_2-I$ chain-ends. This very poorly reversible transfer leads to a significant broadening of the molecular weight distribution. This phenomenon was also observed by Durand et al.[16] and Asandei et al.[17] However, Asandei's group[18] recently demonstrated that addition of $Mn_2(CO)_{10}$ to the photoinitiated ITP of VDF provides a way to reactivate $-CF_2CH_2-I$ PVDF chain-ends. The in situ formed $Mn(CO)_5$• radicals reactivate all iodine-terminated chains, thus affording the synthesis of purer block copolymers (i.e., block copolymers devoid of contamination from PVDF first block). However, the second block is synthesized under free radical conditions, and a broad

polydispersity is obtained. Other controlled polymerization methods have been explored. The use of borane derivatives to polymerize VDF was investigated but did not provide significantly better control than ITP.[19–21]

III. Experimental Section

Materials

All reagents were used as received unless otherwise stated. 1,1-Difluoroethylene (vinylidene fluoride, VDF) was kindly supplied by Arkema (Pierre-Benite, France). O-Ethyl-S-(1-methoxycarbonyl)ethyldithiocarbonate and 1,1,1,3,3-pentafluorobutane (Solkane, PFB) were kindly provided by Solvay. tert-Amyl peroxy-2-ethylhexanoate (purity 95%), (Trigonox 121) was purchased from AkzoNobel (Chalons sur Marne, France). ReagentPlus grade (purity >99%) dimethyl carbonate (DMC), acetonitrile (ACN), and tetrahydrofuran (THF) and laboratory reagent grade hexane (purity >95%) were purchased from Sigma-Aldrich and used as received.

Characterization

Nuclear Magnetic Resonance

Nuclear magnetic resonance (NMR) spectra were recorded on a Bruker AC 400 instrument. Deuterated acetone was used as the solvent in each sample. Coupling constants and chemical shifts are given in hertz (Hz) and parts per million (ppm), respectively. The experimental conditions for recording ^{1}H and ^{19}F NMR spectra were as follows: flip angle, 90° (or 30°); acquisition time, 4.5 s (or 0.7 s); pulse delay, 2 s (or 2 s); number of scans, 128 (or 512); and pulse width, 5 μs (for ^{19}F NMR). 2D NMR spectra were recorded at 25 °C in a Bruker Avance III 400 MHz spectrometer, equipped with a BBFO (broad band fluorine observation) probe. For acquisition of heteronuclear $^{1}H-^{19}F$ (HETCOR: heteronuclear correlation) spectra, QF mode with a pulse delay of 1.5 s, a 2000 TD, and a coupling constant of J_{HF} = 5 Hz were used.

MALDI-TOF Spectrometry

MALDI-TOF mass spectra were recorded using a Bruker Ultraflex III time-of-flight mass spectrometer using a nitrogen laser for MALDI (λ 337 nm). The measurements in positive ion were performed with a voltage and reflector lens potential of 25 and 26.3 kV, respectively. For negative ion mode, the measurements were performed with ion source and reflector lens

potential of 20 and 21.5 kV respectively. Mixtures of peptides were used for external calibration. The matrix and cationizing agent were DCTB (trans-2-[3-(4-tertbutylphenyl)- 2-methylprop-2-enylidene]malononitrile) (10 mg/mL in $CHCL_3$) and LiCl (10 mg/mL in methanol). The polymer concentration was 10 mg/mL in dimethylformamide (DMF). The polymer and matrix were mixed in a 4:10 volume ratio. LiCl was first deposited on the target. After evaporation of solvent, the mixture, composed of polymer and matrix, was placed on the matrix-assisted laser desorption ionization (MALDI) target. The dry droplet sample preparation method was used.

Size-Exclusion Chromatography

Size-exclusion chromatograms (SEC) were recorded using a triple-detection GPC from Agilent Technologies with its corresponding Agilent software, dedicated to multidetector GPC calculation. The system used two PL1113-6300 ResiPore 300 × 7.5 mm columns with DMF (containing 0.1 wt % of LiCl) as the eluent with a flow rate of 0.8 $mL \cdot min^{-1}$ and toluene as the flow rate marker. The detector suite was composed of a PL0390-0605390 LC light scattering detector with two diffusion angles (15° and 90°), a PL0390-06034 capillary viscometer, and a 390-LC PL0390-0601 refractive index detector. The entire SEC-HPLC system was thermostated at 35 °C. PMMA standards were used for calibration. Typical sample concentration was 10 mg/mL.

Differential Scanning Calorimetry

DSC measurements were performed on 10−15 mg samples on a Netzsch DSC 200 F3 instrument using the following heating/cooling cycle: cooling from room temperature (ca. 20 °C) to −50 °C at 20 °C/min, isotherm plateau at −50 °C for 5 min, first heating ramp from −50 °C to 200 °C at 10 °C/min, cooling stage from 200 °C to −50 °C at 10 °C/min, isotherm plateau at −50 °C for 3 min, second heating ramp from −50 °C to 200 °C at 10 °C/min, and last cooling stage from 200 °C to room temperature (ca. 20 °C). Calibration of the instrument was performed with noble metals and checked before analysis with an indium sample. Melting points were determined at the maximum of the enthalpy peaks.

Autoclave

The polymerization of VDF was performed in a 100 mL Hastelloy Parr autoclave system (HC 276) equipped with a mechanical Hastelloy stirring system, a rupture disk (3000 PSI), inlet and outlet valves, and a Parr electronic controller to regulate the stirring speed and heating. Prior to the reaction, the autoclave was pressurized with 30 bar of nitrogen to check for leaks.

The autoclave was then put under vacuum (20×10^{-3} bar) for 30 min to remove any trace of oxygen. A degassed solution of solvent, initiator, and MADIX CTA was introduced via a funnel under vacuum. The reactor was then cooled using a liquid nitrogen bath, and VDF was transferred by double weighing (i.e., the difference of mass before and after filling the autoclave with VDF). After warming to ambient temperature, the autoclave was heated to the target temperature under mechanical stirring.

Synthesis

MADIX Homopolymerization of Vinylidene Fluoride (VDF)

Using the experimental setup described above, a typical polymerization (run 9 in Table II-1) of VDF was performed as follows (Scheme II-1): A solution of tert-amyl peroxy-2-ethylhexanoate (Trigonox 121; 158 mg, 6.87 10^{-4} and O-ethyl-S-(1-methoxycarbonyl)ethyldithiocarbonate (CTA; 1.30 g, 6.25 10^{-3} mol) in dimethylcarbonate (DMC; 60 mL) was degassed by N_2 bubbling during 30 min. This homogeneous solution was transferred into the autoclave using a funnel, VDF gas (19.0 g, 2.97 10^{-1} mol) was introduced in the autoclave at low temperature, and the reactor was gradually heated to 73 °C. The reaction was stopped after 24 h. During the reaction, the pressure increased to a maximum of 25 bar and then decreased to 10 bar after 24 h. The autoclave was cooled to room temperature (ca. 20 °C) and purged of the residual monomers, and DMC was removed under vacuum. The crude product was dissolved in 30 mL of warm THF (ca. 40 °C) and left under vigorous stirring for 30 min. This polymer solution in THF was then precipitated from 400 mL of chilled hexane. The precipitated polymer (white powder) was filtered through a filter funnel and dried under vacuum (15 10^{-3} bar) for 2 h at 50 °C. The polymerization yield was determined by gravimetry (mass of polymers obtained/mass of monomer introduced in the pressure reactor) (yield = 65%). Yields were used as conversion since conversion is very difficult to measure accurately for VDF or other gaseous monomers.

DP and $Mn_{(NMR)}$ Calculations Using End-Group Analysis.

R End-Group Analysis. The degree of polymerization (DP) can be calculated from ^{1}H NMR using the integrals of the signals corresponding to the methyl group of the CTA R-group (1.19 −1.24 ppm), the CH_2 group of the regular VDF additions (HT, 2.70−3.19 ppm), the CH_2 group of the reverse VDF additions (TT, 2.28−2.43 ppm), and that of the terminal VDF units (4.02−4.17 ppm), according to Equation II-1 (see VIII-Supporting Information, SI-Figure II-11, SI-Figure II-12 and SI-Table II-3 for details).

$$\textit{Equation II-1} \quad DP = \frac{\int_{2.70}^{3.19} CH_2(HT) + \int_{2.28}^{2.43} CH_2(TT) + \int_{4.02}^{4.17} CH_2(End-group)}{2/3 \times \int_{1.19}^{1.24} CH_3(R-CTA)}$$

Molecular weight was then calculated using Equation II-2:

$$\textit{Equation II-2} \quad M_{nNMR}(R) = M_nCTA + DP \times M_nVDF$$

Where $M_{n\,CTA}$ = 208.3 g.mol^{-1} and $M_{n\,VDF}$= 64.04 g.mol^{-1}

Z End-Group Analysis. As above, the degree of polymerization (DP) can be calculated from ^{1}H NMR using integrals of the signals centered at 1.45 ppm corresponding to the methyl group (CH_3) of the Z-group of the CTA, the integrals of the signals of the CH_2 group of the normal VDF additions (HT, 2.70−3.19 ppm), that of the CH_2 group of the reverse VDF additions (TT, 2.28−2.43 ppm), and that of the terminal VDF units (4.02−4.17 ppm), according to Equation II-3 (see VIII-Supporting Information, SI-Figure II-11, SI-Figure II-12 and SI-Table II-3 for details).

$$\textit{Equation II-3} \quad DP = \frac{\int_{2.70}^{3.19} CH_2(HT) + \int_{2.28}^{2.43} CH_2(TT) + \int_{4.02}^{4.17} CH_2(End-group)}{2/3 \times \int_{1.40}^{1.46} CH_3(R-CTA)}$$

Molecular weight was then calculated using Equation II-4:

$$\textit{Equation II-4} \quad M_{nNMR}(Z) = M_nCTA + DP \times M_nVDF$$

Theoretical molecular weight was calculated using Equation II-5 with yield = conversion and the $[VDF]_0/[CTA]_0$ ratios listed in Table II-1.

$$\textit{Equation II-5} \quad M_{n(theo)} = \frac{[VDF]_0}{[CTA]_0} \times Yield \times M_nVDF + M_nCTA$$

^{1}H NMR (400 MHz $(CD_3)_2CO$, δ (ppm), Figure II-3) : 1.19-1.24 (d, -CH(C**H$_3$**)(C=O)-, $^3J_{HH}$= 7.1 Hz), 1.40-1.46 (t, C**H$_3$**-CH_2-O-, $^3J_{HH}$= 7.2 Hz), 2.28-2.43 (m,-CF_2-C**H$_2$**-C**H$_2$**-CF_2-, VDF-VDF TT reverse addition), 2.70-3.19 (t, -CF_2-C**H$_2$**-CF_2-, VDF-VDF HT regular addition), 3.60-3.69 (s, -(C=O)-O-C**H$_3$**), 4.02-4.17 (t, -CF_2-C**H$_2$**-S(C=S)OEt, $^3J_{HF}$= 18 Hz), 4.67-4.77 (q, CH_3-C**H$_2$**-O-, $^3J_{HH}$= 7.2 Hz), 6.05-6.45 (tt, $^2J_{HF}$= 55 Hz , $^3J_{HH}$= 4.6 Hz -CH_2-CF_2-**H**)7

^{19}F NMR (376 MHz $(CD_3)_2CO$, δ (ppm),Figure II-4) : -115.63 (-CH_2-CF_2-C**F$_2$**-CH_2-CH_2-, VDF-VDF HH reverse addition), -114.29 ($^2J_{HF}$= 55 Hz, -CH_2-C**F$_2$**-H), -113.34 (-CH_2-C**F$_2$**-CF_2-CH_2-CH_2-, HH reverse addition), -113.09 (CH_2-CF_2-**CF_2**-CH_2-S-), -112.69 (-CH_2-**CF_2**-CF_2-CH_2-S-), -94.79 (-CH_2-CH_2-C**F$_2$**-CH_2-, TT reverse addition), -93.50 (-CH_2-C**F$_2$**-CH_2-CH(CH_3)(C=O)-), -92.12 (-CH_2-C**F$_2$**-CH_2-CF_2H), -91.44 (-CH_2-CH_2-CF_2-CH_2-**CF_2**-CH_2-CF_2-, regular VDF-VDFHT addition), -91.00 (-CH_2-C**F$_2$**-CH_2-, regular VDF-VDF HT addition).

IV. Results and Discussion

Girard et al.[24]have shown that xanthates can be used as chain transfer agents using MADIX experimental protocols to afford some control over the homopolymerization of VDF. Nevertheless, the reaction conditions that they used may not be optimal to afford good control: high $[I]_0/[CTA]_0$ initial molar ratios (equimolar amounts of initiator and chain transfer agent) combined with high radical flux (i.e., high reaction temperature, at which the decomposition half-life of the initiator is close to 1 h). These conditions effectively result in the production of equimolar amounts of radicals to CTA during the course of the polymerization. These conditions (high flux of radicals) are likely to lead to a large number of dead chains (i.e., not terminated by the xanthate moiety), a large number of chains initiated by the initiator rather than by the CTA R-group, and broader molecular weight distributions. Indeed, in a degenerative transfer system, the number of dead chains is dictated by the number of radicals generated from the initiator.[29,30]

These suboptimal conditions had been chosen to increase the polymerization rate and afford a non-negligible amount of polymer. It was thus decided to investigate the polymerization of VDF under MADIX conditions using relatively low initiator to CTA ratios (0.1−0.2) and a polymerization temperature at which the initiator decomposition half-life is about 10 h. The first polymerization was performed in 1,1,1,3,3-pentafluorobutane (run 1,Table II-1). Under these conditions, the yield was low (<10%). The same conditions using acetonitrile as a solvent gave slightly higher yields (25 %, run 2, Table II-1), but they were not efficient enough to afford acceptable monomer conversions and a sufficiently high PVDF molecular weight. Recently, Asandei and co-workers[18b] observed that the radical iodine transfer polymerization of VDF using DMC as the solvent proceeded much faster and with high yields. This is supposedly due to the ability of DMC to better stabilize VDF and to swell PVDF even though it does not dissolve it.[31,32] The authors also stated that while radicals arising from transfer to acetonitrile were not able to reinitiate the polymerization of VDF, those arising from transfer to DMC were more reactive and could reinitiate the polymerization of VDF.[18]

Table II-1: Experimental Conditions and Results for the MADIX Polymerization of VDF[a]

Run	$[VDF]_0/[CTA]_0$	Reaction time Solvent	[b]yield %	[c]$DP_{(NMR)}$ (R)	[d]$M_{n(theo)}$ (g/mol)	[e]$M_{n(NMR)(R)}$ (g/mol)	[f]$M_{n(SEC)}$ (g/mol)	[f]Đ	[c]-CF_2-CH_2-S- %	[c]-CH_2-CF_2-S- %	[c]CF_2H %	Tm (°C)
1	50	24h,PFB	8	18	500	1400	1500	1.05	18	76	6	122
2	50	24h,AcN	25	31	1000	2200	4200	1.33	74	13	13	163
3	50	5h,DMC	< 5	4	n.d	500	*800	*1.05	20	74	6	n.d
4	51	10h,DMC	25	20	1000	1500	3900	1.12	38	47	15	146
5	51	15h,DMC	35	29	1400	2100	4100	1.29	60	29	11	159
6	47	17.5h,DMC	45	41	1600	2800	5300	1.30	86	2	12	170
7	54	20h,DMC	65	47	2400	3200	7200	1.40	85	0	15	171
8	48	24h,DMC	65	44	2200	3000	5000	1.42	86	0	14	171
9	54	64h,DMC	70	44	2600	3000	5200	1.34	86	0	14	170

[a]Reactions conditions: chain transfer agent (CTA) = O-ethyl-S-(1-methoxycarbonyl)ethyldithiocarbonate, initiator (I) = tert-amyl peroxy-2-ethylhexanoate, [I]/[CTA] = 0.1, T = 73 °C. AcN, PFB, and DMC stand for acetonitrile, 1,1,1,3,3-pentafluorobutane, and dimethylcarbonate, respectively. [b]Determined by gravimetry. [c]Determined by ^{1}H NMR (see Equation II-1 in the Experimental Section for details). [d]Calculated using yield as conversion (see Equation II-5 in the Experimental Section for details). [e]Calculated from $DP_{(NMR)}$ (see Equation II-2 in the Experimental Section for details). [f]Determined by SEC.

MADIX polymerizations of VDF in DMC were thus attempted (runs 3−9, Table II-1). As observed by Asandei et al.,[18] polymerizations were much faster in DMC than they were in 1,1,1,3,3-pentafluorobutane or acetonitrile, and the yields were much higher.

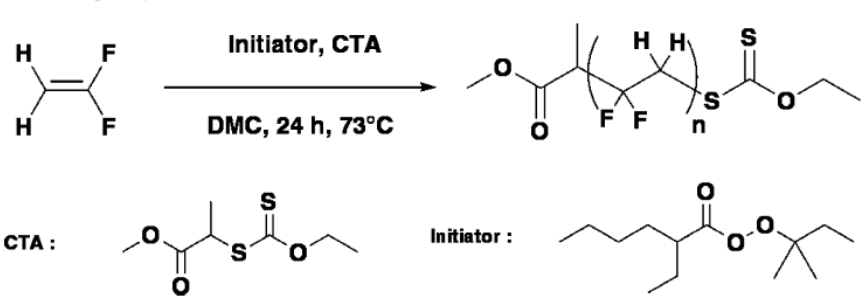

Scheme II-1: Schematic Representation of VDF MADIX Homopolymerization

The polymerizations were, nonetheless, relatively slow and required at least 20 h to reach about 70% yield (runs 7−9, Table II-1), as shown by the first-order kinetics plot (SI-Figure II-13). This plot also revealed three regimes in the MADIX polymerization of VDF: (i) a period between t = 0 and 5 h where the polymerization rate is extremely slow or even negligible, followed by (ii) a polymerization that takes place at a relatively slow rate (between t = 4 and 17 h) and (iii) a significantly higher polymerization rate (after 17 h). The peculiar polymerization kinetics profile may be explained by the only moderate solubility of VDF and PVDF in DMC[18,29,32] and by the effect of the VDF reverse additions on the MADIX

mechanism. The first stage of the polymerization proceeds in solution under dilute conditions, hence resulting in the relatively slow rate of polymerization. Once the PVDF reaches a certain molecular weight, it may not be entirely soluble in the reaction mixture anymore, and the VDF may, at that stage, partition preferentially into the DMC-swollen PVDF (rather than in the DMC or the free volume of the pressure reactor), which may act as nanoreactors with a high local VDF concentration. Once conversion has reached about 50% (at t = 17 h), all of the polymer chains are terminated with a $-CF_2H$ or $-CH_2$-Xa group (vide infra). These xanthate end-groups do not transfer efficiently; thus, the polymerization may take place under free radical conditions, which is faster than MADIX polymerization.[33]

Remarkably, the molecular weight increased linearly with conversion (Figure II-1 and SI-Figure II-14). This proves that the MADIX polymerization of VDF proceeds with some degree of control.

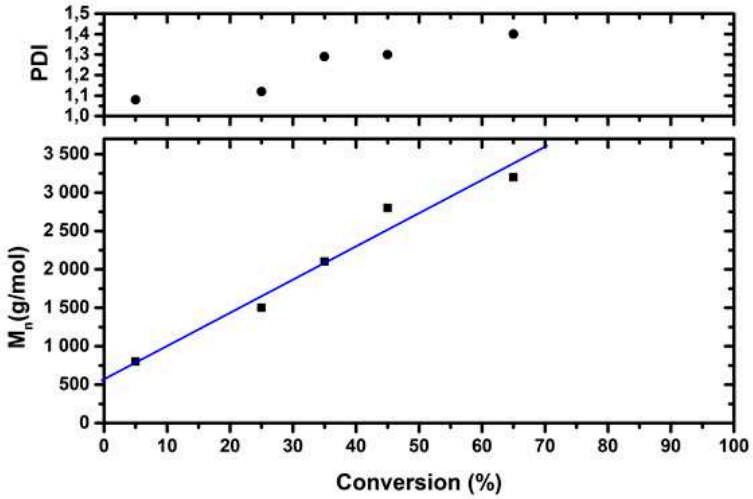

Figure II-1: Evolution of Mn and Đ versus conversion for the MADIX homopolymerization of VDF. Reaction conditions: $[VDF]_0/[CTA]_0/[I]_0$ = 50:1:0.1; CTA = O-ethyl-S-(1-methoxycarbonyl)-ethyldithiocarbonate, I = tert-amyl peroxy-2-ethylhexanoate, solvent = DMC, T = 73 °C. The blue line is a guide to the eye.

However, the molecular weight distribution also increased with conversion (Figure II-1), which suggests that some undesired reactions occurred during the polymerization. Interestingly, a DP of 44 is sufficient to reach the expected melting point of PVDF (171 °C). PVDF radicals are known to be prone to transfer and backbiting,[34] which should cause the formation of lower molecular weight polymers than expected. In addition, VDF polymerization is also known to undergo HH additions, which may lead to unreactive polymer chain-ends and broadening of the molecular weight distribution, ultimately proving to be detrimental to the preparation of well-defined block copolymers. Here, the molecular

weight distributions of the PVDF synthesized were relatively narrow (<1.42) and significantly narrower than those reported by Girard et al.[24] This suggests that the polymerization protocols used here were more efficient than those previously reported. Nonetheless, a thorough characterization of the PVDF synthesized was conducted to better understand the specific phenomena at work in the polymerization of VDF under MADIX conditions.

IV.1 MALDI-TOF Mass Spectrometry

Further characterization of the structures of the PVDF synthesized via MADIX polymerization was performed via matrix-assisted laser desorption/ionization coupled time-of-flight mass spectrometry (MALDI-TOF), using both positive and negative ion modes (run 9, Table II-1). Surprisingly, the positive ion mode mass spectrum displayed only one population of polymer, which corresponded to the expected PVDF chains bearing both the R-(methyl propionyl) and Z-(O-ethyl xanthate) groups of CTA. SI-Table II-4 assigns the different peaks observed in

Figure II-2 with their corresponding calculated molecular weights. Contrary to the previous study by Girard et al.,[24] fragmentation of the ω- chain-end was not observed here.

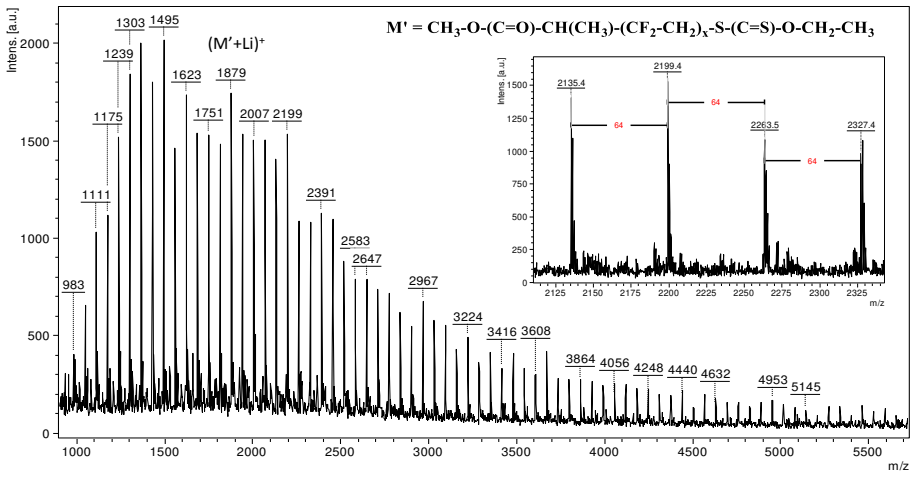

Figure II-2: Positive ion MALDI-TOF mass spectrum of PVDF synthesized by MADIX polymerization (run 9, Table II-1) with DCTB as matrix and LiCl as cationic agent. PVDF: CH_3-O-(C=O)-CH(CH_3)-(CF_2CH_2)$_x$-S(C=S)-O-CH_2CH_3 was detected as a lithium adduct $(M + Li)^+$.

In contrast, the negative ion mode mass spectrum revealed four populations of PVDF (see SI-Figure II-15 to SI-Figure II-17 and SI-Table II-5): (i) PVDF initiated by an initiator fragment and terminated by the O-ethyl xanthate moiety (with methanol), (ii) PVDF initiated by the CTA R group or an initiator fragment and terminated by a thiol or an hydrogen atom (with methanol in the latter case), (iii) PVDF initiated by the CTA R-group and terminated by the

O-ethyl xanthate moiety (with acetone), and (iv) chains initiated by the CTA R-group or an initiator fragment and terminated by a thiol or an hydrogen atom (with acetone and methanol in the case of the thiol-terminated chains or acetone only in the case of the H-terminated chains).

IV.2 NMR Spectroscopy

Using 1D and 2D ^{1}H, ^{19}F, $^{1}H\{^{19}F\}$ and $^{19}F\{1H\}$, COSY ^{1}H–^{1}H, COSY ^{19}F–^{19}F, and HETCOR $^{1}H-^{19}F$ (see VIII-Supporting Information for details) NMR experiments and previously reported studies,[15,28,35] it was possible to perform a thorough structural analysis of the PVDF synthesized under MADIX conditions. Figure II-3 and Figure II-4 respectively display the ^{1}H and ^{19}F NMR spectra of a typical PVDF synthesized in the present study (run 9, Table II-1).

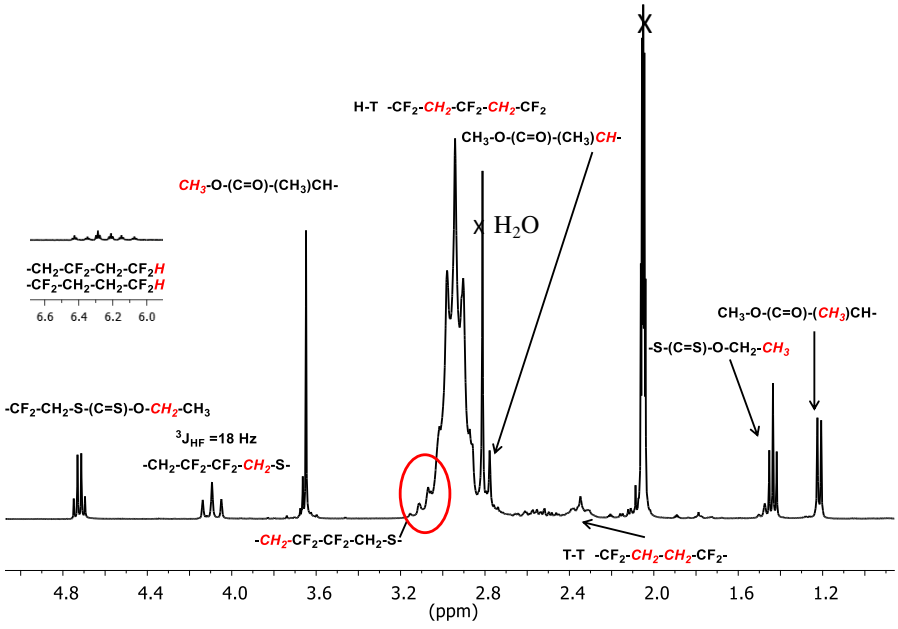

Figure II-3: Expansion of the 1.2–4.9 ppm region of the 1H NMR spectrum in (CD3)2CO of a PVDF homopolymer synthesized via MADIX polymerization (run 9, Table II-1).

The ^{1}H NMR spectrum (Figure II-3) shows (i) a broad multiplet centered at 2.9 ppm corresponding to the methylene of the regular head-to-tail (HT) addition of VDF, (ii) a triplet at 2.3ppm characteristic of the tail-to-tail (TT) addition of VDF, (iii) signals assigned to the R-group of the CTA at 1.2 ppm (doublet), 3.6 ppm (singlet), and 2.8 ppm (partly masked multiplet), (iv) signals assigned to the Z-group of the CTA at 1.4 ppm (triplet, CH_3 of the O-ethyl xanthate) and 4.7 ppm (quartet, $-CH_2-O-$ of the O-ethyl xanthate), (v) signals around 2.1 ppm (broad multiplet) and 2.5 ppm (broad multiplet) assigned to the first two units of VDF on the α-end (i.e., connected to the propionyl moiety of the CTA) of the polymer and a well-

defined triplet at 4.1 ppm corresponding to the last VDF unit on the ω-chain-end (i.e., connected to the O-ethyl xanthate moiety), and (vi) two small triplet of triplets at 6.2 ppm characteristic of -CF_2H end-groups caused by hydrogen abstraction and symptomatic of transfer.

The ^{19}F NMR spectrum (Figure II-4) of the same polymer (run 9, Table II-1) shows (i) the expected intense signal at −91 ppm characteristic of HT addition of VDF, (ii) signals at −115.6, −113.3, −94.8, and −91.4 ppm indicative of chain defects caused by VDF reverse additions, (iii) two quartets of doublets at −114.3 ppm and a small multiplet at −92.1 ppm revealing the presence of small amounts of -CF_2H chain-ends, and (iv) signals at −113.09 and − 112.69 ppm characteristic, respectively, of the ultimate and penultimate VDF units connected to the *O*-ethyl xanthate end-group. Remarkably, *O*-ethyl xanthate groups were capping exclusively HH VDF defects (-CF_2-CH_2-SC(S)OCH_2CH_3 end-group). Regular HT addition terminated with the xanthate group, which would give a -CH_2-CF_2-SC(S)OCH_2CH_3 end-group appearing around −70 ppm in ^{19}F NMR, were not found.

This comprehensive NMR peak assignment was, in large part, made possible by the use of HETCOR 1H−19F 2D experiment (SI-Figure II-18 and SI-Figure II-19), which clearly revealed the connection between fluorinated and hydrogenated moieties.

This NMR study revealed a very important feature: Aside from a small fraction of -CF_2H-terminated chains, the PVDF chains were ending exclusively with a -CF_2-CH_2-Xa group (where Xa = SC(S)OCH_2CH_3). It thus appeared that all PVDF chains were terminated with an HH addition. This is not entirely surprising. Boyer et al.[15] as well as Asandei's group[18b] already reported similar behavior in the case of iodine transfer polymerization of VDF, where CH_2-I end-groups, unable to reinitiate, accumulated in the reaction medium. MADIX, which also proceeds via a degenerative transfer mechanism, is thus likely to suffer from the same phenomenon. The NMR study suggests that VDF reverse additions are more often followed by transfer to the CTA to form unreactive -CF_2-CH_2-Xa chain-ends rather than by another reverse addition (TT addition) onto a VDF molecule.

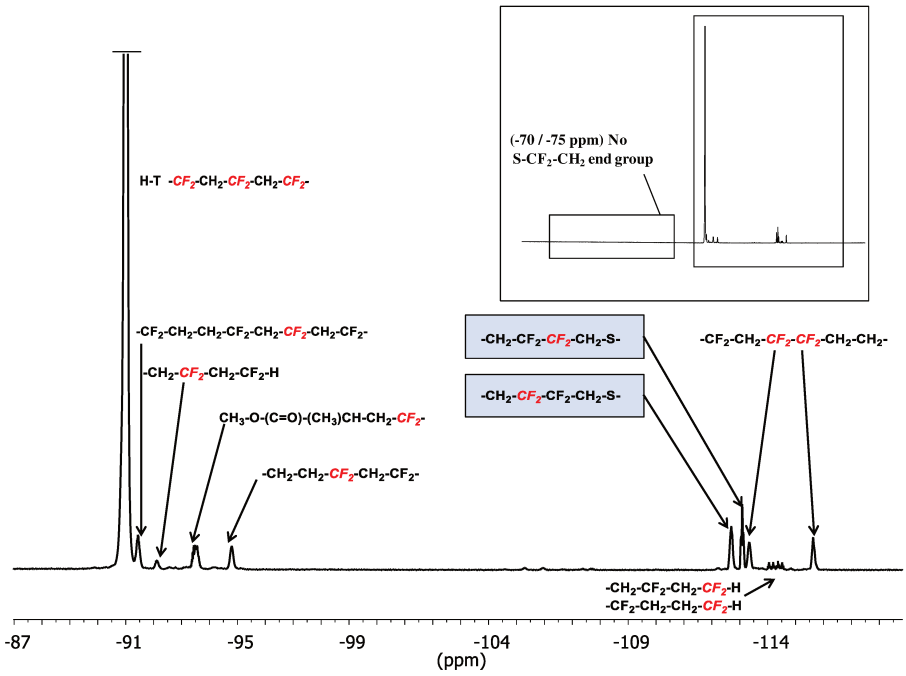

Figure II-4: Expansion of the −87 to −117 ppm region of the ^{19}F NMR spectrum in $(CD_3)_2CO$ of a PVDF homopolymer synthesized via MADIX polymerization (run 9, Table II-1).

IV.3 Mechanism of the MADIX Polymerization of VDF

The previous observations were done on a 64 h MADIX polymerization of VDF, for which the conversion reached 65%. This long polymerization time and high monomer conversion likely favored the formation of -CH_2-Xa end-groups to the detriment of the regular-CF_2-Xa end-groups, which must be the prevailing groups during the polymerization for the polymer to form. An NMR study of the evolution of the PVDF end-groups with conversion was thus carried out on five polymerizations performed under identical conditions (proportions of VDF, CTA, and initiator, temperature, and amount of DMC) but stopped after various reaction times (run 3, 5 h; run 4, 10 h; run 5, 15 h; run 6, 17.5 h; and run 7, 20 h; Table II-1).

Figure II-5 shows the ^1H NMR spectrum of a MADIX polymerization of VDF stopped after 10 h (VDF conversion = 25%). The signal centered at 4.72 ppm corresponding to the -CH_2-O- moiety of the xanthate end-group appeared to be split into two quartets. Similarly, a second triplet can be seen at slightly lower field next to the signal at 1.44 ppm, attributed to the -CH_3 group of the xanthate. The high-field signals (t, 1.44 ppm and q, 4.72 ppm) correspond to a PVDF chain terminated by an inverted VDF unit (HH addition) capped with a xanthate, as shown in Figure II-3. The new lower field signals (triplet at 1.48 ppm and quartet at 4.77 ppm) match a PVDF chain terminated by -CH_2-CF_2-Xa (i.e., a regularly added VDF unit (HT addition) capped with a xanthate).

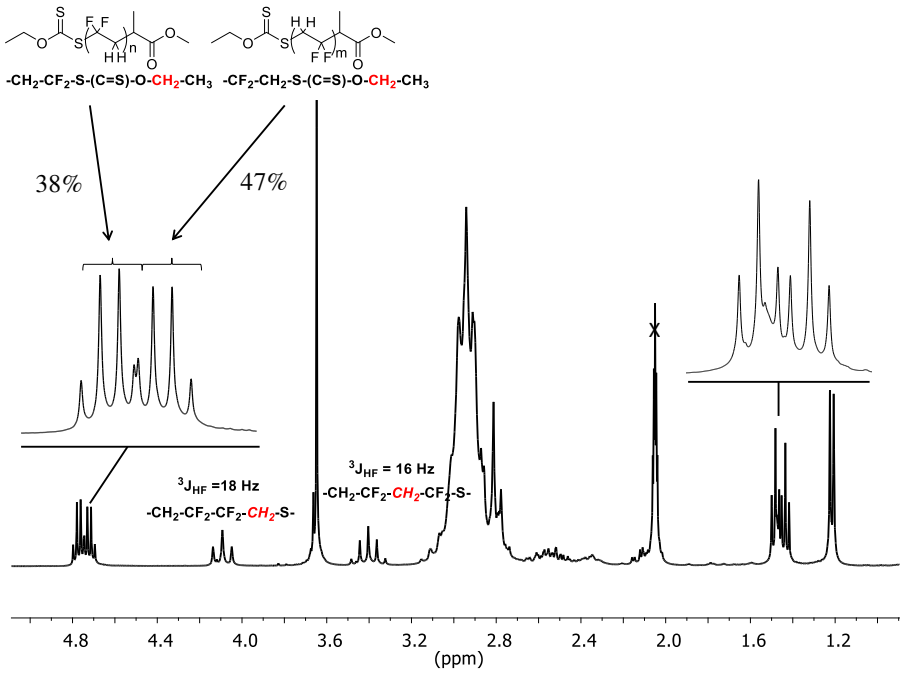

Figure II-5: Expansion of the 1.0−4.9 ppm region of the ^1H NMR spectrum in $(CD_3)_2CO$ of a PVDF homopolymer synthesized via MADIX polymerization (run 4, Table II-1). Polymerization time = 10 h; VDF conversion = 25%.

In addition to these two new signals corresponding to the ethyl group of the xanthate, an extra quintet at 3.4 ppm can also be seen in Figure II-5. This quintet features a 16 Hz coupling constant characteristic of $^3J_{H-F}$ and can be assigned to the methylene protons of the ultimate unit of VDF connected to the xanthate group via regioregular addition (HT). Thanks to the surprisingly strong influence of fluorine atoms on the chemical shifts of other nuclei, the ethyl moiety of the xanthate can be used as a very efficient probe to quantitatively characterize the products of the MADIX polymerization of VDF. Indeed, the chemical shifts of the methyl and methylene of the xanthate end-group are shifted from 1.44 and 4.72 ppm in the case of a -CF_2-CH_2-S- end-group to 1.48 and 4.77 ppm, respectively, in the case of a CH_2-CF_2-S- end-group. Remarkably, this deshielding effect can be seen even for nuclei that are seven covalent bonds away from the fluorine atoms. Using the xanthate moiety as a NMR probe, it was possible to calculate the following proportions of end-groups for the polymer shown in Figure II-5 (run 4, Table II-1): -CF_2-Xa-/-CH_2-Xa/-CF_2H = 38:47:15.

^{19}F NMR spectroscopy also confirmed the presence of a -CH_2-CF_2-Xa end-group shown as a complex signal at −71 ppm (Figure II-6), which was not observed in the ^{19}F NMR spectrum of a PVDF exclusively terminated by a -CF_2-CH_2-Xa group (Figure II-4).

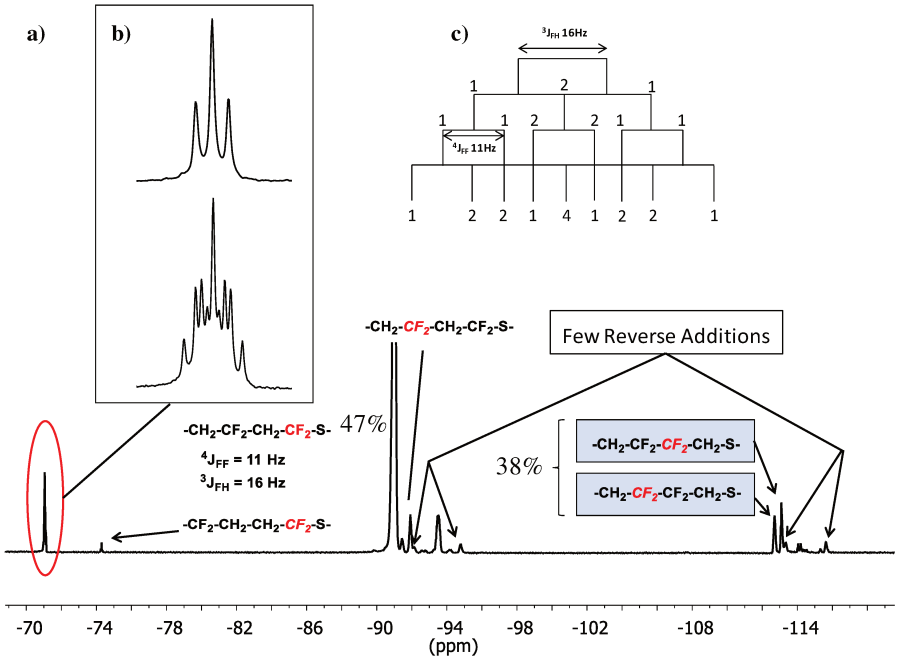

Figure II-6: (a) Expansion of the −70 to −120 ppm region of the ^{19}F NMR spectrum in $(CD_3)_2CO$ of a PVDF homopolymer synthesized via MADIX polymerization (run 4, Table II-1). Polymerization time = 10 h; VDF conversion = 25%. (b) Zoomed in view of the signal of the ω-end terminal CF_2 moiety in $^{19}F\{^1H\}$ NMR (up) and ^{19}F NMR (bottom). (c) Splitting diagram for the ^{19}F NMR signal of the ω-end terminal CF_2 moiety.

After determination of the $^3J_{FH}$ and $^4J_{FF}$ coupling constants using ^1H and $^{19}F\{^1H\}$ NMR experiments, the multiplicity of this signal at −71 ppm was elucidated (Figure II-6). This ^{19}F NMR spectrum was also used to calculate the proportion of each type of chain-ends using the integrals of the signal at −71 ppm, those of the two signals at −113 ppm, and the integral of the signal of -CF_2H end-group at −114.3 ppm. The comparison of the ^1H NMR signal assigned to TT and HT additions (2.3 and 3.0 ppm, respectively) gave indications about the proportion of TT defect present inside the PVDF chains. Similarly, the ^{19}F NMR signals were informative regarding the proportion of HH inside the PVDF chains (−115.63 ppm), of terminal HH addition (i.e., present as the terminal unit) (−112.69 ppm), and of HT regular additions (−91 ppm). SI-Figure II-20 shows the evolution of chain defects versus conversion. This plot reveals that the amounts of intrachain TT and HH reverse additions (SI-Figure II-23 and SI-Equation II-9, SI-Equation II-10, SI-Equation II-11) increase as the polymerization proceeds and that they are strictly equal to each other. This suggests that each intrachain HH reverse addition is immediately followed by a TT reverse addition to reform the normal CF_2· propagating radical. The proportion of terminal HH addition also increases with conversion, but these inversions are not followed by TT additions. This suggests that a large number of

HH additions are immediately followed by transfer to the CTA and do not reinitiate the polymerization (*vide infra*). Finally, the total proportion of chain defects amounts to about 4%. This number is in agreement with the proportion of chain defects observed for PVDF prepared under conventional free radical polymerization.[35] There is no effect of the MADIX polymerization on the total amount of PVDF chain defects, although it appears that a large proportion of these defects are located at the terminal unit of the polymer chain.

To further examine the MADIX polymerization of VDF, the evolution of end-group functionality was monitored as a function of conversion. Figure II-7 shows the evolution of the ω-chain-end $_1$H and $_{19}$F NMR signals with conversion.

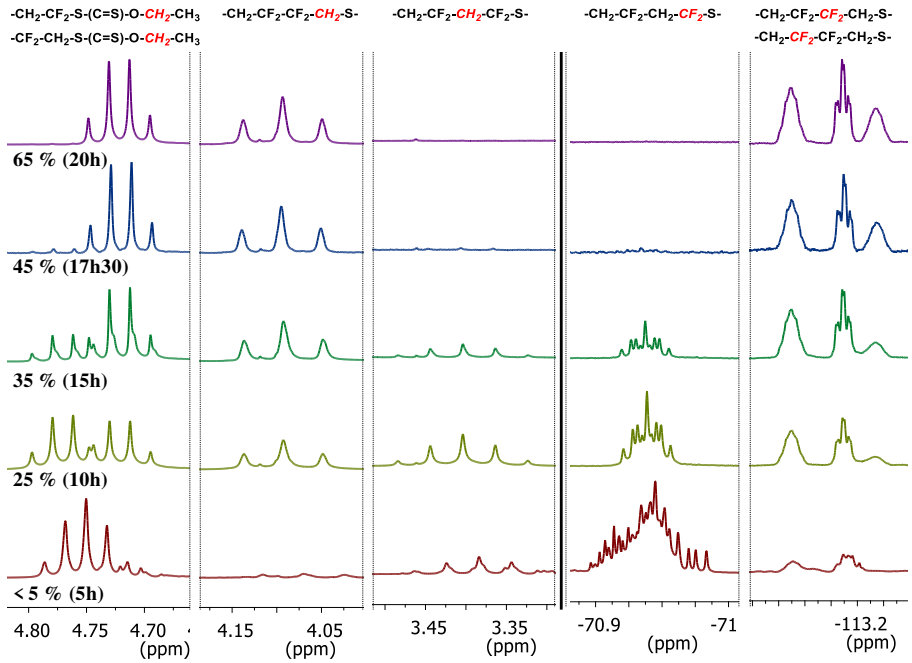

Figure II-7: Evolution of selected ^{1}H and ^{19}F NMR signals with conversion of PVDF homopolymers synthesized via MADIX polymerization. The spectra were recorded in $(CD_3)_2CO$.

It can clearly be seen that at low conversion (beginning of the polymerization) the prevailing ω-chain-end was -CH_2-CF_2-Xa (strong signals at 4.77 and 3.4 ppm in ^{1}H NMR and at −71 ppm in ^{19}F NMR and very weak signals at 4.72 and 4.1 ppm in ^{1}H NMR and at −112.69 and −113.09 ppm in ^{19}F NMR corresponding to a -CF_2-CH_2-Xa chain-end). As the VDF conversion increased, the signals assigned to the -CH_2-CF_2-Xa chain-end decreased, whereas signals corresponding to the -CF_2-CH_2-Xa chain-end appeared and increased in intensity. After 17.5 h of reaction (conversion = 65%), the -CH_2-CF_2-Xa chain-end completely disappeared.

The ^{1}H NMR spectrum of the reaction stopped after 5 h (VDF conversion < 5%) exhibited a surprising quintet instead of the expected quartet at 4.7 ppm. (SI-Figure II-21) At such low conversion, the reaction medium was composed mainly of monoadduct (DP = 1) and few very low molecular weight oligomers. The monoadduct has a very distinctive NMR signature[24] compared to that of oligomers, as shown in the ^{19}F NMR spectrum of this low conversion polymerization (SI-Figure II-22). This also explains the weak intensity of the quintet at 3.4 ppm corresponding to the -CF_2-CH_2-CF_2-Xa end-group. This NMR monitoring of the PVDF chain-end allowed the evolution of chain-end functionality versus conversion in the course of the MADIX polymerization of VDF to be plotted (Figure II-8). Hydrogen abstraction (most likely caused by transfer to DMC even though backbiting[34] and transfer to polymer cannot be completely excluded) occurs throughout the polymerization and increases slowly with conversion to reach about 15% when conversion is at 65%.

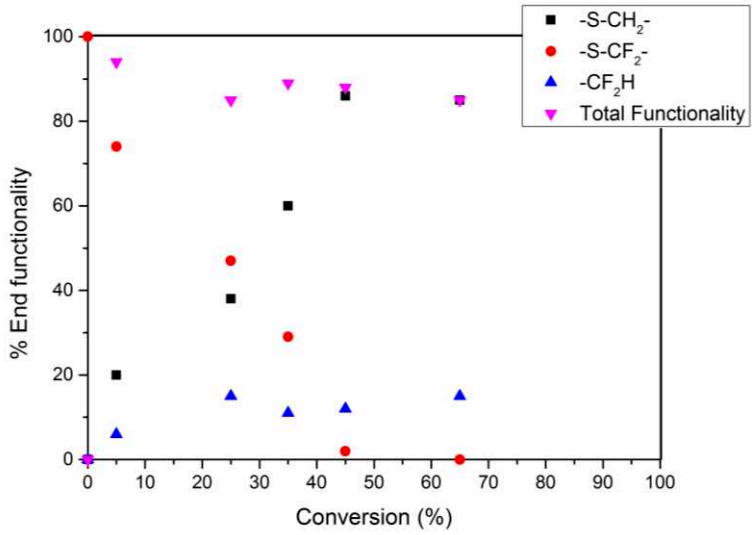

Figure II-8: Evolution of chain-end functionality during VDF MADIX polymerization versus conversion.

Remarkably, the proportion of -CF_2-CH_2-Xa end-groups increases linearly with conversion (to the detriment of the -CH_2-CF_2-Xa end-group, which, conversely, decreases linearly with conversion) and constitutes 100% of the xanthate-terminated end-group when the VDF conversion is only 50%. This accumulation of -CF_2-CH_2-Xa caused by reverse VDF addition immediately followed by transfer to the CTA is reminiscent of the study by Asandei and co-workers[18] who observed exactly the same phenomenon in their study of the ITP of VDF. The present study shows that -CH_2-CF_2-Xa end-groups fragment and reinitiate the polymerization of VDF very readily, whereas -CF_2-CH_2-Xa chain-ends seem to remain inert once they are formed. The accumulation of these nonreactive chain-ends could significantly hinder the

ability to synthesize PVDF-based block copolymers using the MADIX process. Studies focusing on this issue are underway in our laboratory and will be published in due course. In addition, these seemingly nonfragmenting chain-ends are responseble for the broadening of the molecular weight distribution with conversion observed here (SI-Figure II-23). Nonetheless, in spite of this chain-end reactivity difference, Đ remained below 1.5

IV.4 Transfer

Thorough NMR study of the PVDF structure obtained via MADIX polymerization revealed (i) the formation and accumulation in the reaction medium of nonreactive chains (terminated with $-CF_2-CH_2-Xa$ end-groups) caused by reverse addition immediately followed by transfer to the CTA and (ii) the formation of dead chains ($-CH_2-CF_2-H$) by radical transfer reaction from $CF_2\cdot$ radicals to DMC. These DMC radicals produced by hydrogen abstraction are able to reinitiate the polymerization of VDF. They can thus either initiate new PVDF chains or transfer to a CTA. NMR and MALDI-TOF analyses of the PVDF synthesized in the present study did not show any signs of PVDF chains initiated by DMC radicals.

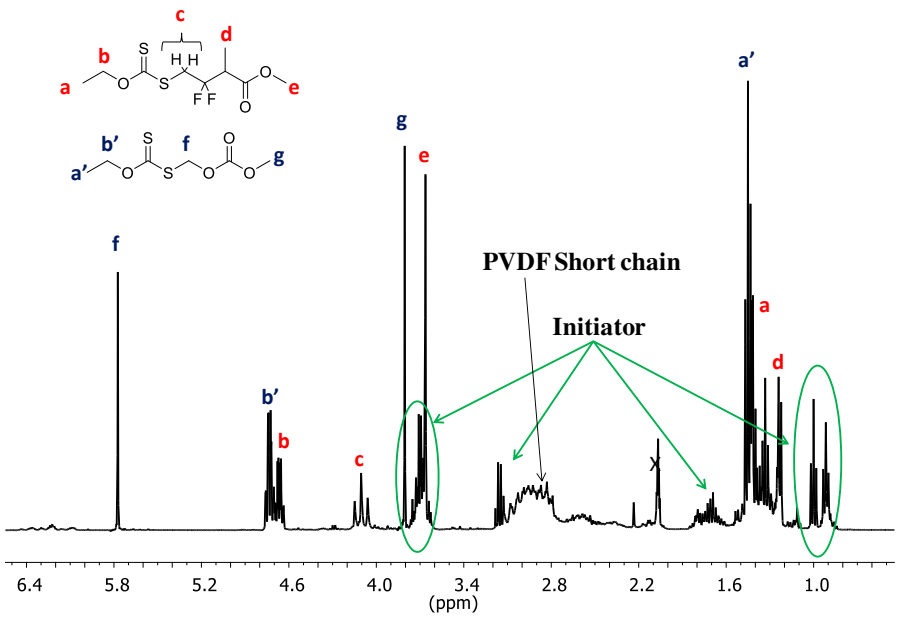

Figure II-9: Expansion of the 0.5−6.5 ppm region of the ^1H NMR spectrum in $(CD_3)_2CO$ of the hexane-soluble residue obtained after precipitation of PVDF synthesized via MADIX polymerization (run 9, Table II-1).

In contrast, the ^1H NMR spectrum (Figure II-9) of the hexanesoluble residue obtained after precipitation of MADIX synthesized (run 9, Table II-1) PVDF revealed the presence of two side products: (i) the adduct of a DMC radical to the CTA and (ii) the VDF−CTA monoadduct

formed by attack of the CTA R-group on the head of VDF (CF_2) followed by transfer to the CTA. The formation of these products was confirmed by NMR analyses of the VDF polymerization medium before precipitation (Figure II-10 and SI-Figure II-24).

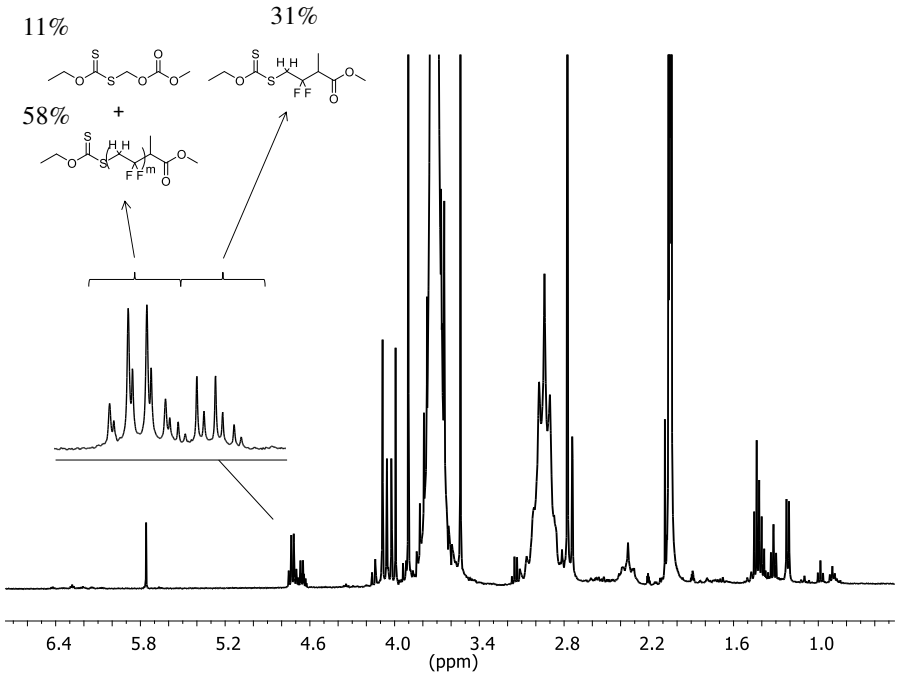

Figure II-10: Expansion of the 0.5−6.7 ppm region of the ^{1}H NMR spectrum in $(CD_3)_2CO$ of a MADIX homopolymerization of VDF (run 9, Table II-1) before precipitation (crude products).

These products do not lead to polymers but actually consume a non-negligible amount of CTA. Indeed, the xanthate moieties in these products are not available anymore to play their role as polymerization control agent. These side reactions thus lead to the combined loss of about 31% of CTA (31% of CTA R-group and 41% of CTA Z-group), as explained in Figure II-10 and Table II-2.

This loss means that the target DP (and $M_{n,theo}$) values shown in Table II-1 have to be recalculated to take into account this irreversible trapping (or consumption) of Xanthate moieties. Table II-2 summarizes this calculation: These recalculated DP_{target} and $M_{n,theo}$ values are in much better agreement with the DP and M_n values calculated by NMR (see Table II-1 and Table II-2).

Table II-2: New Calculation of DP_{target} for Run 8 When Taking into Account the Percentage CTA Loss Caused by Reactions 5 and 6 Presented in Scheme II-2

Run	$[VDF]_0/[CTA]_0$	% CTA Lost		[a]Real DP_{target}	% Yield	(g/mol) [b]$M_{n,Theo}$: DP	(g/mol) $M_{n,NMR}$: DP	
8	48	31 (R)	41 (Z)	69	65	3100:45	3000:44 (R)	3300:48 (Z)

[a]Real DP_{target} calculated using Equation II-6. [b]New $M_{n,theo}$ calculated using Equation II-7.

Equation II-6 $$Real\ DP_{target} = \frac{[VDF]_0/[CTA]_0}{(1-\%\ (R)\ CTA\ Lost)}$$

Equation II-7 $$M_{n,theo} = \left(Real\ DP_{target} \times Yield\right) \times M_{VDF} + M_{CTA}$$

The difference between $M_{n,theo}$ and $M_{n,NMR}$(Z) (calculated using the NMR signal of the CTA Z-group) is caused by the loss of CTA Z-group by transfer onto a DMC radical. This loss due to transfer to DMC also explains the 10% difference between $M_{n,NMR}$(R) and $M_{n,NMR}$(Z) in SI-Table II-3. This in-depth study showed that the MADIX solution polymerization of VDF in DMC proceeds with a degree of control but that the usual elementary reactions occurring during a typical MADIX process are accompanied by a number of side reactions that impair the ability to perfectly control the polymerization of VDF. These side reactions are shown in Scheme II-2

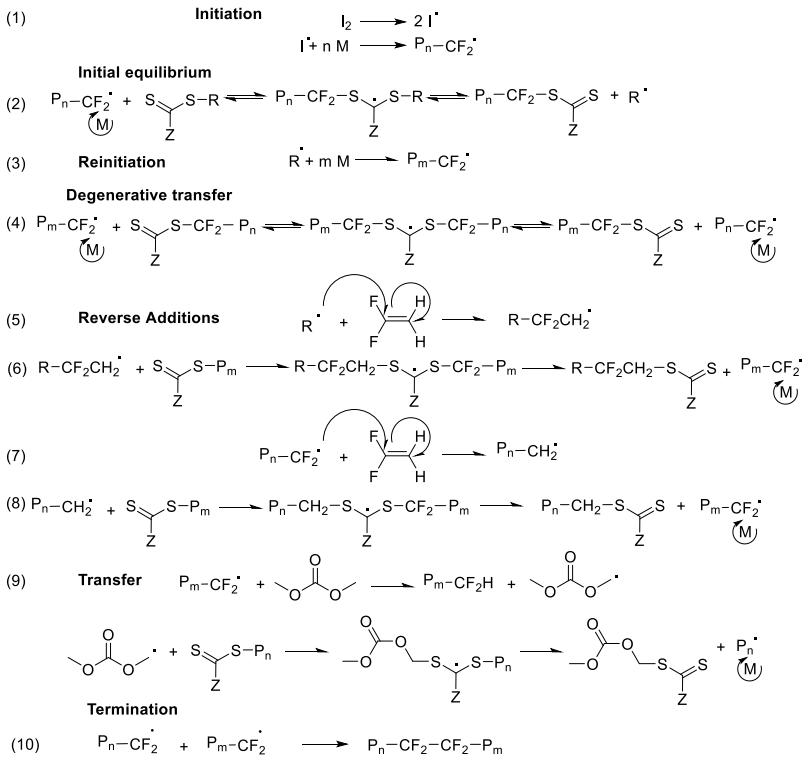

Scheme II-2: Mechanism of Reversible Addition−Fragmentation Chain-Transfer Polymerization (RAFT)/Macromolecular Design via the Interchange of Xanthates MADIX) of VDF. I2 and P_n (or P_m) represent the initiator and a PVDF chain of DP = n (or m), respectively

V. Conclusion

This article presents efficient protocols for the MADIX solution polymerization of VDF in DMC and, for the first time, a comprehensive NMR study with a focus on the end-group functionality of this controlled homopolymerization of VDF. The main goal of this study was to develop a controlled MADIX polymerization of VDF to prepare PVDF polymers featuring high end-group functionality and narrow polydispersity. The linear evolution of molecular weight versus conversion for the MADIX polymerization of VDF was shown for the first time, and evidences of some degree of control were presented. The evolution of the polymer end-groups with conversion was also carefully monitored for the first time and revealed the accumulation in the reaction medium of -CF_2-CH_2-Xaterminated polymer chains throughout the polymerization. This phenomenon demonstrates that, similarly to iodine transfer polymerization (ITP), the MADIX polymerization of VDF suffers from chain defects (head-to-head VDF addition) that lead, after transfer to the CTA, to unreactive chain-ends. As in the case of ITP, this irreversible transfer impairs the control of the polymerization of VDF, causes a broadening of the molecular weight distribution, and could be detrimental to the syntheses of well-defined block copolymers. Furthermore, loss of CTA caused by irreversible transfer onto the CTA from a DMC radical (formed by H-abstraction) or from a reverse addition occurring at the reinitiation stage (attack of the CTA R-group on the head of VDF) was discovered. These unwanted reactions preclude the ability to accurately predict the degree of polymerization (and of the molecular weights) using the usual NMR end-group analyses and affect the control of the polymerization. The extents of these reactions were quantified. As much as 30% of the initial CTA was irreversibly trapped in the reverse addition VDF monoadduct, and the transfer to DMC amounted to about 10% additional irreversible trapping of CTA. This work highlights, for the first time, all the elementary reactions occurring during the course of the MADIX solution polymerization of VDF: transfer to solvent, reverse additions, and irreversible transfer to CTA. Chain defects caused by reverse additions are intrinsic to radical polymerization; therefore, MADIX polymerization could not eliminate this phenomenon. Organometallic-mediated polymerization of VDF may be able to provide a solution to this problem. Nevertheless, in spite of these side reactions and reverse additions, PVDF with 90% chain-end functionality and an acceptable polydispersity (1.4) can be obtained using the MADIX protocols described herein. This study lays the foundation for the MADIX polymerization of VDF and similar monomers (trifluoroethylene,

chlorotrifluoroethylene, etc.) and gives invaluable information for the synthesis of PVDF-based architectures and functional PVDF.

VI. Acknowledgement

The authors thank Arkema (Pierre Bénite, France) and Solvay Fluor S.A (Tavaux, France and Brussels, Belgium) for providing VDF, 1,1,1,3,3-pentafluorobutane, and Xanthate, respectively, and the French Ministry of Science and Technology for the Ph.D. grant attributed to M.G.

VII. References

[1] (a) J. Scheirs, In *Modern Fluoropolymers*, Ed., John Wiley and Sons: New York, 1997. (b) G. Hougham, P. E. Cassidy, K. Johns, J. Davidson, In *Fluoropolymers: Synthesis and Applications*, Ed., Plenum Press: New York, 1999; Vols. **1** and **2**.

[2] B. Ameduri, B. Boutevin, In *Well-Architectured Fluoropolymers*: *Synthesis, Properties and Applications*, Elsevier: Amsterdam, 2004.

[3] J. S. Humphrey, R. Amin-Sanayei, In *Encyclopedia of Polymer Science and Technology*, Wiley: New York, 2006, Vol. **4,** 510−533.

[4] B. Ameduri, *Chem. Rev.,* 2009, **109**, 6632−6686.

[5] (a) J. G. Drobny, In *Technology of Fluoropolymers*, CRC Press, Boca Raton, FL, 2014. (b) D. W. Smith, S. T. Iacono, S. S. Iyer, In *Handbook of Fluoropolymer Science and Technology*, Eds., Wiley: New York, 2014.

[6] F. Boschet, B. Ameduri, *Chem. Rev*., 2014, **114**, 927−980.

[7] G. David, C. Boyer, J. Tonnar, B. Ameduri, P. Lacroix-Desmazes, B. Boutevin, *Chem. Rev.* 2006, **106**, 3936−3981.

[8] M. Tatemoto, *In The First Regular Meeting of Soviet-Japanese Fluorine Chemists*, Tokyo, Japan, February 15−16, 1979.

[9] (a) M. Oka, M. Tatemoto, In *Contemporary Topics in Polymer Science*; Bailey, W. J., Tsuruta, T., Eds., Plenum Press: New York, 1984; Vol. **4**, 763−781. (b) M. Tatemoto, *Int. Polym. Sc. Technol.,* 1985, **12**, 85−98; Nippon Gomu Kyokaishi 1985, **57**, 761−767. (c) M. Tatemoto, In *Polymeric Materials Encyclopedia*, Salamone, J.C., Ed., CRC: Boca Raton, FL, 1996; Vol. **5**, 3847−3862. (d) M. Tatemoto, *Kobunshi Ronbunshu*, 1992, **49**, 765−771. *Chem. Abstr*., **118**, 22655 (e) M. Tatemoto, T. Shimizu, In *Modern Fluoropolymers*, Scheirs, J., Ed., Wiley: New York, 1997, Chapter 30, 565−576.

[10] (a) V. Arcella, G. Brinati, M. Apostolo, *ChimOggi*, 1997, **79**, 345−351. (b) V. Arcella, M. Apostolo, *Rubber World*, 2001, **224**, 27−32.

[11] (a) M. Tatemoto, T. Nakagawa, German Patent 1978/ 2,729,671 (*Chem. Abstr. 88, 137374m*). (b) M. Tatemoto, T. Nakagawa, U.S. Patent 1979/4,158,678. (c) M. Tatemoto, T. Nakagawa, Patent 1991/4,243,770.

[12] (a) D. P. Carlson, Eur. Patent Appl. 1991/0,444,700 and U.S. Patent 1994/5,284,920. (b) D. P. Carlson, A. Nagasawa, Patent WO 1992/020743. (c) M. H. Hung, U.S. Patent 1993/5231154. (d) D. P. Carlson, A. Nagasawa, Patent WO 1993/07704269.

[13] (a) V. Arcella, G. Brinati, M. Albano, V. Tortelli, Eur Patent Appl. 1995/0,661,312 A1. (b) V. Arcella, G. Brinati, M. Albano, V. Tortelli, Eur. Patent Appl. 1995/0,683,186 A1. (c) I. Wlassics, G. Rapallo, M. Apostolo, N. Bellinzago, M. Albano, Eur. Patent Appl. EP,1999/0,979,832 A1. (d) U. Gayer, T. Schuh, V. Arcella, M. Albano, Eur. Patent Appl. EP, 2002/1,231,239 A1.

[14] (a) M. Apostolo, V. Arcella, M. Storti, M. Morbidelli, *Macromolecules*, 1999, **32**, 989−1003. (b) M. Apostolo, V. Arcella, G. Storti, M. Morbidelli, *Macromolecules*, 2002, **35**, 6154−616615.

[15] C. Boyer, D. Valade, L. Sauguet, B. Ameduri, B. Boutevin, *Macromolecules*, 2005, **38**, 10353−10362.

[16] N. Durand, B. Ameduri, B. Boutevin, *J. Polym. Sci., Part A: Polym. Chem.,* 2011, **49**, 82−92.

[17] A. D. Asandei, O. I. Adebolu, C. P. Simpson, J. S. Kim, *Angew. Chem., Int. Ed.,* 2013, **52**, 10027−10030.

[18] (a) A. D. Asandei, O. Adebolu, C. P. Simpson, In *Advances in Fluorine-Containing Polymers*; Smith, D., Iacono, S., Boday, D. J., Eds., American Chemical Society: Washington, DC, 2012, Chapter 4, 47−63. (b) A. D. Asandei, O. I. Adebolu, C. P. Simpson, *J. Am. Chem. Soc.,* 2012, **134**, 6080−6083.

[19] (a) T. C. Chung, A. Petchsuk, *Macromolecules,* 2002, **35**, 7678− 7683. (b) T. C. Chung, A. Petchsuk, U.S. Patent 6,355,749, 2002. (c) T. C. Chung, H. Hong, M. Oka, K. Kubo, U.S. Patent 2005/6,911,509. (d) Z. C. Zhang, T. C. Chung, *Macromolecules,* 2006, **39**, 5187−5194.

[20] (a) Z. C. Zhang, T. C. Chung,. *Macromolecules*, 2007, **40**, 783− 790. (b) Z. C. Zhang, Z. Wang, T. C. Chung, *Macromolecules*, 2007, **40**, 5235−5240.

[21] (a) Z. Zhang, E. Chalkova, M. Fedkin, C. Wang, S. N. Lvov, S. Komarneni, T. C. Chung, *Macromolecules*, 2008, **41**, 9130−9139. (b) M. Chung, Z. Zhang, E. Chalkova, C. Wang, M. Fedkin, S. Komarneni, S. Sharma, S. N. Lvov, *Electr. Chem. Soc. Trans.,* 2007, **11**, 35−45.

[22] (a) M. Destarac, D. Charmot, S. Zard, X. Franck, Patent WO 2000/75207 A1. (b) M. Destarac, W. Bzducha, D. Taton, I. Gauthier-Gillaizeau, S. Z. Zard, *Macromol. Rapid Commun.,* 2002, **23**, 1049−1054. (c) M. J. Monteiro, M; M. Adamy, B. J. Leeuwen, A. M. van Herk, M. Destarac, *Macromolecules*, 2005, **38**, 1538−1541. (d) D. Taton, M. DestaracS. Z. Zard, In *Handbook of RAFT Polymerization*, C. Barner- Kowollik, Ed., Wiley-VCH: Weinheim, 2008; 373−421. (e) M. Destarac*, Macromol. React. Eng*., 2010, **4**, 165−179.

[23] G. Kostov, F. Boschet, J. Buller, L. Badache, S. Brandsadter, B. Ameduri, *Macromolecules*, 2011, **44**, 1841−1855.

[24] E. Girard, J. D. Marty, B. Ameduri, M. Destarac, *ACS Macro Lett.*, 2012, **1**, 270−274.

[25] (a) L. Liu, D. Lu, H. Wang, Q. B. Dong, P. C. Wang, R. K. Bai, *Chem. Commun.,* 2011, **47**, 7839−7841. (b) P. Wang, J. Dai, L. Liu, Q. Dong, B. Jin, R. Bai, *Polym. Chem*., 2013, **4**, 1760−1764.

[26] (a) Y. Patil, B. Ameduri, Patent US2014/0154611. (b) Y. Patil, B. Ameduri, *Polym. Chem.*, 2013, **4**, 2783−2799.

[27] (a) D. Keddie, *Chem. Soc. Rev,*. 2014, **43**, 496. (b) M; R. Hill, R. N. Carmean, B. S. Sumerlin, *Macromolecules*, 2015, **48**, 5459.

[28] E. B. Twum, X. Li, E. F. McCord, P. A. Fox, D. F. Lyons, P. L. Rinaldi, In *Advances in Fluorine-Containing Polymers*, D. Smith, S. Iacono, D. J. Boday, Eds., American Chemical Society: Washington, DC, 2012; 187−213.

[29] G. Gody, T. Maschmeyer, P. B. Zetterlund, S. Perrier, *Macromolecules,* 2014, **47**, 639−649.

[30] G. Moad, E. Rizzardo, S. H. Thang, *Aust. J. Chem.,* 2009, **62**, 1402−1472.

[31] J. Saunier, F. Alloin, J. Y. Sanchez, B. Barriere, *J. Polym. Sci., Part B: Polym. Phys.,* 2004, **42**, 532−543.

[32] Y. Tundo, M. Selva, *Acc. Chem. Res.,* 2002, **35**, 706.

[33] A. Theis, ,A. Feldermann, N. Charton, M; H. Stenzel, T. P. Davis, C. Barner-Kowollik, C. *Macromolecules,* 2005, **38**, 2595−2605.

[34] M. Pianca, E. Barchiesi, G. Esposto, S. J. Radice, Fluorine Chem., 1999, 95, 71−84.

[35] J. Guiot, B. Ameduri, B. Boutevin, B. *Macromolecules*, 2002, **35**, 8694−8707.

VIII. Supporting Information

VIII.1.1 DP and Molar mass

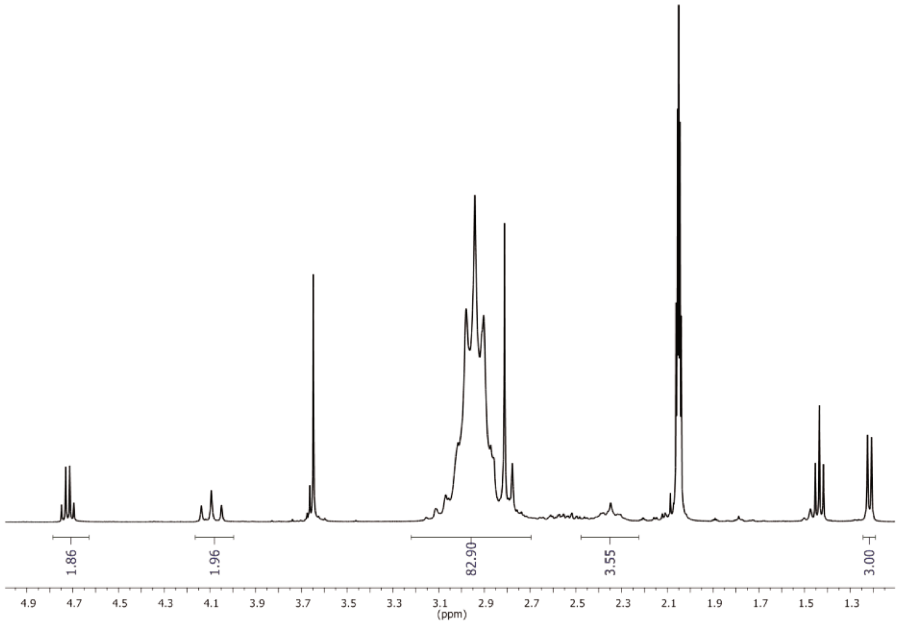

SI-Figure II-11: Expansion of the 1.2 to 4.9 ppm region of the ^{1}H NMR spectrum in $(CD_3)_2CO$ of a PVDF homopolymer synthesized via MADIX polymerization (Run 9, Table II-1).

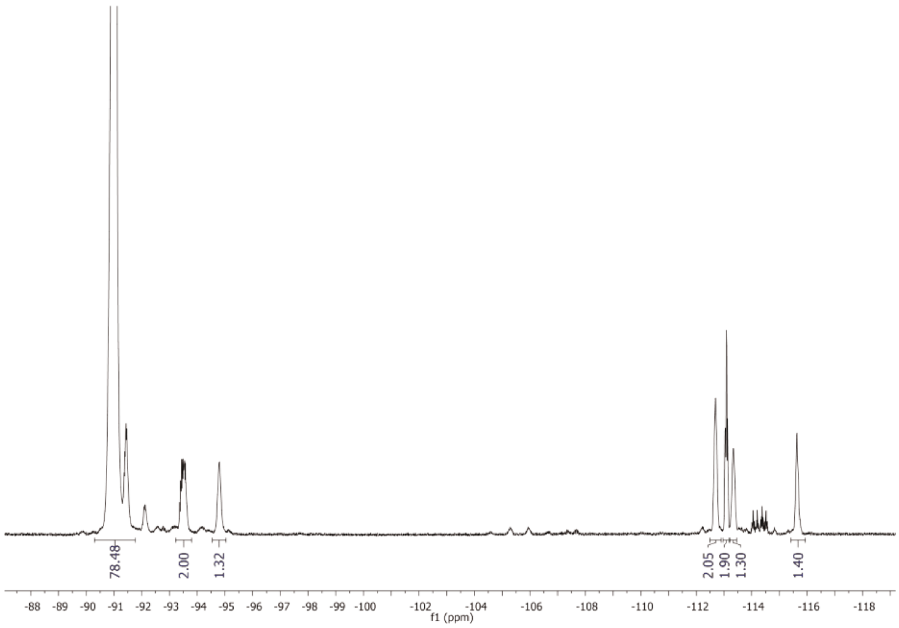

SI-Figure II-12: Expansion of the -87 to -119 ppm region of the ^{19}F NMR spectrum in $(CD_3)_2CO$ of a PVDF homopolymer synthesized by MADIX polymerization (Run 9, Table II-1).

VIII.1.2 Example of calculation of DP and Mn

Note: Molecular weights calculated below using Equation II-1and SI-Equation II-8 were extracted from ^{1}H NMR (SI-Figure II-11) and ^{19}F NMR (SI-Figure II-12) respectively.

Equation II-1 $$DP = \frac{\int_{2.70}^{3.19} CH_2(HT) + \int_{2.28}^{2.43} CH_2(TT) \int_{4.02}^{4.17} + CH_2(End\ Group)}{\frac{2}{3} \times \int_{1.19}^{1.24} CH_3(R-CTA)} =$$

$$\mathrm{DP} = \frac{82.90 + 3.55 + 1.96}{\frac{2}{3} \times 3} = 44$$

$$\mathrm{M_{nNMR}} = \mathrm{M_n CTA} + \mathrm{DP} \times \mathrm{M_n\ VDF\ (64.04\ g.mol^{-1})} = 208.3 + 44 \times 64.04$$
$$= \mathbf{3000\ g/mol}$$

SI-Equation II-8 $DP =$

$$= \frac{\int_{-90.3}^{-91.7} CF_2\,(HT) + \int_{-93.2}^{-93.9} CF_2\,(R\ end\ group) + \int_{-94.6}^{-95.0} CF_2\,(HT) + \int_{-112.5}^{-113.2} CF_2(Z\ end\ group) + \int_{-113.2}^{-113.5} CF_2\,(HH) + \int_{-115.5}^{-115.9} CF_2\,(HH)}{\int_{-93.2}^{-93.9} CF_2\,(R\ end\ group)}$$

$$DP = \frac{78.48 + 2.00 + 1.32 + 1.30 + (2.00 + 1.90) + 1.30 + 1.40}{2.00} = \mathbf{45}$$

$$M_{nNMR} = M_n CTA + DP \times M_n\ VDF\ (64.04\ g.mol^{-1}) = 208.3 + 45 \times 64.04$$
$$= \mathbf{3100\ g/mol}$$

SI-Table II-3: Comparison of the molecular weights calculated by NMR using the signals of the CTA R-group or of the CTA Z-group as references.

Run	DP NMR		M_n NMR (g/mol)		ΔMn NMR (%)
	(R)	(Z)	(R)	(Z)	
1	18	17	1400	1300	8
2	31	31	2200	2200	0
3	4	4	500	500	0
4	20	21	1500	1600	7
5	29	31	2100	2200	5
6	41	45	2800	2900	4
7	47	50	3200	3400	6
8	44	48	3000	3300	10
9	44	48	3000	3300	10

VIII.1.3 Kinetics

Note: The first-order kinetics plot (SI-Figure II-13) and the evolution of molecular weight and Đ versus conversion (Figure II-1) were traced using 4 different polymerizations (runs 5-8 in Table II-1) using the same formulation but stopped at different reaction times.

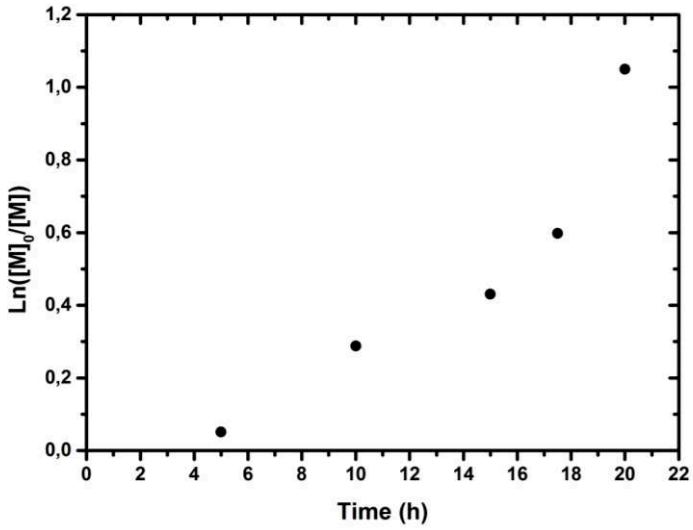

SI-Figure II-13: First order kinetics plot ofr the MADIX polymerization of VDF

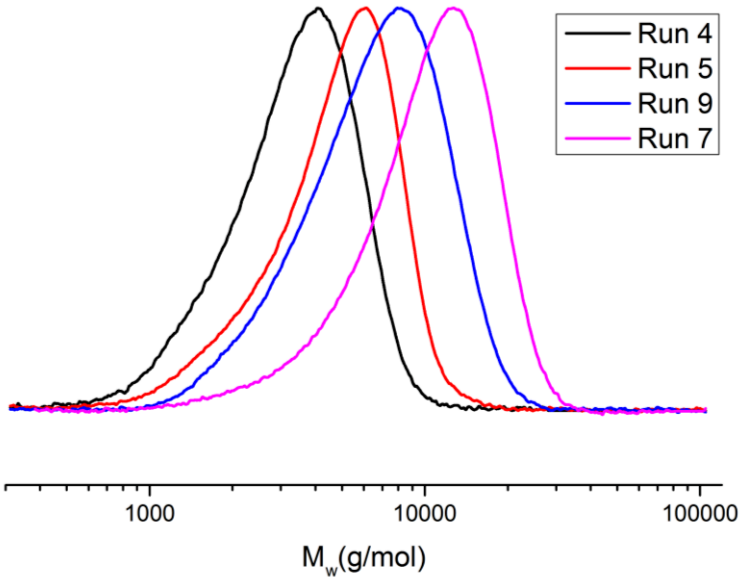

SI-Figure II-14: DMF GPC chromatograms of PVDF – Xanthate synthesized by MADIX homopolymerization of VDF (Run 4, conv = 25% ; Run 5, conv = 35% ; Run 9, conv = 70% ; Run 7, conv = 65%)

VIII.1.4 MALDI-TOF Mass Spectrometry

SI-Table II-4: Peak assignmentsfor the positive mode MALDI-TOF spectrum (

Figure II-2) of PVDF synthesized using MADIX polymerization (run 9,Table II-1). [a] *Theoretical molecular weights were calculated using an isotope pattern profile calculator.*

α end	ω end	Cation	DP	$M_{n,\ theo}$ [a]	$M_{n,\ exp}$
CH_3-O-(C=O)-CH(CH_3)-	-S-(C=S)-O-CH_2-CH_3	Li^+	15	1175.3	1175.2
CH_3-O-(C=O)-CH(CH_3)-	-S-(C=S)-O-CH_2-CH_3	Li^+	17	1303.3	1303.2
CH_3-O-(C=O)-CH(CH_3)-	-S-(C=S)-O-CH_2-CH_3	Li^+	18	1367.3	1367.3
CH_3-O-(C=O)-CH(CH_3)-	-S-(C=S)-O-CH_2-CH_3	Li^+	20	1495.3	1495.3
CH_3-O-(C=O)-CH(CH_3)-	-S-(C=S)-O-CH_2-CH_3	Li^+	22	1623.3	1623.3

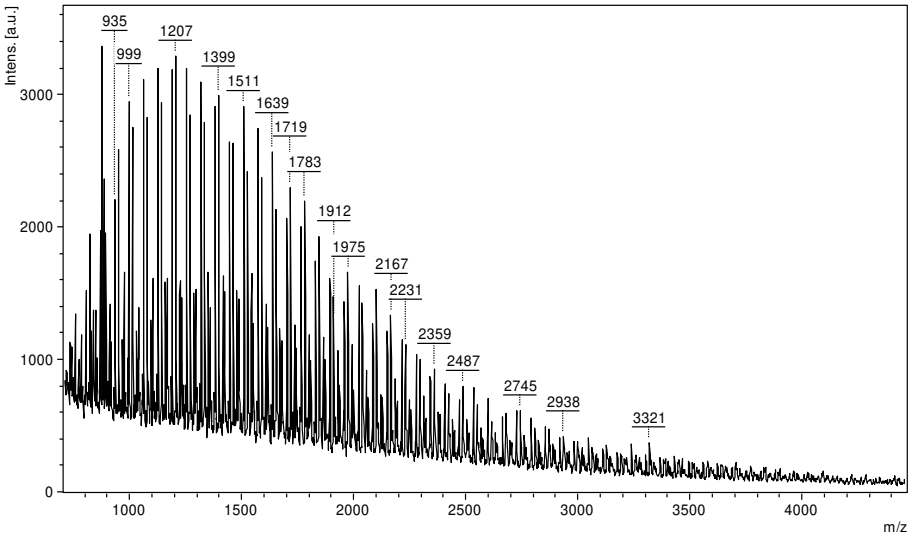

SI-Figure II-15: Negative ion MALDI-TOF mass spectrum of PVDF synthesized by MADIX polymerization (Run 9,Table II-1) with DCTB as matrix and LiCl as cationic agent.

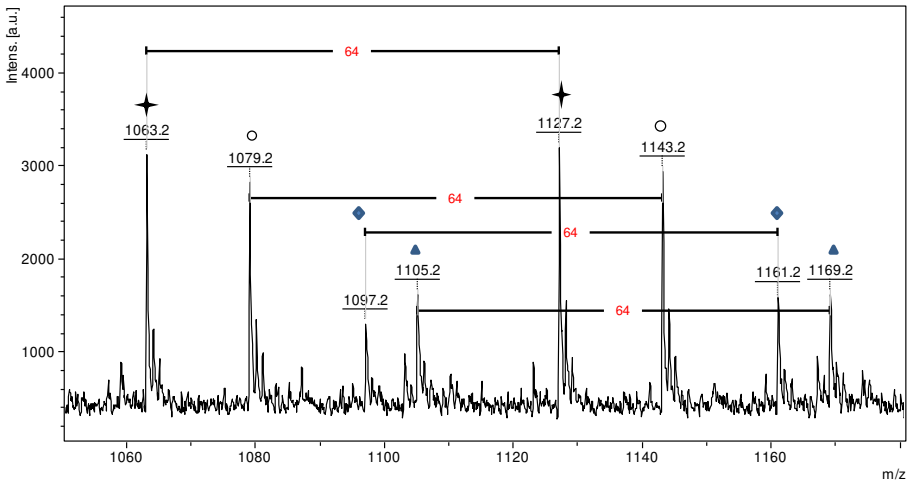

SI-Figure II-16: Expansion of the 1060 to 1260 m/z region of the negative ion MALDI-TOF mass spectrum of PVDF synthesized by MADIX polymerization (Run 9,Table II-1) with DCTB matrix and LiCl as cationic agent.

SI-Table II-5: Peak assignments for the negative mode MALDI-TOF spectrum (SI-Figure II-15 and SI-Figure II-16) of PVDF synthesized using MADIX polymerization (run 9, Table II-1). [a] *Theorical molecular weight was calculated using an isotope pattern profile calculator.*

α end	ω end	DP	$M_{n,\,theo}$ [a]	$M_{n,\,exp}$
CH_3-$(CH_2)_3$-$CH(C_2H_5)$-(C=O)-O- + CH_3OH	-S-(C=S)-O-CH_2-CH_3	12	1063.3	1063.2
CH_3-O-(C=O)-$CH(CH_3)$-	-SH	15	1079.2	1079.2
CH_3-CH_2-$C(CH_3)_2$-O-	-SH	15	1079.2	1079.2
CH_3-O-(C=O)-$CH(CH_3)$-+ CH_3OH	-H	15	1079.3	1079.2
CH_3-CH_2-$C(CH_3)_2$-O- +CH_3OH	-H	15	1079.3	1079.2
CH_3-O-(C=O)-$CH(CH_3)$-+ CH_3-(C=O)-CH_3	-S-(C=S)-O-CH_2-CH_3	13	1097.2	1097.2
CH_3-CH_2-$C(CH_3)_2$-O- + CH_3-(C=O)-CH_3	-S-(C=S)-O-CH_2-CH_3	13	1097.3	1097.2
CH_3-O-(C=O)-$CH(CH_3)$- +CH_3(C=O)-CH_3 + CH_3OH	-SH	14	1105.3	1105.2
CH_3-CH_2-$C(CH_3)_2$-O- +CH_3(C=O)-CH_3 + CH_3OH	-SH	14	1105.3	1105.2
CH_3-O-(C=O)-$CH(CH_3)$- +CH_3(C=O)-CH_3	-H	15	1105.3	1105.2
CH_3-CH_2-$C(CH_3)_2$-O- +CH_3(C=O)-CH_3	-H	15	1105.3	1105.2

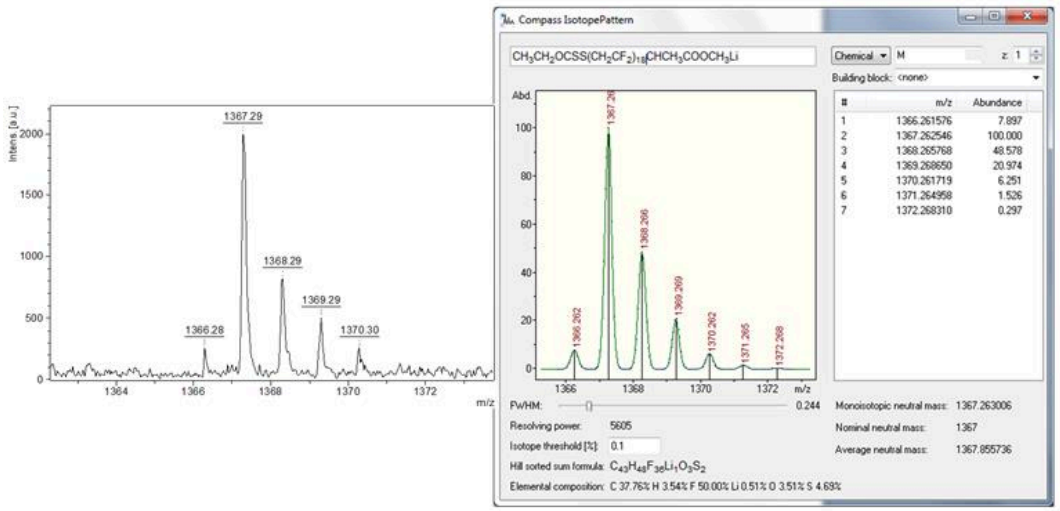

SI-Figure II-17: Comparison of the theoretical and experimental isotopic patterns for a PVDF initiated by $CH_3O(C=O)CH(CH_3)\bullet$ radical and terminated by $-S(C=S)OCH_2CH_3$ in positive mode with Li+ cationization

.

VIII.1.5 HETCOR $^{1}H/^{19}F$

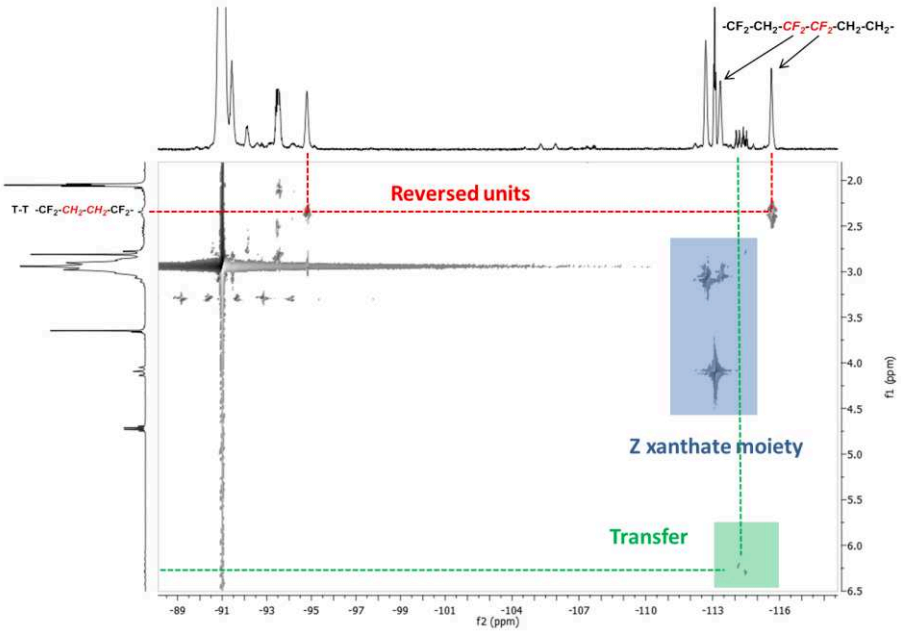

SI-Figure II-18: ^{1}H - ^{19}F HETCOR spectrum in $(CD_3)_2CO$ of PVDF synthesized by MADIX polymerization (Run 9,Table II-1). Vertical axis: ^{1}H NMR spectrum; horizontal axis: ^{19}F NMR spectrum.

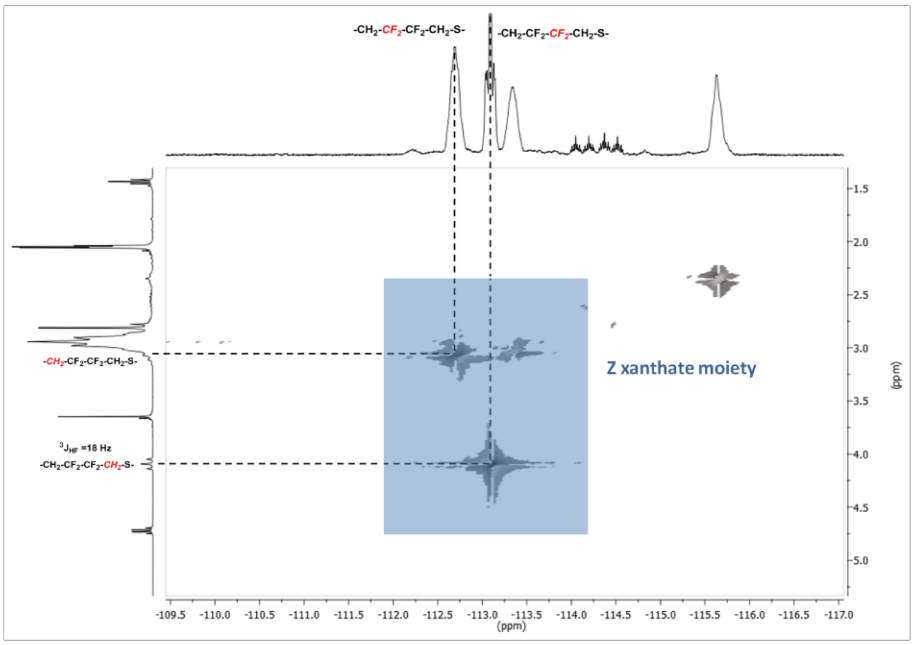

SI-Figure II-19: Expansion of the -110 to -117 ppm region of the ^{1}H-^{19}F HETCOR spectrum in $(CD_3)_2CO$ of PVDF (Run 9, Table II-1).

VIII.1.6 Normal and Reverse additions

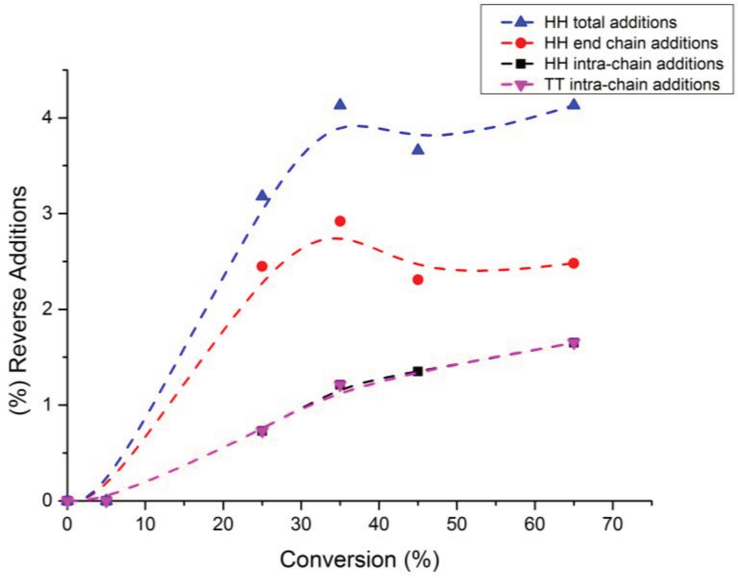

SI-Figure II-20: Evolution of HH additions (Intra chain and as the terminal unit), and of TT additions versus conversion. Dashed line is a guide for eyes

SI-Equation II-9

$$\%\ TT\ (Intra-Chain) = \frac{\int_{-115.4}^{-115.9} CF_2(TT)}{\int_{-70.9}^{-71.2} CF_2(End\ Group)+\int_{-112.4}^{-113.2} CF_2(End\ Group)+\int_{-113.2}^{-113.5} CF_2(HH)+\int_{-90}^{-95} CF_2(HT+TT)+\int_{-115.4}^{-115.9} CF_2(HH)}$$

SI-Equation II-10

$$\%\ HH\ (Intra-Chain) = \frac{\int_{-115.4}^{-115.9} CF_2(HH)}{\int_{-70.9}^{-71.2} CF_2(End\ Group)+\int_{-112.4}^{-113.2} CF_2(End\ Group)+\int_{-113.2}^{-113.5} CF_2(HH)+\int_{-90}^{-95} CF_2(HT+TT)+\int_{-115.4}^{-115.9} CF_2(HH)}$$

SI-Equation II-11

$$\%\ HH\ (End-group) = \frac{\int_{-113.0}^{-113.3} CF_2(HH\ End-group)}{\int_{-70.9}^{-71.2} CF_2(End\ Group)+\int_{-112.4}^{-113.2} CF_2(HH\ End\ Group)+\int_{-113.2}^{-113.5} CF_2(HH)+\int_{-90}^{-95} CF_2(HT+TT)+\int_{-115.4}^{-115.9} CF_2(HH)}$$

VIII.1.7 Mono-adduct

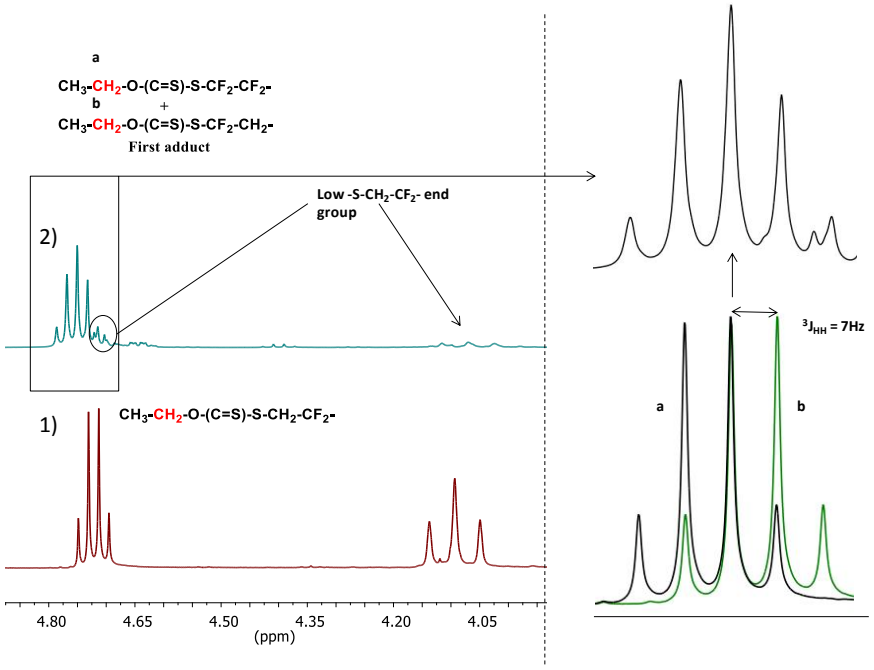

SI-Figure II-21: ^1H NMR spectra in $(CD_3)_2CO$ of PVDF synthesized by MADIX polymerization of VDF. 1) Run 9,Table II-1; 2) Run 3, Table II-1. 3) Expansion (4.65 – 4.8 ppm) of the signal corresponding to the CH_2-CF_2-Xa group.

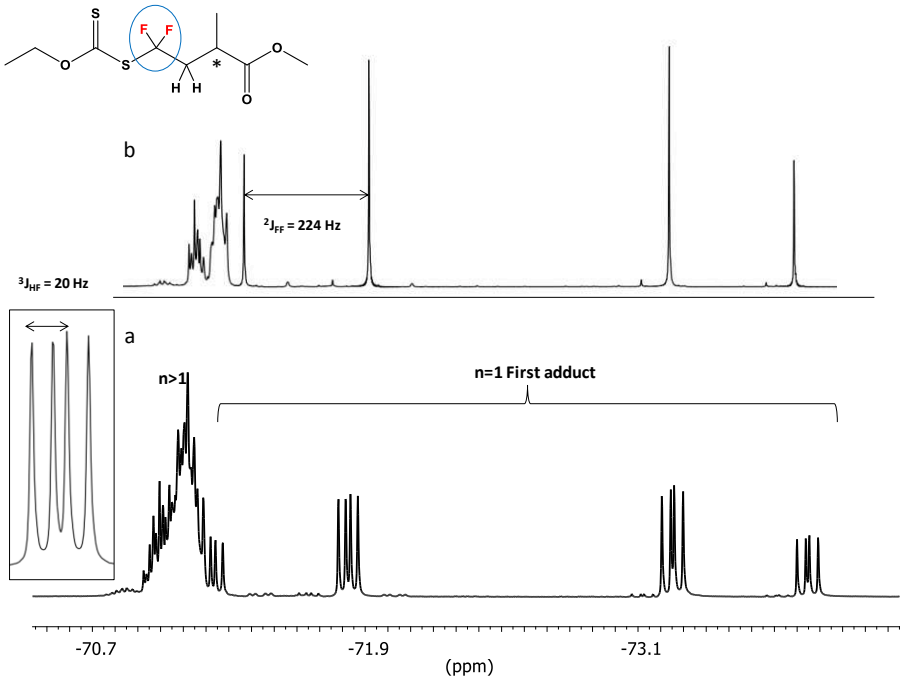

SI-Figure II-22: ^{19}F NMR spectra in $(CD_3)_2CO$ of PVDF (Run 3, Table II-1) with an expansion of the -70 to -74 ppm region corresponding to $-CH_2-CF_2-Xa$ end group of a CTA-VDF monoadduct. a) ^{19}F NMR without any ^1H decoupling b) ^{19}F NMR with ^1H decoupling. The insert is an expansion of the signal centered at -72.1 ppm

VIII.1.8 Others

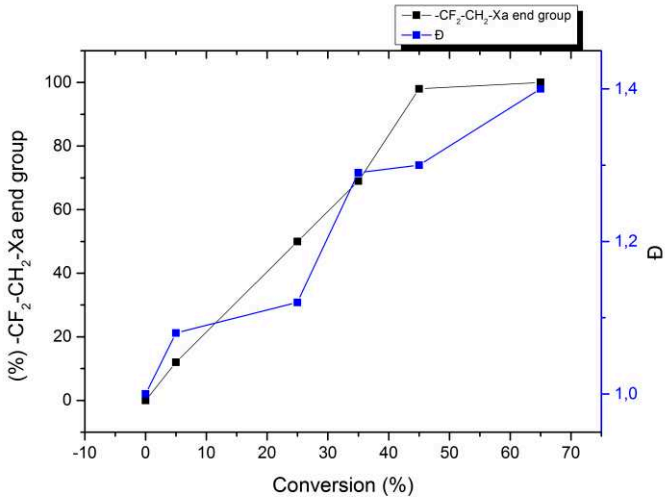

SI-Figure II-23: Evolution of $-CF_2-CH_2-Xa$ end-group and of polydispersity versus conversion during the MADIX VDF homopolymerization.

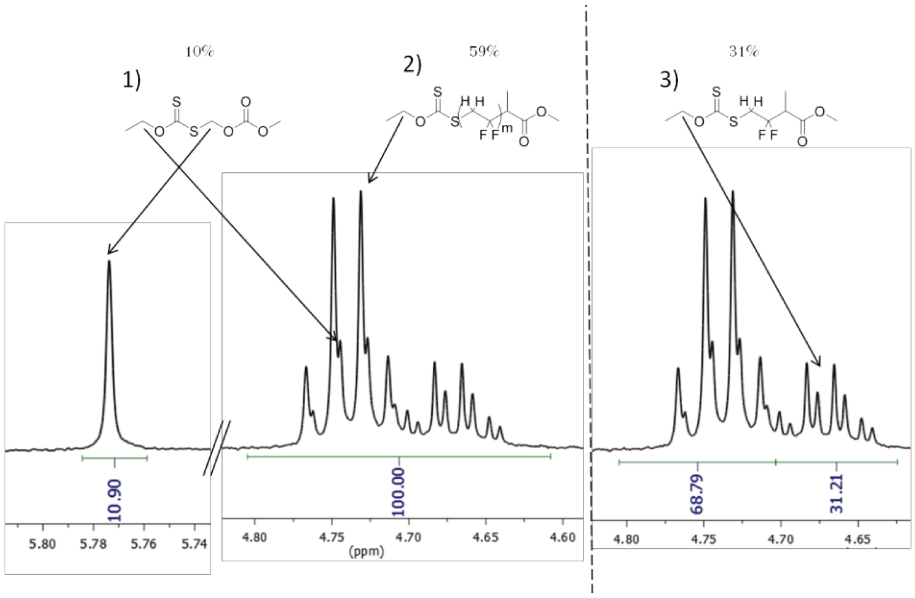

SI-Figure II-24: Expansion of the regions corresponding to the signal assigned to -O-CH_2-CH_3 in the ^1H NMR spectrum in $(CD_3)_2CO$) of a PVDF (Run 8, Table II-1) synthesized by MADIX polymerization before precipitation (crude product) : 1) product of addition of a DMC radical to the CTA, 2) PVDF showing a reverse addition end-group, and 3) VDF-CTA monoadduct formed by attack of the CTA R-group on the head of VDF, followed by transfer to the CTA.

Conclusion Partie 1

La première partie de ce chapitre a montré pour la première fois à travers un suivi cinétique et une étude exhaustive en RMN, le bon contrôle de la polymérisation RAFT du VDF en présence d'agent de transfert de type xanthate. De manière similaire à l'ITP, une accumulation d'extrémités de chaînes moins réactives $–CF_2CH_2$-S-$(C=S)OCH_2CH_3$ (ou $PVDF_T$-XA, avec T et XA correspondant à Tail et Xanthate, respectivement) au détriment des extrémités de chaînes plus réactives $–CH_2CF_2$-S-$(C=S)OCH_2CH_3$ (ou $PVDF_H$-XA, avec H correspondant à Head) a été observée due aux additions tête-tête du VDF. Ces additions inverses ont considérablement affecté le bon contrôle de la polymérisation et ont conduit à un élargissement progressif de la distribution des masses molaires au cours de la polymérisation. Etonnamment, une proportion non négligeable d'agent de transfert (30 %) a été consommée dans les premiers instants de la polymérisation (réamorçage), dû à une mauvaise addition du radical R (issue de l'agent RAFT) sur le VDF, conduisant ainsi à la formation de mono-adduit de VDF porteur des extrémités R et Z de l'agent de transfert. De plus, des réactions de transfert au solvant (DMC) diminuant la fonctionnalité finale, ont également été mises en évidence. Ces réactions de transfert sont responsables de la formation de chaînes mortes CF_2H causées par des réactions de transfert de radicaux $CF_2\cdot$ au solvant. La formation de l'adduit CH_3-$O(C=O)O$-CH_2-XA résultant du transfert d'un radical dimethyl carbonate sur une fraction de la moiétié Z, a également été mise en évidence par RMN.

En dépit de ces difficultés de synthèse, des homopolymères de PVDF avec des degrés de polymérisation (DP) compris entre 4 et 47, possédant une fonctionnalité en xanthate atteignant les 85 % et des dispersités (Đ) inférieures à 1,4 ont pu être préparés.

Partie 2 –

Cette partie vient renforcer l'hypothèse émise dans la précédente partie. En effet, il a été observé dans la partie 1 une consommation surprenante d'agent RAFT (30 % de $[CTA]_0$). Cette perte d'agent RAFT est causée par l'addition du radical R sur le la tête du VDF (CF_2), conduisant à un radical $CH_2^{\cdot}$ qui, suivi par une réaction de transfert sur une fonction xanthate, forme un mono-adduit R-CF_2CH_2-Z qui est éliminé ultérieurement par précipitation (*vide supra*). Cependant, aucune preuve directe par spectroscopie RMN n'a démontré que la totalité des chaînes restantes était réellement amorcées de manière régulière (addition sur la queue du VDF) avec un enchaînement de type : R-CH_2-CF_2-.

Cette partie présente donc une caractérisation approfondie qui détaille par RMN un PVDF synthétisé par RAFT. L'association de spectres RMN du ^{1}H, ^{19}F et ^{13}C couplés et non découplés, ainsi que divers spectres de corrélation hétéronucléaire : 2D $^{1}H\{^{13}C\}$ HSQC, $^{19}F\{^{13}C\}$ HSQC, and $^{19}F\{^{1}H\}$ HETCOR ont permis d'indentifier la microstructure de l'extrémité α du PVDF. Ce travail a été réalisé en collaboration avec le Professeur Gilles Silly de l'Université de Montpellier et a fait l'objet d'un article scientifique publié dans *Macromolecular Chemistry and Physics.*[2]

A Journey into the Microstructure of PVDF Made by RAFT

Marc Guerre,[a] Gérald Lopez,[a] Thibaut Soulestin,[a] Cédric Totée,[b] Bruno Améduri,[a] Gilles Silly,*[c] Vincent Ladmiral[a]*

[a]Institut Charles Gerhardt, Ingénierie et Architectures Macromoléculaires, UMR 5253 – CNRS, Université Montpellier, ENSCM - 8, Rue Ecole Normale, 34296 Montpellier-France.
[b]Institut Charles Gerhardt, PAC, UMR 5253 – CNRS, Université Montpellier, ENSCM - 8, Rue Ecole Normale, 34296 Montpellier-France.
[c]Institut Charles Gerhardt, Chalcogénures et Verres, UMR 5253 – CNRS, Université Montpellier, ENSCM - 8, Rue Ecole Normale, 34296 Montpellier-France.
*Corresponding authors: gilles.silly@umontpellier.fr, vincent.ladmiral@enscm.fr

I. Abstract

Poly(vinylidene fluoride) (PVDF) is a very important fluoropolymer. It possesses high resistances to weathering or ageing and to chemical and thermal aggressions, as well as unique electroactive properties. The reversible-deactivation radical polymerization (RDRP) of VDF can, so far, only be achieved via degenerative transfer using ITP (iodine transfer polymerization) or RAFT (reversible addition‑fragmentation chain transfer). However, due to chain defects, and transfer to solvents, the RAFT polymerization of VDF produces PVDF chains with different chain ends. This article presents the results obtained from advanced ^{1}H, ^{13}C, and ^{19}F NMR spectroscopy experiments using decoupling strategies, to ascertain unequivocally the microstructure of the PVDF chains synthesized using RAFT polymerization. This article provides a very detailed description of the different α- and ω-chain ends of $PVDF_{51}$-XA and reveals an uncommon NMR heteronuclear coupling between the proton of the stereocenter of the CTA R-group and the fluorine atoms of the CF_2 moiety of the first added VDF unit.

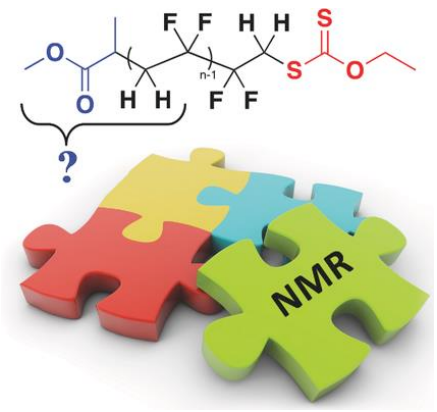

II. Introduction

Fluoropolymers have found many high-tech applications in automotive, aerospace, optical, and microelectronics industries.[1 - 5] Poly(vinylidene fluoride) (PVDF) is a thermoplastic fluoropolymer produced by the radical polymerization of vinylidene fluoride (VDF).[6,7] Thanks to its relatively low melting point (≈170 ° C) compared to other fluoropolymers, PVDF can be more easily melt processed, injected, or molded.[6] This highly chemically resistant fluoropolymer is used in piping, tubing, vessel fabrication, molded valves, and fittings, tower packing, nozzles, and other items for corrosive fluid handling.[6] As a fine powder grade, PVDF is employed as the principal ingredient of high-end weather-resistant paints for metals, stones, or concrete.[6] PVDF membranes are also used for protein immunoblot due to its nonspecific affinity for amino acids.[8] Moreover, PVDF displays strong piezoelectric properties and has a higher dielectric constant in comparison to other fluoropolymers.[9-11] Because of its unique combination of singular properties as well as its processability and low cost (relative to other fluoropolymers), PVDF has become the second largest manufactured fluoropolymer after poly(tetrafluoroethylene).[12] Nevertheless, preparing well-architectured PVDF by reversible-deactivation radical polymerization (RDRP) techniques still remains challenging.[13] In the course of the polymerization, VDF (CH_2CF_2) units undergo head-to-tail (HT) normal additions, and head-to-head (HH) and tail-to-tail (TT) inverse additions, which lead to the formation of $-CF_2CH_2-CF_2CH_2-$, $-CH_2CF_2-CF_2CH_2-$, and $-CF_2CH_2-CH_2CF_2-$ dyads, respectively.[14-16] HH additions result in chain defects that have a detrimental effect on the RDRP of VDF.[17] Recent articles showed that reversible addition-fragmentation chain transfer (RAFT) polymerization[18 - 22] can be used to control the polymerization of VDF, but that HH additions have a crucial influence on the degenerative transfer mechanism, which enables the control of the polymerization.[23,24] PVDF chains terminated by a $-CH_2CF_2-CF_2CH_2$-XA sequence (where XA designates the xanthate moiety of the RAFT chain-transfer agent) seem not susceptible to further reactivation with $-CH_2CF_2\cdot$ terminated radicals. These HH additions terminated PVDF (from now on designated $PVDF_T$-XA) chains thus accumulate in the reaction medium in a similar fashion to what was observed for the iodine transfer polymerization (ITP)[25-30] of VDF.[16,17,31-33] The resulting progressive irreversible trapping of xanthate control agent leads to the broadening of the molar mass distribution and to increased difficulties for the synthesis of well-defined block copolymers.[24,31,34,35] In addition, VDF polymerization is often carried out in

dimethylcarbonate (DMC), because this solvent was shown to provide fast kinetics and high yields.[24,31] In spite of this benefit, this hydrogenated solvent, is nonetheless, prone to transfer reaction. Guerre *et al.*[24] and Asandei *et al.*[31] showed that transfer to DMC did occur in the course of the RAFT (or ITP) polymerization of VDF in DMC, and that this transfer was responsible for a nonnegligible decrease of the end-group functionality of the final PVDF. We indeed showed that transfer to DMC had several consequences: 1) DMC radicals that add to VDF by addition on the head of the monomer form $CH_2\cdot$ radicals which irreversibly trap xanthate groups after transfer to the CTA.[24] 2) DMC radicals can initiate polymerization of VDF and lead to PVDF chains that do not carry the R-group of the CTA. 3) DMC radicals are also strongly suspected to be able to transfer with -CH_2CF_2-XA-terminated chains ($PVDF_H$-XA) and also with $PVDF_T$-XA thus provoking a further decrease of the PVDF functionality.[36] All these observations and discoveries were made possible thanks to careful examination of the polymer microstructure and end groups using ^1H and ^{19}F NMR.[23,24] Progress in the understanding of the RAFT polymerization of VDF thus required accurate and detailed NMR characterization of the PVDF and its various possible end groups. Such an in depth NMR characterization of PVDF-XA had not been carried out. In addition, in previous articles, a number of assumptions were made. For example, the R-group radical was assumed to add preferentially on the tail of VDF, leading to R-CH_2CF_2-α-chain end. The present article thus reports the results of our thorough 1D and 2D NMR analyses of PVDF made by RAFT and presents comprehensive assignments of the ^1H, ^{19}F, and for the first time, ^{13}C NMR signals of this polymer.

III. Experimental section

Materials

All reagents were used as received unless stated otherwise. 1,1-Difluoroethylene (vinylidene fluoride, VDF) was kindly supplied by Arkema (Pierre-Benite, France). *Tert*-Amyl peroxy-2-ethylhexanoate (purity 95%, Trigonox 121) was purchased from AkzoNobel (Chalons-sur-Marne, France). *O*-ethyl-*S*-*(*1- methoxycarbonyl) ethyldithiocarbonate (CTA) was synthesized according to the method described by Liu et al.[37] ReagentPlus grade (purity >99%) dimethyl carbonate (DMC), and laboratory reagent grade hexane (purity >95%) were purchased from Sigma Aldrich.

Nuclear Magnetic Resonance

Instrumentation

NMR spectra of the polymers were collected at 25 °C on a Bruker Avance III 400-MHz spectrometer equipped with two independent broadband (^{15}N-^{31}P and ^{15}N-^{19}F, 300 W) and a high band (^{1}H, 100W) rf channels. A 5 mm $^{1}H/^{19}F/^{13}C$ TXO triple resonance pulsed field gradient probe for which ^{13}C and ^{19}F are on the inner coil and ^{1}H on the outer coil is used for three channels experiments. This probe has a lower background ^{19}F signals compared to standard dual-channel probes. This triple resonance $^{1}H/^{19}F/^{13}C$ probe is capable of producing short 90° pulses 6.5 µs widths on ^{19}F, 9.5 µs for ^{13}C and 9.2 µs for ^{1}H channels. In all experiments, ^{1}H decoupling is realized with waltz16. ^{19}F decoupling is performed with nested loops using 0.5 ms and 1 ms chirped adiabatic pulses with 80 kHz band with in order to desynchronize and minimize decoupling artifacts.

^{1}H 1D NMR

A one pulse 90° (9.25 µs) pulse sequence is used with 2.5 s acquisition time, 3.1 kHz spectral window and 1 transient.

^{19}F 1D NMR

A one pulse 90° (6.5 µs) pulse sequence is used with 0.5 s acquisition time, 11.3 kHz spectral window, 4 transients and 15 s recycle delay.

^{13}C 1D NMR with ^{1}H, ^{19}F and ^{1}H+^{19}F Decoupling

A one pulse 90° pulse sequence is used, acquisition time 1 s and recycle delay 2 s.

^{1}H 2D NMR COSY with ^{19}F Decoupling

The cosygpppqf ^{1}H 2D NMR COSY with ^{19}F Decoupling pulse sequence from Bruker catalog was modified in order to include ^{19}F decoupling over the whole pulse sequence. Acquisition parameters are 1 s acquisition time, 3.2 kHz spectral window in F2 and in F1, 4 transients and recycle delay of 1 s. Processing involves a sine squared window multiplication in F1 and a line broadening of 0.3 Hz in both dimensions.

^{1}H {^{13}C} 2D NMR HSQC with ^{19}F Decoupling

The hsqcetgpsi2 HSQC pulse sequence from Bruker catalog was modified in order to apply ^{19}F decoupling over the whole pulse sequence. Acquisition parameters are 1 s acquisition time, 5.3 kHz spectral window in F2, 30 ms acquisition time, 16.7 kHz spectral window in F1, $^{1}J_{CH}$ =145 Hz, garp decoupling for ^{13}C, 2 transients and recycle delay of 1.5 s. Processing

involves a sine squared window multiplication in F1 and a line broadening of 1 Hz in both dimensions.

^{19}F {^{13}C} 2D NMR HSQC with ^{1}H Decoupling

The pulse sequence described by Li *et al.*[38] (2D NMR studies of a model for Krytox Fluoropolymers) was written from scratch for a Bruker system, the only modifications are ^{1}H decoupling over the whole pulse sequence, ^{13}C decoupling performed with nested loops using 0.5 ms and 1 ms chirped adiabatic pulses with 30 kHz bandwidth in order to desynchronize and minimize decoupling artefacts and echo-antiecho quadrature detection in F1. Acquisition parameters are 0.5 s acquisition time and 11.3 kHz spectral window in F2, 1 s acquisition time and 12.1 kHz spectral window in F1, $^{1}J_{CF} = 275$ Hz, 4 transients and recycle delay of 1 s. Processing involves linear prediction of 1024 points and a sine squared window multiplication in F1 together with a line broadening of 0.3 Hz in both dimensions.

^{19}F {^{13}C} 2D NMR HETCOR with ^{1}H Decoupling

The hfcoqfqn HETCOR pulse sequence from Bruker catalog was modified in order to use a composite adiabatic chirped 180° pulse for refocusing of 2 ms, together with 40 kHz bandwidth. Gradient with amplitudes in the ratio of ^{1}H and ^{19}F gyromagnetic factors are also implemented for quadrature detection in F1 and echo selection. Other parameters are 0.6 s acquisition time, 11.3 kHz spectral window in F2, 3 kHz spectral window in F1, delays of 12.7 ms and 8 ms before and after the last pair of 90° pulses before acquisition, 2 transients and recycle delay of 25 s. Deuterated acetone was used as the solvent for all samples. ^{1}H and ^{13}C NMR chemical shifts are referenced to TMS (in ppm) and ^{19}F to $CFCl_3$ and ^{n}J scalar couplings constants are given in Hertz (Hz).

Synthetic Procedure

Polymerizations of VDF were performed in a 100 mL Hastelloy Parr autoclave systems (HC 276), equipped with a mechanical Hastelloy stirring system, a rupture disk (3000 PSI), inlet and outlet valves, and a Parr electronic controller to regulate the stirring speed and the heating. Prior to reaction, the autoclave was pressurized with 30 bars of nitrogen to check for leaks. The autoclave was then put under vacuum (20 mbar) for 30 min to remove any trace of oxygen. A degassed solution of solvent, initiator, and RAFT CTA was introduced via a funnel under vacuum. The reactor was then cooled down using a liquid nitrogen bath, and VDF was transferred by double weighing (i.e., the difference of mass before and after filling the autoclave with VDF). After warming up to ambient temperature, the autoclave was heated to

the target temperature under mechanical stirring. A typical polymerization of VDF was performed as follows: A solution of *tert*-amyl peroxy-2-ethylhexanoate (Trigonox 121, 158 mg, 6.87 10^{-4} mol) and *O*-Ethyl-*S*-(1-methoxycarbonyl) ethyldithiocarbonate (CTA, 1.30 g, 6.25 10^{-3} mol) in dimethylcarbonate DMC (60 mL), was degassed by N_2 bubbling during 30 min. This homogenous solution was introduced into the autoclave using a funnel, VDF gas (19.0 g, 2.97 10^{-1} mol) was transferred in the autoclave at low temperature, and the reactor was gradually heated to 73 °C. The reaction was stopped after 20 h. During the reaction, the pressure increased to a maximum of 25 bars and then decreased to 10 bars after 20 h. The autoclave was cooled down to room temperature (≈20 °C), purged from the residual monomers and dimethylcarbonate was removed under vacuum. The crude product was dissolved in 30 mL of warm THF (≈40 °C), and left under vigorous stirring for 30 min. This polymer solution was then precipitated from 400 mL of chilled hexane. The precipitated polymer (white powder) was filtered through a filter funnel and dried under vacuum (15 mbar) for two hours at 50 °C. The polymerization yield (65%) was determined by gravimetry (mass of dried precipitated polymers/mass of monomer introduced in the pressure reactor).

^{1}H NMR (400 MHz $(CD_3)_2CO$, δ (ppm)) : 1.19-1.24 (d, -CH(C**H$_3$**)(C=O)-, $^3J_{HH}$= 7.1 Hz), 1.40-1.46 (t, -S(C=S)O-CH_2-C**H$_3$**, $^3J_{HH}$= 7.2 Hz) 1.65-1.85 (m, -CF_2-C**H$_3$**), $^3J_{FH}$= 19.0 Hz), 2.28-2.43 (m,-CF_2-C**H$_2$**-C**H$_2$**-CF_2-, VDF-VDF TT reverse addition), 2.70-3.19 (t, -CF_2-C**H$_2$**-CF_2-, VDF-VDF HT regular addition), 3.60-3.69 (s, -(C=O)-O-C**H$_3$**), 4.02-4.17 (t, -CF_2-C**H$_2$**-S(C=S)OEt, $^3J_{HF}$= 18.0 Hz), 4.67-4.77 (q, (-S(C=S)O-C**H$_2$**-CH_3, $^3J_{HH}$= 7.2 Hz), 6.05-6.45 (tt, $^2J_{HF}$= 55 Hz , $^3J_{HH}$= 4.6 Hz -CH_2-CF_2-**H**)

^{19}F NMR (376 MHz $(CD_3)_2CO$, δ (ppm)) : -115.63 (-CH_2-CF_2-C**F$_2$**-CH_2-CH_2-, VDF-VDF HH reverse addition), -114.29 ($^2J_{HF}$= 55 Hz, -CH_2-C**F$_2$**-H), -113.34 (-CH_2-C**F$_2$**-CF_2-CH_2-CH_2-, HH reverse addition), -113.09 (CH_2-CF_2-**CF$_2$**-CH_2-S-), -112.69 (-CH_2-**CF$_2$**-CF_2-CH_2-S-), -94.79 (-CH_2-CH_2-C**F$_2$**-CH_2-, TT reverse addition), -107.7 (-CF_2-C**H$_3$**), -93.50 (-CH_2-C**F$_2$**-CH_2-CH(CH_3)(C=O)-), -92.12 (-CH_2-C**F$_2$**-CH_2-CF_2H), -91.44 (-CH_2-CH_2-CF_2-CH_2-**CF$_2$**-CH_2-CF_2-, regular VDF-VDF HT addition), -91.00 (-CH_2-C**F$_2$**-CH_2-, regular VDF-VDF HT addition).

^{13}C NMR (100 MHz $(CD_3)_2CO$, δ (ppm)): 13.2 (-S(C=S)O-CH_2-**CH$_3$),** 17.8 (-CH(**CH$_3$**)(C=O)-), 23.1 (-CF_2-**CH$_2$**-CH_2-CF_2-, VDF-VDF TT reverse addition), 29.0 (-CF_2-CH_2-**CH$_2$**-CF_2-, VDF-VDF TT reverse addition), 33.7 (-CF_2-CH_2-**CH**(CH_3)(C=O)-, $^3J_{CF}$ = 3.5 Hz), 34.7 (-CF_2-**CH$_2$**-S(C=S)OEt, $^2J_{CF}$ = 23.0 Hz), 36.8 (t, -**CH$_2$**-CF_2-CF_2-CH_2-S(C=S)OEt,

$^{2}J_{CF}$ = 23.0 Hz), 40.7 (-CF_2-**CH_2**-$CH(CH_3)$(C=O)-, $^{2}J_{CF}$ = 23.0 Hz), 43.7 (t, -CF_2-C**H_2**-CF_2-, VDF-VDF HT regular addition, $^{1}J_{CH}$ = 131 Hz, $^{2}J_{CF}$ = 24.0 Hz**)**, 51.6 (-(C=O)-O-C**H_3**), 71.6 (-S(C=S)O-C**H_2**-CH_3), 113.6 and 113.8 (-CF_2-CH_2-CF_2-CH_2-**CF_2H** and -CH_2-CH_2-CF_2-CH_2-**CF_2H**), 116.2 (-**CF_2**-CH_2-S(C=S)OEt)), 116.9 (-CF_2-**CF_2**-CH_2-S(C=S)OEt) and -CH_2-CF_2-CF_2-CH_2-CH_2-), 118.4 (-CH_2-CF_2-**CF_2**-CH_2-CH_2-), 119.8 (-CH_2-CF_2-CH_2-, $^{1}J_{CF}$ = 245 Hz, $^{2}J_{CH}$ = 4.9 Hz), 119.9 (-CH_2-**CF_2**-CH_2-CF_2H), 121.6 (-CF_2-CH_2-**CF_2**-CH_2-CH_2-), 122.0 (-**CF_2**-CH_2-$CH(CH_3)$(C=O)-).

IV. Result and discussion

Indirect spin–spin coupling is present in almost all the spectra that are reported in this study. It is huge for $^{1}J_{CH}$ (131 Hz) and $^{1}J_{CF}$ (245 Hz), still strong for $^{2,3}J_{CF}$ and $^{2,3}J_{CH}$ with values between 10 Hz and 30 Hz. This can be useful in some 1D experiments as, in ^{13}C NMR for instance, one can suppress either $^{n}J_{CH}$ or $^{n}J_{CF}$ or both, which helps signals assignment. In 2D NMR experiments, however, decoupling of heteronuclei is required because strong *J* couplings lead to multiplets in F1 and F2 dimensions giving muddled maps if not suppressed. For instance, in ^{1}H COSY or ^{19}F{^{1}H} HETCOR experiments broadband, ^{19}F decoupling is required because of $^{n}J_{HF} > n \geq 2$ in the range 10 to 60 Hz. In ^{1}H{^{13}C} (respectively ^{19}F{^{13}C}) HSQC $^{n}J_{HC}$ (respectively $^{n}J_{FC}$) are used to establish correlations during evolution period and suppressed by decoupling during acquisition to enhance resolution but $^{n}J_{FC}$ (respectively $^{n}J_{HC}$) and $^{n}J_{HF}$ have to be suppressed during the whole sequence.

Figure II-25 and Figure II-26 present the ^{1}H and ^{19}F NMR spectra of a typical $PVDF_{51}$-XA prepared by RAFT polymerization of VDF in DMC.[24] The assignments of most of the NMR signals were possible using these simple 1D NMR experiments. As previously reported,[24,36] due to irreversible trapping of the HH chain defects by transfer to the CTA, all the PVDF chains (aside from a small number of H-terminated chains resulting from transfer to DMC, signals *(p)* in Figure II-25 and Figure II-26) feature a -CF_2CH_2-XA ω-chain end. In the PVDF discussed here, CF_2H-terminated chains account for 14% of the total number of chains, while the unavoidable and temperature dependent.[39] HH chain defects amount to about 4.1% of the total number of VDF addition. When they occur, these additions are for their vast majority irreversibly trapped at the chain end by transfer to the CTA (thus leading to $PVDF_T$-XA much less reactive chains), but they can also propagate and add another unit of VDF. In this case, this addition is invariably a tail-to-tail (TT) addition.

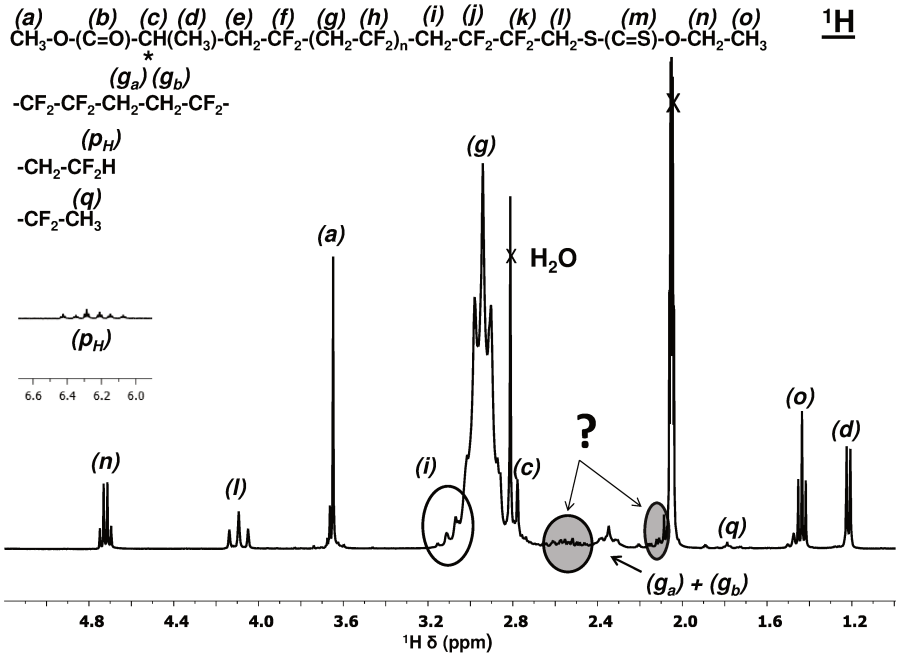

Figure II-25: Expansion of the 1.0–5.1 ppm region of the ^1H NMR spectrum in $(CD_3)_2CO$ of a PVDF homopolymer synthesized via RAFT polymerization. Highlighted signals are suspected to arise from the first VDF unit attached to the CTA R-group (methyl propionyl group): protons (e) .

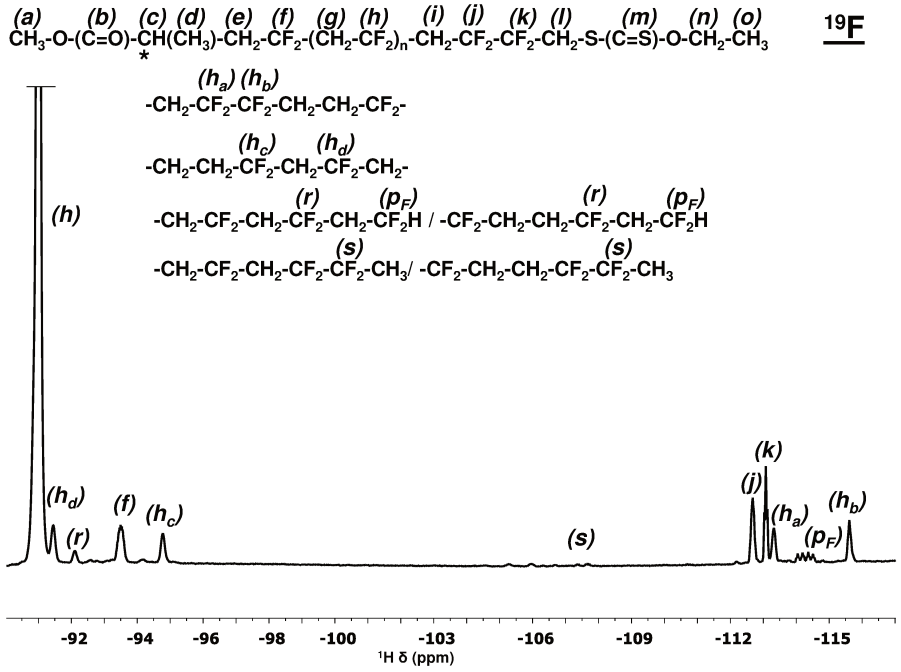

Figure II-26: Expansion of the −90 ppm to −117 ppm region of the 19 F NMR spectrum in (CD 3) 2 CO of a PVDF homopolymer synthesized via RAFT polymerization.

These nonregioregular additions are easily identifiable as intrachain HH and TT defects by NMR (signals *(g_a)* and *(g_b)* in Figure II-25 (TT) and signals *(h_a)*, *(h_b)*, *(h_c)*, and *(h_d)* in Figure II-26 (HH, TT)). The number of intrachain HH reverse addition increases with increasing PVDF molecular weight.[36] In the polymer presented here, they account for 1.65% of the total number of HH defects. $-CF_2CH_2^{\cdot}$ radicals formed via HH addition can also transfer (to a lesser extent compared to transfer to the CTA or propagation to another VDF unit) to the solvent (in the present case DMC) and lead to CH_3-terminated dead chains. Such dead chains can be seen on Figure II-25 (signal *(q)* weak triplet at 1.85 ppm).[40]

The ^1H and ^{19}F NMR signals corresponding to the xanthate group (signals *(n)* and *(o)* in Figure II-25), to the ultimate and to the penultimate VDF units (signals *(l)* and *(i)* respectively in Figure II-25, and signals *(k)* and *(j)* respectively in Figure II-26) were also relatively easily determined. The identification of the signals of the α-chain end was however more difficult. The remaining nonassigned signal in the ^{19}F NMR spectrum of the $PVDF_{51}$-XA (signal *(f)* in Figure II-26) was thought to be that of the first added VDF unit. The ^1H NMR signal of that first added VDF unit, however, was not assigned. Figure II-25 highlights two potential peaks that could correspond to the methylene bridge *(e)* of this first VDF unit. During the polymerization of VDF in the presence of a xanthate CTA, it was observed that when the R-group radical adds onto the head of VDF, the thus formed $R\text{-}CF_2\,CH_2^{\cdot}$ radical transfers immediately to a CTA-VDF monoadduct, which cannot further participate in the polymerization.[24] This small molecule was eliminated when the PVDF was purified by precipitation. It was thus assumed that because of this reaction (which consumes about 31% of the xanthate group) all the PVDF chains initiated by the CTA R-group display an $R\text{-}CH_2CF_2$-α-chain end. This assumption was, however, not supported by spectroscopic evidence. To unequivocally establish the exact chain-end structures of PVDF prepared by RAFT polymerization, we first used $^1H\text{-}^1H$ COSY NMR experiment.

Figure II-27 shows this 2D NMR spectrum. It reveals the correlation pattern of the signals assigned to the CTA Z- and R-group in PVDF. The expected coupling arrangement of the ethyl xanthate can clearly be observed (triplet at 1.43 ppm *(o)* corresponding to the methyl of the ethyl xanthate coupling with the quartet at 4.71 ppm *(n)* of the methylene bridge of the ethyl xanthate) (SI-Figure II-34, VIII-Supporting Information). Starting from the signal of the methyl moiety of the CTA R-group (peak *(d)* in Figure II-25 and Figure II-27) the chemical shift at 2.8 ppm of the signal of proton *(c)* (partly overlapping with the NMR signal of water

contained in deuterated acetone and with that of VDF regular addition in PVDF, in Figure II-25) of the asymmetric center of the CTA R-group can be confirmed. This proton is observed to couple with two weak signals at 2.1 and 2.5 ppm, which also couple with one another. These two signals at 2.1 and 2.5 ppm are thus each thought to be corresponding to one of the protons of the CH_2 moiety of the first added VDF unit *(e)*. The chemical shift difference (0.4 ppm) between these two protons can be explained by the presence of a stereocenter in the CTA R-group. These protons *(e)* are indeed expected to be diastereotopic.

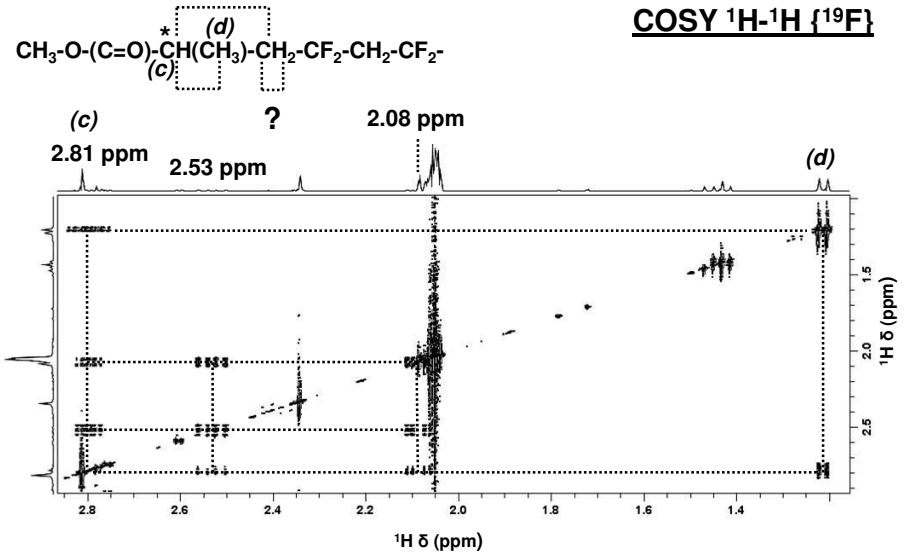

Figure II-27: Expansion region of the 1.15–2.85 ppm region of a ^{19}F decoupled COSY ^{1}H–^{1}H correlation spectrum in $(CD_3)_2CO$ of $PVDF_{51}$-XA. Dashed lines were assigned to a first order correlation between protons of the CTA R-group (CH_3 and CH) and protons of VDF (CH_2).

The assignment of the diastereotopic protons *(e)* was confirmed by the $^{1}H\{^{13}C\}$ with ^{19}F decoupling HSQC correlation spectrum (Figure II-28), which shows that these 2 signals *(e_a)* and *(e_b)* (at 2.5 and 2.1 ppm respectively) correspond to protons carried by the same carbon atom *(e)* (at 40.7 ppm). This $^{1}H\{^{13}C\}$ 2D NMR experiment also allowed the thorough assignment of the ^{13}C NMR signals of $PVDF_{51}$-XA (SI-Figure II-35 and SI-Figure II-36, in VIII-Supporting Information). This had never been reported so far (to the best of our knowledge, only one article[41] shows a ^{13}C NMR spectrum of a PVDF telomer). A more detailed examination of the $PVDF_{51}$-XA chain ends by ^{13}C NMR is presented in Figure II-29 and Figure II-30.

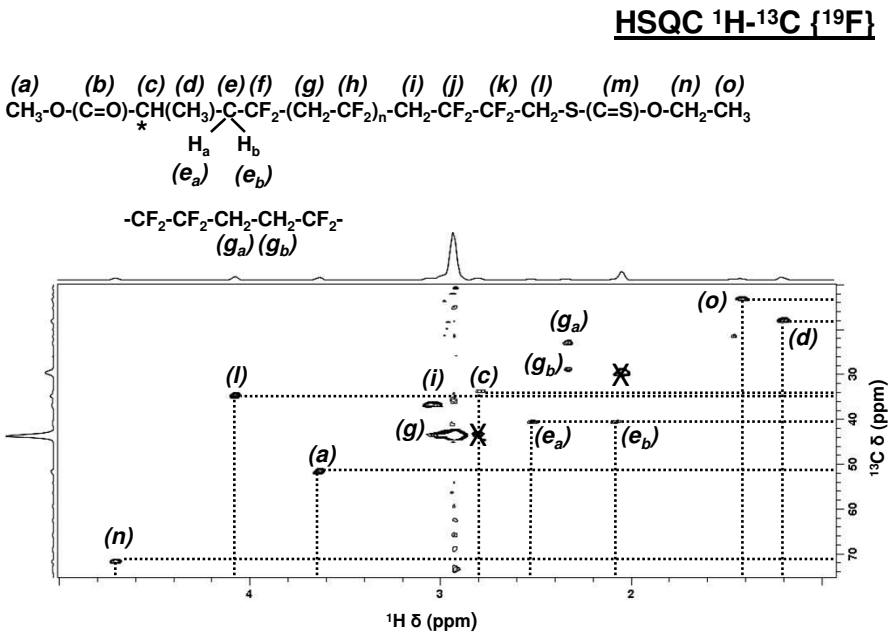

Figure II-28: Expansion region of the 1.0–5.0 (^{1}H) and 10–75 (^{13}C) ppm region of the ^{19}F decoupled HSQC ^{1}H{^{13}C} correlation spectrum in $(CD_3)_2CO$ of $PVDF_{51}$-XA. Vertical axis: ^{13}C NMR chemical shift; horizontal axis: ^{1}H NMR chemical shift. The signal of the acetone-d_6 ($\delta_{(ppm)}$ = (2.05, 29.6)) is crossed-out.

The 2D ^{19}F{^{13}C} with ^{1}H decoupling HSQC NMR spectrum (Figure II-29) was very helpful in achieving this detailed NMR signal assignment. Remarkably, fluorine atoms *(f)* display two symmetrical and very close signals centered at –93.50 ppm and correlated to a unique carbon signal at 122.0 ppm. ^{1}H/ ^{19}F decoupled ^{13}C NMR experiments (Figure II-30) allowed the measurements of carbon-fluorine coupling constants of ^{13}C NMR signals characteristic of the $PVDF_{51}$-XA chain ends. The signals at 36.5 and 34.3 ppm corresponding respectively to the methylene carbons *(i)* and *(l)* of the penultimate and ultimate VDF units (HH addition) appeared as a quintet and a triplet respectively, (with $^{2}J_{CF}$ = 23.0 Hz) in the ^{1}H decoupled ^{13}C NMR spectrum of $PVDF_{51}$-XA (Figure II-30 (middle)). Carbons *(c)* (at 33.5 ppm) and *(e)* (at 40.25 ppm) of the α-chain end CH_3-O-(C=O)**CH**(CH_3)-**CH_2**CF_2- also appeared as triplets in the ^{1}H decoupled ^{13}C NMR spectrum of $PVDF_{51}$-XA (Figure II-30 (middle)) with coupling constants $^{3}J_{CF}$ = 3.5 Hz and $^{2}J_{CF}$ = 23.0 Hz respectively.

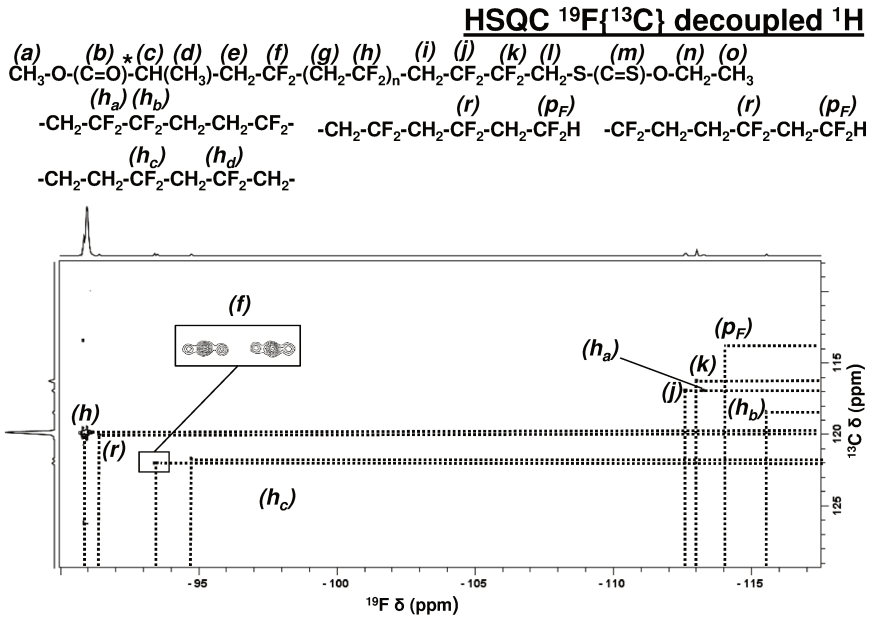

Figure II-29: Expansion region of the -90 to -117.5 (^{19}F) and 108 – 129 (^{13}C) ppm region of the ^{1}H decoupled HSQC $^{19}F\{^{13}C\}$ correlation spectrum in $(CD_3)_2CO$ of $PVDF_{51}$-XA. Vertical axis: ^{13}C NMR chemical shift; horizontal axis: ^{19}F NMR chemical shift.

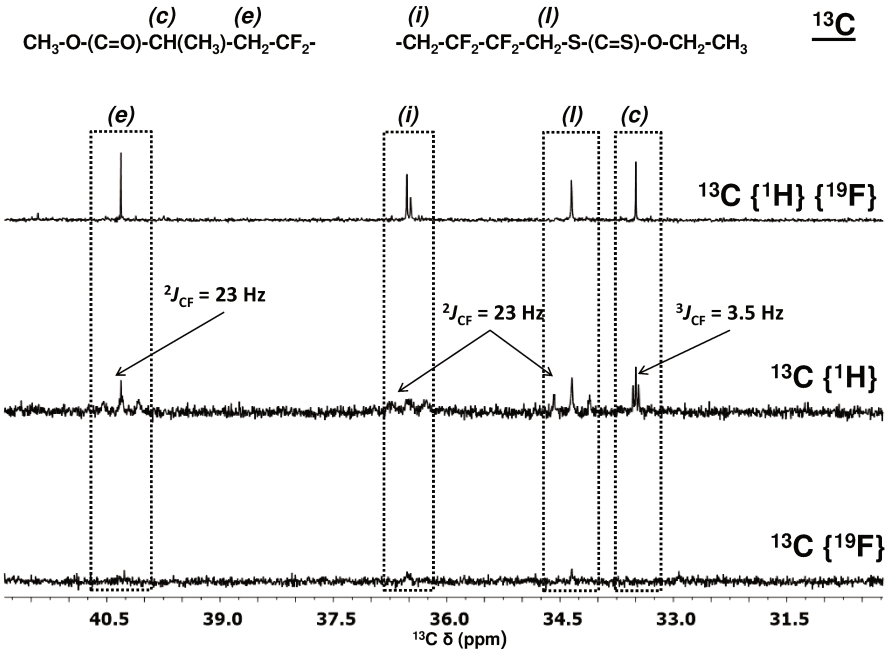

Figure II-30: Expansion of the 30.25 – 41.75 ppm region of the ^{13}C NMR spectra in $(CD_3)_2CO$ of $PVDF_{51}$-XA : ^{19}F decoupled ^{13}C NMR spectrum (bottom), ^{1}H decoupled ^{13}C NMR spectrum (middle), and ^{19}F+^{1}H decoupled ^{13}C NMR spectrum (top).

Figure II-31 shows the $^{19}F\{^{1}H\}$ HETCOR 2D spectrum of $PVDF_{51}$-XA and highlights the connections between proton carrying and fluorine carrying carbons. This 2D NMR spectrum is very informative. The four types of H-terminated chain ends $-CH_2CF_2-CH_2CF_2-CH_2CF_2H$ and $-CF_2CH_2-CH_2CF_2-CH_2CF_2H$ (resulting from transfer of a regioregularly added PVDF radical to DMC), and $-CH_2CF_2-CH_2CF_2-CF_2CH_3$ and $-CF_2CH_2-CH_2CF_2-CF_2CH_3$ (resulting from transfer of an inversely added PVDF radical to DMC) can clearly be seen via the correlation between the proton *(p_H)* and the fluorine atoms *(p_F)* of the terminal CF_2H group and via the correlation between the protons *(q)* and the fluorine atoms *(s)* of the CH_3 group. Importantly, these microstructures had been incorrectly assigned in our previous reports.[24,34] The correct assignments presented here was made possible through the use of $^{19}F\{^{1}H\}$ fully coupled (HETEROCOSY) NMR experiments. The details of this pulse sequence and of its use will be reported in the near future.

The xanthate chain ends are also easily identified via the *(i)-(j)* and *(l)-(k)* correlations at (3.1, -112.69 ppm) and (4.1, -113.09 ppm) corresponding to heteronuclear couplings occurring between the CF_2 and CH_2 bridges of the penultimate and ultimate inversely added (HH) VDF units. The regularly added VDF units inside the PVDF chains produce an intense correlation signal at (-91.0, 2.9 ppm) (signal *(g)-(h)*), while the intrachain inverse additions are revealed by correlation signals at (2.35, -94.79 ppm) and (2.9, -94.79 ppm) (signals *(h_c)-(g_b)* and *(h_c)-(g)*, respectively) and at (2.35, -115.63 ppm) and (3.1, -113.34 ppm) (signals *(g_a)-(h_b)* and *(g)-(h_a)*, respectively). The remaining ^{1}H-^{19}F heteronuclear correlation signals at (2.1, -93.5 ppm), (2.5, -93.5 ppm) and (2.8, -93.5 ppm) were assigned to the α-chain end respectively to the *(e_b)-(f)*, *(e_a)- (f)*, and *(c)-(f)* couplings. These correlation patterns indeed shows that the two diastereotopic protons *(e_a)* and *(e_b)* as well as proton *(c)* are coupling with the fluorine atoms *(f)*.

In addition, the insert in Figure II-31 suggests that the two fluorine atoms on carbon *(f)* are not chemically equivalent. Proton *(c)* couples similarly with both *(f)* fluorine atoms (the *(c)-(f)* correlation spot is symmetrical) while *(e_a)* and *(e_b)* each couple strongly with one of the *(f)* fluorine atoms and weakly with the other one (the correlation spots are asymmetric and the inverse of each other; see insert in Figure II-31).

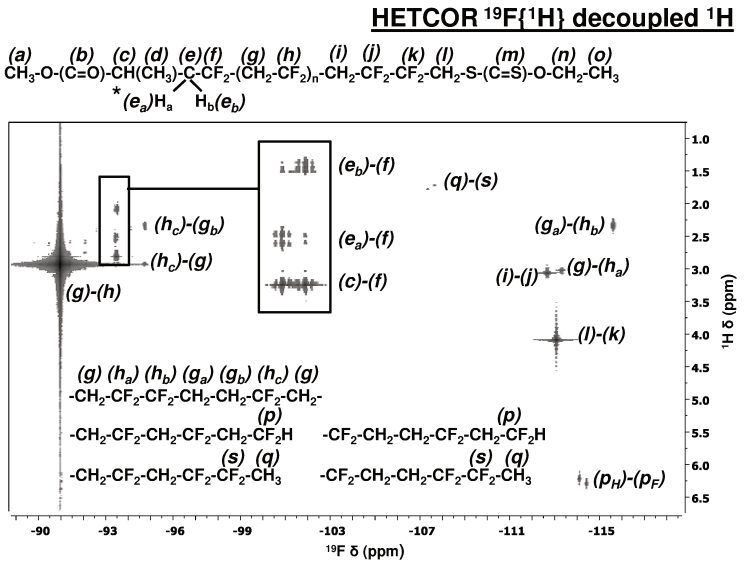

Figure II-31: $^{19}F\{^{1}H\}$ HETCOR spectrum of $PVDF_{51}$-XA in $(CD_3)_2CO$. Vertical axis: ^{1}H NMR chemical shift; horizontal axis: ^{19}F NMR chemical shift decoupled ^{1}H.

The diastereotopicity of protons *(e_a)* and *(e_b)* is confirmed by the ^{19}F decoupled ^{1}H NMR spectrum of the $PVDF_{51}$-XA (Figure II-32), which clearly shows that the signals of these protons are split into doublets of doublets due to coupling with each other (germinal coupling with $^{2}J_{HH}$ = 15.0 Hz) and coupling with the proton *(c)* of the stereocenter of the CTA R group ($^{3}J_{HH}$ = 8.4 Hz for *(e_a)* and $^{3}J_{HH}$ = 4.9 Hz for *(e_b)*). ^{1}H decoupled ^{19}F NMR spectrum of the $PVDF_{51}$–XA (Figure II-33) gave further information on the fluorine atoms *(f)*. In acetone-d_6, the signal of the *(f)* fluorine atoms (at -93.5 ppm) appears as two triplets separated from each other by 36.3 Hz (≈ 0.1 ppm) with an apparent coupling constant $^{4}J_{FF}$ = 8.5-8.6 Hz while in DMF-d_7, the same signal appears as a quartet with an apparent coupling constant of $^{4}J_{FF}$ = 8.8 Hz. These couplings are caused by interactions between the fluorine atoms *(f)* and the fluorine atoms of the second added VDF unit (see Figure II-33). Both chemical shifts and coupling constants can be affected by the deuterated solvent used to record the NMR spectra.[42] It is thus not entirely surprising to observe this difference in NMR signals upon change of solvents. It also suggests that the two fluorine atoms *(f)* are not chemically equivalent due to the influence of the asymmetric carbon *(c)*, but that they surprisingly have identical chemical shift. However, the effect of the stereocenter *(c)* is rather weak and even though the two fl uorine atoms *(f)* are not equivalent, the $^{2}J_{FF}$ is much weaker than usual. Indeed, typical $^{2}J_{FF}$ range from 90 to 300 Hz.[43] In the present case, the $^{2}J_{FF}$ coupling constant is 36.3 Hz in acetone-d_6 and 8.5 Hz in DMF-d_7. To the best of our knowledge, such a long range effect of a stereocenter on fluorine atoms has never been reported.

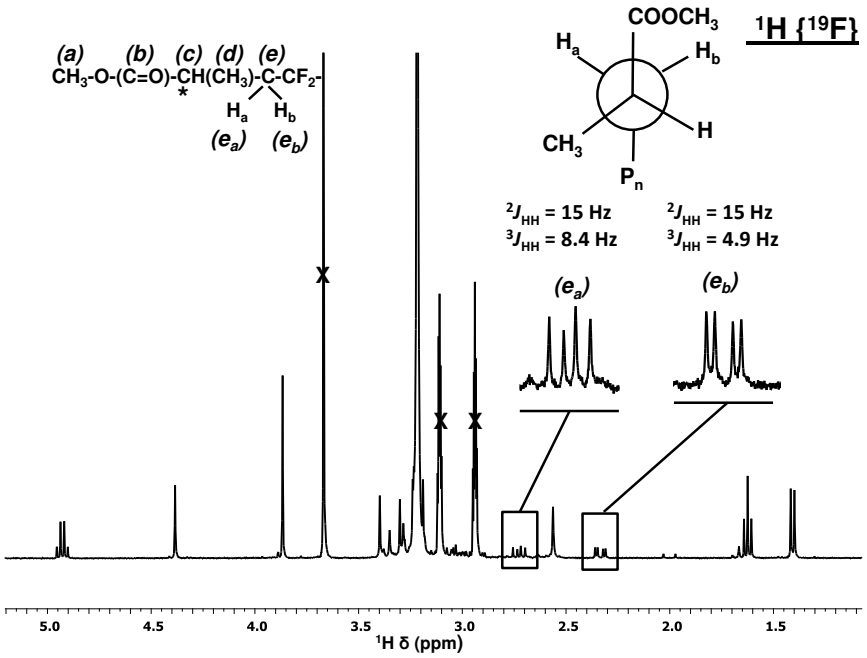

Figure II-32: Expansion of the 1.1 to 5.2 ppm region of the 19F decoupled 1H NMR spectrum in DMF-d 7 of $PVDF_{51}$-XA. The signals of remaining DMF and DMC (respectively at 2.94, 3.11, and 3.67 ppm) are crossed-out.

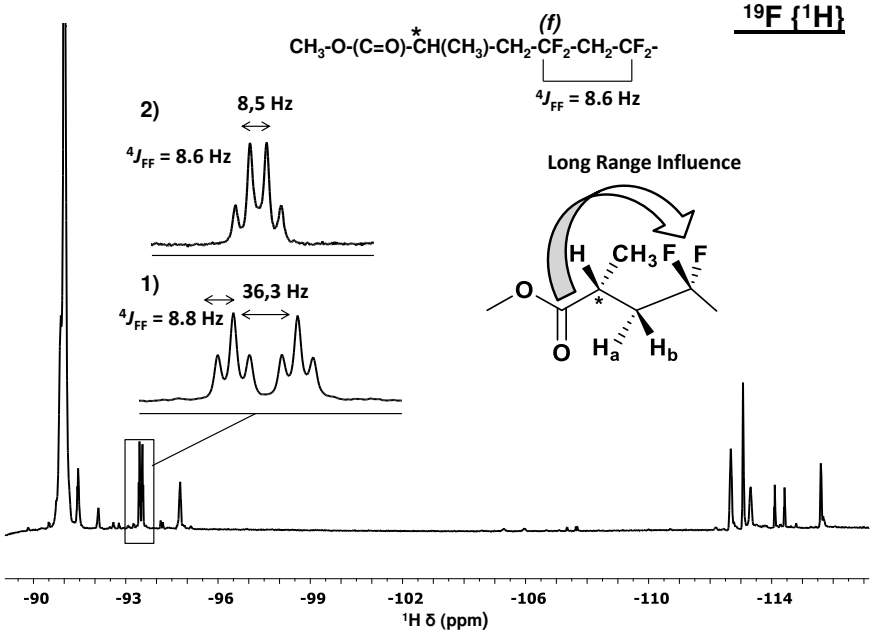

Figure II-33: Expansion of the -89 to -117 ppm region of the ^{1}H decoupled ^{19}F NMR spectrum in $(CD_3)_2CO$ of $PVDF_{51}$-XA. Inserts 1) and 2) show a zoom of the signal of fluorine atoms (f) in acetone-d_6 and in DMF-d_7 respectively.

V. Conclusion

Using 1D ^{1}H, ^{19}F and ^{13}C, and 2D $^{1}H\{^{13}C\}$ HSQC, $^{19}F\{^{13}C\}$ HSQC, and $^{19}F\{^{1}H\}$ HETCOR NMR experiments, as well as decoupling strategies, a comprehensive study of the structure of PVDF synthesized by RAFT ($PVDF_{51}$-XA) was carried out. This article presents the results of this thorough NMR characterization of $PVDF_{51}$-XA with a particular emphasis on the α- and ω-chain ends. It shows so far unreported NMR spectra (^{13}C with and without ^{1}H and ^{19}F decoupling, ^{19}F decoupled HSQC $^{1}H\{^{13}C\}$, ^{1}H decoupled HSQC $^{19}F\{^{13}C\}$) and provides additional NMR signals assignments. Importantly, this article elucidates the structure of the $PVDF_{51}$-XA α-chain end, and demonstrates that the chains initiated by the CTA R group are exclusively composed of R-CH_2CF_2- sequence. This article also suggests that the stereocenter of the CTA R-group exerts an uncommon effect on fluorine atoms carried by a carbon two covalent bonds away. The fluorine atoms indeed seem to be nonequivalent but feature identical chemical shifts and very weak $^{2}J_{FF}$ coupling constant. This article is, to date, the most complete NMR description of PVDF-XA. It paves the way for better characterizations of more complex PVDF-based copolymer and architectures.

VI. Acknowledgements

The authors thank Arkema (Pierre Bénite, France) for providing VDF, and the French Ministry of Science and Technology for the Ph.D. grant attributed to M.G.

VII. References

[1] J. Scheirs, In *Modern Fluoropolymers*, Ed., John Wiley and Sons: New York, 1997.

[2] G. Hougham, P. E. Cassidy, K. Johns, J. Davidson, In *Fluoropolymers: Synthesis and Applications*, Ed., Plenum Press: New York, 1999; Vols. **1** and **2**.

[3] B. Ameduri, B. Boutevin, In *Well-Architectured Fluoropolymers*: Synthesis, Properties and Applications, Elsevier: Amsterdam, 2004.

[4] J. G. Drobny, In *Technology of Fluoropolymers 2nd Ed.*, CRC Press, Boca Raton, FL, 2008.

[5] D. W. Smith Jr., S. T. Iacono, S. S. Iyer, *In Handbook of Fluoropolymer Science and Technology*, Eds., Wiley, New York, 2014.

[6] S. Ebnesajjad, In *Fluoroplastics, Vol. 2: Melt Processible Fluoroplastics, The Definitive User's Guide and Databook*, William Andrew Publishing, Norwich (NY), 2003.

[7] B. Ameduri, *Chem. Rev.,* 2009, **109,** 6632.

[8] ThermoFischer Scientific, PVDF Membranes for Western Blotting, https://www.thermofisher.com/fr/fr/home/life-science/protein-biology/protein-assays analysis/western-blotting/transfer-proteins-western-blot/membranes-transfer-buffers-western-blotting/membranes-western-blotting/pvdf-membranes-western-blotting.html (accessed March 2016)

[9] H. Kawai, *Jpn. J. Appl. Phys.,* 1969, **8**, 975.

[10] T. Soulestin, V. Ladmiral, T. Lannuzel, F. Domingues Dos Santos, B. Ameduri, *Macromolecules,* 2015, **48**, 7861.

[11] I. Katsouras, K. Asadi, M. Li, T. B. van Driel, K. S. Kjær, D. Zhao, T. Lenz, Y. Gu, P. W. M. Blom, D. Damjanovic, M. M. Nielsen, D. M. de Leeuw, *Nat. Mater.,* 2016, **15**, 78.

[12] "Global Fluoropolymer Market", Acmite Market Intelligence, http://www.acmite.fr (accessed March 2016).

[13] B. Ameduri, *Macromolecules,* 2010, **43**, 10163.

[14] N. Durand, B. Ameduri, B. Boutevin, *J. Polym. Sci., Part A: Polym. Chem.,* 2011, **49**, 82.

[15] E. B. Twum, X. Li, E. F. McCord, P. A. Fox, D. F. Lyons, P. L. Rinaldi, In *Advances in Fluorine-Containing Polymers*, Eds, D. W. Smith Jr., S. Iacono, D. J. Boday, American Chemical Society, Washington (DC), 2012, 187.

[16] A. D. Asandei, O. I. Adebolu, C. P. Simpson, J. S. Kim, *Angew. Chem. Int. Ed.,* 2013, **52**, 10027.

[17] C. Boyer, D. Valade, L. Sauguet, B. Ameduri, B. Boutevin, *Macromolecules,* 2005, **38**, 10353.

[18] M. Destarac, D. Charmot, S. Z. Zard, X. Franck (Rhodia Chimie) WO 075207, 2000.

[19] M. Destarac, W. Bzducha, D. Taton, I. Gauthier-Gillaizeau, S. Z. Zard, *Macromol. Rapid Commun.,* 2002, **23**, 1049.

[20] M. J. Monteiro, M. M. Adamy, B. J. Leeuwen, A. M. van Herk, M. Destarac, *Macromolecules,* 2005, **38**, 1538.

[21] D. Taton, M. Destarac, S. Z. Zard, in *Handbook of RAFT Polymerization*, Ed, C. Barner-Kowollik, Wiley-VCH, Weinheim, 2008, 373.

[22] M. Destarac, *Macromol. React. Eng.,* 2010, **4**, 165.

[23] E. Girard, J. D. Marty, B. Ameduri, M. Destarac, *ACS Macro Lett.,* 2012, **1**, 270.

[24] M. Guerre, B. Campagne, O. Gimello, K. Parra, B. Ameduri, V. Ladmiral, *Macromolecules,* 2015, **48**, 7810.

[25] M. Tatemoto, In *The First Regular Meeting of Soviet-Japanese Fluorine Chemists*, Tokyo, Japan, February 15−16, 1979.

[26] M. Oka, M. Tatemoto, In *Contemporary Topics in Polymer Science*, Eds, W. J. Bailey, T. Tsuruta, T., Plenum Press, New York, 1984, 763.

[27] M. Tatemoto, *Int. Polym. Sc. Technol.,* 1985, **12**, 85.

[28] M. Tatemoto, In *Polymeric Materials Encyclopedia*, Ed, J. C. Salamone, CRC Press, Boca Raton, FL, 1996, 3847.

[29] M. Tatemoto, *Kobunshi Ronbunshu,* 1992, **49**, 765.

[30] M. Tatemoto, T. Shimizu, In *Modern Fluoropolymers*, Ed, J. Scheirs, John Wiley and Sons, New York, **1997**, p 565.

[31] A. D. Asandei, O. I. Adebolu, C. P. J. Simpson, *J. Am. Chem. Soc.,* 2012, **134**, 6080.

[32] A. D. Asandei, O. I. Adebolu, C. P. Simpson, in *Advances in Fluorine-Containing Polymers*, Eds, D. W. Smith Jr., S. Iacono, D. J. Boday, American Chemical Society, Washington DC, 2012, 47.

[33] G. Lopez, A. Thenappan, B. Ameduri, *ACS Macro Lett.,* 2015, **4**, 16.

[34] G. Kostov, F. Boschet, F. Buller, J. Badache, S. Brandsadter, B. Ameduri, *Macromolecules,* 2011, **44**, 1841-1855.

[35] Y. Patil, B. Ameduri, *Polym. Chem*., 2013, **4**, 2783-2799.

[36] M. Guerre, S. M. Wahidur Rahaman, B. Ameduri, R. Poli, V. Ladmiral, *Macromolecules,* 2016, **49**, 5386-5396.

[37] X. Liu, O. Coutelier, S. Harisson, T. Tassaing, J-D. Marty, M. Destarac, *ACS Macro Lett.,* 2015, **4**, 89-93.

[38] X. Li, E. F. Mc Cord, S. Baiagern, P. Fox, J. L. Howell, S. K. Sahooc and P. L. Rinaldi, *Magn. Reson. Chem.,* 2011, **49**, 413–424.

[39] P. Pladis, A. H. Alexopoulos, C. Kiparissides, *Ind. Eng. Chem. Res.,* 2014**, 53**, 7352-7364.

[40] M. Duc, B. Ameduri, B. Boutevin, M. Kharroubi, J. M. Sage, *Macromol. Chem. Phys.,* 1998, **199,** 1271-1289.

[41] E. Katoh, K. Ogura, I. Ando, *Polym. J.,* 1994, **26**, 1352-1359

[42] S. L Smith, In *Nonaqueous Chemistry*, Springer: Berlin, Heidelberg, 1972, 117-187.

[43] W. R. Dolbier, In *Guide to Fluorine NMR for organic Chemist*, John Wiley & Sons, Hoboken, 2009, 1-272.

VIII. Supporting Information

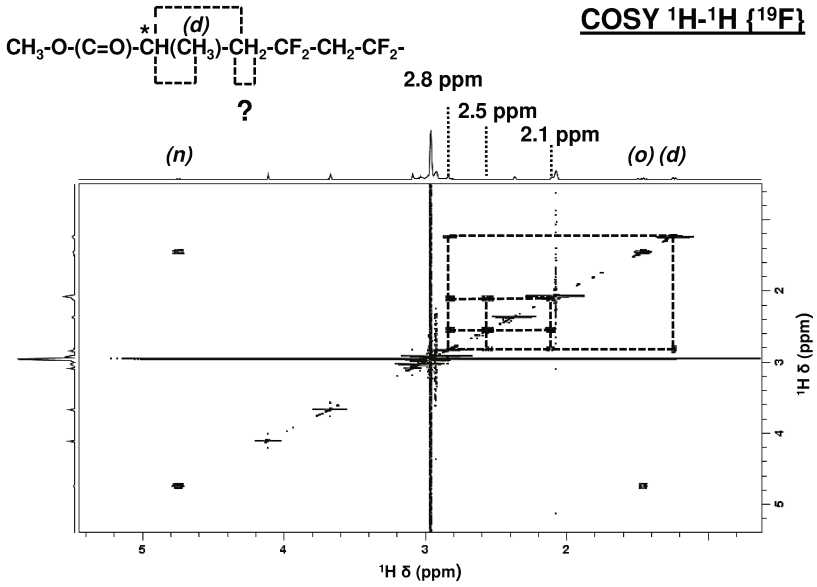

SI-Figure II-34: Expansion region of the 0.5 – 5.5 ppm region of a ^{19}F decoupled COSY ^{1}H-^{1}H correlation spectrum in $(CD_3)_2CO$ of $PVDF_{51}$-XA. Dashed lines were assigned to a first order correlation between protons of the CTA R-group (CH_3 and CH) and protons of VDF (CH_2).

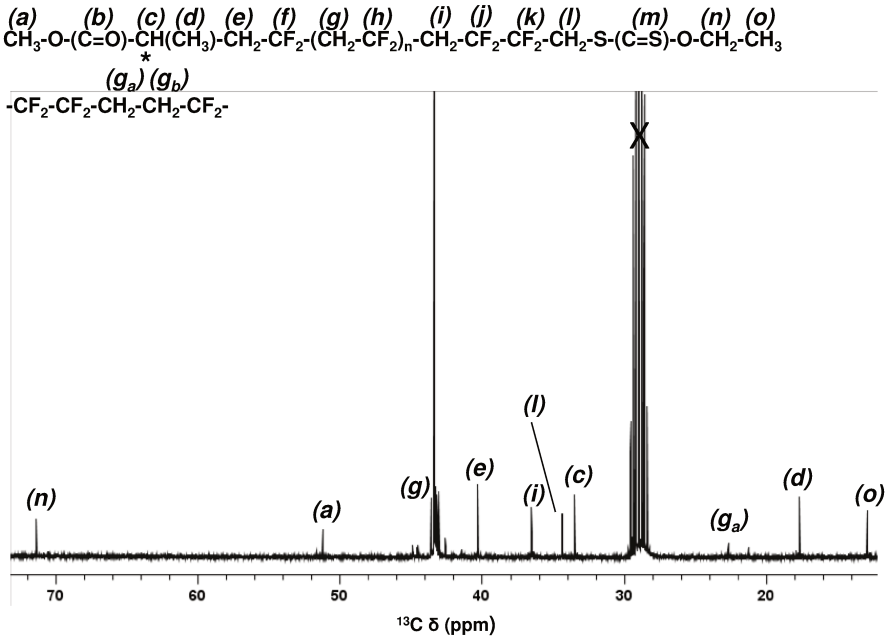

SI-Figure II-35: Expansion of the 12 – 73 ppm region of the ^{1}H + ^{19}F decoupled ^{13}C {} NMR spectrum in $(CD_3)_2CO$ of $PVDF_{51}$-XA

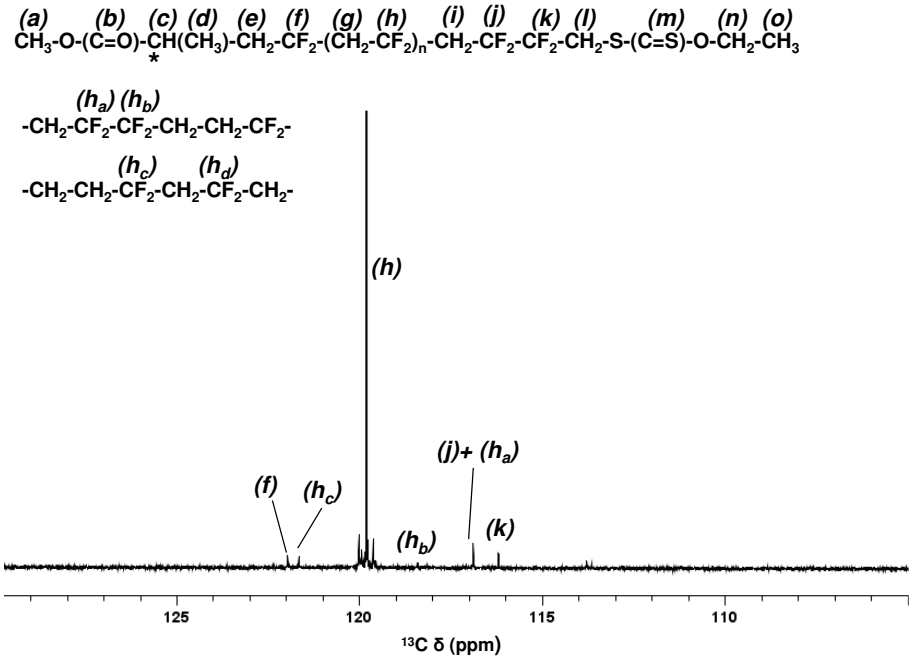

SI-Figure II-36: Expansion of the 105 – 130 ppm region of the $^{1}H + ^{19}F$ decoupled ^{13}C {} NMR spectrum in $(CD_3)_2CO$ of $PVDF_{51}$-XA

Conclusion Partie 2

Par une analyse RMN approfondie, cette deuxième partie a confirmé l'ensemble des signaux RMN préalablement attribué. Elle a également mis en lumière l'importance de la spectrocopie RMN du ^{13}C dans l'authentification des extrémités de chaînes, un noyau qui est trop souvent délaissé en RMN des polymères au profit de la RMN du ^{1}H. Cette deuxième étude a aussi permis d'élucider la microstructure de l'extrémité de chaîne α du PVDF et a démontré que ces bouts de chaînes étaient exclusivement constitués de l'enchaînement R-CH_2-CF_2-. Ces attributions n'ont pu être correctement établis qu'en combinant les spectres 1D ^{1}H, ^{19}F, $^{1}H\{^{19}F\}$, $^{19}F\{^{1}H\}$ et des spectres de correlations 2D : $^{1}H\{^{13}C\}$ HSQC, $^{19}F\{^{13}C\}$ HSQC, et $^{19}F\{^{1}H\}$ HETCOR.

Partie 3 -

Les deux premières parties de ce chapitre ont démontré l'efficacité de la technique RAFT et des agents de transfert de type xanthates, pour contrôler de manière satisfaisante la polymérisation du VDF. Cette première étude a montré pour la première fois la préparation d'agents RAFT macromoléculaires de PVDF hautement fonctionnel (85 %), présentant des dispersités inférieures à 1,4. Cependant, l'étude s'est essentiellement focalisée sur des valeurs de degré de polymérisation (DP) inférieures à 50. De plus, aucune étude n'a été menée, que ce soit par ITP ou par RAFT, sur le devenir du contrôle lorsque la totalité des chaînes est convertie en extrémités $PVDF_T$-XA.

Il y a donc plusieurs objectifs à cette étude. Le premier consiste à vérifier si le contrôle de la polymérisation RAFT du VDF est toujours valable pour des DP supérieurs à 50, et s'il est possible de synthétiser des PVDF-XA fonctionnels de hautes masses molaires. Une attention particulière est donc consacrée au contrôle de la polymérisation pour deux DP visés : 100 et 200. Une évolution du taux d'inversion à l'intérieur et aux extrémités de chaînes, en fonction de la conversion, est également discutée.

Enfin, avec l'appui des expérimentations et des calculs découlant de la Théorie de la fonctionnelle densité (Density Functional Theory, DFT, effectuée en collaboration avec le Professeur Rinaldo Poli) il est démontré que contrairement à l'opinion générale, les extrémités de chaîne $PVDF_T$-XA (ou $PVDF_T$-I, par extrapolation à l'ITP) ne peuvent pas être considérées comme « mortes ». Ce travail a fait l'objet d'un article scientifique publié dans *Macromolecules*.[3]

Limits of Vinylidene Fluoride RAFT Polymerization

Marc Guerre,[a] S. M. Wahidur Rahaman,[b] Bruno Ameduri,[a] Rinaldo Poli,[b§]* Vincent Ladmiral[a]*

[a]Institut Charles Gerhardt, Ingénierie et Architectures Macromoléculaires, UMR 5253 – CNRS, Université Montpellier, ENSCM - 8, Rue Ecole Normale, 34296 Montpellier-France.
[b]CNRS, LCC (Laboratoire de Chimie de Coordination), UPS, INPT, Université de Toulouse, 205 Route de Narbonne, BP 44099, F-31077 Toulouse, Cedex 4, France.
[§]Institut Universitaire de France, 1, rue Descartes, 75231 Paris, Cedex 05, France.
*Corresponding authors: rinaldo.poli@lcc-toulouse.fr, vincent.ladmiral@enscm.fr

I. Abstract

The investigations reported in this article probe the behavior of the RAFT polymerization of vinylidene fluoride (VDF) when degrees of polymerization higher than 50 are targeted: they demonstrate that higher molar mass PVDF (11 000 g mol^{-1}) can indeed be prepared by RAFT polymerization, but only at rather low monomer conversions (<33%). This study more carefully examines the behavior of the reputedly nonreactive -CF_2CH_2-XA chain ends (where XA designates the xanthate group) formed by inverse VDF addition and known to accumulate in the reaction medium during the polymerization. A combination of ^{1}H and ^{19}F NMR spectroscopic monitoring and comprehensive DFT calculations of the various exchange and propagation reactions at work explains the unexpected behavior of this polymerization. The present study disproves entirely the generally accepted belief that -CF_2CH_2-XA-terminated PVDF chains are “dead” and shows how these chains are reactivated, albeit slowly, throughout the polymerization. This activation occurs prevalently and counterintuitively through degenerative exchange by the minority PVDF-CF_2CH_2· radicals. The resulting kinetic scheme rationalizes the experimentally observed absence, after conversion of all the dormant chains into the less reactive -CF_2CH_2-XA end-group, of the longer polymer chains expected from a free radical polymerization mechanism.

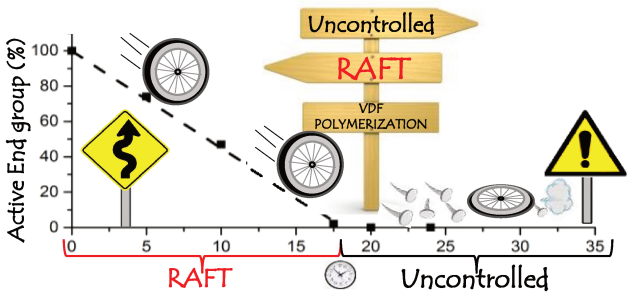

II. Introduction

Fluoropolymers (i.e., polymers the main chain of which is fluorinated), such as polytetrafluoroethylene (PTFE), poly-(vinylidene fluoride) (PVDF), and poly(chlorotrifluoroethylene) (PCTFE), to name just a few, constitute a very important class of polymeric materials and have found numerous high added-value applications.[1,2] Fluoropolymers are usually prepared by radical polymerization. Ironically, while fluoroolefins were among the first monomers polymerized using reversible deactivation radical polymerization (RDRP) techniques,[3] the development of well-defined architectures based on fluoropolymers is clearly lagging behind that of more widespread vinyl monomers (styrene, acrylics, etc.). This is probably due to the fact that most fluoroolefins are gases under standard temperature and pressure, thus requiring less common equipment such as pressure reactors, and to their specific reactivity due to the fluorine atoms, which exert both strong σ- inductive electron-withdrawing and π-donating effects.[4]

PVDF is the second most produced fluoropolymer after PTFE. PVDF and VDF copolymers have found numerous applications, for example in filtration membranes,[5] architectural coatings, fuel hoses, liners, wire and insulation, and their electroactive properties have the potential to open new hightechnology markets.[6–8] Recent years have witnessed a growing interest for the development of efficient preparation methods of well-defined fluoropolymer-based architectures.[9] Iodine transfer polymerization (ITP)[10] and RAFT/MADIX[11] polymerization have emerged as the most efficient techniques to control the polymerization of fluoroolefins[12 – 20] and to prepare well-defined fluoropolymer architectures. We recently reported the results of our detailed investigations of the RAFT polymerization of VDF.[19] That study clearly showed that xanthate chain transfer agents (CTA) are very efficient for preparing PVDF with narrow molar mass distributions (Đ < 1.5). These well-defined xanthate-terminated PVDF can easily be converted into macromonomers, opening the way to novel fluorinated architectures.[21] However, the radical polymerization of VDF is accompanied by a non-negligible amount of chain inversions (head-to-head (HH) and tail-to-tail (TT) VDF additions). These reverse additions are detrimental to the preparation of well-controlled PVDF chains using ITP or RAFT. It has indeed been proven that chain-ends terminated by an inversely added VDF unit accumulate in the reaction medium relatively rapidly.[14,19,22] These PVDF chains are also believed not to be able to participate into further degenerative transfer. Asandei *et al*.[14] reported a method, based on the use of $Mn_2(CO)_{10}$, to

reactivate unreactive iodine-capped chain-ends and to successfully extend PVDF chains under free radical polymerization conditions. In addition, polymerization of VDF in hydrogenated solvents is also affected by undesirable transfer-to solvent reactions. This H-abstraction results in losses of CTA and chain-end functionality and in some cases in the generation of undesired additional polymer chains.[19] Our previous report[19] gave thorough evidence for all these phenomena but restricted the investigation to short polymer chains (target $DP_n < 50$). The present research explores the limits of the RAFT polymerization of VDF and describes how higher molar mass PVDF can be prepared. In the course of these investigations, we were prompted to examine the fate of the PVDF chains that are terminated with an inversely added VDF unit. Our study, combining experimental observations and DFT calculations, proves that these reputedly inactive chains are not "dead" and shows how they are reactivated throughout the polymerization.

III. Experimental Section

Materials

All reagents were used as received unless stated otherwise. 1,1-Difluoroethylene (vinylidene fluoride, VDF) was kindly supplied by Arkema (Pierre-Benite, France). *O*-Ethyl-*S*-(1-methoxycarbonyl) ethyldithiocarbonate (CTA_{XA}) was synthesized according to the method described by Liu *et al*.[23] *tert*-Amylperoxy-2-ethylhexanoate (Trigonox 121, purity 95%) was purchased from AkzoNobel (Chalons-sur-Marne, France). ReagentPlus grade (purity >99%) dimethyl carbonate (DMC) and laboratory reagent grade hexane (purity >95%) were purchased from Sigma-Aldrich and used as received.

Characterization

Nuclear Magnetic Resonance

Nuclear magnetic resonance (NMR) spectra were recorded on a Bruker AC 400 instrument. Deuterated acetone was used as the solvent for all samples. Coupling constants and chemical shifts are given in hertz (Hz) and parts per million (ppm), respectively. The experimental conditions for recording ^1H and ^{19}F NMR spectra were as follows: flip angle 90° (or 30°), acquisition time 4.5 s (or 0.7 s), pulse delay 2 s (or 2 s), number of scans 128 (or 512), and a pulse width of 5 μs for ^{19}F NMR.

Size Exclusion Chromatography

Size exclusion chromatograms (SEC) were recorded using a triple detection GPC from Agilent Technologies with its corresponding Agilent software, dedicated to multidetector GPC calculation. The system used two PL1113-6300 ResiPore 300 × 7.5 mm columns with DMF (containing 0.1 wt % of LiCl) as the eluent with a flow rate of 0.8 mL min^{-1} and toluene as flow rate marker. The detector suite comprised a PL0390-0605390 LC light scattering detector with two diffusion angles (15° and 90°), a PL0390-06034 capillary viscometer, and a 390-LC PL0390-0601 refractive index detector. The entire SEC-HPLC system was thermostated at 35 °C. PMMA standards were used for the calibration. The typical sample concentration was 10 mg/mL.

Autoclave

The polymerizations of VDF were performed in a 100 mL Hastelloy Parr autoclave system (HC 276), equipped with a mechanical Hastelloy stirring system, a rupture disk (3000 PSI), inlet and outlet valves, and a Parr electronic controller to regulate the stirring speed and the heating. Prior to reaction, the autoclave was pressurized with 30 bar of nitrogen to check for leaks. The autoclave was then put under vacuum (20 10^{-3} bar) for 30 min to remove any trace of oxygen. A degassed solution of solvent, initiator, and CTA_{XA} was introduced via a funnel under vacuum. The reactor was then cooled down using a liquid nitrogen bath, and VDF was transferred by double weighing (i.e., mass difference before and after filling the autoclave with VDF). After warming up to ambient temperature, the autoclave was heated to the target temperature under mechanical stirring.

Synthesis

RAFT Homopolymerization of Vinylidene Fluoride (VDF) (Scheme II-3)

Using the experimental setup described above, a typical polymerization (run 5 in Table II-6) of VDF was performed as follows: A solution of Trigonox 121 (158 mg, 6.87 10^{-4} mol) and CTA_{XA} (1.30 g, 6.25 10^{-3} mol) in DMC (60 mL) was degassed by N_2 bubbling for 30 min. This homogeneous solution was introduced into the autoclave using a funnel, VDF gas (19.0 g, 0.297 mol) was transferred in the autoclave at low temperature, and the reactor was gradually heated to 73 °C. The reaction was stopped after 20 h. During the reaction, the pressure increased to a maximum of 25 bar and then decreased to 10 bar after 20 h.

The autoclave was cooled to room temperature (ca. 20 °C), purged from the residual monomers, and the dimethylcarbonate solvent was removed under vacuum. The crude product was dissolved in 30 mL of warm THF (ca. 40 °C) and left under vigorous stirring for 30 min. This polymer solution was then precipitated from 400 mL of chilled hexane. The precipitated polymer (white powder) was filtered through a filter funnel and dried under vacuum (15 10^{-3} mbar) for 2 h at 50 °C. The polymerization yield (65%) was determined gravimetrically (mass of dried precipitated polymers/mass of monomer introduced in the pressure reactor). Yields were used as conversion, since conversion is very difficult to measure accurately for VDF or other gaseous monomers.

^{1}H NMR (400 MHz $(CD_3)_2CO$, δ (ppm)) : 1.19-1.24 (d, -CH(C**H$_3$**)(C=O)-, $^{3}J_{HH}$= 7.1 Hz), 1.40-1.46 (t, -S(C=S)O-CH$_2$-C**H$_3$**, 1.65-1.85 (m, -CF$_2$-C**H$_3$**), $^{3}J_{HH}$= 7.2 Hz), 2.28-2.43 (m,-CF$_2$-C**H$_2$**-C**H$_2$**-CF$_2$-, VDF-VDF TT (tail-to-tail) reverse addition), 2.70-3.19 (t, -CF$_2$-C**H$_2$**-CF$_2$-, VDF-VDF HT (head-to-tail) regular addition), 3.60-3.69 (s, -(C=O)-O-C**H$_3$**), 4.02-4.17 (t, -CF$_2$-C**H$_2$**-S(C=S)OEt, $^{3}J_{HF}$= 18 Hz), 4.67-4.77 (q, (-S(C=S)O-C**H$_2$**-CH$_3$, $^{3}J_{HH}$= 7.2 Hz), 6.05-6.45 (tt, ^{2}J$_{HF}$= 55 Hz , $^{3}J_{HH}$= 4.6 Hz -CH$_2$-CF$_2$-**H**).

^{19}F NMR (376 MHz $(CD_3)_2CO$, δ (ppm)) : -115.63 (-CH$_2$-CF$_2$-C**F$_2$**-CH$_2$-CH$_2$-, VDF-VDF HH reverse addition), -114.29 (^{2}J$_{HF}$= 55 Hz, -CH$_2$-C**F$_2$**-H), -113.34 (-CH$_2$-C**F$_2$**-CF$_2$-CH$_2$-CH$_2$-, HH reverse addition), -113.09 (CH$_2$-CF$_2$-**CF$_2$**-CH$_2$-S-), -112.69 (-CH$_2$-**CF$_2$**-CF$_2$-CH$_2$-S-), -94.79 (-CH$_2$-CH$_2$-C**F$_2$**-CH$_2$-, TT reverse addition), -107.7 (-CF$_2$-C**H$_3$**), -93.50 (-CH$_2$-C**F$_2$**-CH$_2$-CH(CH$_3$)(C=O)-), -92.12 (-CH$_2$-C**F$_2$**-CH$_2$-CF$_2$H), -91.44 (-CH$_2$-CH$_2$-CF$_2$-CH$_2$-**CF$_2$**-CH$_2$-CF$_2$-, regular VDF-VDFHT addition), -91.00 (-CH$_2$-C**F$_2$**-CH$_2$-, regular VDF-VDF HT addition).

Computational Details

The computational work was carried out using the Gaussian09 suite of programs.[24] The geometry optimizations were performed in the gas phase without any symmetry constraint using the B3PW91 functional in combination with the 6-31G(d,p) basis functions for all atoms. The unrestricted formulation was used for all radicals, yielding negligible spin contamination in all cases. The ZPVE, PV, and TS corrections at 298 K were obtained with Gaussian09 from the solution of the nuclear equation using the standard ideal gas and harmonic approximations at T = 298.15 K, which also verified the nature of all optimized geometries as local minima or first-order saddle points. A correction of 1.95 kcal/mol was

applied to all G values to change the standard state from the gas phase (1 atm) to solution (1 M).[25]

Determination of the VDF Concentration in DMC at 73 °C under 33.1 bar.

The autoclave was put under vacuum (20 10^{-3} bar) for 30 min to remove any trace of oxygen. Dimethylcarbonate (37 g, 34.6 mL) was introduced via a funnel under vacuum. The reactor was then cooled down using a liquid nitrogen bath and VDF (21.0 g) was transferred by double weighing. The autoclave was heated up to 73 °C under stirring. After 30 min, a constant pressure of 33.1 bar was recorded. Then the autoclave was cooled down to room temperature (ca. 20 °C), purged from monomers and solvent. Exactly the same volume of lead balls (34.6 mL) was placed in the reactor, and the total weight was recorded. 17 g of VDF was then transferred into the reactor following the protocol described above, and the autoclave was heated up to 73 °C until reaching constant pressure. VDF was then progressively removed from the reactor until the pressure reached 33.1 bar. The reactor was then weighed again. The mass of VDF contained in the free volume of the reactor at P = 33.1 bar and T = 73 °C was calculated to be 9.5 g. The solubility of VDF in DMC at P = 33.1 bar and T = 73 °C was obtained as $(21 - 9.5)/(64.02 \times 34.6 \times 10^{-3}) = 5.2$ mol L^{-1}.

IV. Results and Discussion

IV.1 Assessment of the Apparent Chain Transfer Constant of VDF toward CTA_{XA}

Although RAFT polymerization was shown to efficiently control the polymerization of VDF,[19] there is a clear lack of kinetic data related to this polymerization. We thus assessed the apparent transfer constant of PVDF radicals toward *O*-ethyl-*S*-(1-methoxycarbonyl)ethyldithiocarbonate (CTA_{XA}, Scheme II-3) using O'Brien and Gornick's method (SI-Figure II-45).[26] This method gave a $C_{Tr(app)}$ value of 49 at 73 °C, confirming the efficient transfer of PVDF radicals to the RAFT chain transfer agent used. It is important to note that the transfer constant determination method used here does not take into account the reversibility of the addition onto CTA_{XA}; the real transfer constant is therefore likely higher than 49.[27] The same method used for the ITP of VDF (at 75 °C) reported $C_{Tr(app)}$ values for $HCF_2CF_2CH_2I$ and $C_6F_{13}CH_2CF_2I$ of 0.3 and 7.4 respectively.[28] These results confirm that CTA_{XA} is a much better CTA than alkyl iodides.

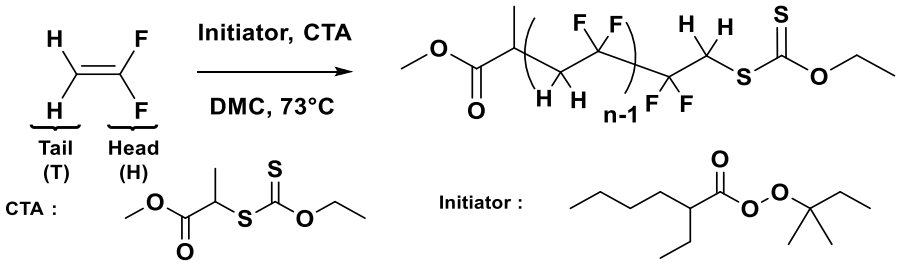

Scheme II-3: Schematic Representation of the RAFT Polymerization of VDF

IV.2 Investigation of the Ability of the RAFT Process to Produce High Molar Mass PVDF

To test the capacity of the RAFT polymerization of VDF to afford high molar mass PVDF, three polymerizations targeting different DP_n (50, 100, and 200) were examined. As reported previously,[19] HH additions were shown to lead to an accumulation of $-CF_2-CH_2$-XA terminated PVDF chains, henceforth noted as $PVDF_T$-XA (where -XA designates the *O*-ethyl xanthate group: $-SC(S)-OCH_2CH_3$). Conversely, $-CH_2CF_2$-XA-terminated chains will be noted $PVDF_H$-XA. The evolution of the PVDF chain-ends was thus carefully monitored by ^{1}H NMR[29] for each polymerization (see Table II-6 and SI-Figure II-46 for the assignment of the ^{1}H NMR signals) and compared to the corresponding first-order kinetic plots (Figure II-37).

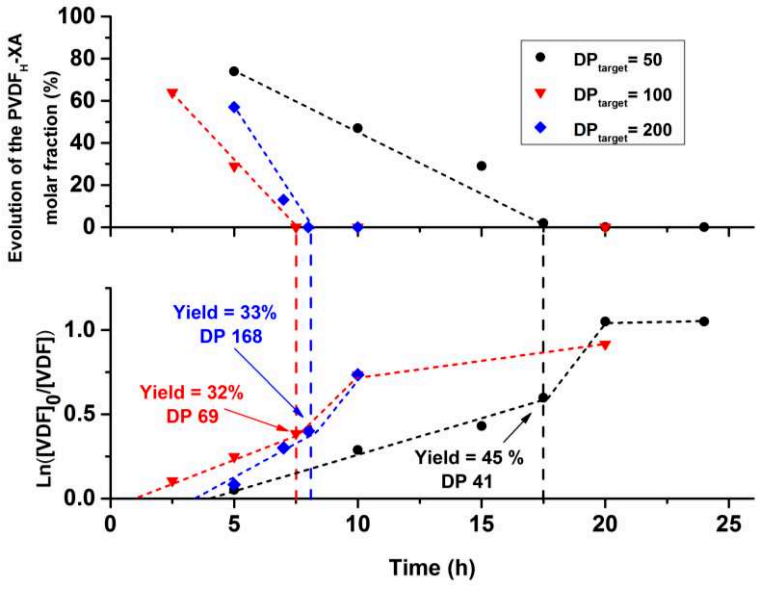

Figure II-37: Correlation between the evolution vs time of the proportion of $PVDF_H$-XA chains ($-CH_2-CF_2$-XA-terminated PVDF chains) (top) and the corresponding first-order kinetic plot (bottom) for three VDF RAFT polymerizations: $DP_{target} = 50$ (black circles), $DP_{target} = 100$ (red triangles), and $DP_{target} = 200$ (blue diamonds).

Table II-6: Experimental Conditions and Results for the RAFT polymerization of VDF in the presence of CTA_{XA}.[a]

Run	$[VDF]_0/[CTA]_0$	Reaction Time (h)	yield[a] %	$DP_{(NMR)(R)}$[b]	$M_{n(theo)}$[c] (g/mol)	$M_{n(NMR)(R)}$[d] (g/mol)	$M_{n(SEC)}$[e] (g/mol)	Đ[e]	$-CF_2-CH_2-XA$[b] %	$-CH_2-CF_2-XA$[b] %	CF_2H[b] %	$-CF_2-CH_3$[b] %	$DMC-CH_2-CF_2-$[b] %	$R-CH_2-CF_2-$[b] %
1	50	5	< 5	4	n.d.	500	800	1.05	20	74	6	0	0	100
2	51	10	25	20	1000	1500	3900	1.12	38	47	15	0	0	100
3	51	15	35	29	1400	2100	4100	1.29	60	29	11	< 1	0	100
4	47	17.5	[f]45	41	1600	2800	5300	1.30	86	2	12	< 1	0	100
5	54	20	65	47	2400	3200	7200	1.40	85	0	n.d	n.d	0	100
6	48	24	65	44	2200	3000	5000	1.42	86	0	n.d	n.d	0	100
7	100	2.5	10	7	900	700	1100	1.10	32	64	4	0	0	100
8	100	5	22	36	1700	2600	3800	1.33	54	26	16	4	0	100
9	100	7.5	[f]32	69	2300	4700	6900	1.43	71	0	25	4	4	96
10	100	10	52	92	3600	6100	8700	1.44	61	0	n.d	n.d	7	93
11	100	20	66	104	4500	6900	10100	1.50	50	0	n.d	n.d	12	88
12	200	5	8	33	1300	2400	6500	1.24	30	57	10	3	0	100
13	200	7	26	56	3600	3800	10100	1.33	63	13	21	3	<1	100
14	200	8	[f]33	168	4500	11000	17000	1.37	59	0	17	24	7	93
15	200	10	52	212	6900	13800	18000	1.41	49	0	n.d	n.d	17	83
16	n.a	16	75	n.a	n.a	n.a	12400	2.10	n.a	n.a	n.a	n.a	n.a	n.a

Reactions conditions: Chain Transfer Agent (CTA) = CTA_{XA}, Initiator (I) = Trigonox 121, [I]/[CTA] = 0.1 (runs 1-15), [I]/[VDF] = 0.005 (run 16), T = 73 °C, Solvent = DMC. [a]Determined gravimetrically. [b]Determined by ^1H NMR using SI-Equation II-12-17SI-Equation II-17. [c]Calculated using yield as conversion. [d]Calculated from $DP_{(NMR)}$. [e]Determined by SEC. [f]Point where all $PVDF_H$-XA have disappeared. n.d stands for not determined. n.a. stands for not applicable.

These kinetic plots($\ln([VDF]_0/[VDF])$ vs time) (Figure II-37, bottom) showed four polymerization regimes: *(i)* an induction period where the polymerization rate is almost negligible[30] may be caused by slow initiation of VDF by the R· radical, followed by *(ii)* polymerization at a relatively slow rate (which increases upon decreasing $[VDF]_0/[CTA]_0$ ratios as is often observed during RAFT polymerizations),[31] *(iii)* a significant increase in the rate of polymerization, and *(iv)* a plateau where the polymerization progresses very slowly or even stops. This plateau, which had not been described in earlier reports, occurs at similar VDF conversions (ca. 65%) and may be caused by the pressure drop inside the reactor below the vapor pressure (and critical pressure) of VDF, which decreases the VDF concentration in solution. The other three phases observed in the RAFT polymerizations of VDF have been described before.[19] However, the sharp increase in the rate of polymerization had been tentatively explained by an increase in the local VDF concentration caused by a change in the solubility of PVDF upon increase of its molar mass. The correlation between the evolution of

$PVDF_H$-XA chains and the polymerization kinetics presented here (Figure II-37) proves this interpretation to be incorrect, even though PVDF is indeed insoluble in DMC, even at 73 °C. Figure II-37 clearly shows that the sharp increase in the rate of polymerization starts exactly when all the PVDF chains have been converted into $PVDF_T$-XA chains (at t = 17.5 h for DP_{target} = 50, t = 7.5 h for DP_{target} = 100, and t = 8 h for DP_{target} = 200). This observation thus rather suggests that the polymerization rate increase is related to a change in the polymerization mechanism. These PVDF chains terminated by an inversely added VDF unit are believed[14,19,22] to be quasiunreactive vis-à-vis the degenerative chain transfer process at the heart of RAFT or ITP. It follows that the degenerative chain transfer (DT) should stop (or become negligible) when the last $PVDF_H$-XA chain has disappeared. If this were true, at this stage the remaining radicals and the newly formed radicals (from the thermal initiator) should have no choice but to polymerize the remaining VDF via free radical polymerization, thus forming PVDF chains that do not bear either R- or Zgroup from the CTA.

This change in the polymerization mechanism from DT to free radical polymerization should also be observed in the plots of the evolutions of molar mass and dispersity versus conversion.

Figure II-38) and in the evolution of the GPC traces versus conversion (Figure II-39).

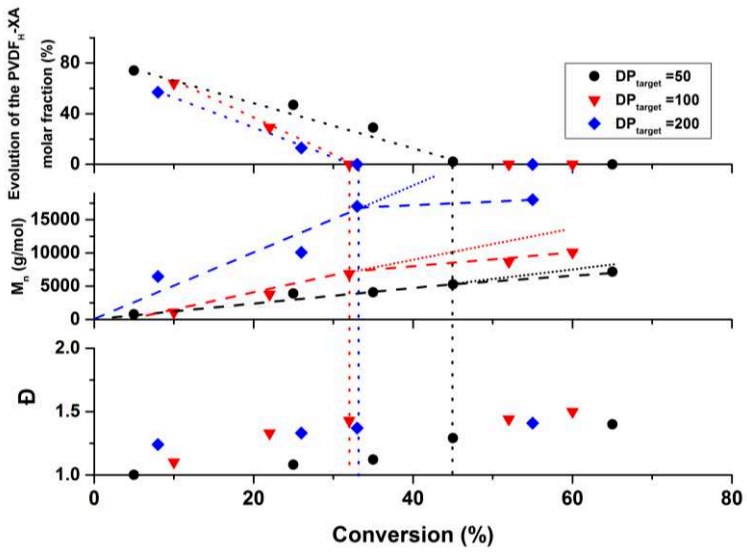

Figure II-38: Correlation between the evolution of the proportion of PVDFH-XA chains (top), of the molar mass (middle), and of the dispersity vs conversion for three VDF RAFT polymerizations: DPtarget = 50 (black circles), 100 (red triangles), and 200 (blue diamonds). Molar masses and dispersity were determined by GPC. Vertical dotted and dashed lines underline the mechanistic transition occurring when all the PVDFH-XA chains have been converted into PVDFT-XA chains.

Figure II-38 does show a slope change in the molar mass evolution versus conversion after the disappearance of the last $PVDF_H$-XA (at conversion = 45% for DP_{target} = 50, 32% for DP_{target} = 100, and 33% for DP_{target} = 200). However, this slope change is toward a slower increase of molar masses with conversion and it is not accompanied by a significant dispersity increase. If free radical polymerization was indeed taking place instead of RAFT polymerization, higher molar masses and dispersities would be expected (run 16, Table II-6).

The evolution of the GPC chromatograms versus conversion (Figure II-39) is also affected by the disappearance of the $PVDF_H$-XA chains. After the transition point (where all xanthate-terminated PVDF chains are $PVDF_T$-XA), the maximum of the chromatograms (M_p) no longer increases monotonously with conversion as it would under an RDRP mechanism.

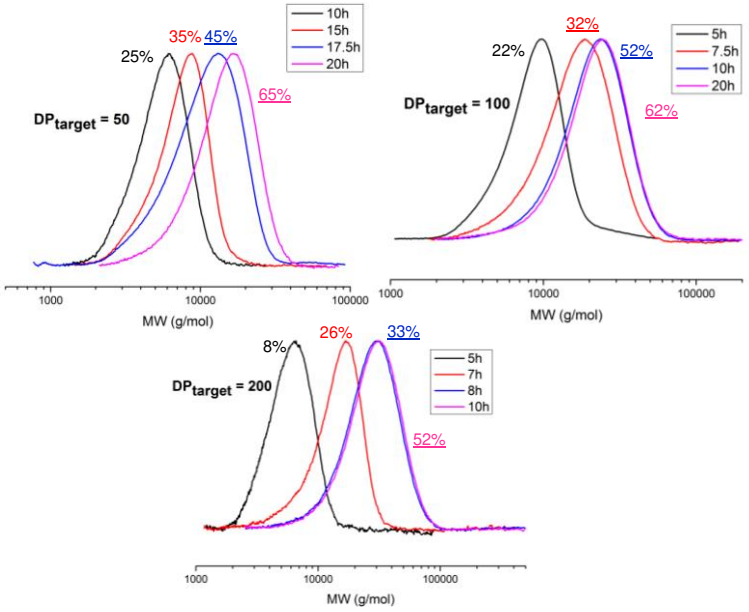

Figure II-39: DMF GPC chromatograms of PVDF prepared by RAFT and targeting three degrees of polymerization: DP_{target} = 50 (top left), DP_{target} = 100 (top right), and DP_{target} = 200 (bottom). Corresponding conversions are shown next to each trace. The underlined conversions correspond to points where the polymerization medium no longer contains any $PVDF_H$-XA.

This is consistent with the end of the DT-controlled chain growth. However, continuation of monomer conversion by free radical polymerization should generate high molar mass new polymer chains, which should appear as secondary molar mass distributions in the chromatograms. Indeed, after the transition points, the polymerizations converted about 20% of VDF. If these polymerizations proceeded by a free radical mechanism, this would imply that the GPC traces of the final PVDF (Figure II-39) correspond to mixtures of PVDF produced by RAFT polymerization and of PVDF produced by free radical polymerization in the following wt % proportions: 69/31 (for DP_{target} = 50), 48/52 (for DP_{target} = 100), and 63/37

(for DP_{target} = 200). Moreover, the VDF/initiator molar ratios at the transition points were calculated to be 840 (DP_{target} = 50), 1030 (DP_{target} = 100), and 2100 (DP_{target} = 200). Such significant ratios and conversions would undoubtedly yield PVDF of high molar mass and broad dispersity.

Such additional high molar mass distributions are not observed, not even as shoulders of the main distribution. These observations (or lack thereof) suggest that beyond the transition point, the VDF polymerization proceeds neither under control by an RDRP mechanism nor as a pure free the propagation, chain inversion, and reactivation rates were investigated using DFT calculations (vide infra). Regardless of this mechanistic transition and its origin, the present study shows that higher molar mass, well-defined PVDF can be prepared using RAFT polymerization. Well-defined PVDF with DP = 41, 69, and 168 were synthesized when DP = 50, 100, and 200 were targeted, respectively (Figure II-37 and Table II-6). However, the study clearly shows that well-controlled PVDF (i.e., with optimum chain-end functionality and containing only negligible quantities of polymer chains formed after the transition point) can only be prepared at relatively low VDF conversion and that the preparation of well-defined high molar mass PVDF can only be done at the detriment of conversion. Indeed, the disappearance of the last $PVDF_H$-XA chain occurs at a conversion around 45% for DP_{target} = 50 and ca. 33 % for DP_{target} = 100 or 200 (Figure II-37 and

Figure II-38).

IV.3 Study of the Chain Defects Evolution during the RAFT Polymerization of VDF

The evolution of the chain defects (head-to-head and tail-to-tail additions) proportion as a function of conversion was also monitored. Since the proportion of defects in PVDF only depends on the reaction temperature,[32] longer chains should display a higher number of intrachain defects than shorter chains prepared at the same temperature. Indeed, the average number of monomer additions occurring per chain between two degenerative transfers increases with increasing $[VDF]_0/[CTA]_0$ initial ratios. Figure II-40 shows the plots of the proportion of intrachain and total HH additions versus conversion. As expected, the amount of intrachain VDF HH additions increases with conversion and with increasing targeted degree of polymerizations (DP_{target}).

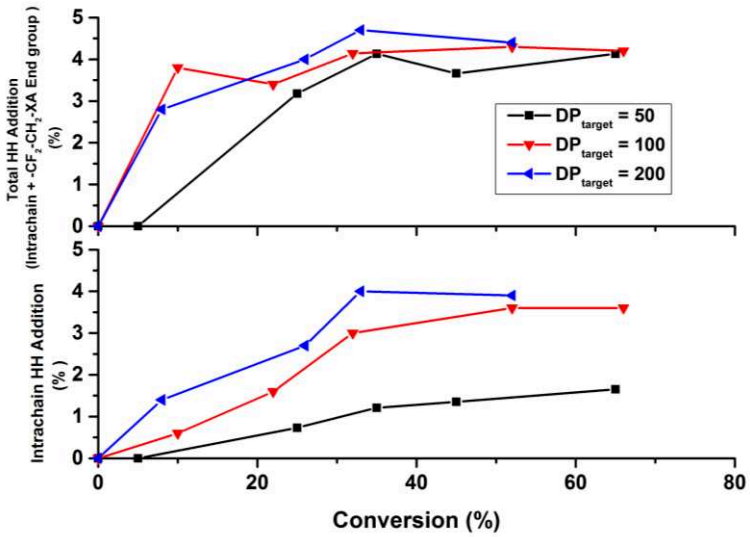

Figure II-40: Evolution of the proportion of intrachain (bottom) and total (top) HH VDF additions vs conversion for three RAFT polymerizations of VDF: DP_{target} = 50 (black squares), DP_{target} = 100 (red triangles) and DP_{target} = 200 (blue triangles).

The total amount of HH VDF additions (intrachain + chain-end) stabilizes to identical proportion (ca. 4.1%) for the three polymerizations examined. This value is in good agreement with the previously reported proportion of defects for polymerizations carried out at similar temperatures.[32,33]

IV.4 Evolution of the Functionality of PVDF Chains Prepared by RAFT

Finally, we monitored by NMR the evolutions of all chain-end groups for the PVDF made by RAFT polymerization with DP_{target} = 50, 100 and 200.The results of this investigation are summarized in Figure II-41. As observed and reported before,[19] $PVDF_H$-XA are progressively converted into $PVDF_T$-XA, and the overall end-group functionality decreases due to a slowly increasing amount of transfer to DMC (H-abstraction). Whereas new polymer chains initiated by the resulting DMC radicals were not observed in our previous study, here on the contrary, DMC-initiated PVDF chains were detected, but only significantly after all the PVDF chains were converted into $PVDF_T$-XA (SI-Figure II-47). These chains give ^{1}H NMR signals characteristic of the CH_3 (singlet at 3.73 ppm) and of the CH_2 (triplet at 3.34 ppm) protons of the CH_3-O(C=O)-O-CH_2-PVDF α-end-group (SI-Figure II-46). Remarkably, the DMC radicals seemed to add exclusively onto the CH_2 of VDF.

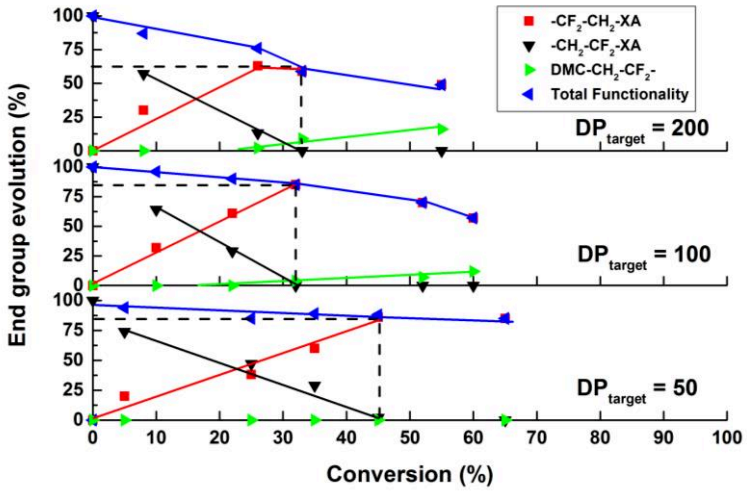

Figure II-41: Evolution of the PVDF chains end-group functionality (-CH_2-CF_2-XA ($PVDF_H$-XA), -CF_2-CH_2-XA, ($PVDF_T$-XA)) and of the proportion of DMC-initiated PVDF chains vs time for three RAFT polymerizations of VDF: DP_{target} = 50 (bottom), DP_{target} = 100 (middle), and DP_{target} = 200 (top).

The formation of these DMC-initiated PVDF chains is accompanied by a progressive disappearance of the chain-ends (loss of xanthate group) of the $PVDF_T$-XA chains. These phenomena start with the mechanistic transition mentioned above (Figure II-37 and Figure II-41). The formation of increasing amounts of -CF_2-CH_3 end-groups after this transition (SI-Figure II-46 and SI-Figure II-48) was also detected. These observations suggest that after the mechanism transition, transfer to DMC becomes more prevalent and that the thus-formed DMC radicals not only initiate new PVDF chains but also readily remove the xanthate groups from the $PVDF_T$-XA chains. This transfer reaction, however, seems to be irreversible and to lead to small DMC-xanthate adducts that are removed from the final polymer upon purification by precipitation, as shown previously.[19]

IV.5 Computational Study

IV.5.1 General Considerations, Choice of Models, and Computation Level.

The above-described, unexpected experimental findings raised several mechanistic questions, the most important one being to understand what happens when all PVDF chains are converted into $PVDF_T$-XA. To shed light on this phenomenon, DFT calculations were carried out on model systems. Previous studies have amply demonstrated the value of DFT for rationalizing unexpected phenomena in RDRP, particularly in RAFT,[34] ATRP,[35] OMRP,[36] and NMP.[37] Calculations on the polymerization of VDF by the RAFT method have not been previously reported, to the best of our knowledge.

To keep the calculations manageable in terms of computational effort while obtaining results of indicative value, the polymer chains were simplified to an H atom beyond the terminal monomer unit. Thus, the PVDF−CH_2CF_2· (or $PVDF_H$·) and PVDF−CF_2CH_2· (or $PVDF_T$·) chains were modeled by CH_3CF_2· and CHF_2CH_2·, respectively. In the xanthate group, for the same reason of computation economy, the ethyl substituent was simplified to a methyl group, -SC(S)OCH_3. These structural modifications are not expected to introduce any major electronic change (polarity, hemolytic strength) or steric effect in the bonds that are involved in the computed processes.

It must be emphasized that the main objective of the computational approach is not that of quantitatively reproducing observed data, but rather to provide insight into the occurring chemical processes. The values of DFT-calculated energy changes associated with chemical processes rarely deviate by less than a couple of kcal/mol from the experimentally available ones. DFT calculations provide better information when comparing data for closely related systems because energy trends are reproduced more faithfully than absolute values. For this reason, we have not made a major effort in testing a variety of different functionals and basis sets in order to choose the most suitable method for the systems of interest. The theory level selected for our study (B3PW91/6-31G(d,p)) is commonly used for high-level calculations on organic and organometallic systems. However, we have initially benchmarked this method against available experimental data. All the results obtained from the computational study (energy, enthalpy, and Gibbs energy at 298.15 K, Gibbs energy extrapolated to 343.5 K, Cartesian coordinates, and views of the optimized geometries) are collected in tabular form in the VIII-Supporting Information.

IV.5.2 Benchmarking on VDF Free Radical Propagation

The values of $k_p/k_t^{1/2}$ (0.14 $L^{1/2}$ $mol^{-1/2}$ $s^{-1/2}$ in 1,1,1,3,3- pentafluorobutane at 74 °C)[28] and k_p (19 400 L mol^{-1} s^{-1} at 60 °C and 1000 bar in supercritical CO_2)[38] for the VDF polymerization have been reported, but individual k_p and k_t values in solution are not available to the best of our knowledge. Notably, it would have been interesting to compare the calculated propagation Gibbs energy barrier ($\Delta G_p^{\ddagger}$) with that derived from k_p using the Eyring equation. However, it is experimentally known that the most probable chain carrier is $PVDF_H$· and that the most probable monomer addition mode is HT, conserving the nature of this reactive chain end, while the HH dyads are present only at a level of 3.5−6 %.[32,39] We have calculated the

profiles for all four possible types of radical addition to monomer, as shown in Figure II-42. Figure II-42a illustrates the energy profiles for the $PVDF_H$· model radical additions to VDF in both HT and HH modes, while Figure II-42b shows the profiles for the TH and TT additions of the $PVDF_T$· model radical.

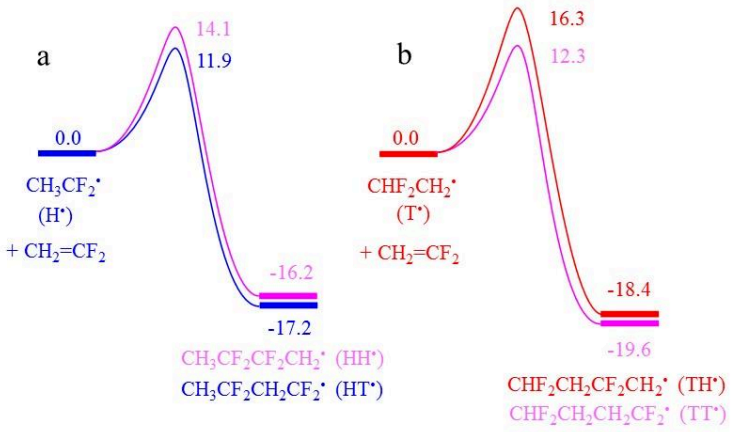

Figure II-42: Energy profiles for (a) the HT and HH additions of the $PVDF_H$• model radical, and (b) the TH and TT additions of the $PVDF_T$• model radical to VDF. The reported values are $\Delta G°_{298.15}$ (1 M standard state) in kcal/mol.

Of all four possible addition modes, the lowest barrier is indeed, as known from the experimental evidence, that of the HT addition (11.9 kcal/mol), while the barrier of the alternative HH addition is ca. 2.2 kcal/mol higher (14.1 kcal/ mol). This $\Delta(\Delta G)$ allows the prediction of a 2.4% HH error probability at 298.15 K or 3.2% after extrapolation of $\Delta(\Delta G)$ to the polymerization temperature (73 °C). These values are quite consistent with the experiment. The energy difference between the two isomeric HT and HH transition states is carried over to the isomeric products. This difference results from the different C-C bond strengths of the CF_2-CH_2 and the CF_2-CF_2 bonds formed by HT and HH coupling, respectively, and/or from the different stabilization of the resulting CH_2· and CF_2·radicals. Concerning the $PVDF_T$· model radical addition, the TT mode is more favored (12.3 kcal/mol) than the TH mode (16.3 kcal/mol). This is again in line with the experimental evidence, since the HT/HH/TT triad is by far much more frequent than the HT/HH/TH triad. This latter triad has indeed never been detected by NMR spectroscopy. Hence, generation of an inverted radical chain end is more likely followed by a TT addition (98.8% probability according to the calculated barriers) to regenerate the preferred $PVDF_H$· chain end. Similar results were also previously obtained, in reference to an uncontrolled VDF telomerization process, at a slightly different computational level (using the B3LYP functional) and with use of CF_3

instead of H as chain end.[40] The *E* barriers reported here with the use of B3PW91 are slightly and systematically smaller (by 0.5-1.5 kcal/mol) than those obtained with B3LYP, but their relative order is the same for both investigations: $\Delta E^{\ddagger}_{p,TT} < \Delta E^{\ddagger}_{p,HT} < \Delta E^{\ddagger}_{p,HH} < \Delta E^{\ddagger}_{p,TH}$.

From our calculated $\Delta G^{\ddagger}_{p,HT}$, a $k_{p,HT}$ value of 1.1 10^4 L mol^{-1} s^{-1} can be derived at 298.15, which becomes 2.3 10^4 L mol^{-1} s^{-1} after extrapolation of $\Delta G^{\ddagger}_{p,HT}$ to the polymerization temperature. This value is actually quite close to that reported by Beueurmann et al. (1.94 10^4 L mol^{-1} s^{-1}) in *sc*CO_2.[38] It also appears reasonable when compared for instance with those reported for tetrafluoroethylene (7.4 10^3 L mol^{-1} s^{-1} at 40 °C)[41] and ethylene (470 L mol^{-1} s^{-1} at 83 °C in benzene).[42] This agreement encouraged us to continue the computational exploration using this level of theory.

IV.5.3 Bond Strengths

The calculated homolytic bond dissociation enthalpy (BDE, $\Delta H°_{298.15}$), in kcal/mol, is 54.5 for CH_3CF_2-XA and 60.7 for CHF_2CH_2-XA, confirming the common perception that the bond is stronger in the T-terminated dormant species obtained after an inverted (HH) monomer addition. The difference between the BDE of the T- and H-terminated dormant chain models almost exactly matches the energy difference of the isomeric radicals: the calculated standard enthalpy of $CHF_2CH_2\cdot$ is 6.6 kcal/mol higher than that of CH_3CF_2. Consequently, the isomeric CTA models are essentially isoenergetic (CH_3CF_2-XA is more stable than CHF_2CH_2-XA by 0.8 kcal/mol; see Figure II-43).

IV.5.4 MacroCTA $PVDF_H$-XA and $PVDF_T$-XA Reactivation: Degenerative and Nondegenerative Chain Transfer.

The computational results on the chain transfer pathway are summarized in Figure II-44. The $CH_3CF_2\cdot$ radical, model of the more probable $PVDF_H\cdot$, adds to the model of the more probable $PVDF_H$-XA macroCTA to undergo degenerative radical exchange via a symmetric CH_3CF_2-SC(OMe)S-CF_2CH_3 intermediate, requiring only 9.0 kcal/mol in activation Gibbs energy. The symmetric intermediate is nearly isoenergetic with the fragmented starting and final degenerate CTA/radical pairs. The nondegenerative exchange leading from the same $PVDF_H$-XA model and the $CHF_2CH_2\cdot$ model of $PVDF_T\cdot$ to the exchanged partners CHF_2CH_2-XA and $CH_3CF_2\cdot$ is thermodynamically favorable because it transforms the more energetic radical to its more stable isomer, whereas the two dormant species are

approximately isoenergetic, as shown in the IV.5.3-Bond Strengths section. This exchange requires an activation Gibbs energy of 9.0 kcal/mol, *i.e.,* the same as for the degenerative exchange of the $PVDF_H\cdot$ radical, and leads to the new partners pair, 6.1 kcal/mol lower in energy. The reverse reactivation of CHF_2CH_2-XA by $CH_3CF_2\cdot$ has a greater associated barrier, 15.1 kcal/mol. Finally, $CHF_2CH_2\cdot$ undergoes degenerative exchange with CHF_2CH_2-XA (red curve in Figure II-44) with an activation barrier of 9.5 kcal/mol.

IV.5.5 Discussion

The lower barrier for the $PVDF_H\cdot$ degenerative chain transfer (9.0 kcal/mol) relative to HT propagation (11.9 kcal/mol, cf. Figure II-44 and Figure II-42) agrees with the experimental observation of efficient control in degenerate transfer polymerization, so long as the growing chain remains $PVDF_H\cdot$. The calculated rate constant ratio k_{CT}/k_p is 1.3 10^2 at 298.15 K according to the Eyring equation. After extrapolation of the two Gibbs energy barriers to the polymerization temperature (73 °C), this ratio is reduced to 70 (k_{CT} increases less than k_p at higher temperatures because the chain transfer activation barrier is characterized by a greater entropy decrease relative to the propagation activation barrier). Actually, the parameters to be compared are the rates, not the rate constants. Since $v_{CT} = k_{CT}[R\cdot][CTA]$ and $v_p = k_p[R\cdot][M]$, the rate ratio depends not only on the rate constant ratio but also on the concentration ratio: $v_{CT}/v_p = (k_{CT}/k_p)\cdot([CTA]/[M])$. A problem in VDF polymerization is that the system is biphasic. The gaseous monomer is only partly dissolved in the polymerization solvent (DMC) where the CTA and macroradical react, and the monomer solubility in this condensed phase was not previously reported. Therefore, we have measured the concentration under conditions close to those of the polymerization (DMC at 70 °C and 33.1 bar; see details in the III-Experimental Section) and found it to be 5.2 mol/L. Thus, although this is a significant concentration, it is unlikely that all the monomer is completely dissolved in the reaction medium; hence [CTA]/[M] > 0.01 for a target DP of 100. The calculated rate ratio would predict comparable rates of chain transfer and propagation, in agreement with a reasonably controlled system.

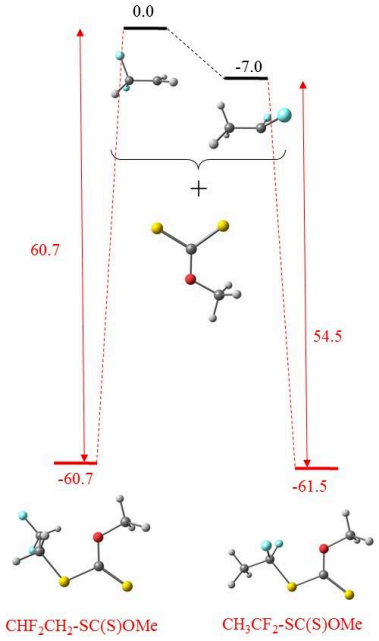

Figure II-43: Relative energies and views of the optimized geometries of the isomeric $CHF_2CH_2^{\bullet}$ and $CH_3CF_2^{\bullet}$ radicals, the $(MeO)C(S)S^{\bullet}$ radical, and the corresponding adducts. The values are the standard enthalpies ($\Delta H°_{298.15}$) in kcal/mol.

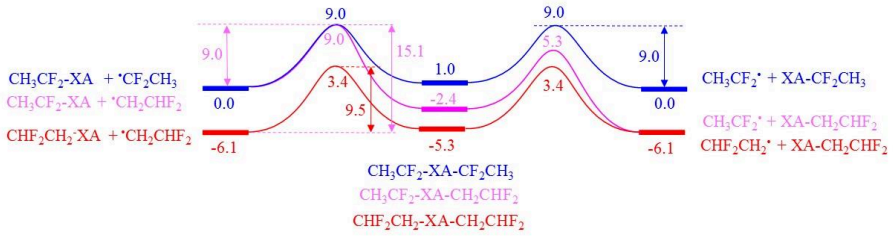

Figure II-44: Energy profiles for the degenerative (H/H and T/T) and non-degenerative (H/T) radical exchange with the dormant chain. The reported values are $\Delta G°_{298.15}$ in kcal/mol.

The major point of interest in this study is the question of the $PVDF_T$-XA reactivation after an inverted monomer addition. This can in principle occur by exchange with either the more abundant $PVDF_H$· radicals or with the $PVDF_T$· radicals. The former has a calculated barrier of 15.1 kcal/mol for the model system. This does not mean that this reactivation cannot occur because this barrier yields a rate constant of 54 M^{-1} s^{-1} under standard conditions, by application of the Eyring relationship. However, after the endothermic nondegenerative head-tail chain transfer process ($\Delta G°_{CT,HT}$ = 6.1 kcal/mol at 298.15 K, $K_{CT,HT}$= 3.4 10^{-5} from the van't Hoff equation), the resulting free tail radicals can be back-trapped with a lower barrier (9.0 kcal/mol) than the subsequent addition to monomer ($\Delta G^{\ddagger}_{p,TT}$ = 12.3 kcal/mol for the more favorable TT addition) needed to re-enter the regular $PVDF_H$· chain growth process.

The Gibbs energy span is thus ($\Delta G°_{CT,HT} + \Delta G^{\ddagger}_{p,TT}$ = 18.4 kcal/mol), which can be extrapolated to 20.1 kcal/mol at 343.15 K, leading to the prediction of an effective activation rate constant $k_{Exch,TH}$ (corresponding to $Kk_{p,TT}$) for the $PVDF_T$-XA chains in VDF homopolymerization of 1.2 $M^{-1}s^{-1}$. Thus, in contrast to what is commonly believed, $PVDF_T$-XA chains cannot be considered dead because the rate constant of their reactivation is significant. Using the estimated [VDF] given above (5.2 M), for instance, a pseudo-first-order decay of ≈ 6 s^{-1} can be calculated for a half-life of ≈ 0.1 s, which naturally increases as the [VDF] is lowered at higher conversions. Although not negligible, this reactivation rate is nevertheless slower by 4 orders of magnitude than the reactivation of the $PVDF_H$-XA chains by the degenerative transfer and also slower than the rate at which the $PVDF_H·$ chains are converted to $PVDF_T·$ by the head-to-head propagation (Figure II-42): $k_{p,HH}$= 6.1 10^2 M^{-1} s^{-1}; $k_{Exch,TH}/k_{p,HH}$ = 2 10^{-3}. This is in agreement with the accumulation of the $PVDF_T$-XA macroCTA as conversion increases.

This relatively slow reactivation would also explain the loss of control observed experimentally when all xanthate-terminated PVDF chains have been converted into $PVDF_T$-XA. However, as alluded to above, the $PVDF_T$-XA dormant chains may also be reactivated by the less numerous $PVDF_T·$ radicals by a degenerative tail−tail process with a lower activation barrier (9.5 kcal/mol), see Figure II-44, for which the estimated rate constant at the polymerization temperature is $k_{Exch,TT}$ = 4.6·10^5 M^{-1} s^{-1}. The relative rates of TT degenerative exchange and TH nondegenerative exchange can be calculated as follows:

$$v_{Exch,TT}/v_{Exch,HT} = (k_{Exch,TT}/k_{Exch,HT})([PVDF_T·]/[PVDF_H·])$$

where the $k_{Exch,TT}/k_{Exch,HT}$ rate constant ratio is 3.8 10^5 and $[PVDF_T·]/[PVDF_H·]$ can be estimated as 0.04, considering a proportion of HH addition of 4% at 343 K. Thus, this calculation yields $v_{Exch,TT}/v_{Exch,HT}$ = 1.5 10^4. Counterintuitively, and in spite of the non-negligible rate constant of the nondegenerate reactivation of $PVDF_T$-XA by $PVDF_H·$ radicals, the computational investigation suggests that the $PVDF_T$-XA chains are actually reactivated much faster by the minority $PVDF_T·$ radicals.

The controlled nature of the VDF polymerization can be appreciated from the comparison of the rate of propagation and the rate of exchange. The rate of propagation would still be dominated by the HT addition, after release of the dormant $PVDF_T$ chain which is converted

into a $PVDF_H\cdot$ radical by the first TT addition: $v_{p,HT} = (1.9\ 10^4\ M^{-1}\ s^{-1})[PVDF_H\cdot][VDF]$. The faster rate of exchange is $v_{Exch,TT} = (4.6\ 10^5\ M^{-1}s^{-1})[PVDF_T\cdot][PVDF_T\text{-XA}]$. By introducing $[PVDFT\cdot] = 0.04[PVDF_H\cdot]$, we derive $v_{p,HT}/v_{Exch,TT} \approx 1.0[VDF]/[PVDF_T\text{-XA}]$. Given that the monomer concentration is greater than the $PVDF_T$-XA concentration, even when the monomer is partially consumed and 100% of the macroCTA is in the $PVDF_T$-XA form, this calculation predicts a much faster propagation than the rate of radical exchange, and thus a loss of control. Scheme II-4 summarizes all the findings of this study.

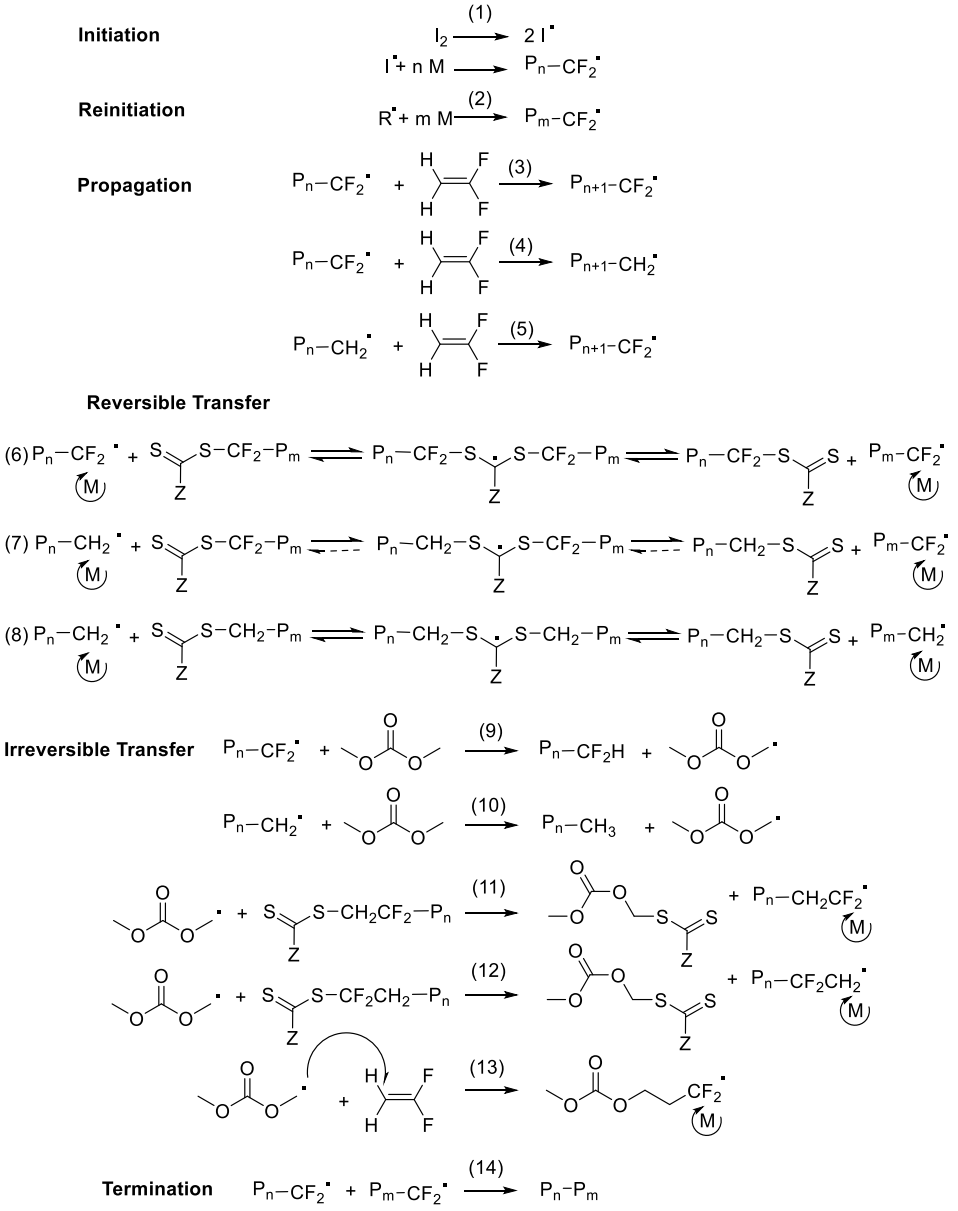

Scheme II-4: Reactions occurring during the RAFT polymerization of VDF.

The VDF RAFT polymerization in DMC gradually leads to the accumulation of $PVDF_T$-XA macroCTA (eqs 4 and 7, Scheme II-4) and undergoes a mechanistic transition from a controlled DT mechanism to an uncontrolled DT mechanism (a DT mechanism too slow to provide control) when no more $PVDF_H$-XA macroCTA remains. During the uncontrolled phase of the polymerization, DT still occurs, but only between the $PVDF_T$-XA macroCTA and the $PVDF_T$· radicals, which are present at low concentration (eq 8, Scheme II-4). The non-DT exchange (eq 7, Scheme II-4), although theoretically nonnegligible, likely does not occur due to a much lower rate compared to the DT exchange between HH-terminated PVDF chains. In addition, during that phase, transfer to DMC (eqs 9 and 10, Scheme II-4) becomes more prominent, and reactions such as chain initiation by DMC radical (eq 13, Scheme II-4) or irreversible exchange between DMC radical and PVDF-XA (eqs 11 and 12, Scheme II-4), which were almost insignificant during the controlled phase of the polymerization, occur more frequently with a growing impact on the PVDF functionality.

V. Conclusion

This study demonstrates that RAFT polymerization of VDF can be used to efficiently prepare well-defined PVDF with high end-group functionality and over a relatively large range of molar masses in spite of the unavoidable accumulation of less reactive $PVDF_T$-XA chains formed by head-to-head VDF addition. However, well-defined high molar mass PVDF can only be prepared at relatively low conversions (<ca. 30%). Indeed, this work shows that controlled polymerization, via a DT mechanism with a sufficiently fast radical exchange, only occurs while regioregularly ended $PVDF_H$-XA chains are still present. When all the xanthate-terminated PVDF chains have been converted into $PVDF_T$-XA chains, the degenerative transfer mechanism slows down dramatically, although it does not stop completely, resulting in a significant loss of polymerization controllability, as the xanthate group exchange rate becomes slower than the propagation rate. DFT calculations suggest that contrary to common belief, the $PVDF_T$-XA dormant chains are not dead and can be reactivated at a non-negligible rate. They further indicate that this reactivation occurs primarily via degenerative transfer with the $PVDF_T$· radicals, in spite of their lower concentrations. In addition, the present study suggests that chain transfer to the solvent, DMC, may be responsible for additional detrimental reactions after the full conversion of all the PVDF active chains into the less reactive $PVDF_T$-XA chains. The resulting DMC radicals seem to both readily initiate new PVDF chains and exchange with the $PVDF_T$-XA chains, thus decreasing the overall end-

group functionality of the final PVDF. In summary, the RAFT polymerization of VDF proceeds through two consecutive regimes marked by a sharp kinetic transition. In the first regime, both $PVDF_H$-XA and $PVDF_T$-XA coexist and polymerize at different rates. $PVDF_H$-XA chains are involved in fast DT mechanism which leads to PVDF with low dispersity, while the $PVDF_T$-XA chains polymerize via a much slower DT mechanism which causes a broadening of the molar masses distribution of the resulting PVDF. In the second part of the polymerization, only the $PVDF_T$-XA chains remain, the slower exchange of which is not sufficient to ensure good control of the polymerization. This study provides a much better understanding of the RAFT polymerization of VDF and clearly delineates the limits of this polymerization technique. Finally, it unambiguously refutes the common belief that the $PVDF_T$-XA chains cannot be reactivated and thus questions the robustness of other RDRP techniques such as ITP, which are also affected by chain inversions of monomers such as vinyl acetate and VDF.

VI. Acknowledgements

The authors thank Arkema (Pierre Bénite, France) for providing VDF and the French Ministry of Science and Technology for the Ph.D. grant attributed to M.G.

VII. References

[1] (a) D. W. Smith, S. T. Iacono, S. I. Suresh,. In *Handbook of Fluoropolymers Science and Technology, Ed.,* John Wiley and Sons: New York, 2014. (b) J. Gardiner, *J. Aust. J. Chem.,* 2015, **68**, 13-22.

[2] B. Ameduri, B. Boutevin, In *Well-Architectured Fluoropolymers: Synthesis, Properties and Applications*, Elsevier: Amsterdam, 2004.

[3] Tatemoto, M. *In The First Regular Meeting of Soviet-Japanese Fluorine Chemists,* Tokyo, Japan, February 15−16, 1979.

[4] W. R. Jr. Dolbier, *Chem. Rev.,* 1996, **96**, 1557-1584.

[5] Z. Cui, E. Drioli, Y. M. Lee, *Prog. Polym. Sc.,* 2014, **39**, 164-198.

[6] T. Soulestin, V. Ladmiral, T. Lannuzel, F. Domingues Dos Santos, B. Ameduri, *Macromolecules*, 2015, **48**, 7861-7871.

[7] I. Katsouras, K. Asadi, M. Li, T. B. van Driel, K. S. Kjær, D. Zhao, T. Lenz, Y. Gu, P. W. M. Blom, D. Damjanovic, M. M. Nielsen, D. M. de Leeuw, *Nat. Mater*., 2016, **15**, 78-84.

[8] B. Ameduri, *Chem. Rev.,* 2009, **109**, 6632-6686.

[9] B. Ameduri, *Macromolecules,* 2010, **43**, 10163-10184.

[10] G. David ; C. Boyer, J. Tonnar, B. Ameduri, P. Lacroix-Desmazes, B. Boutevin, *Chem. Rev.,* 2006, **106**, 3936-3962.

[11] M. R. Hill, R. N. Carmean, B. S. Sumerlin, *Macromolecules,* 2015, **48**, 5459-5469.

[12] L. Liu, D. Lu, H. Wang, Q. Dong, P. Wang, R. Bai, *Chem. Commun*., 2011, **47**, 7839-7841.

[13] G. Kostov, F. Boschet, J. Buller, L. Badache, S. Brandsadter, B. Ameduri, *Macromolecules,* 2011, **44**, 1841−1855.

[14] A. D. Asandei, O. I. Adebolu, C. P. Simpson, *J. Am. Chem. Soc*., 2012, **134**, 6080−6083.

[15] E. Girard, J. D. Marty, B. Ameduri, M. Destarac, *ACS Macro Lett.,* 2012, **1,** 270−274.

[16] P. Wang, J. Dai, L. Liu, Q. Dong, B. Jinand R. Bai, *Polym. Chem*., 2013, **4**, 1760-1764.

[17] A. D. Asandei, O. I. Adebolu, C. P. Simpson, C. P.; J. S. Kim, *Angew. Chem., Int. Ed*., 2013, **52**, 10027−10030.

[18] Y. Patil, B. Ameduri, *Polym. Chem*., 2013, **4**, 2783−2799.

[19] M. Guerre, B. Campagne, O. Gimello, K. Parra, B. Ameduri, V. Ladmiral, *Macromolecules,* 2015, **48**, 7810-7822.

[20] A. D. Asandei, *Chem. Rev.,* 2016, **116**, 2244-2274.

[21] M. Guerre, B. Ameduri, V. Ladmiral, *Polym. Che.,* 2016, **7**, 441-450.

[22] C. Boyer, D. Valade, L. Sauguet, B. Ameduri, B. Boutevin, *Macromolecules*, 2005, **38,** 10353-10362.

[23] X. Liu, O. Coutelier, S. Harrisson, T. Tassaing, J-D. Marty, M. Destarac, *ACS Macro Lett.,* 2015, **4**, 89-93.

[24] M. J. Frisch, G. W. Trucks, H. B. Schlegel, G. E. Scuseria, M. A. Robb, J. R. Cheeseman, G. Scalmani, V. Barone, B. Mennucci, G. A. Petersson, H. Nakatsuji, M. Caricato, X. Li, H. P. Hratchian, A. F. Izmaylov, J. Bloino, G. Zheng, J. L. Sonnenberg, M. Hada, M. Ehara, K. Toyota, R. Fukuda, J. Hasegawa, M. Ishida, T. Nakajima, Y. Honda, O. Kitao, H. Nakai, T. Vreven, J. A. Montgomery Jr., J. E. Peralta, F. Ogliaro, M. Bearpark, J. J. Heyd, E. Brothers, K. N. Kudin, V. N. Staroverov, R. Kobayashi, J. Normand, K. Raghavachari, A. Rendell, J. C. Burant, S. S. Iyengar, J. Tomasi, M. Cossi, N. Rega, J. M. Millam, M. Klene, J. E. Knox, J. B. Cross, V. Bakken, C. Adamo, J. Jaramillo, R. Gomperts, R. E. Stratmann, O. Yazyev, A. J. Austin, R. Cammi, C. Pomelli, J. W. Ochterski, R. L. Martin, K. Morokuma, V. G. Zakrzewski, G. A. Voth, P. Salvador, J. J. Dannenberg, S. Dapprich, A. D. Daniels, Ö. Farkas, J. B. Foresman, J. V. Ortiz, J. Cioslowski and D. J. Fox, Gaussian, Inc., Wallingford, CT, 2009.

[25] V. S. Bryantsev, M. S. Diallo and W. A. Goddard III, *J. Phys. Chem. B*, 2008, **112**, 9709‑9719.

[26] J. L. O'Brien, F. Gornick, *J. Am. Chem. Soc.,* 1955, **77**, 4757.

[27] G. Moad, E. Rizzardo, S. H. Thang, *Aust. J. Chem*., 2009, **62**, 1402. (b) E. Bicciocchi, Y. K. Chong, L. Giorgini, G. Moad, E. Rizzardo, S. H. Thang, *Macromol. Chem. Phys.,* 2010, **211**, 529. (c) D. J. Keddie, C. Guerrero-Sanchez, G. Moad, R. J. Mulder, E. Rizzardo, S. H. Thang, *Macromolecules,* 2012, **45**, 4205.

[28] C. Boyer, D. Valade, B. Ameduri, P. Lacroix Desmazes, B. Boutevin, *J. Polym. Sci., Part A: Polym. Chem.,* 2006, **44**, 5763-5777.

[29] M. Guerre, M.; G. Lopez, T. Soulestin, C. Totée, B. Ameduri, G. Silly, V. Ladmiral, *Macromol. Chem. Phys.,* 2016, **217**, 2275-2285.

[30] G. Pound, J. B. McLeary, J. M. McKenzie, R. F. M. Lange, B. Klumperman, *Macromolecules,* 2006, **39,** 7796

[31] M; H. Stenzel, L. Cummins, G. E. Roberts, T. P. Davis, P. Vana, C. Barner-Kowollik, *Macromol. Chem. Phys.,* 2003, **204**, 1160-1168.

[32] Pladis, A. H. Alexopoulos, K. Kiparissides, *Ind. Eng. Chem. Res.,* 2014, **53**, 7352-7364.

[33] (a) J. Guiot, B. Ameduri, B. Boutevin, *Macromolecules,* 2002, **35**, 8694‒8707. (b) G. Mladenov, B. Ameduri, G. Kostov, R. Mateva, *J. Polym. Sci., Part A: Polym. Chem.,* 2006*,* **44**, 1470-1485.

[34] (a) M. L. Coote and L. Radom, *J. Am. Chem. Soc.,* 2003, **125,** 1490‑1491; (b) M. L. Coote, *Macromolecules,* 2004, **37**, 5023 ‑ 5031; (c) M. L. Coote and L. Radom, *Macromolecules,* 2004, **37,** 590‑596; (d) M. L. Coote, *J. Phys. Chem. A*, 2005, **109**, 1230‑1239; (e) M. L. Coote and D. J. Henry, *Macromolecules*, 2005, **38**, 1415‑1433; (f) M. L. Coote and D. J. Henry, *Macromolecules*, 2005**, 38**, 5774‑5779; (g) K. Matyjaszewski and R.

Poli, *Macromolecules*, 2005, **38**, 8093‑8100; (h) M. L. Coote, E. H. Krenske and E. I. Izgorodina, *Macromol. Rapid Commun.,* 2006, **27**, 473; (i) C. M. R. Abreu, P. V. Mendonça, A. C. Serra, J. F. J. Coelho, V. P. Anatoliy, G. Gryn' ova, M. L. Coote and T. Guliashvili, *Macromolecules,* 2012, **45**, 2200‑2208.

[35] (a) M. B. Gillies, K. Matyjaszewski, P.-O. Norrby, T. Pintauer, R. Poli and P. Richard, *Macromolecules*, 2003, **36**, 8551‑8559; (b) C. Y. Lin, M. L. Coote, A. Petit, P. Richard, R. Poli and K. Matyjaszewski, *Macromolecules*, 2007, **40**, 5985‑5994; (c) W. A. Braunecker, W. C. Brown, B. Morelli, W. Tang, R. Poli and K. Matyjaszewski, *Macromolecules*, 2007, **40**, 8576‑8585; (d) W. Tang, Y. Kwak, W. Braunecker, N. V. Tsarevsky, M. L. Coote and K. Matyjaszewski, *J. Am. Chem. Soc*., 2008, **130**, 10702‑10713; (e) Y. Zhang, K. Schröder, Y. Kwak, P. Krys, A. N. Morin, T. Pintauer, R. Poli and K. Matyjaszewski, *Macromolecules,* 2013, **46**, 5512‑5519.

[36] a) (a) S. Maria, H. Kaneyoshi, K. Matyjaszewski and R. Poli, *Chem. – Eur. J.,* 2007, **13**, 2480; (b) A. Debuigne, Y. Champouret, R. Jérôme, R. Poli and C. Detrembleur, *Chem. – Eur. J*., 2008, **14**, 4046‑4059; (c) A. Debuigne, C. Michaux, C. Jérôme, R. Jérôme, R. Poli and C. Detrembleur, *Chem. – Eur. J*., 2008, **14**, 7623‑7637; (d) Y. Champouret, U. Baisch, R. Poli, L. Tang, J. L. Conway and K. M. Smith, *Angew. Chem., Int. Ed*., 2008, **47**, 6069‑ 6072; (e) A. Debuigne, R. Poli, J. De Winter, P. Laurent, P. Gerbaux, P. Dubois, J.-P. Wathelet, C. Jérôme and C. Detrembleur, *Chem. – Eur. J.,* 2010, **16**, 1799‑1811; (f) A. Debuigne, R. Poli, J. De Winter, P. Laurent, P. Gerbaux, J.-P. Wathelet, C. Jérôme and C. Detrembleur, *Macromolecules,* 2010, **43**, 2801‑2813; (g) Y. Champouret, K. C. MacLeod, U. Baisch, B. O. Patrick, K. M. Smith and R. Poli, *Organometallics*, 2010, **29**, 167‑176; (h) Y. Champouret, K. C. MacLeod, K. M. Smith and R. Poli, *Organometallics*, 2010, **29**, 3125‑3132; (i) A. Debuigne, A. N. Morin, A. Kermagoret, Y. Piette, C. Detrembleur, C. Jérôme and R. Poli, *Chem. – Eur. J*., 2012, **18**, 12834‑12844; (j) Y. Piette, A. Debuigne, C. Jérôme, V. Bodart, R. Poli and C. Detrembleur, *Polym. Chem*., 2012**, 3**, 2880‑2891.

[37] C. M. R. Abreu, P. V. Mendonça, A; C. Serra, B. B. Noble, T. Guliashvili, J. Nicolas, M. L. Coote, J. F. J. Coelho, *Macromolecules,* 2016, **49**, 490-498.

[38] R. Siegmann, M. Drache, S. Beuermann, *Macromolecules,* 2013, **46**, 9507-9514.

[39] (a) M. A. Bachmann, W. L. Gordon, J. L. Koening, J. B. Lando, *J. Appl. Phys.,* 1979, **50**, 6106. (b) D. E. Mattern, L. Fu-Tyan, D. M. Hercules, *Anal. Chem,* 1984, **56**, 2762-2769. (c) A. J. Lovinger, D. D. Davis, R. E. Cais, J. M. Kometani, *Polymer,* 1987, **28**, 617-626.

[40] P. Laflamme, F. Porzio, B. Ameduri, A. Soldera, *Polym. Chem.,* 2012, **3**, 652-657.

[41] A. N. Plyusnin, N. M. Chirkor, *Theor. Eksp. Khimiya*, 1966, **2**, 777.

[42] Z. Litia, Z. Machacek, *J. Polym. Sci.,* 1959, **38**, 459.

VIII. Supporting Information

VIII.1.1 Equations

SI-Equation II-12

$$(\%) - CF_2 - CH_2 - XA = \frac{\frac{1}{2}\int_{4.02}^{4.17} -CF_2 - CH_2 - XA}{\frac{1}{3}\int_{1.71}^{1.87} -CF_2 - CH_3 + \frac{1}{2}\int_{3.26}^{3.52} -CH_2 - CF_2 - XA + \int_{6.01}^{6.48} -CH_2 - CF_2H + \frac{1}{2}\int_{4.02}^{4.17} -CF_2 - CH_2 - XA}$$

SI-Equation II-13

$$(\%) - CH_2 - CF_2 - XA = \frac{\frac{1}{2}\int_{3.26}^{3.52} -CH_2 - CF_2 - XA}{\frac{1}{3}\int_{1.71}^{1.87} -CF_2 - CH_3 + \frac{1}{2}\int_{3.26}^{3.52} -CH_2 - CF_2 - XA + \int_{6.01}^{6.48} -CH_2 - CF_2H + \frac{1}{2}\int_{4.02}^{4.17} -CF_2 - CH_2 - XA}$$

SI-Equation II-14

$$(\%) - CH_2 - CF_2H = \frac{\int_{6.01}^{6.48} -CH_2 - CF_2H}{\frac{1}{3}\int_{1.71}^{1.87} -CF_2 - CH_3 + \frac{1}{2}\int_{3.26}^{3.52} -CH_2 - CF_2 - XA + \int_{6.01}^{6.48} -CH_2 - CF_2H + \frac{1}{2}\int_{4.02}^{4.17} -CF_2 - CH_2 - XA}$$

SI-Equation II-15

$$(\%) - CF_2 - CH_3 = \frac{\frac{1}{3}\int_{1.71}^{1.87} -CF_2 - CH_3}{\frac{1}{3}\int_{1.71}^{1.87} -CF_2 - CH_3 + \frac{1}{2}\int_{3.26}^{3.52} -CH_2 - CF_2 - XA + \int_{6.01}^{6.48} -CH_2 - CF_2H + \frac{1}{2}\int_{4.02}^{4.17} -CF_2 - CH_2 - XA}$$

SI-Equation II-16

$$(\%)R - CH_2 - CF_2 - = \frac{\frac{1}{3}\int_{1.19}^{1.25} R - PVDF}{\frac{1}{3}\int_{1.19}^{1.25} R - PVDF + \frac{1}{2}\int_{4.30}^{4.39} DMC - PVDF}$$

SI-Equation II-17

$$(\%)DMC - CH_2 - CF_2 - = \frac{\frac{1}{2}\int_{4.30}^{4.39} DMC - PVDF}{\frac{1}{3}\int_{1.19}^{1.25} R - PVDF - + \frac{1}{2}\int_{4.30}^{4.39} DMC - PVDF}$$

Equations used to calculate the proportions of chain-ends and to construct Figure II-40 (the evolution of the proportion of intrachain and total HH VDF additions *vs* conversion for three RAFT polymerizations) were calculated using the equations described in our earlier report.[19]

VIII.1.2 Chain Transfer Constant

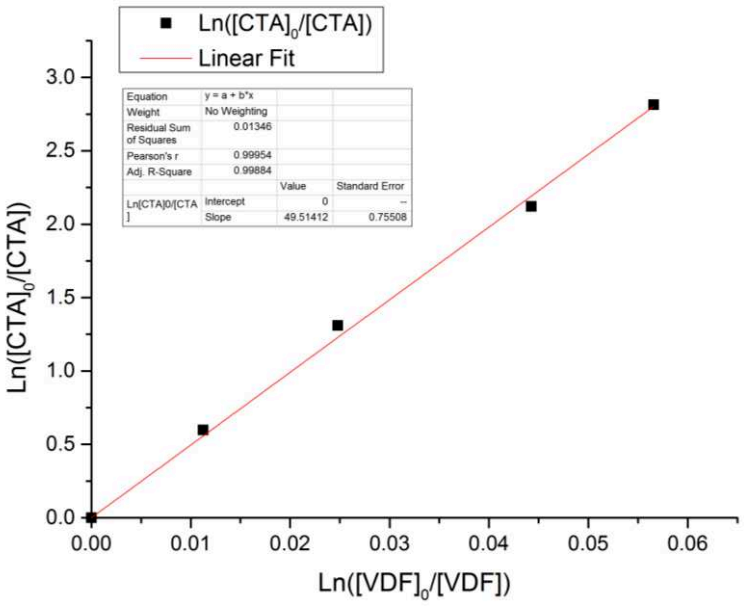

SI-Figure II-45: Determination of the transfer constant of O-ethyl-S-(1-methoxycarbonyl)ethyldithiocarbonate CTA with VDF using O'Brien and Gornick's method.[26]

SI-Figure II-45 displays the plots of $Ln([CTA]_0/[CTA])$ versus Ln $([VDF]_0/[VDF])$. The slope of the linear fit of this plot provides the $C_{Tr(app)}$, using SI-Equation II-18 :

SI-Equation II-18 $$Ln(\frac{[CTA]_0}{[CTA]}) = C_{Tr(app)}\, Ln(\frac{[VDF]_0}{[VDF]})$$

$C_{Tr(app)} = 49$ at 73 °C

VIII.1.3 NMR

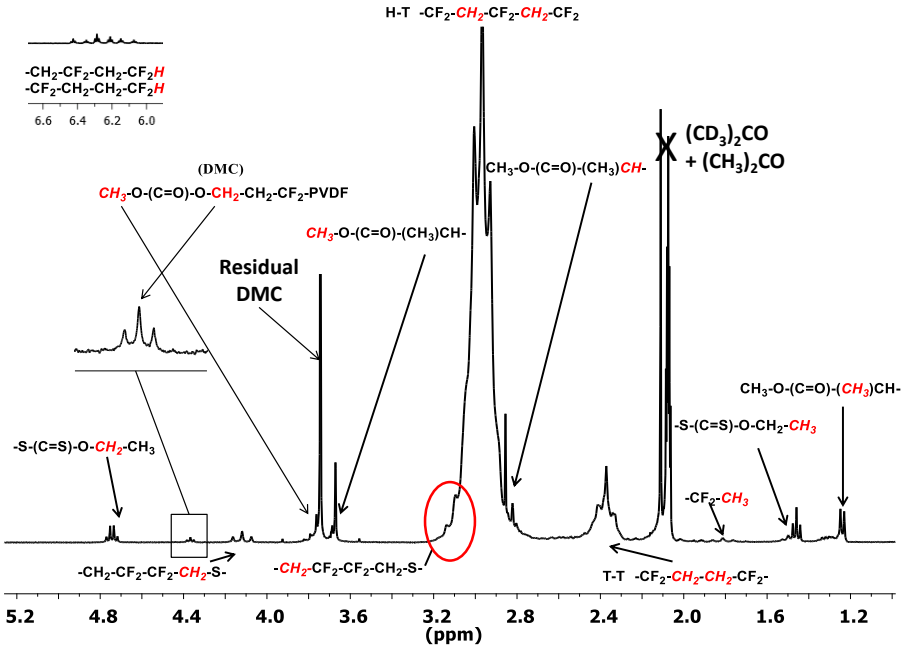

SI-Figure II-46: Expansion of the 1.0 - 5.2 ppm region of the ^{1}H NMR spectrum in $(CD_3)_2CO$ of PVDF homopolymer (run 13, Table II-6) synthesized via RAFT polymerization.

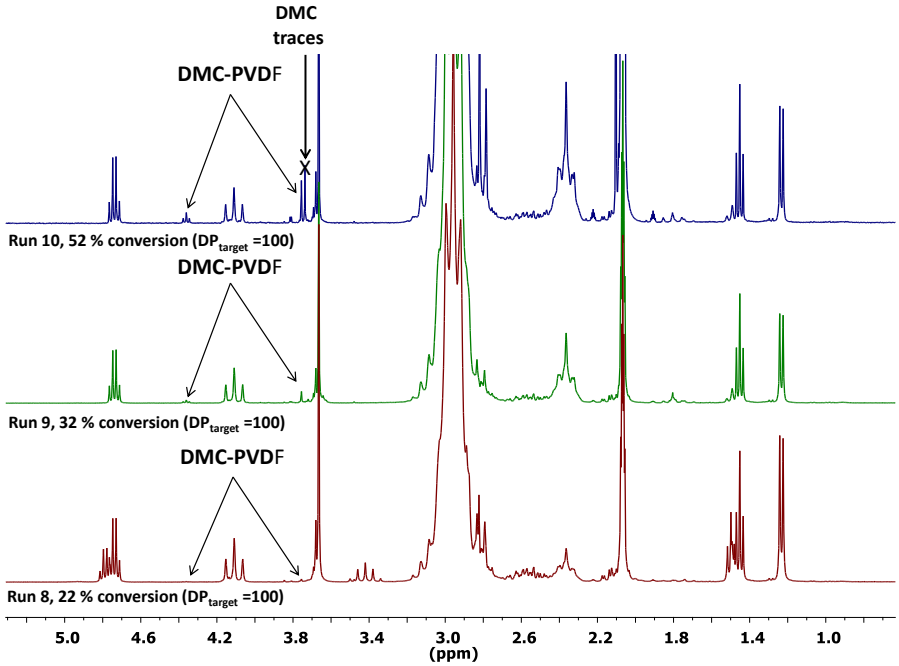

SI-Figure II-47: Evolution of the PVDF chains initiated by DMC radicals (DMC-PVDF) during the course of a VDF RAFT polymerization (DP_{target} =100). The DMC moiety at the α-chain-end is characterized by two ^{1}H NMR signals at 3.73 and 4.34 ppm. The ^{1}H NMR spectra were recorded in $(CD_3)_2CO$.

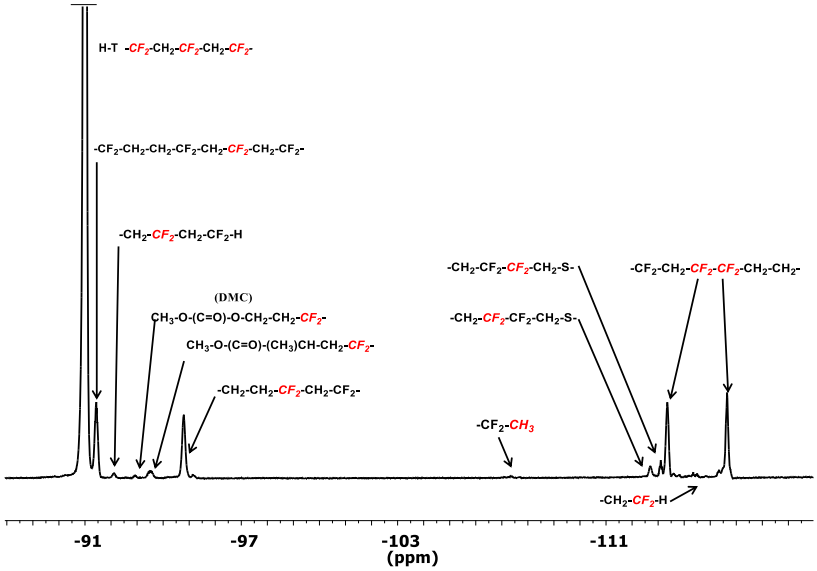

SI-Figure II-48: Expansion of the -88 to -119 ppm region of the ^{19}F NMR spectrum in $(CD_3)_2CO$ of PVDF homopolymer (run 13, Table II-6) synthesized via RAFT polymerization.

VIII.1.4 Computational

SI-Table II-7: Energies, enthalpies, Gibbs energies of all optimized geometries

Compound	E (hartrees)	$H_{298.15}$ (hartrees)	$G_{298.15}$ (hartrees)	$G_{343.15}$ (hartrees)[a]
(a) Radicals				
$CHF_2CH_2^{\bullet}$	-277.3819182	-277.330618	-277.363927	-277.3689544
$CH_3CF_2^{\bullet}$	-277.3942109	-277.341757	-277.374487	-277.379427
$(MeO)C(S)S^{\bullet}$	-949.1387931	-949.081962	-949.119578	-949.1252554
(b) Monomers				
$CH_2=CF_2$	-276.8179418	-276.77658	-276.807351	-276.8119953
(c) Chain transfer agents				
CHF_2CH_2-SC(S)(OMe)	-1226.623079	-1226.509289	-1226.558343	-1226.565747
CH_3CF_2-SC(S)(OMe)	-1226.623112	-1226.510636	-1226.559231	-1226.566565
(d) VDF propagation				
(d_1) Head to tail				
$CH_3CF_2^{\cdots}CH_2CF_2^{\bullet}$ TS	-554.2069944	-554.112686	-554.159811	-554.1669236
CH_3CF_2-$CH_2CF_2^{\bullet}$	-554.2596083	-554.162115	-554.206273	-554.2129378
(d_2) Head to head				
$CH_3CF_2^{\cdots}CF_2CH_2^{\bullet}$ TS	-554.204510	-554.110865	-554.156331	-554.1631932
CH_3CF_2-$CF_2CH_2^{\bullet}$	-554.2563001	-554.161183	-554.204725	-554.2112968
(d_3) Tail to tail				
$CHF_2CH_2^{\cdots}CH_2CF_2^{\bullet}$ TS	-554.1966673	-554.102442	-554.148653	-554.1556277
CHF_2CH_2-$CH_2CF_2^{\bullet}$	-554.2540946	-554.155206	-554.19951	-554.2061968
(d_4) Tail to Head				
$CHF_2CH_2^{\cdots}CF_2CH_2^{\bullet}$ TS	-554.190701	-554.09724	-554.142244	-554.1490365
CHF_2CH_2-$CF_2CH_2^{\bullet}$	-554.249403	-554.15306	-554.197573	-554.2042914
(e) MacroCTA degenerative and non-degenerative radical exchange				
(e_1) Head-head (degenerative)				
CH_3CF_2-SC(OMe)$S^{\cdots}{}^{\bullet}CF_2CH_3$ TS	-1504.017061	-1503.851318	-1503.916319	-1503.92613
CH_3CF_2-$SC^{\bullet}$(OMe)S-CF_2CH_3	-1504.033495	-1503.866567	-1503.929195	-1503.938647
(e_2) Head-tail (non-degenerative)				
CH_3CF_2-SC(OMe)$S^{\cdots}{}^{\bullet}CH_2CHF_2$ TS	-1504.006925	-1503.841794	-1503.905873	-1503.915544
CH_3CF_2-$SC^{\bullet}$(OMe)S-CH_2CHF_2	-1504.028759	-1503.860603	-1503.924011	-1503.933581
$CH_3CF_2^{\cdots}$SC(OMe)S-CH_2CHF_2 TS	-1504.013737	-1503.846844	-1503.911662	-1503.921445
(e_3) Tail-tail (degenerative)				
CHF_2CH_2-SC(OMe)$S^{\cdots}{}^{\bullet}CH_2CHF_2$ TS	-1504.007386	-1503.840705	-1503.904122	-1503.913694
CHF_2CH_2-$SC^{\bullet}$(OMe)S-CH_2CHF_2	-1504.023796	-1503.854494	-1503.918067	-1503.927662

[a]Extrapolation done on the basis $G_{343.15} \approx H_{298.15} - 343.15 \cdot S_{298.15}$.

Si-Table II-8:Cartesian coordinates and views of all optimized geometries

(a) Radicals

$CHF_2CH_2^{\bullet}$

6	1.394001000	-0.107134000	-0.085236000
6	-0.012319000	0.007573000	0.354372000
1	1.605256000	-0.523019000	-1.065566000
1	-0.126101000	0.065360000	1.446414000
1	2.185777000	0.377679000	0.476297000
9	-0.595048000	1.137805000	-0.178214000
9	-0.733288000	-1.062544000	-0.096448000

$CH_3CF_2^{\bullet}$

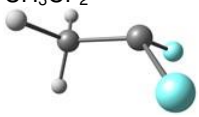

6	0.059485000	0.000229000	-0.305567000
6	-1.386581000	0.000075000	0.044979000
1	-1.526760000	0.000221000	1.137790000
1	-1.870565000	0.890101000	-0.366469000
1	-1.869553000	-0.890889000	-0.365766000
9	0.735032000	1.098602000	0.064360000
9	0.734907000	-1.098742000	0.064303000

$(MeO)C(S)S^{\bullet}$

16	1.736278000	-0.629578000	-0.000015000
6	0.122262000	-0.147474000	0.000058000
8	-0.840806000	-1.050048000	0.000022000
16	-0.059249000	1.524074000	-0.000003000
6	-2.203329000	-0.590138000	-0.000024000
1	-2.405410000	0.006032000	-0.896070000
1	-2.405500000	0.005896000	0.896092000
1	-2.808709000	-1.497813000	-0.000123000

(b) Monomers

$CF_2=CH_2$

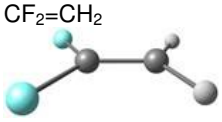

6	-1.386768000	0.002088000	0.000517000
6	-0.062812000	0.000473000	-0.000250000
9	0.699065000	1.082140000	0.000097000
9	0.695002000	-1.084340000	-0.000050000
1	-1.924716000	-0.937027000	-0.000253000
1	-1.924408000	0.941462000	-0.001776000

(c) Chain transfer agents

CHF_2CH_2-SC(S)(OMe)

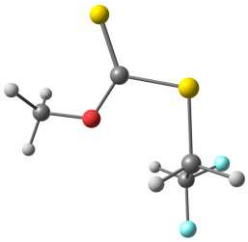

6	-1.388504000	-0.272977000	0.878223000
6	-2.139901000	0.290759000	-0.311861000
1	-1.514938000	0.912329000	-0.965455000
16	0.039507000	-1.312514000	0.424652000
6	1.315328000	-0.152852000	0.073669000
8	0.907451000	1.115151000	0.186556000
16	2.818127000	-0.673688000	-0.340214000
6	1.871772000	2.153075000	-0.054321000
1	2.256150000	2.082942000	-1.076646000
1	2.705447000	2.065589000	0.649297000
1	1.325110000	3.085697000	0.097855000
1	-1.061251000	0.538475000	1.533052000
1	-2.065970000	-0.928721000	1.436919000
9	-2.670438000	-0.720824000	-1.051412000
9	-3.171613000	1.053457000	0.158884000

CH_3CF_2-SC(S)(OMe)

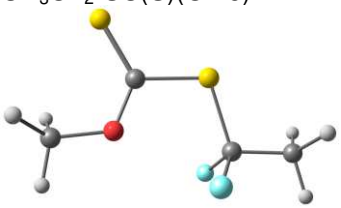

6	-1.739920000	0.093570000	-0.000102000
6	-3.070870000	-0.619464000	-0.000207000
1	-3.858173000	0.141307000	-0.000444000
1	-3.174583000	-1.241038000	-0.893661000
1	-3.174924000	-1.240682000	0.893459000
9	-1.641560000	0.894919000	-1.093022000
9	-1.642260000	0.895670000	1.092355000
16	-0.382514000	-1.168765000	0.000561000
6	1.124096000	-0.245886000	0.000132000
8	0.933171000	1.065294000	0.000332000
16	2.556679000	-1.052479000	-0.000251000
6	2.090846000	1.914417000	0.000030000
1	2.696436000	1.728319000	-0.892552000
1	2.696846000	1.728387000	0.892371000
1	1.691865000	2.930133000	0.000106000

(d) VDF propagation

d_1. Head to tail

$CH_3CF_2^{\cdots}CH_2CF_2^{\bullet}$ TS

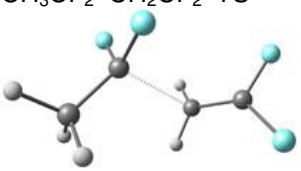

6	-2.158405000	1.207936000	0.047492000
1	-1.574520000	2.050013000	-0.335116000
6	-1.358932000	-0.046126000	-0.045633000
6	0.657535000	0.082305000	1.153753000
6	1.677277000	0.049552000	0.277680000
1	-2.427143000	1.404482000	1.089606000

1	-3.084703000	1.128328000	-0.542083000
9	-0.940210000	-0.333394000	-1.291850000
9	-1.975705000	-1.126313000	0.475005000
1	0.406299000	1.030245000	1.614796000
1	0.369504000	-0.838078000	1.647436000
9	2.188369000	-1.055216000	-0.240560000
9	2.217070000	1.121924000	-0.284193000

CH_3CF_2-$CH_2CF_2^{\bullet}$

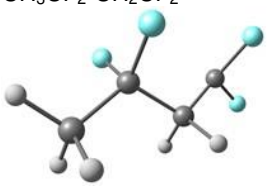

6	2.352301000	-0.619137000	-0.572377000
1	2.359051000	-0.494871000	-1.659387000
6	1.090199000	-0.034673000	0.019506000
6	-0.205844000	-0.661011000	-0.484407000
1	-0.182032000	-1.735621000	-0.277347000
1	-0.260780000	-0.529879000	-1.577292000
6	-1.432006000	-0.097764000	0.162578000
9	-2.521939000	-0.867131000	0.026501000
9	-1.720436000	1.168778000	-0.143918000
1	2.431724000	-1.683584000	-0.332158000
1	3.213755000	-0.093994000	-0.149706000
9	1.136308000	-0.168255000	1.385084000
9	1.062776000	1.312547000	-0.240546000

d_2 Head to head

$CH_3CF_2^{\cdots}CF_2CH_2^{\bullet}$ TS

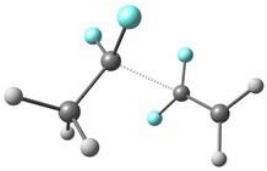

6	1.560248000	1.287506000	-0.330611000
1	1.232692000	2.040159000	0.391370000
6	1.013457000	-0.043277000	0.052733000
6	-1.255145000	0.055866000	0.015317000
6	-1.581038000	0.767576000	1.116467000
9	-1.364521000	-1.269951000	-0.048813000
9	-1.287949000	0.582123000	-1.213663000
1	-1.654650000	0.266309000	2.072941000
1	-1.618625000	1.848336000	1.062336000
1	1.201817000	1.562044000	-1.325580000
1	2.659521000	1.262548000	-0.342228000
9	1.324937000	-0.436538000	1.296438000
9	1.300213000	-1.029570000	-0.809771000

CH_3CF_2-$CF_2CH_2^{\bullet}$

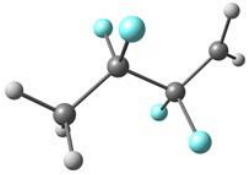

6	-1.546077000	-1.146382000	0.048530000
1	-1.319949000	-1.683404000	0.972568000
6	-0.739621000	0.122913000	-0.017998000
6	0.790337000	-0.076506000	0.006120000
6	1.573209000	1.175666000	-0.030580000
1	-1.303983000	-1.782413000	-0.806343000
1	-2.608819000	-0.889717000	0.023648000
9	-1.039052000	0.813291000	-1.159569000
9	-1.052605000	0.939394000	1.037376000
9	1.079842000	-0.798540000	1.147868000
9	1.122616000	-0.878252000	-1.051994000
1	1.200517000	2.059703000	0.472528000
1	2.567926000	1.158640000	-0.461960000

d_3 Tail to tail

$CHF_2CH_2^{\cdots}CH_2CF_2^{\bullet}$ TS

9	-2.875243000	-0.166590000	-0.808372000
9	-1.825636000	0.874191000	0.828245000
6	-1.627059000	0.083165000	-0.277944000
1	-1.068415000	0.671503000	-1.019233000
6	-0.953191000	-1.174583000	0.109315000
1	-0.549421000	-1.793729000	-0.686980000
1	-1.352531000	-1.689853000	0.980438000
6	1.054238000	-0.353007000	1.069772000
1	1.254540000	-1.315441000	1.524110000
1	0.438363000	0.367289000	1.593110000
6	1.886274000	0.083953000	0.108770000
9	2.780549000	-0.667245000	-0.512652000
9	1.822095000	1.284428000	-0.446213000

CHF_2CH_2-$CH_2CF_2^{\bullet}$

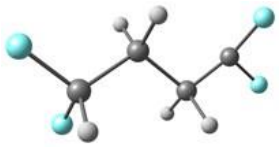

9	-2.862340000	0.853176000	-0.116868000
9	-2.167248000	-1.242727000	-0.148715000
6	-1.886139000	0.009726000	0.326858000
1	-1.941927000	-0.030221000	1.425270000
6	-0.545296000	0.468713000	-0.194117000
1	-0.360260000	1.482832000	0.178402000
1	-0.616610000	0.527766000	-1.287184000
6	0.587436000	-0.468354000	0.219272000
1	0.409619000	-1.476077000	-0.171379000
1	0.632993000	-0.556416000	1.320292000
6	1.917319000	-0.005094000	-0.276451000
9	2.929997000	-0.848195000	-0.038490000
9	2.259175000	1.240210000	0.090876000

d_4 Tail to head

$CHF_2CH_2^{\cdots}CF_2CH_2^{\bullet}$ TS

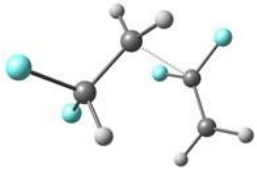

9	-2.795715000	0.551306000	-0.005202000
9	-1.435116000	-1.164521000	-0.280439000
6	-1.550438000	0.060687000	0.319078000
1	-1.527002000	-0.087853000	1.407860000
6	-0.491674000	0.974100000	-0.170238000
1	-0.311338000	1.877259000	0.407400000
1	-0.388650000	1.057178000	-1.250392000

6	1.514295000	-0.075097000	0.074862000
6	1.418863000	-0.611269000	1.314945000
9	2.197708000	1.039993000	-0.173371000
9	1.395091000	-0.798675000	-1.030880000
1	1.666271000	-0.007044000	2.178717000
1	0.956719000	-1.582993000	1.433568000

CHF_2CH_2-$CF_2CH_2^{\bullet}$

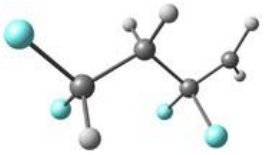

9	2.486165000	-0.827517000	-0.068382000
9	1.605801000	1.189307000	-0.191796000
6	1.385351000	-0.079532000	0.247794000
1	1.283412000	-0.055863000	1.339907000
6	0.180163000	-0.680419000	-0.448223000
1	0.153436000	-1.751166000	-0.217443000
1	0.310374000	-0.568019000	-1.530292000
6	-1.145309000	-0.064793000	-0.026238000
6	-2.344589000	-0.705492000	-0.616745000
9	-1.157520000	1.270991000	-0.326758000
9	-1.221232000	-0.138462000	1.362722000
1	-2.372656000	-1.777631000	-0.780691000
1	-3.247184000	-0.114780000	-0.733091000

(e) MacroCTA degenerative and non-degenerative radical exchange

e_1 Head-head (degenerative)

CH_3CF_2-SC(OMe)$S^{\cdots}{}^{\bullet}CF_2CH_3$ TS

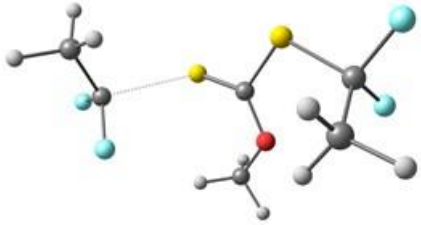

6	-2.807691000	-0.392322000	0.229687000
6	-2.568589000	-0.426759000	1.715561000
16	-1.345727000	-0.801172000	-0.844229000
6	-0.184783000	0.507732000	-0.613656000
8	-0.612813000	1.475967000	0.204955000
6	0.283122000	2.565379000	0.470123000
1	0.534414000	3.087101000	-0.458969000
1	1.199835000	2.193688000	0.938812000
16	1.280671000	0.421883000	-1.369011000
6	3.042866000	-0.510122000	0.325948000
6	2.982271000	-1.994919000	0.350186000
1	-1.833633000	0.330185000	1.995035000
1	-2.210837000	-1.415330000	2.013441000
1	-3.518070000	-0.216943000	2.220367000
1	3.209792000	-2.387940000	-0.644091000
1	1.978033000	-2.319304000	0.635385000
1	3.707736000	-2.405592000	1.070095000
9	2.697524000	0.085944000	1.482297000
9	4.196593000	0.004827000	-0.116315000
9	-3.343651000	0.796117000	-0.138434000
9	-3.699470000	-1.367115000	-0.117744000
1	-0.266016000	3.223150000	1.146812000

CH_3CF_2-$SC^{\bullet}$(OMe)S-CF_2CH_3

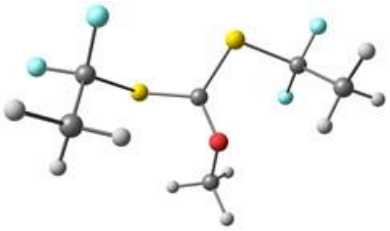

6	-2.692916000	-0.373753000	0.035881000
6	-3.118673000	0.164007000	1.375317000
16	-0.972894000	-1.086513000	-0.028379000
6	-0.012072000	0.344211000	-0.292943000
8	-0.295484000	1.415583000	0.504869000
6	-0.188056000	2.699399000	-0.119644000
1	-0.925441000	2.786355000	-0.926326000
1	0.819829000	2.858459000	-0.520920000
16	1.501402000	0.195347000	-1.145080000
6	2.676818000	-0.396970000	0.186012000
6	2.888052000	0.559316000	1.328338000
1	-2.455164000	0.978875000	1.671865000
1	-3.072073000	-0.629581000	2.125587000
1	-4.148570000	0.529599000	1.295773000
1	1.934750000	0.773876000	1.818486000
1	3.573915000	0.101189000	2.049692000
1	3.320137000	1.492540000	0.958367000
9	3.845239000	-0.620936000	-0.476115000
9	2.238957000	-1.594220000	0.661988000
9	-2.816370000	0.588939000	-0.917561000
9	-3.496788000	-1.414613000	-0.321258000
1	-0.397901000	3.432898000	0.662613000

e_2 Head-tail (non-degenerative)

CH_3CF_2-SC(OMe)$S^{\cdots}{}^{\bullet}CH_2CHF_2$ TS

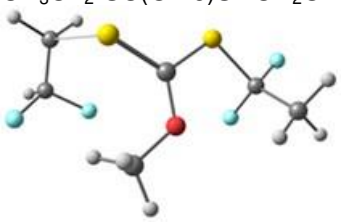

6	2.704670000	-0.179030000	0.397924000
6	3.412880000	1.019732000	-0.173786000
16	1.412381000	-0.959491000	-0.690278000
6	0.104621000	0.211621000	-0.821333000
8	0.305972000	1.334604000	-0.135460000
6	-0.734985000	2.327679000	-0.148586000
1	-1.661911000	1.903971000	0.243995000
1	-0.897223000	2.691880000	-1.168417000
16	-1.229206000	-0.189774000	-1.710041000
1	4.179820000	1.337522000	0.541189000
1	-0.363644000	3.126723000	0.495907000
1	3.887677000	0.755998000	-1.121959000
1	2.704173000	1.834640000	-0.331869000
9	3.591758000	-1.204488000	0.565161000
9	2.183661000	0.108753000	1.613804000
6	-2.920198000	-1.488062000	-0.150076000
1	-3.694116000	-1.577223000	-0.906519000
1	-2.273818000	-2.343004000	0.020838000
6	-3.173693000	-0.580902000	0.988614000
1	-3.850853000	-1.003646000	1.753117000
9	-3.745881000	0.594316000	0.566319000
9	-2.003810000	-0.263213000	1.633156000

CH_3CF_2-$SC^{\bullet}$(OMe)S-CH_2CHF_2

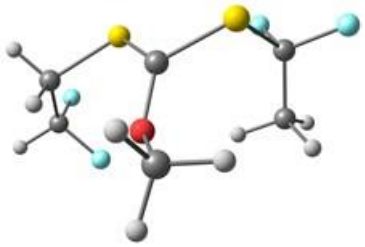

6	-2.561743000	0.338966000	-0.815491000
6	-3.255134000	-0.289894000	0.375786000
16	-0.929742000	-0.403548000	-1.159936000
6	0.166306000	0.853132000	-0.610863000
8	-0.296715000	1.635587000	0.408132000
6	0.327705000	2.910722000	0.554966000
1	0.227065000	3.502230000	-0.364330000
1	1.392076000	2.803930000	0.796091000
9	-2.500237000	-0.169379000	1.500397000
9	-3.462195000	-1.618650000	0.147318000
1	-2.425659000	1.409417000	-0.640166000
1	-3.186764000	0.195194000	-1.703354000
16	1.863004000	0.600136000	-0.911426000
6	2.354201000	-0.768076000	0.276327000
6	1.956280000	-0.545927000	1.710050000
1	2.435834000	0.356348000	2.097786000
1	2.280326000	-1.410962000	2.299251000
9	3.709958000	-0.842270000	0.152167000
9	1.846794000	-1.949844000	-0.165418000
1	0.870818000	-0.442297000	1.790889000
1	-4.232992000	0.179201000	0.567229000
1	-0.193747000	3.404566000	1.378523000

$CH_3CF_2^{\bullet\cdots}SC(OMe)S\text{-}CH_2CHF_2$ TS

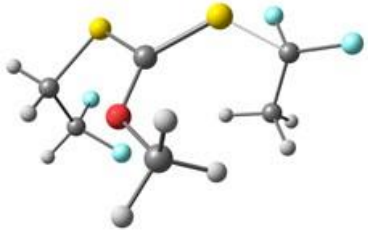

6	-2.798208000	0.149650000	-0.470829000
6	-2.842776000	-0.971204000	0.548816000
16	-1.247097000	0.193748000	-1.430182000
6	-0.174239000	1.199786000	-0.454341000
8	-0.803847000	1.838415000	0.545190000
6	-0.028268000	2.715517000	1.366292000
1	0.420675000	3.511182000	0.761734000
1	0.769217000	2.164169000	1.875700000
9	-1.813525000	-0.858782000	1.438387000
9	-2.731442000	-2.179177000	-0.067584000
1	-2.944558000	1.113461000	0.023837000
1	-3.604697000	-0.000763000	-1.196710000
16	1.435472000	1.255906000	-0.813511000
6	2.588557000	-0.898725000	0.117475000
6	1.880131000	-1.285626000	1.366163000
1	2.024005000	-0.510760000	2.123764000
1	2.272288000	-2.237574000	1.756594000
9	3.866089000	-0.523615000	0.279203000
9	2.505252000	-1.789970000	-0.875651000
1	0.809897000	-1.400239000	1.172353000
1	-3.784192000	-0.962143000	1.119680000
1	-0.734424000	3.128398000	2.089970000

$CHF_2CH_2\text{-}SC(OMe)S^{\cdots\bullet}CH_2CHF_2$ TS

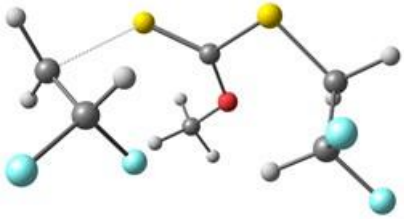

6	2.392511000	-0.611062000	-0.402674000
6	2.314008000	0.757616000	0.248399000
16	0.924558000	-0.995779000	-1.411168000
6	-0.288597000	-1.428782000	-0.211594000
8	0.216653000	-1.582915000	1.015679000
6	-0.693297000	-1.864745000	2.089799000
1	-1.238670000	-2.793475000	1.894945000
1	-1.397947000	-1.036412000	2.203590000
16	-1.875171000	-1.566746000	-0.658039000
6	-2.932832000	0.787730000	-0.365777000
6	-1.757377000	1.656006000	-0.147714000
1	1.428289000	0.892368000	0.880171000
1	-1.050217000	1.667904000	-0.986371000
1	2.535962000	-1.383921000	0.356023000
1	3.243946000	-0.623671000	-1.092220000
1	-3.561877000	0.579662000	0.495584000
1	-3.407412000	0.816338000	-1.341884000
9	2.305140000	1.724853000	-0.712848000
9	3.434943000	0.932307000	1.009340000
9	-1.064615000	1.246871000	0.977656000
9	-2.144395000	2.954496000	0.096351000
1	-0.061631000	-1.962395000	2.974911000

$CHF_2CH_2\text{-}SC^{\bullet}(OMe)S\text{-}CH_2CHF_2$

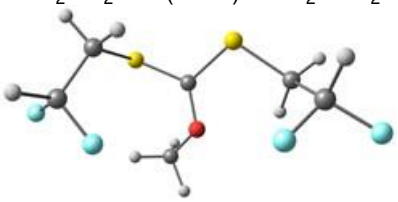

6	-2.696617000	0.710198000	0.167481000
6	-3.143813000	-0.497003000	-0.634701000
16	-1.187168000	1.493032000	-0.487674000
6	0.079684000	0.888703000	0.582633000
8	-0.220311000	-0.242923000	1.263609000
6	0.636694000	-0.583106000	2.355158000
1	0.709068000	0.248569000	3.067364000
1	1.634867000	-0.850906000	1.995775000
9	-2.233321000	-1.500688000	-0.551098000
9	-4.320676000	-0.949801000	-0.102314000
1	-2.519100000	0.406725000	1.203155000
1	-3.489349000	1.465159000	0.144539000
16	1.694564000	1.422080000	0.210488000
6	2.239175000	0.432939000	-1.265544000
1	2.994139000	1.046653000	-1.770035000
1	1.386441000	0.303176000	-1.940048000
6	2.837494000	-0.912106000	-0.925731000
9	1.910008000	-1.713631000	-0.325398000
9	3.882745000	-0.769269000	-0.061656000
1	3.205925000	-1.436984000	-1.821205000
1	-3.311361000	-0.270593000	-1.697600000
1	0.168999000	-1.447448000	2.832577000

e_3 Tail-tail (degenerative)

Conclusion Partie 3

L'ultime partie de ce chapitre a démontré l'efficacité de la polymérisation RAFT pour synthétiser des PVDF-XA fonctionnels et de hautes masses molaires (>10k $g.mol^{-1}$), en dépit des additions inverses et des réactions de transfert irréversibles au solvant qui détériorent le contrôle de la polymérisation. La fonctionnalité et le contrôle sont seulement conservés pour des conversions inférieures à 45 %, 32 % et 33 % (pour des DP visés de 50, 100 et 200 respectivement), ce qui rend cette technique difficilement transposable pour l'industrie.

Contrairement à l'idée reçue, cette étude révèle aussi par l'expérience et les calculs DFT que les extrémités de chaînes $PVDF_T$-XA sont en réalité actives et ne peuvent pas être considérées comme « mortes ». En effet, le contrôle de la polymérisation reste optimal dans la première partie de la polymérisation, avec une accumulation progressive d'extrémités de chaînes $PVDF_T$-XA au détriment des extrémités plus réactives : $PVDF_H$-XA. Cependant, lorsque toutes les chaînes ont été transformées en $PVDF_T$-XA, le transfert dégénératif, qui est essentiel pour assurer le bon contrôle de la polymérisation, est considérablement diminué. Cela a pour conséquence, une nette diminution du contrôle et un élargissement de la distribution des masses molaires. En définitive, après cette transition, un deuxième transfert dégénératif mettant en jeu les radicaux $PVDF_T^{\cdot}$ (en large minorité car ils ne sont générés qu'en cas d'addition tête-tête du VDF, environ 4% des additions) et les chaînes $PVDF_T$-XA opère. Cette situation correspond donc à une polymérisation pour laquelle la propagation est prépondérante par rapport au transfert dégénératif, et donc une polymérisation qui n'est ni conventionnelle, ni contrôlée, mais qui se rapproche d'une polymérisation RAFT utilisant un agent de transfert peu efficace.

Conclusion Chapitre II

Dans ce second chapitre, la synthèse, la caractérisation d'homopolymères de PVDF ($PVDF_T$-Xa et $PVDF_H$-XA) et les limites de la polymérisation RAFT du VDF ont été étudiées. Ces travaux ont montré le fort potentiel de la polymérisation RAFT dans la préparation d'homopolymères PVDF hautement fonctionnels. Bien que l'accumulation des chaînes moins réactives $PVDF_T$-XA et les réactions de transfert au solvant affectent fortement la polymérisation, et conduisent à un élargissement de la distribution en masse et à une diminution de la fonctionnalité, cette dernière méthode reste à ce jour la meilleure pour synthétiser des PVDF fonctionnels, pouvant atteindre 10 $kg.mol^{-1}$ et présentant une dispersité inférieure à 1,4.

En outre, cette partie a également révélé par l'appui de calculs DFT, le mécanisme détaillé de la polymérisation RAFT du VDF et l'effet de l'accumulation de chaînes $PVDF_T$-XA sur le contrôle de la polymérisation. Cette étude constitue une contribution non négligeable à la compréhension du mécanisme de polymérisation du VDF par RAFT. De plus, cette compréhension du mécanisme peut facilement s'extrapoler à l'ITP du VDF, et de manière encore plus fortuite, à la polymérisation RAFT de l'acétate de vinyle (VAc). En effet, le VAc possède une réactivité très similaire à celle du VDF, avec 1.23 % d'inversion à 20 °C et 1.95 % à 110 °C. Bien que ces invertions soient bien connues des polymeristes, l'effet de celles-ci sur le contrôle de la polymérisation du VAc par RAFT n'a été que très peu décrit dans la littérature. Il ne fait donc aucun doute que de manière similaire à la RAFT du VDF, l'augmentation de la dispersité de la polymérisation RAFT du VAc (qui se rapproche généralement de 1,3) est très fortement liée à l'accumulation des chaînes $PVAc_T$-XA.

Enfin, le développement de la RAFT du VDF donne accès de par les fonctions thiocarbonythio des extrémités de chaînes, à une large gamme de modifications chimiques post-polymérisation. L'aminolyse des fonctions xanthate du PVDF suivie de l'addition de Michael sur un composé acrylate/méthacrylate fait l'objet du chapitre suivant.

Chapitre III. Synthèse d'un Macromonomère à base de PVDF

Table des Matières

Introduction Chapitre III

Le chapitre précédent a démontré l'efficacité de la polymérisation RAFT dans la préparation de PVDF bien défini et hautement fonctionnel. Cette avancée permet, à travers la chimie bien connue des composés soufrés, la préparation de nouvelles architectures de PVDF. Par exemple, la préparation de macromonomère représente un enjeu de taille et donne accès à de nouvelles architectures. De plus, la préparation de macromonomère de PVDF n'a été que très rarement rapportée dans la littérature. Seulement deux articles utilisant des télomères (avec 1 à 8 unités de VDF) comme précurseurs, ont rapporté la synthèse de macromonomères PVDF. Les méthodes de synthèses employées, étaient également très laborieuses et nécessitaient pour la plupart, plusieurs étapes de synthèse. Il convient donc de saisir cette opportunité et de développer une méthode de synthèse facile, efficace et adaptée à la préparation de macromonomères PVDF, le tout, en utilisant les extrémités fonctionnelles RAFT.

Ainsi, ce chapitre décrit la synthèse d'un macromonomère PVDF de type méthacrylate en utilisant un procédé en une seule étape. L'extrémité xanthate réagit dans un premier temps avec une amine primaire par aminolyse, générant *in situ* un thiol PVDF-SH, qui réagit de manière sélective sur l'acrylate d'un monomère acrylate-méthacrylate, générant ainsi un PVDF-méthacrylate. Dans cette étude, deux composés permettant la formation du thiol par attaque nucléophile ont été étudiés et comparés : l'Hexylamine et le l'azoture de sodium NaN_3. Ce travail a fait l'objet d'une publication scientifique publié dans *Polymer Chemistry*.[3]

One-pot synthesis of Poly(Vinylidene Fluoride) Methacrylate Macromonomers *via* thia-Michael addition.

Marc Guerre,[a] Bruno Améduri,[a] and Vincent Ladmiral[a]*

[a]Institut Charles Gerhardt, Ingénierie et Architectures Macromoléculaires, UMR 5253 – CNRS, Université Montpellier, ENSCM - 8, Rue Ecole Normale, 34296 Montpellier-France.
*Corresponding authors: gilles.silly@umontpellier.fr, vincent.ladmiral@enscm.fr

I. Abstract

This study presents a new synthetic route to prepare original PVDF macromonomers and PVDF-based architectures. A poly(vinylidene fluoride), PVDF, synthesized using MADIX controlled polymerization in the presence of *O*-ethyl-*S*-(1-methoxycarbonyl)ethyldithiocarbonate was chemically modified *via* two strategies and fully characterized. Using a one-pot procedure, the xanthate end-groups of the PVDF were converted into thiols which were immediately added onto the acrylate moieties of 3-(acryloyloxy)-2-hydroxypropyl methacrylate (AHPMA) *via* regioselective thia-Michael addition to form new PVDF-MA macromonomers. Two methods of elimination of the thiocarbonylthio group were tested and compared: aminolysis, and elimination using sodium azide. These reactions were thoroughly examined *via* ^{1}H and ^{19}F NMR spectroscopy and SEC-HPLC. The aminolysis procedure was shown to give better coupling efficiency and better-defined macromonomers. The PVDF-MA macromonomers with the highest functionality were further polymerized by RAFT. The RAFT homopolymerization of PVDF-MA revealed that a non-negligible amount of macromonomers did not react. In contrast RAFT copolymerization of PVDF-MA and MMA resulted in the total conversion of the macromonomers and allowed the synthesis of novel methacrylic copolymers and block copolymers.

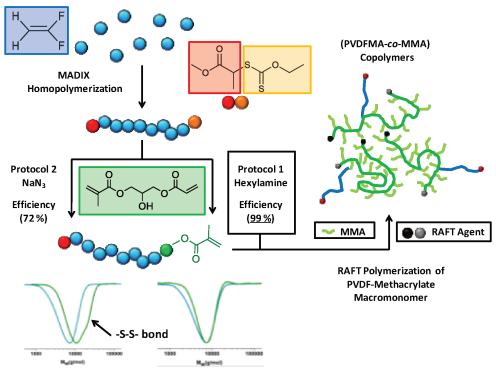

II. Introduction

PVDF-based materials have found many applications as paints and coatings, materials for packaging, high performance elastomers and separators in lithium batteries.[1] Since the late 1970s, and Tatemoto's[2] pioneering work on iodine transfer polymerization (ITP) of fluoroalkenes, the study of controlled radical polymerization of fluorine-containing monomers has been reported in a number of articles. Many studies deal with controlled radical polymerization (CRP) of fluorinated styrene,[3] (meth)acrylate monomers,[4-6] and vinyl esters[7] but only a few articles describe convincingly the CRP of fluoroalkenes (alkenes bearing fluorine atoms directly on the vinylic carbons).[8-17] Fluorinated block copolymers have recently been synthesized[18] by ATRP,[10-24] RAFT/MADIX polymerization,[10-13] photomediated ITP,[14-16] or via the use of the combination of CRP[25] or of functional initiator[26] and click chemistry. These developments represent significant progress towards the synthesis of well-defined PVDF with predetermined molecular weights, narrow molecular weight distributions, sophisticated architectures, and useful end-functionalities. Nonetheless, the synthesis of VDF-based polymers with perfect end-group fidelity is still very difficult, and so far only moderately welldefined block and copolymers have been prepared. The synthesis of PVDF-based macromonomers has been scarcely reported.[27] In 2004, Ameduri *et al.*[28] achieved the synthesis of a PVDF-based acrylate bearing from 1 to 8 VDF units via the combination of VDF telomerisation, and end group modification. Huang *et al.*[29] revisited this procedure and synthesized monoacrylates containing one or two VDF units. However, for all its merits, this method yielded PVDF macromonomers with only a few VDF units and required several synthetic steps.

Our recent work[14] on the RAFT/MADIX homopolymerization of VDF opens new opportunities to prepare PVDF macromonomers, by harnessing the chemistry of the xanthate chain end-group. The end-group removal and modification of RAFT polymers, have been well studied over the last 10 years.[30,31] Indeed, the sulphur-containing end-group could lead to unwanted colouring, or odors (caused by decomposition), and undesirable residual chemical reactivity. To achieve this goal, several ways have been studied: thermolysis,[32-34] radical induced end-group removal,[35] hetero-Diels Alder chemistry,[36,37] reduction,[38] and nucleophilic substitution usually using primary amines.[39] This latter technique does not remove the terminal sulphur atom from the polymer. This remaining terminal thiol or thiolate can nonetheless be very useful for further chemical modification owing to the rich chemistry of thiols and their derivatives.

Thiol‑ene and thiol‑yne reactions for example have been very successfully used to prepare a range of functional polymers.[40-45] Another attractive reaction, is the thia-Michael addition which can be considered as an example of click chemistry. This reaction efficiently catalysed by phosphines[46-48] allows the introduction of a functional group, and synthesize uncommon architectures, using mild conditions. For example, Lowe et al.[47] reported the synthesis of star polymers using *thia*-Michael addition of a polyacrylamide synthesized by RAFT on a triacrylate core. The same team[46] also described the post-functionalization of polyacrylamides into allyl and propargyl function using the same method. This *thia*-Michael addition was also shown to be a very facile and powerful method to synthesize monomers[49-51] and macromonomers[52] using 3-(acryloyloxy)-2-hydroxypropylmethacrylate (AHPMA), a dissymmetric telechelic molecule featuring both a methacrylate and an acrylate functional group. Thiols add with total regioselectivity onto the acrylate group to form a new methacrylate (macro)monomer.

The main goal of this work was to develop a robust and facile method to synthesise PVDF macromonomers. Two onepot strategies of PVDF macromonomer synthesis have thus been investigated and compared: protocol 1: using hexylamine to remove xanthate end-groups, and protocol 2: using sodium azide as a nucleophile. The PVDF macromonomers obtained by the most efficient method were homopolymerized and copolymerized with MMA by RAFT polymerization.

III. Experimental Section

Materials

4-Cyano-4-(2-phenylethanesulfanylthiocarbonyl)sulfanyl pentanoicacid (PETTC) CTA was synthesized according to the method described by Semsarilar et al.[53] 2,2′ -Azobis-isobutyronitrile (AIBN) purchased from Sigma Aldrich was recrystallized in methanol prior to use. All other reagents were used as received unless stated otherwise. 1,1-Difluoroethylene (vinylidene fluoride, VDF) was kindly supplied by Arkema (Pierre-Benite, France). *O*-Ethyl-*S*-(1-methoxycarbonyl)ethyldithiocarbonate, was kindly provided by Solvay SA. *tert*-Amyl peroxy-2- ethylhexanoate (purity 95%, Trigonox 121), 4,4′ -azobis-4-cyanopentanoic acid (ACVA, >98%) and azobisisobutyronitrile (AIBN>98%) were purchased from AkzoNobel (Chalons-sur-Marne, France). ReagentPlus grade (purity >99%) dimethyl carbonate (DMC), 2-phenylethanethiol, dimethylformamide (DMF), 3-(acryloyloxy)-2-hydroxypropyl

methacrylate (AHPMA), sodium azide (NaN_3), dimethylphenylphosphine (DMPP), triethylamine (TEA), hexylamine, methyl methacrylate (MMA), methanol (MeOH), tetrahydrofuran (THF), ethyl acetate and laboratory reagent grade hexane and diethyl ether (purity>95%) were purchased from Sigma Aldrich.

Nuclear Magnetic Resonance (NMR)

The Nuclear Magnetic Resonance (NMR) spectra were recorded on a Bruker AC 400 instrument. Deuterated acetone was used as the solvent in each sample. Coupling constants and chemical shifts are given in hertz (Hz) and part per million (ppm), respectively. The experimental conditions for recording ^{1}H, and ^{19}F NMR, spectra were as follows: flip angle 90° (or 30°), acquisition time 4.5 s (or 0.7 s), pulse delay 2 s (or 5 s), number of scans 128 (or 512), and a pulse width of 5 μs for ^{19}F

Size Exclusion Chromatography (SEC)

Size exclusion chromatograms were recorded using a triple detection GPC from Agilent Technologies with its corresponding Agilent software, dedicated to multi-detector GPC calculation. The system used two PL1113-6300 ResiPore 300 × 7.5 mm columns (all range of M_w) with DMF as the eluent with a flow rate of 0.8 mL min^{-1} and toluene as a flow rate marker. The detector suite comprised a PL0390-0605390 LC light scattering detector with 2 diffusion angles (15° and 90°), a PL0390-06034 capillary viscometer, and a 390-LC PL0390-0601 refractive index detector. The entire SEC-HPLC system was thermostated at 35 °C. PMMA narrow standards were used for the calibration. Typical sample concentration was 10 mg mL^{-1}.

Autoclave

The radical polymerizations of VDF were performed in a 100 mL Hastelloy Parr autoclave system (HC 276), equipped with a mechanical Hastelloy stirring system, a rupture disk (3000 PSI), inlet and outlet valves, and a Parr electronic controller to regulate the stirring speed and the heating. Prior to reaction, the autoclave was pressurized with 30 bars of nitrogen to check for leaks. The autoclave was then placed under vacuum (20 10^{-3} bar) for 30 minutes to remove any trace of oxygen. A degassed solution of solvent, initiator and xanthate CTA was introduced via a funnel. The reactor was then cooled down in liquid nitrogen to about -80 °C, and the desired quantity of VDF was transferred by double weighing (i.e. the difference of weight before and after filling the autoclave with VDF). After warming up to ambient

temperature (ca. 20 °C), the autoclave was heated to the targeted temperature under mechanical stirring.

Thermogravimetric analysis (TGA)

TGA analyses were carried out on 10‑15 mg samples on a TGA Q50 apparatus from TA Instruments from 20 °C to 580 °C, in platinum pans, at a heating rate of 10 °C min^{-1}, under air.

Synthetic procedures

MADIX homopolymerization of vinylidene fluoride

Using the experimental setup described above, a typical polymerization of VDF was performed as follows: a solution of *tert*-amyl peroxy-2-ethylhexanoate (158 mg, 6.87 10^{-4} mol) and *O*-ethyl-*S*-(1-methoxycarbonyl)ethyldithiocarbonate (1.30 g, 6.25 10^{-3} mol) in dimethylcarbonate (DMC, 60 mL), was degassed by N_2 bubbling for 30 min. This homogeneous solution was introduced in the autoclave using a funnel, and VDF gas (19 g, 2.97 10^{-1} mol) was transferred into the autoclave at a low temperature, and then the reactor was gradually heated to 73 °C. The reaction was stopped after 24 h. During the reaction, the pressure was increased to a maximum of 25 bar and then decreased to 10 bar over 24 h. The autoclave was cooled down to room temperature (ca. 20 °C), purged from the residual monomers, and dimethylcarbonate was removed under vacuum. The crude product was dissolved in 30 mL of warm THF (ca. 40 °C), and left under vigorous stirring for 30 minutes. This polymer solution in THF was then precipitated dropwise into 400 mL of chilled hexane. The polymer (white powder) was filtered through a filter funnel and dried under vacuum (15 10^{-3} bar) for two hours at 50 °C. The polymerization yield (yield = 65%) was determined by gravimetry (mass of polymers obtained/mass of monomers introduced in the pressure reactor). Yields were used as conversion, since conversion is very difficult to be measured accurately for VDF and other gaseous monomers.

The degree of polymerization (DP) can be calculated from ^{1}H NMR using the integrals of the signals corresponding to: the methyl of the CTA R-group (1.19‑1.24 ppm), the CH_2 of the regular VDF additions (head-to-tail, HT, 2.70‑3.19 ppm), the CH_2 of the reverse VDF additions (tail-to-tail, TT, 2.28‑2.43 ppm), and the CH_2 of the terminal VDF units (4.02‑4.17 ppm), according to Equation II-1:

$$\textit{Equation III-1} \quad DP = \frac{\int_{2.70}^{3.19} CH_2(HT) + \int_{2.28}^{2.43} CH_2(TT) + \int_{4.02}^{4.17} CH_2(End-group)}{2/3 \times \int_{1.19}^{1.24} CH_3(R-CTA)}$$

Molecular weight was then calculated using Equation II-2:

$$\textit{Equation III-2} \quad M_{nNMR}(R) = M_nCTA + DP \times M_nVDF$$

Where $M_{n\,CTA}$ = 208.3 g.mol^{-1} and $M_{n\,VDF}$= 64.04 g.mol^{-1}

^{1}H NMR (400 MHz $(CD_3)_2CO$, δ (ppm)) Figure III-1a: 1.19-1.24 (d, -CH(**CH**$_3$)(C=O)-, $^3J_{HH}$= 7.1 Hz), 1.40-1.46 (t, **CH$_3$**-CH_2-O-, $^3J_{HH}$= 7.2 Hz), 2.28-2.43 (m,-CF_2-**CH$_2$-CH$_2$**-CF_2-, VDF-VDF TT reverse addition), 2.70-3.19 (t, -CF_2-**CH$_2$**-CF_2-, VDF-VDF HT normal addition), 3.60-3.69 (s, -(C=O)-O-**CH$_3$**), 4.02-4.17 (t, -(C=S)-S-**CH$_2$**-CF_2-, $^3J_{HF}$ = 18 Hz), 4.67-4.77 (q, CH_3-**CH$_2$**-O-, $^3J_{HH}$= 7.2 Hz), 6.05-6.45 (tt, $^2J_{HF}$ = 55 Hz , $^3J_{HH}$= 4.5 Hz -CH_2-CF_2-**H,** about 14 mol %)

^{19}F NMR (376 MHz $(CD_3)_2CO$, δ (ppm)) SI-Figure III-11: -115.63 (-CH_2-CF_2-**CF$_2$**-CH_2-CH_2-, VDF-VDF HH reverse addition), -114.29 (-CH_2-CF_2-**H**), -113.34 (-CH_2-**CF$_2$**-CF_2-CH_2-CH_2-, HH reverse addition), -113.09 (-S-CH_2-**CF$_2$**-CF_2-CH_2-), -112.69 (-S-CH_2-CF_2-**CF$_2$**-CH_2-), -94.79 (-CH_2-CH_2-**CF$_2$**-CH_2-, TT reverse addition), -93.50 (-CH_2-**CF$_2$**-CH_2-CH(CH_3)(C=O)-), -92.12 (-CH_2-**CF$_2$**-CH_2-CF_2H), -91.44 (-CH_2-**CF$_2$**-CH_2-CF_2-CH_2-CH_2-, regular VDF-VDF HT addition), -91.00 (-CH_2-**CF$_2$**-CH_2-, regular VDF-VDF HT addition).

HH, HT and TT stand for head-to-head, head-to-tail, and tail-to-tail, respectively.

(M_{nSEC} = 5100 g.mol^{-1}, Đ = 1.34, M_{nNMR} = 3000 g.mol^{-1})

Macromonomer Synthesis (PVDF-MA)

Hexylamine protocol

The aminolysis and subsequent Michael addition were conducted using a one-pot protocol described by McKee *et al*.[52] In a typical reaction $PVDF_{54}$-XA, where XA represents the ethylxanthate group, (1.00 g, 3.33 10^{-4} mol) and 3-(acryloyloxy)-2-hydroxypropyl methacrylate, AHPMA, (0.214 g, 1.00 10^{-3} mol) were dissolved in DMF (23 mL). The solution was degassed by nitrogen bubbling for 10 min and a degassed mixture of *n*-hexylamine (0.135 g, 1.33 10^{-3} mol), triethylamine (0.056 g, 5.00 10^{-4} mol) and 0.1 mL of DMPP in 1 mL of DMF was injected into the reaction mixture. Nitrogen bubbling was continued for a further 10 min and the reaction solution was then stirred at 25 °C for 16 h. The dark solution was precipitated twice from chilled methanol, and the resulting solid was

filtered through a filter funnel and dried under high vacuum at 70 °C until constant weight to remove traces of DMF (yield = 76%).

^{1}H NMR (400 MHz $(CD_3)_2CO$, δ (ppm)) Figure III-1d: 1.19-1.24 (d, -CH(**CH_3**)(C=O)-, $^{3}J_{HH}$= 7.1 Hz), 1.85-1.96 (s, H_2C=C(**CH_3**)), 2.28-2.43 (m,-CF_2-**CH_2-CH_2**-CF_2-, VDF-VDF TT reverse addition), 2-.70-3.19 (t, -CF_2-**CH_2**-CF_2-, VDF-VDF HT normal addition), 3.25-3.40 (t, -CF_2-CF_2-**CH_2**-S-, $^{3}J_{HF}$ = 18 Hz), 3.60-3.69 (s, -(C=O)-O-**CH_3**), 4.00-4.55 (m, -O-**CH_2-CH**(OH)-**CH_2**-O-), 5.60-5.68 (s, **H**-CH=C(CH_3)-), 6.05-6.14 (s, **H**-CH=C(CH_3)-), 6.05-6.45 (tt, $^{2}J_{HF}$ = 55 Hz , $^{3}J_{HH}$= 4.5 Hz -CH_2-CF_2-**H,** about 14 mol %)

^{19}F NMR (376 MHz $(CD_3)_2CO$, δ (ppm)) Figure III-2d : -115.63 (-CH_2-CF_2-**CF_2**-CH_2-CH_2-, VDF-VDF HH reverse addition), -114.29 (-CH_2-CF_2-**H**), -114.24 (-CH_2-CF_2-**CF_2**-CH_2-S-), -113.34 (-CH_2-**CF_2**-CF_2-CH_2-CH_2-, HH reverse addition), -112.83 (-CH_2-**CF_2**-CF_2-CH_2-S-),-94.79 (-CH_2-CH_2-**CF_2**-CH_2-, TT reverse addition), -93.50 (-CH_2-**CF_2**-CH_2-CH(CH_3)(C=O)-), -92.12 (-CH_2-**CF_2**-CH_2-CF_2H), -91.44 (-CH_2-**CF_2**-CH_2-CF_2-CH_2-CH_2-, regular VDF-VDF HT addition), -91.00 (-CH_2-**CF_2**-CH_2-, regular VDF-VDF HT addition).

(M_{nSEC} = 6000 gmol^{-1}, Đ = 1.22, M_{nNMR} = 3000 gmol^{-1})

NaN_3 protocol

As above, the conversion of the xanthate end-group and the Michael addition were conducted using a one-pot protocol. The removal of the xanthate group was performed using NaN_3 instead of amines as described by Wu *et al*.[54]

In a typical reaction, $PVDF_{54}$-XA (1.00 g, 3.33 10^{-4} mol) and 3-(acryloyloxy)-2-hydroxypropyl methacrylate, AHPMA, (0.214 g, 1.00 × 10^{-3} mol) were dissolved in DMF (23 mL). The solution was degassed by nitrogen bubbling for 10 min and a degassed solution of NaN_3 (0.130 g, 2.00 × 10^{-3} mol) and 0.1 mL of DMPP in a mixture of 1 mL of DMF and 1 mL of distilled water was injected into the reaction mixture. Nitrogen bubbling was continued for a further 10 min and the reaction solution was then stirred at 25 °C for 16 h. The red solution was precipitated twice from chilled methanol, and the resulting solid was filtered through a filter funnel and dried under high vacuum at 70 °C until constant weight to remove traces of DMF (yield = 80%).

(M_{nSEC} = 8800 g mol^{-1}, Đ = 1.41, M_{nNMR} = 3000 g mol^{-1}).

RAFT homopolymerization of PVDF-MA macromonomer

In a typical reaction, $PVDF_{54}$-MA (1.00 g, 2.78 10^{-4} mol), AIBN (1.2 mg, 7.3 10^{-6} mol) and PETTC (9.55 mg, 2.81 10^{-5} mol) were dissolved in 5 mL of DMF. The solution was degassed by nitrogen bubbling for 15 min and left under stirring at 70 °C for 24 h. The crude reaction was precipitated in a large excess of methanol and the resulting solid was dried under vacuum at 70 °C until constant weight (yield = 95%).

RAFT copolymerization of PVDF-MA macromonomer and methyl methacrylate

A mixture of $PVDF_{54}$-MA (0.10 g, 2.78 10^{-5} mol), MMA (136 mg, 1.36 × 10^{-3} mol), PETTC (9.40 mg, 2.70 × 10^{-5} mol), and AIBN (1.00 mg, 5.60 10^{-6} mol) was dissolved in 2 mL of DMF. The solution was degassed by N_2 bubbling for 15 min and left under stirring at 70 °C for 24 h. The crude reaction was precipitated in a large excess of methanol and the resulting was dried under vacuum at 70 °C until constant weight (yield = 85%).

Synthesis of poly[(PVDF-MA-*co*-MMA)-*b*-PMMA] block copolymer

Poly(PVDF-MA-*co*-MMA) copolymer (20 mg, 4.0 10^{-6} mol), MMA (80 mg, 8.0 10^{-4} mol) and AIBN (0.15 mg, 9.1 10^{-7} mol) were dissolved in 0.5 mL of DMF. The solution was degassed by N_2 bubbling for 15 min and left under stirring at 70 °C for 24 h. The crude reaction was precipitated in a large excess of methanol and the resulting solid was dried under vacuum at 70 °C until constant weight (yield = 51%).

IV. Results and Discussion

IV.1 Comparison of methods

Special care was paid to the thiocarbonylthio group removal step. Indeed, PVDF is relatively sensitive to bases which can cause dehydrofluorination.[55-58] This sensitivity may be a significant limitation to PVDF chemical modification strategies. In the presence of a base, PVDF solutions readily turn black as a consequence of dehydrofluorination reaction creating conjugated C=C bonds within the PVDF backbone. However, it has been shown that only 0.1% of dehydrofluorination is sufficient to cause a deep black coloration of PVDF.[54] This undesired reaction was partially investigated with several alkaline compounds, and should also occur with primary amine.[57] However, the very fast and quantitative reaction of primary amines with xanthate groups and the mild conditions used (low temperature, short reaction time, amine/xanthate group molar ratios) should limit this phenomenon. Furthermore, the

conjugated C=C bonds in dehydrofluorinated PVDF can be easily assigned in ^{1}H NMR as distinctive signals at 6 ppm.[57,59]

Using sodium azide[54] instead of amine could be an efficient way to prepare thiol-terminated PVDF while avoiding the undesired dehydrofluorination reaction. The synthesis of the PVDF macromonomer was achieved using the experimental protocols depicted in Scheme III-1. In these reactions, NaN_3 and hexylamine played the role of nucleophilic thiocarbonylthio-group removal agents, while DMPP was used as a catalyst, TEA as a proton sponge for the *thia*-Michael addition, and AHPMA as a Michael acceptor. Protocol 1 yielded black polymers while protocol 2 delivered reddish polymers. These observations suggest that dehydrofluorination probably occurred in parallel to the xanthate removal. However, this dehydrofluorination could not be detected by either ^{1}H or ^{19}F NMR *(vide infra)*. The extent of the dehydrofluorination is thus likely negligible. Figure III-1 displays the ^{1}H NMR spectra of: (a) xanthate-functionalized PVDF (PVDF-XA) synthesized by MADIX polymerization, (b) the thiol-functionalized PVDF (PVDF-SH) formed by aminolysis of PVDF-XA using hexylamine, (c) the thiol-functionalized PVDF (PVDF-SH) formed via NaN_3 elimination, (d) the PVDF methacrylate macromonomer (PVDF-MA) synthesized using protocol 1 (Scheme III-1) and (e) the PVDF methacrylate macromonomer (PVDF-MA) synthesized using protocol 2 (Scheme III-1).

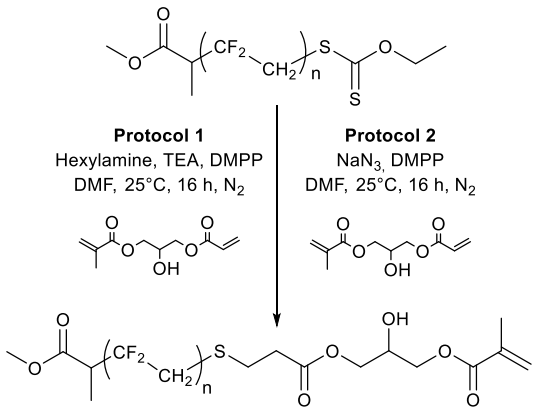

Scheme III-1: Synthesis of PVDF-MA macromonomer from PVDF-XA according to two strategies.

As reported previously,[14] the ^{1}H NMR spectrum of the PVDF-XA (Figure III-1a) shows the characteristic signals of the *O*-ethyl xanthate terminal group (a triplet at 1.4 ppm (CH_3 of the *O*-ethyl xanthate) and a quartet at 4.7 ppm (-CH_2-O- of the O-ethyl xanthate)), and a well-defined triplet centered at 4.1 ppm corresponding to the CH_2 group of the last VDF unit connected to the *O*-ethyl xanthate moiety (-CF_2-CH_2-S-). Indeed, MADIX polymerization of

VDF leads to an accumulation of PVDF chains terminated by -CF_2-CH_2-Xa moieties.[14] The PVDF used here was exclusively composed of such -CF_2-CH_2-Xa-terminated chains.

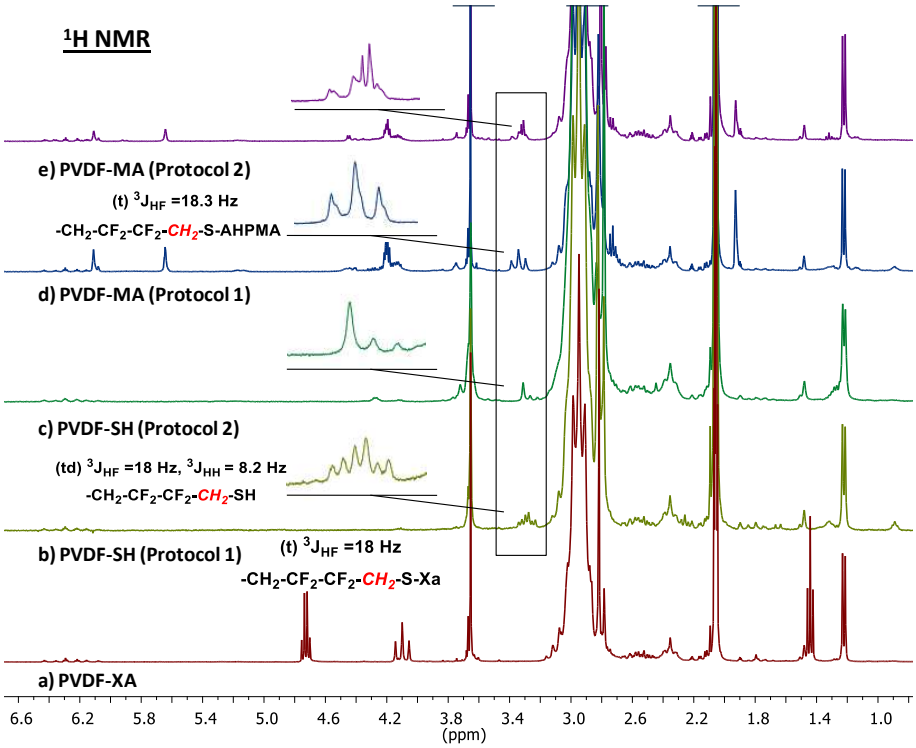

Figure III-1: ^{1}H NMR spectra in $(CD_3)_2CO$ of: (a) PVDF-XA, (b) PVDF-SH prepared using hexylamine (protocol 1), (c) PVDF-SH prepared using sodium azide (protocol 2), (d) PVDF-MA macromonomer prepared using protocol 1, and (e) PVDF-MA macromonomer prepared using protocol 2.

After aminolysis, the ^{1}H NMR spectrum of the PVDF-SH (Figure III-1b) shows the elimination of the ω-chain end group (complete disappearance of the triplet and quartet of the *O*-ethyl xanthate at 1.4 and 4.7 ppm, respectively); and the formation of the thiol end-group revealed by the shift of the signal of the methylene of the terminal VDF unit from 4.1 ppm to 3.3 ppm. This signal is also split into a doublet of triplets (with a coupling constant $^3J_{HH}$ = 8.2 Hz) in agreement with a -CH_2-SH motif. After the Michael addition, this coupling between the proton of the thiol and the CH_2 of the terminal VDF unit disappears (Figure III-1d). Instead, a triplet can be seen at 3.3 ppm on the ^{1}H NMR spectrum of the polymer isolated after the reaction following the one-pot aminolysis and thia-Michael addition protocol, thus confirming the synthesis of the PVDF methacrylate macromonomer. The ^{1}H NMR spectra of the PVDF-SH (Figure III-1c) obtained using NaN_3 as a nucleophile and of PVDF-MA (Figure III-1e) prepared via protocol 2 (one-pot reaction using sodium azide in the presence of AHPMA and DMPP) are very different from the corresponding PVDF-SH (Figure III-1c) and PVDF-MA (Figure III-1d) prepared using hexylamine and protocol 1 respectively. The well-

resolved triplet observed at 3.3 ppm on the ^{1}H NMR spectrum of the PVDF-MA synthesized via protocol 1 (Figure III-1d), appears as a multiplet in the case of the PVDF-MA synthesized using protocol 2 (Figure III-1e). This difference suggests that the *thia*-Michael addition did not proceed quantitatively in protocol 2 or that it is accompanied by undesired side reactions. The comparison of the intensity of the signals of the methacrylic protons (at 5.63, 6.10, and 1.90 ppm, in Figure III-1d and e) with that of the (-CH-**CH$_3$**) signal at 1.2 ppm (Figure III-1) or that of the ((C=O)-O-**CH$_3$**) signal at 3.6 ppm (Figure III-1a) of the MADIX CTA R-group at the α-end of the PVDF chain allows the calculation of the extent of the replacement of the xanthate moiety into methacrylate (see Equation III-3below). However, as reported in a previous work,[14] the PVDF-XA chains initiated by the CTA R-group radicals were not all terminated by the xanthate Z-group. Transfer to the DMC occurred in the course of the polymerisation, leading to around 14% of dead chains terminated with by a -CF_2H group.

Therefore, a correction factor (α = 0.86) was introduced in Equation III-3 to calculate accurately the percentage of end group functionality.

$$\textit{Equation III-3} \quad \textit{Functionality (\%)} = \frac{\int_{6.04}^{6.13}(H) + \int_{5.56}^{5.68}(H) + \int_{1.86}^{1.96}(CH_3)}{\frac{5}{3}\int_{1.18}^{1.25}(CH_3)} \times \alpha$$

This calculation shows a total functionality of 85% and 62% with a coupling efficiency of 99% and 72% for protocol 1 and protocol 2, respectively (see SI-Figure III-9 and SI-Figure III-10 for details). The aminolysis-Michael addition method is thus confirmed to be more efficient than the method utilizing sodium azide.

The same comparative study was carried out using ^{19}F NMR spectroscopy. Figure III-2 presents the -111.5 to -117 ppm region of the ^{19}F NMR spectra of: (a) PVDF-XA (b) PVDF-SH, formed by aminolysis of PVDF-XA using hexylamine, (c) PVDF-SH, formed via NaN_3 elimination, (d) PVDF-MA synthesized using protocol 1, (e) PVDF-MA synthesized using protocol 2 (full NMR spectra are provided in SI-Figure III-11and SI-Figure III-12). The effect of the aminolysis can easily be seen by monitoring the −112 ppm −117 ppm region where the signals corresponding to the ultimate and penultimate VDF unit appear (-CH_2-CF_2-**CF_2**-CH_2-S-: -113.09 ppm, and -CH_2-**CF_2**-CF_2-CH_2-S-: −112.69 ppm).

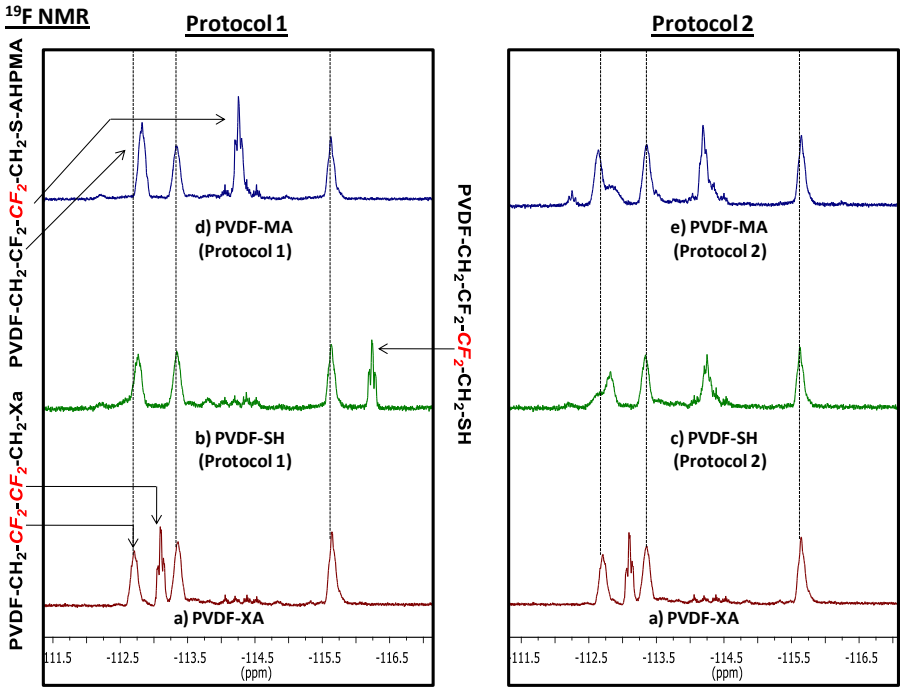

Figure III-2: Expansion of the -111.5 - -117 ppm region of the ^{19}F NMR spectra in $(CD_3)_2CO$ of : a) PVDF-XA, b) PVDF-SH prepared by aminolysis, c) PVDF-SH prepared by action of NaN_3, d) PVDF-MA prepared following protocol 1 and e) PVDF-MA prepared following protocol 2

On the spectrum of PVDF-SH (Figure III-2b) a surprising highfield shift of the signal of the CF_2 terminal VDF unit from -113.09 ppm to -116.4 was observed following aminolysis. This shielding was caused by the removal of the xanthate group. This end-group removal also had a small influence on the CF_2 of the penultimate VDF unit (which shifted from -112.69 to -112.77 ppm). Similarly to what was observed by ^1H NMR spectroscopy, ^{19}F NMR also shows that the end-group removal by aminolysis was quantitative. The spectrum of PVDF-MA prepared via protocol 1 (Figure III-2d) shows the deshielding of the signals of the CF_2 of the ultimate VDF unit from -116.4 ppm in PVDF-SH to -114.24 ppm and the shielding of the signal of the CF_2 of the penultimate VDF unit from -112.77 ppm (in PVDF-SH) to -112.83 ppm. The complete shifts of these ^{19}F NMR signals confirm the quantitative coupling of the AHPMA onto the ω-end of the PVDF chains. The study of the ^{19}F NMR spectra of the product obtained using protocol 2 revealed significant differences (Figure III-2c and e). For PVDF-SH, the signal of the CF_2 of the ultimate VDF unit shifted from -113.09 to -114.19 ppm and the peak assigned to the CF_2 of the penultimate VDF unit observed at -112.73 in PVDF-XA was split into two distinctive peaks at -112.66 ppm and −112.84 ppm after treatment with NaN_3 (Figure III-2c). This feature can also be seen in the ^{19}F NMR spectrum of PVDF-MA prepared using protocol 2 (Figure III-2e). This difference may be ascribed to differences in the xanthate group removal reaction.

The mechanism of the reaction involving NaN_3 was proposed by Wu *et al.*[54] and this reaction was reported to be extremely fast (quantitative in 3 - 5 min). The formation of disulfide linkages was readily observed by Wu *et al.* in their study. In the case of PVDF-XA, the reaction was also observed to be very fast and the GPC traces (Figure III-3) of PVDF-SH and of PVDF-MA also suggest the formation of substantial amounts of PVDF-SS-PVDF, even when the reaction was carried out in the presence of a reducing agent such as DMPP.

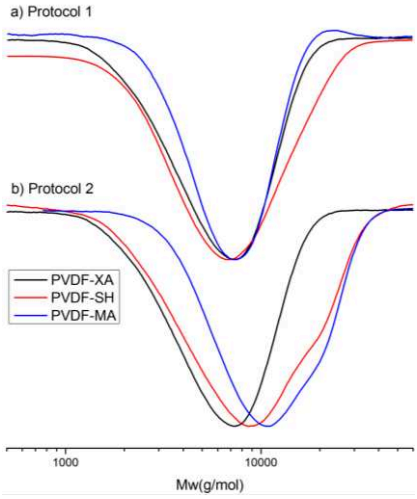

Figure III-3: RI GPC traces of: a) PVDF-XA, PVDF-SH prepared by aminolysis, and PVDF-MA prepared following protocol 1; b) PVDF-XA, PVDF-SH prepared by action of NaN_3 and PVDF-MA prepared following protocol

McKee *et al.*[52] showed that the reaction rate of the *thia*-Michael additions was faster than that of the aminolysis reaction. Consequently, as soon as a thiol was formed by aminolysis, it reacted immediately on the Michael acceptor. This one pot reaction (Aminolysis/*thia*-Michael addition) is an efficient method to decrease the thiol concentration in the reaction medium, which in turn impairs the formation of disulfide bond.

The lower efficiency of protocol 2 compared to protocol 1 may lie in the large difference of the reaction rate between the *thia*-Michael additions and the xanthate end-group removal effected by sodium azide. Indeed, this reaction is very fast. The hypothesis is that it releases, in a very short time, a large quantity of thiols which are not immediately consumed by *thia* Michael addition, but form disulfide bonds instead. If this hypothesis is true, then protocol 2 may, in a way, be considered as a two-step process where PVDF-XA are first converted into PVDF-SH which can then react either on themselves to form disulfides or on AHPMA to yield PVDF-MA. In conclusion, protocol 1 is a better method to efficiently synthesise PVDF methacrylates with high chain-end functionality.

IV.2 RAFT Homopolymerization and copolymerization of PVDF-MA macromonomer with methyl methacrylate

Typical polymerizations of PVDF-MA macromonomer and synthetic procedure of copolymerization with methyl methacrylate are summarized and depicted in Table III-1 and : b

Scheme III-2.

Table III-1: Experimental conditions ofr the RAFt (co)polymerization of PVDF-MA macromonomer

Run	$\frac{[PVDF\text{-}MA]_0}{[CTA]_0}$	$\frac{[MMA]_0}{[CTA]_0}$	Conversion PVDF-MA[a] (%)	Conversion MMA[b] (%)	$M_n$theo[c] (g/mol)	M_nNMR[d] (g/mol)	M_nSEC[e] (g/mol)	Đ[e]
1	10	0	59	0	18300	21000	9700	1.48
2	1	49	100	52	5600	5000	9800	1.33
3	1*	200	0	45	12000	9500	14100	1.35

[a]Measured by ^{1}H NMR. [b]Measured by gravimetry. [c]$M_{n,theo} = ([M]_0/[CTA]_0 \times M_w$ monomer × conversion)/100 + $M_{n,CTA}$. [d]Calculated from the degree of polymerization determined by ^{1}H NMR. [e]SEC data based on PMMA narrow standard calibration (solvent: DMF). *Poly($PVDF_{54}$-MA-*co*-MMA_{20}) (run 2) used as MacroCTA. Reaction conditions: [I]/[CTA] = 0.2, T = 70 °C, with: CTA = 4-cyano-4-(2-phenylethanesulfanylthiocarbonyl)-sulfanylpentanoicacid, initiator = AIBN, solvent = DMF.

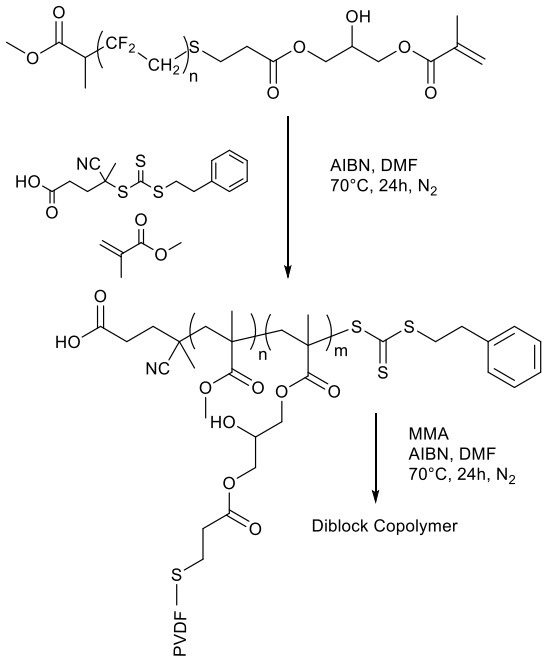

: b

Scheme III-2: RAFT copolymerization of PVDF-MA macromonomer

The RAFT homopolymerization of the PVDF-MA macromonomer (run 1, Table III-1) did not reach high conversion (59% only in 24 h), probably due to the lack of reactivity of the methacrylate group of PVDF-MA caused by steric hindrance and lack of chain mobility. In addition, the purification of the oligo (PVDF-MA) obtained (elimination of the excess macromonomer) was quite difficult. The GPC traces (Figure III-4a) of the PVDF-MA and of

the oligo(PVDF-MA) obtained after 24 hours of polymerization clearly show that a significant amount of PVDF-MA did not react. However, when RAFT polymerization was carried out on a 50/1 mixture of MMA/PVDF-MA, total conversion of the PVDF-MA was achieved (Table III-1, run 2 and Figure III-5). The GPC trace of the corresponding copolymer of PVDF-MA and MMA is displayed inFigure III-4b (red chromatogram). The significant shift of the GPC trace towards higher molecular weights suggests that the copolymerization proceeded under good control.

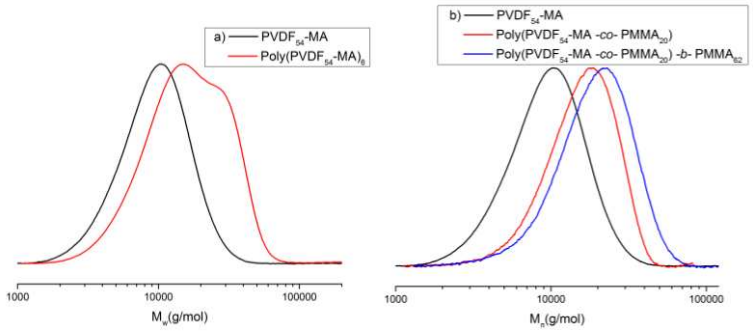

Figure III-4: a) GPC traces (viscometric detector) of $PVDF_{54}$-MA (black trace) and poly($PVDF_{54}$-MA)$_6$ (red trace) prepared by RAFT polymerization. (b) GPC traces (viscometric detector) of PVDF-MA (black trace), poly- ($PVDF_{54}$-MA-co-MMA_{20}) (red trace) and of poly[($PVDF_{54}$-MA-co- MMA_{20})-b-$PMMA_{62}$] (blue trace).

The ^{1}H NMR spectrum of the poly(PVDF-MA-*co*-MMA) copolymer (Figure III-5) attests the complete conversion of the PVDF-MA (complete disappearance of the methacrylic protons in the 5.6 to 6.1 ppm range). The chain extension of the poly-(PVDF-MA-*co*-MMA) with methyl methacrylate was also carried out (run 3, Table III-1). This polymerization reached 45% conversion. The GPC trace of the resulting poly[(PVDF-MA-*co*-MMA)-b-PMMA] (Figure III-4b, blue chromatogram) suggests the efficient chain extension of the copolymers with a PMMA block.

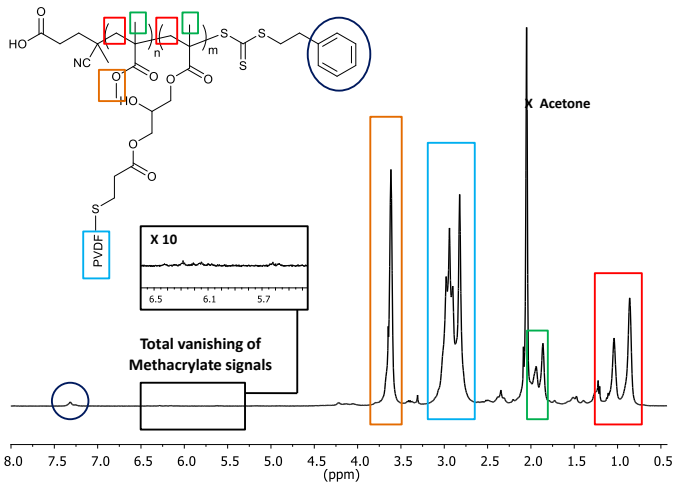

Figure III-5: 1H NMR spectrum of the RAFT copolymerizatio of MMA with PVDF-MA in (CD3)2CO.

IV.3 Thermal stability

The thermal stabilities of PVDF-XA, PVDF-MA and poly- (PVDF-MA-*co*-MMA) copolymer were determined by thermogravimetric analysis under air (Figure III-6). As expected, PVDF polymers (PVDF-MA and PVDF-XA) exhibited good thermal stabilities with no significant weight loss until 336 °C and 350 °C, respectively. The superior thermal stability of PVDF-MA is most likely due to the higher stability of the methacrylate group, compared to the thiocarbonylthio end group.[60] Above 380 °C, decomposition of the PVDF via dehydrofluorination is rapidly observed.

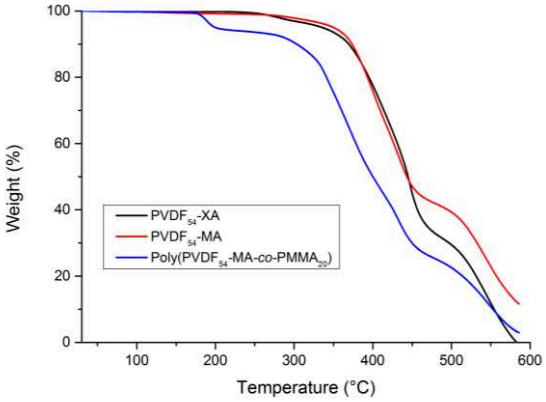

Figure III-6: Thermogravimetric analysis under air of PVDF-XA, PVDF-MA, and poly(PVDF-MA-co-MMA) copolymers.

The TGA profile of the poly(PVDF-MA-*co*-MMA) copolymer showed several weight loss stages, indicating a complex thermal decomposition mechanism.[61] The first decomposition stage (occurring at about 200 °C) is due to the scissions of the head-to-head linkages in the PMMA segments. The second decomposition stage (occurring at 330 °C) is caused by unzipping depolymerization from vinylidene ends (both PMMA and PVDF chains) and dehydrofluorination of the PVDF segments, and the third stage (500 °C) corresponds to random scissions within the polymethacrylic and PVDF backbones.

V. Conclusion

This article presents and compares two one-pot methods to prepare well-defined PVDF-based methacrylate macromonomers prepared from PVDF (synthesized by MADIX homopolymerization of VDF) and 3-(acryloyloxy)-2-hydroxypropyl methacrylate (AHPMA).

The aminolysis/thia Michael addition combination (protocol 1) proved to be very efficient to afford well-defined PVDF-MA macromonomers and to be superior to the sodium azide treatment/thia Michael addition combination (protocol 2). Indeed, protocol 2 did not provide total functionalization of the polymer end-group in contrast to protocol 1 which allowed the transformation of 99% of the xanthate chain-ends into methacrylate for a total polymer functionality of 85% as shown by detailed ^{1}H and ^{19}F NMR characterization. The PVDF-MA macromonomers prepared were black, due to some dehydrofluorination caused by attack of the PVDF by the primary amine. The extent of this dehydrofluorination was nonetheless not detected either by ^{1}H or ^{19}F NMR and was not detrimental to either the macromonomer synthesis or its polymerization. RAFT homopolymerization of PVDF-MA did not proceed with high conversion but a welldefined poly(PVDF-MA-*co*-MMA) copolymer and a poly-[(PVDF-MA-*co*-MMA)-*b*-PMMA] block copolymer were easily synthesized by RAFT polymerization. The aminolysis/thia Michael addition one-pot protocol is thus very efficient to prepare well-defined PVDF methacrylate macromonomers. These novel macromonomers open the way to the synthesis of new PVDF-based architectures such as block copolymers, graft copolymers and bottle brush copolymers for example.

VI. Acknowledgement

The authors thank Arkema S.A (Pierre Bénite, France) and Solvay S.A (Lyon, France) for providing VDF and Xanthate, respectively and the “Ministère Francais de l’Education Nationale, de l’ Enseignement supérieur et de la Recherche” for the Ph.D Grant attributed to MG.

VII. References

[1] B. Ameduri, *Chem. Rev.,* 2009, **109**, 6632−6686.

[2] M. Tatemoto, In *The First Regular Meeting of Soviet-Japanese Fluorine Chemists*, Tokyo, February 15–16, 1979.

[3] N.M. Hansen, K. Jankova, S. Hvilsted, *Eur. Polym. J.,* 2007*,* **43**, 255-293.

[4] B.P. Koiry, A. Chakrabarty and N.K. Singha, *RSC Adv.,* 2015, **5**, 15461.

[5] S. Chen, W.H. Binder, *Polym Chem.,* 2015, **6**, 448-458.

[6]W. Yao, Y. Li, X. Huang, *Polymer*, 2014, **55**, 6197-6211.

[7] E. Girard, X. Liu, J.D. Marty, M. Destarac, *Polym Chem.*, 2014, **5**, 1013-1022

[8] D. Valade, C. Boyer, B. Ameduri, B. Boutevin, *Macromolecules*, 2006, **39**, 8639–8651

[9] A. Meskini, M. Raihane, I. Stevenson-Royaud, G. Boiteux, G. Seytre, B. Ameduri, *J. Non-Cryst. Solids*, 2010, **356**, 688–694.

[10] G. Laruelle, E. Nicol, B. Ameduri, J. F. Tassin, N. Ajellal, *J. Polym. Sci. Part A: Polym. Chem.*, 2011, **49**, 3960–3969.

[11] G. Kostov, F. Boschet, J. Buller, L. Badache, S. Brandsadter, B. Ameduri, *Macromolecules*, 2011, **44**, 1841–1855.

[12] E. Girard, J.-D. Marty, B. Ameduri, M. Destarac*, ACS Macro Lett.*,2012, **1**, 270–274.

[13] Y. Patil, B. Ameduri, *Polym. Chem*., 2013, **4**, 2783–2799.

[14] M. Guerre, B. Campagne, O. Gimello, K. Parra, B. Ameduri, V. Ladmiral, *Macromolecules*, 2015, **49**, 5386-5396

[15] A. D. Asandei, O. I. Adebolu, C. P. Simpson*, J. Am. Chem. Soc.*, 2012, **134**, 6080–6083.

[16] A. D. Asandei, O. I. Adebolu, C. P. Simpson, J.-S. Kim,*Angew. Chem. Int. Ed.,* 2013, **52**, 10027–10030.

[17] P. Cernoch, S. Petrova, Z. Cernochova, J.-S Kim, C.P. Simpson,A.D. Asandei, *Eur. Polym. J.*, 2015, **68**, 460 – 470.

[18] V. S. D. Voet, G.T. Brinke, K. Loos, *J. Polym. Sci., Part A: Polym. Chem.,* 2014, **52**, 2861–2877.

[19] Z. B. Zhang, S. K. Ying, Z. Q. Shi, *Polymer*, 1999, **40**, 1341–1345.

[20] S. M. Jol, W. S. Lee, B. S. Ahn, K. Y. Park, K. A. Kim, I. S. Rhee Paeng, *Polym. Bull.,* 2000, **44**, 1–8.

[21] M. Duc, B. Ameduri, G. David, B. Boutevin, *J. Fluorine Chem.*,2007, **128**, 144–149.

[22] (a) Z. Q. Shi, S. Holdcroft, *Macromolecules*, 2004, **37**, 2084–2089. (b) Z. Q. Shi, S. Holdcroft, *Macromolecules*, 2005, **38**, 4193–4201.

[23] K. Xu, K. Li, P. Khanchaitit, Q. Wang, Chem. Mater., 2007, **19**, 5937–5945.

[24] (a) V. S. D. Voet, D. Hermida-Merino, G. ten Brinke, K. Loos, *RSC Adv.*, 2013, **3**, 7938–7946. (b) V. S. D. Voet, M. Tichelaar, S. Tanase, M. C. Mittelmeijer-Hazeleger, G. ten Brinke, K. Loos, *Nanoscale*, 2013, **5**, 184–192.

[25] *R.* Vukicevic, U. Schwadtke, S. Schmucker, P. Schafer, D. Kuckling, S. Beuermann, *Polym. Chem., 2012, **3**, 409–414.*

[26] V. S. D. Voet, G. O. R. Alberda van Ekenstein, N. L.Meereboer, A. H. Hofman, G. ten Brinke, K. Loos, *Polym. Chem.*, 2014, **5**, 2219–2230.

[27] A. Vitale, R. Bongiovanni, B. Ameduri, *Chem. Rev.*, 2015, **115**, 8835-8866.

[28] F. Montefusco, R. Bongiovanni, A. Priola, B. Ameduri, *Macromolecules*, 2004, **37**, 9804-9813.

[29] J.Q. Huang, W.D. Meng, F.L. Qing, *J. Fluorine Chem.*, 2007, **128**, 1469−1477

[30] Y. K. Chong, G. Moad, E. Rizzardo, S. H. Thang,*Macromolecules*, 2007, **40**, 4446–4455.

[31] H. Willcock, R. K. O'Reilly, *Polym. Chem.*, 2010, **1**, 149–157

[32] B. Chong, G. Moad, E. Rizzardo, M. Skidmore, S. H. Thang, *Aust. J. Chem.*, 2006, **59**, 755–762.

[33] A. Postma, T. P. Davis, G. Moad and M. S. O'Shea, *Macromolecules*,2005, **38,** 5371–5374.

[34] L. Chugaev, *Chem. Ber.*, 1899, **32**, 3332.

[35] S. Perrier, P. Takolpuckdee and C. A. Mars, Macromolecules, 2005,38, 2033–2036.

[36] A. J. Inglis, S. Sinnwell, T. P. Davis, C. Barner-Kowollik and M. H. Stenzel, *Macromolecules*, 2008, **41**, 4120–4126.

[37] S. Sinnwell, A. J. Inglis, T. P. Davis, M. H. Stenzel and C. Barner-Kowollik, *Chem. Commun.*, 2008,**17**, 2052–2054.

[38] B. J. Kim, S. Given-Beck, J. Bang, C. J. Hawker and E. J. Kramer, *Macromolecules*, 2007, **40**, 1796–1798.

[39] M. Deletre, G. Levesque, *Macromolecules*, 1990, **23**, 4733–4741.

[40] A. Cornille, V. Froidevaux, C. Negrell, S. Caillol, B. Boutevin, *Polymer*, 2014, **55**, 5561-5570.

[41] R. Auvergne, M. Desroches, S. Clerc, S. Carlotti, S. Caillol, B. Boutevin, *Reactive & Functional Polymers,*2012, **72**, 393–401.

[42] M. Semsarilar, V. Ladmiral, S. Perrier, *Macromolecules*, 2010, **43**, 1438-1443.

[43] A. B. Lowe, C.E. Hoyle, C. N. Bowman, *J. Mater. Chem.,* 2010, **20**, 4745-4750.

[44] A.B. Lowe, *Polym. Chem.*, 2010, **1**, 17-36.

[45] H. Li, B. Yu, H. Matsushima, C. E. Hoyle, A. B Lowe, *Macromolecules*, 2009, **42**, 6537-6542.

[46] J. W. Chan, B. Yu, C. E. Hoyle, A.B. Lowe, *Chem. Commun.*, 2008, **40**, 4959–4961

[47] B. Yu, J. W. Chan, C.E. Hoyle, A. B. Lowe, *J. Polym. Sci.: Part A: Polym. Chem.*, 2009, **47**, 3544–3557

[48] G. Z Li, R. K. Randev, A. H. Soeriyadi, G. Rees, C. Boyer, Z. Tong, T. P. Davis, C. R. Becer, D. M. Haddleton, *Polym. Chem.*, 2010, **1**, 1196–1204

[49] V. Ladmiral, A. Charlot, M. Semsarilar, S. P. Armes, *Polym. Chem*., 2015, **6**, 1805–1816

[50] V. Ladmiral, M. Semsarilar, I. Canton, S. P. Armes, *J. Am. Chem. Soc.*, 2013, **135**, 13574-13581.

[51] A. M. Alswieleh, N. Cheng, I. Canton, B. Ustbas, X. Xue, V. Ladmiral, S. Xia, R. E. Ducker, O. E. Zumir, M. L. Cartron, C. N. Hunter, G. J. Legget, S. P. Armes, *J. Am. Chem. Soc.*, 2014, **136,** 9404−9413.

[52] J. R. McKee, V. Ladmiral, J. Niskanen, H. Tenhu, S. P. Armes, *Macromolecules*, 2011, **44,** 7692–7703.

[53] M. Semsarilar, V. Ladmiral, A. Blanazs, S. P. Armes, *Langmuir*, 2012, **28**, 914.

[54] Y. Wu, Y. Zhou, J. Zhu, W. Zhang, X. Pan, Z. Zhang, X. Zhu, *Polym. Chem*, 2014, **5**, 5546−5550

[55] J. Scheirs, In *Modern fluoropolymers: High performance polymers for diverse applications*, Chichester: Wiley, 1997, 18-19

[56] H. Kise, H. Ogata, M. Nakata, *Angew. Makromolek. Chem.,* 1989, **168,** 205-216.

[57] A. Taguet, L. Sauguet, B. Ameduri, B. Boutevin, *J. Fluorine Chem.*, 2007, **128**, 619-630.

[58] A. Taguet, B. Ameduri, B. Boutevin, *Adv.Polym. Sci.*, 2005,**184**, 127–211.

[59] S. Tan, J. Li, G. Gao, H. Li, Z. Zhang, *J. Mater. Chem*., 2012, **22**, 18496.

[60] T. M. Legge, A. T. Slark, S. Perrier, *J. Polym. Sci. Part A: Polym. Chem.*, 2006, **44**, 6980-6987.

[61]T. Kashiwagi, A. Inaba, J. E. Brown, K. Hatada, T. Kitayama, E. Masuda, *Macromolecules*, 1986, ***19***, *2160-2168.*

VIII. Supporting Information

VIII.1 NMR

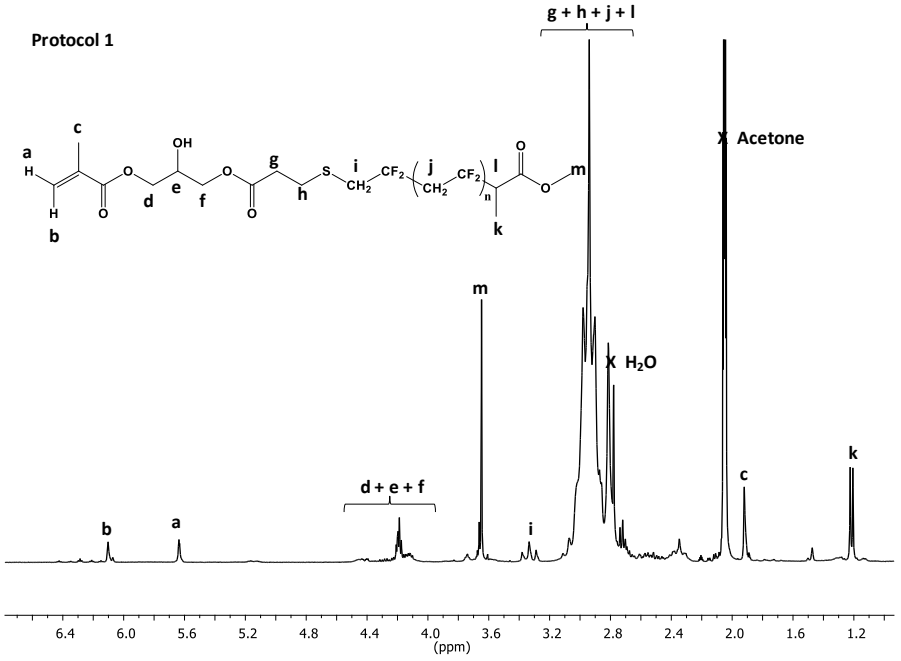

SI-Figure III-7: ^{1}H NMR spectrum (with signal assignment) in $(CD_3)_2CO$ of PVDF-MA macromonomer synthesized using protocol 1.

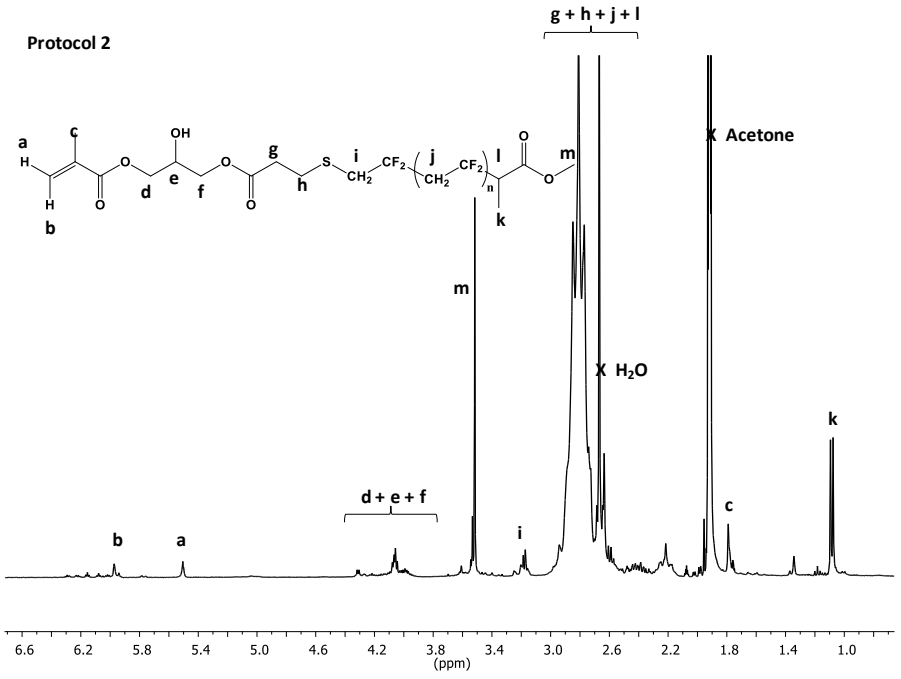

SI-Figure III-8: ^{1}H NMR spectrum (with signal assignments) in $(CD_3)_2CO$ the PVDF-MA macromonomer synthesized using protocol 2.

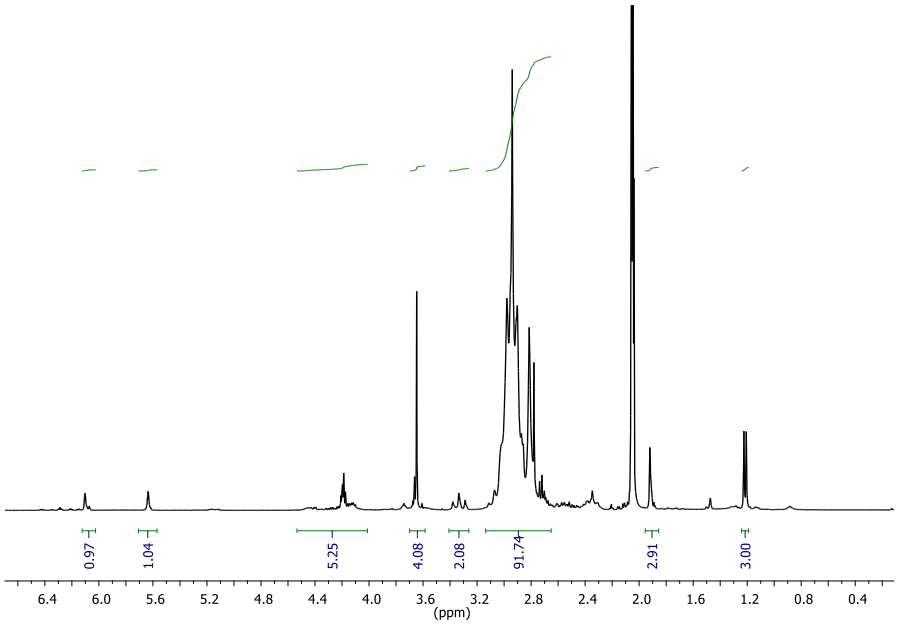

SI-Figure III-9: ntegration of the ^{1}H NMR spectrum signals of the PVDF-MA synthesized using protocol 1.

$$\text{Assessment of Functionality (\%)} = \frac{\int_{6.04}^{6.13}(\text{H}) + \int_{5.56}^{5.68}(\text{H}) + \int_{1.86}^{1.96}(\text{CH}_3)}{\frac{5}{3}\int_{1.18}^{1.25}(\text{CH}_3)} \times \alpha$$

$$= \frac{0.97 + 1.04 + 2.91}{\frac{5}{3} \times 3.00} \times 0.86 = 85\ \%$$

$$\text{Determination of Coupling efficiency (\%)} = \frac{\int_{6.04}^{6.13}(\text{H}) + \int_{5.56}^{5.68}(\text{H}) + \int_{1.86}^{1.96}(\text{CH}_3)}{\frac{5}{3}\int_{1.18}^{1.25}(\text{CH}_3)}$$

$$= \frac{0.97 + 1.04 + 2.91}{\frac{5}{3} \times 3.00} = 99\ \%$$

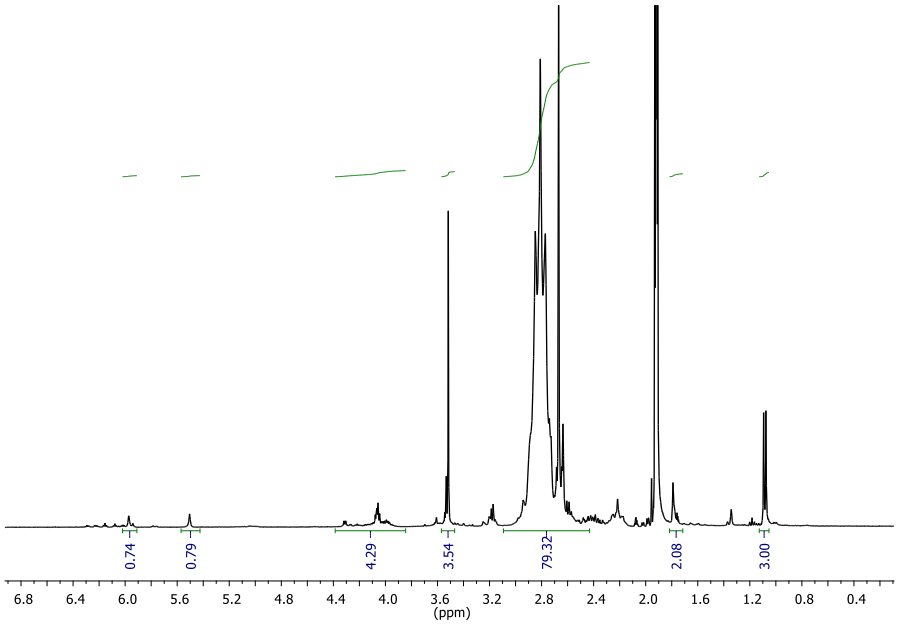

SI-Figure III-10: Integration of the ^{1}H NMR spectrum signals of the PVDF-MA synthesized using protocol 2.

$$\text{Assessment of Functionality (\%)} = \frac{\int_{6.04}^{6.13}(\text{H}) + \int_{5.56}^{5.68}(\text{H}) + \int_{1.86}^{1.96}(\text{CH}_3)}{\frac{5}{3}\int_{1.18}^{1.25}(\text{CH}_3)} \times \alpha$$

$$= \frac{0.74 + 0.79 + 2.08}{\frac{5}{3} \times 3.00} \times 0.86 = 62\ \%$$

$$\text{Determination of Coupling efficiency (\%)} = \frac{\int_{6.04}^{6.13}(\text{H}) + \int_{5.56}^{5.68}(\text{H}) + \int_{1.86}^{1.96}(\text{CH}_3)}{\frac{5}{3}\int_{1.18}^{1.25}(\text{CH}_3)}$$

$$= \frac{0.74 + 0.79 + 2.08}{\frac{5}{3} \times 3.00} \times 0.86 = 72\ \%$$

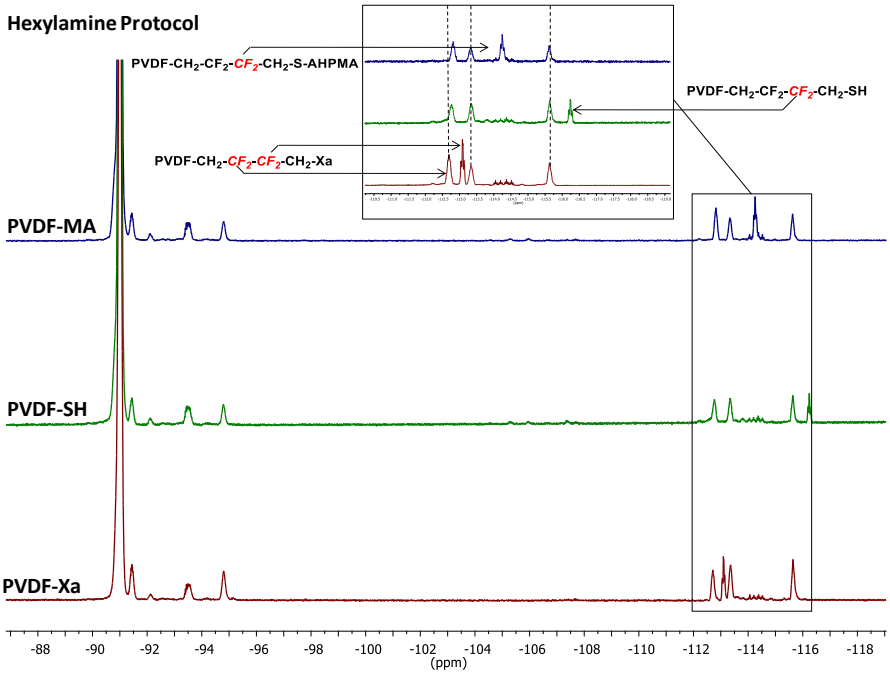

SI-Figure III-11: ^{19}F NMR spectra in $(CD_3)_2CO$ of: PVDF-XA, PVDF-SH synthesized via aminolysis using hexylamine, and of PVDF-MA prepared following protocol 1.

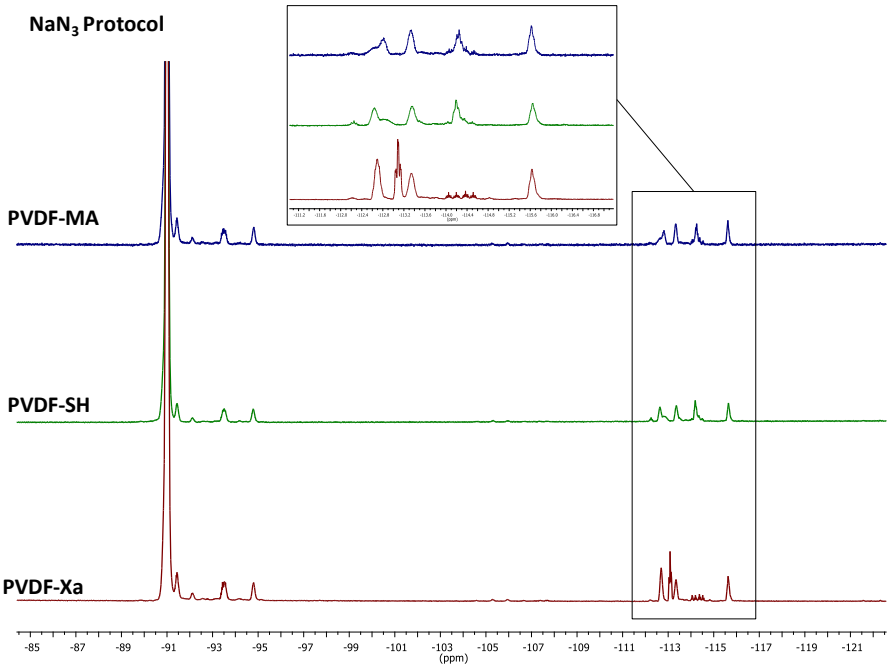

SI-Figure III-12: ^{19}F NMR spectra in $(CD_3)_2CO$ of: PVDF-XA, PVDF-SH synthesized using NaN_3 as end-group removal agent, and of PVDF-MA prepared following protocol 2.

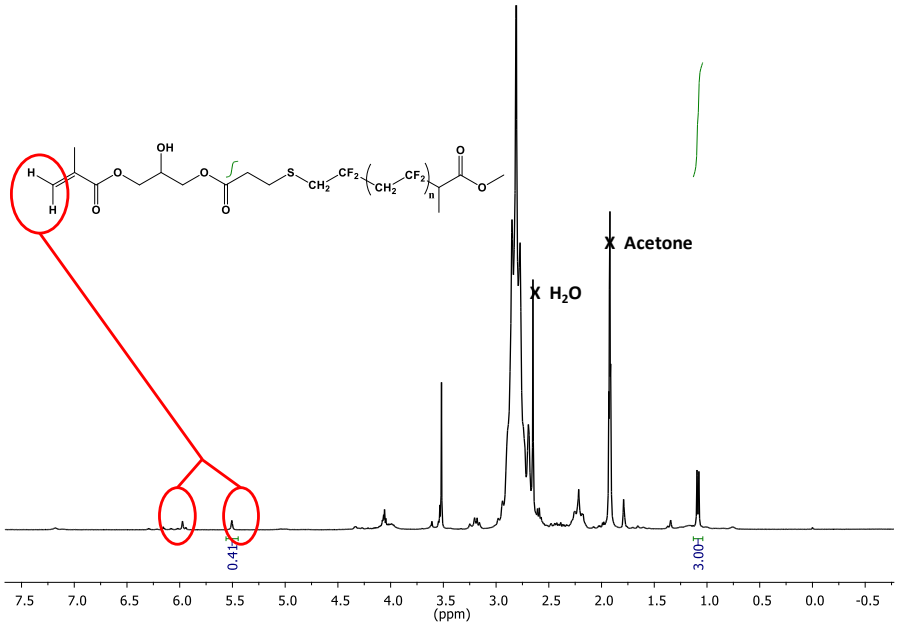

SI-Figure III-13: ^1H NMR spectrum in $(CD_3)_2CO$ of PVDF-MA homopolymer prepared by RAFT polymerization.

$$Conversion = 1 - \frac{\int_{5.60}^{5.68} \boldsymbol{H}CH{=}C(CH_3)\ Methacrylate\ end\ group}{\frac{1}{3}\times \int_{1.19}^{1.24} C\boldsymbol{H}_3{-}CH\ R\ CTA\ end\ group} = 1 - \frac{0.41}{\frac{1}{3}\times 3.00} = 59\ \%$$

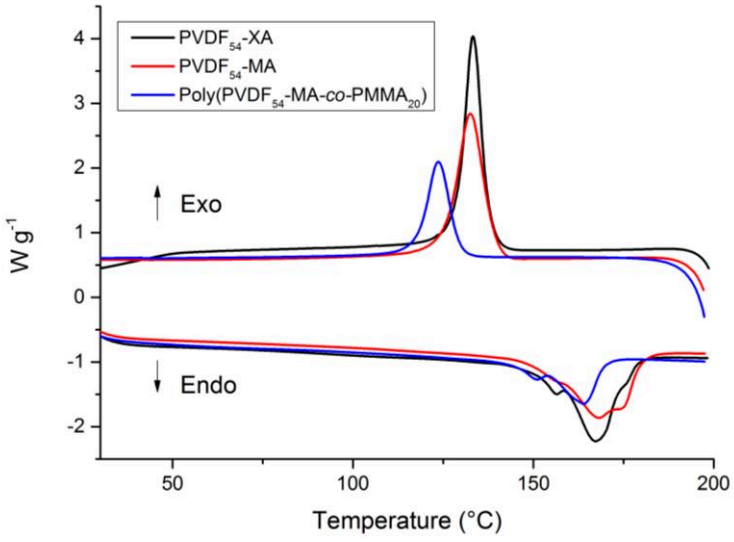

SI-Figure III-14: DSC thermogram for PVDF-XA, PVDF-MA synthesized using Protocol 1 and poly(PVDF-MA-co-MMA) copolymer.

Conclusion Chapitre 3

Ce chapitre démontre en utilisant un PVDF synthétisé par RAFT, l'efficacité des réactions d'aminolyse et d'addition de Michael pour la préparation de macromonomère PVDF de type méthacrylate. En effet, il a été montré au cours de ce chapitre que la méthode utilisant l'azoture de sodium (NaN_3) comme agent nucléophile, contrairement à celle utilisant l'hexylamine, ne permet pas une transformation quantitative des extrémités xanthate en méthacrylate. En effet, l'attaque nucléophile de l'azoture de sodium sur les extrémités xanthate est très rapide (3-5 min), et génère une grande quantité de thiol très rapidement. En dépit d'agent réducteur (Dimethylphenylphosphine), ces PVDF thiols tendent à former des ponts disulfures conduisant à des copolymères diblocs de PVDF-S-S-PVDF. Ces copolymères diblocs ne peuvent plus être fonctionnalisés en méthacrylate et apparaissent sur la trace de chromatographie d'exclusion stérique par un épaulement à une masse molaire double de celle du précurseur de PVDF initial. Contrairement à l'azoture de sodium, la réaction nucléophile mettant en jeu l'Hexylamine est plus lente, et libère de manière progressive des PVDF thiols qui réagissent instantanément avec l'acrylate par addition de Michael. Cette stratégie permet de diminuer fortement la concentration en thiol dans le milieu réactionnel et donc limite la formation de ponts disulfures. Ainsi, le protocole 1 et l'héxylamine conduit à une transformation quantitative des extrémités xanthate en méthacrylate.

De manière prévisible, en raison de la très longue chaîne de PVDF, et donc de la faible mobilité de celle-ci, l'homopolymérisation RAFT du macromonomère de PVDF méthacrylate n'a pu atteindre 100 % de conversion. Ce macromonomère a donc été copolymérisé par polymérisation RAFT de manière quantitative avec un comonomère de méthyl méthacrylate (MMA) permettant ainsi la formation de nouvelles architectures à base de PVDF: poly[(PVDF-MA-*co*-MMA)-*b*-PMMA].

Cette méthode très versatile ne se limite pas au macromonomère de PVDF mais permet, de par sa facilité de mise en œuvre ainsi que du grand nombre de composés acrylates commercialement disponibles, la préparation d'une large gamme de PVDF fonctionnels.

La préparation de copolymères à blocs à base de PVDF qui attirent également beaucoup d'intérêts depuis ces dernières années est abordée dans le chapitre suivant.

Chapitre IV.Synthèses et Caractérisations de Copolymères Diblocs de PVDF

Table des Matières

Introduction Chapitre IV

Les précédents chapitres ont établi les fondations du mémoire à travers la synthèse d'homopolymères de VDF fonctionnel par polymérisation RAFT, et la préparation de macromonomère PVDF-méthacrylate. Cependant, en se recentrant sur l'objectif principal du mémoire qui est l'étude de l'auto-assemblage de copolymères à base de PVDF, il est primordial de développer de nouvelles architectures amphiphiles. Une voie facile à mettre en œuvre consiste à réaliser des extensions de chaînes d'un premier bloc de PVDF synthétisé par RAFT. Ainsi, en sélectionnant judicieusement le monomère, il est possible de préparer des copolymères diblocs PVDF-*b*-PX par polymérisation RAFT séquentielle. Les synthèses de copolymères à blocs à partir de PVDF-XA ainsi que les différentes problématiques rencontrées dans cette étude sont décrites dans la Partie 1 de ce chapitre.

Une méthode analogue à la précédente consiste à préparer le premier bloc hydrogéné puis de réaliser l'extension de chaînes du VDF dans un second temps. Un agent de transfert RAFT bien adapté à la polymérisation des deux blocs doit être judicieusement choisi pour préparer des copolymères diblocs PX-*b*-PVDF suffisamment définis. Cette méthodologie est décrite dans la Partie 2 de ce Chapitre.

Partie 1 -

Les copolymères diblocs contenant une séquence PVDF et un bloc hydrogéné comme second bloc, ont reçu un regain d'intérêt au début des années 2000 avec le développement des techniques de polymérisation radicalaire contrôlées. Ces copolymères ont été préparés *via* des télomères de PVDF (avec des extrémités de type Br ou Cl) ou à partir de PVDF synthétisé par ITP, qui ont ensuite été employés comme macro-amorceurs dans des polymérisations à transfert d'atome (Atom Transfer Radical Polymerization, ATRP). Par ailleurs, des amorceurs fonctionnels ont également été employés dans la polymérisation conventionnelle du PVDF pour la préparation de copolymères à blocs. Cependant, les inconvénients majeurs de ces méthodes, qui sont en définitive ceux de la polymérisation du VDF, sont : *(i)* les faibles masses molaires atteignables *(ii)* un mauvais contrôle sur la polydispersité (ITP, télomerisation et particulièrement pour la polymérisation conventionnelle) *(iii)* des distributions de masses bimodales (ITP, télomérisation).

Dans le cas de l'ITP, et pour contourner cette distribution bimodale de masse molaire due à la réactivité quasi nulle des extrémités -CF_2-CH_2-I, le groupe d'Asandei a proposé l'utilisation de composés à base de Manganèse : $Mn_2(CO)_{10}$. Ce composé photoclivable, libérant des radicaux du type $Mn(CO)_5^{\bullet}$ active de manière irréversible la liaison -CH_2-I et permet ainsi de réamorcer ces chaînes communément considérées comme « mortes ». Cependant, la formation du second bloc s'effectue par polymérisation conventionnelle et les polydispersités qui en résultent sont nécessairement supérieures à 1,5.

Cette partie présente l'ensemble des copolymères diblocs qui ont été synthétisé à partir de PVDF préparé par polymérisation RAFT. Une collaboration avec le Professeur Rinaldo Poli s'est avérée déterminante afin de rationaliser par des calculs DFT, les différences de réactivations observées expérimentalement. Ce travail a fait l'objet d'un article scientifique publié dans *Polymer Chemistry.*[4]

RAFT synthesis of well-defined PVDF-*b*-PVAc block copolymers

Marc Guerre,[a] S. M. Wahidur Rahaman,[b] Bruno Améduri,[a] Rinaldo Poli,[b§]* Vincent Ladmiral[a]*

[a]Institut Charles Gerhardt, Ingénierie et Architectures Macromoléculaires, UMR 5253 – CNRS, Université Montpellier, ENSCM - 8, Rue Ecole Normale, 34296 Montpellier-France.
[b]CNRS, LCC (Laboratoire de Chimie de Coordination), UPS, INPT, Université de Toulouse, 205 Route de Narbonne, BP 44099, F-31077 Toulouse, Cedex 4, France.
[§]Institut Universitaire de France, 1, rue Descartes, 75231 Paris, Cedex 05, France.
*Corresponding authors: rinaldo.poli@lcc-toulouse.fr, vincent.ladmiral@enscm.fr

I. Abstract

RAFT polymerization of vinylidene fluoride (VDF), leading to relatively well defined poly(vinylidene fluoride) (PVDF), is negatively affected by chain inversion resulting in less easily reactivatable $PVDF_T$-XA dormant chains (terminated with the tail end of an inversely added VDF unit; XA = xanthate moiety). Although slow reactivation of these chains by PVDF· radicals (in contrast to general belief) was recently demonstrated, slow radical exchange leads to progressive loss of chain growth control. This article deals with the possibility of synthesizing block copolymers from PVDF-XA macroCTAs by sequential addition. The investigations show that only $PVDF_H$-XA (chains terminated with the head end of regularly added VDF) can be reactivated by PNVP· (poly(*N*-vinylpyrrolidone)) radicals and that $PVDF_T$-XA chains are completely unreactive in the presence of PNVP·, PB· (poly(butylacrylate)) or PDM· (poly(*N,N'*-dimethylacrylamide)). However, both $PVDF_H$-XA and $PVDF_T$-XA can be reactivated by PVAc· (poly(vinyl acetate)) radicals. The reactivation of the $PVDF_T$-XA, albeit slower than that of the $PVDF_H$-XA, is sufficiently fast to allow the synthesis of unprecedented well-defined PVDF-*b*-PVAc block copolymers with relatively high end-group fidelity. DFT calculations rationalize this behavior on the basis of faster radical exchange in the order $PVDF_H$-XA/VAc > $PVDF_H$-XA/NVP > $PVDF_T$-XA/VAc >> $PVDF_T$-XA/NVP. The success of the chain extension also relies on faster activation relative to homopropagation of the chain extending monomer, as well as fast addition of the released $PVDF_H$· and $PVDF_T$· to the monomer.

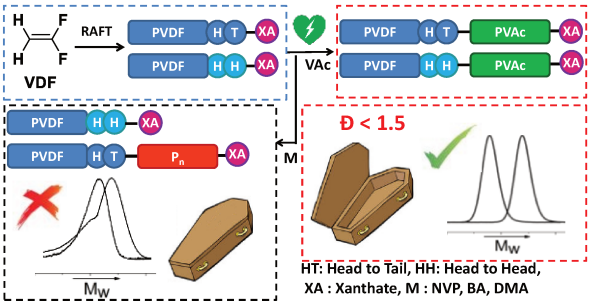

II. Introduction

Owing to its remarkable thermal, chemical and electroactive properties,[1-3] poly(vinylidene fluoride) (PVDF) is a very important fluorinated polymer. The radical polymerization of VDF is relatively well-known, but the use of reversible deactivation radical polymerization (RDRP) techniques to prepare well-defined PVDF is still a very challenging topic in polymer chemistry.[4] Iodine transfer polymerization (ITP), also known as iodine degenerative transfer (IDT) has been relatively well studied over the last two decades but, in spite of its simplicity, it affords only moderate control in VDF polymerization.[5-7] Recently, our team has made an important contribution to VDF RDRP[8,9] with a thorough study of VDF RAFT[10–12] polymerization. Similarly to what Asandei showed for ITP,[13] this study revealed that VDF head-to-head additions lead to the accumulation of much less reactive -CF_2-CH_2-XA (where XA stands for xanthate) terminated PVDF chains resulting in broader molar mass distributions, difficulties in the synthesis of block copolymers, and limitation of the accessible range of molar masses. Moreover, the occurrence of transfer reactions (mainly from the CF_2· radical to the solvent), which cause a 10 % loss in chain-end functionality and consumption of a significant amount of the chain transfer agent (CTA), was also demonstrated.[8] Nonetheless, RAFT is, so far, arguably the best technique to synthesize PVDF with good control and relatively high chain-end functionality. This technique was also shown to open the way to the preparation of well-defined PVDF-based architectures.[14] A crucial step towards more sophisticated architectures is the preparation of well-defined diblock copolymers.[15] The first studies on PVDF-containing block copolymers described the use of brominated PVDF telomers as macroinitiators for the ATRP of styrene[16] or that of iodine-terminated PVDF for the ATRP of MMA.[17] In both cases, relatively broad and bimodal molar mass distributions (ca. 1.6) were observed. A few articles dealing with the synthesis of PVDF-based block architectures using telomerization[18-21] or conventional radical polymerization from functionalized initiators[22-25] were then published. PVDF telomerization resulted in a very

limited degree of polymerization and broad dispersities were observed in the case of peroxide-initiated radical polymerization. ITP[26,27] has been extensively studied for the synthesis of PVDF-containing block copolymers. Pioneered at Daikin in the late 70s,[4] this process led to the production of fluorinated block copolymers as commercial products. Valade et al.[28] attempted the synthesis of PVDF-*b*-PS block copolymers by sequential addition of VDF and styrene on a fluorinated alkyl iodide. However, broad dispersity (1.8–2.0) and a bimodal GPC trace were observed due to the presence of $-CF_2-CH_2-I$ end groups which did not reactivate efficiently during the polymerization of styrene. This phenomenon was also identified in other articles dealing with the ITP of VDF.[6,29] In particular, Asandei's group[7,30,31] recently demonstrated that the addition of $Mn_2(CO)_{10}$ to the photomediated ITP of VDF offers an elegant solution to this problem. *In situ* generated $Mn(CO)_5\cdot$ radicals reactivate all the iodine-terminated chains and thus afford purer block copolymers (i.e. block copolymers devoid of contamination from PVDF homopolymer chains). However, the second block is synthesized under conventional radical polymerization conditions and broad dispersities are obtained. RAFT was also used to prepare VDF-containing block copolymers[32–34] with moderate success, probably because of partial reactivation of the end-groups as in ITP.

We recently reported that the reputedly completely unreactive PVDF-CF_2-CH_2-XA ($PVDF_T$-XA) chains are actually reactivated, albeit at a slower rate than the PVDF-CH_2-CF_2-XA ($PVDF_H$-XA) chains, by PVDF· radicals.[35] That study demonstrated that the VDF RAFT polymerization proceeds via two regimes: a first stage where $PVDF_H$-XA are still present, with good chain growth control; and a second stage when all the dormant chains have been transformed into $PVDF_T$-XA, for which transfer with PVDF· radicals is slower than propagation leading to poor control.

This study examines the phenomena at work in the block extension of RAFT-synthesized PVDF[8] with a range of vinyl monomers including vinyl acetate (VAc) and reports the surprising synthesis of well-defined PVDF-*b*-PVAc block copolymers by sequential monomer addition. The analysis of the radical exchange process on the xanthate transfer agent and of the radical addition to the monomer, carried out by DFT calculations on suitable molecular model systems, provides a framework of understanding and allows rationalizing this unexpected result.

III. Experimental Section

Materials

All reagents were used as received unless stated otherwise. 1,1- Difluoroethylene (vinylidene fluoride, VDF) was kindly supplied by Arkema (Pierre-Benite, France). *O*-Ethyl-*S*-*(*1-methoxycarbonyl) ethyldithiocarbonate (CTA_{XA}) was synthesized according to the method described by Liu et al.[36]tert-Amyl peroxy-2-ethylhexanoate (Trigonox 121, purity 95%) was purchased from AkzoNobel (Chalons-sur-Marne, France). ReagentPlus grade (purity >99%) 2,2-azoisobutyronitrile (AIBN), vinyl acetate (VAc), butyl acrylate (BA), *N*-vinylpyrrolidone (NVP), *N,N*-dimethylacrylamide (DMA), dimethyl carbonate (DMC), dimethylformamide (DMF), acetonitrile (ACN), tetrahydrofuran, (THF), methanol (MeOH), and laboratory reagent grade hexane (purity >95%) were purchased from Sigma Aldrich and used as received. AIBN was purified by recrystallization from methanol twice before use.

Nuclear Magnetic Resonance

The Nuclear Magnetic Resonance (NMR) spectra were recorded on a Bruker AC 400 instrument. Deuterated acetone or DMSO was used as the solvent in each sample. Coupling constants and chemical shifts are given in hertz (Hz) and parts per million (ppm), respectively. The experimental conditions for recording ^{1}H and ^{19}F NMR spectra were as follows: flip angle 90° (or 30°), acquisition time 4.5 s (or 0.7 s), pulse delay 2 s (or 2 s), number of scans 128 (or 512), and a pulse width of 5 μs for ^{19}F NMR. *In situ* NMR experiments were recorded with a pulse delay of 1 s, acquisition times of 4 s and 0.87 s, and 8 and 16 scans for ^{1}H and ^{19}F NMR, respectively.

Size Exclusion Chromatography

Size exclusion chromatograms (SEC) were recorded using a triple detection GPC from Agilent Technologies with its corresponding Agilent software, dedicated to multi-detector GPC calculation. The system used two PL1113-6300 ResiPore 300 × 7.5 mm columns with DMF (containing 0.1 wt % of LiCl) as the eluent with a flow rate of 0.8 mL min^{-1} and toluene as flow rate marker. The detector suite comprised a PL0390-0605390 LC light scattering detector with 2 diffusion angles (15° and 90°), a PL0390-06034 capillary viscosimeter, and a 390-LC PL0390-0601 refractive index detector. The entire SEC-HPLC system was thermostated at 35 °C. PMMA standards were used for the calibration. The typical sample concentration was 10 mg mL^{-1}.

Differential Scanning Calorimetry

DSC measurements were performed on 10‑15 mg samples on a Netzsch DSC 200 F3 instrument using the following heating/ cooling cycle: cooling from room temperature (ca. 20 °C) to -50 °C at 20 °C min^{-1}, isotherm plateau at -50 °C for 5 min, first heating ramp from -50 to 200 °C at 10 °C min^{-1}, cooling stage from 200 to -50 °C at 10 °C min^{-1}, isotherm plateau at -50 °C for 3 min, second heating ramp from −50 °C to 200 °C at 10 °C min^{-1} and last cooling stage from 200 °C to room temperature (ca. 20 °C). The instrument was calibrated with noble metals and checked before analysis with an indium sample. Melting points were determined at the maximum of the enthalpy peaks.

Thermogravimetric analyses

TGA analyses were carried out on 10‑15 mg samples on a TGA Q50 apparatus from TA Instruments from 20 °C to 580 °C, in platinum pans, at a heating rate of 10 °C min^{-1}, in air. A thermal degradation temperature at 5% weight loss (T_d 5%) was arbitrarily chosen.

Autoclave

The polymerizations of VDF were performed in a 100 mL Hastelloy Parr autoclave systems (HC 276), equipped with a mechanical Hastelloy stirring system, a rupture disk (3000 PSI), inlet and outlet valves, and a Parr electronic controller to regulate the stirring speed and the heating. Prior to reaction, the autoclave was pressurized with 30 bars of nitrogen to check for leaks. The autoclave was then kept under vacuum (20 10^{-3} bar) for 30 minutes to remove any trace of oxygen. A degassed solution of an initiator and CTA_{XA} was introduced via a funnel under vacuum. The reactor was then cooled using a liquid nitrogen bath and the VDF was transferred by double weighing (i.e. mass difference before and after filling the autoclave with VDF). After warming to ambient temperature, the autoclave was heated to the target temperature under mechanical stirring.

Syntheses

MacroRAFT PVDF-XA with the characteristics listed in Table IV-1 (entries 1‑3) were generated on the basis of previously published protocols.[8,9,35] The synthetic details and the equations used to determine the proportion of each chain end ($PVDF_T$-XA, $PVDF_H$-XA and PVDF-H) are reported in the VI.1-Supporting Informations. All the proportions reported in this article are in mol %.

RAFT Polymerization of VAc

In a 50 mL round bottom flask, *O*-ethyl-*S*-*(*1-methoxycarbonyl) ethyldithiocarbonate (1.613 g, 7.744 10^{-3} mol) and AIBN (0.254 g, 1.55 10^{-3} mol) were dissolved in 25 mL of anhydrous ACN and the solution was degassed by N_2 bubbling for 15 min. A degassed solution of VAc (20.0 g, 2.32 10^{-1} mol) was then introduced into the reaction vessel and the reaction medium was left under vigorous stirring at 60 °C for 14 hours. The ACN was then removed under vacuum; the viscous residue was then dissolved in 20 mL of acetone and precipitated from chilled hexane. The resulting polymer was dried until constant weight under vacuum at 50 °C to remove traces of solvent (yield = 73%) (entry 4, Table IV-1).

^{1}H NMR (400 MHz $(CD_3)_2CO$, δ (ppm)): 1.06-1.17 (-CH(C**H$_3$**)(C=O)-), 1.37-1.46 (-S(C=S)O-CH_2-C**H$_3$**), 1.68-1.91 (-CH(OAc)-C**H$_2$**-CH(OAc)-), 1.91-2.04 (-CH(O**Ac)**-), 2.16-2.35 (-C**H$_2$**-CH(OAc)-S(C=S)OEt), 2.38-2.62 (-C**H**(CH_3)(C=O)-O-CH_3), 3.18-3.51 (-CH(OAc)-C**H$_2$**-S(C=S)OEt), 3.56-3.74 (-CH(CH_3)-(C=O)-O-C**H$_3$**), 3.95-4.13 (-CH_2-(CH_3(C=O)O)C**H$_2$**), 4.57-4.75 (-S(C=S)O-C**H$_2$**-CH_3), 4.76-5.14 (-CH_2-C**H(**OAc)-CH_2-), 5.13-5.24 (-C**H(**OAc)-CH_2-S(C=S)OEt), 6.50-6.70 (-CH_2-C**H(**OAc)-S(C=S)OEt).

Synthesis of PVDF-*b*-PVAc block copolymers using PVDF-XA as macroCTA

A typical synthesis of a PVDF-b-PVAc block copolymer was performed as follows (Scheme IV-1): PVDF-XA macroCTA (entry 1, Table IV-1) (1.00 g, 3.33 10^{-4} mol) and AIBN (10.9 mg, 6.66 10^{-5} mol) were dissolved in 5 mL of DMF. The solution was stirred and bubbled with N_2 for 20 min, and a degassed solution of VAc (5.74 g, 6.66 10^{-2} mol) was injected. The septum was carefully replaced by a glass stopper and firmly closed with a keck joint clip. The solution was then stirred and heated at 70 °C for 24 h. The viscous reaction was diluted with 5 mL of acetone and precipitated in a large excess of hexane. The resulting solid was dried until constant weight under vacuum at 40 °C (yield = 88%) (entry 8, Table IV-1). The equations used to determine the proportions of each type of PVAc chain (PVAc-CH_2CH(OAc)-XA, PVAc-CH(OAc)CH_2-XA, and PVAc-CH_2-CH_2(OAc) denoted $PVAc_T$-XA, $PVAc_H$-XA and PVAc-H respectively) are detailed in the Supporting information. The attempted syntheses of PVDF-*b*-X (where X stands for NVP, BA and DMA) (entries 5‑7, Table IV-1) were carried out using the same experimental protocol as the one used for the synthesis of PVDF-*b*-PVAc block copolymer.

DP and $M_{n(NMR)}$ calculation

The degree of polymerization (DP) can be calculated from ^{1}H NMR using the integrals of the signals corresponding to: the methyl group of the CTA R-group (1.19‑1.24 ppm), the CH of the PVAc backbone (4.76‑5.14 ppm) and the CH_2 group end-capped with xanthate moieties of the reverse VAc additions (HH, 3.22‑3.46 ppm). However, as reported in a previous work,[14] the PVDF-XA chains initiated by R-radicals from the CTA were not all terminated by a CTA Z-group. Transfer to the DMC occurred in the course of the polymerization, leading to around 14% of dead chains terminated by a -CF_2H group. Therefore, a correction factor (α = 0.86) was introduced in Equation IV-1 to calculate a more accurate DP and molar mass for the PVAc block:

$$\textit{Equation IV-1} \quad DP = \frac{\int_{4.76}^{5.14} CH + 1/2 \int_{3.22}^{3.46} CH_2(HH\ End-group)}{\frac{\alpha}{3} \times \int_{1.19}^{1.24} CH_3(R-CTA_{XA})}$$

The molar mass was then calculated using equation (2):

$$\textit{Equation IV-2} \quad M_{n,NMR}(R) = M_{n,PVDF-XA} + (DP \times M_{n,VAc})$$

where M_nPVDF$_{51}$-XA = 3500 g.mol^{-1}, M_n PVDF$_{85}$-XA = 5700 g.mol^{-1} and M_n VAc= 86.09 g.mol^{-1}.

^{1}H NMR (400 MHz $(CD_3)_2CO$, δ (ppm), Figure IV-1) : 1.19-1.24 (d, -CH(C**H$_3$**)(C=O)-, $^3J_{HH}$ = 7.1 Hz), 1.40-1.46 (t, (-S(C=S)O-CH_2-C**H$_3$**), 1.63-1.92 (m, -CH(OAc)-C**H$_2$**-CH(OAc)-, VAc), 1.92-2.03 (m, -CH(O**Ac)**-, VAc), 2.28-2.43 (m,-CF_2-C**H$_2$**-C**H$_2$**-CF_2-, VDF-VDF TT reverse addition), 2.70-3.19 (t, -CF_2-C**H$_2$**-CF_2-, regular VDF-VDF HT addition), 3.21-3.42 (m, -CH(OAc)-C**H$_2$**-S(C=S)OEt, VAc HH reverse addition), 3.60-3.69 (s, -(C=O)-O-C**H$_3$**), 3.95-4.13 (-CH_2-C**H$_2$(**OAc), VAc), 4.63-4.72 (q, (-S(C=S)O-C**H$_2$**-CH_3, $^3J_{HH}$ = 7.2 Hz), 4.76-5.14 (-CH_2-C**H(**OAc)-CH_2-), 6.05-6.45 (tt, $^2J_{HF}$ = 55 Hz , $^3J_{HH}$ = 4.6 Hz -CH_2-CF_2-**H**).

^{19}F NMR (376 MHz $(CD_3)_2CO$, δ (ppm), Figure IV-2) : -115.63 (-CH_2-CF_2-C**F$_2$**-CH_2-CH_2-, VDF-VDF HH reverse addition), -115.43 (-CH_2-CF_2-**CF$_2$**-CH_2-CH_2-CH(OAc)-), -114.29 ($^2J_{HF}$ = 55 Hz, -CH_2-C**F$_2$**-H), -113.34 (-CH_2-C**F$_2$**-CF_2-CH_2-CH_2-, HH reverse addition), -94.79 (-CH_2-CH_2-C**F$_2$**-CH_2-, TT reverse addition), -93.50 (-CH_2-C**F$_2$**-CH_2-CH(CH_3)(C=O)-), -92.12 (-CH_2-C**F$_2$**-CH_2-CF_2H), -91.44 (-CH_2-CH_2-CF_2-CH_2-**CF$_2$**-CH_2-CF_2-, regular VDF-VDF HT addition), -91.00 (-CH_2-C**F$_2$**-CH_2-, regular VDF-VDF HT addition).

Kinetic of PVDF-XA reactivation

A primary solution of VAc, a PVDF macroRAFT agent, an initiator and DMF targeting a desired DP was prepared and divided into various glass tubes previously purged with nitrogen. The tubes were then placed in a shaking oil bath thermostated at 70 °C. The tubes were then taken off at different desired times and the reaction was quenched by immersion of the tube in liquid nitrogen. The crude product was then analyzed without purification by ^{1}H, ^{19}F NMR and SEC. *In situ* ^{1}H and ^{19}F NMR experiments were performed using a similar procedure. An aliquot of the required reaction mixture was placed in an NMR tube previously purged with nitrogen. The initial ^{1}H and ^{19}F NMR spectra were recorded at 25 °C. The spectrometer was then heated at 70 °C, the NMR tube was then placed in the spectrometer and spectra were recorded every 2 minutes and 7 s for 5 hours using the above described acquisition parameters.

Computational details

The computational work was carried out using the Gaussian09 suite of programs.[37] The geometry optimizations were performed in the gas phase without any symmetry constraint using the B3PW91 functional in combination with the 6-31G (d,p) basis functions for all atoms. The unrestricted formulation was used for all radicals, yielding negligible spin contamination in all cases. The ZPVE, PV and TS corrections at 298 K were obtained with Gaussian09 from the solution of the nuclear equation using the standard ideal gas and harmonic approximations at T = 298.15 K, which also verified the nature of all optimized geometries as local minima or first order saddle points. A correction of 1.95 kcal mol^{-1} was applied to all G values to change the standard state from the gas phase (1 atm) to solution (1 M).[38] Geometry optimizations in solvent using the SMD polarizable continuum model[39] were also carried out for selected calculations (see IV-Results and Discussion) in vinyl acetate (ε = 4.2) and in acetonitrile (ε = 35.7).

IV. Results and Discussion

IV.1.1 Block synthesis tests

PVDF-XA macroCTAs featuring different chain-ends were first prepared according to published procedures (Table IV-1, entries 1−3).[8] As mentioned in our previous publications, the different ω-chain-ends of these macroCTAs originate from the head-to-tail (HT) and head-to-head (HH) additions of VDF, which lead to easily reactivated $PVDF_H$-XA and much less

reactive $PVDF_T$-XA respectively, and from transfer to the solvent resulting in PVDF-H dead chains.[8,9,35]

The synthesis protocols used in the present study (solution polymerization in DMC) cannot produce pure $PVDF_H$-XA macroCTAs. The transfer reactions to the DMC are unavoidable. The formation of $PVDF_T$-XA is intrinsic to the radical polymerization of VDF with accumulation in the reaction medium as the polymerization reaction progresses. It is possible to minimize the proportions of the less reactive $PVDF_T$-XA chains by stopping the polymerization at low VDF conversion.[35]

To probe the possibility of synthesizing block copolymers from $PVDF_T$-XA, a range of monomers including *N*-vinylpyrrolidone (NVP, entry 5, Table IV-1), *N,N*-dimethyl acrylamide (DMA, entry 6, Table IV-1), butyl acrylate (BA, entry 7, Table IV-1), and vinyl acetate (VAc, entry 8, Table IV-1) were tested in RAFT polymerization in the presence of the $PVDF_T$-XA macroCTA obtained from entry 1 (DP = 51). VAc and NVP are good examples of "less activated" monomers (LAM) for which polymerization can be controlled using xanthate CTAs.[40] *N,N*-Dimethyl acrylamide is an example of "more activate" monomers (MAM), the polymerization of which, in the presence of xanthate CTAs, was recently claimed to proceed with satisfactory control.[10,41] Butyl acrylate is also a "more activated" monomer and its polymerization cannot be controlled using xanthate CTAs. These two MAMs were thus tested to see whether PVDF-XA could be reactivated by their radicals. The polymerizations of these monomers were carried out for 24 h and the resulting crude polymers were analyzed by ^1H and ^{19}F NMR spectroscopies and SEC-HPLC (see SI-Figure IV-9 to SI-Figure IV-11, respectively). In the case of NVP, DMA and BA, $PVDF_T$-XA did not take part in the polymerization reactions. This can be clearly seen by comparing the ^1H (SI-Figure IV-9) and ^{19}F NMR (SI-Figure IV-10) spectra of $PVDF_T$-XA with those of the corresponding chain extension reaction products. In the ^1H NMR spectra, the well-defined triplet centered at 4.10 ppm of the VDF unit adjacent to the xanthate moiety did not disappear while the ^{19}F NMR resonances at -113.09 and -112.69 ppm corresponding to the ultimate and penultimate VDF units of the xanthate-terminated PVDF chains did not decrease in intensity relatively to the main PVDF signal at -91 ppm, and no new signal appeared. In addition, the GPC traces (SI-Figure IV-11) of the polymers resulting from the chain extension of $PVDF_T$-XA with NVP, DMA and BA are bimodal and feature broad dispersities ($Đ > 1.8$). These results demonstrate that the $PVDF_T$-XA chains behaved as spectators during the conventional radical polymerizations of these monomers.

Table IV-1: Experimental conditions and results for the syntheses of PVDF and the chain extension reactions

Entry	CTA	M	$[M]_0$ / $[CTA]_0$	Reaction time (h), Solvent	yield [a](%)	$DP_{(NMR)}$ [b] $_{(R)}$	$M_{n(theo)}$ [c] (g/mol)	$M_{n(NMR)(R)}$ [d] (g/mol)	M_{nSEC} [e] (g/mol)	Đ[e]	End Group (%)					
											f	g	h	i	j	k
1	CTA_{XA}	VDF	51	18, DMC	65	51	2400	3400	8300	1.40	86	0	14	n.a.	n.a	n.a.
2	CTA_{XA}	VDF	100	24, DMC	60	85	4100	5700	10100	1.50	49	0	51	n.a.	n.a.	n.a.
3	CTA_{XA}	VDF	51	10, DMC	25	20	1000	1500	3900	1.12	38	47	15	n.a.	n.a	n.a.
4	CTA_{XA}	VAc	30	14, ACN	73	28	2100	2600	4000	1.20	n.a.	n.a.	n.a.	25	63	12
5	$PVDF_{51}$-XA	NVP	150	24, DMF	80	n.a.	16800	n.a.	35500	2.10	86	0	14	n.a.	n.a	n.a.
6	$PVDF_{51}$-XA	DMA	100	24, DMF	73	n.a.	10700	n.a.	100000	1.79	86	0	14	n.a.	n.a	n.a.
7	$PVDF_{51}$-XA	BA	200	24, DMF	80	n.a.	24000	n.a.	58300	1.95	86	0	14	n.a.	n.a	n.a.
8	$PVDF_{51}$-XA	VAc	200	24, DMF	88	219	18600	22300	19100	1.40	0	0	14	33	0	53
9	$PVDF_{51}$-XA	VAc	100	14, DMF	85	103	10800	12300	10200	1.41	0	0	14	36	0	50
10	$PVDF_{51}$-XA	VAc	150	14, DMF	91	172	15200	18300	17500	1.34	0	0	14	35	0	49
11	$PVDF_{51}$-XA	VAc	200	14, DMF	93	217	19500	22100	19500	1.39	0	0	14	40	0	46
12	$PVDF_{51}$-XA	VAc	250	14, DMF	89	270	22700	26700	24200	1.35	0	0	14	32	0	54
13	$PVDF_{51}$-XA	VAc	300	0.5, DMF	46	120	15300	13700	n.a	n.a	55	0	14	15	2	14
14	$PVDF_{51}$-XA	VAc	300	3, DMF	59	238	18600	23900	17100	1.38	46	0	14	20	0	20
15	$PVDF_{51}$-XA	VAc	300	6, DMF	73	273	22200	26900	22300	1.36	0	0	14	30	0	56
16	$PVDF_{20}$-XA (Entry 3)	VAc	100	5, DMF	95	112	10000	11400	11300	1.33	5	0	15	53	5	22
17[l]	$PVDF_{20}$-XA (Entry 3)	NVP	200	14, DMF	50	n.a.	12600	n.a.	8000	1.98	n.a.	n.a.	n.a.	n.a.	n.a	n.a.
18	$PVDF_{85}$-XA (Entry 2)	VAc	250	14, DMF	65	318	17500	30100	18400	2.02	0	0	51	14	0	35

Reactions conditions: (i) (entries 1‑3) VDF homopolymerization, [I]/[CTAXA] = 0.1 with I = Trigonox 121 and CTA_{XA} = *O*-ethyl-*S*-(1-methoxycarbonyl)ethyldithiocarbonate, T = 73 °C; (ii) (entry 4) VAc homopolymerization, [I]/[CTAXA] = 0.1 with I = AIBN and CTAXA = *O*-ethyl-*S*-(1-methoxycarbonyl)ethyldithiocarbonate, T = 60 °C; (iii) (entries 5‑18) chain extension from PVDF-XA, [I]/[PVDF-XA] = 0.2 with I = AIBN, T = 70 °C. [a]Determined gravimetrically. [b]Determined by ^{1}H NMR using SI-Equation IV-8 for VDF and Equation IV-1 for VAc. c Calculated using the yield as conversion and the equation: $M_{n,theo} = [M]_0/[CTA_{XA}]_0 \times$ yield $\times M_n$ (M) + $M_n(CTA_{XA})$. [d]Calculated from DP_{NMR} using SI-Equation IV-9 for VDF and Equation IV-2 for VAc. [e]Determined by SEC (RI detector). [f] -CF_2-CH_2-XA, calculated using SI-Equation IV-10. [g] -CH_2-CF_2-XA, calculated using SI-Equation IV-11. [h]-CF_2H, calculated using SI-Equation IV-12. [i]-AcOCH-CH_2-XA, calculated using SI-Equation IV-13. [j]-CH_2-AcOCH‑XA, calculated using SI-Equation IV-14. [k]-CH_2-$AcOCH_2$, calculated using SI-Equation IV-15. [l]The PNVP-XA end-groups could not be identified by ^{1}H NMR. However, since only $PVDF_H$-XA were reactivated they should correspond to 47% of the total molar fraction of end-groups while $PVDF_T$-XA and PVDF-H correspond to 38% and 15% of end groups respectively. n.a.: not applicable.

Interestingly, when the PVDF-XA macroCTA from entry 3, containing both $PVDF_T$-XA (38 mol%) and $PVDF_H$-XA (47 mol %), was used in a chain extension reaction with NVP (entry 17, Table IV-1), a block copolymer was formed. The ^{19}F NMR spectrum of this block copolymer (SI-Figure IV-12) shows the complete disappearance of the signal of the $PVDF_H$-XA end group (at -71 ppm). This proves the total reactivation of this type of end-groups by exchange with the PNVP· radical and the formation of block copolymers. In this case as well, the signals at -113.09 and -112.69 ppm assigned to the ultimate and penultimate VDF units in $PVDF_T$-XA remained unchanged (SI-Figure IV-12).

This experiment shows that only the $PVDF_H$-XA macroCTA can be reactivated under these RAFT polymerization conditions. Consequently, the resulting polymer is a binary mixture of $PVDF_T$-XA and PVDF-*b*-PNVP, the latter containing exclusively a -CH_2CF_2-NVP- moiety at

the block junction. The unreacted PVDF chains can easily be seen on the GPC trace of the diblock copolymer (low molar mass shoulder in SI-Figure IV-13).

IV.1.2 PVDF-*b*-PVAc block copolymers

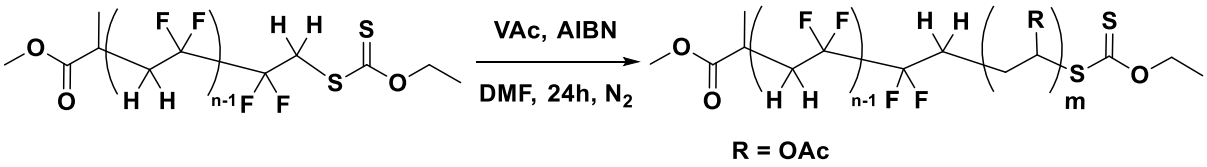

Scheme IV-1:Synthesis of PVDF-b-PVAc block copolymers

In contrast with the above described chain extension attempts with NVP, DMA and BA, the chain extension of $PVDF_T$-XA with VAc displayed a surprisingly narrow trace (Đ = 1.40, SI-Figure IV-11), and a clear molar mass shift towards higher molar masses, suggesting the formation of a relatively well-defined PVDF-*b*-PVAc block copolymer. Figure IV-1 displays the ^{1}H spectrum of the PVDF-*b*-PVAc block copolymer synthesized by chain extension of $PVDF_T$-XA with VAc (entry 8, Table IV-1); and shows:

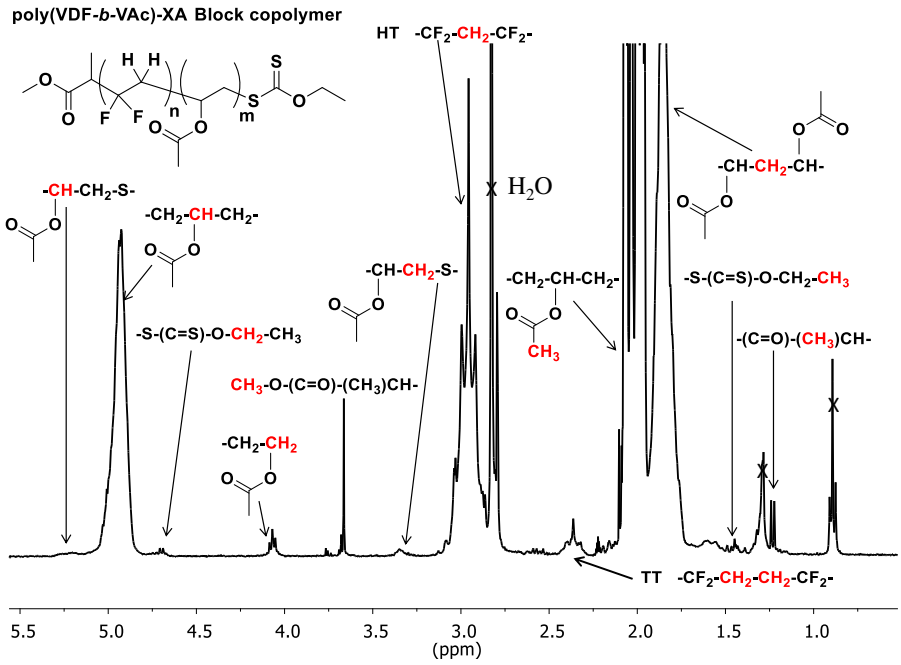

Figure IV-1: Expansion of the 0.3-5.5 ppm region of the ^{1}H NMR spectrum of a PVDF-b-PVAc block copolymer synthesized via RAFT polymerization (entry 8, Table IV-1) recorded in $(CD_3)_2CO$. Crossed-out signals are assigned to residual hexane and water.

(i) typical broad peaks centered at 1.75, 2.00, and 4.92 ppm corresponding to the CH_2, CH_3 and CH of PVAc, respectively, *(ii)* a broad triplet at 2.9 ppm assigned to the methylene of regular VDF head-to-tail (HT) additions and a triplet at 2.3 ppm characteristic of VDF tail-to-

tail (TT) additions, *(iii)* signals assigned to the CTA R-group at 1.2 ppm (doublet) and 3.6 ppm (singlet), *(iv)* signals of the CTA Z-group at 1.4 ppm (triplet) and 4.65 ppm (quartet), *(v)* a small peak centered at 3.3 ppm corresponding to a VAc head-to-head (HH) addition terminated by the xanthate group and, (vi) a triplet at 4.0 ppm characteristic of a -CH_2-CH_2(OAc) end-group caused by transfer of a $^{-}CH_2CH(OAc)^{\cdot}$ radical to the solvent.[42,43] Remarkably, the welldefined triplet at 4.10 ppm (coupling constant $^3J_{HF}$ = 18 Hz) characteristic of $PVDF_T$-XA chains, which remained unchanged when similar experiment were carried out with other monomers, completely disappeared in the presence of VAc. This spectrum suggests the successful chain extension of $PVDF_T$-XA by VAc.

This successful chain extension was further confirmed by comparing the ^{19}F NMR spectra of the polymers before and after chain extension with VAc (Figure IV-2).

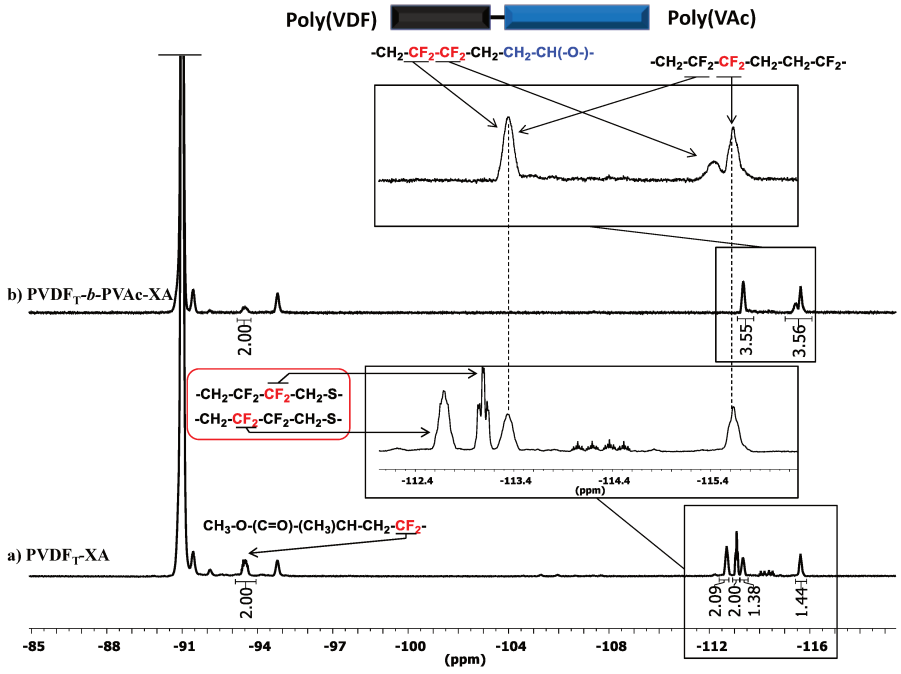

Figure IV-2: Expansion of the -85 to -119.5 ppm region of the ^{19}F NMR spectra recorded in $(CD_3)_2CO$ of: (a) $PVDF_T$-XA synthesized via RAFT polymerization (entry 1, Table IV-1), (b) PVDF-b-PVAc block copolymer synthesized via RAFT polymerization (entry 8, Table IV-1).

The expanded ^{19}F NMR spectrum between -112 and -116.3 ppm (inserts in Figure IV-2) clearly showed the shift of the signal at -112.69 ppm (assigned to the penultimate VDF unit) to -113.34 ppm. This signal at -113.34 overlaps with that of the VDF internal reverse (HH) addition. Similarly, the signal of the VDF ultimate unit (at -113.09 ppm) completely shifted to -115.43 ppm, close to the second peak (at -115.63 ppm) of the VDF internal reverse (HH)

addition. The signal integrals are also in very good agreement with these chemical shift changes. These shieldings are caused by the complete reactivation of the $PVDF_T$-XA chains and formation of the $-CH_2CF_2CF_2CH_2-CH_2CH(OAc)-$ linkage. A range of $PVDF_{51}$-*b*-PVAc block copolymers with different PVAc block lengths was prepared (entries 9‑12 in Table IV-1) from the $PVDF_T$-XA macroCTA of entry 1. The corresponding viscosimetric GPC traces (Figure IV-3a) show narrow molar mass distributions (Đ < 1.4) and an increase to high molar masses (in agreement with the PVAc chain length), indicating the quantitative reactivation of the reputedly inactive $PVDF_T$-XA chains.

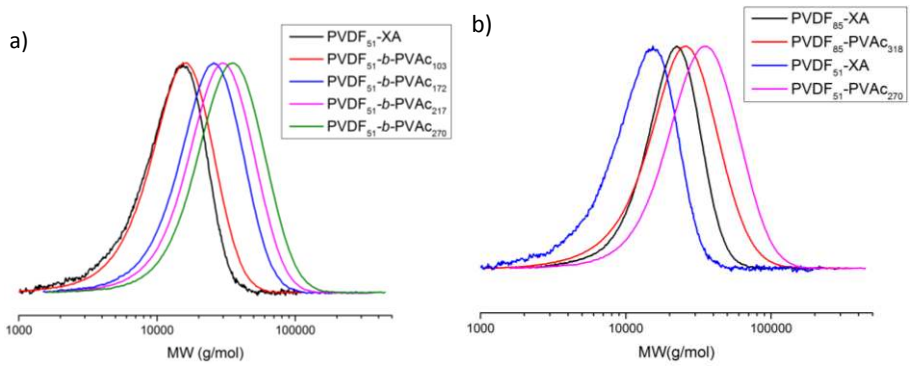

Figure IV-3: a) Normalized GPC traces (viscosimetric detector) of $PVDF_{51}$-XA (entry 1, Table IV-1) homopolymer, $PVDF_{51}$-b-$PVAc_{103}$ (entry 9, Table IV-1), $PVDF_{51}$-b-$PVAc_{172}$ (entry 10, Table IV-1), $PVDF_{51}$-b-$PVAc_{217}$ (entry 11, Table IV-1) and $PVDF_{51}$-b-$PVAc_{270}$ (entry 12, Table IV-1) block copolymers. (b) Normalized GPC traces (viscosimetric detector) of $PVDF_{51}$-XA (entry 1, Table IV-1), $PVDF_{85}$-XA (entry 2, Table IV-1), $PVDF_{51}$-b-$PVAc_{270}$ (entry 12, Table IV-1) and $PVDF_{85}$-b-$PVAc_{318}$ (entry 18, Table IV-1).

Figure IV-3b displays the viscosimetric GPC traces of $PVDF_{51}$-XA (entry 1, Table IV-1), $PVDF_{85}$-XA composed of 49% $PVDF_T$-XA and 51% of $-CF_2H$-terminated PVDF chains (PVDF-H) (entry 2, Table IV-1), and the diblock copolymers resulting from the chain extensions of these PVDF-XA macroCTAs with VAc targeting a PVAc block length of 250 units and carried out under identical experimental conditions (entries 12 and 18, Table IV-1). The $PVDF_{85}$-*b*-PVAc diblock copolymer is clearly of poor quality (high dispersity) and contains a significant amount of PVDF homopolymer (the completely unreactive PVDF-H chains formed by transfer to DMC[8] throughout the polymerization of VDF). In contrast, the chain extension of $PVDF_{51}$-XA, which contained only 14 mol% of PVDF-H, led to a relatively well-defined block copolymer. The chain-end functionality of the starting PVDF macroCTA is thus a crucial parameter for the synthesis of welldefined PVDF-*b*-PVAc block copolymers.

IV.1.3 Reactivation kinetics

$PVDF_T$-XA chains are thermodynamically stable, hard to activate, and commonly considered as dead chains, whereas $PVDF_H$-XA chains are considered as easily reactivatable by PVDF radicals. However, we have recently demonstrated that these assumptions are wrong.[35] $PVDF_T$-XA chains cannot be considered dead; they can be reactivated by $PVDF_T$· and $PVDF_H$· radicals, albeit at a slower rate than $PVDF_H$-XA chains. In the case of VDF RAFT homopolymerization, this reactivation slowdown leads to the accumulation of $PVDF_T$-XA chains, which ultimately leads to loss of polymerization control. However, these chains can still be extended.

The reactivation kinetics of the two different type of PVDF-XA chains were examined using *in situ* NMR monitoring of the polymer chain-ends during the VAc chain extension of the $PVDF_{20}$-XA macroCTA obtained from entry 3 (Table IV-1), composed of 38% of $PVDF_T$-XA, 47% of $PVDF_H$-XA and 15% of PVDF-H. SI-Figure IV-14/15 show, respectively, the stacked ^1H and ^{19}F NMR spectra of this PVDF-*b*-PVAc synthesis attempt. Figure IV-4 shows the evolution of the polymer chain-ends during this PVAc block synthesis experiment.

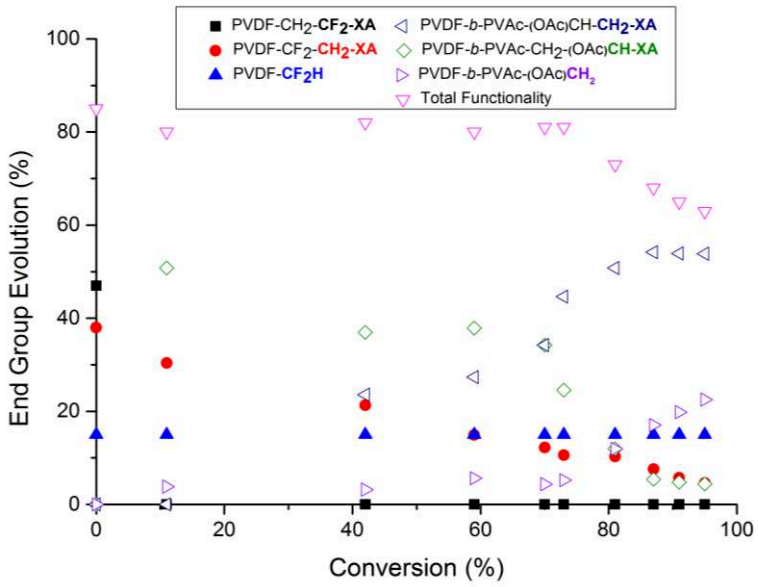

Figure IV-4: Evolution of chain-end functionality of $PVDF_{20}$-b-PVAc during the PVAc block synthesis (target DP = 100) from PVDF20-XA (entry 3, Table IV-1) extracted from in situ NMR experiment. $PVDF_H$-XA, $PVDF_T$-XA, $PVDF_H$-H designate PVDF-CH_2CF_2-XA, PVDF-CF_2CH_2-XA and PVDF-CH_2CF_2-H, respectively; and PVDF-b -$PVAc_H$-XA, PVDF-b-$PVAc_T$XA, PVDF-b-$PVAc_H$-H stand for PVDF-b-PVAc-CH_2-CH(OAc)-XA, PVDF-b- PVAc-CH(OAc)-CH_2-XA, PVDF-b-PVAc-CH_2-CH(OAc)-H, respectively.

These chain-end monitorings revealed the extremely rapid reactivation of the $PVDF_H$-XA chains and the much slower reactivation of the $PVDF_T$-XA chains. The $PVDF_H$-XA reactivation was already quantitative at only 11% of VAc conversion (2 min and 7 s, second point in the *in situ* NMR monitoring in Figure IV-4) as evidenced by the total disappearance of the ^{19}F NMR signal at -71 ppm and the appearance of a new signal at -93.14 ppm (SI-Figure IV-16). After the same reaction time, the $PVDF_T$-XA reactivation had reached only 7.6%. The effect of the VAc target DP on the $PVDF_T$-XA reactivation was also studied. Two $PVDF_{51}$-XA chain extensions, targeting $DP_{VAc} = 100$ and $DP_{VAc} = 300$, were monitored by ^1H and ^{19}F NMR spectroscopies. The results of this study, summarized in SI-Figure IV-17, did not reveal any significant influence of the targeted DP on the reactivation of the $PVDF_T$-XA, although the reactivation seemed to be completed at slightly lower conversions for the higher targeted DP.

The much slower reactivation of this type of chain-end thus occurred throughout the polymerization and was actually still incomplete when the NMR monitoring was stopped after 5 h (5% of residual $PVDF_T$-XA, Fig. S10).

It is important to note that the RAFT polymerizations of VAc and VDF are very similar. In both cases monomer reverse additions (TT) lead to the accumulation of much less reactive species. For VAc, this has been mentioned in the past by several research groups but never studied in detail.[10,44] We recently demonstrated that for PVDF, this accumulation is even faster and leads to a more pronounced broadening of the dispersity and slowdown of the degenerative chain transfer mechanism.[35] Figure IV-4 shows the fast accumulation of $PVAc_T$-XA (-$CH(OAc)CH_2$-XA-terminated PVAc chains) throughout the polymerization of VAc. At 42% VAc conversion, these $PVAc_T$-XA already represent 37% of the xanthate-terminated PVAc chains; and at 87% VAc conversion 70% of the xanthate-terminated PVAc chains are $PVAc_T$-XA. It is worth noting that when the VAc conversion reached around 70%, a surprising increase of transfer to solvent was observed. In consequence, the total functionality decreased drastically towards the end of the PVAc block synthesis (see Figure IV-4).

Figure IV-5 displays the evolution of the viscosimetric GPC traces of the PVAc block synthesis targeting $DP_{VAc} = 300$ from a $PVDF_{51}$-XA macroCTA (DP = 51, entry 1, Table IV-1) constituted only by $PVDF_T$-XA and PVDF-H chains ($PVDF_T$-XA/PVDF-H = 86/14).

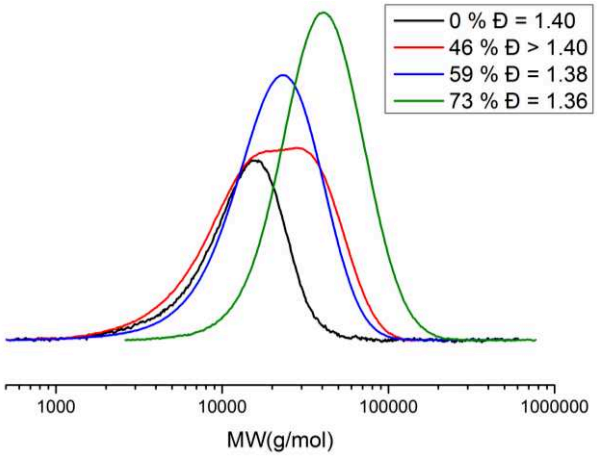

Figure IV-5: GPC traces scaled to $Conv_{(VAc)}$ (viscosimetric detector) of the $PVDF_{51}$-b-PVAc block copolymers resulting from PVAc (target DP = 300) block synthesis from $PVDF_{51}$-XA (entry 1 in Table IV-1: $-CF_2-CH_2-XA/-CH_2-CF_2-XA/-CF_2H$ = 86/0/14). Proportions of xanthate-terminated PVAc chains: red trace (entry 13, Table IV-1) $Conv_{(VAc)}$ = 46%, $PVAc_H$-XA/$PVAc_T$-XA = 10/90; blue trace (entry 14, Table IV-1) $Conv_{(VAc)}$ = 59%, $PVAc_H$-XA/$PVAc_T$-XA = 0/100, green trace (entry 15, Table IV-1) $Conv_{(VAc)}$ = 73%, $PVAc_H$-XA/$PVAc_T$-XA = 0/100. Note: the determination of the molar mass and molar mass distribution of the diblock copolymers using GPC was not possible because it requires a concentration detector such as a RI detector. In the cases of PVDF and PVAc, this cannot be used because of the negative response of PVDF and the positive response of PVAc in DMF. This is particularly true for the GPC trace corresponding to $Conv_{(VAc)}$ = 46%.

At $Conv_{(VAc)}$ = 46%, a bimodal trace was observed. However, at higher conversions, the GPC traces appeared monomodal again and the dispersity did not increase significantly (initial Đ = 1.4, final Đ = 1.36). This surprising evolution may be explained by the chain inversions occurring during VAc polymerization and by the large incidence of transfer to the solvent. At $Conv_{(VAc)}$ = 46%, only a part of the starting $PVDF_T$-XA has been reactivated ($PVDF_T$-XA = 55%, $PVAc_T$-XA = 15%, $PVAc_H$-XA = 2%) and the GPC trace is bimodal because it is the sum of the traces of the growing diblock copolymer and of the residual starting $PVDF_T$-XA (and of the PVDF-H dead chains). As the polymerization carries on, the $PVDF_T$-XA chains are gradually reactivated. Meanwhile, the PVAc growing block undergoes more and more chain inversion and $PVAc_T$-XA chains accumulate in the polymerization medium. Indeed, at $Conv_{(VAc)}$ = 46%, the $PVAc_H$-XA/$PVAc_T$-XA ratio is 10/90, and at higher VAc conversion ($Conv_{(VAc)}$ = 59% and 73%) the PVAc-XA segments are only composed of inversely added chain-ends ($PVAc_H$-XA/$PVAc_T$-XA = 0/100, $Conv_{(VAc)}$ = 59%: $PVDF_T$-XA = 46%, $PVAc_T$-XA = 20%, $PVAc_H$-XA = 0%, PVAc-H = 20%; $Conv_{(VAc)}$ = 73%: $PVDF_T$-XA = 0%, $PVAc_T$-XA = 30%, $PVAc_H$-XA = 0%, PVAc-H = 56%). These $PVAc_T$-XA chains tend to reactivate more slowly than the regularly-added chain-ends ($PVAc_H$-XA). The PVAc block formed from slowly activating chains originating from $PVDF_T$-XA, and thus likely terminated by a -$CH_2CH(OAc)$-XA group ($PVAc_H$-XA), grows faster than the polymer chains that have been

reactivated before them and that have already been converted to the less reactive $PVAc_T$-XA form.

In addition, the increasing amount of PVAc-H dead chains (formed by transfer reaction) observed at higher VAc conversion (PVAc-H = 56% at $VAc_{(Conv)}$ = 73%) do not grow while the $PVDF_T$-XA are still being reactivated. Consequently, the observed intermediate molar mass distribution broadening, eventually narrows down again. A thorough simulation of the RAFT polymerization of VDF, VAc and of the synthesis of PVDF-*b*-PVAc block copolymer using PREDICI will be undertaken in due time to test this hypothesis.

IV.1.4 Assessment of the VAc chain transfer constant (C_{Tr}) to $PVDF_H$-Xa and $PVDF_T$-XA

The O' Brien and Gornick method,[45] previously used by Chong et al.[46] in the RAFT polymerization of styrene and by Boyer et al.[47] in the ITP of VDF, was employed to determine the apparent transfer constants $C_{Tr(app)}$ of the two types of PVDF macroCTAs ($PVDF_T$-XA and $PVDF_H$-XA) towards VAc. This simple method provides an estimate of the real transfer constants which are likely higher than the $C_{Tr(app)}$ determined here.[48]

SI-Figure IV-19 and SI-Figure IV-20 show the plots of $\ln([CTA]_0/[CTA])$ versus $\ln([VAc]_0/[VAc])$ using data acquired from the *in situ* NMR experiments. Linear fitting of these plots provide the $C^{Tr(app)}$, using Equation IV-3:

$$Ln(\frac{[CTA]_0}{[CTA]}) = C_{Tr(app)}\, Ln(\frac{[VAc]_0}{[VAc]}) \qquad \textit{Equation IV-3}$$

This simple method allows the determination of both $C_{Tr(app)}$ from the data of a single experiment. As mentioned earlier, the $PVDF_H$-XA reactivation is extremely fast, yielding only two useful data points. The corresponding transfer constant was thus calculated to be at least 39 at 73 °C (SI-Figure IV-19). In the case of the $PVDF_T$-XA chains, which reactivated much more slowly, the in situ NMR experiment yielded many more usable data points and the corresponding $C_{Tr(app)}$ was more accurately estimated at 0.8 at 73 °C (Fig. S12). This large difference in the $C_{Tr(app)}$ of the two types of PVDF macroCTAs confirms the observation that the $PVDF_H$-XA chains reactivate much faster than the $PVDF_T$-XA chains, but the latter is nonetheless reactivated at a significant rate. Indeed, 0.8 is very close to 1, which is considered as the theoretical limit value to achieve controlled polymerization (linear increase of the molar

masses versus monomer conversion).[48] This value (which characterizes the radical transfer reaction from a vinyl acetate radical onto a $PVDF_T$-XA macroCTA) is comparable to the chain transfer constant observed in the polymerization of styrene carried out in the presence of CTA_{XA} (C_{Tr} = 0.67 at 60 °C) and which does not afford narrow dispersity polystyrene (Đ = 2.0).[49] However, in the case presented here, this transfer only has to occur once; after reactivation and switching toward a VAc-terminated radical chain, the subsequent transfer reactions are those of the PVAc· radicals under the RAFT operating conditions, which are known to afford adequate control (C_{Tr} = 25 at 70 °C with CTA_{XA} as RAFT agent and AIBN as initiator).[50]

IV.1.5 Thermal Analysis

The thermal stability of the new well-defined PVDF-*b*-PVAc block copolymers was determined by thermogravimetric analysis (TGA) in air. The thermograms are displayed in SI-Figure IV-21. As described in a previous study,[14] PVDF-XA exhibited good thermal stability with no significant weight loss until 350 °C whereas PVAc-XA homopolymers start to decompose at 270 °C. The PVDF-*b*-PVAc block copolymers presented intermediate thermal stabilities between those of the PVDF and of the PVAc homopolymers, with no significant degradation below 310 °C.

Differential scanning calorimetry (DSC) experiments were also performed, with specific attention to PVDF crystallization. The corresponding DSC thermograms are shown in Figure IV-6. The $PVDF_{51}$-XA exhibited a typical melting temperature at 170 °C. However, the expected PVDF glass transition at -40 °C [33] was not detected. In agreement with previous DSC studies on PVDF/PVAc blends,[51] complete disappearance of the melting temperature was noticed for the block copolymers (in PVDF-*b*-PVAc, with $DP_{PVAc} > 100$). An exothermic transition was observed at 100 °C for $PVDF_{51}$-*b*-$PVAc_{103}$. This surprising phenomenon may be considered as a cold crystallization transition[52] probably caused by the higher PVDF content in this diblock compared to the other diblock copolymers examined. The disappearance of the PVDF melting temperature and the increase of the glass transition temperature with increasing PVAc weight fraction in PVDF-*b*-PVAc copolymers indicate the miscibility of PVDF and PVAc.

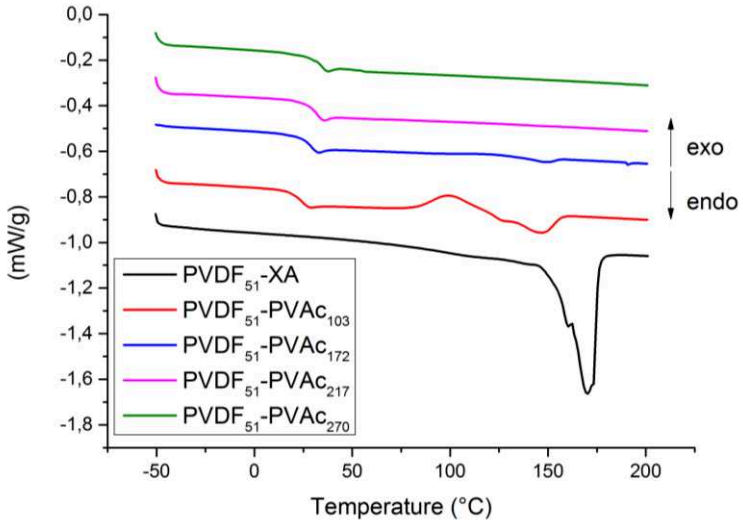

Figure IV-6: DSC thermograms (second heating) for: $PVDF_{51}$-XA homopolymer (black), $PVDF_{51}$-b-$PVAc_{103}$ (red), $PVDF_{51}$-b-$PVAc_{172}$ (blue), $PVDF_{51}$-b- $PVAc_{217}$ (pink) and $PVDF_{51}$-b-$PVAc_{270}$ (green) block copolymers.

IV.2 Computational study

IV.2.1 General considerations, choice of models and computation level

DFT calculations have amply provided insight into the mechanistic issues associated with RDRP, particularly in RAFT,[53] ATRP,[54] OMRP,[55] and NMP.[56] The above described, partly unexpected experimental findings raised several mechanistic questions, the most important one being to understand which property makes VAc special for the reactivation of the less reactive $PVDF_T$-XA dormant chains. In order to shed light on this phenomenon, DFT calculations were carried out on model systems. Related calculations on the homopolymerization of VDF by the RAFT method have been published by us in a recent article.[35] In order to keep the calculations manageable in terms of computational effort while obtaining results of indicative value, the polymer chains were simplified to an H atom beyond the terminal monomer unit.

Thus, the PVDF-$CH_2CF_2^{\bullet}$ (or $PVDF_H^{\bullet}$) and PVDF-$CF_2CH_2^{\bullet}$ (or $PVDF_T^{\bullet}$) chains were modeled respectively by $CH_3CF_2^{\bullet}$ and $CHF_2CH_2^{\bullet}$, the PVAc-$CH_2CH(OAc)$• (or $PVAc_H$•) and PVAc-$CH(OAc)CH_2^{\bullet}$ (or $PVAc_T$•) were modeled respectively by $CH_3CH(OAc)^{\bullet}$ and $(AcO)CH_2CH_2^{\bullet}$, and so forth. In the xanthate group, for the same reason of computational economy, the ethyl substituent in the xanthate group was simplified to a methyl group, -$SC(S)OCH_3$. These structural modifications should not introduce major changes (polarity, homolytic strength, steric effects) in the bonds that are the focus of our investigations.

We stress that we do not aim at quantitatively reproducing observed data. The calculated energies associated with chemical reactions are rarely in agreement with the experimental ones by less than a couple of kcal mol^{-1}. Rather, the main objective of our computational approach is to provide insight into the occurring chemical processes. Energy trends within closely related systems are reproduced more faithfully than absolute values by the DFT calculations. For this reason, we have not tested different functionals and basis sets in order to find the most suitable method for our system. We have continued using B3W91/6-31G(d,p) as in our recent contribution on the closely related VDF RAFT homopolymerization, allowing us to make direct comparisons between the two systems.[35] In that contribution, the method was benchmarked against the known VDF homopropagation rate constant and monomer inversion (head-to-head, or HH) errors, providing acceptable agreement between experimental and computational results. Additional benchmarking has now been carried out here on the VAc homopropagation process.

Experimental values, although showing much scatter depending on the investigation method, are available for the VAc propagation rate constant: 895, 1000 and 4600 M^{-1} s^{-1} in bulk at 25 °C,[57] 117 M^{-1} s^{-1} in benzene and 8 M^{-1} s^{-1} in benzonitrile.[58] From these values, standard activation free energies ($\Delta G^{\ddagger}$) in the range 12.4–16.2 kcal mol^{-1} can be derived using the Eyring equation. The calculations for the $CH_3CH(OAc)\cdot$ addition to CH_2=CH(OAc) to yield $CH_3CH(OAc)CH_2CH(OAc)\cdot$ (regular head-to-tail (HT) addition) yield standard activation barriers ($\Delta G^{\ddagger}$ 298) of 17.6 kcal mol^{-1} from the gas phase calculations, 18.1 kcal mol^{-1} in bulk (vinyl acetate as solvent, ε = 4.2) and 18.1 kcal mol^{-1} in acetonitrile (ε = 35.7). We consider this agreement satisfactory, while the very small corrections observed for solvent models of disparate polarity, reflecting the uncharged nature of radicals, justified pursuing our exploration with the less time consuming and less problematic gas phase optimizations.

Another benchmarking was carried out on the basis of the VDF–VAc reactivity ratios, which were given in different contributions as 0.075 ± 0.015 and 6 ± 1 at 40 °C in water,[59] and essentially zero (± 0.04) and 1.67 (± 0.6) at 45 °C in supercritical CO_2,[60] for r_{VDF} and r_{VAc}, respectively. From the calculated homo- and cross-propagation barriers restricted to the more favorable HT additions (*vide infra*) and the Eyring equation, the computationally predicted reactivity ratios are 0.06 and 1.8 at the operational polymerization temperature of 70 °C. Once again, the agreement can be considered satisfactory.

Comprehensive tables of energy and structural data for the geometry optimized molecules investigated in this study are provided in the VI.1-Supporting Informations (SI-Table IV-3and SI-Table IV-4, respectively).

IV.2.2 Bond strengths

Before presenting the results on the dormant chain activation processes, we briefly analyze the strength of the bonds linking the PVAc chain with the xanthate function. The calculated homolytic bond dissociation enthalpy

(BDE, $\Delta H°_{298:15}$) for the $CH_3CH(OAc)$-XA and $CH_2(OAc)CH_2$-XA bonds, models of the $PVAc_H$-XA and $PVAc_T$-XA chains, are 48.7 and 55.6 kcal mol^{-1}, respectively, confirming the common perception that the bond is stronger in the T-terminated dormant species obtained after an inverted (HH) monomer addition. This situation parallels that reported for the CH_3CF_2-XA and CHF_2CH_2-XA bonds,[35] models of the $PVDF_H$-XA and $PVDF_T$-XA chains (54.5 and 60.7 kcal mol^{-1}).

The BDE difference between the $PVAc_T$-XA and $PVAc_H$-XA models corresponds almost exactly to the energy difference of the isomeric radicals: the calculated standard enthalpy of $CH_2(OAc)CH_2\cdot$ is 6.8 kcal mol^{-1} higher than that of $CH_3CH(OAc)\cdot$. Consequently, the isomeric CTA models are essentially isoenergetic, ($CH_3CH(OAc)$-XA is more stable than $CH_2(OAc)CH_2$-XA by 0.4 kcal mol^{-1}); see SI-Figure IV-22where the energetic profile of the related PVDF model systems[35] is also shown for comparison. Note that the BDE values are greater for the VDF systems than for the VAc systems with equivalent terminal monomer orientation. This is consistent with the notion that the VDF radical ($CH_3CF_2\cdot$) is more reactive than the VAc radical ($CH_3CH(OAc)\cdot$). Less expectedly, the BDE is also lower for VAc than for VDF when comparing the bonds generated by the tail monomer end, although both chain ends involve a primary methylene radical. This suggests that the β-C atom substituents (CF_2 *vs*. CH(OAc)) also have a significant influence on radical stability and reactivity.

IV.2.3 VAc homopolymerization: radical exchange vs. propagation

The results of the calculations for the VAc homopolymerization are summarized in Figure IV-7. The figure shows the energy profiles associated with the radical exchange process (chain transfer) in part a, and the addition to monomer (chain propagation) in part b.

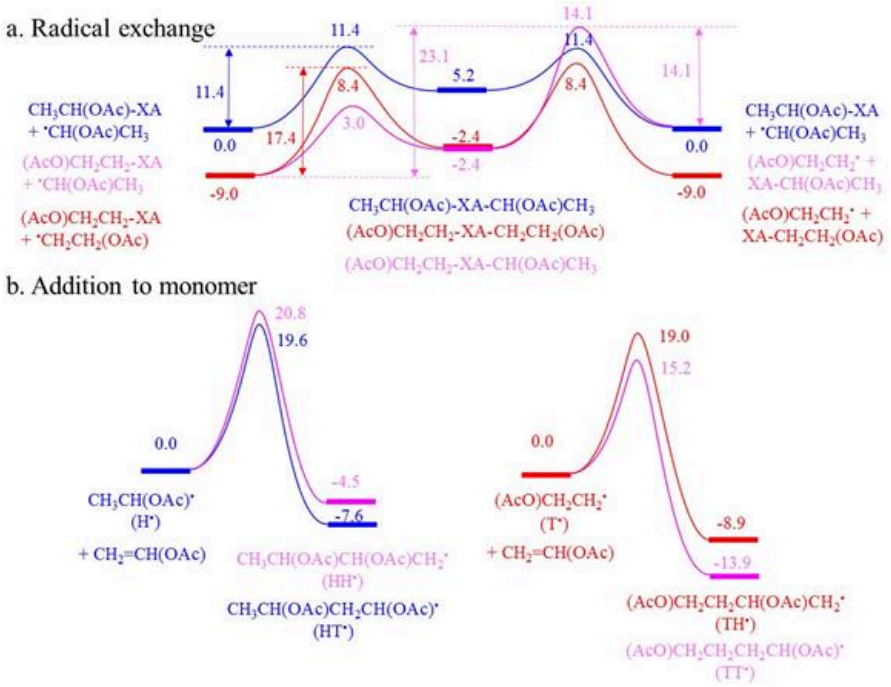

Figure IV-7: Energy profiles for (a) the degenerative (HH and TT) and nondegenerative (HT) radical exchange with the dormant chain and (b) for the different modes of radical addition to monomer in RAFT VAc homopolymerization. The reported values are ΔG (343.15 K) in kcal mol^{-1}.

The scenario for the RAFT VAc homopolymerization is quite similar to that of the VDF homopolymerization.[35] The degenerative (HH and TT) and non-degenerative (HT and reverse TH) radical exchange processes go through associative PVAc-XA-PVAc radical intermediates, the energy of which is very close to those of the separate radical and dormant chain. The main difference relative to the VDF RAFT system is that all barriers are higher, both for the radical exchange and for the monomer addition processes. In terms of radical addition to the monomer (Figure IV-7b), the regular H-$CH_2CH(OAc)\cdot$ radical (model of $PVAc_H\cdot$) prefers the HT addition mode (blue profile in Figure IV-7b, $\Delta G^{\ddagger}_{p;HT}$= 19.6 kcal mol^{-1}). The calculated $k_{p,HT}/k_{p,HH}$ ratio is 5.8 at 70 °C which, predicts a 15% probability of inverted monomer additions. The experimentally reported inverse addition frequency is in the 1-2 % range.[44b,61]

The $PVAc_T\cdot$ model radical species adds to monomer more favorably in the TT mode ($\Delta G^{\ddagger}_{p;TT}$ = 15.2 kcal mol^{-1} *vs.* $\Delta G^{\ddagger}_{p;TH}$ = 19.0 kcal mol^{-1}) to regenerate the regular chain-end (99.6% probability). The energy difference between the isomeric HH and HT (or TH and TT)

products reflects the greater C-C bond strength in CH(X)-CH_2 relative to CH(X)-CH(OAc) (X = H for the HT and HH addition; OAc for the TH and TT addition).

As previously found for the VDF RAFT system,[35] the barrier to the degenerative exchange between the regular $PVAc_H$· radicals on the xanthate CTA (blue profile in Figure IV-7a, $\Delta G^{\ddagger}_{Exch;HH}$ = 11.4 kcal mol^{-1}) is smaller than the monomer addition barrier, which is a necessary condition to insure good control by degenerative transfer. Application of the Eyring relationship yields the rate constants $k_{p,HT}$ = 2.4 M^{-1} s^{-1} for HT homopropagation and $k_{Exch,HH}$ = 4.0 10^5 M^{-1} s^{-1} for the degenerative radical exchange at 70 °C. Thus, the $k_{Exch,HH}/k_{p,HT}$ ratio is 1.7 10^5.

The competing rates of the degenerative exchange and addition to the monomer for the same radical depend not only on the rate constant ratio but also on the concentration ratio:

$$\frac{v_{Exch,HH}}{v_{p,HT}} = \frac{k_{Exch,HH}}{k_{p,HT}} \frac{[PVAc_H - XA]}{[VAc]} \qquad \textit{Equation IV-4}$$

which is in favor of the monomer and therefore favors propagation. However, even for high target DPs (e.g. [VAc]/[PVAc-XA] > 10^3), the $v_{Exch,HH}/v_{p,HT}$ ratio would still be in favor of exchange, guaranteeing controlled chain growth.

After an inverted monomer addition, the resulting $PVAc_T$· radical yield the more stable $PVAc_T$-XA dormant chain by a thermodynamically favorable exchange with $PVAc_H$-XA, which has a calculated barrier ($\Delta G^{\ddagger}_{Exch;HT}$), for the model system, of 14.1 kcal mol^{-1} (pink profile in Figure IV-7a). Reactivation of this dormant chain with ultimate regeneration of the regular$PVAc_H$· radical requires release of the $PVAc_T$· radical from the dormant chain and TT monomer addition. This can be accomplished by exchange with the more abundant $PVAc_H$· radical (pink profile in Figure IV-7a, $\Delta G^{\ddagger}_{Exch;TH}$ = 23.1 kcal mol^{-1}) followed by TT addition to the monomer. The profile involves a competing back-trapping (barrier of 14.1 kcal mol^{-1}, $k_{Exch,HT}$ = 7.6 10^3 M^{-1} s^{-1}) and TT addition to the monomer (barrier of 15.2 kcal mol^{-1}, $k_{p,TT}$ = 1.5 10^3 M^{-1} s^{-1}) for the intermediate$PVAc_T$· radical. Although the rate constant is greater for backtrapping, the concentration factor ([VAc] > [$PVAc_H$-XA]) is in favor of propagation. The complete rate expression for $PVAc_T$-XA reactivation, under the steady state approximation for the $PVAc_T$· intermediate, is:

$$v_{act}(PVAc_T - XA) = \frac{k_{Exch,TH} k_{p,TT} [PVAc_H^{\bullet}][PVAc_T - XA][VAc]}{k_{Exch,HT}[PVAc_H - XA] + k_{p,TT}[VAc]} \quad \textit{Equation IV-5}$$

which under saturation conditions ([VAc] >> [$PVAc_H$-XA]) leading to faster propagation than back-trapping ($k_{p,TT[VAc]} >> k_{Exch,HT[PVAcH-XA]}$) simplifies to:

$$v_{act}(PVAc_T - XA) = k_{Exch,TH}[PVAc_H^{\bullet}][PVAc_T - XA] = v_{Exch,TH} \quad \textit{Equation IV-6}$$

This means that the reactivation of the $PVAc_T$-XA dormant chain by the more abundant $PVAc_H$· radical is likely limited by the non-degenerative exchange ($\Delta G^{\ddagger}_{Exch;TH}$ = 23.1 kcal mol^{-1}, $k_{Exch,TH}$ = 1.43 10^{-2} M^{-1} s^{-1}). On the other hand, for the VDF system, back-trapping was predicted faster than homopropagation, with a reactivation rate also affected by the subsequent propagation barrier.[35] The larger barrier for reactivation of $PVAc_T$-XA relative to $PVAc_H$-XA agrees with the polymerization slowdown and poorer control following the inverted monomer addition in the RAFT homopolymerization of VAc.[62,63]

It can also be imagined that the less abundant $PVAc_T$· radical contributes to the reactivation of the less reactive $PVAc_T$-XA chains (red energy profile inFigure IV-7a, $\Delta G^{\ddagger}_{Exch;TT}$ of 17.4 kcal mol^{-1} at 70 °C). Indeed, in the recent VDF RAFT polymerization study,[35] the reactivation and chain extension of the $PVDF_T$-XA chains (though with poor control) was shown to be dominated by the degenerative exchange with the less abundant $PVDF_T$· radical. The degenerative exchange rate constant for the $PVAc_T$-XA/$PVAc_T$· reaction is $k_{Exch,TT}$ = 60.6 M^{-1} s^{-1}. However, the actual exchange rate has a first order dependence on the less abundant $PVAc_T$· radical concentration (estimated as 1-2 % of the total PVAc· concentration from the experimentally known fraction of inverted monomers in the polymer chain). The relative rates of TT degenerative exchange and TH non-degenerative exchange for the same $PVAc_T$-XA dormant chain can be calculated as:

$$\frac{v_{Exch,TT}}{v_{Exc,TH}} = \frac{k_{Exch,TT}}{k_{Exch,TH}} \frac{[PVAc_T^{\bullet}]}{[PVAc_H^{\bullet}]} \quad \textit{Equation IV-7}$$

Insertion of the rate constant ratio (4.2 10^3) and the above estimated radical ratio into this expression yields a rate ratio of 42‑84. This suggests that, like in the recently reported VDF RAFT system and counterintuitively, the $PVAc_T$-XA dormant chains are reactivated more rapidly by the degenerative exchange with the less abundant $PVAc_T$· radicals.

IV.2.4 VDF/comonomer cross-exchange with xanthate and crosspropagation.

The investigation of the reactivation process of the PVDF-XA macroCTAs ($PVDF_H$-XA, $PVDF_T$-XA) in the block copolymerization experiments used the same approach described in the previous section: *(i)* determination of the Gibbs energy profile leading from the macroCTA models (CH_3CF_2-XA and CHF_2CH_2-XA, respectively) and the model of the active radical chain generated from the added monomer ($CH_3CH(OAc)\cdot$ for $PVAc_H\cdot$, $CH_3CH(COOMe)\cdot$ for PBA$\cdot$, $CH_3CHCO(NMe_2)\cdot$ for PDMA$\cdot$, and $CH_3CH\cdot N(cyclo\text{-}COCH_2CH_2CH_2)$ for PNVP$\cdot$) to the liberation of the desired $CH_3CF_2\cdot$ or $CHF_2CH_2\cdot$ free radical; *(ii)* investigation of the subsequent addition of these liberated radicals to the monomer of interest, yielding the chain-end switched new radical; *(iii)* analysis of the full energy profile with identification of the ratelimiting transition state of the overall process; *(iv)* derivation, through the Eyring relationship, of the effective rate constant for the macroCTA activation rate; *(v)* comparison with the activation barrier of the primary radical homopropagation. All the relevant results are collected in Table IV-2, in which the Gibbs equilibrium and activation energies are reported at the polymerization temperature (70 °C).

Table IV-2: Summary of the calculated Gibbs energy changes for the propagation barriers, radical exchange and back-trapping barriers, radical exchange equilibrium, and addition of the liberated radical to monomer (in kcal mol^{-1} at 70 °C), and predicted effective rate constants (in M^{-1} s^{-1}), for the reactivation of the CH_3CF_2-XA and CHF_2CH_2-XA macroCTA models by different monomers

MacroCTA model	M[a]	$\Delta G^{\ddagger}_{p}$[b]	k_p[c]	$\Delta G^{\ddagger}_{Exch}$[d]	k_{Exch}[c]	$\Delta G^{\ddagger}_{bt}$[e]	ΔG_{Exch}[f]	$\Delta G^{\ddagger}_{add}$[g]	Experimental observations
CH_3CF_2-XA	VAc	19.6	2.4	19.4	3.2	11.0	6.5	11.6	Fast reactivation
CHF_2CH_2-XA				23.5	$8.0\cdot10^{-3}$		12.6	12.2	Slow reactivation
CH_3CF_2-XA	NVP	12.9	$4.4\cdot10^{4}$	21.4	0.17	10.0	11.9	11.0	Reactivation
CHF_2CH_2-XA				27.9	$1.3\cdot10^{-5}$		17.9	11.3	No reactivation
CH_3CF_2-XA	MA	16.0	$4.7\cdot10^{2}$	23.3	$1.1\cdot10^{-2}$	9.7	12.3	9.9	n.d.[h]
CHF_2CH_2-XA				28.1	$9.4\cdot10^{-6}$		18.4	11.4	No reactivation
CH_3CF_2-XA	DMA	17.1	94	17.2	81	11.4	16.2	10.7	n.d.[h]
CHF_2CH_2-XA				33.7	$2.6\cdot10^{-9}$		16.2	12.0	No reactivation

[a]Only the predominant addition of the liberated radical to the tail end of the monomer is considered. [b]Activation free energy for M homopropagation at 343.15 K. [c]Calculated from the corresponding $\Delta G^{\ddagger}$ by the Eyring relationship at 343.15 K. [d]Activation free energy for the radical exchange from the macroCTA model + H-M$\cdot$ to H-M-XA and the macroradical model at 343.15 K. [e]Activation free energy for the back-trapping process leading from CH_3CF_2 or $CHF_2CH_2\cdot$ and H-M-XA to the starting macroCTA model and HM$\cdot$. [f]Gibbs energy change for the radical exchange process at 343.15 K. [g]Activation barrier for the $CH_3CF_2\cdot$ or $CHF_2CH_2\cdot$addition to M at 343.15 K. [h]n.d. = not determined.

Fig. 8 reports the results of the chain extension with VAc, limited to the reactivation by the more abundant $PVAc_H\cdot$ chains and of the addition of the resulting $PVDF_H\cdot$ and $PVDF_T\cdot$ model radicals to the tail end of the VAc monomer, yielding the HT and the TT coupled

products, respectively. Complete energy diagrams including the activations by the minority $PVAc_T\cdot$ model and the $PVDF\cdot$ HH and TH additions to VAc are in the Supporting Informations (SI-Figure IV-23and SI-Figure IV-24). As seen previously for the VDF[35] and above for the VAc homopolymerizations, the HH addition is less favored than the HT addition and the TH addition is less favored than the TT addition.

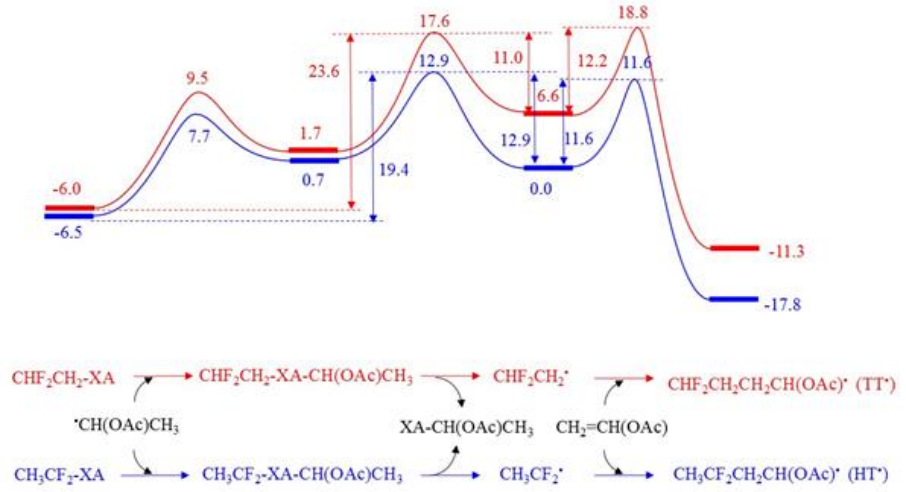

Figure IV-8: Energy profiles for the model $PVDF_H$-XA and $PVDF_T$-XA reactivation processes in the chain extension with VAc. The reported values are ΔG (343.15 K) in kcal mol^{-1}, with the zero energy reference being the $CH_3CF_2\cdot$ radical.

Activation of the regular chain-end model, CH_3CF_2-XA, has a large barrier ($\Delta G^{\ddagger}_{Exch}$= 19.4 kcal mol^{-1}), the intermediate adduct fragmentation being the rate-limiting step. This barrier is much greater than those of the degenerative reactivations of CH_3CF_2-XA by $CH_3CF_2\cdot$ (10.6 kcal mol^{-1})[35] and of $CH_3CH(OAc)$-XA by $CH_3CH(OAc)\cdot$ (11.4 kcal mol^{-1}, Figure IV-7a). However, contrary to these degenerative processes in VDF and VAc homopolymerizations, the subsequent addition of the $CH_3CF_2\cdot$radical to the VAc monomer has a lower barrier ($\Delta G^{\ddagger}_{add}$ =11.6 kcal mol^{-1}) than the back-trapping process ($\Delta G^{\ddagger}_{bt}$ =12.9 kcal mol^{-1}). In addition, the concentration ratio ([VAc] > > [PVAc-XA]) plays further in favor of propagation. Therefore, once the $PVDF_H\cdot$radical is generated, it is immediately transformed into a $PVAc_H\cdot$radical which then undergoes RAFT homopolymerization according to the profile in Figure IV-7. Hence, the activation rate is limited by the non-degenerative exchange process with k_{Exch} = 3.2 M^{-1} s^{-1} for the $PVDF_H$-XA macroCTA. This is actually a greater rate than for the reactivation of the $PVAc_T$-XA macroCTA in VAc homopolymerization *(vide supra)* and is thus compatible with a fast reactivation process. It is also competitive with VAc homopropagation ($\Delta G^{\ddagger}_{p}$ = 19.6 kcal mol^{-1}). The relative rate of $PVAc\cdot$ addition to $PVDF_H$-

XA, leading to macroCTA reactivation, and addition to VAc, leading to homopropagation, is $v_{Exch/vp} = (k_{Exch}/k_p)([PVDF_H\text{-}XA]/[VAc])$, with the rate constant ratio being 1.3. This is an important point, because the efficiency of chain extension depends on how rapidly the new radical can generate the chain from the macroCTA before leading to significant homopropagation. The reactivation of the $PVDF_T$-XA macroCTA by VAc involves, according to the calculations on the model system, a greater exchange barrier ($\Delta G^{\ddagger}_{Exch}$ = 23.6 kcal mol^{-1}), while TT coupling of the liberated $PVDF_T$· radical to VAc has a slightly greater barrier ($\Delta G^{\ddagger}_{add}$ = 12.2 kcal mol^{-1}) than back-trapping ($\Delta G^{\ddagger}_{bt}$ = 11.0 kcal mol^{-1}), yielding a rate constant ratio k_{add}/k_{bt} = 0.17.

However, like for the previously analyzed VAc homopolymerization, the concentration factor acts in favor of radical addition to the monomer and thus the dormant chain activation is likely limited by the exchange process, yielding an estimated k_{Exch} of 8.0 10^{-3} M^{-1} s^{-1}. Hence, the regular $PVDF_H$-XA macroCTA is reactivated 400 times faster than the $PVDF_T$-XA macroCTA. This ratio is qualitatively consistent with the results of the apparent transfer constant determination (>39 and 0.8, SI-Figure IV-19 and SI-Figure IV-20). In addition, since VAc homopropagation is now much faster (k_p = 2.4 M^{-1} s^{-1}) than the macroCTA reactivation, the switching process is not predicted to lead to a diblock copolymer with a narrow molecular weight distribution. On the basis of the calculated rate constants, the ratio between propagation and activation rates is $v_p/v_{Exch} = 300([VAc]/[PVDF_T\text{-}XA])$, meaning for instance that for a [VAc]/[$PVDF_T$-XA] ratio of 100 as in entry 16, the PVAc· radical should add on average thirty thousand monomer molecules before activating the macroCTA. This is not in perfect agreement with the experiment since the PVDF-*b*-PVAc resulting from entries 8‑16 (Table IV-1) has a relatively narrow molecular weight distribution, but the discrepancy can be rationalized not only by a possible computational overestimation of the activation barrier, greater than the overestimation of the propagation barrier, but also by the contribution to activation by the less abundant $PVAc_T$· radicals (after an inverted VAc addition), since the activation barrier is in this case lower (19.8 kcal mol^{-1}, see SI-Figure IV-24). The key to the reactivation of both $PVDF_H$-XA and $PVDF_T$-XA by VAc is that $\Delta G^{\ddagger}_{add}$ is low for both head and tail PVDF· radicals, *i.e.* the VDF-to-VAc monomer switch is faster than either VDF or VAc homopropagation.

IV.2.5 Reactivation of PVDF-XA by NVP, BA and DMA

The last question addressed by the DFT calculations is the failure of the NVP, BA and DMA monomers to afford well-defined block copolymers starting from the PVDF-XA macroCTA. As a reminder, none of these monomers is able to extend the $PVDF_T$-XA chains, but for NVP reactivation of the $PVDF_H$-XA chains occurs.

Concerning the $PVDF_T$-XA reactivation by NVP and by the other monomers, the exchange barriers are higher (27.9, 28.1 and 33.7 kcal mol^{-1}, respectively) than for the reactivation by Vac (23.5 kcal mol^{-1}, see Table IV-2). Furthermore, once activated, the back-trapping has a smaller activation barrier than the addition to the monomer and the two processes will compete. The energy profiles for these reactivation processes are provided in the Supporting Informations (SI-Figure IV-25). From the calculated k_{bt}/k_{add} value (6.7 for NVP, 12 for MA, 2.4 for DMA), activation should still be limited by the exchange for high [monomer]/[macroCTA] ratios, but even in the most favorable case of an exchangelimited kinetics, the reactivation of $PVDF_T$-XA by these monomers is at least two orders of magnitude slower than the reactivation by VAc (Table IV-2). These rates are much slower than those of homopropagation, thus once generated from the initiating $R_0\cdot$ radicals, the new $R_0M\cdot$ radicals lead to preferred homopropagation instead of exchange to release the $PVDF_T\cdot$ radicals. This justifies the experimentally observed inability of these monomers to reactivate the $PVDF_T$-XA chains.

Finally, for each monomer, the radical exchange involving the $PVDF_H$-XA chains has a lower thermodynamic penalty by *ca.* 6 kcal mol^{-1}, than the radical exchange involving the $PVDF_T$-XA chains according to the DFT calculations on the model systems. For NVP, the calculated exchange barrier is slightly higher (21.4 kcal mol^{-1}) than for the exchange involving VAc (19.4 kcal mol^{-1}) but lower than that of the $PVDF_T$-XA reactivation by VAc (23.5 kcal mol^{-1}). The subsequent $PVDF_{H\cdot}$ addition to NVP, though having a slightly greater barrier (11.0 kcal mol^{-1}) than back-trapping, should not be rate-limiting because of the concentration factor as in the other situations examined above. This is consistent with the observed reactivation of $PVDF_H$-XA by NVP. However, according to the calculations, the homopropagation of NVP is much faster than the exchange, in contrast to the reactivation of $PVDF_H$-XA by VAc, which yields faster exchange than homopropagation as shown above. This could in part rationalize the high dispersity of the PVDF-*b*-PNVP product (entry 17 in Table IV-1). The calculations also predict that it may be possible to reactivate the $PVDF_H$-XA macroCTA with MA and

DMA (see the data in Table IV-2 and the Gibbs energy profiles in SI-Figure IV-26). This phenomenon has not been investigated experimentally since xanthate-based RAFT agents are known to poorly control the homopolymerization of acrylates or acrylamides.

V. Conclusion

This article deals with the possibility of synthesizing block copolymers from PVDF-XA macroCTA via sequential addition of monomers. It shows that PVDF macroCTAs terminated by regularly added VDF units ($PVDF_H$-XA) are efficiently reactivated by both PVAc· and PNVP· radicals, thus leading to well-defined block copolymers. In contrast, PVDF macroCTAs terminated with an inversely added VDF unit ($PVDF_T$-XA) were not reactivated by PNVP· radicals. However, in the case of VAc, these less reactive $PVDF_T$-XA macroCTAs are reactivated sufficiently fast to afford relatively well-defined PVDF-*b*-PVAc block copolymers. A thorough ^{1}H and ^{19}F NMR spectroscopic characterization of the block copolymers demonstrated this surprising complete reactivation of the reputedly "dead" $PVDF_T$-XA chains. This difference in reactivation speed was confirmed by calculation of the corresponding apparent transfer constants ($C_{Tr(app)} > 39$ for $PVDF_H$-XA and $C_{Tr(app)} = 0.8$ for $PVDF_T$-XA at 73 °C) using O'Brien and Gornick's method. DFT calculations on model systems rationalize the observed behavior on the basis of differences in radical exchange kinetics ($\Delta G^{\ddagger}_{Exch}$ = 19.4 and 23.5 kcal mol^{-1} for $PVDF_H$-XA and $PVDF_T$-XA with VAc; 21.4 kcal mol^{-1} for $PVDF_H$-XA with NVP), whereas the barriers to addition of the liberated $PVDF_H$· and $PVDF_T$· radicals to VAc and NVP are similar and yield competitive addition rates relative to the thermodynamically favorable back-trapping. In addition, the macroCTA reactivation rates are competitive with the homopropagation rate of the chain extending monomer, particularly for the extension of $PVDF_H$-XA with VAc. The lack of $PVDF_T$-XA reactivation by NVP, BA and DMA is rationalized by the fact that the rate of exchange is much lower than that of monomer homopropagation.

VI. References

[1] B. Ameduri, B. Boutevin, In *Well-Architectured Fluoropolymers: Synthesis, Properties and Applications*, Ed., Elsevier: Amsterdam, 2004.

[2] B. Ameduri, *Chem. Rev*., 2009, **109**, 6632−6686.

[3] F. Boschet, B. Ameduri, *Chem. Rev*., 2014, **114**, 927-980.

[4] M. Tatemoto, In *The First Regular Meeting of Soviet Japanese Fluorine Chemists*, Tokyo, 1979.

[5] (a) N. Durand, B. Ameduri, B. Boutevin, *J. Polym. Sci.: Part A: Polym. Chem*., 2011, **49**, 82–92. (b) C. Boyer, D. Valade, L. Sauguet, B. Ameduri, B. Boutevin, *Macromolecules*, 2005, **38**, 10353-10362.

[6] B. Ameduri, *Macromolecules*, 2010, **43**, 10163-10184.

[7] (a) A. D. Asandei, O. I. Adebolu, C. P. Simpson, J. S. Kim, *Angew. Chem. Int. Ed*., 2013, **52**, 10027-10030. (b) A. D. Asandei, *Chem. Rev.*, 2016, **116**, 2244-2274.

[8] M. Guerre, B. Campagne, O. Gimello, L. Parra, B. Ameduri, V. Ladmiral, *Macromolecules*, 2015, **48**, 7810-1822.

[9] M. Guerre, G. Lopez, T. Soulestin, C. Totée, B. Ameduri, G. Silly, V. Ladmiral, *Macromol. Chem. Phys*., 2016, **217**, 2275-2285.

[10] S. Harrisson, X. Liu, J-N. Ollagnier, O. Coutelier, J-D. Marty, M. Destarac, *Polymers*, 2014, **6**, 1437-1488.

[11] M. R. Hill, R. N. Carmean, B. S. Summerlin, *Macromolecules*, 2015, **48**, 5459-5469.

[12] S. Perrier, P. J. Takolpuckdee, *Polym. Sci.: Part A: Polym. Chem*., 2005, **43**, 5347-5393.

[13] A. D. Asandei, O. Adebolu, C. P. Simpson, *J. Am. Chem. Soc.,* 2012, **134,** 6080-6083.

[14] M. Guerre, B. Ameduri, V. Ladmiral, *Polym. Chem.*, 2016, **7**, 441-450.

[15] V. S. D. Voet, G. ten Brinke, K. Loos, *J. Polym. Sci.: Part A: Polym. Chem*., 2014, **52**, 2861-2877.

[16] Z. B. Zhang, S. K. Ying, Z. Q. Shi, *Polymer*, 1999, **40**, 1341–1345.

[17] S. M. Jol, W. S. Lee, B. S. Ahn, K. Y. Park, K. A. Kim, I. S. Rhee Paeng, *Polym. Bull.*, 2000, **44**, 1–8.

[18] M. Destarac, K. Matyjaszewski, E. Silverman, B. Ameduri, B. Boutevin, *Macromolecules*, 2000, **33**, 4613–4615.

[19] Z. Q. Shi, S. Holdcroft, *Macromolecules*, 2004, **37**, 2084–2089.

[20] Z. Q. Shi, S. Holdcroft, *Macromolecules*, 2005, **38**, 4193–4201.

[21] G. Laruelle, E. Nicol, B. Ameduri, J. F. Tassin; N. Ajellal*, J. Polym. Sci.: Part A: Polym. Chem.*, 2011, **49**, 3960-3969.

[22] K. Xu, K. Li, P. Khanchaitit, Q. Wang, *Chem. Mater.,* 2007, **19**, 5937–5945.

[23] C. Chanthad, K. A. Masser, K. Xu, J. Runt, Q. J. Wang, *Mater. Chem*., 2012, **22**, 341–344.

[24] V. S. D. Voet, M. Tichelaar, S. Tanase, M. C. Mittelmeijer-Hazeleger, G. ten Brinke, K. Loos, *Nanoscale,* 2013, **5**, 184–192.

[25] V. S. D. Voet, D. Hermida-Merino, G. ten Brinke, K. Loos, *RSC Adv*., 2013, **3**, 7938–7946.

[26] A. Meskini, M. Raihane, I. Stevenson-Royaux, G. Boiteux, G. Seytre, B. Ameduri, *J. Non-Cryst. Solids*, 2010, **356**, 688-694.

[27] G. David, C. Boyer, J. Tonnar, B. Ameduri, P. Lacroix-Desmazes, B. Boutevin, *Chem. Rev.*, 2006, **106,** 3936-3981.

[28] D. Valade, C. Boyer, B. Ameduri, B. Boutevin, *Macromolecules*, 2006, **39**, 8639-8651.

[29] G. Lopez, A. Thenappan, B. Ameduri, *ACS Macro. Lett.,* 2015, **4**, 16-20.

[30] a) P. Černoch, S. Petrova, Z. Černochová, J-S. Kim, C. P. Simpson, A. D. Asandei*, Eur. Polym. J.,* 2015, **68**, 460-470. b) P. Černoch, Z. Cernochová, S. Petrova, D. Kaňková, J-S. Kim, V. Vasu, A. D. Asandei, *RSC Adv.*, 2016, **6**, 55374-55381.

[31] C. P. Simpson, A. I. Abdelou, J. S. Kim, V. Vasu, A. D. Asandei, *Macromolecules*, 2015, **48**, 6404-6420.

[32] G. Kostov, F. Boschet, J. Buller, L. Badache, S. Brandstadter, B. Ameduri, *Macromolecules*, 2011, **44**, 1841-1855.

[33] E. Girard, J-D. Marty, B. Ameduri, M. Destarac, *ACS Macro Lett.*, 2012, **1**, 270-274.

[34] Y. Patil. B. Ameduri, *Polym. Chem*., 2013, **4**, 2783-2799.

[35] M. Guerre, W. S. M. Rahaman, B. Ameduri, R. Poli, V. Ladmiral, *Macromolecules*, 2016, 49, 5386-5396.

[36] X. Liu, O. Coutelier, S. Harrisson, T. Tassaing, J-D. Marty, M. Destarac, *ACS Macro Lett.* 2015, **4**, 89-93

[37] M. J. Frisch, G. W. Trucks, H. B. Schlegel, G. E. Scuseria, M. A. Robb, J. R. Cheeseman, G. Scalmani, V. Barone, B. Mennucci, G. A. Petersson, H. Nakatsuji, M. Caricato, X. Li, H. P. Hratchian, A. F. Izmaylov, J. Bloino, G. Zheng, J. L. Sonnenberg, M. Hada, M. Ehara, K. Toyota, R. Fukuda, J. Hasegawa, M. Ishida, T. Nakajima, Y. Honda, O. Kitao, H. Nakai, T. Vreven, J. A. Montgomery, Jr., J. E. Peralta, F. Ogliaro, M. Bearpark, J. J. Heyd, E. Brothers, K. N. Kudin, V. N. Staroverov, R. Kobayashi, J. Normand, K. Raghavachari, A. Rendell, J. C. Burant, S. S. Iyengar, J. Tomasi, M. Cossi, N. Rega, J. M. Millam, M. Klene, J. E. Knox, J. B. Cross, V. Bakken, C. Adamo, J. Jaramillo, R. Gomperts, R. E. Stratmann, O. Yazyev, A. J. Austin, R. Cammi, C. Pomelli, J. W. Ochterski, R. L. Martin, K. Morokuma, V. G. Zakrzewski, G. A. Voth, P. Salvador, J. J. Dannenberg, S. Dapprich, A. D. Daniels, Ö. Farkas, J. B. Foresman, J. V. Ortiz, J. Cioslowski, and D. J. Fox, Gaussian, Inc., Wallingford CT, 2009.

[38] V. S. Bryantsev, M. S. Diallo, W. A. Goddard, III *J. Phys. Chem. B*, 2008, **112**, 9709-9719.

[39] A. V. Marenich, C. J. Cramer, D. G. Truhlar, *J. Phys. Chem. B,* 2009, **113**, 6378-6396.

[40] G. Moad, E. Rizzardo, S. H. Thang, Aust. J. Chem., 2012, **65**, 985-1076.

[41] M. Destarac, D. Charmot. X. Franck, S. Z. Zard, *Macromol. Rapid. Commun*., 2000, **21**, 1035-1039.

[42] W. R. Jr. Dolbier, *Top. Curr. Chem.,* 1997, **192**, 97-163.

[43] J. Demarteau, A. Kermagoret, I. German, D. Cordella, K. Robeyns, J. De Winter, P. Gerbaux, C. Jerome, A. Debuigne, C. Detrembleur, *Chem. Comm*., 2015, **51**, 14334.

[44] (a) Y. Kwak, A. Goto, T. Fukuda, Y. Kobayashi, S. Yamago, Macromolecules, 2006, **39**, 4671–4679. (b) A. N. Morin, C. Detrembleur, C. Jérôme, P. D. Tullio, R. Poli, A. Debuigne, Macromolecules, 2013, **46**, 4303-4312.

[45] J. L. O'Brien, F. Gornick, J. Am. Chem. Soc., 1955, **77**, 4757.

[46] Y. K. Chong, J. Krstina, T. P. T. Le, G. Moad, A. Postma, E. Rizzardo, S. H. Thang, Macromolecules, 2003, **36**, 2256–2272.

[47] C. Boyer, D. Valade, P. Lacroix-Desmazes, B. Ameduri, B. Boutevin, J. Polym. Sci.: Part A: Polym. Chem., 2006, **44**, 5763-5777.

[48] (a) G. Moad, E. Rizzardo, S. H. Thang, Aust. J. Chem. 2009, 62, 1402. (b) E. Bicciocchi, Y. K. Chong, L. Giorgini, G. Moad, E. Rizzardo, S. H. Thang, Macromol. Chem. Phys., 2010, **211**, 529. (c) D. J. Keddie, C. Guerrero-Sanchez, G. Moad, R. J. Mulder, E. Rizzardo, S. H. Thang, Macromolecules, 2012, **45**, 4205.

[49] M. Adamy AM. van Herk, M. Destarac M. J. Monteiro, Macromolecules, 2003, **36**, 2293-2301.

[50] P-E. Dufils, G. David, B. Boutevin, G. Woodward, G. Otter, A. Guinaudeau, S. Mazières, M. Destarac, J. Polym. Sci.: Part A: Polym. Chem., 2012, **50**, 1997-2007.

[51] R. Baskaran, S. Selvasekarapandian, N. Kuwata, J. Kawamura, T. Hattori, Mat. Chem. and Phy., 2006, **98**, 55-61.

[52] (a) Y. Chen, X. Chen, D. Zhou, Q. Shen, W. Hu, Polymer, 2016, **84**, 319-327. (b) J. You, H. Fu, W. Dong, L. Zhao, X. Cao, Y. Li, ACS Appl. Mater. Interfaces, 2012, **4**, 4825−4831.

[53] (a) M. L. Coote, L. Radom, J. Am. Chem. Soc., 2003, **125**, 1490-1491. (b) M. L. Coote, Macromolecules, 2004, **37**, 5023-5031. (c) M. L. Coote, L. Radom, Macromolecules, 2004, **37**, 590-596. (d) M. L. Coote, J. Phys. Chem. A, 2005, **109**, 1230-1239. (e) M. L. Coote, D. J. Henry, Macromolecules, 2005, **38**, 1415-1433. (f) M. L. Coote, D. J. Henry, Macromolecules, 2005, **38**, 5774-5779. (g) K. Matyjaszewski, R. Poli, Macromolecules, 2005, **38,** 8093-8100. (h) M. L. Coote, E. H. Krenske, E. I. Izgorodina, Macromol. Rapid Comm., 2006, **27**, 473. (i) C. M. R. Abreu, P. V. Mendonça, A. C. Serra, J. F. J. Coelho, V. P. Anatoliy, G. Gryn'ova, M. L. Coote, T. Guliashvili, Macromolecules, 2012, **45**, 2200-2208.

[54] (a) M. B. Gillies, K. Matyjaszewski, P-O. Norrby, T. Pintauer, R. Poli, P. Richard, Macromolecules, 2003, **36**, 8551-8559. (b) C. Y. Lin, M. L. Coote, A. Petit, P. Richard, R.

Poli, K. Matyjaszewski, Macromolecules, 2007, **40**, 5985-5994. (c) W. A. Braunecker, W. C. Brown, B. Morelli, W. Tang, R. Poli, K. Matyjaszewski, Macromolecules, 2007, **40**, 8576-8585. (d) W. Tang, Y. Kwak, W. Braunecker, N. V. Tsarevsky, M. L. Coote, K. Matyjaszewski, J. Am. Chem. Soc., 2008, **130**, 10702-10713. (e) Y. Zhang, K. Schröder, Y. Kwak, P. Krys, A. N. Morin, T. Pintauer, R. Poli, K. Matyjaszewski, Macromolecules, 2013, **46**, 5512-5519.

[55] (a) S. Maria, H. Kaneyoshi, K. Matyjaszewski, R. Poli, Chem. Eur. J., 2007, **13**, 2480. (b) A. Debuigne, Y. Champouret, R. Jérôme, R. Poli, C. Detrembleur, C. Chem. Eur. J., 2008, **14**, 4046-4059. (c) A. Debuigne, C. Michaux, C. Jérôme, R. Jérôme, R. Poli, C. Detrembleur, Chem. Eur. J., 2008, **14**, 7623-7637. (d) Y. Champouret, U. Baisch, R. Poli, L. Tang, J. L. Conway, K. M. Smith, Angew. Chem. Int. Ed. Engl., 2008, **47**, 6069-6072. (e) A. Debuigne, R. Poli, J. De Winter, P. Laurent, P. Gerbaux, P. Dubois, J-P. Wathelet, C. Jérôme, C. Detrembleur, Chem. Eur. J., 2010, **16**, 1799-1811. (f) A. Debuigne, R. Poli, J. De Winter, P. Laurent, P. Gerbaux, J-P.; Wathelet, C. Jérôme, C. Detrembleur, Macromolecules, 2010, **43**, 2801-2813. (g) Y. Champouret, K. C. MacLeod, U. Baisch, B. O. Patrick, K. M. Smith, R. Poli, Organometallics, 2010, **29**, 167-176. (h) Y. Champouret, K. C. MacLeod, K. M. Smith, R. Poli, Organometallics, 2010, **29**, 3125-3132. (i) A. Debuigne, A. N. Morin, A. Kermagoret, Y. Piette, C. Detrembleur, C. Jérôme, R. Poli, Chem. Eur. J., 2012, **18**, 12834-12844. (j) Y. Piette, A. Debuigne, C. Jérôme, V. Bodart, R. Poli, C. Detrembleur, Polym. Chem., 2012, **3**, 2880-2891..

[56] C. M. R. Abreu, P. V. Mendonça, A. C. Serra, B. B. Noble, T. Guliashvili, J. Nicolas, M. L. Coote, J. F. J. Coelho, Macromolecules, 2016, **49**, 490-498.

[57] (a) W. J. Bengough, H. W. Melville, Proc. R. Soc. London, Ser. A, 1955, **230**, 429. (b) H. Kwart, H. S. Broadbent, P. D. Bartlett, J. Am. Chem. Soc., 1950, **72**, 1060. (c) G. Dixon-Lewis, Proc. R. Soc. London, Ser. A, 1949, **198**, 510.

[58] K. Kamachi, D. J. Liaw, S. Nozakura, Polym. J., 1979, **11**, 921.

[59] T. L. Latypov, A. A. Yul'chibayev, Kuzieva Kh. Yu. Uzb. Khim. Zh., 1983, **62**.

[60] B. Baradie, M. S. Shoichet, Macromolecules, 2002, **35**, 3569-3575.

[61] P. J. Flory, F. S. Leutner, Journal of Polymer Science, 1948, **3**, 880. (b) D. Britton, F. Heatley, P. A. Lovell, Macromolecules, 1998, **31**, 2828.

[62] K. Koumura, K. Satoh, M. Kamigaito, Macromolecules, 2009, **42**, 2497-2504.

[63] K. Koumura, K. Satoh, M. Kamigaito, Polymer Journal, 2009, **41**, 595-603.

VI.1 Supporting Informations

VI.1.1 RAFT Homopolymerization of VDF

Using the experimental setup described above, a typical polymerization (entry 1 in Table 1) of VDF was performed as follows: A solution of Trigonox 121 (158 mg, 6.87 10^{-4} mol) and CTA_{XA} (1.30 g, 6.25 10^{-3} mol) in DMC (60 mL), was degassed by N_2 bubbling during 30 min. This homogenous solution was introduced into the autoclave using a funnel, VDF gas (19.0 g, 2.97 10^{-1} mol) was transferred in the autoclave at low temperature, and the reactor was gradually heated to 73 °C. The reaction was stopped after 18 h. During the reaction, the pressure increased to a maximum of 25 bars and then decreased to 10 bars after 24 h. The autoclave was cooled down to room temperature (ca. 20 °C), purged from the residual monomers and DMC was removed under vacuum. The crude product was dissolved in 30 mL of warm THF (ca. 40 °C), and left under vigorous stirring for 30 minutes. This polymer solution was then precipitated from 400 mL of chilled hexane. The precipitated polymer (white powder) was filtered through a filter funnel and dried under vacuum ($15 \cdot 10^{-3}$ bar) for two hours at 50°C. The polymerization yield (65%) was determined gravimetrically (mass of dried precipitated polymers / mass of monomer introduced in the pressure reactor). Yields were used as conversion, since conversion is very difficult to measure accurately for VDF or other gaseous monomers.

DP and $M_{n(NMR)}$ calculations:

The degree of polymerization (DP) of PVDF can be calculated according to equations (S1) and SI-Equation IV-8 and SI-Equation IV-9:[8]

SI-Equation IV-8
$$DP = \frac{\int_{2.70}^{3.19} CH_2(HT) + \int_{2.28}^{2.43} CH_2(TT) + \int_{4.02}^{4.17} CH_2(End-group)}{2/3 \times \int_{1.19}^{1.24} CH_3(R-CTAXA)}$$

SI-Equation IV-9
$$M_{n,NMR}(R) = M_{n,CTA} + (DP \times M_{n,VDF})$$

Where $M_{n\,CTA}$ = 208.3 g.mol^{-1} and $M_{n\,VDF}$= 64.04 g.mol^{-1}

^{1}H NMR (400 MHz $(CD_3)_2CO$, δ (ppm)) : 1.19-1.24 (d, -CH(C**H$_3$**)(C=O)-, $^3J_{HH}$ = 7.1 Hz), 1.40-1.46 (t, -S(C=S)O-CH_2-C**H$_3$**, $^3J_{HH}$ = 7.2 Hz), 2.28-2.43 (m,-CF_2-C**H$_2$**-C**H$_2$**-CF_2-, VDF-VDF TT reverse addition), 2.70-3.19 (t, -CF_2-C**H$_2$**-CF_2-, VDF-VDF HT regular addition), 3.60-3.69 (s, -(C=O)-O-C**H$_3$**), 4.02-4.17 (t, -CF_2-C**H$_2$**-S(C=S)OEt, $^3J_{HF}$ = 18 Hz), 4.67-4.77

(q, (-S(C=S)O-C**H$_2$**-CH$_3$, $^3J_{HH}$ = 7.2 Hz), 6.05-6.45 (tt, $^2J_{HF}$ = 55 Hz , $^3J_{HH}$ = 4.6 Hz -CH$_2$-CF$_2$-**H**).

^{19}F NMR (376 MHz $(CD_3)_2CO$, δ (ppm)) : -115.63 (-CH$_2$-CF$_2$-C**F$_2$**-CH$_2$-CH$_2$-, VDF-VDF HH reverse addition), -114.29 ($^2J_{HF}$ = 55 Hz, -CH$_2$-C**F$_2$**-H), -113.34 (-CH$_2$-C**F$_2$**-CF$_2$-CH$_2$-CH$_2$-, HH reverse addition), -113.09 (CH$_2$-CF$_2$-**CF$_2$**-CH$_2$-S-), -112.69 (-CH$_2$-**CF$_2$**-CF$_2$-CH$_2$-S-), -94.79 (-CH$_2$-CH$_2$-C**F$_2$**-CH$_2$-, TT reverse addition), -93.50 (-CH$_2$-C**F$_2$**-CH$_2$-CH(CH$_3$)(C=O)-), -92.12 (-CH$_2$-C**F$_2$**-CH$_2$-CF$_2$H), -91.44 (-CH$_2$-CH$_2$-CF$_2$-CH$_2$-**CF$_2$**-CH$_2$-CF$_2$-, regular VDF-VDF HT addition), -91.00 (-CH$_2$-C**F$_2$**-CH$_2$-, regular VDF-VDF HT addition).

VI.1.2 Equations used to determine the degree of polymerization and molar mass of PVAc macro-CTAs

VI.1.2.1 PVDF

SI-Equation IV-10

$$(\%) - CF_2 - CH_2 - XA = \frac{\frac{1}{2}\int_{4.02}^{4.17} -CF_2-CH_2-XA}{\frac{1}{2}\int_{3.26}^{3.52} -CH_2-CF_2-XA+\int_{6.01}^{6.48} -CH_2-CF_2H+\frac{1}{2}\int_{4.02}^{4.17} -CF_2-CH_2-XA}$$

SI-Equation IV-11

$$(\%) - CH_2 - CF_2 - XA = \frac{\frac{1}{2}\int_{3.26}^{3.52} -CH_2-CF_2-XA}{\frac{1}{2}\int_{3.26}^{3.52} -CH_2-CF_2-XA+\int_{6.01}^{6.48} -CH_2-CF_2H+\frac{1}{2}\int_{4.02}^{4.17} -CF_2-CH_2-XA}$$

SI-Equation IV-12

$$(\%) - CH_2 - CF_2H = \frac{\int_{6.01}^{6.48} -CH_2-CF_2H}{\frac{1}{2}\int_{3.26}^{3.52} -CH_2-CF_2-XA+\int_{6.01}^{6.48} -CH_2-CF_2H+\frac{1}{2}\int_{4.02}^{4.17} -CF_2-CH_2-XA}$$

Note : -CF$_2$-CH$_3$ end group were not taken into consideration in the calculation because, as described in a previous study,[35] irreversible transfers reactions between CH$_2$ radical and solvent were exclusively observed for a targeted DP higher than 100.

VI.1.2.2 PVAc

SI-Equation IV-13

$$(\%) - CH(OAc) - CH_2 - XA = \frac{\frac{1}{2}\int_{3.18}^{3.51} -CH(OAc)-CH_2-XA}{\frac{1}{2}\int_{3.18}^{3.51} -CH(OAc)-CH_2-XA+\int_{6.01}^{6.48} -CH_2-CF_2H+\frac{1}{2}\int_{3.95}^{4.13} -CH_2-(OAc)CH_2+\int_{6.50}^{6.70} -CH_2-CH(OAc)-XA}$$

SI-Equation IV-14

$$(\%) - CH_2 - CH(OAc) - XA = \frac{\int_{6.50}^{6.70} -CH_2-CH(OAc)-XA}{\frac{1}{2}\int_{3.18}^{3.51} -CH(OAc)-CH_2-XA+\int_{6.01}^{6.48} -CH_2-CF_2H+\frac{1}{2}\int_{3.95}^{4.13} -CH_2-(OAc)CH_2+\int_{6.50}^{6.70} -CH_2-CH(OAc)-XA}$$

SI-Equation IV-15

$$(\%) - CH_2 - (OAc)CH_2 = \frac{\frac{1}{2}\int_{3.95}^{4.13} -CH_2-(OAc)CH_2}{\frac{1}{2}\int_{3.18}^{3.51} -CH(OAc)-CH_2-XA+\int_{6.01}^{6.48} -CH_2-CF_2H+\frac{1}{2}\int_{3.95}^{4.13} -CH_2-(OAc)CH_2+\int_{6.50}^{6.70} -CH_2-CH(OAc)-XA}$$

VI.1.3 Further Characterization

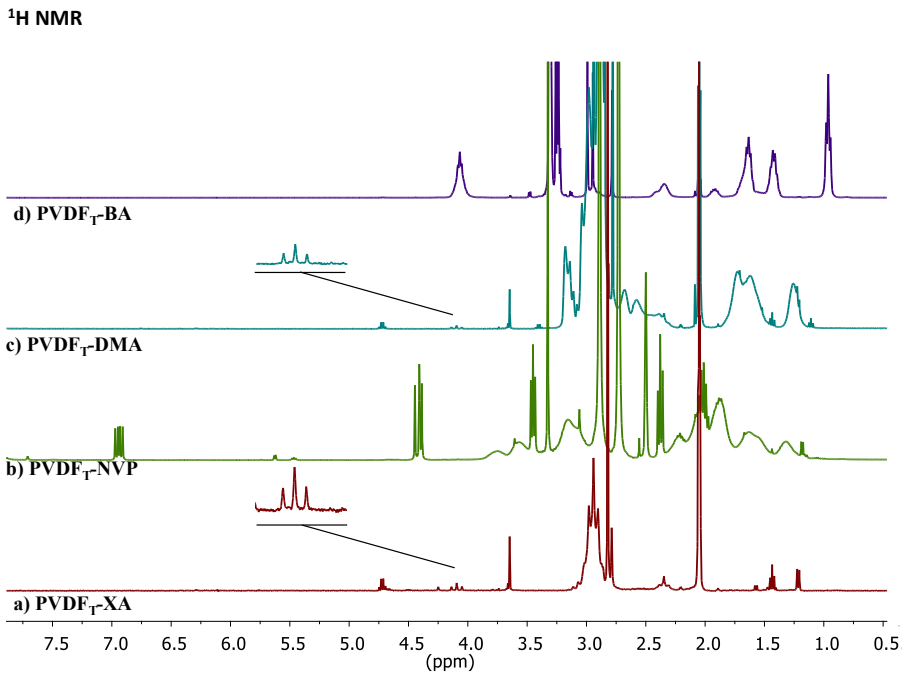

SI-Figure IV-9: Expansion of the 0.5 to 8.5 ppm region of the ^{1}H NMR spectrum of : a) PVDF$_T$-XA (entry 1, Table IV-1), b) chain extension with NVP (entry 5, Table IV-1), c) chain extension with DMA (entry 6, Table IV-1), d) chain extension with BA (entry 7, Table IV-1). Spectra a), c) and d) recorded in $(CD_3)_2CO$, spectrum b) recorded in $(CD_3)_2SO$. All polymers were purified by precipitation in cold hexane.

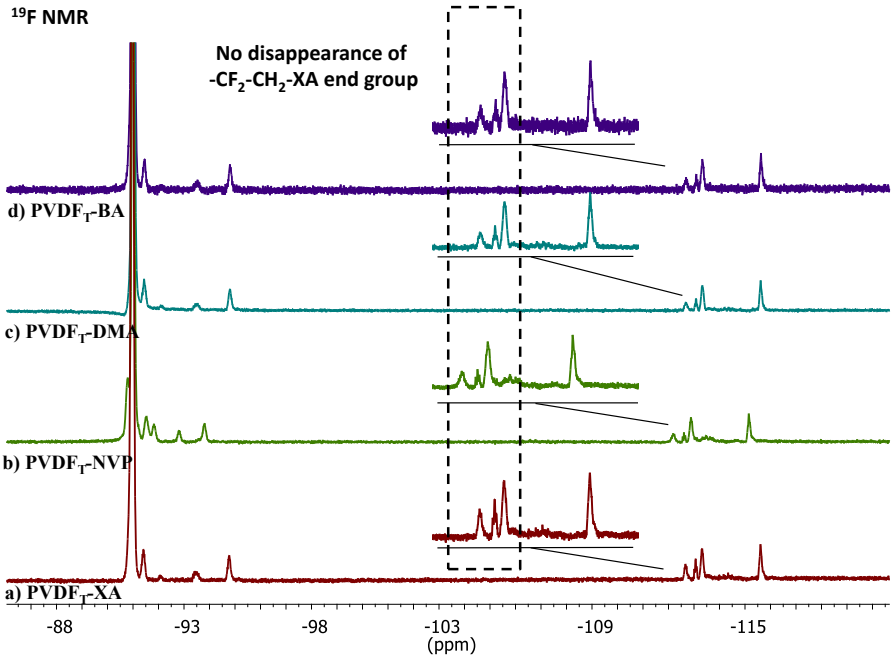

SI-Figure IV-10: Expansion of the -86 to -120.5 ppm region of the ^{19}F NMR spectrum of : a) $PVDF_T$-XA (entry 1, Table IV-1b) chain extension with NVP (entry 5, Table IV-1), c) chain extension with DMA (entry 6, Table IV-1), d) chain extension with BA (entry 7, Table IV-1). Spectra a), c) and d) recorded in $(CD_3)_2CO$, spectrum b) recorded in $(CD_3)_2SO$. All polymers were purified by precipitation in cold hexane.

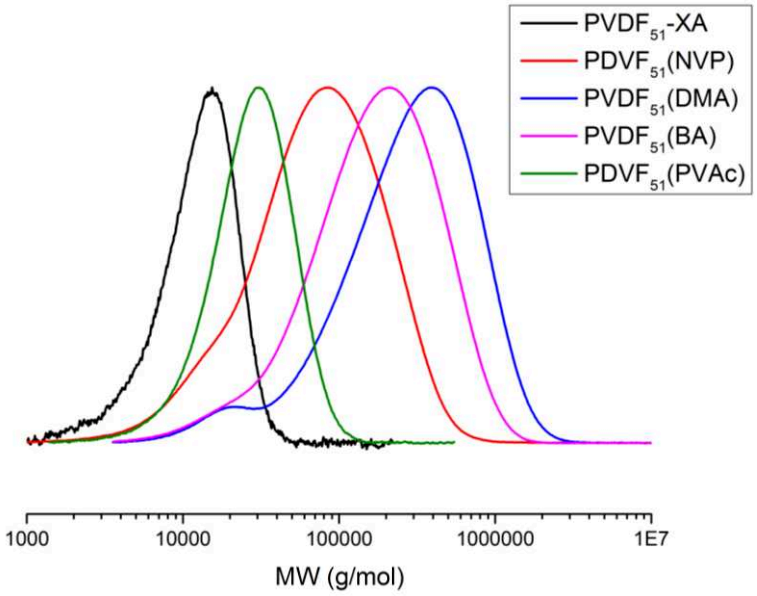

SI-Figure IV-11: Normalized GPC traces (viscometric detector) of $PVDF_{51}$-XA (black trace) and of the polymers obtained by chain extension of this $PVDF_T$-XA with: 1) NVP: $PVDF_{51}$(NVP) (red trace), 2) DMA: $PVDF_{51}$(DMA) (blue trace), 3) BA: $PVDF_{51}$(BA) (pink trace), and 4) VAc: $PVDF_{51}$(PVAc) (green trace).

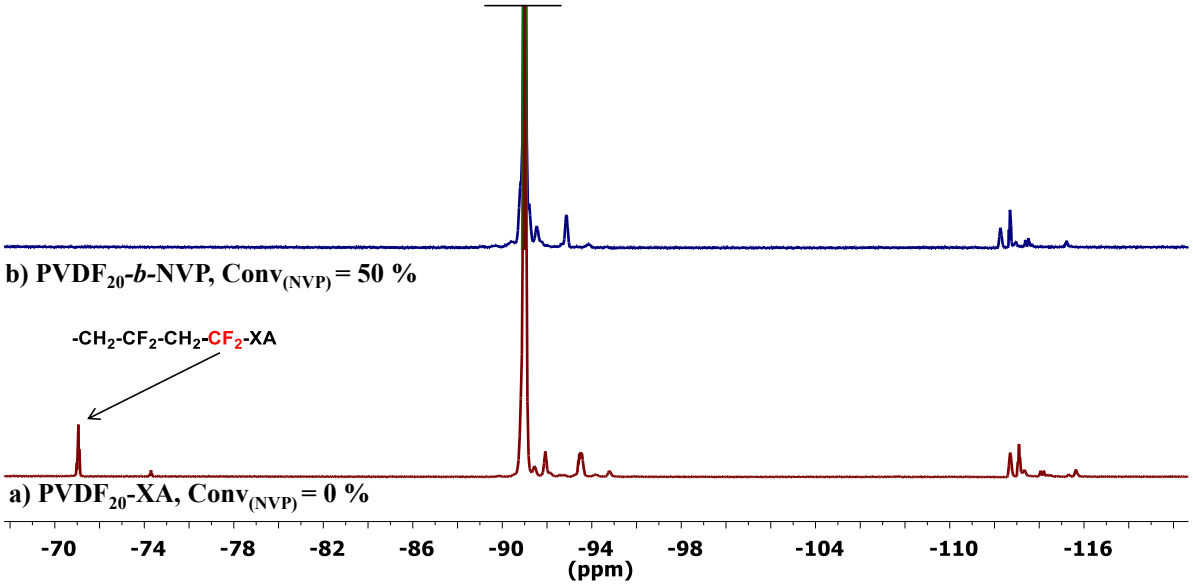

SI-Figure IV-12: Expansion of the -68 to -118 ppm region of the ^{19}F NMR: a) $PVDF_{20}$-XA synthesized via RAFT polymerization (entry 3, Table IV-1) composed of 38 % of $PVDF_T$-XA, 47 % of $PVDF_H$-XA and 14 % of PVDF-H chains, b) $PVDF_{20}$-b-PNVP block copolymer synthesized via RAFT polymerization after 14 hours of polymerization (entry 17, Table IV-1). ($Conv_{(NVP)}$ = 50 %) Spectrum a) recorded in $(CD_3)_2CO$ and spectrum b) recorded in $(CD_3)_2SO$.

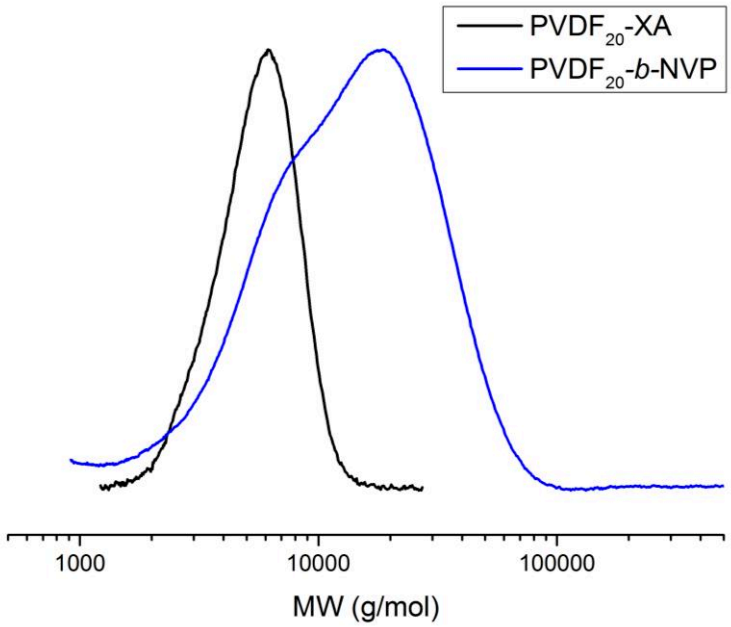

SI-Figure IV-13: Normalized GPC traces (viscometric detector) of $PVDF_{20}$-XA (black trace) and of the polymers obtained by chain extension of this $PVDF_{20}$-XA composed of 38 % of $PVDF_T$-XA, 47 % of $PVDF_H$-XA and 14 % of PVDF-H chains (blue trace).

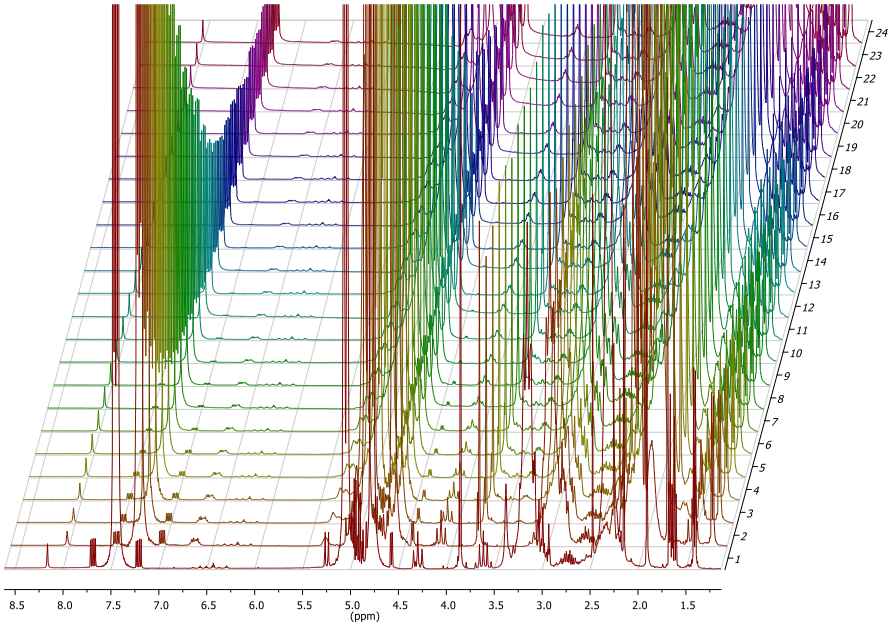

SI-Figure IV-14: Stacked ^{1}H NMR spectra in deuterated DMF of the chain extension of $PVDF_{20}$-XA (entry 3, Table IV-1) with VAc (Target DP = 100) via RAFT polymerization (entry 16, Table IV-1).

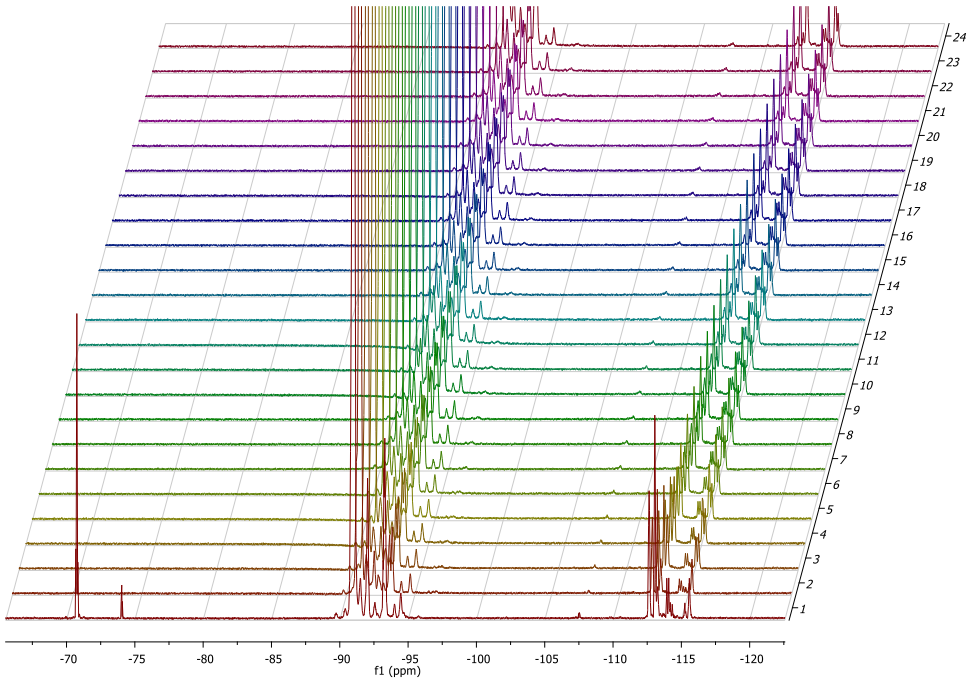

SI-Figure IV-15: Stacked ^{19}F NMR spectra in deuterated DMF of the chain extension of $PVDF_{20}$-XA (entry 3, Table IV-1) with VAc (Target DP = 100) via RAFT polymerization (entry 16, Table IV-1).

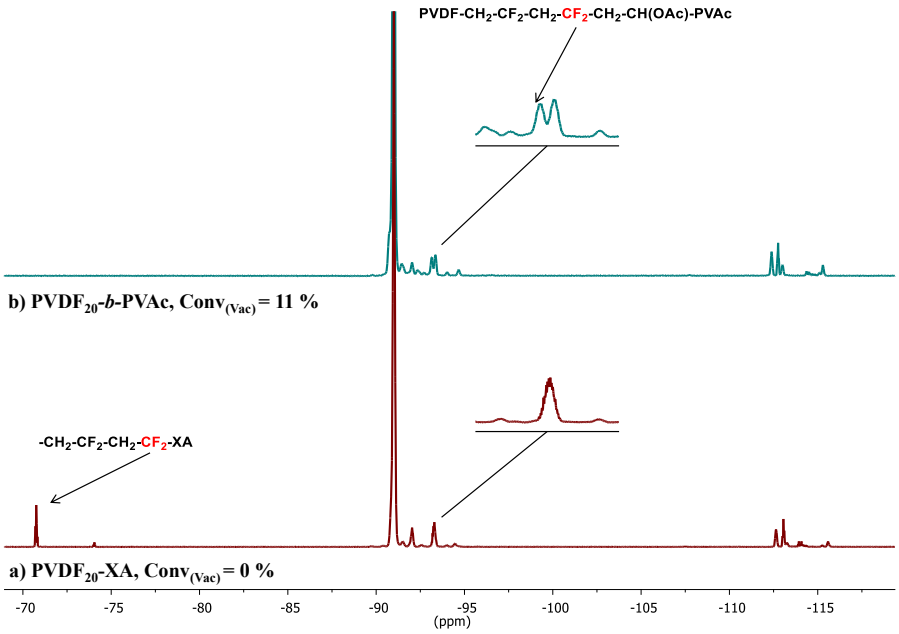

SI-Figure IV-16: Expansion of the -68 to -118 ppm region of the ^{19}F NMR: a) $PVDF_{20}$-XA synthesized via RAFT polymerization (entry 3, Table IV-1) composed of 38 % of $PVDF_T$-XA, 47 % of $PVDF_H$-XA and 14 % of PVDF-H chains, b) $PVDF_{20}$-b-PVAc block copolymer synthesized via RAFT polymerization after 2 min and 7 s, second point in the in situ NMR monitoring (entry 16, Table IV-1). ($Conv_{(VAc)}$ = 11 %) Spectra recorded in d_7-DMF and spectrum.

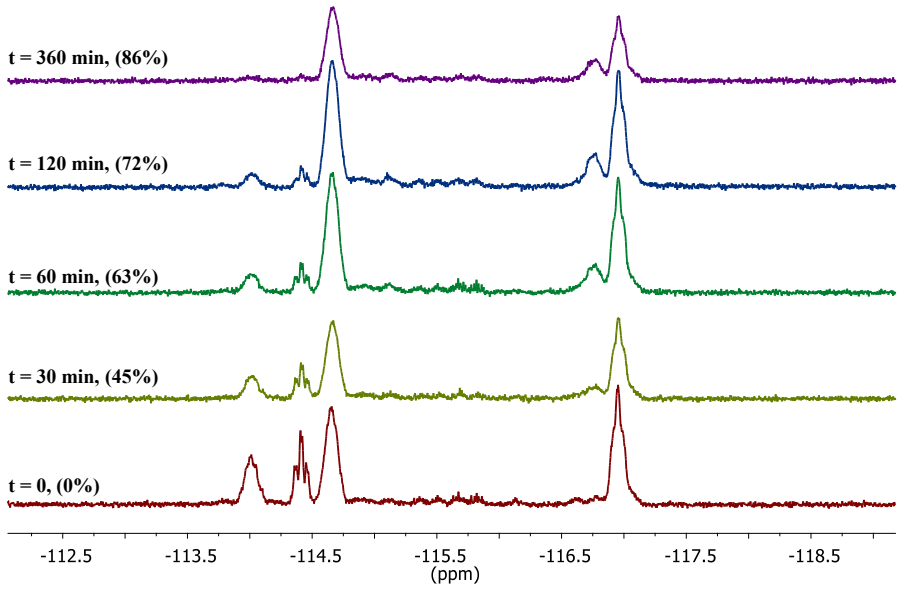

SI-Figure IV-17: Expansion of selected ^{19}F NMR signals with conversion of $PVDF_{20}$-XA chain extension monitored by in situ NMR Spectroscopy recorded in d_7-DMF. The conversion of VAc is shown in brackets after the reaction time for each spectrum.

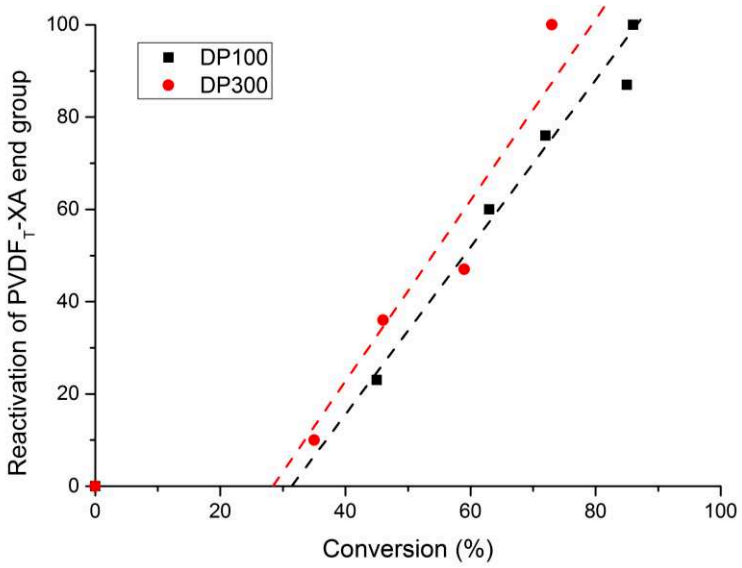

SI-Figure IV-18: Reactivation of PVDF$_T$-XA (entry 1, Table IV-1) vs VAc conversion during the syntheses of PVAc block with VAc target DP = 100 and 300.

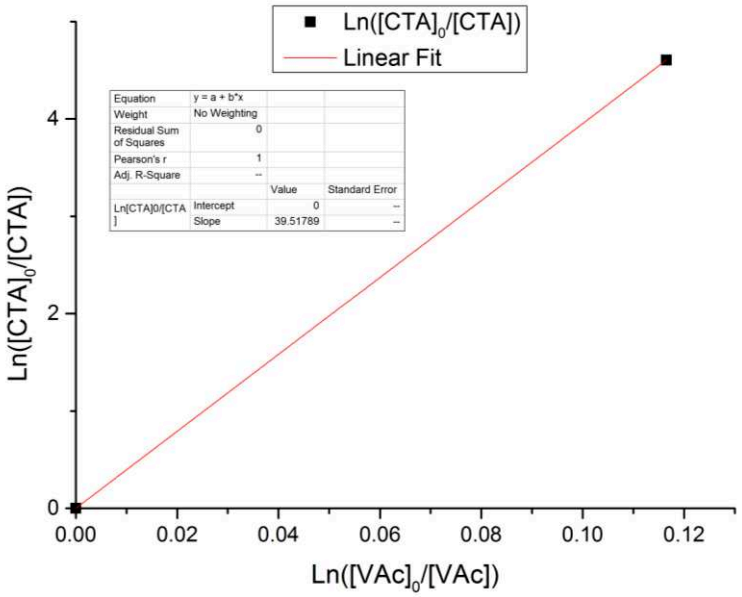

SI-Figure IV-19: Determination of the apparent transfer constant of PVDF$_H$-XA macroCTA with VAc using O'Brien and Gornick's method.[45]

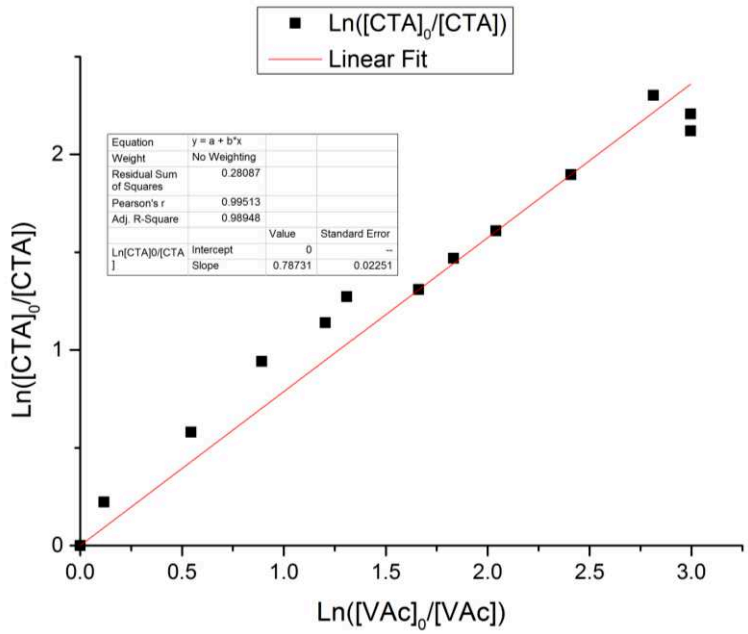

SI-Figure IV-20: Determination of the apparent transfer constant of $PVDF_T$-XA macroCTA with VAc using O'Brien and Gornick's method.[45]

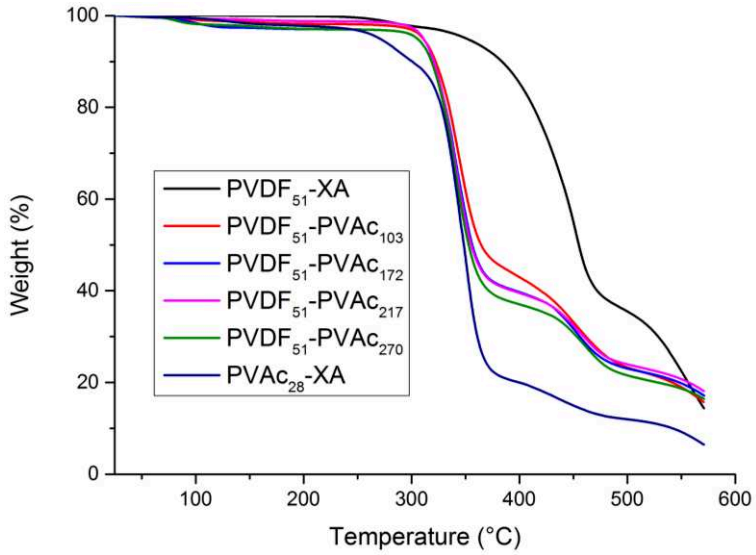

SI-Figure IV-21: TGA thermograms of $PVDF_{51}$-XA (black), $PVAc_{28}$-XA (dark blue) homopolymer, $PVDF_{51}$-b-$PVAc_{103}$ (red), $PVDF_{51}$-b-$PVAc_{172}$ (blue), $PVDF_{51}$-b-$PVAc_{217}$ (pink) and $PVDF_{51}$-b-$PVAc_{270}$ (green).

VI.1.4 Computational

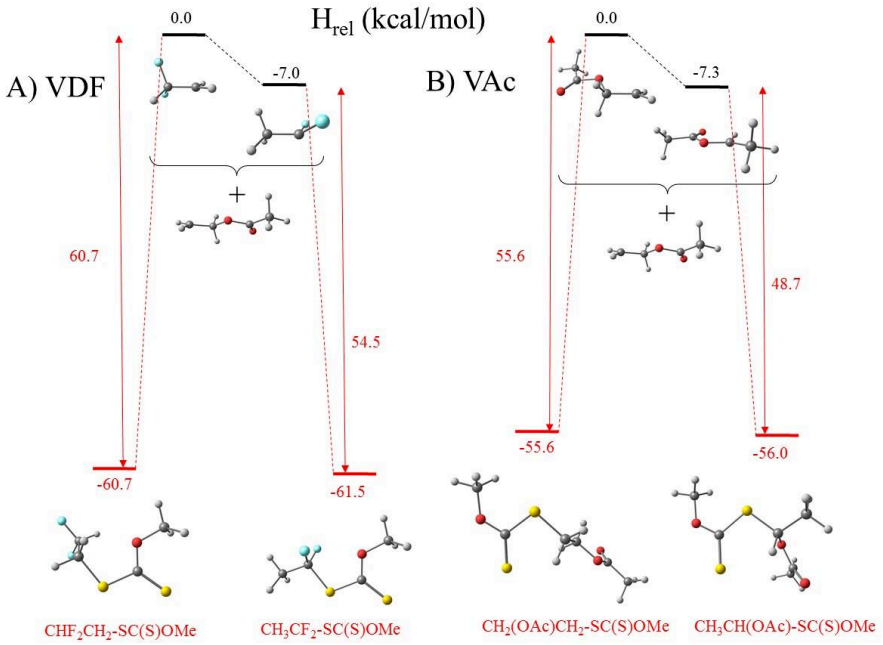

SI-Figure IV-22: Relative energies and views of the optimized geometries of the isomeric $CHF_2CH_2^{\bullet}$ and $CH_3CF_2^{\bullet}$ radicals, the isomeric $CH_2(OAc)CH_2^{\bullet}$ and $CH_3CH(OAc)^{\bullet}$ radicals, the $(MeO)C(S)S^{\bullet}$ radical, and the corresponding adducts. The values are the standard enthalpies ($\Delta H°_{298.15}$) in kcal/mol.

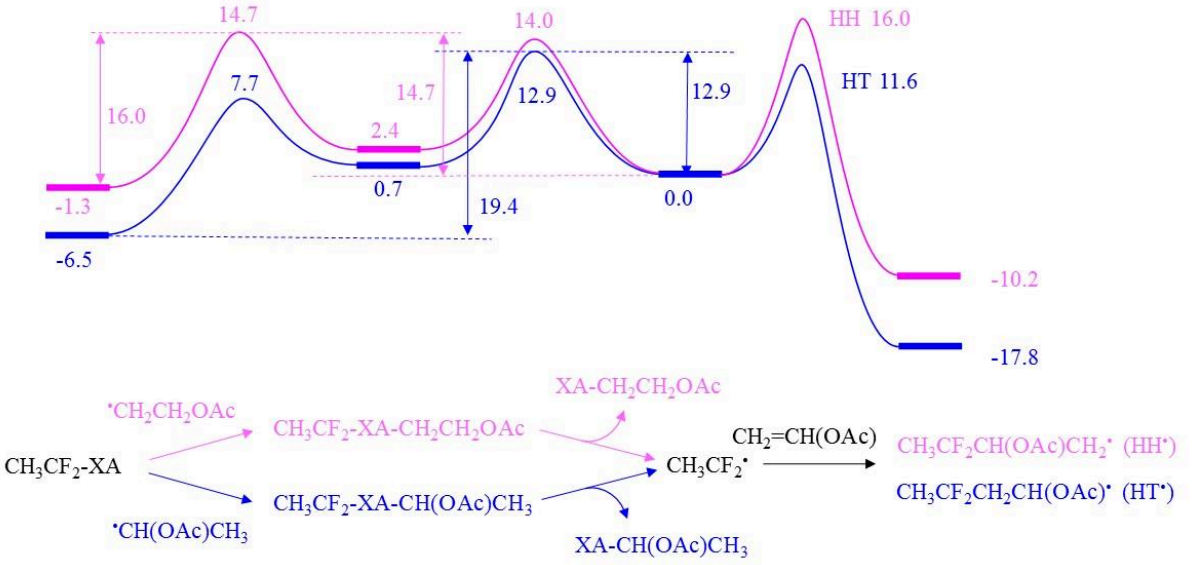

SI-Figure IV-23: Energy profiles (ΔG at 343.5 K in kcal/mol) for the model $PVDF_H$-XA reactivation by both head and tail $PVAc^{\bullet}$ model radicals in the chain extension with VAc.

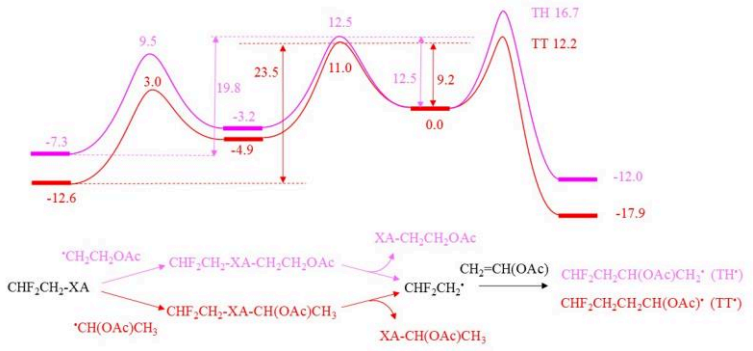

SI-Figure IV-24: . Energy profiles (ΔG at 343.5 K in kcal/mol) for the model PVDF$_T$-XA reactivation by both head and tail PVAc• model radicals in the chain extension with VAc.

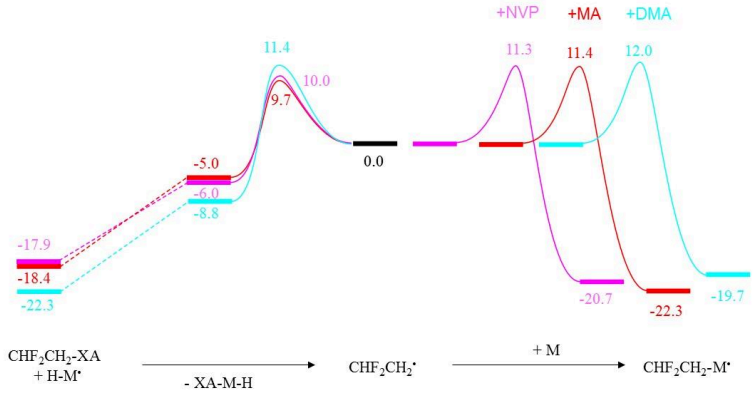

SI-Figure IV-25: Energy profiles (ΔG at 343.5 K in kcal/mol) for the model PVDF$_T$-XA reactivation by the H-M• model radicals in the chain extension with NVP, MA (model of BA), and DMA. Only the rate-determining transition state corresponding to the intermediate fragmentation was optimized.

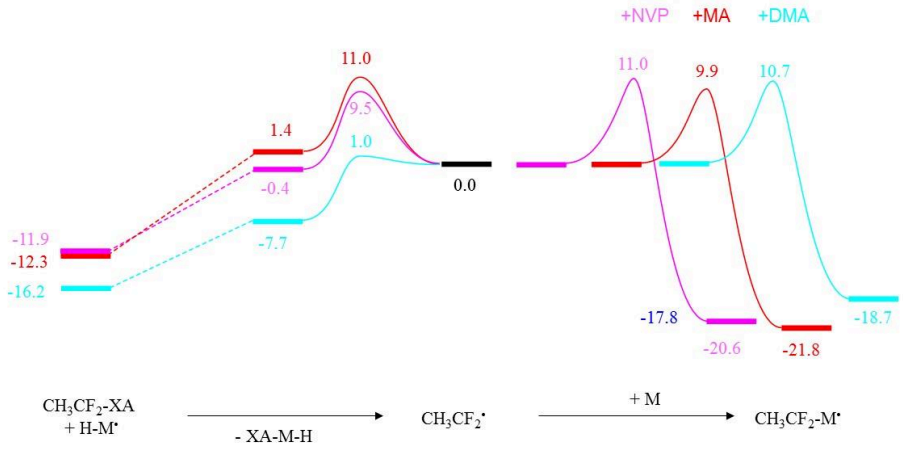

SI-Figure IV-26: Energy profiles (ΔG at 343.5 K in kcal/mol) for the model PVDF$_H$-XA reactivation by the H-M• model radicals in the chain extension with NVP, MA (model of BA), and DMA. Only the rate-determining transition state corresponding to the intermediate fragmentation was optimized.

SI-Table IV-3: Energies, enthalpies, Gibbs energies of all optimized geometries (N-pyr = N-substituted pyrrolidone).

Compound	E (hartrees)	$H_{298.15}$ (hartrees)	$G_{298.15}$ (hartrees)	$G_{343.15}$ (hartrees)[a]
(a) (a) Radicals				
$CH_3CF_2^{\bullet}$	-277.3942109	-277.341757	-277.374487	-277.379427
$CHF_2CH_2^{\bullet}$	-277.3819182	-277.330618	-277.363927	-277.368954
$CH_3CH(OAc)^{\bullet}$	-306.748937	-306.637180	-306.678902	-306.685199
$CH_3CH(OAc)^{\bullet}$ (in vinyl acetate, ε = 4.2)	-306.748869	-306.637110	-306.678314	-306.684533
$CH_3CH(OAc)^{\bullet}$ (in acetonitrile, ε = 35.7)	-306.748832	-306.637082	-306.678154	-306.684353
$AcOCH_2CH_2^{\bullet}$	-306.736664	-306.625483	-306.668129	-306.674566
$CH_3CH(N\text{-}pyr)^{\bullet}$	-364.248303	-364.086106	-364.128929	-364.135392
$CH_3CH(COOMe)^{\bullet}$	-306.752227	-306.639465	-306.679787	-306.685873
$CH_3CH(CONMe_2)^{\bullet}$	-326.159236	-326.004772	-326.048889	-326.055548
$(MeO)C(S)S^{\bullet}$	-949.138793	-949.081962	-949.119578	-949.125255
(b) (b) Monomers				
CH_2=CH(OAc)	-306.174665	-306.072904	-306.111829	-306.117704
CH_2=CH(OAc) (in vinyl acetate, ε = 4.2)	-306.174615	-306.072872	-306.111505	-306.117336
CH_2=CH(OAc) (in acetonitrile, ε = 35.7)	-306.174590	-306.072872	-306.111386	-306.117199
CH_2=CH(N-pyr)	-363.667907	-363.515781	-363.556191	-363.562290
CH_2=CH(COOMe)	-306.170160	-306.067512	-306.105545	-306.111285
CH_2=CH($CONMe_2$)	-325.581015	-325.436666	-325.478491	-325.484804
(c) Chain transfer agents				
CH_3CF_2-SC(S)(OCH_3)	-1226.623079	-1226.509289	-1226.558343	-1226.565747
CHF_2CH_2-SC(S)(OCH_3)	-1226.623112	-1226.510636	-1226.559231	-1226.566565
$CH_3CH(OAc)$-SC(S)(OCH_3)	-1255.969930	-1255.796755	-1255.853426	-1255.861979
$AcOCH_2CH_2$-SC(S)(OCH_3)	-1255.969996	-1255.796001	-1255.853922	-1255.862664
$CH_3CH(N\text{-}pyr)$-SC(S)(OCH_3)	-1313.459406	-1313.236059	-1313.294756	-1313.303615
$CH_3CH(COOMe)$-SC(S)(OCH_3)	-1255.962630	-1255.788557	-1255.844913	-1255.853419
$CH_3CH(CONMe_2)$-SC(S)(OCH_3)	-1275.36569	-1275.149574	-1275.208001	-1275.216819
(d) VAc homopropagation				
d_1 Head-to-tail				
$CH_3CH(OAc)^{\bullet}\cdots CH_2$=CH(OAc) TS	-612.9146473	-612.699775	-612.759644	-612.768680
$CH_3CH(OAc)^{\bullet}\cdots CH_2$=CH(OAc) TS (in vinyl acetate, ε = 4.2)	-612.9141652	-612.700268	-612.757935	-612.766639
$CH_3CH(OAc)^{\bullet}\cdots CH_2$=CH(OAc) TS (in acetonitrile, ε = 35.7)	-612.9140444	-612.700163	-612.757689	-612.766371
$CH_3CH(OAc)$-$CH_2CH(OAc)^{\bullet}$	-612.9604502	-612.742476	-612.802898	-612.812018
$CH_3CH(OAc)$-$CH_2CH(OAc)^{\bullet}$ (in vinyl acetate, ε = 4.2)	-612.9603017	-612.742385	-612.802230	-612.811262
$CH_3CH(OAc)$-$CH_2CH(OAc)^{\bullet}$ (in acetonitrile, ε = 35.7)	-612.9602412	-612.742284	-612.801606	-612.810560
d_2 head-to-head				
$CH_3CH(OAc)^{\bullet}\cdots CH(OAc)=CH_2$ TS	-612.912089	-612.697544	-612.757623	-612.766691
$CH_3CH(OAc)$-$CH(OAc)CH_2^{\bullet}$	-612.9550274	-612.737817	-612.797963	-612.807041
d3. Tail-to-tail				
$AcOCH_2CH_2^{\bullet}\cdots CH_2$=CH(OAc) TS	-612.9068575	-612.69188	-612.755489	-612.765090
$AcOCH_2CH_2$-$CH_2CH(OAc)^{\bullet}$	-612.9593542	-612.740662	-612.802093	-612.811365
d4. Tail-to-head				
$AcOCH_2CH_2^{\bullet}\cdots CH(OAc)=CH_2$ TS	-612.9020385	-612.687388	-612.749543	-612.758924
$AcOCH_2CH_2$-$CH(OAc)CH_2^{\bullet}$	-612.9517277	-612.733705	-612.794286	-612.803430
(e) Other monomers homopropagation (all head-to-tail)				
$CH_3CH(N\text{-}pyr)^{\bullet}\cdots CH_2$=CH(N-pyr) TS	-727.9168423	-727.600943	-727.664546	-727.674146
CH3CH(N-pyr)-CH2CH(N-pyr)$^{\bullet}$	-727.9554137	-727.636386	-727.698752	-727.708165
$CH_3CH(COOMe)^{\bullet}\cdots CH_2$=CH(COOMe) TS	-612.9160239	-612.699270	-612.759524	-612.768618

$CH_3CH(COOMe)$-$CH_2CH(COOMe)^{\bullet}$	-612.9565734	-612.736780	-612.796156	-612.805118
$CH_3CH(CONMe_2)^{\bullet\cdots}CH_2$=$CH(CONMe_2)$ TS	-651.7337656	-651.433334	-651.500074	-651.510147
$CH_3CH(CONMe_2)$-$CH_2CH(CONMe_2)^{\bullet}$	-651.7734329	-651.469831	-651.535584	-651.545508
(e) VAc RAFT: MacroCTA degenerative and non-degenerative radical exchange				
e_1 Head-head (degenerative)				
$CH_3CH(OAc)$-$SC(OMe)S^{\cdots\bullet}CH(OAc)CH_3$ TS	-1562.725753	-1562.438808	-1562.514567	-1562.526001
$CH_3CH(OAc)$-$SC^{\bullet}(OMe)S$-$CH(OAc)CH_3$	-1562.739448	-1562.450252	-1562.524707	-1562.535945
e2. Head-tail (non-degenerative)				
$CH_3CH(OAc)$-$SC(OMe)S^{\cdots\bullet}CH_2CH_2OAc$ TS	-1562.704885	-1562.418258	-1562.498879	-1562.511047
$CH_3CH(OAc)$-$SC^{\bullet}(OMe)S$-CH_2CH_2OAc	-1562.735275	-1562.445479	-1562.525252	-1562.537292
$CH_3CH(OAc)^{\bullet\cdots}SC(OMe)S$-$CH_2CH_2OAc$ TS	-1562.724235	-1562.436581	-1562.516658	-1562.528744
e_3 Tail-tail (degenerative)				
$AcOCH_2CH_2$-$SC(OMe)S^{\cdots\bullet}CH_2CH_2OAc$ TS	-1562.702989	-1562.415461	-1562.494514	-1562.506446
$AcOCH_2CH_2$-$SC^{\bullet}(OMe)S$-CH_2CH_2OAc	-1562.724562	-1562.434221	-1562.511981	-1562.523717
(f) $PVDF_H$-XA reactivation				
f_1 By VAc (head)				
CH_3CF_2-$SC(OMe)S^{\cdots\bullet}CH(OAc)CH_3$ TS	-1533.370507	-1533.144785	-1533.215404	-1533.226063
CH_3CF_2-$SC^{\bullet}(OMe)S$-$CH(OAc)CH_3$	-1533.384941	-1533.157036	-1533.226742	-1533.237263
$CH_3CF_2^{\bullet\cdots}SC(OMe)S$-$CH(OAc)CH_3$ TS	-1533.362805	-1533.136301	-1533.207169	-1533.217865
f_2 By VAc (tail)				
CH_3CF_2-$SC(OMe)S^{\cdots\bullet}CH_2CH_2OAc$ TS	-1533.359134	-1533.133279	-1533.204875	-1533.215681
CH_3CF_2-$SC^{\bullet}(OMe)S$-CH_2CH_2OAc	-1533.382418	-1533.153724	-1533.224516	-1533.235201
$CH_3CF_2^{\bullet\cdots}SC(OMe)S$-$CH_2CH_2OAc$ TS	-1533.360834	-1533.13358	-1533.205937	-1533.216858
f_3 By NVP (head)				
CH_3CF_2-$SC^{\bullet}(OMe)S$-$CH(N\text{-}pyr)CH_3$	-1590.875069	-1590.596986	-1590.66974	-1590.680721
$CH_3CF_2^{\bullet\cdots}SC(OMe)S$-$CH(N\text{-}pyr)CH_3$ TS	-1590.857208	-1590.580442	-1590.653796	-1590.664867
f_4 By MA (head)				
CH_3CF_2- $SC^{\bullet}(OMe)S$-$CH(COOMe)CH_3$	-1533.373768	-1533.145211	-1533.216727	-1533.227521
$CH_3CF_2^{\bullet\cdots}SC(OMe)S$-$CH(COOMe)CH_3$ TS	-1533.355094	-1533.127949	-1533.201246	-1533.212309
f_5 By DMA (head)				
CH_3CF_2-$SC^{\bullet}(OMe)S$-$CH(CONMe_2)CH_3$	-1552.789602	-1552.519183	-1552.594241	-1552.605570
$CH_3CF_2^{\bullet\cdots}SC(OMe)S$-$CH(CONMe_2)CH_3$ TS	-1552.774757	-1552.505650	-1552.580418	-1552.591703
(g) $PVDF_T$-XA reactivation				
g_1 By VAc (head)				
CHF_2CH_2-$SC(OMe)S^{\cdots\bullet}CH(OAc)CH_3$ TS	-1533.368746	-1533.141749	-1533.212515	-1533.223196
CHF_2CH_2-$SC^{\bullet}(OMe)S$-$CH(OAc)CH_3$	-1533.383938	-1533.154939	-1533.225124	-1533.235717
$CHF_2CH_2^{\bullet\cdots}SC(OMe)S$-$CH(OAc)CH_3$ TS	-1533.354954	-1533.128909	-1533.19973	-1533.210419
g_2 By VAc (tail)				
CHF_2CH_2-$SC(OMe)S^{\cdots\bullet}CH_2CH_2OAc$ TS	-1533.358868	-1533.131644	-1533.202796	-1533.213535
CHF_2CH_2-$SC^{\bullet}(OMe)S$-CH_2CH_2OAc	-1533.382549	-1533.152609	-1533.223061	-1533.233694
$CHF_2CH_2^{\bullet\cdots}SC(OMe)S$-$CH_2CH_2OAc$ TS	-1533.353517	-1533.126535	-1533.197946	-1533.208724
g_3 By NVP (head)				
CHF_2CH_2-$SC^{\bullet}(OMe)S$-$CH(N\text{-}pyr)CH_3$	-1590.874868	-1590.595518	-1590.66815	-1590.679112
$CHF_2CH_2^{\bullet\cdots}SC(OMe)S$-$CH(N\text{-}pyr)CH_3$ TS	-1590.846518	-1590.570249	-1590.642649	-1590.653576
g_4 By MA (head)				
CHF_2CH_2- $SC^{\bullet}(OMe)S$-$CH(COOMe)CH_3$	-1533.376416	-1533.146421	-1533.216746	-1533.227360
$CHF_2CH_2^{\bullet\cdots}SC(OMe)S$-$CH(COOMe)CH_3$ TS	-1533.346591	-1533.119745	-1533.192852	-1533.203886
g_5 By DMA (head)				
CHF_2CH_2-$SC^{\bullet}(OMe)S$-$CH(CONMe_2)CH_3$	-1552.783000	-1552.511104	-1552.585599	-1552.596843
$CHF_2CH_2^{\bullet\cdots}SC(OMe)S$-$CH(CONMe_2)CH_3$ TS	-1552.746166	-1552.477343	-1552.553144	-1552.564585
(h) $PVDF_H^{\bullet}$ addition to monomer				

h_1 To VAc (tail)				
$CH_3CF_2^{\bullet}\cdots CH_2=CHOAc$ TS	-583.5661989	-583.411501	-583.467199	-583.475606
CH_3CF_2-$CH_2CH^{\bullet}$(OAc)	-583.6184335	-583.461508	-583.514463	-583.522456
h_2 To VAc (head)				
$CH_3CF_2^{\bullet}\cdots$ CH(OAc)=CH_2 TS	-583.5632561	-583.408942	-583.460804	-583.468632
CH_3CF_2-CH(OAc)$CH_2^{\bullet}$	-583.6070571	-583.450876	-583.502591	-583.510396
h_3 To NVP (tail)				
$CH_3CF_2^{\bullet}\cdots CH_2$=CH(N-pyr) TS	-641.0626328	-640.857376	-640.912834	-640.921204
CH_3CF_2-CH_2CH(N-pyr)$^{\bullet}$	-641.1172897	-640.909599	-640.963287	-640.971390
h_4 To MA (tail)				
$CH_3CF_2^{\bullet}\cdots CH_2$=CH(COOMe) TS	-583.565874	-583.409888	-583.46379	-583.471926
CH_3CF_2-CH_2CH(COOMe)$^{\bullet}$	-583.6214092	-583.463503	-583.514737	-583.522470
h_5 To DMA (tail)				
$CH_3CF_2^{\bullet}\cdots CH_2$=CH($CONMe_2$) TS	-602.9768097	-602.779299	-602.835686	-602.844196
CH_3CF_2-CH_2CH($CONMe_2$)$^{\bullet}$	-603.0274511	-602.827802	-602.882699	-602.890985
(i) $PVDF_T^{\bullet}$ addition to monomer				
i_1 To VAc (tail)				
$CHF_2CH_2^{\bullet}\cdots CH_2$=CHOAc TS	-583.5556446	-583.401323	-583.455898	-583.464135
CHF_2CH_2-$CH_2CH^{\bullet}$(OAc)	-583.6092704	-583.450861	-583.504152	-583.512195
i_2 To VAc (head)				
$CHF_2CH_2^{\bullet}\cdots$ CH(OAc)=CH_2 TS	-583.549514	-583.395363	-583.448964	-583.457054
CHF_2CH_2-CH(OAc)$CH_2^{\bullet}$	-583.5993171	-583.441958	-583.494767	-583.502738
i_3 To NVP (tail)				
$CHF_2CH_2^{\bullet}\cdots CH_2$=CH(N-pyr) TS	-641.0502614	-640.845362	-640.901730	-640.910238
CHF_2CH_2-CH_2CH(N-pyr)$^{\bullet}$	-641.1080386	-640.899154	-640.953059	-640.961200
i_4 To MA (tail)				
$CHF_2CH_2^{\bullet}\cdots CH_2$=CH(COOMe) TS	-583.5518487	-583.396475	-583.450774	-583.458969
CHF_2CH_2-CH_2CH(COOMe)$^{\bullet}$	-583.6118974	-583.452544	-583.504878	-583.512777
i_5 To DMA (tail)				
$CHF_2CH_2^{\bullet}\cdots CH_2$=CH($CONMe_2$) TS	-602.9642969	-602.767117	-602.823126	-602.831580
CHF_2CH_2-CH_2CH($CONMe_2$)$^{\bullet}$	-603.0191477	-602.818125	-602.873759	-602.882156

[a]Extrapolation done on the basis of $G_{343.15} \approx H_{298.15} - 343.15 \cdot S_{298.15}$.

SI-Table IV-4: Cartesian coordinates and views of all optimized geometries.

(a) Radicals

$CH_3CF_2^{\bullet}$

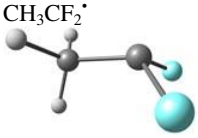

6	0.059485000	0.000229000	-0.305567000
6	-1.386581000	0.000075000	0.044979000
1	-1.526760000	0.000221000	1.137790000
1	-1.870565000	0.890101000	-0.366469000
1	-1.869553000	-0.890889000	-0.365766000
9	0.735032000	1.098602000	0.064360000
9	0.734907000	-1.098742000	0.064303000

$CHF_2CH_2^{\bullet}$

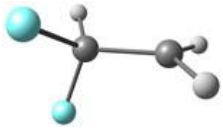

6	1.394001000	-0.107134000	-0.085236000
6	-0.012319000	0.007573000	0.354372000
1	1.605256000	-0.523019000	-1.065566000
1	-0.126101000	0.065360000	1.446414000
1	2.185777000	0.377679000	0.476297000
9	-0.595048000	1.137805000	-0.178214000
9	-0.733288000	-1.062544000	-0.096448000

$CH_3CH(OAc)^{\bullet}$

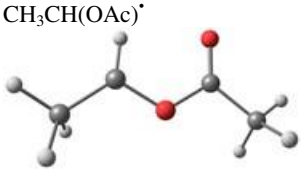

6	-1.317193000	0.378626000	0.127296000
1	-1.138269000	1.439541000	-0.011959000
6	-2.612320000	-0.308037000	-0.059108000
1	-2.688219000	-1.200343000	0.577045000
1	-3.435138000	0.367766000	0.196880000
1	-2.770382000	-0.643370000	-1.099745000
6	1.021800000	0.159756000	-0.010070000
6	2.102555000	-0.884143000	-0.016208000
1	3.059268000	-0.411321000	-0.244154000
1	2.161285000	-1.361742000	0.969438000
1	1.881530000	-1.669032000	-0.746692000
8	-0.211172000	-0.433592000	0.050058000
8	1.181282000	1.358753000	-0.036592000

$AcOCH_2CH_2^{\bullet}$

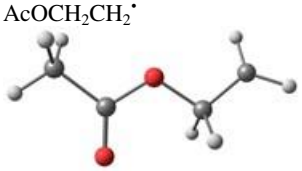

6	2.590296000	0.428611000	-0.053564000
1	2.563545000	1.366036000	-0.600509000
6	-0.972335000	-0.148153000	-0.005656000
1	3.548517000	0.027284000	0.260812000
6	1.372092000	-0.397371000	0.063337000
1	1.372485000	-1.008668000	0.977953000
1	1.254996000	-1.110042000	-0.772854000
8	0.224291000	0.475481000	0.073181000
6	-2.097558000	0.852835000	0.012625000
1	-1.978617000	1.571953000	-0.805039000
1	-3.049920000	0.329379000	-0.084528000
1	-2.078954000	1.420145000	0.949875000
8	-1.097669000	-1.351933000	-0.076451000

$CH_3CH(N\text{-}pyr)^{\bullet}$

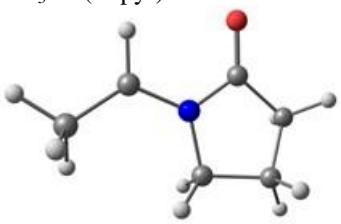

6	1.604229000	0.573915000	0.058455000
6	-0.799941000	0.867325000	0.001853000
6	0.003647000	-1.358441000	0.174567000
6	-2.016788000	-0.037628000	0.109161000
6	-1.477724000	-1.429332000	-0.228391000
1	0.159975000	-1.677167000	1.217567000
1	0.646067000	-1.976840000	-0.462951000
1	-2.402551000	0.017944000	1.137908000
1	-2.814038000	0.311917000	-0.553885000
1	-2.001034000	-2.242239000	0.284891000
1	-1.555828000	-1.609778000	-1.307192000
8	-0.769686000	2.087317000	-0.063960000
7	0.330620000	0.055363000	0.026685000
1	1.635803000	1.654445000	-0.026985000
6	2.807955000	-0.285920000	-0.062264000
1	2.921980000	-0.740047000	-1.063883000
1	3.707209000	0.311757000	0.118402000
1	2.817288000	-1.115585000	0.660730000

$CH_3CH(COOMe)^{\bullet}$

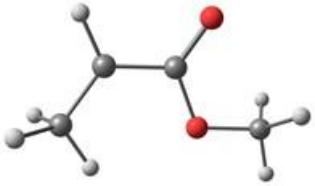

6	-0.072335000	0.527703000	-0.000007000
6	1.378554000	0.516345000	-0.000018000
8	-0.762975000	1.545644000	0.000018000
8	-0.611279000	-0.741331000	-0.000013000
6	-2.054762000	-0.771908000	0.000002000
1	-2.454698000	-0.268927000	-0.893760000
1	-2.324426000	-1.835020000	-0.000041000
1	-2.454677000	-0.269009000	0.893820000
1	1.833847000	1.509781000	0.000009000
6	2.237822000	-0.696024000	0.000000000
1	1.642705000	-1.617667000	-0.000288000
1	2.908037000	-0.705031000	-0.881227000
1	2.907570000	-0.705330000	0.881586000

$CH_3CH(CONMe_2)^{\bullet}$

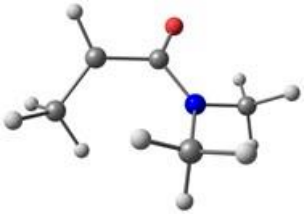

6	-2.320376000	0.525191000	0.432044000
1	-3.085277000	0.026269000	1.046289000
1	-1.715383000	1.150478000	1.095816000
1	-2.872779000	1.189726000	-0.252335000
6	-1.507709000	-0.484340000	-0.302939000
1	-2.029606000	-1.285350000	-0.822810000

8	0.321146000	-1.914228000	-0.111385000
6	-0.073003000	-0.741279000	-0.142815000
7	0.789292000	0.321432000	0.045065000
6	2.169585000	0.035726000	0.375848000
1	2.830113000	0.183514000	-0.492808000
1	2.510965000	0.697421000	1.183631000
1	2.238993000	-1.006218000	0.693664000
6	0.513301000	1.667827000	-0.405670000
1	0.538473000	2.393450000	0.421005000
1	1.264983000	1.978402000	-1.147544000
1	-0.465479000	1.717353000	-0.888088000

(MeO)C(S)S$^{\bullet}$

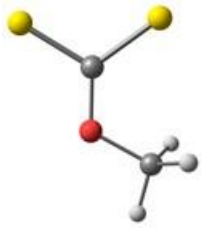

16	1.736278000	-0.629578000	-0.000015000
6	0.122262000	-0.147474000	0.000058000
8	-0.840806000	-1.050048000	0.000022000
16	-0.059249000	1.524074000	-0.000003000
6	-2.203329000	-0.590138000	-0.000024000
1	-2.405410000	0.006032000	-0.896070000
1	-2.405500000	0.005896000	0.896092000
1	-2.808709000	-1.497813000	-0.000123000

(b) Monomers

CH_2=CH(OAc)

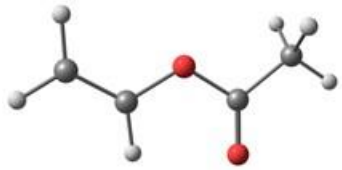

6	-1.405642000	0.278115000	-0.000006000
1	-1.228064000	1.350183000	0.000023000
6	-2.598642000	-0.307743000	0.000029000
1	-2.705080000	-1.388925000	0.000009000
1	-3.495708000	0.302694000	0.000116000
6	0.943656000	0.169181000	-0.000018000
6	2.071051000	-0.823171000	0.000023000
1	3.023078000	-0.290578000	-0.000909000
1	2.002784000	-1.468808000	0.882637000
1	2.001784000	-1.470211000	-0.881468000
8	-0.257894000	-0.489091000	-0.000078000
8	1.050228000	1.372510000	0.000005000

CH_2=CH(N-pyr)

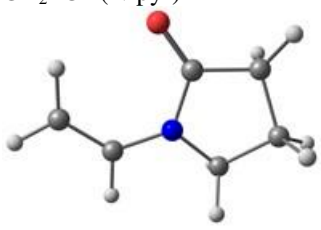

6	-2.686331000	-0.133135000	0.037509000
1	-3.651156000	-0.631901000	0.045072000
1	-2.647440000	0.948852000	0.061135000
6	-1.578855000	-0.884401000	0.003226000
1	-1.649499000	-1.971584000	-0.016936000
6	0.169019000	0.877452000	-0.014475000
6	0.852539000	-1.387584000	-0.143278000
6	1.688522000	0.867245000	-0.136517000
6	2.087518000	-0.560326000	0.239250000
1	0.913661000	-1.754316000	-1.180439000
1	0.703727000	-2.255138000	0.511245000
1	1.944277000	1.107677000	-1.178398000
1	2.125534000	1.646414000	0.494482000
1	2.992374000	-0.914470000	-0.264226000
1	2.255703000	-0.629824000	1.320706000
8	-0.552422000	1.859212000	0.036674000
7	-0.251755000	-0.442130000	-0.000047000

CH_2=CH(COOMe)

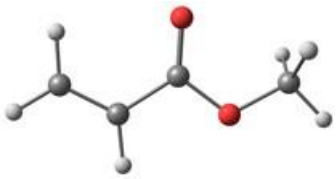

6	2.485397000	-0.007753000	-0.000081000
1	3.431200000	-0.543770000	-0.000088000
1	2.510442000	1.080322000	-0.000318000
6	1.314034000	-0.647934000	0.000107000
6	0.042467000	0.113825000	0.000027000
1	1.240816000	-1.733426000	0.000118000
8	-0.063509000	1.324420000	0.000076000
8	-1.015214000	-0.729120000	-0.000013000
6	-2.292455000	-0.085382000	-0.000056000
1	-3.031182000	-0.889324000	0.000507000
1	-2.408895000	0.544089000	0.888622000
1	-2.409261000	0.543173000	-0.889324000

CH_2=CH($CONMe_2$)

6	-2.285341000	0.589878000	0.452633000
1	-1.795719000	1.178881000	1.226516000
1	-3.360473000	0.720320000	0.346714000
6	-1.614308000	-0.278807000	-0.308982000
1	-2.142507000	-0.898765000	-1.032580000
8	0.060136000	-1.891137000	-0.045550000
6	-0.186688000	-0.688020000	-0.121408000
7	0.785252000	0.273756000	0.000771000
6	2.138636000	-0.154695000	0.296292000
1	2.802518000	0.020042000	-0.563145000
1	2.534216000	0.402383000	1.156494000
1	2.118720000	-1.222293000	0.522099000
6	0.628090000	1.675839000	-0.325983000
1	0.786279000	2.314114000	0.556132000
1	1.367026000	1.966992000	-1.086977000
1	-0.370242000	1.865952000	-0.721553000

(c) Chain transfer agents

CH_3CF_2-SC(S)(OCH_3)

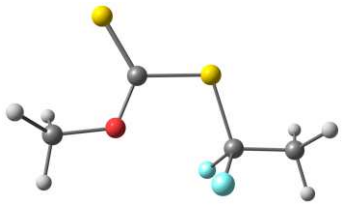

6	-1.739920000	0.093570000	-0.000102000
6	-3.070870000	-0.619464000	-0.000207000
1	-3.858173000	0.141307000	-0.000444000
1	-3.174583000	-1.241038000	-0.893661000
1	-3.174924000	-1.240682000	0.893459000
9	-1.641560000	0.894919000	-1.093022000
9	-1.642260000	0.895670000	1.092355000
16	-0.382514000	-1.168765000	0.000561000
6	1.124096000	-0.245886000	0.000132000
8	0.933171000	1.065294000	0.000332000
16	2.556679000	-1.052479000	-0.000251000
6	2.090846000	1.914417000	0.000030000
1	2.696436000	1.728319000	-0.892552000
1	2.696846000	1.728387000	0.892371000
1	1.691865000	2.930133000	0.000106000

CHF_2CH_2-SC(S)(OCH_3)

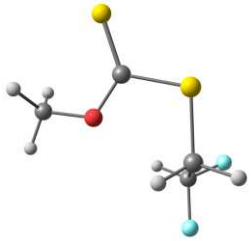

6	-1.388504000	-0.272977000	0.878223000
6	-2.139901000	0.290759000	-0.311861000
1	-1.514938000	0.912329000	-0.965455000
16	0.039507000	-1.312514000	0.424652000
6	1.315328000	-0.152852000	0.073669000
8	0.907451000	1.115151000	0.186556000
16	2.818127000	-0.673688000	-0.340214000
6	1.871772000	2.153075000	-0.054321000
1	2.256150000	2.082942000	-1.076646000
1	2.705447000	2.065589000	0.649297000
1	1.325110000	3.085697000	0.097855000
1	-1.061251000	0.538475000	1.533052000
1	-2.065970000	-0.928721000	1.436919000
9	-2.670438000	-0.720824000	-1.051412000
9	-3.171613000	1.053457000	0.158884000

CH_3CH(OAc)-SC(S)(OCH_3)

16	0.785871000	1.772068000	0.822287000
6	1.633161000	0.530039000	0.166306000
8	2.917159000	0.702222000	-0.161754000
6	3.701159000	-0.358456000	-0.721666000
1	3.291733000	-0.685763000	-1.684825000
1	3.763931000	-1.209083000	-0.032518000
16	1.013752000	-1.108091000	-0.177284000
6	-0.719661000	-0.997320000	0.375073000
1	4.693935000	0.070739000	-0.869132000
1	-0.744433000	-0.383305000	1.282664000
6	-1.257925000	-2.397547000	0.608134000
1	-1.239612000	-2.989968000	-0.313033000
1	-0.676975000	-2.914787000	1.378618000
1	-2.293346000	-2.309588000	0.951967000
6	-2.544085000	0.372869000	-0.225708000
6	-3.124393000	1.178155000	-1.353549000
1	-4.108624000	1.550717000	-1.065002000
1	-2.460932000	2.025709000	-1.561926000
1	-3.191369000	0.578525000	-2.266485000
8	-1.457775000	-0.331055000	-0.654280000
8	-2.954108000	0.338425000	0.912044000

$AcOCH_2CH_2$-SC(S)(OCH_3)

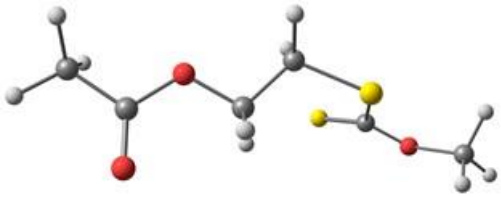

16	1.496067000	1.940834000	0.081796000
6	2.171592000	0.446881000	-0.015408000
8	3.406804000	0.308853000	-0.501811000
6	4.040069000	-0.973135000	-0.600643000
1	3.474955000	-1.641675000	-1.260851000
1	4.156688000	-1.432729000	0.388072000
16	1.417223000	-1.090809000	0.487952000
6	-0.223927000	-0.556829000	1.047017000
1	5.022193000	-0.770774000	-1.031746000
1	-0.112606000	0.423904000	1.523602000
6	-3.522347000	-0.079958000	-0.369307000
1	-0.529547000	-1.294490000	1.797703000
6	-1.219998000	-0.497307000	-0.097615000
1	-1.328475000	-1.466839000	-0.597714000
1	-0.914674000	0.243393000	-0.845289000
8	-2.473006000	-0.110403000	0.488157000
6	-4.773084000	0.372499000	0.335333000
1	-4.661645000	1.416105000	0.651292000
1	-5.623037000	0.284481000	-0.343142000
1	-4.943463000	-0.225051000	1.236901000
8	-3.432157000	-0.374653000	-1.540228000

CH_3CH(N-pyr)-SC(S)(OCH_3)

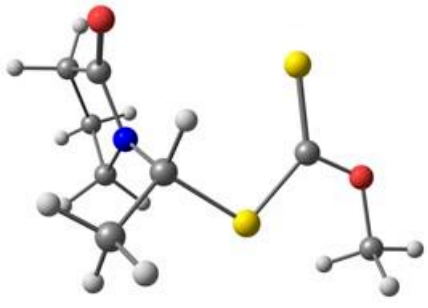

16	-1.171040000	-1.921352000	0.625972000
6	-1.925753000	-0.583858000	0.059034000
8	-3.137397000	-0.686940000	-0.503307000
6	-3.844980000	0.459395000	-0.988379000
1	-3.293553000	0.953273000	-1.797586000
1	-4.040903000	1.175075000	-0.180893000
16	-1.296722000	1.084157000	0.110607000
6	0.376871000	0.910448000	0.883172000
1	-4.789695000	0.068209000	-1.371207000
1	0.286033000	0.174768000	1.692436000
6	0.742944000	2.290757000	1.429388000
1	0.811076000	3.044958000	0.636618000

1	0.004865000	2.628175000	2.164253000
1	1.718237000	2.219297000	1.923363000
7	1.352544000	0.374054000	-0.020467000
6	3.221985000	-0.835196000	-0.738678000
1	4.182086000	-0.365012000	-0.483943000
1	3.403626000	-1.908495000	-0.845860000
6	2.555048000	-0.175637000	-1.948289000
1	1.916840000	-0.901508000	-2.465141000
1	3.264921000	0.228701000	-2.676494000
6	1.674963000	0.923408000	-1.328512000
1	2.221330000	1.877145000	-1.238992000
1	0.761122000	1.111608000	-1.904438000
6	2.258974000	-0.577168000	0.414044000
8	2.288660000	-1.063353000	1.530208000

$CH_3CH(COOMe)$-SC(S)(OCH_3)

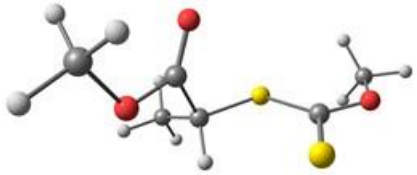

16	-0.790895000	1.824988000	-0.796460000
6	-1.601251000	0.533117000	-0.183868000
8	-2.870727000	0.671862000	0.209027000
6	-3.602870000	-0.425340000	0.767438000
1	-3.123359000	-0.791724000	1.682986000
1	-3.701809000	-1.242843000	0.042846000
16	-0.950862000	-1.108342000	0.014499000
6	0.746553000	-0.921083000	-0.607406000
1	-4.588747000	-0.019653000	1.001942000
1	0.693154000	-0.360108000	-1.546681000
6	1.329793000	-2.321057000	-0.838994000
1	1.375228000	-2.894693000	0.093412000
1	0.730035000	-2.877730000	-1.566114000
1	2.347023000	-2.221046000	-1.231783000
6	3.594548000	1.115977000	0.512444000
1	4.368202000	1.470960000	-0.170809000
1	3.092603000	1.959259000	0.996959000
1	4.026740000	0.469636000	1.283317000
6	1.624070000	-0.140107000	0.370313000
8	1.468054000	-0.058185000	1.566274000
8	2.665671000	0.385393000	-0.299583000

$CH_3CH(CONMe_2)$-SC(S)(OCH_3)

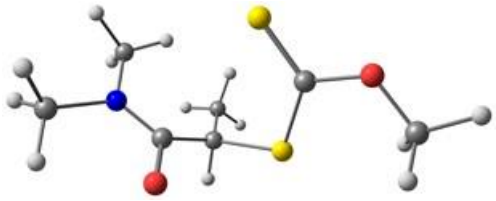

6	-1.697839000	0.550607000	-0.113274000
6	0.613747000	-0.488744000	2.235624000
1	1.657960000	-0.531108000	2.564705000
1	0.258506000	0.542603000	2.301423000
1	0.023024000	-1.096508000	2.929991000
16	-0.700311000	1.860458000	-0.073707000
8	-2.967706000	0.720032000	-0.497302000
6	-3.876488000	-0.383666000	-0.593652000
1	-3.525421000	-1.118427000	-1.327898000
1	-4.015307000	-0.866364000	0.381280000
16	-1.280988000	-1.118635000	0.283326000
6	0.470041000	-1.066811000	0.830046000
1	0.639493000	-2.151769000	0.912364000
8	1.216252000	-1.406051000	-1.389479000
6	1.406317000	-0.749426000	-0.370121000
7	2.506037000	0.050203000	-0.227943000
6	3.476506000	0.022079000	-1.311980000
1	3.318614000	0.858316000	-2.008469000
1	4.487274000	0.100809000	-0.893071000
1	3.370063000	-0.912546000	-1.864054000
6	2.695143000	1.130342000	0.723963000
1	3.427384000	0.870158000	1.502369000
1	3.072930000	2.008117000	0.184325000
1	1.750317000	1.424221000	1.176996000
1	-4.819240000	0.053783000	-0.927643000

d) VAc homopropagation

d_1 Head-to-tail

$CH_3CH(OAc)^{\bullet}\cdots CH_2=CH(OAc)$ TS

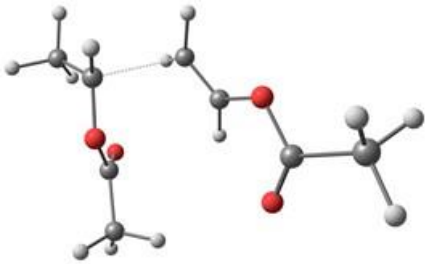

6	1.585616000	1.206690000	-0.081789000
6	1.748714000	-0.991150000	0.850453000
1	1.286717000	-1.524968000	1.679046000
8	1.415706000	0.349645000	0.967002000
6	1.027754000	2.559345000	0.261910000
1	1.234246000	2.823681000	1.303026000
1	1.444391000	3.306578000	-0.416206000
1	-0.061205000	2.524481000	0.129841000
8	2.082749000	0.896587000	-1.142456000
6	0.272262000	-1.797956000	-0.828491000
1	1.086446000	-1.760358000	-1.543804000
1	0.118100000	-2.717326000	-0.270105000
6	-0.715046000	-0.882302000	-0.935531000
1	-0.673852000	0.011444000	-1.548993000
8	-1.848290000	-1.006850000	-0.153999000
6	-2.632677000	0.098327000	0.001637000
8	-2.355471000	1.188865000	-0.446976000
6	-3.868914000	-0.245186000	0.783617000
1	-4.415463000	0.669691000	1.017497000
1	-4.507505000	-0.912143000	0.192457000
1	-3.605369000	-0.777333000	1.703555000
6	3.127114000	-1.381848000	0.437861000
1	3.210354000	-2.474689000	0.436010000
1	3.376659000	-0.996250000	-0.554397000
1	3.879992000	-0.994299000	1.145501000

$CH_3CH(OAc)$-$CH_2CH(OAc)^{\bullet}$

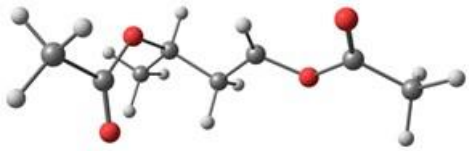

6	2.300214000	0.918783000	-0.308441000
6	1.443043000	-1.147908000	0.636123000
1	1.199128000	-1.406068000	1.674221000
8	1.903950000	0.224824000	0.781204000
6	2.709419000	2.315094000	0.086155000
1	3.457118000	2.282794000	0.885517000
1	3.109970000	2.834625000	-0.785793000

1	1.841500000	2.860522000	0.474042000
8	2.316478000	0.484886000	-1.441508000
6	0.159853000	-1.228968000	-0.193441000
1	0.394530000	-0.972286000	-1.239711000
1	-0.171698000	-2.279308000	-0.200965000
6	-0.918975000	-0.370389000	0.351819000
1	-0.769250000	0.572728000	0.866304000
8	-2.157112000	-0.573616000	-0.204718000
6	-3.145756000	0.333092000	0.077085000
8	-2.970809000	1.310851000	0.767287000
6	-4.432294000	-0.080173000	-0.579188000
1	-5.183536000	0.694890000	-0.419722000
1	-4.280994000	-0.244134000	-1.651530000
1	-4.784119000	-1.026359000	-0.151444000
6	2.547945000	-2.068798000	0.139338000
1	2.225039000	-3.112276000	0.235870000
1	2.790506000	-1.867566000	-0.907045000
1	3.451052000	-1.937519000	0.745432000

d_2 Head-to-head

$CH_3CH(OAc)^{\bullet}\cdots CH(OAc)=CH_2$ TS

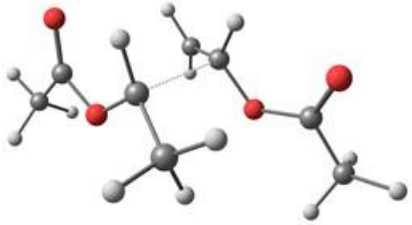

6	-2.773507000	0.063602000	-0.005780000
6	-0.631297000	0.904839000	-0.502962000
1	-0.958836000	0.802941000	-1.536589000
8	-1.648893000	0.717263000	0.413413000
6	-3.717819000	-0.138414000	1.146155000
1	-3.903746000	0.810253000	1.661014000
1	-4.655406000	-0.556931000	0.776892000
1	-3.270997000	-0.823118000	1.876049000
8	-2.961765000	-0.278824000	-1.151943000
6	-0.262887000	-1.977206000	-0.140054000
1	-0.316709000	-2.352841000	0.877522000
1	-0.998185000	-2.310816000	-0.863925000
6	0.615473000	-0.991753000	-0.479736000
1	0.889760000	-0.751514000	-1.503399000
8	1.604430000	-0.679069000	0.457869000
6	2.761318000	-0.131341000	-0.005727000
8	2.963125000	0.142864000	-1.167991000
6	3.736620000	0.057138000	1.123330000
1	4.605401000	0.610430000	0.763321000
1	3.265141000	0.587723000	1.956828000
1	4.056051000	-0.921740000	1.499675000
6	0.283897000	2.009877000	-0.114927000
1	0.669795000	1.861975000	0.901108000
1	1.127670000	2.063655000	-0.809479000
1	-0.235907000	2.981661000	-0.131595000

$CH_3CH(OAc)\text{-}CH(OAc)CH_2^{\bullet}$

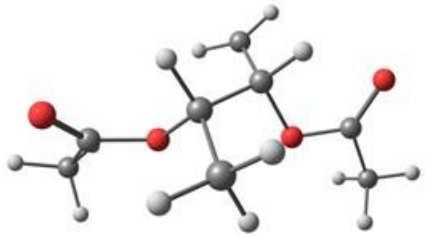

6	2.761344000	0.252559000	-0.016055000
6	0.663808000	-0.858993000	0.143249000
1	1.221990000	-1.651063000	-0.372552000
8	1.412485000	0.370565000	0.003260000
6	3.409410000	1.606962000	-0.130769000
1	3.221893000	2.182645000	0.783015000
1	4.484549000	1.484422000	-0.271043000
1	2.978114000	2.171134000	-0.964005000
8	3.349907000	-0.804481000	0.060437000
6	-0.526674000	-0.276381000	-2.005524000
1	0.304146000	0.346073000	-2.322979000
1	-1.344357000	-0.466049000	-2.693500000
6	-0.662554000	-0.674446000	-0.583317000
1	-1.233375000	-1.609406000	-0.509468000
8	-1.423422000	0.340585000	0.155713000
6	-2.768947000	0.230615000	0.082548000
8	-3.346060000	-0.638671000	-0.535819000
6	-3.434606000	1.335645000	0.860673000
1	-4.513100000	1.170353000	0.875330000
1	-3.042734000	1.376306000	1.882247000
1	-3.215792000	2.300643000	0.389317000
6	0.516817000	-1.207332000	1.615248000
1	0.018945000	-0.395317000	2.153493000
1	-0.078402000	-2.120818000	1.731285000
1	1.503260000	-1.384685000	2.053816000

d_3 Tail-to-tail

$AcOCH_2CH_2^{\bullet}\cdots CH_2=CH(OAc)$ TS

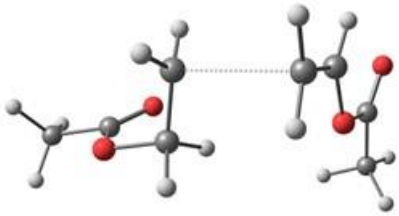

6	-1.079938000	1.851066000	-0.341750000
1	-0.961182000	1.465779000	-1.350932000
6	-2.877603000	-0.735904000	-0.160422000
1	-1.461750000	2.866520000	-0.251415000
6	-1.370253000	0.875549000	0.738228000
1	-1.345864000	1.338999000	1.729492000
1	-0.674837000	0.030909000	0.706296000
8	-2.730935000	0.341872000	0.639061000
6	-4.321112000	-1.168441000	-0.207659000
1	-4.922816000	-0.391932000	-0.693889000
1	-4.403000000	-2.100487000	-0.769307000
1	-4.715812000	-1.299130000	0.805284000
8	-1.967667000	-1.271563000	-0.758472000
6	1.249030000	2.334449000	0.072840000
1	1.161314000	3.220415000	-0.546856000
1	1.000207000	2.425889000	1.126231000
6	1.987461000	1.297832000	-0.375639000
1	2.386047000	1.193212000	-1.380399000
8	2.202538000	0.215302000	0.446743000
6	2.948065000	-0.824018000	-0.055650000
8	3.459081000	-0.807533000	-1.149494000
6	3.002208000	-1.946840000	0.938694000
1	3.741841000	-2.680770000	0.615027000
1	3.246766000	-1.569658000	1.936683000
1	2.017805000	-2.426533000	0.999216000

$AcOCH_2CH_2\text{-}CH_2CH(OAc)^{\bullet}$

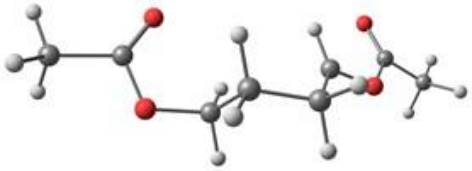

6	-0.907968000	1.234132000	-0.632528000
1	-1.113525000	0.516149000	-1.436841000
6	-3.376731000	-0.581019000	0.068485000
1	-1.438592000	2.161989000	-0.881431000
6	-1.463356000	0.679053000	0.671644000
1	-1.268987000	1.363702000	1.505100000
1	-1.024730000	-0.298961000	0.897630000
8	-2.897271000	0.557474000	0.621923000
6	-4.882666000	-0.586490000	0.090353000
1	-5.270558000	0.282773000	-0.451945000
1	-5.249100000	-1.506339000	-0.367939000
1	-5.243570000	-0.513063000	1.122175000
8	-2.675742000	-1.465499000	-0.374120000
6	0.596910000	1.513884000	-0.550952000
1	0.913723000	2.017851000	-1.484021000
1	0.808200000	2.235888000	0.253765000
6	1.396950000	0.284715000	-0.325306000
1	1.182931000	-0.684892000	-0.766567000
8	2.695175000	0.502462000	0.065444000
6	3.563382000	-0.559424000	0.047307000
8	3.250567000	-1.664616000	-0.329540000
6	4.908360000	-0.138833000	0.568159000
1	5.621162000	-0.952244000	0.423653000
1	5.255541000	0.765285000	0.057166000
1	4.836385000	0.097182000	1.636628000

d_4 Tail-to-head

$AcOCH_2CH_2^{\bullet\cdots}CH(OAc)=CH_2$ TS

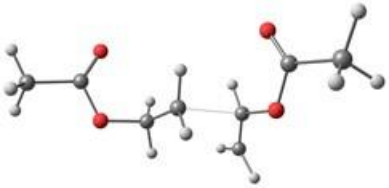

6	-0.212966000	0.198998000	-0.463050000
1	-0.094283000	-0.770697000	0.016145000
6	-3.240276000	-0.414406000	0.122840000
1	0.116080000	0.270795000	-1.498046000
6	-1.363446000	1.040378000	-0.040465000
1	-1.282420000	2.059547000	-0.429923000
1	-1.462534000	1.063628000	1.050369000
8	-2.621590000	0.549213000	-0.595335000
6	-4.513493000	-0.846420000	-0.558483000
1	-4.281834000	-1.285357000	-1.535505000
1	-5.027095000	-1.580815000	0.064056000
1	-5.162266000	0.017917000	-0.735968000
8	-2.818421000	-0.860376000	1.168562000
6	1.563877000	2.488035000	0.239474000
1	2.043320000	2.961169000	-0.612318000
1	0.930118000	3.089440000	0.882735000
6	1.661831000	1.150085000	0.453438000
1	1.369532000	0.657661000	1.377124000
8	2.591164000	0.445351000	-0.303100000
6	2.884544000	-0.830179000	0.090353000
8	2.379296000	-1.370638000	1.046422000
6	3.907994000	-1.432043000	-0.830421000
1	4.157043000	-2.437188000	-0.487278000
1	3.514359000	-1.473215000	-1.852216000
1	4.807994000	-0.807969000	-0.853681000

$AcOCH_2CH_2$-$CH(OAc)CH_2^{\bullet}$

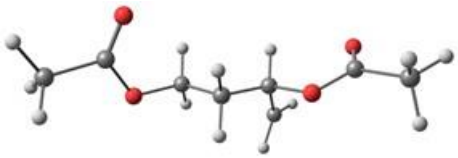

6	-0.289765000	0.215484000	-0.435059000
1	-0.431054000	-0.855514000	-0.250870000
6	-3.298967000	-0.444626000	0.189831000
1	-0.328107000	0.378942000	-1.520497000
6	-1.414459000	0.989996000	0.238708000
1	-1.311781000	2.067957000	0.076031000
1	-1.435891000	0.785960000	1.315575000
8	-2.690373000	0.647797000	-0.331065000
6	-4.621871000	-0.685545000	-0.487485000
1	-4.473889000	-0.823612000	-1.564147000
1	-5.093222000	-1.571322000	-0.058989000
1	-5.274167000	0.185145000	-0.358392000
8	-2.829642000	-1.118410000	1.081360000
6	1.450855000	2.032837000	-0.226406000
1	1.145912000	2.474654000	-1.173171000
1	2.178368000	2.557780000	0.384643000
6	1.078017000	0.631745000	0.094154000
1	1.149551000	0.466445000	1.176881000
8	2.029874000	-0.298373000	-0.533786000
6	3.198857000	-0.470860000	0.122783000
8	3.489371000	0.098055000	1.153625000
6	4.071185000	-1.463870000	-0.601291000
1	5.012377000	-1.580579000	-0.061699000
1	3.560229000	-2.430159000	-0.674893000
1	4.264736000	-1.119207000	-1.622963000

(e) Other monomers homopropagation (all head-to-tail)

$CH_3CH(N\text{-}pyr)^{\bullet\cdots}CH_2=CH(N\text{-}pyr)$ TS

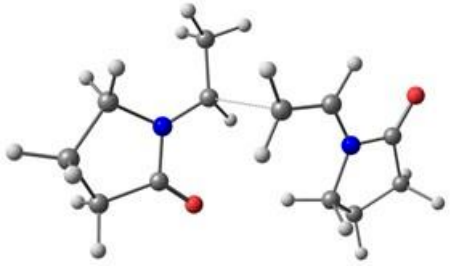

6	1.470492000	1.201836000	0.806511000
6	-2.337504000	-1.113711000	-0.331740000
6	-3.579840000	0.846176000	0.155031000
6	-3.719941000	-1.570948000	0.102856000
6	-4.308004000	-0.344157000	0.803976000
1	-4.149517000	1.270064000	-0.686002000
1	-3.388609000	1.656636000	0.868575000
1	-4.292184000	-1.852817000	-0.793119000
1	-3.649555000	-2.461221000	0.735093000
1	-5.394775000	-0.259482000	0.706507000
1	-4.071804000	-0.378302000	1.874220000
8	-1.387239000	-1.813493000	-0.668296000
7	-2.327490000	0.269254000	-0.321547000
6	-1.345165000	2.427899000	-1.091900000
1	-1.871623000	2.548622000	-2.054052000
1	-1.887372000	3.025285000	-0.347532000
1	-0.349680000	2.870340000	-1.205714000
6	-1.202333000	0.996909000	-0.692370000
1	-0.499944000	0.378994000	-1.245529000

6	0.164856000	1.045372000	1.176431000
1	-0.348891000	1.899834000	1.608120000
1	-0.236578000	0.065415000	1.420779000
1	1.952568000	2.173240000	0.726782000
7	2.293792000	0.171608000	0.390077000
6	3.610251000	0.394140000	0.009127000
8	4.138726000	1.492306000	-0.060227000
6	1.934176000	-1.242330000	0.432174000
1	0.933586000	-1.407435000	0.014691000
1	1.930046000	-1.595145000	1.476083000
6	3.043108000	-1.911413000	-0.396875000
1	2.728532000	-1.970158000	-1.445560000
1	3.248449000	-2.930544000	-0.055215000
6	4.238198000	-0.964935000	-0.258996000
1	4.872610000	-1.220210000	0.602354000
1	4.888958000	-0.918687000	-1.137368000

CH3CH(N-pyr)-CH2CH(N-pyr)$^{\bullet}$

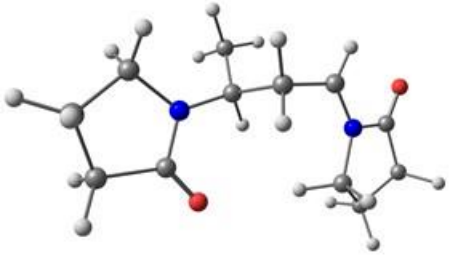

6	1.367141000	1.193609000	0.745124000
6	-2.389073000	-1.099413000	-0.277665000
6	-3.394249000	0.998502000	0.163722000
6	-3.869776000	-1.368288000	-0.039765000
6	-4.366476000	-0.093929000	0.648818000
1	-3.787829000	1.534596000	-0.714462000
1	-3.190626000	1.746319000	0.941230000
1	-4.347589000	-1.529134000	-1.016419000
1	-4.005811000	-2.282733000	0.544567000
1	-5.407905000	0.153406000	0.420975000
1	-4.280766000	-0.202341000	1.736737000
8	-1.518566000	-1.923463000	-0.538278000
7	-2.193687000	0.251227000	-0.177050000
6	-0.959946000	2.149561000	-1.174981000
1	-1.470714000	2.020722000	-2.136054000
1	-1.487474000	2.924381000	-0.603626000
1	0.052488000	2.517410000	-1.374033000
6	-0.880568000	0.834177000	-0.408935000
1	-0.354901000	0.093009000	-1.024553000
6	-0.088864000	0.967900000	0.927580000
1	-0.509871000	1.797881000	1.512343000
1	-0.275072000	0.048971000	1.502339000
1	1.815918000	2.178438000	0.668003000
7	2.208892000	0.172962000	0.368459000
6	3.531546000	0.410491000	0.002114000
8	4.026506000	1.523633000	-0.100297000
6	1.906397000	-1.255558000	0.486233000
1	0.909559000	-1.490954000	0.095455000
1	1.934980000	-1.552437000	1.546862000
6	3.034194000	-1.919944000	-0.317085000
1	2.728423000	-2.014947000	-1.365867000
1	3.260662000	-2.923742000	0.055519000
6	4.201830000	-0.938714000	-0.195646000
1	4.825763000	-1.147524000	0.686200000
1	4.867878000	-0.912363000	-1.063574000

$CH_3CH(COOMe)^{\bullet}\cdots CH_2=CH(COOMe)$ TS

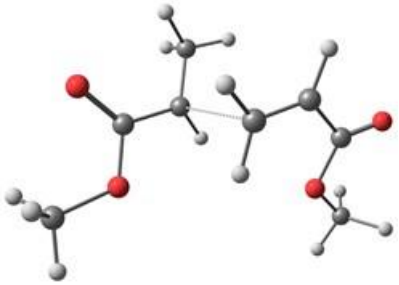

6	1.448646000	-0.941874000	-0.987474000
6	-0.971993000	-2.170293000	1.017545000
1	-1.396714000	-2.382077000	2.012138000
1	-1.562752000	-2.735834000	0.289815000
1	0.061267000	-2.533003000	1.022834000
6	-1.038529000	-0.712937000	0.732800000
1	-0.392153000	-0.030139000	1.279381000
6	0.226674000	-0.381177000	-1.205002000
1	-0.517737000	-0.910135000	-1.796076000
1	0.074163000	0.683500000	-1.051000000
1	1.661918000	-1.969868000	-1.270672000
6	2.572938000	-0.257613000	-0.333837000
8	3.684207000	-0.739689000	-0.204323000
8	2.242819000	0.977899000	0.119513000
6	3.315539000	1.689342000	0.741622000
1	3.708780000	1.130309000	1.597406000
1	4.132900000	1.857949000	0.032131000
1	2.891220000	2.641205000	1.067708000
8	-3.204624000	-0.811477000	-0.260265000
8	-2.271564000	1.201846000	0.222798000
6	-3.449530000	1.813172000	-0.307817000
1	-3.287007000	2.890170000	-0.229583000
1	-3.604230000	1.523151000	-1.352890000
1	-4.333747000	1.517674000	0.267496000
6	-2.277515000	-0.157210000	0.193752000

$CH_3CH(COOMe)\text{-}CH_2CH(COOMe)^{\bullet}$

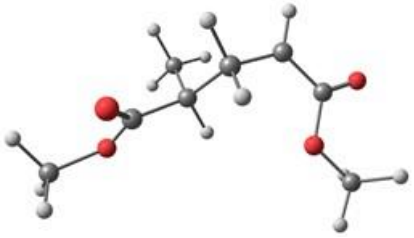

6	-1.583188000	1.234258000	-0.489422000
6	0.953965000	1.637622000	1.225656000
1	1.611168000	1.332411000	2.045402000
1	1.417164000	2.489510000	0.711764000
1	0.003979000	1.977034000	1.653474000
6	0.716229000	0.474036000	0.252517000
1	0.255115000	-0.354901000	0.807353000
6	-0.213020000	0.852588000	-0.923476000
1	0.249742000	1.672452000	-1.485474000
1	-0.264942000	-0.011122000	-1.599141000
1	-1.892626000	2.275603000	-0.450041000
6	-2.603987000	0.291838000	-0.075176000
8	-3.732596000	0.603150000	0.281578000
8	-2.173471000	-1.000270000	-0.124153000
6	-3.152721000	-1.965882000	0.262342000
1	-3.482016000	-1.796852000	1.293531000
1	-4.029157000	-1.914902000	-0.392985000
1	-2.664546000	-2.938539000	0.171353000
8	2.386888000	-0.014768000	-1.453262000
8	2.799041000	-0.554566000	0.698681000
6	4.075026000	-1.054734000	0.282308000

1	4.561332000	-1.418333000	1.189648000
1	3.954151000	-1.868229000	-0.440658000
1	4.670418000	-0.261067000	-0.180955000
6	2.036250000	-0.044965000	-0.292419000

$CH_3CH(CONMe_2)^{\bullet\cdots}CH_2=CH(CONMe_2)$ TS

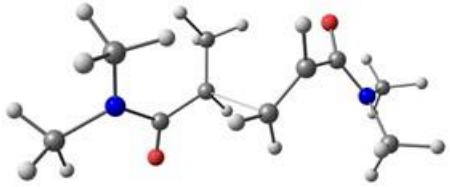

6	1.201225000	0.280466000	1.150487000
6	-0.828087000	1.756348000	-0.959599000
1	-1.022493000	2.094286000	-1.989944000
1	-1.499303000	2.321153000	-0.307721000
1	0.207370000	2.037529000	-0.724850000
6	-1.002705000	0.269363000	-0.892824000
1	-0.395944000	-0.276799000	-1.613121000
6	0.249182000	-0.640759000	0.811903000
1	-0.616340000	-0.788230000	1.453212000
1	0.476617000	-1.465243000	0.140532000
1	0.971854000	1.055333000	1.881105000
6	2.415743000	0.580472000	0.344319000
8	2.576627000	1.736783000	-0.062412000
8	-2.558447000	-1.365803000	-1.505037000
6	-2.297085000	-0.434982000	-0.732841000
7	-3.188923000	-0.052006000	0.248092000
7	3.290695000	-0.428994000	0.038838000
6	-4.496184000	-0.675944000	0.274085000
1	-4.647442000	-1.229930000	1.212376000
1	-5.289445000	0.081291000	0.191929000
1	-4.559287000	-1.368076000	-0.567397000
6	-2.927304000	0.895229000	1.307856000
1	-3.471214000	1.842036000	1.162971000
1	-3.252838000	0.470284000	2.268584000
1	-1.861587000	1.114044000	1.382947000
6	3.304203000	-1.731018000	0.672363000
1	3.095761000	-2.533875000	-0.049997000
1	4.293956000	-1.921744000	1.112112000
1	2.558980000	-1.770302000	1.468699000
6	4.398604000	-0.142845000	-0.851123000
1	5.356479000	-0.190583000	-0.312889000
1	4.427393000	-0.872773000	-1.671661000
1	4.264083000	0.862773000	-1.253568000

$CH_3CH(CONMe_2)$-$CH_2CH(CONMe_2)^{\bullet}$

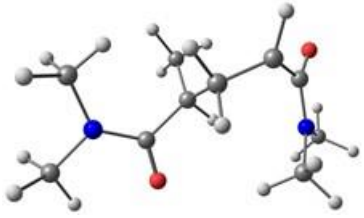

6	-1.410483000	1.222088000	-1.059102000
6	0.630486000	1.579716000	1.295024000
1	1.031778000	1.280149000	2.270135000
1	1.257512000	2.390387000	0.908845000
1	-0.371347000	1.993821000	1.458410000
6	0.525178000	0.372865000	0.354117000
1	-0.232083000	-0.289604000	0.788624000
6	0.007946000	0.738801000	-1.064570000
1	0.637241000	1.511867000	-1.524897000
1	0.120659000	-0.155286000	-1.698823000
1	-1.625234000	2.221036000	-1.432259000
6	-2.503080000	0.685589000	-0.230131000
8	-3.200706000	1.498059000	0.395948000
8	1.516609000	-1.781725000	0.521059000
6	1.724049000	-0.587142000	0.296358000
7	2.984113000	-0.137299000	-0.007560000
7	-2.680812000	-0.670603000	-0.115785000
6	4.082568000	-1.085660000	0.022117000
1	4.525338000	-1.199757000	-0.977880000
1	4.867615000	-0.739567000	0.708984000
1	3.693413000	-2.048084000	0.357690000
6	3.352444000	1.206452000	-0.395316000
1	3.953770000	1.701621000	0.382119000
1	3.953919000	1.173778000	-1.314902000
1	2.474610000	1.818298000	-0.595048000
6	-2.053044000	-1.644295000	-0.988868000
1	-1.142220000	-2.081512000	-0.552799000
1	-2.765182000	-2.455026000	-1.186603000
1	-1.805535000	-1.184609000	-1.950240000
6	-3.625211000	-1.174241000	0.861277000
1	-4.476666000	-1.666255000	0.368954000
1	-3.140813000	-1.903043000	1.525419000
1	-3.992248000	-0.328595000	1.446186000

(e) VAc RAFT: MacroCTA degenerative and non-degenerative radical exchange

e_1 Head-head (degenerative)

$CH_3CH(OAc)$-$SC(OMe)S^{\cdots\bullet}CH(OAc)CH_3$ TS

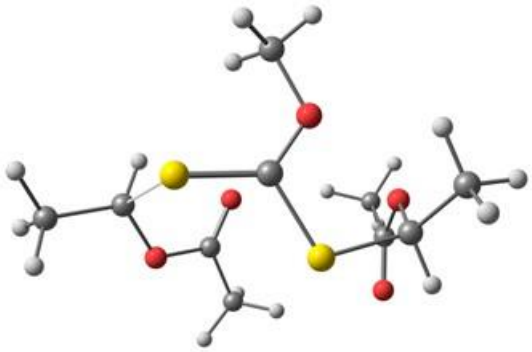

6	2.484098000	-0.634868000	-0.807774000
16	0.758250000	-0.816034000	-1.444623000
6	-0.180960000	-1.581485000	-0.160883000
8	0.530849000	-1.862155000	0.940834000
6	-0.169013000	-2.373907000	2.077021000
1	-0.678820000	-3.312201000	1.831528000
1	-0.903807000	-1.643071000	2.430188000
16	-1.813456000	-1.780317000	-0.369799000
6	-3.109910000	0.257929000	0.250744000
1	0.600663000	-2.538623000	2.834236000
1	-2.898234000	0.223497000	1.317010000
6	-4.449524000	-0.095994000	-0.284456000
1	-4.414418000	-0.228481000	-1.371996000
1	-4.800497000	-1.028683000	0.169608000
1	-5.192928000	0.687867000	-0.065654000
6	-1.456133000	1.931427000	0.173091000
6	-0.937187000	3.047801000	-0.683223000
1	-0.869458000	3.958807000	-0.079124000
1	0.078405000	2.799082000	-1.014533000
1	-1.574573000	3.221512000	-1.552164000
8	-2.533016000	1.323890000	-0.404024000
8	-1.001898000	1.588893000	1.246889000
1	2.939535000	-0.051260000	-1.618502000
6	3.220501000	-1.937079000	-0.571368000

1	3.231539000	-2.530763000	-1.490514000
1	4.255159000	-1.718911000	-0.281348000
1	2.744822000	-2.516430000	0.222909000
8	2.535368000	0.131487000	0.393425000
6	2.470767000	1.482868000	0.256890000
6	2.379114000	2.150350000	1.596391000
1	2.737810000	3.178769000	1.517602000
1	1.318734000	2.159686000	1.883004000
1	2.937499000	1.599264000	2.357655000
8	2.451365000	2.042797000	-0.819342000

$CH_3CH(OAc)\text{-}SC^{\bullet}(OMe)S\text{-}CH(OAc)CH_3$

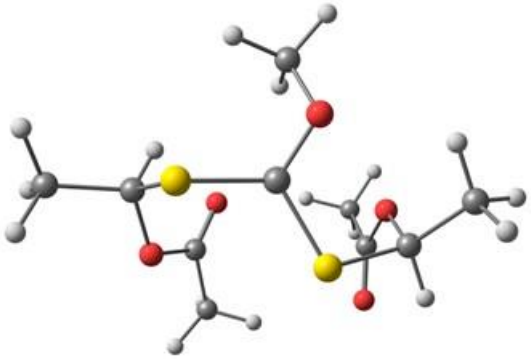

6	2.390269000	-0.770216000	-0.746858000
16	0.700746000	-0.972511000	-1.473603000
6	-0.309847000	-1.398123000	-0.103627000
8	0.266174000	-2.158392000	0.865893000
6	-0.239975000	-1.940444000	2.183307000
1	-1.300121000	-2.219706000	2.243923000
1	-0.115569000	-0.889424000	2.470503000
16	-2.031944000	-1.525126000	-0.454149000
6	-2.711617000	0.062155000	0.209069000
1	0.344999000	-2.585770000	2.843524000
1	-2.382463000	0.178715000	1.245176000
6	-4.220491000	0.025272000	0.071484000
1	-4.513700000	-0.083392000	-0.978298000
1	-4.637415000	-0.810360000	0.642954000
1	-4.645767000	0.959046000	0.455164000
6	-1.288298000	1.962896000	0.037324000
6	-0.822127000	3.039773000	-0.898905000
1	-0.801684000	3.994006000	-0.363978000
1	0.205465000	2.809012000	-1.205332000
1	-1.457367000	3.110411000	-1.783860000
8	-2.219378000	1.170634000	-0.548844000
8	-0.890352000	1.809362000	1.176330000
1	2.903210000	-0.209079000	-1.538144000
6	3.092605000	-2.074974000	-0.431888000
1	3.146819000	-2.693557000	-1.333160000
1	4.112584000	-1.864873000	-0.087756000
1	2.555107000	-2.626333000	0.342818000
8	2.375741000	0.022247000	0.439736000
6	2.447706000	1.371158000	0.275698000
6	2.393525000	2.077022000	1.598211000
1	2.884767000	3.048433000	1.508804000
1	1.335852000	2.233523000	1.847110000
1	2.854099000	1.479959000	2.389596000
8	2.520295000	1.906708000	-0.810351000

e_2 Head-tail (non-degenerative)

$CH_3CH(OAc)\text{-}SC(OMe)S^{\cdots}\text{-}^{\bullet}CH_2CH_2OAc$ TS

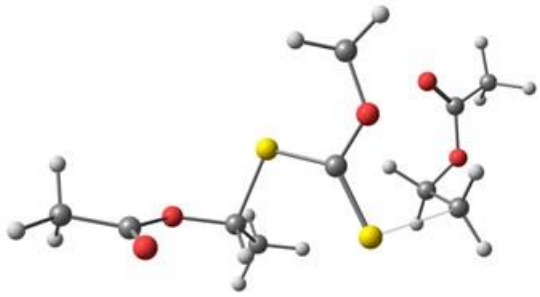

6	2.540046000	-0.980503000	1.626213000
6	2.600000000	-1.370777000	0.196440000
16	0.037699000	-0.548209000	1.997506000
6	-0.144136000	0.685336000	0.907536000
8	0.558313000	1.807988000	1.103484000
6	0.638137000	2.818384000	0.090540000
1	-0.356568000	3.201594000	-0.167950000
1	1.151197000	2.424411000	-0.793608000
16	-1.117138000	0.647043000	-0.576228000
6	-2.166296000	-0.858930000	-0.317340000
1	2.403225000	-2.436702000	0.050860000
1	1.236112000	3.616893000	0.533717000
1	-2.332828000	-0.926998000	0.763225000
1	2.717376000	-1.725249000	2.397932000
1	2.777441000	0.049040000	1.878839000
1	1.906426000	-0.779809000	-0.413014000
8	3.940691000	-1.172342000	-0.364566000
6	4.180885000	0.036720000	-0.906156000
8	3.365386000	0.935520000	-0.976806000
6	5.602382000	0.124364000	-1.400716000
1	5.736071000	1.048967000	-1.964853000
1	6.288641000	0.115133000	-0.545897000
1	5.846940000	-0.741738000	-2.023949000
6	-1.553798000	-2.107141000	-0.907124000
1	-2.226406000	-2.956499000	-0.738195000
1	-1.389043000	-1.994591000	-1.983585000
1	-0.600398000	-2.313418000	-0.412242000
8	-3.390613000	-0.601646000	-0.999395000
6	-4.390313000	-0.022592000	-0.264110000
6	-5.592638000	0.223097000	-1.131372000
1	-5.354558000	0.988269000	-1.879302000
1	-5.867747000	-0.687959000	-1.672644000
1	-6.423419000	0.562826000	-0.511125000
8	-4.289658000	0.241322000	0.909518000

$CH_3CH(OAc)\text{-}SC^{\bullet}(OMe)S\text{-}CH_2CH_2OAc$

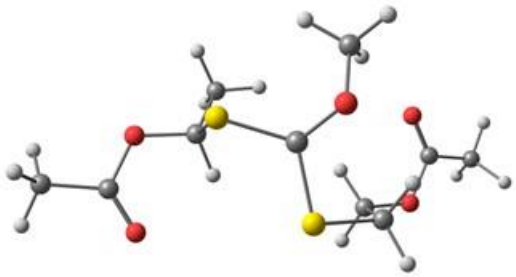

6	-2.012421000	-0.334956000	-1.621921000
6	-2.118961000	-1.324307000	-0.471687000
16	-0.267504000	0.059512000	-2.000967000
6	0.067682000	1.197458000	-0.698850000
8	-0.795690000	2.247455000	-0.630925000
6	-1.063212000	2.760603000	0.678949000
1	-0.130263000	3.002164000	1.202688000
1	-1.650441000	2.034420000	1.253808000
16	1.749297000	1.445094000	-0.231030000
6	2.028728000	-0.061301000	0.825192000

1	-1.691025000	-2.293874000	-0.742876000
1	-1.645949000	3.673111000	0.528864000
1	1.603037000	-0.911536000	0.281445000
1	-2.443739000	-0.744961000	-2.541603000
1	-2.521808000	0.603167000	-1.381341000
1	-1.610001000	-0.929452000	0.413508000
8	-3.498837000	-1.588104000	-0.152030000
6	-4.071759000	-0.762206000	0.753397000
8	-3.493477000	0.154338000	1.299551000
6	-5.509589000	-1.143554000	0.982472000
1	-5.944481000	-0.487685000	1.738127000
1	-6.071971000	-1.057593000	0.046042000
1	-5.576155000	-2.187820000	1.306144000
6	1.477278000	0.082278000	2.225272000
1	1.650752000	-0.841465000	2.791307000
1	1.958995000	0.914102000	2.749935000
1	0.398935000	0.267482000	2.184909000
8	3.444033000	-0.211497000	0.910303000
6	4.016080000	-1.165748000	0.117179000
6	5.512211000	-1.122255000	0.256362000
1	5.893191000	-0.203856000	-0.205350000
1	5.800766000	-1.101663000	1.312101000
1	5.948601000	-1.988894000	-0.242634000
8	3.389801000	-1.924118000	-0.584566000

$CH_3CH(OAc)^{\bullet}\cdots SC(OMe)S\text{-}CH_2CH_2OAc$ TS

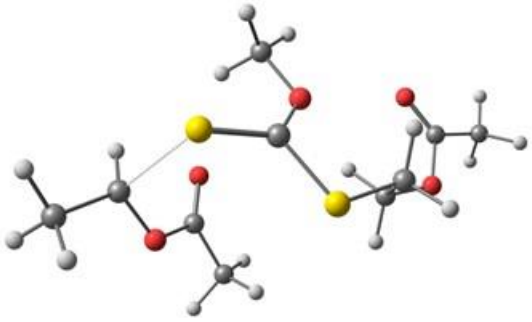

6	1.860870000	-0.736996000	-1.401607000
6	2.190774000	0.618716000	-0.793178000
16	0.081408000	-0.940065000	-1.768784000
6	-0.621634000	-1.353390000	-0.197375000
8	0.273400000	-1.273797000	0.793658000
6	-0.168326000	-1.504130000	2.137410000
1	-0.609756000	-2.502268000	2.230570000
1	-0.899858000	-0.741072000	2.419604000
16	-2.230310000	-1.725237000	-0.073418000
6	-3.608988000	0.308464000	0.428050000
1	1.862557000	1.430937000	-1.448917000
1	0.735928000	-1.417625000	2.742512000
1	-3.450100000	0.284885000	1.503514000
1	2.362548000	-0.857356000	-2.369132000
1	2.178195000	-1.543395000	-0.734710000
1	1.726083000	0.716123000	0.192090000
8	3.617028000	0.783101000	-0.678651000
6	4.187660000	0.286942000	0.446864000
8	3.573202000	-0.279394000	1.324041000
6	5.671015000	0.545232000	0.442160000
1	6.113230000	0.139580000	1.353348000
1	6.131249000	0.079942000	-0.436442000
1	5.865037000	1.621550000	0.378484000
6	-4.919961000	-0.047865000	-0.170124000
1	-5.679733000	0.727773000	0.022575000
1	-4.835044000	-0.172938000	-1.255425000
1	-5.284806000	-0.986623000	0.260432000
8	-2.984883000	1.355557000	-0.212531000
6	-1.915135000	1.940314000	0.401724000
6	-1.341088000	3.018381000	-0.472054000
1	-0.899226000	2.563944000	-1.367083000
1	-2.126868000	3.702991000	-0.808129000
1	-0.574855000	3.564670000	0.080462000
8	-1.509157000	1.611997000	1.496014000

e_3 Tail-tail (degenerative)

$AcOCH_2CH_2\text{-}SC(OMe)S^{\cdots\bullet}CH_2CH_2OAc$ TS

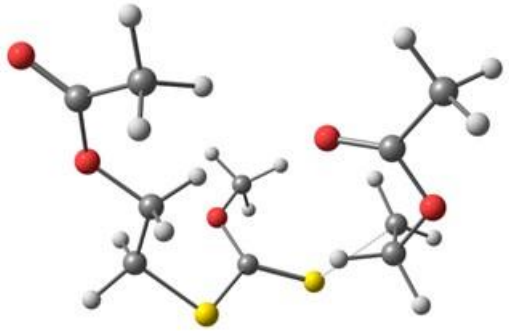

6	1.174883000	-2.093457000	-1.027259000
6	1.775069000	-0.770839000	-0.574634000
16	-0.566135000	-1.897719000	-1.542925000
6	-1.452006000	-1.873738000	-0.018638000
8	-0.707078000	-2.264287000	1.023543000
6	-1.327877000	-2.335933000	2.312697000
1	-2.157667000	-3.050392000	2.296852000
1	-1.705066000	-1.353890000	2.614942000
16	-3.029427000	-1.376418000	0.026507000
6	-2.960954000	1.164792000	0.490276000
1	1.801063000	-0.060660000	-1.411715000
1	-0.538546000	-2.671408000	2.988223000
1	-2.392510000	1.081336000	1.412644000
6	-0.543548000	3.124209000	0.088368000
1	1.700350000	-2.482932000	-1.906352000
1	1.234882000	-2.840350000	-0.231581000
1	-4.033047000	1.315423000	0.590582000
6	-2.252725000	1.668602000	-0.712272000
1	-2.917571000	1.757728000	-1.574748000
1	-1.399159000	1.033879000	-0.972298000
8	-1.743778000	3.029984000	-0.506651000
6	-0.138928000	4.565519000	0.257103000
1	-0.841645000	5.069274000	0.930453000
1	0.868965000	4.618070000	0.671862000
1	-0.180925000	5.087471000	-0.704599000
8	0.119496000	2.167167000	0.446669000
1	1.170160000	-0.327443000	0.225757000
8	3.092342000	-1.071680000	-0.106984000
6	3.949977000	-0.077829000	0.266306000
8	5.016980000	-0.391942000	0.735803000
6	3.515875000	1.349375000	0.034883000
1	4.269425000	2.003586000	0.476433000
1	3.458456000	1.555705000	-1.041935000
1	2.529543000	1.572660000	0.458155000

$AcOCH_2CH_2\text{-}SC^{\bullet}(OMe)S\text{-}CH_2CH_2OAc$

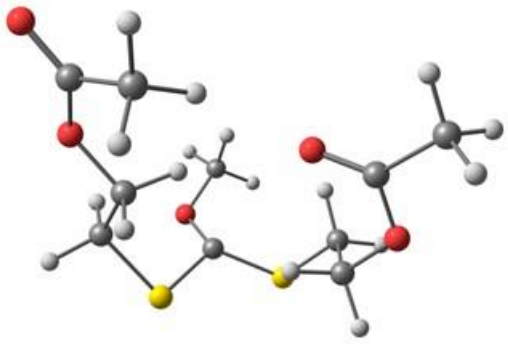

6	1.105603000	-2.165526000	-0.857540000
6	1.785960000	-0.831348000	-0.597178000
16	-0.599212000	-1.942185000	-1.482278000
6	-1.469632000	-1.680107000	0.023882000
8	-1.231282000	-2.630513000	0.970448000
6	-1.496689000	-2.265996000	2.324173000
1	-2.548936000	-1.987125000	2.457359000
1	-0.852751000	-1.432538000	2.635434000
16	-3.050503000	-0.893556000	-0.066419000
6	-2.615598000	0.844962000	0.344169000
1	1.909013000	-0.279722000	-1.539290000
1	-1.269238000	-3.151432000	2.922411000
1	-1.949684000	0.848254000	1.212284000
6	-0.484601000	3.132262000	0.145948000
1	1.642946000	-2.738875000	-1.620466000
1	1.059232000	-2.768959000	0.053363000
1	-3.560723000	1.327013000	0.622213000
6	-1.969434000	1.560771000	-0.830167000
1	-2.658030000	1.627733000	-1.677171000
1	-1.055914000	1.045017000	-1.140024000
8	-1.660342000	2.927543000	-0.482557000
6	-0.271249000	4.595523000	0.422037000
1	-1.123419000	5.004423000	0.975059000
1	0.648134000	4.729967000	0.993830000
1	-0.204260000	5.145566000	-0.523409000
8	0.290607000	2.241833000	0.436859000
1	1.179796000	-0.214984000	0.079774000
8	3.055580000	-1.133486000	-0.009135000
6	3.960341000	-0.149637000	0.259729000
8	4.989098000	-0.454445000	0.814045000
6	3.620964000	1.256111000	-0.174493000
1	4.426139000	1.912781000	0.158915000
1	3.545369000	1.314119000	-1.267894000
1	2.664494000	1.601069000	0.236120000

(f) $PVDF_H$-XA reactivation

f_1 By VAc (head)

CH_3CF_2-SC(OMe)S···•$CH(OAc)CH_3$ TS

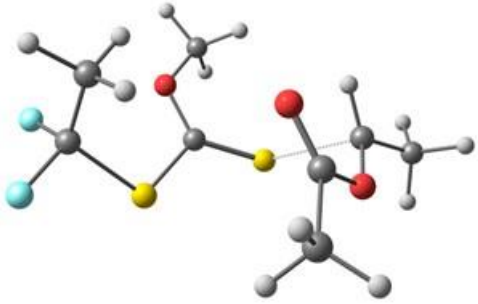

6	2.631789000	0.626291000	-0.004428000
6	2.245614000	0.952316000	1.412421000
16	1.237574000	0.183351000	-1.149409000
6	0.438628000	-1.210421000	-0.420109000
8	1.190649000	-1.836660000	0.500124000
6	0.660599000	-3.018859000	1.104559000
1	0.456753000	-3.779652000	0.343124000
1	-0.265552000	-2.799011000	1.646731000
16	-1.099380000	-1.608451000	-0.888296000
6	-2.867047000	-0.312835000	0.346836000
1	1.870910000	0.056296000	1.909685000
1	1.467682000	1.718290000	1.433283000
1	3.140978000	1.309913000	1.933114000
9	3.590601000	-0.332482000	-0.028429000
9	3.156826000	1.731873000	-0.615829000
1	1.437841000	-3.359358000	1.791940000
1	-2.461394000	-0.464299000	1.344458000
6	-4.094682000	-1.009228000	-0.113766000
1	-4.198041000	-0.946472000	-1.203751000
1	-4.058109000	-2.064834000	0.173447000
1	-5.000723000	-0.565739000	0.330669000
6	-1.861329000	1.809714000	0.480968000
6	-1.788312000	3.119120000	-0.246631000
1	-1.393393000	3.886638000	0.422064000
1	-1.101772000	3.007067000	-1.095582000
1	-2.765098000	3.412634000	-0.640465000
8	-2.771353000	0.980152000	-0.113920000
8	-1.201745000	1.488885000	1.445518000

CH_3CF_2-SC•(OMe)S-$CH(OAc)CH_3$

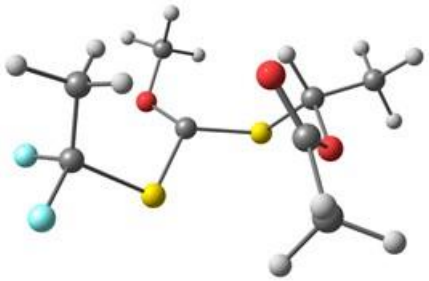

6	2.446529000	0.687510000	0.057042000
6	2.024708000	0.774162000	1.498028000
16	1.132993000	0.180444000	-1.149749000
6	0.358864000	-1.165179000	-0.329670000
8	1.214652000	-2.152369000	0.055545000
6	0.727989000	-3.100497000	1.004515000
1	-0.088126000	-3.700217000	0.585318000
1	0.376139000	-2.598837000	1.915963000
16	-1.284003000	-1.568720000	-0.840820000
6	-2.306785000	-0.470065000	0.229808000
1	1.771519000	-0.221749000	1.868041000
1	1.158881000	1.429962000	1.614074000
1	2.872203000	1.162997000	2.073007000
9	3.526355000	-0.129229000	-0.063293000
9	2.831113000	1.916014000	-0.404318000
1	1.578959000	-3.743813000	1.240409000
1	-1.842546000	-0.425366000	1.219239000
6	-3.725861000	-1.003885000	0.262880000
1	-4.150842000	-1.049569000	-0.745941000
1	-3.750579000	-2.005939000	0.702223000
1	-4.349660000	-0.337493000	0.868580000
6	-1.748799000	1.843432000	0.400110000
6	-1.769520000	3.132116000	-0.370713000
1	-1.560179000	3.964449000	0.303470000
1	-0.991820000	3.088408000	-1.142539000
1	-2.730213000	3.272570000	-0.874509000
8	-2.337107000	0.852161000	-0.319532000
8	-1.269737000	1.689006000	1.503771000

$CH_3CF_2^{\bullet\cdots}SC(OMe)S\text{-}CH(OAc)CH_3$ TS

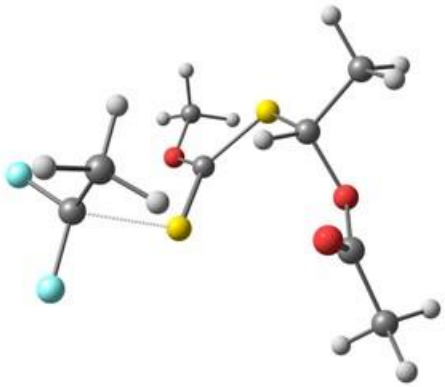

6	-2.605402000	-1.237757000	0.342422000
6	-1.915576000	-1.896165000	1.483795000
16	-0.887221000	0.093253000	-1.049302000
6	-0.334732000	1.549934000	-0.510241000
8	-1.000952000	2.670340000	-0.843101000
6	-0.581430000	3.951332000	-0.370650000
1	0.426755000	4.197460000	-0.727342000
1	-0.610403000	4.001897000	0.725158000
16	1.084004000	1.821781000	0.543166000
6	1.657979000	0.126508000	0.877225000
1	-1.622629000	-1.141539000	2.219359000
1	-1.021724000	-2.417318000	1.129329000
1	-2.583832000	-2.620792000	1.975176000
9	-3.622263000	-0.435194000	0.679503000
9	-2.989002000	-2.070809000	-0.634342000
1	-1.299430000	4.660021000	-0.788606000
1	0.782002000	-0.495127000	1.087958000
6	2.627844000	0.154035000	2.045426000
1	3.509974000	0.760811000	1.814790000
1	2.145594000	0.552045000	2.944217000
1	2.950265000	-0.872579000	2.247986000
6	2.132643000	-1.708395000	-0.529792000
6	2.692246000	-2.080650000	-1.872504000
1	2.782406000	-3.165957000	-1.942106000
1	2.005780000	-1.722743000	-2.649000000
1	3.660966000	-1.600176000	-2.039327000
8	2.304890000	-0.378804000	-0.294626000
8	1.594275000	-2.463483000	0.250235000

f_2 By VAc (tail)

$CH_3CF_2\text{-}SC(OMe)S^{\cdots\bullet}CH_2CH_2OAc$ TS

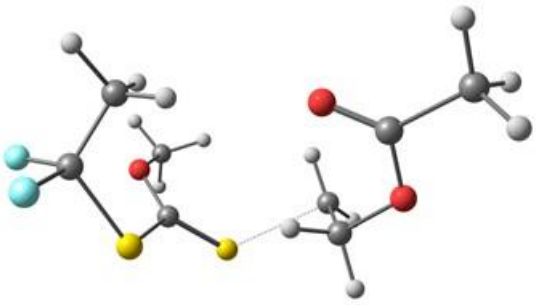

6	-1.986383000	-1.704741000	-0.103089000
6	-1.101769000	-1.951224000	1.088143000
16	-1.460683000	-0.309307000	-1.217688000
6	-1.427676000	1.127251000	-0.199055000
8	-2.159570000	1.010754000	0.915439000
6	-2.234085000	2.141694000	1.791874000
1	-2.669622000	2.999338000	1.268534000
1	-1.239326000	2.414517000	2.159599000
16	-0.532626000	2.437598000	-0.664103000
6	1.917944000	1.937660000	0.083007000
1	-0.057669000	-2.058107000	0.784283000
1	-2.877682000	1.820413000	2.613095000
1	1.660718000	1.621389000	1.090491000
6	3.458109000	-0.789031000	0.328245000
1	2.299245000	2.949907000	-0.029829000
6	2.296592000	0.890903000	-0.899154000
1	2.487677000	1.308744000	-1.890653000
1	1.529545000	0.113262000	-0.968658000
8	3.558927000	0.242038000	-0.531793000
6	4.816426000	-1.372547000	0.621946000
1	5.470391000	-0.603830000	1.048032000
1	4.712896000	-2.204066000	1.320913000
1	5.284986000	-1.719319000	-0.305582000
8	2.411592000	-1.190203000	0.798830000
1	-1.185695000	-1.119321000	1.790033000
1	-1.444185000	-2.869426000	1.578279000
9	-1.945058000	-2.771743000	-0.954530000
9	-3.277262000	-1.548997000	0.278840000

$CH_3CF_2\text{-}SC^{\bullet}(OMe)S\text{-}CH_2CH_2OAc$

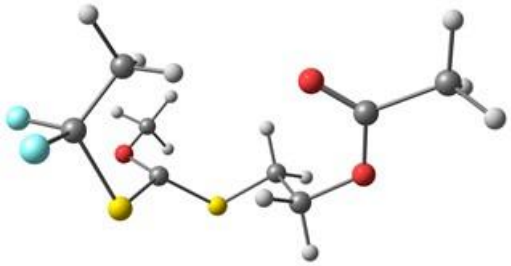

6	-1.924309000	-1.695600000	-0.051083000
6	-1.037428000	-1.807435000	1.159081000
16	-1.515169000	-0.315692000	-1.223349000
6	-1.303567000	1.043480000	-0.134993000
8	-2.412857000	1.348417000	0.592598000
6	-2.250021000	2.220073000	1.710345000
1	-1.991896000	3.236028000	1.390669000
1	-1.471862000	1.848264000	2.390096000
16	-0.174317000	2.320791000	-0.600193000
6	1.430330000	1.651830000	-0.005723000
1	0.015177000	-1.874656000	0.873870000
1	-3.215942000	2.224937000	2.221053000
1	1.279010000	1.184865000	0.971849000
6	3.434563000	-0.722862000	0.343753000
1	2.080503000	2.526720000	0.116987000
6	2.048071000	0.668162000	-0.987837000
1	2.191081000	1.133643000	-1.967355000
1	1.420524000	-0.221505000	-1.092671000
8	3.368719000	0.286410000	-0.553360000
6	4.866209000	-1.043947000	0.678661000
1	5.388845000	-0.142517000	1.015723000
1	4.895768000	-1.809828000	1.455094000
1	5.384592000	-1.404021000	-0.217164000
8	2.463214000	-1.288174000	0.801764000
1	-1.179253000	-0.934752000	1.801292000
1	-1.331862000	-2.705960000	1.712378000
9	-1.815271000	-2.810607000	-0.832216000
9	-3.225685000	-1.611418000	0.332617000

$CH_3CF_2^{\bullet\cdots}SC(OMe)S\text{-}CH_2CH_2OAc$ TS

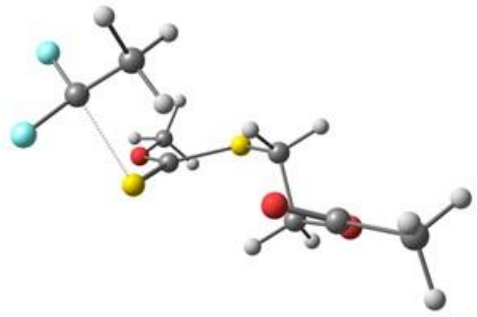

6	1.360508000	2.537070000	0.225118000
6	0.205969000	2.675628000	1.152092000
16	1.141405000	0.311829000	-1.071980000
6	1.635829000	-1.090446000	-0.361449000
8	2.913809000	-1.487045000	-0.502385000
6	3.406819000	-2.656800000	0.151987000
1	2.879052000	-3.557601000	-0.186555000
1	3.325680000	-2.567781000	1.242567000
16	0.643273000	-2.168492000	0.663800000
6	-0.952675000	-1.307525000	0.750962000
1	-0.727999000	2.479622000	0.617736000
1	4.458930000	-2.722625000	-0.133163000
1	-0.769423000	-0.242576000	0.922366000
6	-3.527225000	0.128197000	-0.140049000
1	-1.438215000	-1.740075000	1.634599000
6	-1.836315000	-1.509659000	-0.474278000
1	-1.859180000	-2.561681000	-0.772545000
1	-1.480540000	-0.888364000	-1.301701000
8	-3.206962000	-1.186828000	-0.168361000
6	-5.001144000	0.308228000	0.108051000
1	-5.309935000	-0.248760000	0.998811000
1	-5.222263000	1.369684000	0.229702000
1	-5.569802000	-0.091939000	-0.739120000
8	-2.725956000	1.022738000	-0.304081000
1	0.307885000	1.957953000	1.971132000
1	0.171959000	3.690095000	1.580047000
9	1.332216000	3.361094000	-0.830454000
9	2.565703000	2.586860000	0.807233000

f_3 By NVP (head)

CH_3CF_2-SC$^{\bullet}$(OMe)S-CH(N-pyr)CH_3

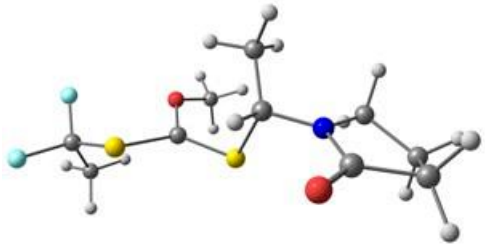

9	-4.475546000	-1.782985000	0.056268000
9	-4.216662000	0.182062000	0.982559000
6	-3.826694000	-0.587353000	-0.066400000
6	-1.194625000	0.430283000	-0.273274000
6	3.608193000	-1.236354000	0.017725000
6	3.616002000	1.143150000	0.060689000
6	5.001423000	-0.785819000	-0.401153000
6	4.822560000	0.686994000	-0.778640000
1	3.929895000	1.573952000	1.024707000
1	2.998055000	1.887407000	-0.456510000
1	5.672349000	-0.916945000	0.459522000
1	5.378340000	-1.420526000	-1.208074000
1	5.709054000	1.300086000	-0.589548000
1	4.577561000	0.771522000	-1.844047000
8	3.200463000	-2.376020000	0.153695000
7	2.869400000	-0.091423000	0.264695000
6	1.190166000	0.715782000	1.891641000
1	1.776340000	0.381578000	2.757494000
1	1.420485000	1.770362000	1.701352000
1	0.128856000	0.639881000	2.146941000
6	-4.203070000	0.079295000	-1.362890000
1	-3.670023000	1.027016000	-1.464162000
1	-3.957572000	-0.569954000	-2.206418000
1	-5.281220000	0.272423000	-1.349623000
16	-2.041489000	-1.058879000	0.098207000
8	-1.726077000	1.540536000	0.320964000
6	-1.277224000	2.808196000	-0.149376000
1	-0.218110000	2.967632000	0.083678000
1	-1.417314000	2.898751000	-1.234539000
16	0.441756000	0.322063000	-0.838958000
6	1.511554000	-0.153910000	0.691986000
1	1.299074000	-1.211652000	0.879202000
1	-1.890767000	3.548083000	0.370597000

$CH_3CF_2^{\bullet\cdots}$SC(OMe)S-CH(N-pyr)CH_3 TS

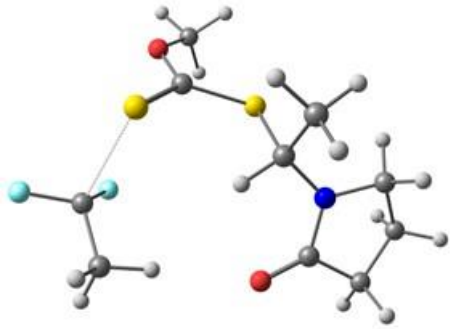

9	4.013539000	1.879536000	-0.002503000
9	2.456517000	1.199403000	-1.386386000
6	2.694415000	1.711120000	-0.169118000
6	1.400784000	-1.424773000	0.177849000
6	-2.434791000	1.368968000	-0.203875000
6	-3.582678000	-0.692541000	0.078857000
6	-3.843992000	1.567398000	-0.744354000
6	-4.373022000	0.144441000	-0.942568000
1	-4.120489000	-0.786742000	1.035079000
1	-3.368728000	-1.705428000	-0.285320000
1	-4.418454000	2.125712000	0.008120000
1	-3.819857000	2.174954000	-1.653287000
1	-5.453865000	0.052814000	-0.799452000
1	-4.138166000	-0.201453000	-1.956054000
8	-1.543107000	2.199554000	-0.139798000
7	-2.351512000	0.069377000	0.249150000
6	-1.428767000	-1.134870000	2.202220000
1	-1.917879000	-0.440398000	2.896836000
1	-2.063194000	-2.019354000	2.078574000
1	-0.476236000	-1.445884000	2.641261000
6	1.855378000	2.881014000	0.196221000
1	0.795232000	2.635291000	0.084734000
1	2.052374000	3.164961000	1.234041000
1	2.091287000	3.741488000	-0.450760000
16	2.003242000	-0.394017000	1.315621000
8	2.253232000	-2.219511000	-0.493500000
6	1.798534000	-3.069643000	-1.546518000
1	1.075063000	-3.808823000	-1.179924000
1	1.352586000	-2.486810000	-2.362266000
16	-0.300484000	-1.567535000	-0.324540000
6	-1.168426000	-0.432061000	0.879896000
1	-0.482871000	0.413819000	1.010385000
1	2.693540000	-3.580052000	-1.908587000

f_4 By MA (head)

CH_3CF_2- SC$^{\bullet}$(OMe)S-CH(COOMe)CH_3

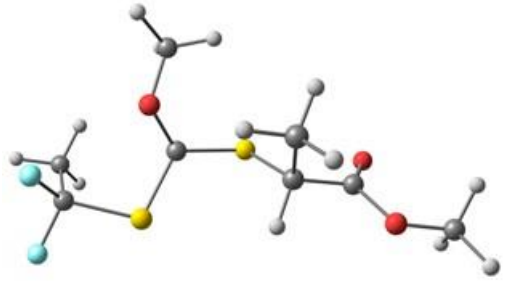

9	-3.932043000	-1.950021000	0.060452000
9	-3.675019000	-0.104041000	1.205799000
6	-3.356084000	-0.711850000	0.034819000
6	-0.808563000	0.477729000	-0.282704000
6	1.859448000	0.786550000	1.614990000
1	2.486457000	0.343766000	2.397977000
1	2.238944000	1.788842000	1.386178000
1	0.838316000	0.877736000	1.998681000
6	-3.887869000	0.088379000	-1.124199000
1	-3.414028000	1.072088000	-1.147492000
1	-3.693008000	-0.432518000	-2.064433000
1	-4.967814000	0.212418000	-0.989514000
16	-1.542909000	-1.092924000	-0.029245000
8	-1.311769000	1.470222000	0.510282000
6	-1.010347000	2.813684000	0.134097000
1	0.065466000	3.012477000	0.193421000
1	-1.352758000	3.019492000	-0.888519000
16	0.781865000	0.538821000	-1.003058000
6	1.876482000	-0.098438000	0.369559000
1	1.533648000	-1.107735000	0.627585000
8	3.658657000	0.327979000	-1.230863000
6	3.271801000	-0.209785000	-0.216304000
1	-1.550556000	3.445199000	0.843399000
8	4.046794000	-0.983364000	0.568507000
6	5.402757000	-1.127552000	0.122504000
1	5.900064000	-0.153186000	0.079410000
1	5.887195000	-1.774216000	0.856292000
1	5.433113000	-1.583146000	-0.872367000

$CH_3CF_2^{\bullet\cdots}SC(OMe)S-CH(COOMe)CH_3$ TS

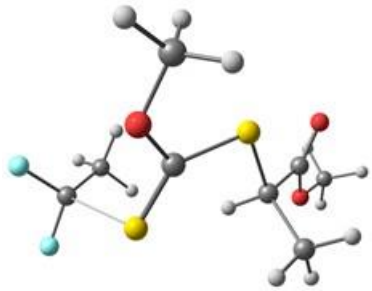

9	-3.308292000	-2.370953000	0.749848000
9	-3.903741000	-0.930722000	-0.790903000
6	-2.871230000	-1.582903000	-0.243728000
6	-0.855021000	1.380300000	0.274497000
6	2.003966000	0.482083000	1.976648000
1	2.462588000	-0.381762000	2.470426000
1	2.716633000	1.313690000	1.979181000
1	1.113322000	0.771777000	2.542371000
6	-1.974043000	-2.254756000	-1.222299000
1	-1.579794000	-1.518710000	-1.928515000
1	-1.140682000	-2.726624000	-0.695472000
1	-2.519540000	-3.027305000	-1.786923000
16	-1.518258000	0.146432000	1.154373000
8	-1.645954000	2.405860000	-0.088052000
6	-1.141605000	3.494158000	-0.865380000
1	-0.328103000	4.013426000	-0.344341000
1	-0.792666000	3.153930000	-1.848716000
16	0.810093000	1.483505000	-0.350296000
6	1.602902000	0.103313000	0.548923000
1	0.864429000	-0.708773000	0.586998000
8	3.308669000	0.284272000	-1.182639000
6	2.802517000	-0.334640000	-0.271841000
1	-1.989869000	4.169755000	-0.993416000
8	3.255723000	-1.519334000	0.177681000
6	4.423889000	-2.013364000	-0.493011000
1	5.254436000	-1.307627000	-0.390579000
1	4.662672000	-2.961408000	-0.007934000
1	4.219751000	-2.165806000	-1.557599000

f_5 By DMA (head)

CH_3CF_2-SC$^{\bullet}$(OMe)S-CH($CONMe_2$)CH_3

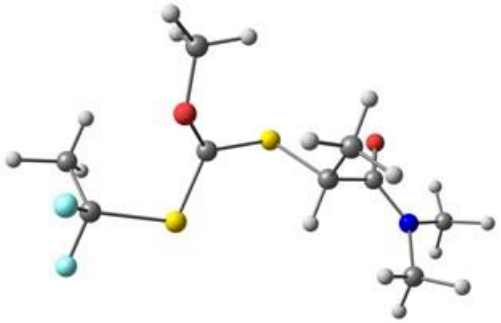

9	-3.948484000	-2.137986000	-0.230803000
9	-3.811275000	-0.495439000	1.207620000
6	-3.485632000	-0.863914000	-0.058060000
6	-1.063489000	0.596398000	-0.254052000
6	1.678910000	1.052520000	1.626442000
1	2.332975000	0.613554000	2.392206000
1	2.050546000	2.056582000	1.395135000
1	0.670990000	1.132452000	2.046891000
6	-4.133686000	0.064911000	-1.049973000
1	-3.750704000	1.078898000	-0.917576000
1	-3.932278000	-0.271536000	-2.069575000
1	-5.213907000	0.061542000	-0.868458000
16	-1.650891000	-1.056162000	-0.228578000
8	-1.648828000	1.416814000	0.670876000
6	-1.489611000	2.821776000	0.472208000
1	-0.437228000	3.118497000	0.542512000
1	-1.876770000	3.123904000	-0.509792000
16	0.512051000	0.897038000	-0.944097000
6	1.661900000	0.196768000	0.362204000
1	1.282854000	-0.807323000	0.578624000
8	3.319537000	1.013979000	-1.150278000
6	3.033520000	0.162016000	-0.311192000
7	3.917351000	-0.813582000	0.068625000
6	3.690336000	-1.835057000	1.069493000
1	4.504442000	-1.824095000	1.807908000
1	2.754271000	-1.673734000	1.604807000
1	3.661972000	-2.836002000	0.613891000
6	5.216572000	-0.857575000	-0.577683000
1	5.367037000	-1.829593000	-1.067622000
1	5.255135000	-0.061245000	-1.322610000
1	6.020101000	-0.711657000	0.157773000
1	-2.070220000	3.298245000	1.265837000

$CH_3CF_2^{\bullet\cdots}SC(OMe)S-CH(CONMe_2)CH_3$ TS

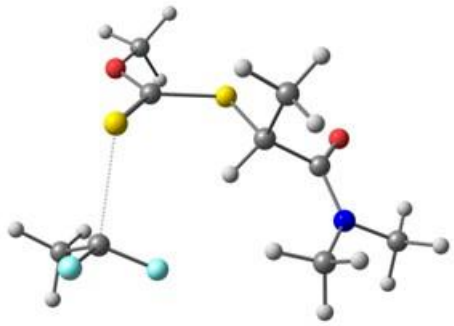

9	0.714187000	2.336078000	-0.692617000
9	2.309871000	3.052832000	0.629650000
6	1.993559000	2.139690000	-0.300010000
6	1.508887000	-1.352628000	0.266536000
6	-1.389988000	-0.739676000	2.078307000
1	-1.963449000	0.091497000	2.507995000
1	-1.962992000	-1.663140000	2.211403000
1	-0.443764000	-0.815224000	2.622583000
6	2.962956000	2.023181000	-1.420548000
1	3.957913000	1.812273000	-1.020469000
1	2.667401000	1.201941000	-2.079156000
1	3.001615000	2.953890000	-2.008194000
16	1.972363000	-0.010164000	1.122362000
8	2.473622000	-2.161773000	-0.213171000
6	2.145642000	-3.331864000	-0.966277000
1	1.537175000	-4.027790000	-0.375563000
1	1.615335000	-3.075382000	-1.892061000
16	-0.140170000	-1.839999000	-0.164546000
6	-1.121957000	-0.487727000	0.593892000
1	-0.512259000	0.411292000	0.462836000
8	-2.868399000	-1.502113000	-0.685605000
6	-2.432779000	-0.461941000	-0.192458000
7	-3.104940000	0.726171000	-0.271391000
6	-2.687569000	1.985381000	0.314277000
1	-3.236850000	2.201827000	1.243221000
1	-1.617843000	2.001699000	0.524689000
1	-2.893438000	2.797384000	-0.394726000
6	-4.417954000	0.732065000	-0.892071000
1	-4.444695000	1.454927000	-1.718453000
1	-4.621885000	-0.269557000	-1.273665000
1	-5.190703000	1.010979000	-0.161710000
1	3.104831000	-3.795178000	-1.207045000

(g) $PVDF_T$-XA reactivation

g_1 By VAc (head)

CHF_2CH_2-SC(OMe)S···•CH(OAc)CH_3 TS

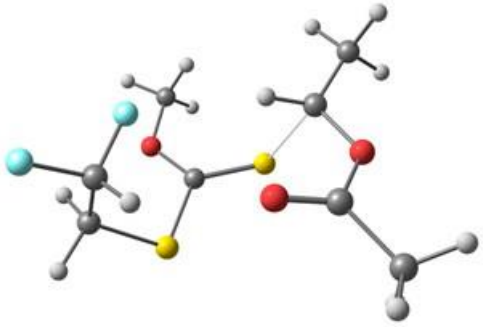

6	-2.456219000	-1.184842000	-0.558141000
6	-1.785572000	-1.705876000	0.698885000
16	-1.284594000	-0.357433000	-1.685112000
6	-0.949761000	1.159089000	-0.838840000
8	-2.035850000	1.630968000	-0.204965000
6	-1.895098000	2.813913000	0.581560000
1	-1.565173000	3.654137000	-0.039183000
1	-1.169687000	2.658153000	1.387771000
16	0.559162000	1.836606000	-0.859586000
6	1.990764000	0.702654000	0.928572000
1	-0.899851000	-2.320118000	0.502317000
1	-2.888509000	3.003824000	0.993958000
1	1.155196000	0.155267000	1.358067000
6	2.628533000	1.849840000	1.622257000
1	3.252991000	2.433104000	0.934770000
1	1.862435000	2.509710000	2.040066000
1	3.276147000	1.510579000	2.448154000
6	2.518763000	-1.346005000	-0.109036000
6	3.535671000	-1.957929000	-1.027353000
1	4.551769000	-1.675910000	-0.736683000
1	3.420825000	-3.043455000	-1.025994000
1	3.365198000	-1.584823000	-2.045062000
8	2.883943000	-0.069958000	0.225098000
8	1.502405000	-1.873648000	0.283888000
1	-3.277137000	-0.513204000	-0.291449000
1	-2.859964000	-2.031381000	-1.123965000
9	-2.702003000	-2.439671000	1.402011000
9	-1.402863000	-0.661063000	1.497191000

CHF_2CH_2-SC•(OMe)S-CH(OAc)CH_3

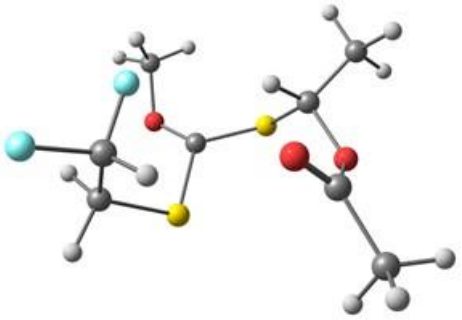

6	2.240232000	1.067198000	-0.776957000
6	1.847419000	1.628313000	0.574579000
16	0.879978000	0.227872000	-1.661288000
6	0.689680000	-1.210031000	-0.675659000
8	1.808263000	-1.973473000	-0.550257000
6	1.979074000	-2.640484000	0.704397000
1	1.142621000	-3.319815000	0.908135000
1	2.066812000	-1.905542000	1.512719000
16	-0.895799000	-1.952926000	-0.520195000
6	-1.741969000	-0.790290000	0.635128000
1	0.942198000	2.245479000	0.555835000
1	2.904998000	-3.213954000	0.613272000
1	-0.970087000	-0.266324000	1.206941000
6	-2.714621000	-1.552750000	1.514190000
1	-3.456048000	-2.086338000	0.908920000
1	-2.181453000	-2.277535000	2.136923000
1	-3.244507000	-0.849243000	2.166383000
6	-2.191675000	1.480913000	0.036726000
6	-2.990002000	2.322386000	-0.919570000
1	-2.928692000	3.370859000	-0.622988000
1	-2.572810000	2.204325000	-1.926830000
1	-4.032215000	1.991313000	-0.954298000
8	-2.488137000	0.168939000	-0.132111000
8	-1.387432000	1.902742000	0.841074000
9	1.637307000	0.608649000	1.467493000
9	2.893501000	2.371681000	1.050073000
1	2.553020000	1.890716000	-1.427887000
1	3.081649000	0.376750000	-0.658153000

CHF_2CH_2•···SC(OMe)S-CH(OAc)CH_3 TS

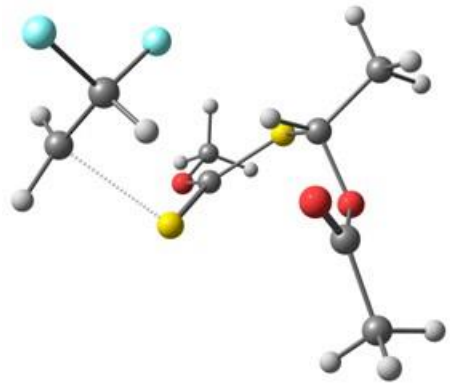

6	1.598314000	-2.434420000	-0.830300000
6	2.347515000	-1.670857000	0.189020000
16	-0.307153000	-0.742437000	-1.527901000
6	-1.620392000	-0.708380000	-0.529641000
8	-2.645075000	-1.538582000	-0.776395000
6	-3.797347000	-1.571779000	0.071383000
1	-4.316072000	-0.605211000	0.072353000
1	-3.526378000	-1.850298000	1.097098000
16	-1.836597000	0.321248000	0.903183000
6	-0.249860000	1.215963000	1.015189000
1	2.674847000	-0.678899000	-0.145779000
1	-4.446576000	-2.336500000	-0.359485000
1	0.555174000	0.494729000	0.854055000
6	-0.155876000	1.860543000	2.386524000
1	-0.961786000	2.585080000	2.545693000
1	-0.191143000	1.101495000	3.174489000
1	0.804374000	2.382665000	2.452619000
6	0.989641000	2.418499000	-0.599776000
6	0.850543000	3.370309000	-1.753719000
1	1.840030000	3.698125000	-2.076520000
1	0.349421000	2.853715000	-2.580762000
1	0.231342000	4.229132000	-1.477113000
8	-0.218812000	2.214993000	-0.006625000
8	2.017690000	1.894637000	-0.231707000
9	1.568106000	-1.500789000	1.313280000
9	3.465283000	-2.370833000	0.597775000
1	1.994794000	-2.471931000	-1.840557000
1	0.985826000	-3.266121000	-0.494373000

g_2 By VAc (tail)

CHF_2CH_2-SC(OMe)S$^{\cdots}$$^{\bullet}CH_2CH_2OAc$ TS

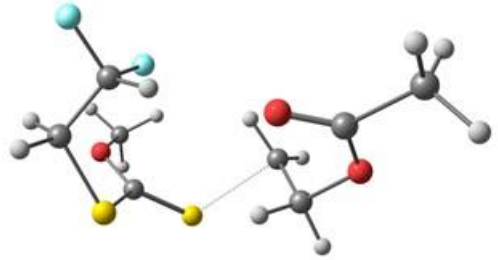

6	-1.586477000	1.899325000	0.894516000
6	-0.526845000	2.207685000	-0.148272000
16	-1.366787000	0.253017000	1.647614000
6	-1.914134000	-0.843610000	0.375112000
8	-2.865782000	-0.306816000	-0.393848000
6	-3.333624000	-1.062624000	-1.515511000
1	-3.786691000	-2.002192000	-1.181679000
1	-2.507847000	-1.284027000	-2.199546000
16	-1.240086000	-2.343889000	0.219069000
6	1.075547000	-1.786052000	-0.836300000
1	0.501437000	2.089661000	0.211834000
1	-4.075105000	-0.423868000	-1.999518000
1	0.727257000	-0.875819000	-1.317174000
6	3.437028000	0.140846000	-0.001549000
9	-0.687930000	1.388223000	-1.234409000
9	-0.715916000	3.493294000	-0.574409000
1	-1.497057000	2.613630000	1.719976000
1	-2.582642000	1.991140000	0.452815000
1	1.178553000	-2.668430000	-1.464140000
6	1.910903000	-1.655268000	0.383568000
1	2.074069000	-2.617186000	0.876568000
1	1.474476000	-0.943897000	1.090746000
8	3.265709000	-1.191536000	0.056110000
6	4.857462000	0.481479000	-0.373734000
1	5.042954000	0.188916000	-1.413821000
1	5.015325000	1.555800000	-0.264778000
1	5.563080000	-0.074032000	0.252117000
8	2.562276000	0.958341000	0.210495000

CHF_2CH_2-SC$^{\bullet}$(OMe)S-CH_2CH_2OAc

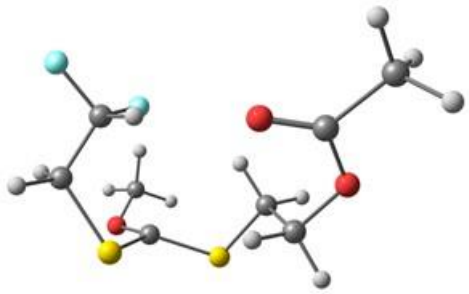

6	-1.735014000	1.773367000	0.881136000
6	-0.661367000	2.225491000	-0.086743000
16	-1.415576000	0.139085000	1.633324000
6	-1.711989000	-0.919343000	0.269021000
8	-2.964305000	-0.849368000	-0.256315000
6	-3.062636000	-1.023592000	-1.673620000
1	-2.693963000	-2.010398000	-1.978122000
1	-2.494229000	-0.240926000	-2.190001000
16	-0.746984000	-2.372213000	0.051847000
6	0.850355000	-1.667732000	-0.533767000
1	0.358342000	2.148052000	0.306435000
1	-4.125881000	-0.937420000	-1.911532000
1	0.633959000	-0.721808000	-1.038701000
6	3.317881000	0.265102000	-0.040100000
9	-0.721020000	1.480122000	-1.239870000
9	-0.915192000	3.523565000	-0.436578000
1	-1.783176000	2.480720000	1.716030000
1	-2.706821000	1.760313000	0.376897000
1	1.256020000	-2.379324000	-1.262787000
6	1.827995000	-1.467027000	0.614271000
1	2.009261000	-2.407540000	1.143386000
1	1.453246000	-0.714145000	1.314051000
8	3.116224000	-1.063000000	0.106686000
6	4.698514000	0.536458000	-0.574289000
1	4.821308000	0.059442000	-1.552983000
1	4.849107000	1.613250000	-0.664343000
1	5.452111000	0.105452000	0.093654000
8	2.492474000	1.112975000	0.229361000

$CHF_2CH_2^{\bullet\cdots}SC(OMe)S$-$CH_2CH_2OAc$ TS

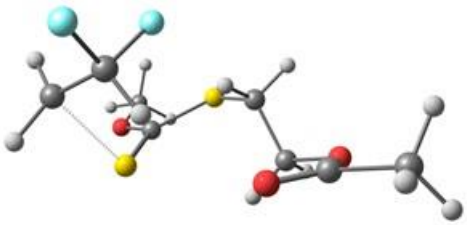

6	-0.404403000	2.913549000	0.441843000
6	0.877672000	2.610126000	-0.229117000
16	-1.197724000	0.595666000	1.356835000
6	-2.187003000	-0.303858000	0.390383000
8	-3.516602000	-0.151157000	0.493244000
6	-4.417418000	-0.878532000	-0.346790000
1	-4.320107000	-1.959999000	-0.190100000
1	-4.252403000	-0.640025000	-1.404591000
16	-1.676543000	-1.478099000	-0.845447000
6	0.134078000	-1.334742000	-0.851766000
1	1.580672000	2.032090000	0.382274000
1	-5.415034000	-0.552863000	-0.045507000
1	0.396693000	-0.272823000	-0.842574000
6	3.015939000	-1.189545000	0.355624000
9	0.644630000	1.903628000	-1.389975000
9	1.509741000	3.778176000	-0.611442000
1	-0.369157000	3.329455000	1.444431000
1	-1.252631000	3.178124000	-0.183306000
1	0.421701000	-1.761407000	-1.820826000
6	0.821377000	-2.100460000	0.271792000
1	0.451227000	-3.128302000	0.332254000
1	0.681285000	-1.586992000	1.227263000
8	2.225863000	-2.224993000	-0.019179000
6	4.451958000	-1.466693000	0.000722000
1	4.551624000	-1.594766000	-1.082858000
1	5.075154000	-0.635823000	0.334655000
1	4.783604000	-2.398934000	0.470517000
8	2.604876000	-0.189364000	0.902529000

g_3 By NVP (head)

CHF_2CH_2-SC$^{\bullet}$(OMe)S-CH(N-pyr)CH_3

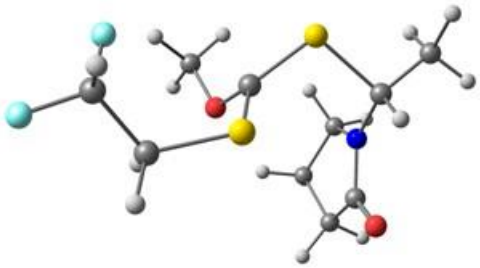

6	2.807695000	0.951856000	0.736220000
6	3.996170000	0.087651000	0.372613000
16	1.379571000	0.008089000	1.360646000
6	0.631234000	-0.546505000	-0.123075000
8	0.629989000	0.350248000	-1.155174000
6	0.908161000	-0.206296000	-2.444483000
1	0.202914000	-1.012320000	-2.683462000
1	1.933555000	-0.590868000	-2.474833000
16	-0.458124000	-1.896274000	-0.070609000
6	-2.079145000	-1.216917000	0.690007000
1	4.328378000	-0.563238000	1.192606000
1	0.791895000	0.612692000	-3.159440000
1	-1.866237000	-1.012419000	1.744399000
6	-3.101923000	-2.332813000	0.533865000
1	-3.306800000	-2.551614000	-0.520438000
1	-2.740383000	-3.252242000	1.007074000
1	-4.040822000	-2.042653000	1.020402000
9	3.704413000	-0.704371000	-0.701412000
9	5.034976000	0.901306000	0.013137000
1	3.096607000	1.638191000	1.539036000
1	2.498560000	1.537931000	-0.134703000
7	-2.470481000	0.027649000	0.123614000
6	-2.918688000	2.313562000	-0.062805000
1	-3.973329000	2.532627000	0.157004000
1	-2.346691000	3.224307000	0.135869000
6	-2.725398000	1.730674000	-1.464833000
1	-1.705647000	1.937560000	-1.808889000
1	-3.426747000	2.123019000	-2.207762000
6	-2.883113000	0.214782000	-1.258441000
1	-3.924746000	-0.112476000	-1.405753000
1	-2.245267000	-0.375326000	-1.927941000
6	-2.465169000	1.194531000	0.865773000
8	-2.179799000	1.275836000	2.048470000

$CHF_2CH_2^{\bullet\cdots}SC(OMe)S$-$CH(N\text{-}pyr)CH_3$ TS

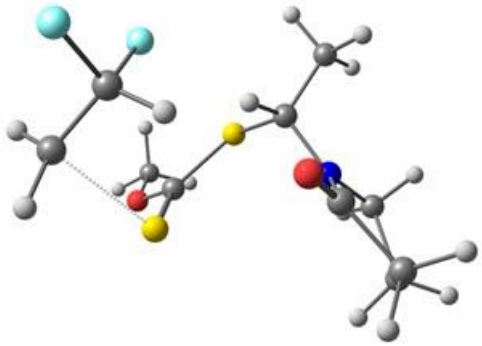

6	-3.033248000	-0.901667000	-1.020586000
6	-2.588005000	-1.780748000	0.080501000
16	-0.835912000	0.483671000	-1.573292000
6	-0.559013000	1.761819000	-0.573010000
8	-1.044720000	2.970067000	-0.908322000
6	-0.875372000	4.106494000	-0.056947000
1	0.186074000	4.349139000	0.077223000
1	-1.344342000	3.943158000	0.921076000
16	0.313058000	1.728573000	0.974642000
6	0.786394000	-0.048425000	1.219933000
1	-1.682071000	-2.355351000	-0.143976000
1	-1.376679000	4.927286000	-0.574083000
1	-0.108606000	-0.645465000	1.019798000
6	1.190068000	-0.164566000	2.690011000
1	2.051739000	0.466998000	2.936337000
1	0.356935000	0.114674000	3.342704000
1	1.455406000	-1.207669000	2.894600000
9	-2.339609000	-1.026012000	1.209955000
9	-3.589381000	-2.668124000	0.427448000
1	-3.065768000	-1.311337000	-2.025653000
1	-3.707358000	-0.083951000	-0.782310000
7	1.798379000	-0.500864000	0.313094000
6	2.956312000	-1.913257000	-1.145495000
1	3.539694000	-2.690892000	-0.632834000
1	2.725497000	-2.287241000	-2.147125000
6	3.651058000	-0.549565000	-1.116936000
1	3.346722000	0.042811000	-1.987450000
1	4.743553000	-0.612302000	-1.116386000
6	3.110243000	0.111552000	0.162138000
1	3.751378000	-0.102860000	1.032722000
1	3.017235000	1.200391000	0.071458000
6	1.670806000	-1.699972000	-0.357300000
8	0.718852000	-2.460070000	-0.282909000

g_4 By MA (head)

CHF_2CH_2- SC$^{\bullet}$(OMe)S-CH(COOMe)CH_3

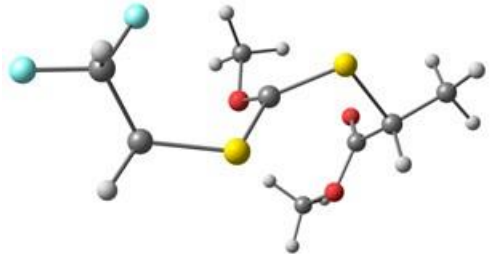

6	2.742505000	-0.665564000	-0.856574000
6	3.704023000	0.239866000	-0.115492000
16	1.258137000	0.192650000	-1.476682000
6	0.318920000	0.389793000	-0.009118000
8	0.320431000	-0.689617000	0.817342000
6	0.101400000	-0.428970000	2.210974000
1	-0.924377000	-0.088453000	2.386321000
1	0.819563000	0.314901000	2.573118000
16	-0.859430000	1.654369000	0.082038000
6	-2.480836000	0.937546000	-0.586164000
1	3.990212000	1.132216000	-0.688949000
1	0.266260000	-1.384898000	2.714162000
1	-2.371237000	0.860709000	-1.671737000
6	-3.578356000	1.910827000	-0.183883000
1	-3.705708000	1.908691000	0.902776000
1	-3.342831000	2.927550000	-0.517139000
1	-4.529584000	1.615613000	-0.642779000
6	-2.418487000	-2.732439000	-0.391234000
1	-2.227749000	-3.374249000	-1.253397000
1	-1.652470000	-2.887379000	0.375490000
1	-3.404053000	-2.939093000	0.037202000
9	3.159949000	0.649828000	1.066287000
9	4.834894000	-0.472180000	0.176256000
1	3.244066000	-1.074831000	-1.739816000
1	2.442092000	-1.490531000	-0.203812000
6	-2.695443000	-0.436991000	0.001804000
8	-3.107746000	-0.665589000	1.121538000
8	-2.350113000	-1.389268000	-0.884117000

$CHF_2CH_2^{\bullet\cdots}SC(OMe)S$-CH(COOMe)$CH_3$ TS

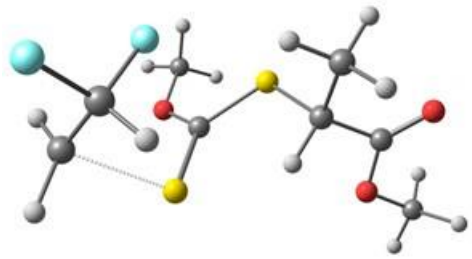

6	3.373198000	-0.101370000	1.094878000
6	3.174488000	-1.293283000	0.247725000
16	0.897567000	0.710708000	1.581868000
6	0.325646000	1.425231000	0.207131000
8	0.759489000	2.654099000	-0.101927000
6	0.314851000	3.330315000	-1.283627000
1	-0.772083000	3.474698000	-1.270993000
1	0.608539000	2.781076000	-2.186370000
16	-0.786550000	0.727405000	-0.991405000
6	-1.200284000	-0.915447000	-0.283194000
1	2.579045000	-2.080849000	0.728718000
1	0.817101000	4.299308000	-1.261341000
1	-0.704122000	-0.913037000	0.698720000
6	-0.698890000	-2.039481000	-1.176745000
1	-1.184418000	-2.012279000	-2.156776000
1	0.383938000	-1.961805000	-1.302448000
1	-0.938888000	-3.005357000	-0.716632000
6	-4.488223000	-0.244507000	1.256090000
1	-4.612827000	0.332988000	2.173710000
1	-5.009837000	0.238637000	0.423334000
1	-4.885375000	-1.257079000	1.380598000
9	2.551737000	-0.946181000	-0.929016000
9	4.385355000	-1.854204000	-0.108837000
1	3.618314000	-0.248393000	2.142391000
1	3.720899000	0.808998000	0.615761000
6	-2.709253000	-0.966333000	-0.084922000
8	-3.480416000	-1.550476000	-0.814947000
8	-3.076521000	-0.282870000	1.011948000

g_5 By DMA (head)

CHF_2CH_2-SC$^{\bullet}$(OMe)S-CH(CONMe$_2$)CH_3

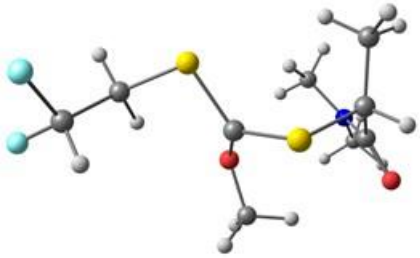

6	2.842524000	-0.488228000	0.869511000
6	0.477343000	0.169315000	-0.430577000
6	-2.125583000	2.326296000	0.811556000
1	-3.078843000	2.301954000	1.356013000
1	-1.326417000	2.076016000	1.514544000
1	-1.951312000	3.355249000	0.479729000
6	3.912152000	-0.258545000	-0.178146000
1	3.511961000	-0.201827000	-1.199885000
16	1.531532000	0.780730000	0.835791000
8	0.263525000	-1.176566000	-0.392627000
6	-0.216321000	-1.792130000	-1.595581000
1	-1.235724000	-1.468094000	-1.833037000
1	0.445053000	-1.557686000	-2.438793000
16	-0.530651000	1.271728000	-1.306081000
6	-2.182735000	1.408341000	-0.406217000
1	-2.751291000	1.912453000	-1.197020000
8	-3.556167000	-0.286782000	-1.332981000
6	-2.916565000	0.061710000	-0.339051000
7	-2.907742000	-0.696051000	0.801310000
1	3.305344000	-0.444585000	1.861149000
1	2.383356000	-1.470641000	0.731987000
9	4.807780000	-1.290514000	-0.118157000
9	4.587484000	0.893922000	0.084350000
6	-3.764013000	-1.868463000	0.839295000
1	-3.177455000	-2.791904000	0.723222000
1	-4.286958000	-1.911753000	1.803565000
1	-4.484511000	-1.803595000	0.022878000
6	-1.993732000	-0.578327000	1.919717000
1	-2.511405000	-0.249730000	2.832603000
1	-1.538637000	-1.557702000	2.117287000
1	-1.177188000	0.107747000	1.703784000
1	-0.200534000	-2.866589000	-1.396473000

$CHF_2CH_2^{\bullet\cdots}SC(OMe)S$-CH(CONMe$_2$)$CH_3$ TS

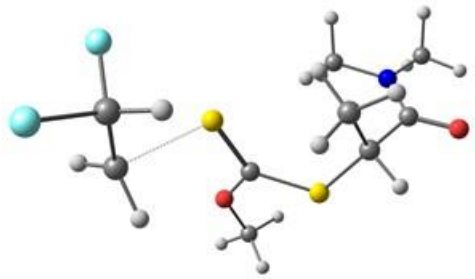

6	-3.659677000	0.308624000	-0.243969000
6	-0.276766000	1.459540000	0.206390000
6	0.495630000	-1.632112000	-1.124201000
1	0.935272000	-2.525414000	-1.585541000
1	0.205230000	-1.870422000	-0.100734000
1	-0.408499000	-1.366411000	-1.679932000
6	-3.933658000	-1.143373000	-0.239399000
1	-3.263155000	-1.719424000	-0.892075000
16	-1.270114000	0.328996000	0.891181000
8	-0.543932000	2.752743000	0.463423000
6	0.256959000	3.822490000	-0.052551000
1	1.298579000	3.732996000	0.277405000
1	0.217963000	3.856260000	-1.147958000
16	1.082999000	1.248182000	-0.910384000
6	1.541822000	-0.526761000	-1.227036000
1	1.796336000	-0.420867000	-2.287264000
8	3.797411000	-1.190652000	-1.452379000
6	2.919856000	-0.906600000	-0.638800000
7	3.120889000	-0.962461000	0.706985000
1	-4.146974000	0.913382000	0.514872000
1	-3.398681000	0.784525000	-1.184274000
9	-5.227089000	-1.394757000	-0.656789000
9	-3.829792000	-1.644591000	1.030541000
6	4.441500000	-1.325685000	1.189425000
1	4.856638000	-0.518089000	1.808161000
1	4.387705000	-2.236860000	1.800962000
1	5.088345000	-1.500437000	0.328511000
6	2.145362000	-0.672686000	1.734992000
1	2.078794000	-1.517666000	2.434485000
1	2.435220000	0.220083000	2.307888000
1	1.150532000	-0.502490000	1.321941000
1	-0.187758000	4.730001000	0.360677000

(h) $PVDF_H^{\bullet}$ addition to monomer

h_1 To VAc (tail)

$CH_3CF_2^{\bullet\cdots}CH_2$=CHOAc TS

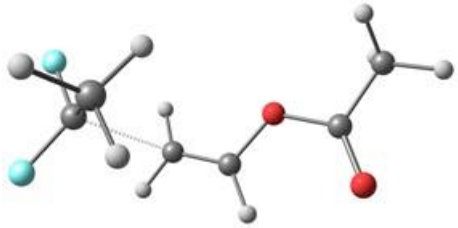

6	-2.304435000	0.200626000	0.085604000
6	-1.734179000	1.105977000	1.118348000
1	-0.971224000	1.745085000	0.666082000
1	-1.270895000	0.513112000	1.911850000
6	-0.562982000	-1.168903000	-0.865639000
1	-1.216667000	-2.007816000	-0.649618000
1	-0.743631000	-0.601125000	-1.774132000
6	0.610590000	-1.071270000	-0.210127000
1	0.917582000	-1.674682000	0.638788000
8	1.510930000	-0.090828000	-0.578164000
6	2.668503000	0.012869000	0.145203000
8	2.928934000	-0.686412000	1.096340000
6	3.536583000	1.098900000	-0.424023000
1	4.428657000	1.210218000	0.194032000
1	3.825520000	0.845893000	-1.450544000
1	2.985944000	2.044904000	-0.466038000
1	-2.515554000	1.742477000	1.560467000
9	-2.822705000	0.831186000	-0.984960000
9	-3.204309000	-0.683334000	0.554683000

CH_3CF_2-$CH_2CH^{\bullet}$(OAc)

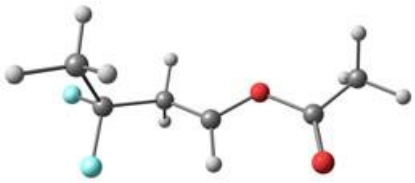

6	2.124552000	-0.045160000	0.009035000
6	2.246930000	0.045240000	1.511313000
1	2.216747000	-0.955144000	1.953768000
1	1.424625000	0.639660000	1.919918000
6	0.833644000	-0.651214000	-0.532629000
1	0.979083000	-0.756726000	-1.622688000
1	0.719159000	-1.664670000	-0.128581000
6	-0.360802000	0.162258000	-0.206352000
1	-0.448430000	1.229917000	-0.375726000
8	-1.529647000	-0.542631000	-0.084166000
6	-2.701812000	0.168402000	0.011895000
8	-2.745652000	1.375326000	-0.025094000
6	-3.863952000	-0.769164000	0.169909000
1	-4.790430000	-0.193461000	0.192026000
1	-3.888798000	-1.489618000	-0.654974000
1	-3.762011000	-1.341535000	1.099169000
1	3.199018000	0.519914000	1.765905000
9	3.173077000	-0.786166000	-0.482282000
9	2.258263000	1.218158000	-0.523691000

h_2 To VAc (head)

$CH_3CF_2^{\bullet\cdots}$ CH(OAc)=CH_2 TS

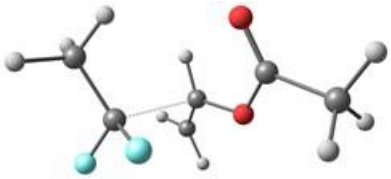

6	-1.394511000	-0.489168000	-0.176924000
6	-1.763098000	-1.351670000	0.980319000
1	-2.339602000	-0.769763000	1.705608000
1	-0.852874000	-1.722861000	1.458418000
6	-0.743941000	2.374375000	0.220156000
1	-0.559679000	2.888263000	-0.718214000
1	-1.561367000	2.714184000	0.847124000
6	-0.063892000	1.248540000	0.553788000
1	-0.081300000	0.798633000	1.543443000
8	1.056920000	0.921689000	-0.202097000
6	1.808543000	-0.132454000	0.219154000
8	1.574824000	-0.766741000	1.224375000
6	2.934258000	-0.386137000	-0.741274000
1	3.639453000	-1.091559000	-0.298960000
1	2.523167000	-0.811845000	-1.664308000
1	3.438392000	0.548548000	-1.005457000
1	-2.376069000	-2.203736000	0.650300000
9	-0.623332000	-1.103511000	-1.095944000
9	-2.437582000	0.084581000	-0.796000000

CH_3CF_2-CH(OAc)$CH_2^{\bullet}$

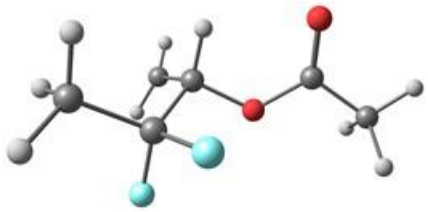

6	1.353415000	-0.364753000	0.038529000
6	2.606352000	-0.311129000	-0.803088000
1	3.114307000	0.648873000	-0.671769000
1	2.359103000	-0.443211000	-1.860660000
6	0.789799000	2.086152000	0.068739000
1	1.385270000	2.242254000	0.963374000
1	0.389757000	2.949317000	-0.454099000
6	0.323080000	0.723761000	-0.282310000
1	0.051487000	0.643662000	-1.342002000
8	-0.869729000	0.419512000	0.490254000
6	-1.952007000	-0.007011000	-0.211888000
8	-2.001544000	-0.069640000	-1.420077000
6	-3.063102000	-0.383002000	0.729988000
1	-3.972877000	-0.578408000	0.160084000
1	-2.776689000	-1.282895000	1.286303000
1	-3.232220000	0.413489000	1.461570000
1	3.276514000	-1.117278000	-0.490206000
9	0.750204000	-1.584497000	-0.127071000
9	1.697609000	-0.275379000	1.365536000

h_3 To NVP (tail)

$CH_3CF_2^{\bullet}\cdots CH_2$=CH(N-pyr) TS

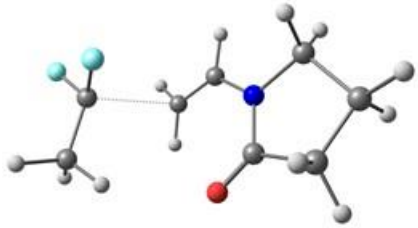

6	-2.627696000	1.483018000	-0.113349000
1	-1.640195000	1.952531000	-0.079863000
6	-2.466532000	0.014317000	-0.278036000
6	-0.857651000	-0.762541000	1.467394000
1	-1.618153000	-1.449786000	1.825505000
1	-0.857215000	0.256652000	1.832719000
6	0.197560000	-1.270992000	0.790927000
1	0.224039000	-2.324254000	0.518050000
6	1.469753000	0.806287000	0.321202000
6	2.353617000	-1.252954000	-0.435869000
6	2.756631000	1.116287000	-0.433061000
6	3.490127000	-0.224032000	-0.493495000
1	1.989504000	-1.517183000	-1.441211000
1	2.643827000	-2.179982000	0.072871000
1	2.482323000	1.483634000	-1.432487000
1	3.307780000	1.917569000	0.067878000
1	4.112255000	-0.348085000	-1.385218000
1	4.135839000	-0.338546000	0.385407000
8	0.704256000	1.620375000	0.819222000
7	1.304531000	-0.565750000	0.315338000
9	-3.598023000	-0.702992000	-0.133267000
9	-1.855383000	-0.354543000	-1.418265000
1	-3.147383000	1.692576000	0.826133000
1	-3.212583000	1.913603000	-0.941424000

CH_3CF_2-CH_2CH(N-pyr)$^{\bullet}$

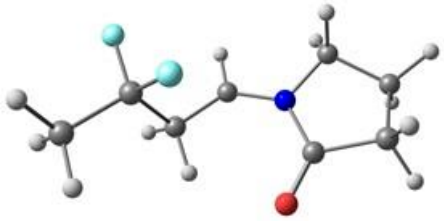

6	-3.435717000	0.865568000	-0.139385000
1	-3.111082000	1.907082000	-0.221168000
6	-2.236949000	-0.054013000	-0.137196000
6	-1.253833000	0.150497000	1.018507000
1	-1.809259000	-0.043597000	1.946804000
1	-0.926795000	1.194222000	1.019301000
6	-0.075635000	-0.753750000	0.933270000
1	-0.206116000	-1.824593000	1.054878000
6	1.598570000	0.909299000	0.150647000
6	2.072797000	-1.400740000	-0.078042000
6	2.939115000	0.786308000	-0.557070000
6	3.392938000	-0.642400000	-0.255564000
1	1.708192000	-1.824153000	-1.025934000
1	2.139334000	-2.215922000	0.653012000
1	2.779171000	0.948994000	-1.633103000
1	3.623269000	1.565283000	-0.207850000
1	4.016399000	-1.083854000	-1.039234000
1	3.963698000	-0.665614000	0.680594000
8	1.021791000	1.947977000	0.446428000
7	1.134126000	-0.379731000	0.392790000
1	-4.074906000	0.621565000	-0.993333000
1	-4.012055000	0.742807000	0.782646000
9	-1.563277000	0.092804000	-1.326983000
9	-2.682366000	-1.360864000	-0.111748000

h_4 To MA (tail)

$CH_3CF_2^{\bullet}\cdots CH_2$=CH(COOMe) TS

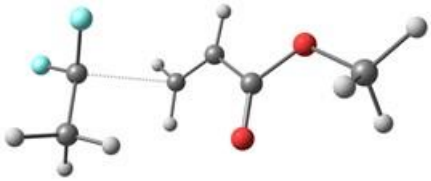

6	2.001610000	1.449351000	-0.573498000
1	0.936615000	1.695318000	-0.616268000
6	2.189128000	0.176313000	0.169602000
6	0.408385000	-1.425595000	-0.911698000
1	1.117334000	-2.244864000	-0.827112000
1	0.506877000	-0.751673000	-1.759546000
6	-0.659182000	-1.327336000	-0.098297000
6	-1.619358000	-0.223488000	-0.264712000
1	-0.836605000	-2.026216000	0.715352000
8	-1.495449000	0.723562000	-1.024459000
8	-2.685475000	-0.379478000	0.552965000
6	-3.667651000	0.655268000	0.463294000
1	-4.447476000	0.387980000	1.179305000
1	-3.231386000	1.627575000	0.716563000
1	-4.080555000	0.712688000	-0.549561000
1	2.379467000	1.340052000	-1.593881000
1	2.546547000	2.272104000	-0.084478000
9	1.766536000	0.186092000	1.438600000
9	3.415572000	-0.363061000	0.104004000

CH_3CF_2-CH_2CH(COOMe)$^{\bullet}$

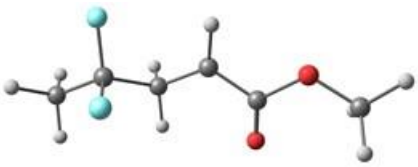

6	3.285981000	0.804252000	-0.091035000
1	3.127550000	1.787069000	0.362668000
6	2.045815000	-0.046184000	0.053455000
6	0.787829000	0.510805000	-0.605394000
1	1.015821000	0.638610000	-1.677266000
1	0.562388000	1.506589000	-0.206605000
6	-0.393756000	-0.368251000	-0.437174000
6	-1.689888000	0.207633000	-0.143273000
1	-0.300807000	-1.445273000	-0.544708000
8	-1.908180000	1.403329000	0.009564000
8	-2.654019000	-0.743356000	-0.058177000
6	-3.958731000	-0.240846000	0.234678000
1	-4.612177000	-1.114789000	0.273930000
1	-3.966623000	0.286828000	1.194845000
1	-4.293208000	0.453094000	-0.544521000
1	3.539261000	0.934650000	-1.147374000
1	4.118523000	0.307850000	0.416070000
9	2.299009000	-1.292862000	-0.478599000
9	1.794698000	-0.244790000	1.389080000

h_5 To DMA (tail)

$CH_3CF_2^{\bullet}\cdots CH_2{=}CH(CONMe_2)$ TS

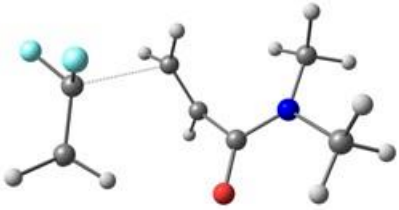

6	-0.348524000	-0.425783000	-1.341985000
6	2.314572000	-0.014269000	0.271010000
6	0.489013000	-1.312093000	-0.755440000
1	1.233660000	-1.851172000	-1.337177000
1	0.334051000	-1.650960000	0.267065000
1	-0.178910000	-0.108236000	-2.370086000
6	-1.293829000	0.452418000	-0.593275000
8	-1.134563000	1.675692000	-0.664161000
7	-2.275505000	-0.113602000	0.175309000
6	-2.647836000	-1.512256000	0.145218000
1	-2.473549000	-1.994446000	1.118415000
1	-3.716920000	-1.610960000	-0.093214000
1	-2.070468000	-2.038163000	-0.616763000
6	-3.110417000	0.750961000	0.985593000
1	-4.150694000	0.735191000	0.629594000
1	-3.098923000	0.420858000	2.033426000
1	-2.720926000	1.768006000	0.913236000
9	1.934242000	0.012320000	1.558989000
9	3.430449000	-0.754966000	0.154464000
6	2.347093000	1.308511000	-0.402451000
1	1.340709000	1.740473000	-0.417386000
1	3.032929000	1.993468000	0.118877000
1	2.691430000	1.184499000	-1.432955000

CH_3CF_2-$CH_2CH(CONMe_2)^{\bullet}$

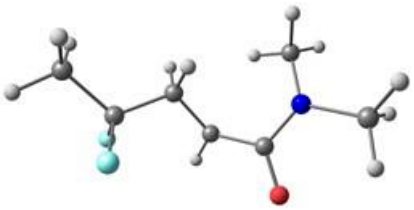

6	-0.111302000	0.433768000	-0.785236000
6	2.182360000	-0.063878000	0.112219000
6	0.822006000	-0.627447000	-0.304891000
1	1.025538000	-1.370801000	-1.094867000
1	0.400413000	-1.173815000	0.547205000
1	0.305978000	1.244514000	-1.376556000
6	-1.457325000	0.700173000	-0.267933000
8	-1.804225000	1.874498000	-0.097273000
7	-2.267670000	-0.359475000	0.090061000
6	-2.149021000	-1.685145000	-0.476457000
1	-1.986739000	-2.451758000	0.295787000
1	-3.068985000	-1.947139000	-1.021133000
1	-1.324208000	-1.723502000	-1.191709000
6	-3.517020000	-0.069217000	0.763156000
1	-4.372417000	-0.139837000	0.073367000
1	-3.676558000	-0.781066000	1.584039000
1	-3.469784000	0.947922000	1.156277000
9	2.719984000	0.609342000	-0.962284000
9	1.992529000	0.868698000	1.099197000
6	3.187198000	-1.086166000	0.592929000
1	3.394921000	-1.819205000	-0.192421000
1	4.117338000	-0.573463000	0.855122000
1	2.807993000	-1.606395000	1.477701000

(i) $PVDF_T^{\bullet}$ addition to monomer

i_1 To VAc (tail)

$CHF_2CH_2^{\bullet}\cdots CH_2{=}CHOAc$ TS

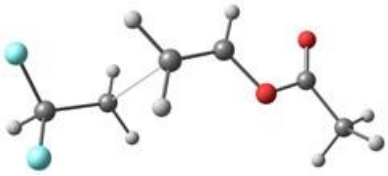

6	-1.798123000	0.066931000	1.123956000
6	-0.442862000	-0.470412000	-0.841534000
1	-1.139469000	-1.283581000	-1.011611000
1	-0.718966000	0.515245000	-1.202456000
6	0.818012000	-0.749251000	-0.461401000
1	1.192049000	-1.727302000	-0.172675000
8	1.737101000	0.271585000	-0.359380000
6	2.994965000	-0.046952000	0.084980000
8	3.329064000	-1.163850000	0.401802000
6	3.858387000	1.181447000	0.105769000
1	4.844727000	0.924258000	0.494476000
1	3.951450000	1.589933000	-0.906880000
1	3.398623000	1.957389000	0.727562000
1	-1.643156000	-0.839788000	1.700707000
6	-3.117038000	0.248248000	0.480899000
9	-3.502107000	-0.902773000	-0.162800000
1	-1.265940000	0.959401000	1.438603000
9	-3.064069000	1.253352000	-0.453059000
1	-3.933112000	0.507294000	1.179624000

CHF_2CH_2-$CH_2CH^{\bullet}(OAc)$

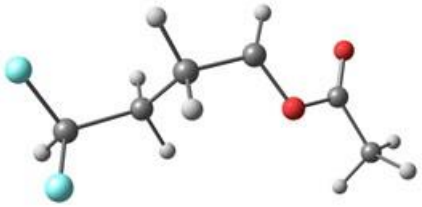

6	-1.364040000	-0.055276000	0.693837000
6	-0.700139000	-0.558712000	-0.605838000
1	-1.229094000	-1.454335000	-0.951531000
1	-0.832690000	0.212150000	-1.377847000
6	0.736382000	-0.881452000	-0.454376000
1	1.143381000	-1.838912000	-0.145752000
8	1.561771000	0.205771000	-0.294753000
6	2.866895000	-0.019608000	0.062008000
8	3.311802000	-1.122419000	0.281045000
6	3.623409000	1.277003000	0.114320000
1	4.613732000	1.099886000	0.536800000
1	3.727358000	1.686698000	-0.897569000
1	3.082535000	2.018284000	0.711739000
1	-1.301893000	-0.820673000	1.477870000
6	-2.818716000	0.303347000	0.499273000
9	-3.515560000	-0.783776000	0.044482000
1	-0.837749000	0.833591000	1.062954000
9	-2.941009000	1.289292000	-0.442472000
1	-3.307789000	0.655040000	1.419571000

i_2 To VAc (head)

$CHF_2CH_2^{\bullet}\cdots CH(OAc)=CH_2$ TS

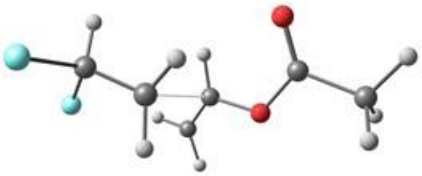

6	-0.952576000	-0.555990000	-0.516344000
6	-2.243159000	-0.481557000	0.204570000
1	-2.150607000	-0.634508000	1.289777000
6	-0.132924000	2.236778000	0.055617000
1	0.190695000	2.800390000	-0.814486000
1	-1.008335000	2.571514000	0.599421000
6	0.446880000	1.055344000	0.381377000
1	0.298880000	0.537871000	1.325566000
8	1.612053000	0.702648000	-0.287424000
6	2.297325000	-0.386246000	0.170371000
8	1.928264000	-1.067139000	1.099929000
6	3.541736000	-0.596169000	-0.643803000
1	4.087509000	-1.457441000	-0.256056000
1	3.278773000	-0.761666000	-1.694557000
1	4.172906000	0.298360000	-0.604148000
9	-2.851168000	0.728232000	-0.004145000
9	-3.112205000	-1.444958000	-0.267011000
1	-0.305612000	-1.392124000	-0.262598000
1	-0.960094000	-0.228897000	-1.553281000

CHF_2CH_2-$CH(OAc)CH_2^{\bullet}$

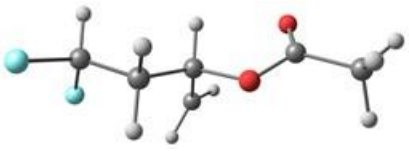

6	-1.051803000	-0.639923000	-0.209126000
6	-2.367283000	-0.196985000	0.390092000
1	-2.307549000	0.023509000	1.466373000
6	0.010981000	1.637255000	-0.562270000
1	-0.595594000	1.785319000	-1.450314000
1	0.654242000	2.441448000	-0.218974000
6	0.108920000	0.304843000	0.079931000
1	0.256949000	0.425780000	1.162287000
8	1.296775000	-0.409995000	-0.416107000
6	2.465885000	-0.093138000	0.185888000
8	2.568596000	0.715141000	1.084098000
6	3.602941000	-0.873168000	-0.420944000
1	4.512482000	-0.695332000	0.155085000
1	3.368411000	-1.942386000	-0.441649000
1	3.756177000	-0.552562000	-1.457862000
9	-2.837459000	0.921921000	-0.239385000
9	-3.293362000	-1.185792000	0.211333000
1	-0.815561000	-1.627832000	0.203012000
1	-1.192982000	-0.757569000	-1.290852000

i_3 To NVP (tail)

$CHF_2CH_2^{\bullet}\cdots CH_2$=CH(N-pyr) TS

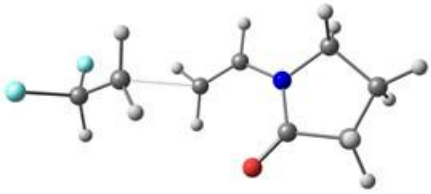

9	4.375938000	0.828201000	0.756925000
9	3.740084000	-0.943267000	-0.388294000
6	3.353742000	0.326285000	-0.026934000
1	3.311092000	0.940618000	-0.936996000
6	2.082653000	0.288381000	0.720794000
1	1.475644000	1.186413000	0.764196000
1	2.008849000	-0.422307000	1.539170000
6	0.584013000	-0.833171000	-0.939414000
1	1.398400000	-1.531980000	-1.096290000
1	0.593409000	0.115347000	-1.461611000
6	-0.525577000	-1.266706000	-0.296562000
1	-0.556397000	-2.264179000	0.139166000
6	-1.899205000	0.798357000	-0.344891000
6	-2.816692000	-1.145189000	0.653754000
6	-3.280259000	1.167052000	0.181543000
6	-3.977759000	-0.178193000	0.386553000
1	-2.583726000	-1.215752000	1.728030000
1	-3.013258000	-2.158416000	0.283827000
1	-3.147493000	1.713559000	1.126312000
1	-3.784125000	1.842130000	-0.516166000
1	-4.708010000	-0.177956000	1.201480000
1	-4.499138000	-0.474165000	-0.531578000
8	-1.098950000	1.545165000	-0.884842000
7	-1.696190000	-0.545706000	-0.069648000

CHF_2CH_2-CH_2CH(N-pyr)$^{\bullet}$

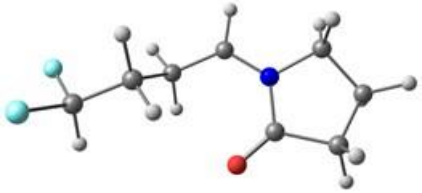

9	3.750353000	0.976686000	0.918517000
9	3.784525000	-0.744771000	-0.463064000
6	3.050949000	0.347766000	-0.074411000
1	2.989884000	1.031305000	-0.933973000
6	1.701967000	-0.086617000	0.441744000
1	1.149412000	0.810031000	0.741825000

1	1.868370000	-0.707428000	1.331540000
6	0.894296000	-0.854727000	-0.622674000
1	1.481079000	-1.723963000	-0.943875000
1	0.762713000	-0.200487000	-1.493512000
6	-0.427623000	-1.347937000	-0.147731000
1	-0.543529000	-2.362933000	0.219366000
6	-1.679326000	0.794879000	-0.294040000
6	-2.775355000	-1.120517000	0.562901000
6	-3.098710000	1.207561000	0.067270000
6	-3.862311000	-0.112583000	0.171480000
1	-2.669911000	-1.209952000	1.655037000
1	-2.953112000	-2.123597000	0.157192000
1	-3.069595000	1.746447000	1.025741000
1	-3.491792000	1.902252000	-0.681308000
1	-4.683627000	-0.093178000	0.894683000
1	-4.281582000	-0.382813000	-0.805059000
8	-0.794108000	1.521770000	-0.729805000
7	-1.548953000	-0.559147000	-0.007932000

i_4 To MA (tail)

$CHF_2CH_2^{\bullet}\cdots CH_2=CH(COOMe)$ TS

9	3.965149000	-1.080016000	-0.275093000
9	3.302863000	0.996999000	0.057180000
6	2.930964000	-0.314276000	0.216297000
1	2.851243000	-0.518995000	1.292749000
6	1.687225000	-0.588141000	-0.536190000
1	1.058796000	-1.421064000	-0.237821000
1	1.641246000	-0.249365000	-1.567184000
6	0.125425000	1.141330000	0.437264000
1	0.898177000	1.862477000	0.189534000
1	0.229408000	0.574625000	1.360361000
6	-1.035310000	1.070835000	-0.246686000
6	-2.083973000	0.122402000	0.172783000
1	-1.228988000	1.676436000	-1.129101000
8	-1.990613000	-0.681903000	1.082748000
8	-3.188397000	0.251403000	-0.597838000
6	-4.261400000	-0.630735000	-0.257662000
1	-5.065188000	-0.407054000	-0.961877000
1	-3.948621000	-1.676260000	-0.351154000
1	-4.593693000	-0.458137000	0.771604000

CHF_2CH_2-$CH_2CH(COOMe)^{\bullet}$

9	3.814240000	0.835375000	-0.640718000
9	3.305035000	-0.797572000	0.755452000
6	2.873427000	-0.109914000	-0.347080000
1	2.826654000	-0.819086000	-1.186770000
6	1.553357000	0.562327000	-0.049872000
1	1.255721000	1.138124000	-0.934615000
1	1.727756000	1.277180000	0.764960000
6	0.459178000	-0.448314000	0.329941000
1	0.827203000	-1.033647000	1.188304000
1	0.277376000	-1.153342000	-0.491102000
6	-0.825666000	0.199293000	0.685540000
6	-2.050812000	-0.141311000	-0.010086000
1	-0.871735000	0.942333000	1.479660000
8	-2.138819000	-0.947094000	-0.928429000
8	-3.113137000	0.548448000	0.480049000
6	-4.356081000	0.258030000	-0.161427000
1	-5.102462000	0.875822000	0.342181000
1	-4.311496000	0.504683000	-1.228095000
1	-4.607255000	-0.803794000	-0.062188000

i_5 To DMA (tail)

$CHF_2CH_2^{\bullet}\cdots CH_2=CH(CONMe_2)$ TS

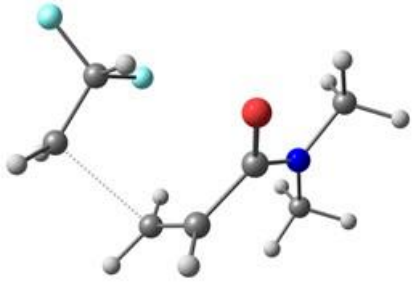

6	-0.553526000	1.469780000	0.794822000
6	2.440968000	1.026482000	-0.007744000
6	0.197442000	1.965793000	-0.217368000
1	0.659797000	2.946915000	-0.137139000
1	0.200605000	1.499166000	-1.199312000
1	-0.553668000	1.958157000	1.768792000
6	-1.143271000	0.096776000	0.811029000
8	-0.738822000	-0.691797000	1.671369000
7	-2.076420000	-0.248335000	-0.124492000
6	-2.695742000	0.668683000	-1.057738000
1	-2.414384000	0.435250000	-2.095147000
1	-3.789921000	0.597589000	-0.979569000
1	-2.396873000	1.694016000	-0.833783000
6	-2.545419000	-1.619651000	-0.168467000
1	-3.625232000	-1.666239000	0.030816000
1	-2.354937000	-2.057447000	-1.157897000
1	-2.010305000	-2.188558000	0.593871000
6	2.137054000	-0.422530000	0.009205000
1	1.559923000	-0.742121000	0.884721000
1	2.728723000	1.498447000	0.927063000
1	2.849219000	1.438919000	-0.928101000
9	1.423645000	-0.762688000	-1.117759000
9	3.306081000	-1.154353000	-0.032938000

CHF_2CH_2-$CH_2CH(CONMe_2)^{\bullet}$

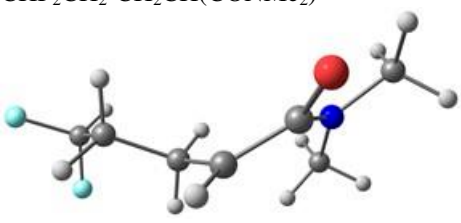

6	0.552810000	0.602628000	0.905033000
6	-1.800112000	0.639721000	0.025351000
6	-0.579682000	-0.221838000	0.387224000
1	-0.905776000	-0.955079000	1.144337000
1	-0.262148000	-0.801525000	-0.490073000
1	0.324891000	1.390275000	1.621693000
6	1.889651000	0.724685000	0.311795000
8	2.393758000	1.850988000	0.218549000
7	2.510846000	-0.398558000	-0.193132000
6	2.204715000	-1.745469000	0.237183000
1	1.888641000	-2.384060000	-0.600863000
1	3.093623000	-2.206226000	0.694103000

1	1.414363000	-1.735952000	0.991303000
6	3.751863000	-0.230959000	-0.920867000
1	4.616895000	-0.538186000	-0.313184000
1	3.740451000	-0.838998000	-1.835578000
1	3.861154000	0.824523000	-1.176869000
6	-2.965146000	-0.184308000	-0.469501000
1	-2.745986000	-0.750539000	-1.387490000
1	-1.539412000	1.369020000	-0.751200000
1	-2.145650000	1.204390000	0.900923000
9	-3.343715000	-1.084399000	0.491562000
9	-4.033133000	0.628576000	-0.719437000

Conclusion Partie 1

Cette Partie 1 détaille la synthèse par polymérisation séquentielle RAFT de copolymères diblocs à partir de PVDF-XA. Des extensions de chaînes de PVDF-XA en présence de VAc, *N*-VinylPyrrolidone (NVP), Butyl Acrylate (BA) et *N,N*-Dimethyl acrylamide (DMA) ont été testées. Les extrémités de chaînes $PVDF_H$-XA ont été rapidement réactivées en présence de VAc et NVP, contrairement aux extrémités $PVDF_T$-XA, qui ont été exclusivement réactivées par le VAc. Bien que la réactivation des extrémités $PVDF_T$-XA par le VAc soit relativement lente et s'effectue de manière progressive le long de la polymérisation du bloc PVAc, il est néanmoins possible de synthétiser des copolymères à blocs PVDF-*b*-PVAc bien définis. De plus, comme discuté dans la conclusion du Chapitre II, le VAc possède une réactivité très similaire à celle du VDF avec la formation d'additions tête-tête. Par une étude RMN *in situ*, consistant à effectuer une extension de chaîne d'un PVDF-XA en présence de VAc directement dans le spectromètre RMN, il a pu être montré une accumulation progressive des extrémités PVDF-*b*-$PVAc_T$-XA lau cours de la polymérisation. L'accumulation de ces chaînes $PVAc_T$-XA moins réactives ainsi que la différence de réactivités des extrémités $PVDF_T$-XA et $PVDF_H$-XA vis à vis du VAc et des autres monomères utilisés, ont été parfaitement rationalisés par des calculs DFT.

Afin d'étendre la gamme de copolymères à blocs à base de PVDF, et de pallier la faible versatilité des agents RAFT macromoléculaires PVDF-XA, une autre méthode combinant deux polymérisations RAFT (cationique et radicalaire) est présentée dans la Partie 2 de ce chapitre.

Partie 2 –

La précédente partie a démontré la surprenante réactivité des extrémités de chaînes PVDF-XA, qui a permis la formation de nouveaux copolymères à blocs bien définis PVDF-*b*-PVAc. Cependant, bien qu'il s'agisse du premier bloc de PVDF correctement contrôlé, cette synthèse reste limitée.

L'intérêt s'est donc porté sur la méthode inverse: amorçage du VDF par des macro-agents RAFT hydrogénés. Notre attention s'est tournée vers les travaux de l'équipe du Professeur Masami Kamigaito, qui a très récemment développé la polymérisation RAFT cationique. Cette technique s'est avérée être particulièrement efficace et robuste pour contrôler la polymérisation cationique des éthers vinyliques. Ainsi, j'ai eu l'opportunité de réaliser un séjour de trois mois dans le laboratoire du Professeur Kamigaito (Université de Nagoya, au Japon) pour y synthétiser les agents RAFT macromoléculaires poly(éther vinylique). Cette bourse m'a été attribuée par la Japan Society for the Promotion of Science (JSPS) dans le cadre d'un programme d'été ayant pour but de nouer des collaborations entre les laboratoires Japonais et des laboratoires étrangers. Cette partie présente donc la synthèse originale de copolymères diblocs PEVE-*b*-PVDF réalisée en combinant la polymérisation RAFT cationique des éthers vinyliques préparés au Japon, et la polymérisation RAFT radicalaire du VDF. La polymérisation RAFT cationique étant optimale en présence d'agent dithiocarbamate, une étude cinétique de la polymérisation RAFT du VDF avgec un agent dithiocarbamate a été indispensable. Ce travail a fait l'objet d'un article scientifique publié dans *ACS Macro Letters*.[5]

Combination of cationic and radical RAFT polymerization: A versatile route to well-defined poly(vinyl ethyl ether)-*block*-poly(vinylidene fluoride) block copolymers

Marc Guerre,[a] Mineto Uchiyama,[b] Enrique Folgado,[a,c] Mona Semsarilar,[c] Bruno Ameduri,[a] Kotaro Satoh,[b,d] Masami Kamigaito,[b]* Vincent Ladmiral[a]*

[a]Institut Charles Gerhardt, Ingénierie et Architectures Macromoléculaires, UMR 5253 – CNRS, Université Montpellier, ENSCM - 8, Rue Ecole Normale, 34296 Montpellier-France.
[b]Department of Applied Chemistry Graduate School of Engineering, Nagoya University Furo-cho, Chikusa-ku, Nagoya 464-8603-Japan
[c]Institut Européen des Membranes, IEM, UMR5635, UM-ENSCM-CNRS, Place Eugène Bataillon, 34095 Montpellier cedex 5, France.
[d]Precursory Research for Embryonic Science and Technology, Japan Science and Technology Agency, 4-1-8 Honcho, Kawaguchi, Saitama 332-0012, Japan.

*Corresponding authors: kamigait@apchem.nagoya-u.ac.jp, vincent.ladmiral@enscm.fr

I. Abstract

Poly(vinylidene fluoride)-containing block copolymers are difficult to prepare, and still very rare in spite of their potential use in high added value applications. This communication describes in details the synthesis of unprecedented poly(ethyl vinyl ether)-*block*-poly(vinylidene fluoride) (PEVE-*b*-PVDF) block copolymers (BCP) via the sequential combination of cationic RAFT polymerization of vinyl ethers and of radical RAFT polymerization of vinylidene fluoride (VDF). Dithiocarbamates chain transfer agents were found to efficiently control the radical RAFT polymerization of VDF and to be very suitable for the preparation of (PEVE-*b*-PVDF) BCP. These new block copolymers composed of incompatible polymer segments may find applications owing to their phase segregation and self-assembly behaviour.

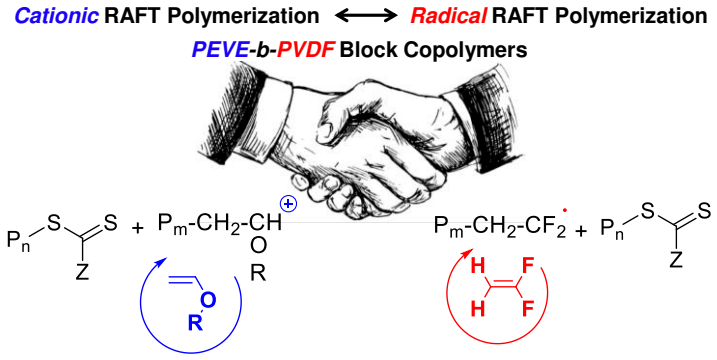

II. Introduction

Fluoropolymers are an intriguing class of materials which attract much curiosity in the field of materials science, owing to their chemical inertness, thermal stability, and low surface energy.[1,2] Poly(vinylidene fluoride) (PVDF) is a fluorinated semi-crystalline polymer endowed with exceptional electroactive properties with potential uses in many high value-added electronic devices.[3] PVDF is usually prepared by conventional radical polymerization in aqueous dispersed medium (in suspension, or emulsion).[4] The preparation of PVDF block copolymers[5] has so far been achieved via three main strategies: using functional PVDF telomers,[6-11] functional initiators,[12-15] or Reversible Deactivation Radical Polymerization (RDRP) techniques such as Iodine Transfer Polymerization (ITP)[16] for example.[17-19] However, these methods are somewhat limited as they often only achieve low molar masses, high dispersities or bimodal SEC traces.

Recently, the reversible addition-fragmentation chain transfer (RAFT) polymerization of VDF in dimethyl carbonate has been thoroughly investigated, and has been shown to be an efficient method to prepare PVDF with predictable molar mass, narrow molar mass distribution and high end-group fidelity.[20-22] However, the RAFT of VDF suffers from the accumulation of less reactive end-groups (-CF_2-CH_2-S(S)OCH_2CH_3 termini) resulting from VDF head-to-head addition and transfer to the RAFT chain transfer agent (CTA). These less reactive chain-ends are responsible for a slowdown of the degenerative chain transfer process which leads to a broadening of the molar mass distribution,[20,22] and to a reduced reactivity towards radicals which impairs the synthesis of a wide range of block copolymers. So far, PVDF RAFT macromolecular chain transfer agents (macro-CTAs) could only be efficiently chain extended with vinyl acetate (VAc) to form PVDF-*b*-PVAc[23] (and its poly(vinyl alcohol) derivative[24]). Similarly, few RAFT macro-CTAs are able to produce well-defined PVDF-containing block copolymers. VDF RAFT dispersion polymerization protocols in the presence of PVAc macro-CTAs allowed the polymerization-induced self-assembly (PISA) of PVAc-*b*-PVDF block copolymers and resulted into original crystalline block copolymer morphologies.[25] Moreover, VDF behaves as a Less Activated monomer (LAM) and its polymerization is only adequately controlled by xanthate RAFT agents. Therefore, the synthesis of well-defined PVDF-based block copolymers is still very challenging.

In 2015, Kamigaito's group reported the cationic RAFT polymerization of vinyl ether (which do not homopolymerize under radical polymerization conditions), using thiocarbonylthio

compounds as CTAs, and a small amount of a strong Brønsted acid acting as the initiator.[26,27] This cationic polymerization proceeds through the degenerative chain transfer of growing carbocationic species to dormant thiocarbonylthio species. Very efficient control of the polymerization of vinyl ethers was demonstrated using trithiocarbonate and dithiocarbamate RAFT agents, which remain at the chain-ends even after isolation of the resulting poly(vinyl ethers) (PVE).

This communication reports the development of a facile strategy for the synthesis of unprecedented PVDF-containing block copolymers. This strategy, which relies on the combination of cationic RAFT polymerization and radical RAFT polymerization, produces well-defined PVDF-*b*-PVE block copolymers (BCPs). Xanthate CTAs, which are well-suited for the radical RAFT polymerization of VDF, are not very efficient in controlling the cationic polymerization of vinyl ethers,[26] and lead to poorly defined PVE with relatively high dispersity (Đ = 1.50). Dithiocarbamate CTAs thus appeared as a better choice, provided that they also control the radical polymerization of VDF, since they offer efficient control over the cationic polymerization of VEs. In consequence, the still unreported RAFT of VDF using dithiocarbamates was carefully examined using ^{1}H and ^{19}F NMR spectroscopy and size exclusion chromatography (SEC).

III. Results and Discussion

RAFT polymerization of VDF in the presence of *N*,*N*-diethyldithiocarbamate (CTA_1) was performed according to Scheme IV-2 (SI-Table IV-5, runs 1-7).

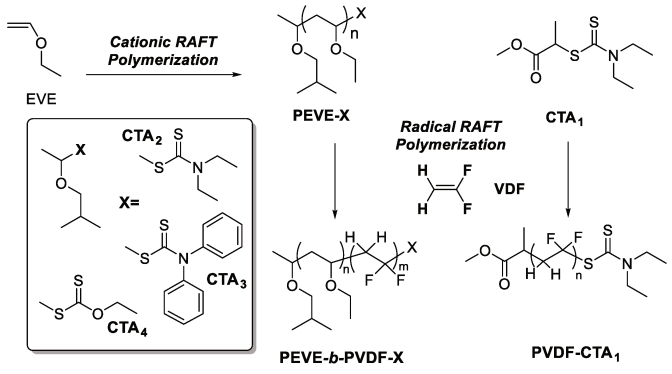

Scheme IV-2: Schematic representation of the vinylidene fluoride (VDF) radical RAFT homopolymerization using methyl 2-((N,N-diethylcarbamothioyl)thio)propanoate (CTA_1) and the synthesis of PEVE–b-PVDF block copolymers via sequential cationic RAFT polymerization of EVE (ethyl vinyl ether) and radical RAFT polymerization of VDF.

The first-order kinetic plot and the evolutions of the molar mass and of the dispersity of the resulting PVDF versus VDF conversion for this radical RAFT polymerization of VDF (SI-Table IV-5) are displayed in SI-Figure IV-34 and Figure IV-27, respectively. The first order kinetic plot (SI-Figure IV-34) exhibted the three different regimes of polymerization already observed by Guerre *et al*. in the case of the xanthate RAFT polymerization of VDF.[20,22] However, this RAFT polymerization proceeded at a surprisingly slower rate (initial molar ratio $[M]_0/[CTA]_0 = 100$, inhibition time = 8h and first order kinetic slope = 0.029) compared to the RAFT polymerization of VDF using xanthate CTA ($[M]_0/[CTA]_0 = 50$, inhibition time = 5h and first order kinetic slope = 0.041[20]). This slowdown of the polymerization is thought to arise from the presence of the nitrogen atom which causes the strong stabilization of the intermediate radical (compared to the *O*-ethyl moiety). The apparent transfer constant $C_{Tr(app)}$ of the PVDF$^{\bullet}$ radicals towards CTA_1 was determined using O'Brien's and Gornick's method (SI-Figure IV-35). This method gave $C_{Tr(app)} = 32$ at 73 °C, a slightly inferior value to that determined with a xanthate CTA ($C_{Tr(app)} = 49$ at 73 °C)[22] but high enough to ensure fast transfer to the CTA and efficient control.

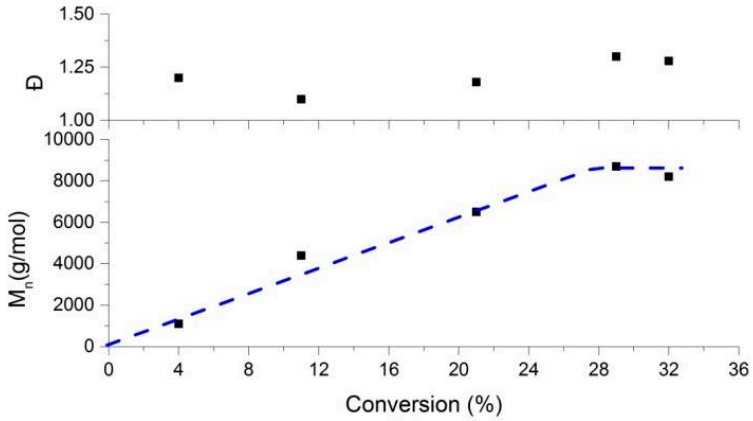

Figure IV-27: Evolution of molar mass and of dispersity with VDF conversion of the radical RAFT polymerization of VDF using methyl 2-((N,N-diethylcarbamothioyl)thio)propanoate as chain transfer agent (CTA_1) (SI-Table IV-5). Reaction conditions: $[VDF]_0/[CTA_1]_0/[I]_0$ = 100/1/0.1, I = Trigonox® 121, T = 73 °C, solvent : DMC.

As in the xanthate-CTA-mediated polymerization of VDF, the molar mass of the resulting PVDF increased linearly with conversion for the most part of the polymerization and the dispersity remained below 1.3 throughout the polymerization (Figure IV-27 and SI-Figure IV-36) suggesting that the dithiocarbamate CTA_1 efficiently controls the polymerization of VDF. As in the VDF RAFT polymerization controlled by xanthate, the slope of the "M_n *vs*

conversion" plot changed abruptly in the later stage of the polymerization.[22] This is likely caused by the disappearance of the last $PVDF_H$-CTA end-group (where $PVDF_H$-CTA designates PVDF chains terminated with a head-to-tail (regular) addition: $-CH_2CF_2-CH_2CF_2-S-C(S)NEt_2$) which leads to a slowdown of the degenerative chain transfer and marks the onset of a less efficient control of the polymerization.[22] This analogy with the xanthate mediated RAFT polymerization of VDF was further confirmed by NMR. Typical ^{1}H NMR spectrum recorded after 10 h of polymerization (run 1, SI-Table IV-5) is displayed in Figure IV-28. This spectrum shows the typical doublet at 1.22 ppm and singlet at 3.65 ppm assigned, respectively, to the -O-**CH_3** and **CH_3**-CH of the CTA R-group at the PVDF α-chain-end.

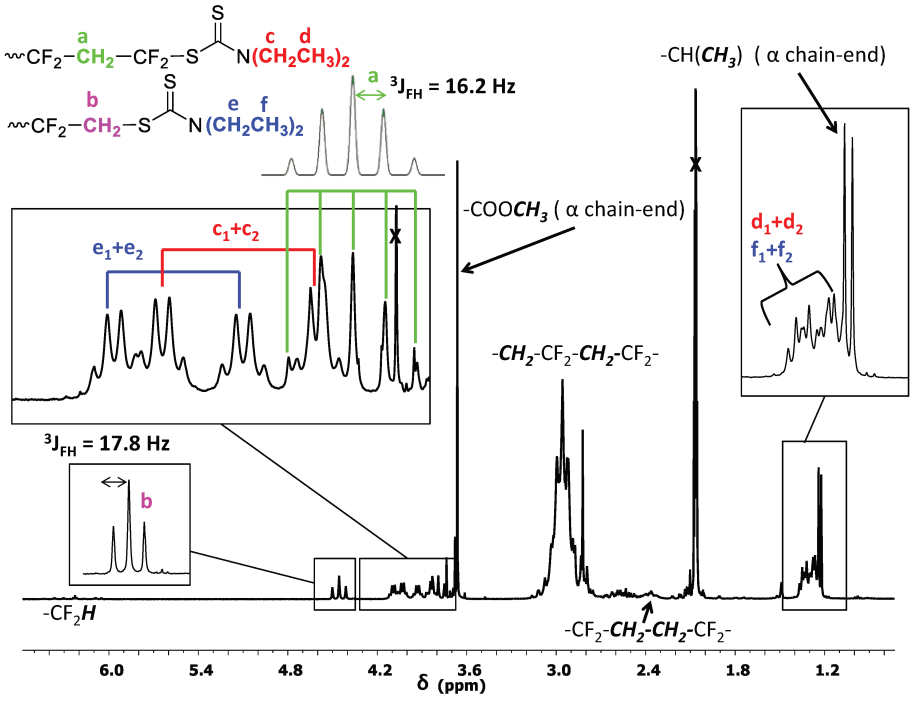

Figure IV-28: ^{1}H NMR spectrum of PVDF-CTA$_1$ (run 1, Table IV-1) synthesized by radical RAFT polymerization using CTA$_1$. Reaction conditions: $[VDF]_0/[CTA_1]_0/[I]_0 = 100/1/0.1$, I = Trigonox® 121, T = 73°C, solvent : DMC, t = 10 h.

The complex signal (two doublets of quartets) between 3.76 and 4.17 ppm was assigned to the $-N(\mathbf{CH_2}CH_3)_2$ protons of the Z-group of the CTA at the PVDF ω-chain-end. This signal splitting also observed in the ^{1}H NMR spectrum of CTA_1 (SI-Figure IV-32) is likely caused by the slow configuration inversion of the nitrogen atom in the dithiocarbamate functional group and also by the presence of two different chain-ends consisting of $-CH_2-CF_2-S(C=S)N(CH_2CH_3)_2$ ($PVDF_H$-CTA_1) and $CF_2-CH_2-S(C=S)N(CH_2CH_3)_2$ ($PVDF_T$-CTA_1). The CH_2 of the VDF terminal unit in the $PVDF_T$-CTA chains (PVDF chains terminated with a

(inverse) head-to-head addition: -CH_2CF_2-CF_2CH_2-S-C(S)N(CH_2CH_3)$_2$) was clearly identified at 4.44 ppm with a typical $^3J_{HF}$ = 17.8 Hz coupling constant while the CH_2 of the terminal VDF unit in the $PVDF_H$-CTA chains at 3.77 ppm overlapped with the protons c of the CTA Z-group (–N(**CH_2**CH_3)$_2$). A simulation of this multiplet is provided in Figure IV-28, for clarity. The presence of these two types of end-groups confirms that the RAFT polymerization of VDF in the presence of CTA_1 proceeds, just like the RAFT polymerization mediated by xanthate, with the progressive accumulation of $PVDF_T$-CTA.

In addition, the usual signals corresponding to the head-to-tail (HT) and tail-to-tail (TT) additions of PVDF were observed at 2.94 ppm (broad signal) and 2.35 ppm, respectively. The ^{19}F NMR spectrum of this PVDF-CTA_1 (SI-Figure IV-37) displayed the expected signals previously reported for the xanthate-mediated RAFT VDF polymerization:[20] signal at -93.51 ppm of the CF_2 of the first-added VDF unit (connected to the R-group of CTA_1), and signals of the CF_2 of the ultimate and penultimate VDF units at the ω-end of the PVDF (-69.1 ppm and -91.65 ppm, respectively for $PVDF_H$-CTA_1 and -112.3 and -112.7 ppm, respectively for $PVDF_T$-CTA_1).

Since well-defined PVDF can be successfully synthesized using dithiocarbamate CTA, a series of poly(ethyl vinyl ether) (PEVE) macro-CTAs was synthesized via cationic RAFT polymerization using different CTAs: CTA_2 (Z-group = diethylcarbamate), CTA_3 (Z-group = diphenylcarbamate), and CTA_4 (Z-group = xanthate) (Scheme IV-2 and SI-Table IV-6).

The narrowest dispersities ($Đ$ < 1.1) were obtained for the diethylcarbamate and diphenylcarbamate CTAs ($Đ_{CTA2}$= 1.08 and $Đ_{CTA3}$ = 1.09, SI-Table IV-6), whereas the xanthate CTA_4 led to broader dispersity ($Đ_{CTA4}$ = 1.52). Indeed, dithiocarbamate CTAs with electron-donating nitrogen atoms are most effective at controlling the molar masses, most likely through the formation of a more stabilized cationic intermediate, in contrast to the oxygen atom of an ester group.[26] The structures of the resulting PEVE macro-CTAs were further characterized by ^1H and ^{13}C NMR spectroscopy (Figure IV-29, SI-Figure IV-38/SI-Figure IV-42).

The ^1H NMR spectrum of PEVE-CTA_2 (Figure IV-29) shows typical signals corresponding to the CH_2 (l_1 and l_2) and CH_3 (m_1 and m_2) of the –N(CH_2CH_3)$_2$ CTA Z-group at 3.78-4.13 ppm and 1.21-1.33 ppm, respectively. The signal assigned to the ultimate EVE unit adjacent to the diethylcarbamate end-group was easily identified at 6.11 ppm. Signals corresponding to the CH_3 and CH_2 of the isobutyl vinyl ether moiety were also identified at 0.9 ppm and

3.28/3.06 ppm, respectively (two peaks were observed for the CH_2 due to their diastereotopicity). As reported by Kamigaito et al.,[26] the small peak (signal n) at 4.6 ppm was assigned to the -C**H**(OEt)OCH_3 ω-chain-end originating from quenching of the polymerization by methanol. The functionality of PEVE-CTA_2 was calculated to be 83 % (while those of PEVE-CTA_3 and PEVE-CTA_4 were estimated at 95 and 91 %, respectively, SI-Table IV-6, SI-Equation IV-23).

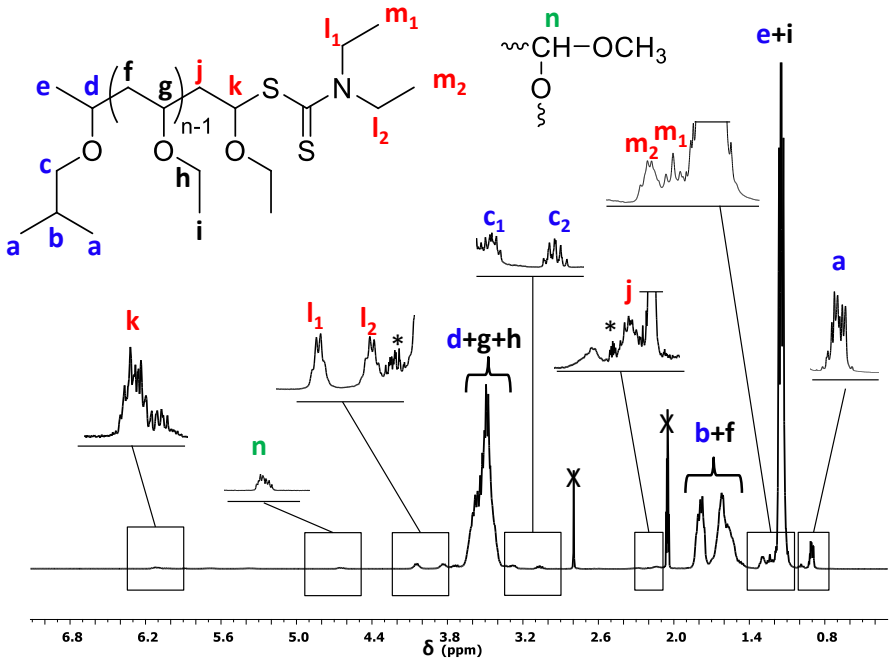

*Figure IV-29: ^{1}H NMR spectrum of PEVE-CTA2 (run 1, SI-Table IV-6) synthesized by cationic RAFT polymerization. Crossed-out peaks correspond to residual acetone and water. *spinning side bands. Reaction conditions: $[EVE]_0/[CTA_2]_0/[I]_0 = 50/1/0.05$, T = - 40 °C, solvent : DMC.*

These PEVE macroCTAs were then used in the radical RAFT polymerization of VDF (SI-Scheme V-2). SI-Figure IV-43 shows the ^{1}H NMR spectrum of the resulting PEVE-*b*-PVDF-CTA_2 BCP. The expected chain-ends signals already observed for the PVDF synthesized by RAFT polymerization using CTA_1 (Figure IV-28) were clearly identified in the ^{1}H NMR spectrum of this block copolymer.

This suggests that the PVDF chains formed were efficiently end-capped by the dithiocarbamate group, and that the RAFT polymerization of VDF proceeded with a degree of control. However, a large quantity of dead chains (58 mol % of -CF_2H ω-chain-ends) likely caused by transfer to DMC and often observed during VDF polymerization in DMC for high target DP[22] can be seen at 6.3 ppm. The important signal to ascertain the formation of block copolymer and corresponding to the connection between the PEVE and PVDF blocks

was only observed in the ^{19}F NMR spectrum of the BCP at -93.4 ppm (Figure IV-30). These ^{19}F signals are also visible in the ^{19}F NMR spectra of the PEVE-*b*-PVDF block copolymers synthesized using PEVE-CTA$_3$ and PEVE-CTA$_4$ as macro-CTAs (SI-Figure IV-44). The efficient chain extension was also confirmed by SEC (Figure IV-31).

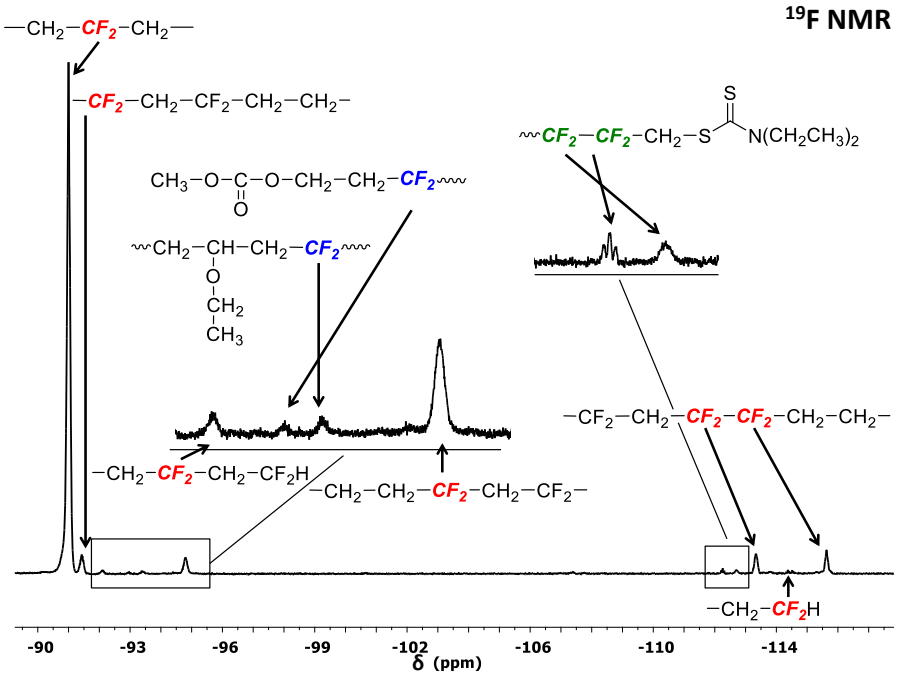

Figure IV-30: Expansion of the -90 to -118 ppm region of the ^{19}F NMR spectrum in $(CD_3)_2CO$ of the purified PEVE-b-PVDF-CTA$_2$ block copolymer (run 1, SI-Table IV-7) synthesized by RAFT polymerization of VDF using PEVE-CTA$_2$ as the CTA.

The SEC trace of the crude PEVE-*b*-PVDF-CTA$_2$ BCP (Figure IV-31b, left) shows the presence of a large amount of unreacted PEVE (at 2000 g.mol^{-1}) and indicates the relatively poor reactivation of PEVE-CTA$_2$ macro-CTA by PVDF$^{\bullet}$ radicals. In contrast, PEVE-CTA$_3$ macro-CTA was better reactivated by PVDF$^{\bullet}$ radicals. The SEC trace of the crude PEVE-*b*-PVDF-CTA$_3$ (Figure IV-31b, middle) only showed a small PEVE-CTA$_3$ macro-CTA residual peak. Finally PEVE-CTA$_4$, although of higher dispersity than its dithiocarbamate analogs, was entirely reactivated by PVDF$^{\bullet}$ radicals (Figure IV-31b, right). To further investigate this contamination caused by the suboptimal reactivation of the PEVE-CTA, the ^{1}H NMR spectra of the crude and purified BCP (precipitated in hexane, good solvent for PEVE and bad solvent for PVDF) were compared (SI-Figure IV-47SI-Figure IV-49). The residual fraction of PEVE-CTA$_2$ (peak at 6.1 ppm in SI-Figure IV-47), which was not reactivated by PVDF$^{\bullet}$ radicals, was eliminated by this precipitation (SI-Figure IV-47 and SI-Figure IV-49). This observation strongly supports the hypothesis of a slow reactivation of PEVE-CTA$_2$

macroCTA by PVDF$^{\bullet}$ radicals compared to PEVE-CTA_3 and PEVE-CTA_4, and is in agreement with the slowdown of the polymerization observed for the VDF RAFT polymerization mediated by CTA_1. In addition, the PEVE-O-CH_3 dead chains (peak at 4.6 ppm in Figures SI-Figure IV-47and SI-Figure IV-49), formed by quenching by methanol and which did not take part in the RAFT polymerization of VDF, were also removed in the precipitation process.

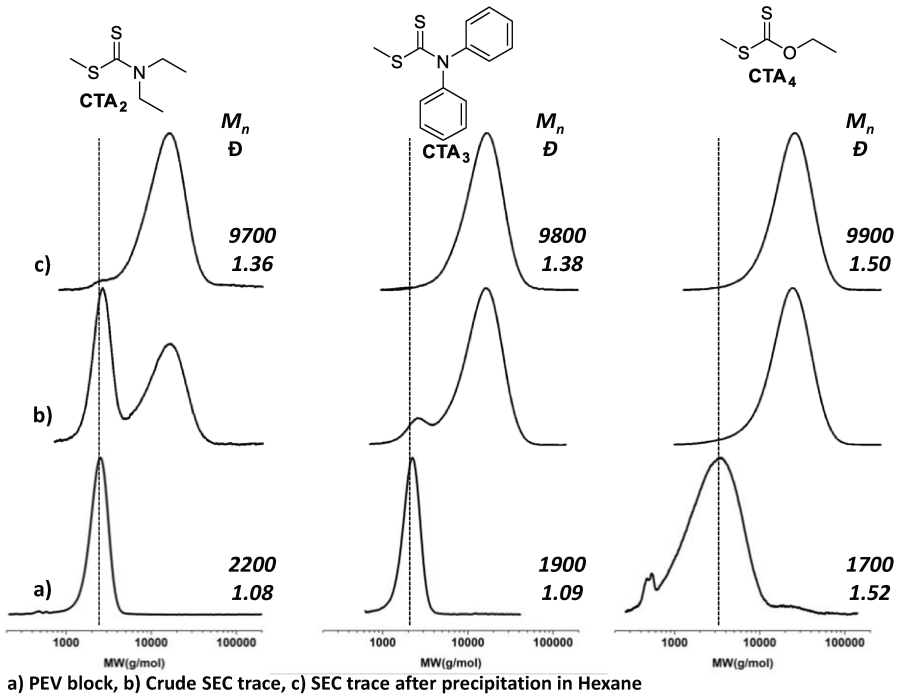

Figure IV-31: SEC traces of polymers synthesized using different CTAs (from left to right: CTA_2, CTA_3, CTA_4): a) PEVE-CTA, b) crude PEVE-b-PVDF-CTA, c) PEVE-b-PVDF-CTA after precipitation in hexane (good solvent for PEVE and bad solvent for PVDF).

It is also important to note the absence of the characteristic signal of the xanthate end-group in the ^{1}H NMR spectrum of the purified PEVE-*b*-PVDF-CTA_4 BCP (SI-Figure IV-49). The *O*-ethyl signals observed at 1.39 ppm and 4.65 ppm in the ^{1}H NMR of the crude BCP disappeared after precipitation. This means that side reactions occurred on the *O*-ethyl xanthate end-group during the VDF polymerization. These reactions also affect the dithiocarbamate-functionalized polymers, but at a much slower rate. DMC radicals produced by proton abstraction by -$CF_2^{\bullet}$ radicals were shown to either initiate new PVDF chains (as observed on all BCPs ^{1}H NMR spectra : peaks at 3.71 and 4.31 ppm corresponding to the CH_3 and CH_2 of the DMC moiety, respectively), or to transfer to the PVDF xanthate ω-end-group.[20,22] In the present case, these transfer reactions likely consume entirely the remaining xanthate end-group to form ($CH_3O(C{=}O)OCH_2$-S(C=S)-OCH_2CH_3) adducts which are

eliminated by precipitation. In comparison, the functionalities of PEVE-*b*-PVDF-CTA_2 (58%) and PEVE-*b*-PVDF-CTA_3 (80 %) are much higher.

The PEVE-*b*-PVDF block copolymers were analyzed by differential scanning calorimetry (DSC) to investigate the miscibility of PEVE and PVDF. The DSC thermograms of all BCPs display a melting temperature at *ca.* 160-170 °C corresponding to the melting point of PVDF (SI-Figure IV-50). In addition, the glass transition (T_g) of PEVE at -35 °C was also observed on all thermograms. These results strongly suggest the immiscibility of the PVDF and of the PEVE segments.

IV. Conclusion

This communication describes the successful use of sequential cationic RAFT polymerization and radical RAFT polymerization to prepare novel well-defined PEVE-*b*-PVDF block copolymers. Dithiocarbamates RAFT agents are particularly well-suited for this synthesis which leads to block copolymers containing incompatible blocks. These new block copolymers could be very useful as compatibilizers, for example for electronic devices. The study of the self-assembly of these block copolymers in selective solvents[28] and in the bulk[5] are underway and will be published in due course.

V. Acknowledgements

The authors thank Arkema (Pierre Benite, France) for providing VDF, the Ministère de l'Education Nationale et de l'Enseignement Supérieur et de la Recherche for the Ph.D grant awarded to MG, the Japan Society for the Promo-tion of Science (JSPS) for the JSPS Summer program Fellow-ship 2016 awarded to MG and the PhD grant awarded to EF by the Institut Carnot Chimie Balard and the LABEX CheMISyst (ANR-10-LABX-05-01).

VI. References

[1] D. W. Smith, S. T. Iacono, S. I. Suresh, In *Handbook of Fluoropolymers Science and Technology*, Eds., John Wiley & Sons, Inc.: New York, 2004.

[2] J. Gardiner, *Aust. J. Chem,*. 2015, **68**, 13−22.

[3] B. Améduri, B. Boutevin, In *Well-Architectured Fluoropolymers: Synthesis, Properties and Applications*, Eds.; Elsevier: Amsterdam, 2004.

[4] B. Ameduri, *Chem. Rev*., 2009, **109**, 6632−6686.

[5] V. S. D. Voet. G. ten Brinke, K. Loos, K. *J. Polym. Sci., Part A: Polym. Chem*., 2014, **52**, 2861–2877.

[6] Z. B. Zhang, S. K. Ying, Z. Q. Shi, *Polymer*, 1999, **40**, 1341–1345.

[7] S. M. Jol, W. S. Lee, B. S. Ahn, K; Y. Park, K. A. Kim, I. S. Rhee Paeng, *Polym. Bull*., 2000, **44**, 1–8.

[8] M. Destarac, K. Matyjaszewski, E. Silverman, B. Améduri, B. Boutevin, *Macromolecules*, 2000, **33**, 4613–4615.

[9] Z. Q. Shi, S. Holdcroft, *Macromolecules*, 2004, **37**, 2084–2089.

[10] Z. Q. Shi, S. Holdcroft, *Macromolecules*, 2005, **38**, 4193–4201.

[11] G. Laruelle, E. Nicol, B. Améduri, J. F. Tassin, N. J. and Ajellal, *J. Polym. Sci., Part A: Polym. Chem.*, 2011, **49**, 3960–3969.

[12] K; Xu, K. Li, P. Khanchaitit, Q. Wang, *Chem. Mater*., 2007, **19,** 5937–5945.

[13] C. Chanthad, K. A. Masser, K. Xu, J. Runt, Q. J. Wang, *Mater. Chem*., 2012, **22**, 341–344.

[14] V. S. D. Voet, M. Tichelaar, S. Tanase, M. C. Mittelmeijer- Hazeleger, G. ten. Brinke, K. Loos, *Nanoscale*, 2013, **5**, 184–192.

[15] V. S. D. Voet, D. Hermida-Merino, G. ten. Brinke and K. Loos, *RSC Adv*., 2013, **3**, 7938–7946.

[16] G. David, C. Boyer, J. Tonnar, B. Ameduri, P. Lacroix-Desmazes, B. Boutevin, *Chem. Rev*., 2006, **106**, 3936–3981

[17] M. Tatemoto, In *The First Regular Meeting of Soviet Japanese Fluorine Chemists*, Tokyo, 1979.

[18] D. Valade, C. Boyer, B. Ameduri, B. Boutevin, *Macromolecules*, 2006, **39**, 8639–8651.

[19] A. D. Asandei, O. I. Adebolu, C. P. Simpson, *J. Am. Chem. Soc*., 2012, **134**, 6080−6083.

[20] M. Guerre, B. Campagne, O. Gimello, K. Parra, B. Ameduri, V. Ladmiral, *Macromolecules*, 2015, **48**, 7810-2799.

[21] M. Guerre, T. Soulestin, G. Lopez, C. Totée, B. Améduri, G. Silly, V. Ladmiral, *Macromol. Chem. Phys.*, 2016, **217**, 2275–2285.

[22] M. Guerre, S. M. W. Rahaman, B. Améduri, R. Poli. V. Ladmiral, *Macromolecules*, 2016, **49**, 5386–5396.

[23] M. Guerre, S. M. W. Rahaman, B. Améduri, R. Poli, V. Ladmiral, *Polym. Chem.,* 2016, **7,** 6918–6933.

[24] M. Guerre, J. Schmidt, Y. Talmon, B. Ameduri, V. Ladmiral, *Polym. Chem*., 2017, **8**, 1125-1128.

[25] M. Guerre, M. Semsarilar, F. Godiard, B. Ameduri, V. Ladmiral*, Polym. Chem*., 2017, DOI: 10.1039/c6py02203k.

[26] M. Uchiyama, K. Satoh, M. Kamigaito, *Angew. Chem. Int. Ed.*, 2015, **54**, 1924-1928.

[27] T. G. McKenzie, Q. Fu, M. Uchiyama, K. Satoh, J. Xu, C. Boyer, M. Kamigaito, G. G. Qiao*, Adv. Sci*., 2016, **3**, 1500394.

[28] Y. Mai, A. Eisenberg, *Chem. Soc. Rev*., 2012, **41**, 5969-5985.

[29] X. Liu, O. Coutelier, S. Harrisson, T. Tassaing, J-D. Marty, M. Destarac, *ACS Macro Lett*., 2015, **4**, 89−93.

[30] J. L., O'Brien, F. Gornick*, J. Am. Chem. Soc*., 1955, **77**, 4757.

VII. Supporting Informations

VII.1 Materials

Radical RAFT

All reagents were used as received unless stated otherwise. 1,1- Difluoroethylene (vinylidene fluoride, VDF) was kindly supplied by Arkema (Pierre-Bénite, France). tert-Amyl peroxy-2-ethylhexanoate (Trigonox® 121, purity 95%) was purchased from AkzoNobel (Chalons-sur-Marne, France). Methyl 2-((diethylcarbamothioyl)thio)propanoate (CTA_1) was synthesized according to the method described by Liu et al.[29] slightly modified (The potassium ethyl xanthogenate salt was replaced by sodium diethyldithiocarbamate trihydrate salt).

Ethyl vinyl ether (EVE), methyl 2-bromopropionate, dimethyl Carbonate (DMC), methanol (MeOH), acetone ($(CH_3)_2CO$), ethanol (EtOH) and n-hexane (Hex) (>99 %) were purchased from Sigma Aldrich and used as received.

Cationic RAFT

Ethyl vinyl ether (EVE) (TCI, 98%) was distilled over calcium hydride under reduced pressure before use. Trifluoromethanesulfonic (Triflic) acid (TfOH) (TCI,>98.0%) was used as received. *S-1*-Isobutoxyethyl *N,N*-diethyl dithiocarbamate[29] (CTA_2), *S-1*-isobutoxyethyl *N,N*-diphenyl dithiocarbamate[26] (CTA_3) and *S-1*-isobutoxyethyl *O*-ethyl xanthate[26] (CTA_4) were synthesized according to previously published protocols. Toluene (KANTO, >99.5%; H_2O <10 ppm), *n*-hexane (KANTO, >96%; H_2O <10 ppm), diethyl ether (KANTO, >99.5%; H_2O <50 ppm), and dichloromethane (KANTO, >99.5%; H_2O <0.005%) were dried and deoxygenized by passage through column of Glass Contour Systems before use.

VII.2 Characterization

Nuclear magnetic resonance (NMR)

The Nuclear Magnetic Resonance (NMR) spectra were recorded on a Bruker AC 400 instrument. Deuterated acetone was used as the solvent. Coupling constants and chemical shifts are given in Hertz (Hz) and part per million (ppm), respectively. The experimental conditions for recording ^1H, ^{19}F, spectra were as follows: flip angle 90° (or 30°), acquisition

time 4.5 s (or 0.7 s), pulse delay 2 s (or 2 s), number of scans 128 (or 512), and a pulse width of 5 μs for ^{19}F NMR.

Size Exclusion Chromatography (SEC)

Size exclusion chromatograms were recorded using a Triple detection GPC from Agilent Technologies with its corresponding Agilent software, dedicated to multi-detector GPC calculation. The system used two PL1113-6300 ResiPore 300 x 7.5 mm columns (all range of Mw) with DMF as the eluent with a flow rate of 0.8 mL/min and toluene as flow rate marker. The detector suite comprised a PL0390-0605390 LC light scattering detector with 2 diffusion angles (15° and 90°), a PL0390-06034 capillary viscometer, and a 390-LC PL0390-0601 refractive index detector. The entire SEC-HPLC system was thermostated at 35°C. PMMA narrow standards were used for the calibration. Typical sample concentration was 10 mg/mL.

Differential scanning calorimetry (DSC)

DSC measurements were performed on 10 - 15 mg samples on a Netzsch DSC 200 F3 instrument using the following heating/ cooling cycle: cooling from room temperature (ca. 20 °C) to -50 °C at 20 °C min^{-1}, isotherm plateau at -50 °C for 5 min, first heating ramp from -50 to 200 °C at 10 °C min^{-1}, cooling stage from 200 to -50 °C at 10 °C min^{-1}, isotherm plateau at -50 °C for 3 min, second heating ramp from -50 °C to 200 °C at 10 °C min^{-1} and last cooling stage from 200 °C to room temperature (ca. 20 °C). The instrument was calibrated with noble metals and checked before analysis with an indium sample. Melting points were determined at the maximum of the enthalpy peaks.

Autoclave

The radical polymerizations of VDF were performed in a 100 mL Hastelloy Parr autoclave systems (HC 276), equipped with a mechanical Hastelloy stirring system, a rupture disk (3000 PSI), inlet and outlet valves, and a Parr electronic controller to regulate the stirring speed and the heating. Prior to reaction, the autoclave was pressurized with 30 bars of nitrogen to check for leaks. The autoclave was then put under vacuum (20.10^{-3} mbar) for 30 minutes to remove any trace of oxygen. A degassed solution of solvent, initiator and CTA was introduced via a funnel. The reactor was then cooled down in liquid nitrogen to about -80°C, and the desired quantity of VDF was transferred by double weighing (i.e. the difference of weight before and after filling the autoclave with VDF). After warming up to

ambient temperature (*ca.* 20 °C), the autoclave was heated to the target temperature under mechanical stirring.

VII.3 Syntheses

Methyl 2-((diethylcarbamothioyl)thio)propanoate (CTA_1)

^{1}H NMR (400 MHz $(CD_3)_2CO$, (δ ppm), SI-Figure IV-32): 1.18 – 1.34 (-N(CH_2**CH_3**)$_2$), 1.49-1.58 (d, (**CH_3**)CH-(C=O)), 3.65-3.72 (s, -(C=O)O**CH_3**), 3.73-3.86 (q, (-N(**CH_2**CH_3)$_2$), 3.96-4.10 (q, (-N(CH_2CH_3)$_2$), 4.66-4.79 (q, (CH_3)**CH**-(C=O)).

^{13}C NMR (100 MHz $(CD_3)_2CO$, (δ ppm), SI-Figure IV-33): 11.63 (-N(CH_2**CH_3**)$_2$), 12.75 (-N(CH_2**CH_3**)$_2$), 17.85 ((**CH_3**)CH-(C=O)), 47.53 (-N(**CH_2**CH_3)$_2$), 49.41 ((CH_3)**CH**-(C=O)), 50.16 (-N(**CH_2**CH_3)$_2$), 52.68 (-(C=O)O**CH_3**), 172.70 (-(**C=S**)S-), 193.43 (**C=O**).

RAFT Homopolymerization of Vinylidene Fluoride (VDF) with CTA_1

Using the experimental setup described above, a typical polymerization of VDF was performed as follows: A solution of Trigonox® 121 (158 mg, 6.87×10^{-4} mol) and CTA_1 (1.47 g, 6.25×10^{-3} mol) in DMC (60 mL) was degassed by N_2 bubbling for 30 min. This homogeneous solution was introduced into the autoclave using a funnel, VDF gas (19.0 g, 0.297 mol) was transferred in the autoclave at low temperature, and the reactor was gradually heated to 73 °C. The reaction was stopped after 20 h. During the reaction, the pressure increased to a maximum of 25 bar and then decreased to 10 bar after 20 h. The autoclave was cooled to room temperature (ca. 20 °C), purged from the residual monomers, and the dimethylcarbonate solvent was removed under vacuum. The crude product was dissolved in 30 mL of warm THF (ca. 40 °C) and left under vigorous stirring for 30 min. This polymer solution was then precipitated from 400 mL of chilled hexane. The precipitated polymer (white powder) was filtered through a filter funnel and dried under vacuum (15×10^{-3} mbar) for 2 h at 50 °C. The polymerization yield (24%) was determined gravimetrically (mass of dried precipitated polymers/mass of monomer introduced in the pressure reactor). Yields were used as conversion, since conversion is very difficult to measure accurately for VDF and other gaseous monomers.

Typical Cationic RAFT Polymerization of EVE

The cationic RAFT polymerization of EVE was carried out by the syringe technique under dry nitrogen in baked glass tubes equipped with a three-way stopcock. A typical example for the polymerization procedure is given below. The reaction was initiated by addition of TfOH (4.3 mL of 0.65 mM in Et_2O) via dry syringe into monomer solution (43.17 mL) containing EVE (27.7 mM), *S-1*-isobutoxyethyl *N,N*-diethyl dithiocarbamate (0.55 mM), and toluene (0.97 mL) in *n*-hexane/CH_2Cl_2 mixture (8/1 vol) at –40 ºC. At predetermined intervals, the polymerization was terminated with methanol (15.0 mL) containing small amount of triethylamine. The monomer conversion was determined from the concentration of residual monomer measured by ^{1}H NMR with toluene as an internal standard (e.g., for 25 sec, 90% conversion). The quenched reaction mixture was washed with distilled water to remove initiator residues, evaporated to dryness under reduced pressure, and vacuum-dried to yield a viscous oil (Yield = 99%).

Typical Block copolymers synthesis (PEVE-*b*-PVDF) via RAFT radical polymerization

Radical RAFT chain extension reactions were carried out in thick 8 mL Carius tubes in which a solution of the initiator (Trigonox® 121, 2.7 mg, 1.17 10^{-5} mol) and the macro-CTA (PEVE)-CTA_2, 0.225 mg, 5.85 10^{-5} mol) in DMC (5 mL), was added and then degassed by performing at least three freeze−pump−thaw cycles. The gaseous monomer was introduced into the Carius tube at the liquid nitrogen temperature (VDF, 1.5 g, 2.34 10^{-2}, mol, 1 ΔP) using a custom-made manifold that enables accurate measurement of quantities of gas (using “pressure drop *vs* mass of monomer” calibration curves). The tube was then sealed under dynamic vacuum at the temperature of liquid nitrogen, before being placed horizontally in a shaking water bath thermostated at 73 °C. After 24 h, the tube was placed into liquid nitrogen, opened, and then the solvent was evaporated at 50 °C under reduced pressure. Conversion was determined gravimetrically after drying under vacuum for 16 hours until constant weight. The unreacted PEVE macro-CTA was then eliminated by dissolving the powder in 2 mL of acetone and precipitation in 50 mL of chilled pentane (good solvent for PEVE, bad solvent for PVDF). The PVDF was then isolated as a white powder by centrifugation, and dried at 40 °C and 8 mbar for 2h in a vacuum.

VII.4 Figures

(CTA1) : Methyl 2-((N,N-diethylcarbamothioyl)thio)propanoate

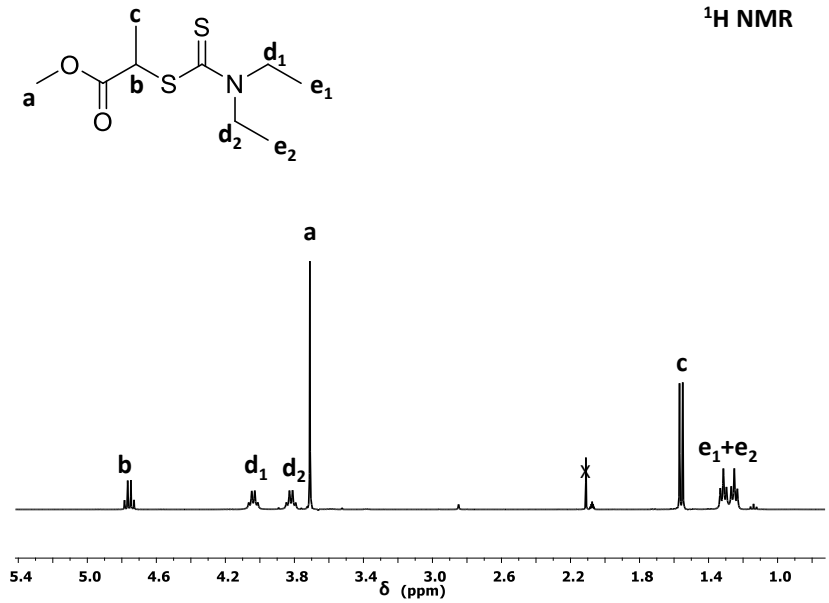

SI-Figure IV-32: Expansion of the 0.7 to 5.4 ppm region of [1]H NMR of Methyl 2-((N, N-diethylcarbamothioyl)thio)propanoate (CTA_1) in $(CD_3)_2CO$. The crossed-out peak is assigned to residual solvent (acetone).

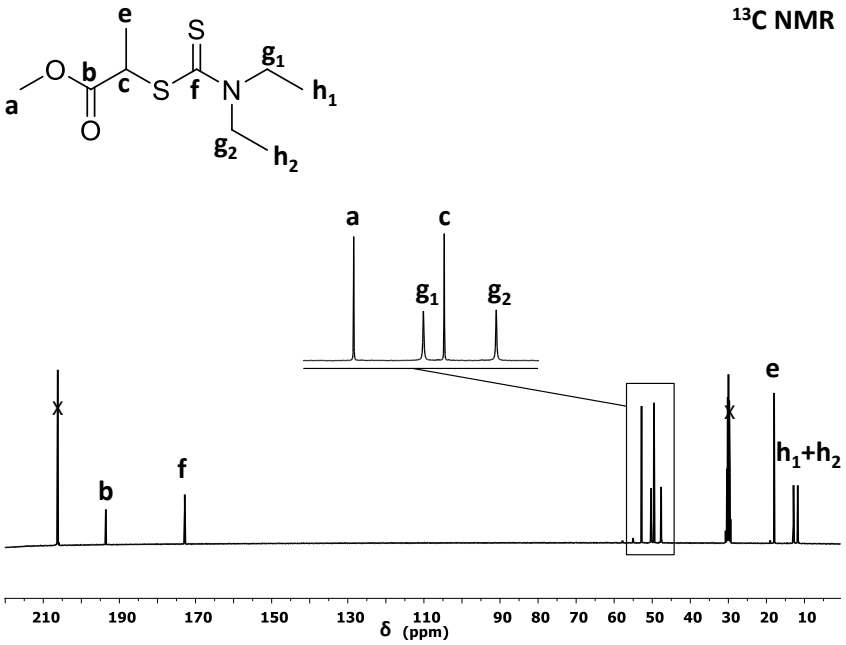

SI-Figure IV-33: Expansion of the 0 to 220 ppm region of the [13]C NMR of Methyl 2-((N, N-diethylcarbamothioyl)thio)propanoate (CTA_1) in $(CD_3)_2CO$. The crossed-out peak is assigned to residual solvent (acetone).

Radical RAFT polymerization of VDF with CTA_1:

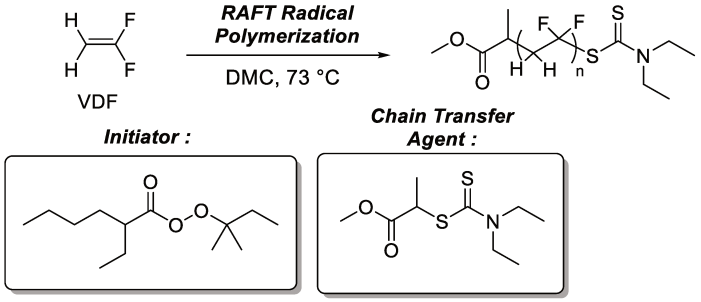

SI-Scheme IV-3: Schematic Representation of VDF RAFT VDF polymerization with CTA_1

SI-Table IV-5: Experimental conditions and results for the radical RAFT polymerization of VDF using CTA_1[a]

Entry	M	$[M]_0/[CTA]_0/[I]_0$	Time (h)	Yield[b] (%)	$M_{n(theo)}$[c] (g/mol)	$M_{n(NMR)}$[d] (g/mol)	$M_{n(SEC)}$[e] (g/mol)	$Đ$[e]
1	VDF	100/1/0.11	10	4	370	1300	1100	1.20
2	VDF	100/1/0.11	15	11	600	1600	4400	1.10
3	VDF	100/1/0.11	17.5	29	1200	4000	8700	1.30
4	VDF	100/1/0.11	20	21	900	2700	6500	1.18
5	VDF	100/1/0.11	24	32	1300	4500	8200	1.28
6	VDF	50/1/0.1	24	24	1000	1700	4600	1.08
7	VDF	200/1/0.1	24	32	4300	5500	11100	1.31

[a]Reactions conditions: Initiator (I) = Trigonox® 121, T= 73 °C, solvent = DMC. [b]Determined gravimetrically. [c]Calculated using yield as conversion and SI-Equation IV-16. [d]Calculated using equations SI-Equation IV-17and SI-Equation IV-18. [e]Determined by SEC calibrated using with PMMA narrow standards.

SI-Equation IV-16
$$M_{n(theo)} = \frac{[M]_0}{[CTA]_0} \times Yield \times M_{n,VDF} + M_nCTA$$

SI-Equation IV-17
$$DP = \frac{\int_{2.70}^{3.19} CH_2(HT) + \int_{2.28}^{2.43} CH_2(TT) + \int_{4.37}^{4.52} CH_2(End-group)}{2/3 \times \int_{1.19}^{1.24} CH_3(R-CTA)}$$

SI-Equation IV-18
$$M_{nNMR} = M_nCTA + DP \times M_nVDF$$

With $M_{n\ CTA} = 235.07$ g.mol^{-1} and $M_{n,VDF} = 64.04$ g.mol^{-1}

1st order kinetic plot:

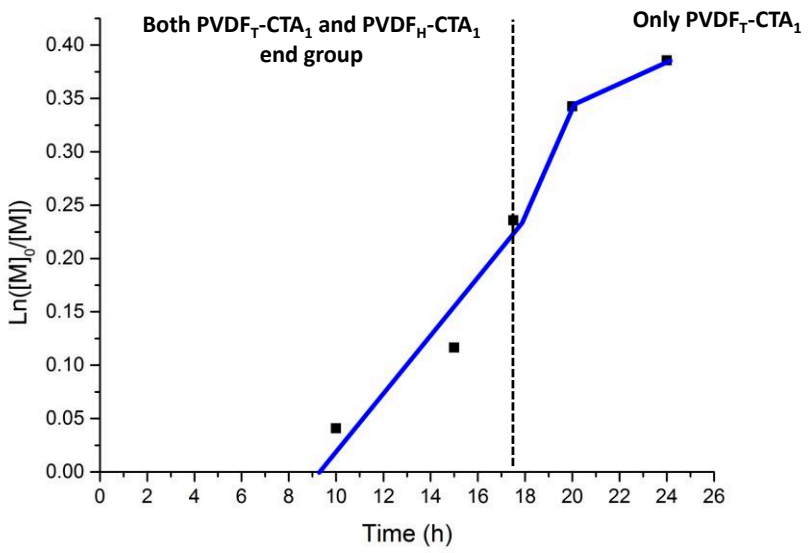

SI-Figure IV-34: First order kinetic plot of the RAFT polymerization of VDF using methyl 2-((N, N-diethylcarbamothioyl)thio)propanoate (CTA_1) as CTA. Reaction conditions: $[M]_0/[CTA]_0/[I]_0$ =100/1/0.1, T = 73 °C.

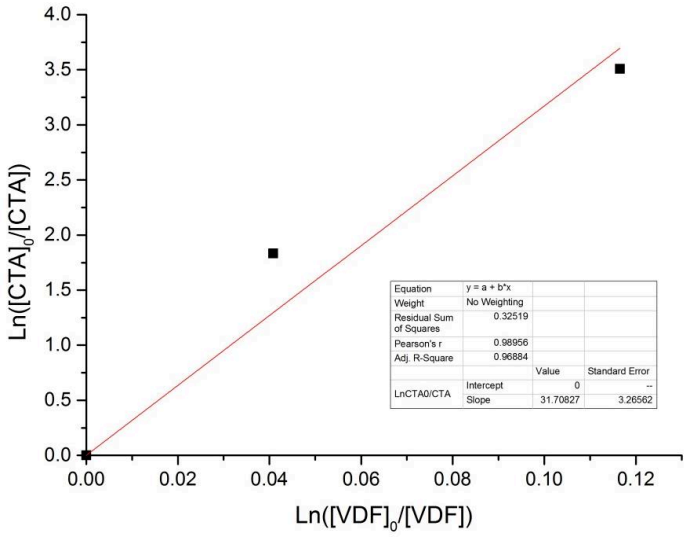

SI-Figure IV-35: Determination of the transfer constant of methyl 2-((N,N-diethylcarbamothioyl)thio)propanoate (CTA_1) with VDF using O'Brien's and Gornick's method.[30] Figure displays the plots of Ln($[CTA]_0/[CTA]$) versus Ln($[VDF]_0/[VDF]$). The slope of the linear fit of this plot provide the $C_{Tr(app)}$ value using SI-Equation IV-19:

SI-Equation IV-19 $$Ln\left(\frac{[CTA]_0}{[CTA]}\right) = C_{Tr(app)} Ln\left(\frac{[VDF]_0}{[VDF]}\right)$$

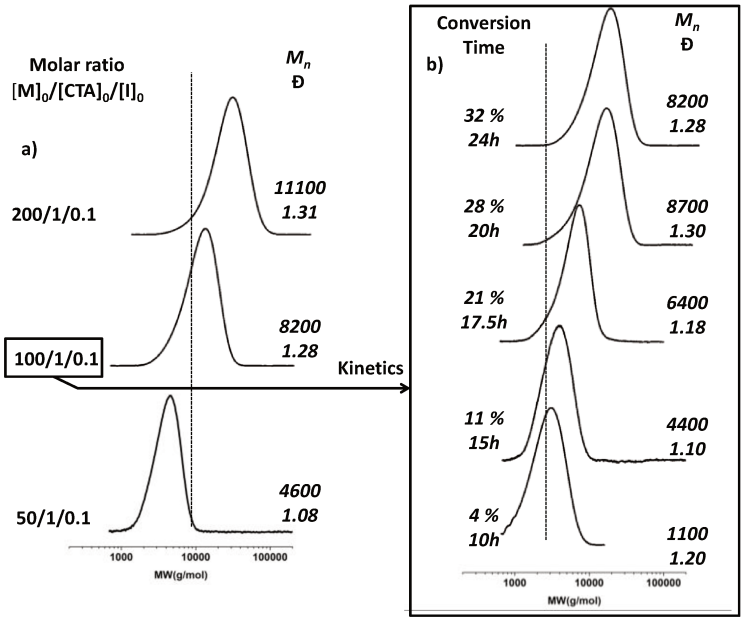

SI-Figure IV-36: a) SEC traces of the PVDF synthesized by RAFT polymerization in the presence of CTA_1 and using 3 different initial molar ratio $[M]_0/[CTA]_0/[I]_0$ = 50/1/0.1; 100/1/0.1; 200/1/0.1. b) Evolution of the SEC trace of the PVDF formed during the RAFT polymerization of VDF carried out in the presence of CTA_1. Reaction conditions: $[VDF]_0/[CTA_1]_0/[I]_0$ =100/1/0.1.

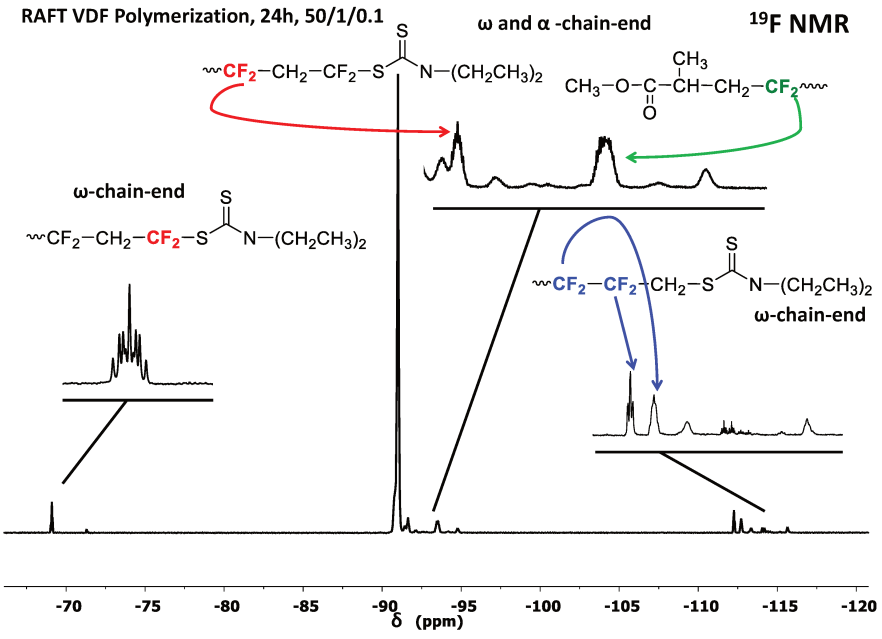

SI-Figure IV-37: Expansion of the -66 to -120 ppm region of the ^{19}F NMR spectrum in $(CD_3)_2CO$ of PVDF-CTA_1 homopolymer (run 1, SI-Table IV-5) synthesized by RAFT polymerization using CTA_1.

Cationic RAFT polymerization of Ethyl Vinyl Ether (EVE) with CTA_2, CTA_3, CTA_4

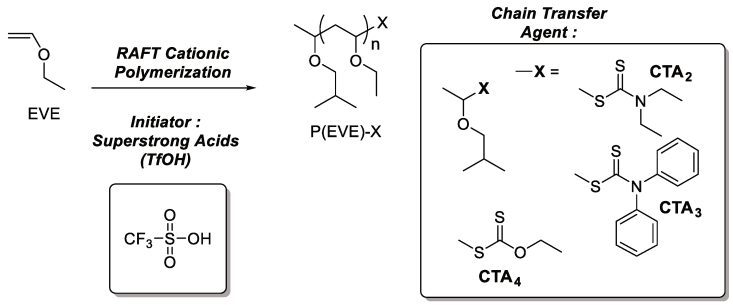

SI-Scheme IV-4: Schematic representation of the EVE cationic RAFT polymerization using CTA_2, CTA_3 or CTA_4.

SI-Table IV-6: Experimental conditions and results for the RAFT cationic polymerization of EVE homopolymers[a]

Entry	CTA	$[M]_0/[CTA]_0/[I]_0$	Time (h)	Conversion[b] (%)	$M_{n(theo)}$[c] (g/mol)	$M_{n(NMR)}$[d] (g/mol)	$M_{n(SEC)}$[e] (g/mol)	$Đ$[e]	Functionality[f]
1	CTA_2	50/1/0.005	1	99	3870	3970	2200	1.08	83
2	CTA_3	50/1/0.005	1	99	3970	4000	1900	1.09	95
3	CTA_4	50/1/0.005	45	85	3300	3950	1700	1.52	91

[a]Reactions conditions: Initiator (I) = TfOH, T = -40 °C for entry 1 and 2, -78 °C for entry 3, solvent : Hexane/CH_2Cl_2/Et_2O (80:10:10). [b]Determined from the residual monomer concentration measured by ^{1}H NMR with toluene as an internal standard. [c]Calculated using SI-Equation IV-20. [d]Calculated using equation SI-Equation IV-21and SI-Equation IV-22. [e]Determined by SEC calibrated using PMMA narrow standards. [f]Determined using SI-Equation IV-23.

SI-Equation IV-20
$$M_{n(theo)} = \frac{[M]_0}{[CTA]_0} \times Conv. \times M_{n,EVE} + M_nCTA$$

SI-Equation IV-21
$$DP = \frac{[\int_{1.38}^{1.91} CH_2\ PEVE(backbone) - 1H(CH\ R-CTA)] + \int_{5.94}^{6.21} CH-CTA\ (end\ group)}{1/3 \times \int_{0.87}^{0.94} (CH_3)_2 (R-CTA)}$$

SI-Equation IV-22
$$M_{nNMR} = M_nCTA + DP \times M_nEVE$$

SI-Equation IV-23
$$Functionality\ (\%) = \frac{\int_{5.93}^{6.24} CH-CTA\ (k)}{\int_{5.93}^{6.24} CH-CTA\ (k) + \int_{4.56}^{4.71} CH-OCH_3\ (n)} \times 100$$

With $M_{n,CTA2}$ = 249.43 g.mol^{-1}, $M_{n,CTA3}$ = 345.52 g.mol^{-1}, $M_{n,CTA4}$ = 222.36 g.mol^{-1} and $M_{n,EVE}$ = 72.11 g.mol^{-1}

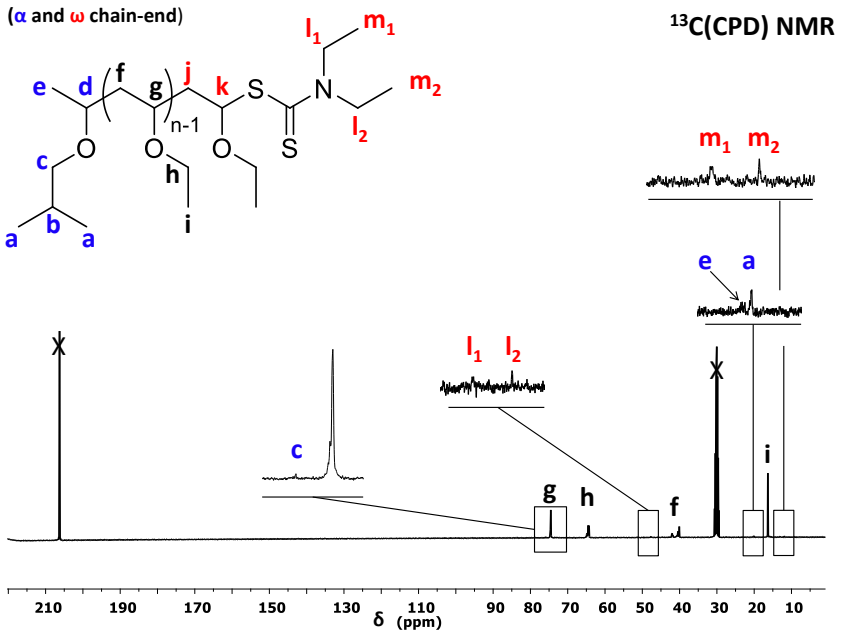

SI-Figure IV-38: Expansion of the 0 to 220 ppm region of the ^{1}H decoupled ^{13}C NMR spectrum of PEVE-diethylcarbamate homopolymer (run 1, SI-Table IV-6) synthesized by RAFT polymerization using CTA_2 in $(CD_3)_2CO$. Highlighted signals were assigned to PEVE α- and ω-CTA end-groups.

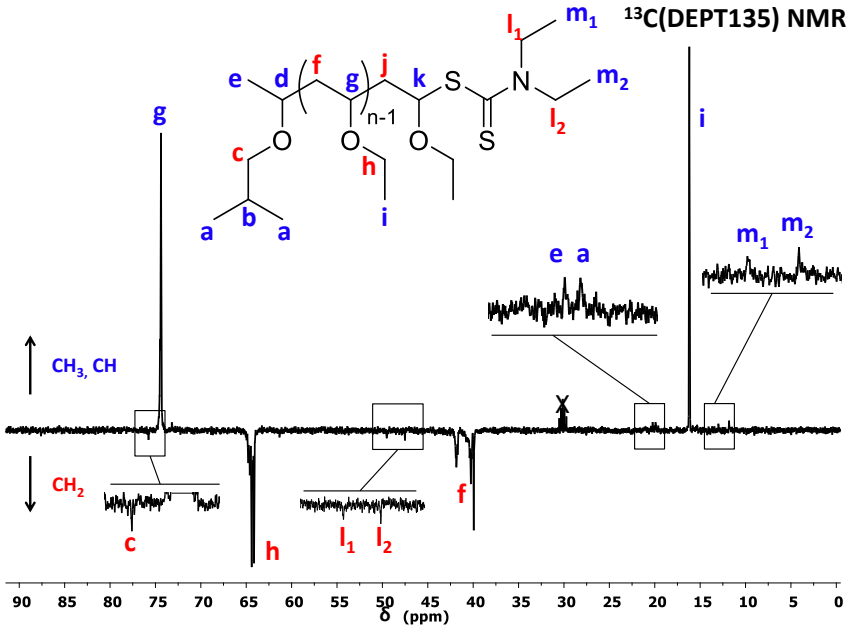

SI-Figure IV-39: pansion of the 0 to 90 ppm region of the DEPT135 ^{13}C NMR spectrum of PEVE-diethylcarbamate homopolymer (run 1, SI-Table IV-6) synthesized by RAFT polymerization using CTA_2 in $(CD_3)_2CO$. Highlighted signals were assigned to PEVE α- and ω-CTA end-groups.

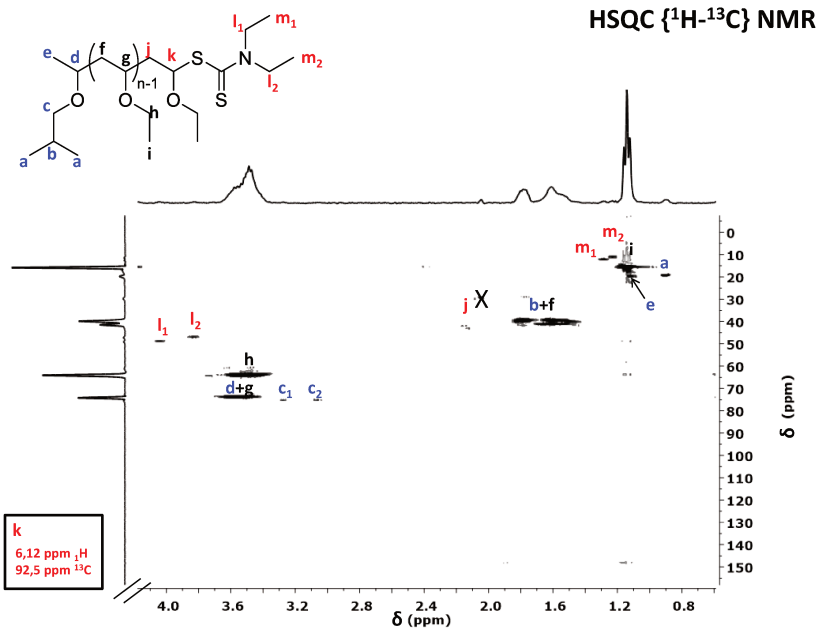

SI-Figure IV-40: HSQC ^{1}H-^{13}C NMR correlation spectrum of PEVE-diethylcarbamate homopolymer (run 1, SI-Table IV-6) synthesized by RAFT polymerization using CTA_2 in $(CD_3)_2CO$.

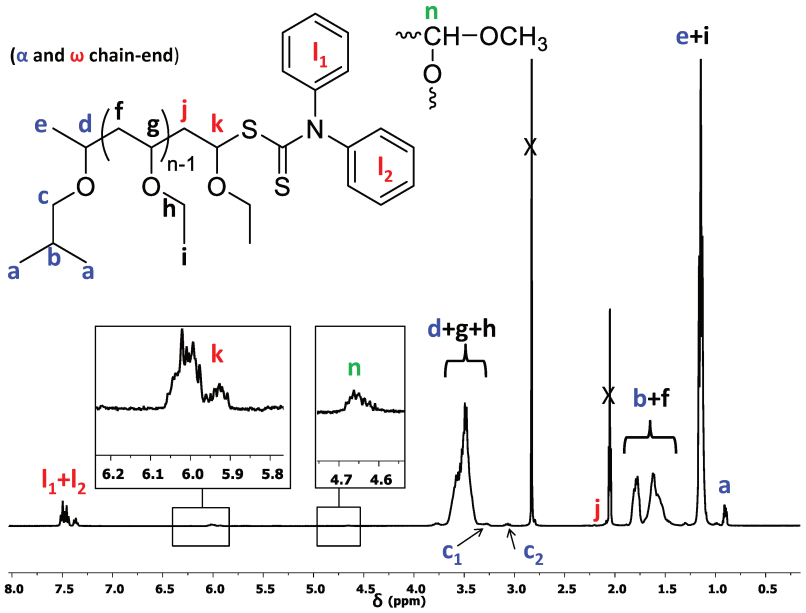

SI-Figure IV-41: Expansion of the 0 to 8 ppm region of the ^{1}H NMR spectrum of PEVE-diphenylcarbamate homopolymer (run 2, SI-Table IV-6) synthesized by RAFT polymerization using CTA_3 in $(CD_3)_2CO$. Highlighted signals were assigned to PEVE α- and ω-CTA end-groups.

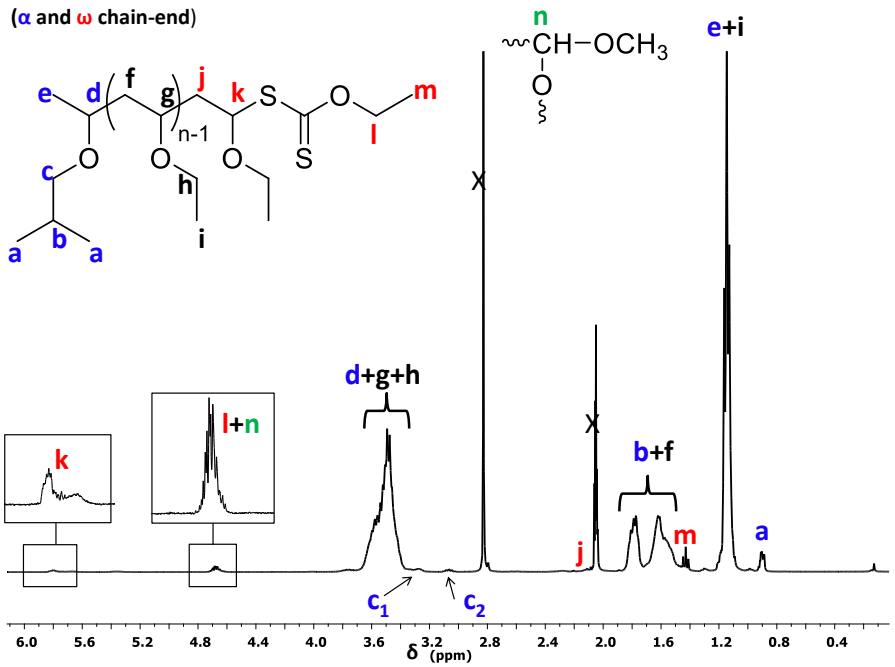

SI-Figure IV-42: Expansion of the 0 to 6 ppm region of the ^{1}H NMR spectrum of PEVE-xanthate homopolymer (run 3, SI-Table IV-6) synthesized by RAFT polymerization using CTA$_4$ in (CD$_3$)$_2$CO. Highlighted signals were assigned to PEVE α- and ω-CTA end-groups.

Radical RAFT polymerization of VDF with PEVE-CTA$_{2,3,4}$:

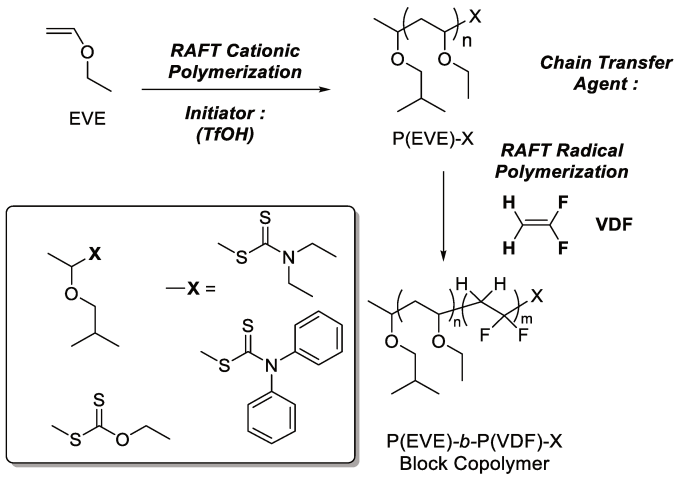

SI-Scheme IV-5: Schematic representation of VDF radical RAFT polymerization using PEVE-CTA$_2$, CTA$_3$ or CTA$_4$.

SI-Table IV-7: Experimental conditions and results for the chain extension of PEVE-CTA by RAFT radical polymerization of VDF[a]

Entry	Macro-CTA	M	$[M]_0/[CTA]_0/[I]_0$	Yield[b] (%)	$M_{n(theo)}$[c] (g/mol)	$M_{n(NMR)}$[d] (g/mol)	$M_{n(SEC)}$[e] (g/mol)	$Đ$[e]
1	PEVE-CTA$_2$	VDF	400/1/0.1	33	12500	33100	9700	1.36
2	PEVE-CTA$_3$	VDF	400/1/0.1	57	16600	31600	9800	1.38
3	PEVE-CTA$_4$	VDF	400/1/0.1	60	19400	68700	9900	1.50

[a]Reactions conditions: Initiator (I) = Trigonox® 121, T= 73 °C, solvent = DMC. [b]Determined gravimetrically. [c]Calculated using yields as conversion following SI-Equation IV-24. [d]Calculated using equation SI-Equation IV-25 and SI-Equation IV-26. [e]Determined by SEC with PMMA standard.

SI-Equation IV-24
$$M_{n(theo)} = \frac{[M]_0}{[PEVE-CTA]_0} \times Yield \times M_{n,VDF} + M_nPEVE - CTA$$

SI-Equation IV-25
$$DP = \frac{\int_{2.70}^{3.19} CH_2(HT) + \int_{2.28}^{2.43} CH_2(TT) + \int_{4.02}^{4.17} CH_2(End-group)}{1/3 \times \int_{0.87}^{0.94} (CH_3)_2(R-CTA\ PEVE\ block)}$$

SI-Equation IV-26
$$M_{nNMR} = M_nPEVE - CTA + DP \times M_nVDF$$

With $M_{n,PEVE\text{-}CTA2}$ = 3970 g.mol^{-1}, $M_{n,PEVE\text{-}CTA3}$ = 4000 g.mol^{-1}, $M_{n,PEVE\text{-}CTA4}$ = 3950 g.mol^{-1} and $M_{n,VDF}$ = 64.04 g.mol^{-1}.

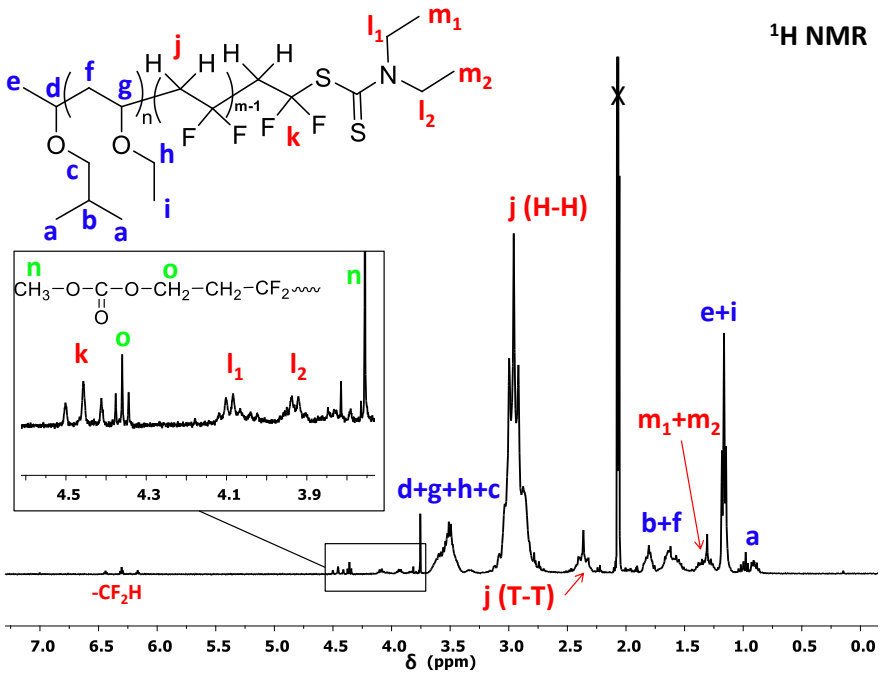

SI-Figure IV-43: Expansion of the 0 to 7.5 ppm region of the ^{1}H NMR spectrum in $(CD_3)_2CO$ of the purified PEVE-b-PVDF-CTA$_2$ block copolymer (run 1, SI-Table IV-7) synthesized by RAFT polymerization using PEVE-CTA$_2$. H-H and T-T stand for head-to-head and tail-to-tail, respectively.

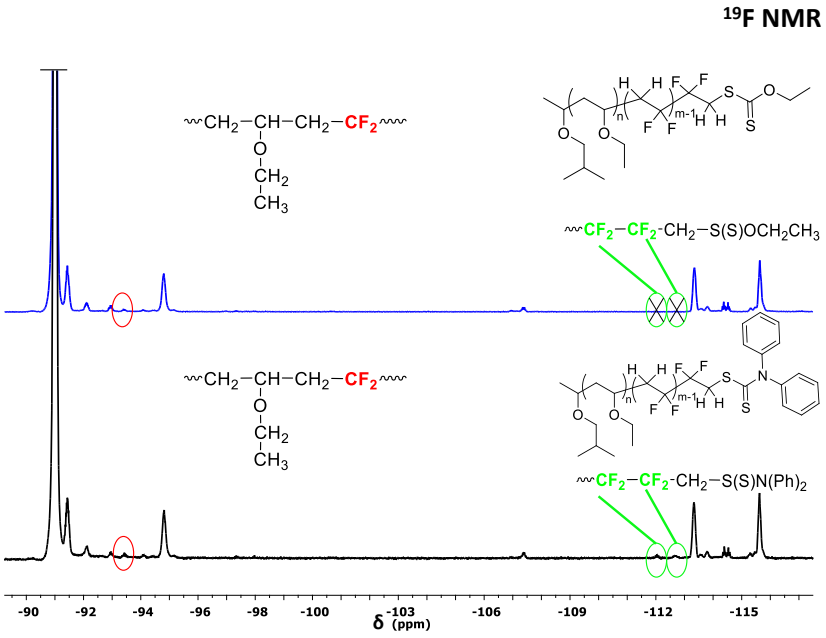

SI-Figure IV-44: Expansion of the -89 to -117 ppm region of the ^{19}F NMR spectra in $(CD_3)_2CO$ of the purified PEVE-b-PVDF-CTA$_3$ (bottom) and of PEVE-b-PVDF-CTA$_4$ (top) block copolymer (run 2 and 3, SI-Table IV-7) synthesized by RAFT polymerization using PEVE-CTA$_3$ and PEVE-CTA$_4$, respectively.

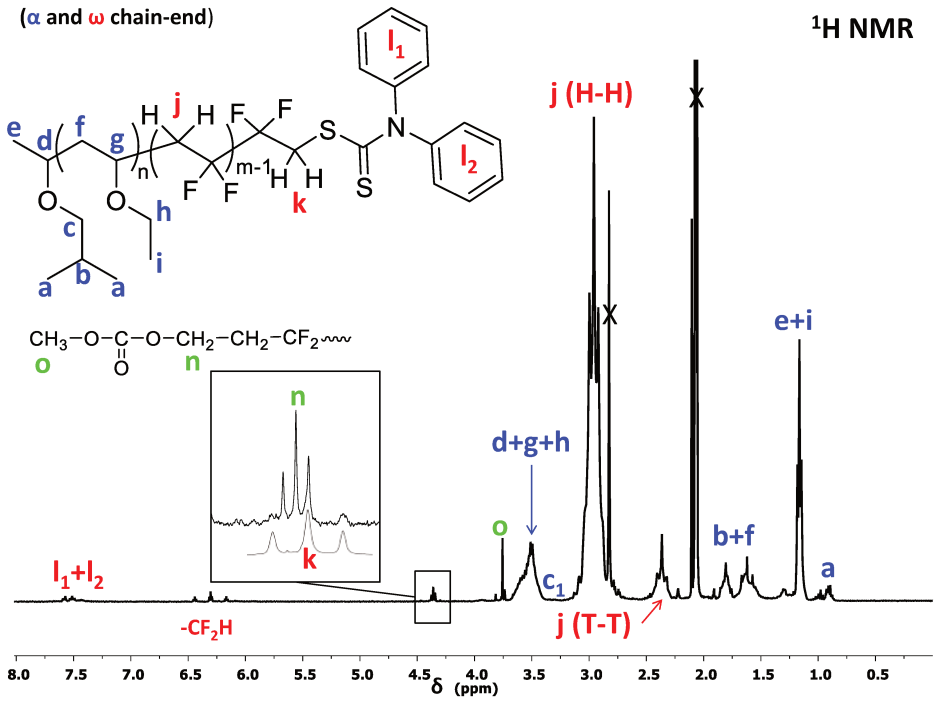

SI-Figure IV-45: Expansion of the 0 to 8 ppm region of the ^{1}H NMR spectrum in $(CD_3)_2CO$ of the purified PEVE-b-PVDF-CTA$_3$ (run 2, SI-Table IV-7) synthesized by RAFT polymerization using PEVE-CTA$_3$.

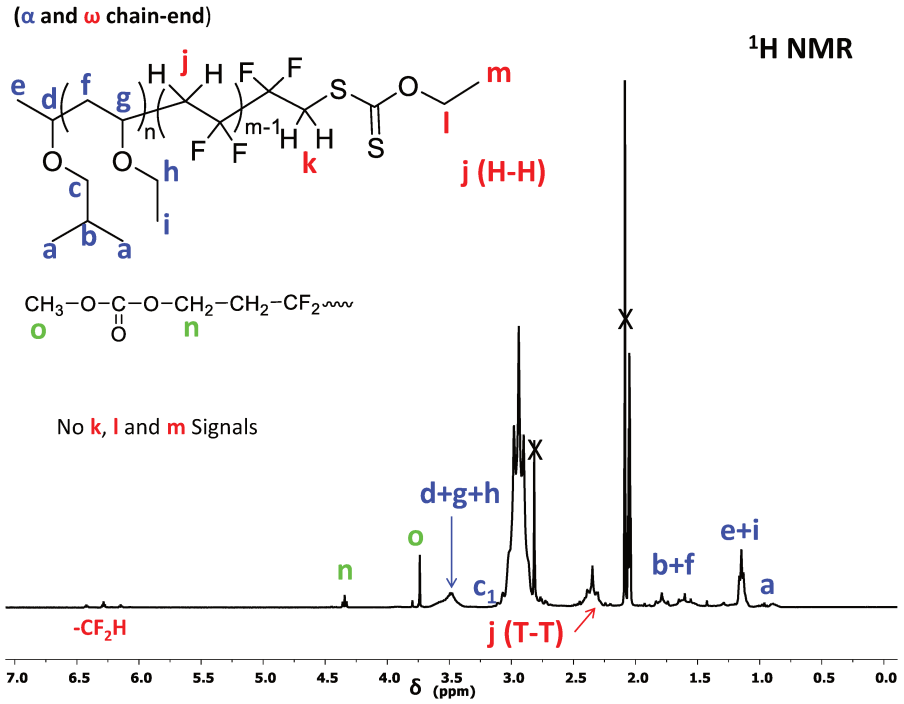

SI-Figure IV-46: Expansion of the 0 to 7 ppm region of the ^{1}H NMR spectrum in $(CD_3)_2CO$ of the purified PEVE-b-PVDF-CTA$_4$ (run 3, SI-Table IV-7) synthesized by RAFT polymerization using PEVE- CTA$_4$.

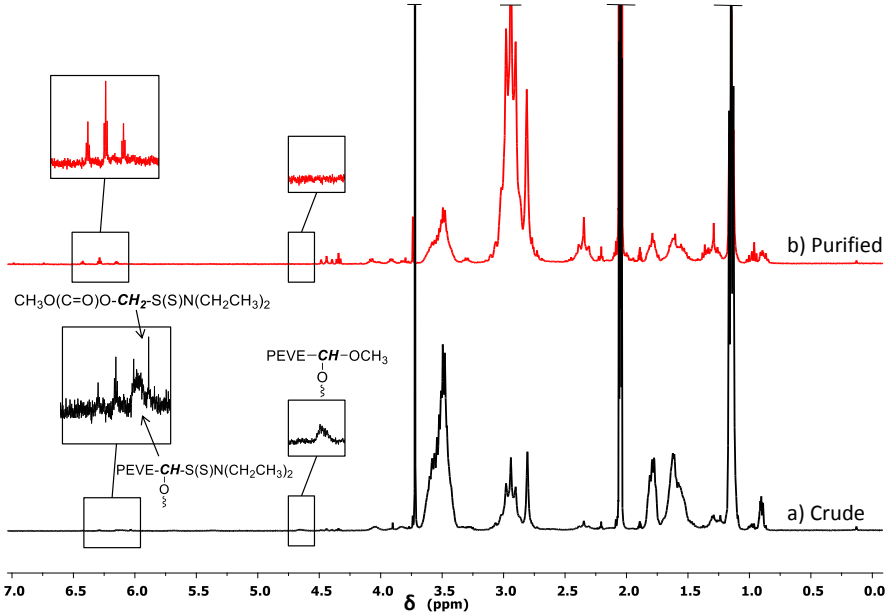

SI-Figure IV-47: . Expansion of the 0 to 7 ppm region of the ^{1}H NMR spectrum in $(CD_3)_2CO$ of a) crude and b) purified PEVE-b-PVDF- CTA_2 block copolymer (run 1, SI-Table IV-7) synthesized by RAFT polymerization using PEVE-CTA_2.

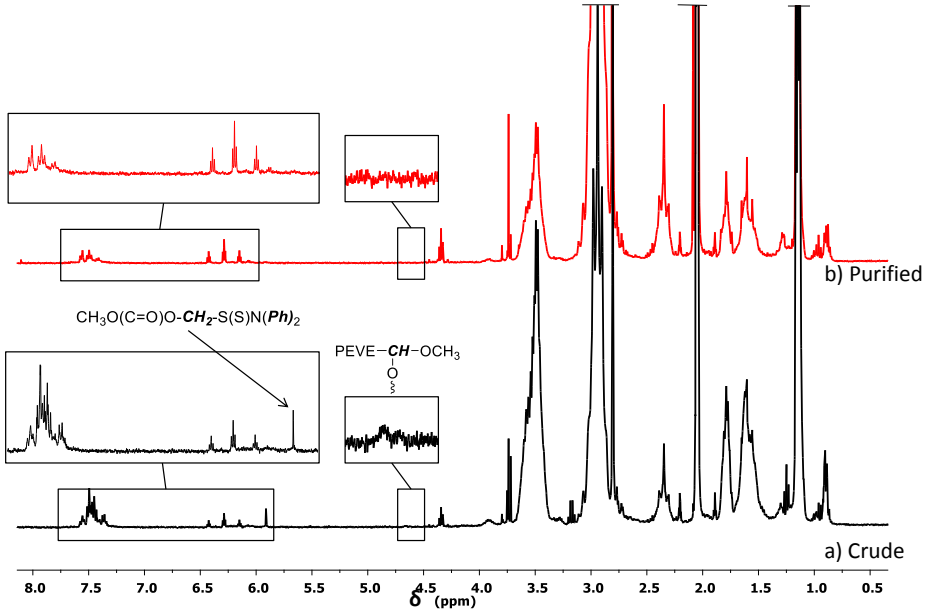

SI-Figure IV-48: Expansion of the 0 to 8 ppm region of the ^{1}H NMR spectrum in $(CD_3)_2CO$ of a) crude and b) purified PEVE-b-PVDF-CTA_3 block copolymer (run 2, SI-Table IV-7) synthesized by RAFT polymerization using PEVE-CTA_3.

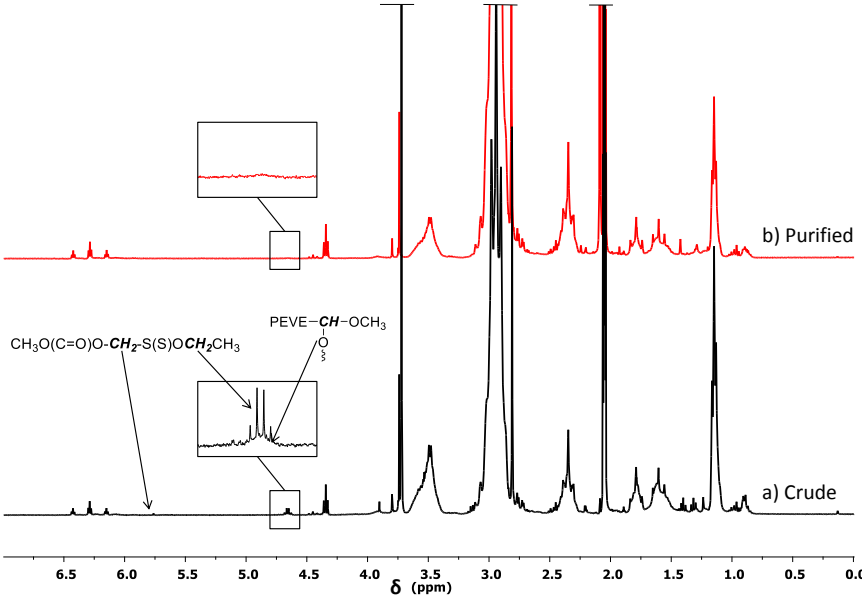

SI-Figure IV-49: Expansion of the 0 to 7 ppm region of the ^{1}H NMR spectrum in $(CD_3)_2CO$ of a) crude and b) purified PEVE-b-PVDF-CTA$_4$ block copolymer (run 3, SI-Table IV-7) synthesized by RAFT polymerization using PEVE-CTA$_4$.

Differential Scanning Calorimetry:

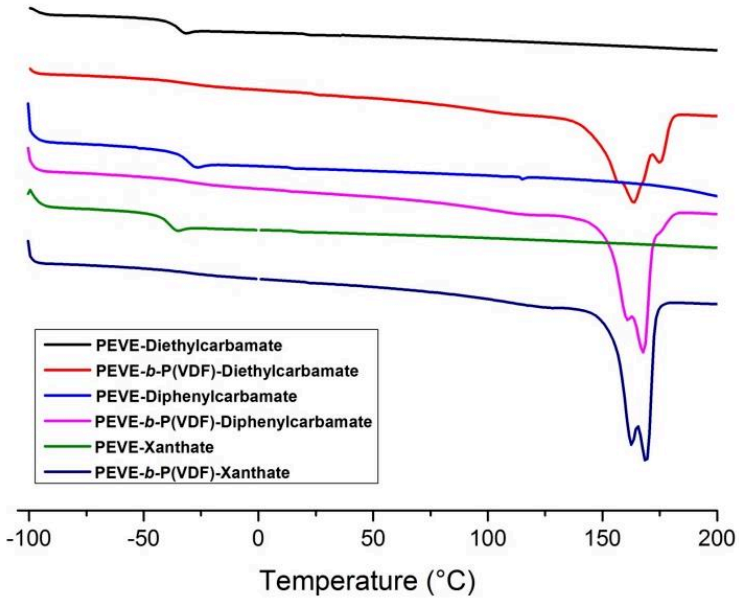

SI-Figure IV-50: DSC thermograms (second heating) of PEVE-CTA$_{2,3,4}$, PEVE-b-PVDF-CTA$_2$, PEVE-b-PVDF-CTA$_3$ and PEVE-b-PVDF-CTA$_4$.

Conclusion Partie 2

Cette partie a montré par combinaison des polymérisations RAFT radicalaire et cationique, une voie totalement inédite pour la préparation de copolymères diblocs PEVE-*b*-PVDF bien définis. Trois agents macromoléculaires poly(ethyl vinyl ether) (PEVE) possédant différents agents de transfert ont été préalablement synthétisés par polymérisation RAFT cationique: PEVE-diethylcarbamate, PEVE-diphenylcarbamate et PEVE-xanthate. Cependant, il s'avère que la polymérisation RAFT cationique des éthers vinyliques est très mal contrôlée par les xanthates (Đ = 1.52) et présente un contrôle optimal en présence de diethylcarbamate (Đ = 1,08). Une étude similaire à celle des xanthates décrite dans la Partie 1, Chapitre II ce mémoire a dû être effectué afin de vérifier le comportement de la RAFT du VDF avec des agents RAFT carbamates. Il a été montré que les agents RAFT de type dithiocarbamates étaient effectivement capables de contrôler de manière semblable aux xanthates la polymérisation du VDF, bien que la cinétique de polymérisation soit considérablement ralentie. Cet effet a été d'autant plus significatif lors de l'extension de chaînes d'agents RAFT macromoléculaires poly(éther vinylique) avec une réactivation très lente des agents macromoléculaires PEVE-diethyl carbamate, contrairement au PEVE-Xanthate. En dépit de cette lente réactivation, il a été possible de préparer des PEVE-*b*-PVDF bien définis par précipitation sélective de la fraction PEVE non réactivée : PEVE-*b*-PVDF-Diethyl carbamate (Đ = 1,36), PEVE-*b*-PVDF-Diphenyl carbamate (Đ = 1,38) et PEVE-*b*-PVDF-Xanthate (Đ = 1,52),

Conclusion Chapitre IV

Ce chapitre a exposé deux nouvelles stratégies de polymérisation RAFT pour la préparation de copolymères diblocs à base de PVDF. L'une d'elle permet de préparer des PVDF-*b*-PVAc par polymérisation RAFT séquentielle du VDF et du VAc. Bien que les réactivités des extrémités $PVDF_H$-XA et $PVDF_T$-XA soient très différentes, il a été possible de produire des copolymères diblocs relativement bien définis. L'autre méthode a consisté à associer la RAFT cationique des éthers vinyliques développés par le groupe du Professeur Kamigaito et la RAFT radicalaire du VDF. Cette combinaison des polymérisations RAFT cationique et RAFT radicalaire a conduit à des copolymères à blocs PEVE-*b*-PVDF contrôlés. Cette étude a également révélé l'efficacité des carbamates pour contrôler la polymérisation du VDF.

Le chapitre suivant décrit la synthèse et l'auto-assemblage de copolymère amphiphiles PVDF-*b*-PVA.

Chapitre V. Synthèse et Auto-assemblage de Copolymère Dibloc PVDF-*b*-PVA

Table des Matières

Introduction Chapitre V

Le chapitre précédent a proposé deux nouvelles méthodes permettant la synthèse de copolymère à blocs bien définis : PVDF-*b*-PVAc et PEVE-*b*-PVDF. Cette profonde avancée dans la synthèse d'architectures contrôlées à base de PVDF, permet à présent de se projeter dans le deuxième axe de recherche de ce mémoire qui est d'étudier l'auto-assemblage en solution des copolymères de PVDF.

Les copolymères amphiphiles se définissent comme l'association, au sein d'une même molécule, de polymères à propriétés antagonistes, l'un (ou les uns) hydrophobe(s), l'autre (ou les autres) hydrophile(s), ce qui leur permet de former des auto-assemblages en milieu aqueux. Ce type de copolymères peut être obtenu à partir de la combinaison de blocs de polymères hydrophiles et hydrophobes. La synthèse de copolymères amphiphiles d'architectures variables apparaît de plus en plus intéressante, puisqu'elle permet de moduler finement les propriétés physico-chimiques des édifices formés en milieu aqueux.

Une des voies les plus simples pour préparer un copolymère amphiphile de PVDF consiste à saponifier en milieu basique les copolymères diblocs PVDF-*b*-PVAc préalablement synthétisés. Le nouveau copolymère à bloc PVDF-*b*-PVA ainsi formé devrait, *via* le bloc PVA, présenter des propriétés amphiphiles. La synthèse, la caractérisation et l'auto-assemblage de ce copolymère dibloc sont détaillés dans ce chapitre. Ce travail a fait l'objet d'un article scientifique publié dans *Polymer Chemistry*.[7]

An amphiphilic poly(vinylidene fluoride)-*b*-poly(vinyl alcohol) block copolymer; synthesis and self-assembly in water

Marc Guerre,[a] Judith Schmidt,[b] Yeshayahu Talmon,[b] Bruno Ameduri,[a] Vincent Ladmiral[a]*

[1]Institut Charles Gerhardt, Ingénierie et Architectures Macromoléculaires, UMR 5253 – CNRS, Université Montpellier, ENSCM - 8, Rue Ecole Normale, 34296 Montpellier-France.
[2]Department of Chemical Engineering, Technion-Israel Institute of Technology, Haifa 3200003, Israel.
*Corresponding authors: vincent.ladmiral@enscm.fr

I. Abstract

This study is the first report of the synthesis and self-assembly in water of an amphiphilic PVDF-*b*-PVA block copolymer. The block copolymer was prepared by sequential RAFT polymerization of VDF and VAc followed by saponification of the PVAc block and was haracterized by ^{1}H NMR and FTIR. The self-assembled nanoparticles were characterized by DLS and cryo-TEM.

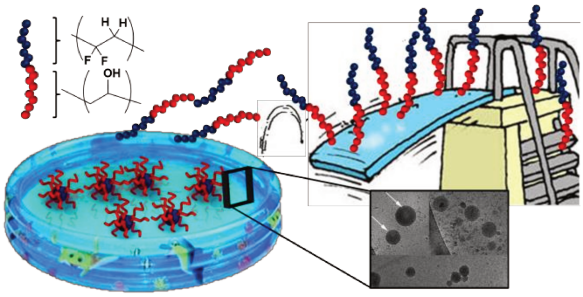

II. Introduction

Poly(vinylidene fluoride) (PVDF) is the second most produced fluoropolymers. It possesses remarkable thermal, chemical and electroactive properties.[1–4] In industry, it is prepared by radical polymerization of VDF in dispersed aqueous media. Although PVDF is a relatively well-known polymer, welldefined architectures such as block, or graft copolymers for example, have been very rarely reported[5–13] in comparison to other vinyl polymers. The reversible deactivation radical polymerization (RDRP) of VDF is indeed more challenging than that of (meth)acrylates or styrenics, for example, because of the formation and accumulation of much less reactive PVDF chains resulting from VDF head-to-head (HH) addition.[14] We recently reported a detailed study on the RAFT polymerization of VDF which

highlights the generation of these less reactive PVDF chains.[14,15] In previous articles, we also showed that RAFT polymerization can be used to prepare PVDF-methacrylate macromonomers,[16] or fluorinated dendrimers,[17] and reported a comprehensive study of the effect of these less reactive chains ($PVDF_T$-XA, chains terminated with a $-CF_2-CH_2$-XA end-sequence, where XA represents the xanthate moiety) on the mechanism of the RAFT polymerization of VDF.[18] This latter work also showed how relatively high molar mass PVDF with high end-group functionality could be synthesized. These PVDF chains, thought to be unreactive, were indeed experimentally observed to be involved in the RAFT polymerization of VDF and to react via degenerative and non-degenerative transfer reactions with PVDF• radicals, albeit at a much slower rate than their highly reactive regularly terminated counterparts, $PVDF_H$-XA (chains terminated with a $-CH_2-CF_2$-XA endsequence). This behaviour was rationalized using DFT calculations.[18] The resulting accumulation of these $PVDF_T$-XA chains results in the gradual broadening of the molar mass distribution of the PVDF, and eventually to a degradation of the control of the polymerization, when all PVDF chains have been converted into $PVDF_T$-XA, which are mediocre chain transfer agents. These studies provide a much better understanding of the RAFT of VDF, and allow the preparation of a well-defined PVDF with high chain end fidelity and a relatively high degree of polymerization.[18] Building on this improved understanding, PVDF-based diblock copolymers[19-21] were synthesized by sequential addition of monomers using PVDF macroCTAs.[22] We recently showed that $PVDF_H$-XA can readily be reactivated by poly(N-vinyl pyrrolidone) and poly(vinyl acetate) (PVAc) radicals, while $PVDF_T$-XA only reacted with PVAc•, and prepared unprecedented well-defined PVDF-*b*-PVAc diblock copolymers.[22] The present Communication reports the preparation of a PVDF-*b*-PVA (where VA stands for vinyl alcohol) amphiphilic diblock copolymer and its self-assembly in water.

III. Results and Discussion

This novel amphiphilic PVDF-*b*-PVA diblock copolymer was prepared from a PVDF-*b*-PVAc precursor by hydrolysis of the ester groups of the VAc units (Scheme V-1). The hydrophobic PVDF macroCTA (2) was synthesized by RAFT polymerization of VDF (1) following a procedure published previously.[14] This polymerization afforded a well-defined PVDF (2) (Đ= 1.40, DP = 51) with a high functionality (86 % of $PVDF_T$-XA active end-group and 14 % of $-CF_2H$ dead chains). The PVDF-*b*-PVAc (3) block copolymer was prepared by chain extension of this PVDF macroCTA using RAFT polymerization of VAc.[22]

The resulting well-defined $PVDF_{51}$-*b*-$PVAc_{172}$ diblock copolymer (3) (Đ = 1.34, SI-Figure V-6) was then dispersed in an ethanol solution and the PVAc block was hydrolyzed into PVA by basic hydrolysis using an aqueous/alcoholic solution of K_2CO_3.[23,24]

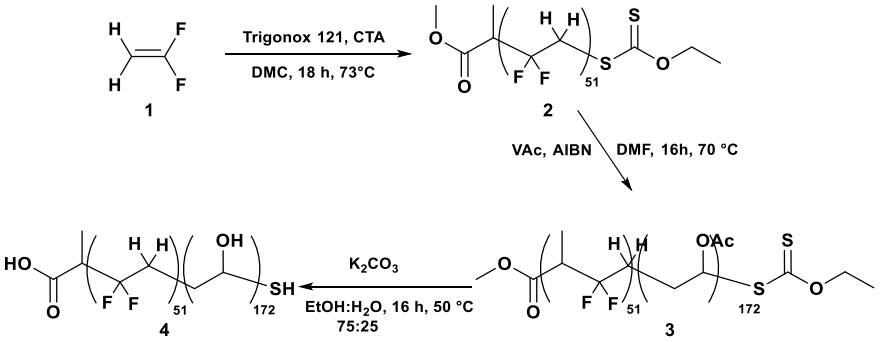

Scheme V-1: Schematic representation of the synthesis of PVDF-b-PVA block copolymer.

FTIR spectra of the $PVDF_{51}$-*b*-PVA_{172} block copolymer and of its precursor (Figure V-1) show the quantitative hydrolysis of the ester bonds of the VAc units (complete disappearance of the carbonyl signal of PVAc at 1735 cm^{-1}).

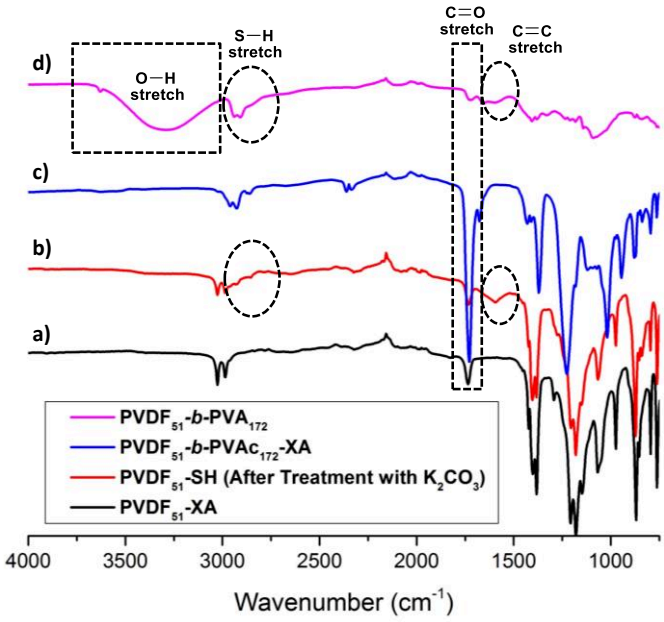

Figure V-1: . FTIR spectra of: a) the $PVDF_{51}$-XA (black), b) $PVDF_{51}$-SH after K_2CO_3 treatment (red), c) $PVDF_{51}$-b-$PVAc_{172}$ (blue), d) $PVDF_{51}$-b-PVA_{172} (pink) copolymers.

The spectrum of the amphiphilic diblock copolymer displays the characteristic stretching bands of PVA[25,26] (Figure V-1d and SI-Figure V-10,† OH vibration band at 3293 cm^{-1} and C-H signal at 1396 cm^{-1}), as well as a broad stretching band at 2590 cm^{-1} corresponding to the S-H bonds formed by the hydrolysis of the xanthate group.[27,28] The disappearance of the

vibration assigned to the C=S band (1000–1200 cm^{-1}) was, however, difficult to see. Chain–chain coupling via disulfide bond formation may occur, but it could not be seen on the FTIR spectrum, as it falls outside of the analysis window (400–500 cm^{-1}). However, disulfide linkage formation was not observed in previous studies on the hydrolysis of PVAc-XA.[23,24] As expected, a small signal assigned to the -CH=CF- double bond at 1630 cm^{-1} appeared after basic treatment.[29–32] PVDF is relatively prone to dehydrofluorination in the presence of bases.[2] The hydrolysis of PVAc was thus accompanied by some dehydrofluorination, which generated internal carbon–carbon double bonds within the PVDF backbone, and gave a dark color to the resulting material.[16,33] The hydrolysis of the PVAc block was also confirmed by ^{1}H NMR spectroscopy (Figure V-2).

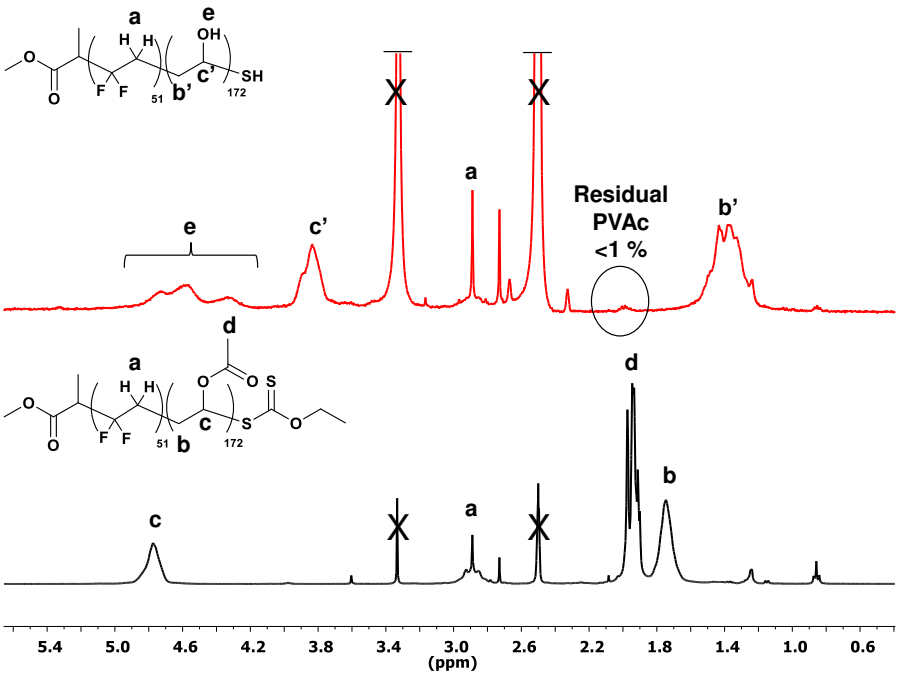

Figure V-2: Expansion of the 0.4–5.7 ppm region of the ^{1}H NMR spectra of PVDF-b-PVAc-XA (bottom) and PVDF-b-PVA (top) block copolymers recorded in DMSO-d_6. The crossed-out signals are those of water (3.33 ppm) and DMSO (2.5 ppm).

The signals corresponding to the CH_2 (signal b, in Figure V-2) and to the CH (signal c in Figure V-2) of the PVAc backbone were, as expected, quantitatively shifted from 1.74 and 4.77 ppm to 1.37 and 3.83 ppm, respectively, upon hydrolysis of the acetate groups. The signal centered at 1.94 ppm (signal d in Figure V-2), assigned to the CH_3 of the acetate of the VAc units, almost entirely disappeared (only 1% of the original signal remained), and a new broad signal (probably caused, in part, by the tacticity of the PVA segments) corresponding to the hydroxyl groups of PVA appeared around 4.5 ppm (e, in Figure V-2). The signals of the PVDF segments remained untouched at 2.89 ppm.[13,15,18]

It is however important to note that although DMSO efficiently solubilizes the PVA block, it is only a moderately good solvent of PVDF (compared to acetone for example). This solubility difference can be easily seen on the PVDF NMR signal at 2.89 ppm in acetone, (PVDF-*b*-PVAc, SI-Figure V-6) and in DMSO (PVDF-*b*-PVAc bottom and PVDF-*b*-PVA top, Figure V-2). Consequently, in DMSO, the amphiphilic block copolymer is probably not entirely soluble, and could be already somewhat self-assembled into loose nanoobjects with a PVDF core and a PVA corona (the ratio of the integrals of the signals of the PVDF and PVAc blocks is 0.22 in the PVDF-*b*-PVAc copolymers, whereas the PVDF/PVA integral ratio is estimated to be 0.16 in the amphiphilic copolymer). The signals of the *O*-ethyl xanthate end-group at 1.63 and 4.63 ppm overlapped with the signals of the CH and OH of PVA, respectively. The complete end-group removal thus cannot be confirmed by NMR spectroscopy on the PVDF-*b*-PVA NMR spectrum. On the other hand, the *O*-ethyl xanthate endchain signals have totally disappeared from the ^{1}H NMR spectrum of treated PVDF (PVDF having undergone the same PVDF-*b*-PVAc hydrolysis conditions) (SI-Figure V-11). This indirectly proves the ω-chain-end elimination after hydrolysis.

In addition, the C=C double bonds arising from the dehydrofluorination reaction and barely identifiable in FTIR (1630 cm^{-1}, Figure V-1) could not be seen by ^{1}H or ^{19}F NMR spectroscopy (SI-Figure V-11and SI-Figure V-12). To the best of our knowledge such NMR signals (caused by dehydrofluorination of PVDF) have never been reported anywhere.[30,33,34] In the case of the diblock copolymer studied here, this may also be explained by the reduced solubility of the PVDF block in DMSO, by the small quantity of these double bonds, and the sensitivity limits of NMR spectroscopy. Therefore, a PVDF homopolymer was treated under the same conditions as the PVDF-*b*-PVAc block copolymer, and subsequently analyzed by FTIR, ^{1}H and ^{19}F NMR in deuterated acetone (good solvent for PVDF, Fig. S9). After treatment with K_2CO_3, a new weak and broad signal appeared around 7 ppm on the ^{1}H NMR spectrum. However, this signal was not intense enough to quantify accurately the extent of the dehydrofluorination reactions caused by the base. These results suggest that the extent of dehydrofluorination of the PVDF-b-PVA diblock copolymer is not significant.

To study the self-assembly behaviour in the solution of the new PVDF-*b*-PVA amphiphilic fluorinated block copolymer, a good solvent for both blocks was required. However, due to the large difference of solubility of each block, and the high crystallinity of PVDF and PVA, the PVDF-*b*-PVA copolymer was particularly difficult to solubilize in any solvent. PVDF is usually solubilized in polar solvents such as DMF, DMAc, NMP, acetone or to a lesser extent

DMSO, while PVA is only soluble in hot water or DMSO. The diblock copolymer was thus dissolved in hot DMSO (80 °C) at a concentration of 2.2 g L^{-1} to improve the solubility of the PVDF block. The resulting polymer solution was then filtered (using 0.45 µm filters) and self-assembled in water using the dialysis method[35,36] with a final concentration of 1.16 g L^{-1}. The dispersion of the selfassembled objects was analyzed by dynamic light scattering and cryo-TEM. The intensity-average hydrodynamic diameter distribution displayed in Figure V-3 shows an almost monomodal peak centered at 147 nm. A few larger objects (2 populations with a hydrodynamic diameter ranging from 500 nm to 1 µm and around 7 µm) were also detected. These larger aggregates may be caused by aggregation of a minor fraction of the self-assembled nano-objects. The smaller PVDF-*b*-PVA selfassembled nano-objects were spherical and displayed a relatively large diameter distribution (from 70 nm to 350 nm), as observed both by DLS and cryo-TEM (Figure V-3b-e).

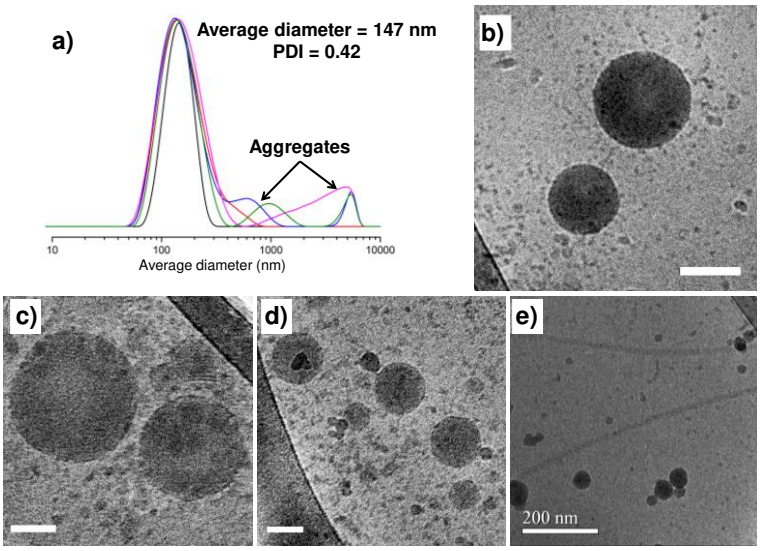

Figure V-3: a) Intensity-average hydrodynamic diameter distribution of $PVDF_{51}$-b-PVA_{172} amphiphilic block copolymers self-assembled in water (c = 1.16 mg mL^{-1}) measured by DLS. (b, c, d, and e) Cryo-TEM micrographs of the $PVDF_{51}$-b-PVA_{172} nano-objects self-assembled in water.

IV. Conclusion

In this Communication we have described the synthesis of the first PVDF-*b*-PVA block copolymer via sequential RAFT polymerization and basic hydrolysis, and the self-assembly of this original amphiphilic fluorinated block copolymer in water. The first PVDF block was prepared by RAFT polymerization of VDF in the presence of xanthate. Chain extension with VAc was then successfully performed, leading to a PVDF-*b*-PVAc block copolymer. The

acetate groups of this copolymer were finally hydrolysed with K_2CO_3 to form the unprecedented PVDF-*b*-PVA amphiphilic fluorinated block copolymer. This amphiphilic block copolymer was subsequently self-assembled in water using the dialysis method. The quantitative hydrolysis was confirmed by FTIR and ^{1}H NMR spectroscopies. Although dehydrofluorination of the PVDF backbone caused by the basic treatment could be seen on the FTIR spectrum and from the polymer colour change (from white to dark brown), NMR spectroscopy failed to detect clearly the expected CF=CH double bonds. This is likely due to the very small extent of the dehydrofluorination reaction under the conditions used here for the hydrolysis of PVAc. The self-assembly of the diblock copolymer in water, which was studied by DLS and cryo-TEM, led to the formation of a major population of spherical nanoobjects constituted of a PVDF core and a PVA shell with diameters centered around 147 nm. Minor particle aggregation was also observed. This first foray into the synthesis and selfassembly of fluorinated amphiphilic PVDF- and PVA-containing block copolymers opens new opportunities in the study of fluorinated colloids.

V. Acknowledgements

The authors thank Arkema S.A (Pierre Bénite, France) for providing VDF and the Ministère de l'Education Nationale, de l'Enseignement Supérieur et de la Recherche for the Ph.D. Grant attributed to MG. The cryo-TEM work was done at the Technion Laboratory for Electron Microscopy of Soft Materials, Supported by the Technion Russell Berrie Nanotechnology Institute (RBNI).

VI. References

[1] B. Ameduri, B. Boutevin, B. In *Well-Architectured Fluoropolymers: Synthesis, Properties and Application*, Elsevier: Amsterdam, 2004.

[2] B. Ameduri, *Chem. Rev*., 2009, **109**, 6632−6686.

[3] I. Katsouras, K. Asadi, M. Li, T. B. van Driel, K. S. Kjær, D. Zhao, T. Lenz, Y. Gu, P. W. M. Blom, D. Damjanovic, M. M. Nielsen, D. M. de Leeuw, *Nat. Mater*. 2016, **15**, 78-84.

[4] M. Li, H. J. Wondergem, M-J. Spijkman, K. Asadi, I. Katsouras, P. W. M. Blom, D. M. de Leeuw, *Nat. Mater*., 2013, **12**, 433-438.

[5] (a) A. D. Asandei, O. I. Adebolu and C. P. Simpson, J. Am. Chem. Soc., 2012, **134**, 6080‑6083. (b) A. D. Asandei, O. I. Adebolu, C. P. Simpson, J. S. Kim, *Angew. Chem., Int. Ed.*, 2013, **52**, 10027−10030. (c) P. Černoch, Z. Černochová, S. Petrova, D. Kaňková, J-S. Kim, V. Vasu, A. D. Asandei, *RSC Adv.*, 2016, **6**, 55374-55381.

[6] (a) V. S. D. Voet, D. Hermida-Merino, G. ten Brinke and K. Loos, RSC Adv., 2013, **3**, 7938‑7946; (b) V. S. D. Voet, M. Tichelaar, S. Tanase, M. C. Mittelmeijer-Hazeleger, G. ten Brinke and K. Loos, *Nanoscale*, 2013, **5**, 184‑192. (c) V. S. D. Voet, G. T. Brinke and K. Loos, *J. Polym. Sci., Part A: Polym. Chem*., 2014, **52**, 2861‑2877

[7] R. Vukicevic, U. Schwadtke, S. Schumucker, P. Schafer, D. Kuckling, S. Beuermann, *Polym. Chem.,* 2012, **3**, 409-414.

[8] D. Valade, C. Boyer, B. Ameduri, B. Boutevin, *Macromolecules*, 2006, **39**, 8639-8651.

[9] C. Boyer, D. Valade, L. Sauguet, B. Ameduri, B. Boutevin, *Macromolecules*, 2005, **38**, 10353−10362.

[10] N. Durand, B. Ameduri, B. Boutevin, *J. Polym. Sci., Part A: Polym. Chem.,* 2011, **49**, 82−92.

[11] G. Kostov, F. Boschet, J. Buller, L. Badache, S. Brandstadter, B. Ameduri, *Macromolecules*, 2011, **44**, 1841-1855.

[12] E. Girard, J. D. Marty, B. Ameduri, M. Destarac, *ACS Macro Lett.*, 2012, **1**, 270-274.

[13] Y. Patil, B. Ameduri, *Polym. Chem.,* 2013, **4**, 2783-2799.

[14] M. Guerre, B. Campagne, O. Gimello, K. Parra, B. Ameduri, V. Ladmiral, *Macromolecules*, 2015**, 48,** 7810-1822

[15] M. Guerre, G. Lopez, T. Soulestin, C. Totée, B. Ameduri, G. Silly, V. Ladmiral, *Macromol. Chem. Phys*., 2016, **217**, 2275-2285.

[16] M. Guerre, B. Ameduri, V. Ladmiral, Polym. Chem., 2016, **7**, 441-450.

[17] E. Folgado, M. Guerre, C. Bijani, V. Ladmiral, A-M. Caminade, B. Ameduri, A. Ouali, *Polym. Chem*., 2016, **7**, 5625-5629.

[18] M. Guerre, W. Rahaman, B. Ameduri, R. Poli, V. Ladmiral, *Macromolecules*, 2016, **49**, 5386-5396.

[19] A. D. Asandei, *Chem. Rev*., 2016, **116**, 2244-2274.

[20] C. P. Simpson, O. I. Adelou, J-S. Kim, V. Vasu, A. D. Asandei, *Macromolecules*, **48**, 6404-6420.

[21] P. Cernoch, S. Petrova, Z. Cernochova, J-S. Kim, C. P. Simpson, A. D. Asandei, *Eur. Polym. J.*, 2015, **68**, 460-470.

[22] M. Guerre, W. Rahaman, B. Ameduri, R. Poli, V. Ladmiral, *Polym. Chem*., 2016,**7**, 6918-6933.

[23] J. Bernard, A. Favier, T. P. Davis, C. Barner-Kowollik, M. H. Stenzel, *Polymer*, 2006, **47**, 1073-1080.

[24] M. H. Stenzel, T. P. Davis, C. Barner-Kowollik, *Chem. Commun*., 2004, 1546-1547.

[25] E. R. Blout, R. Karplus*, J. Am. Chem. Soc.,* 1948, **70**, 862-864.

[26] H. S. Mansur, C. M. Sadahira, A. N. Souza, A. A. P. Mansur, *Materials Science and Engineering*, 2008, **28**, 539-548.

[27] H. Willcock, R. K. O'Reilly, *Polym Chem.,* 2010, **1**, 149-157.

[28] M. F. Llauro, J. Loiseau, F. Boisson, F. Delolme, C. Ladaviere, J. Claverie, *J. Polym. Sci., Part A: Polym. Chem*., 2004, **42,** 5439–5462.

[29] H. Kise, H. Ogata and M. Nakata, *Angew. Makromol. Chem*., 1989, **168**, 205–216.

[30] A. Taguet, L. Sauguet, B. Ameduri and B. Boutevin, *J. Fluorine Chem*., 2007, **128**, 619–630

[31] J. Wootthikanokkhan, P. Changsuwan, *JOM*, 2008, **18**, 57-62.

[32] S. Subianto, N. R. Choudhury, N. Dutta, *Nanomaterials*, 2014, **4**, 1-18.

[33] J. Scheirs, In *Modern fluoropolymers: High performance polymers for diverse applications*, Wiley, Chichester, 1997, 18–19.

[34] A. Taguet, B. Ameduri and B. Boutevin, *Adv. Polym. Sci*., 2005, **184**, 127–211

[35] I. Fuentes, B. Blanco-Fernandez, N. Alvarado, A. Leiva, D. Radic, C. Alvarez-Lorenzo, A. Concheiro, *Langmuir,* 2016, **32**, 3331-3339.

[36] P. Zhang, H. Zhang, W. He, D. Zhao, A. Song, Y. Luan*, Biomacromolecules*, 2016, **17**, 1621-1632.

[37] Liu, X.; Coutelier, O.; Harrisson, S.; Tassaing, T.; Marty, J.-D.; Destarac, M., *ACS Macro Lett.*, **4**, 89-93.

VII. Supporting Informations

VII.1 Experimental Section

VII.1.1 Materials

All reagents were used as received unless stated otherwise. 1,1-Difluoroethylene (vinylidene fluoride, VDF) was kindly supplied by Arkema (Pierre-Benite, France). *O*-ethyl-*S*-(1-methoxycarbonyl)ethyldithiocarbonate (CTA_{XA}) was synthesized according to the method described by Liu et al.[37] *Tert*-amyl peroxy-2-ethylhexanoate (Trigonox 121, purity 95%) was purchased from AkzoNobel (Chalons-sur-Marne, France). ReagentPlus grade (purity > 99%) Poly(vinyl alcohol) M_w= 89000 – 98000 g/mol 99+% hydrolyzed, 2,2-azoisobutyronitrile (AIBN), vinyl acetate (VAc), dimethyl carbonate (DMC), dimethylformamide (DMF), tetrahydrofuran, (THF), ethanol (EtOH), potassium carbonate (K_2CO_3) and laboratory reagent grade hexane (purity > 95%) were purchased from Sigma Aldrich and used as received. AIBN was purified by recrystallization from methanol twice before use.

VII.1.2 Characterization

Nuclear Magnetic Resonance

The Nuclear Magnetic Resonance (NMR) spectra were recorded on a Bruker AC 400 instrument. Deuterated acetone was used as the solvent in each sample. Coupling constants and chemical shifts are given in Hertz (Hz) and parts per million (ppm), respectively. The experimental conditions for recording ^1H and ^{19}F NMR spectra were as follows: flip angle 90° (or 30°), acquisition time 4.5 s (or 0.7 s), pulse delay 2 s (or 2 s), number of scans 128 (or 512), and a pulse width of 5 μs for ^{19}F NMR. *In situ* NMR experiments were recorded with a pulse delay of 1 s, acquisition times of 4 s and 0.87 s, and 8 and 16 scans for ^1H and ^{19}F NMR, respectively.

Size Exclusion Chromatography

Size exclusion chromatograms (SEC) were recorded using a triple detection GPC from Agilent Technologies with its corresponding Agilent software, dedicated to multi-detector GPC calculation. The system used two PL1113-6300 ResiPore 300 x 7.5 mm columns with DMF (containing 0.1 wt % of LiCl) as the eluent with a flow rate of 0.8 $mL.min^{-1}$ and toluene as flow rate marker. The detector suite comprised a PL0390-0605390 LC light scattering detector with 2 diffusion angles (15° and 90°), a PL0390-06034 capillary viscosimeter, and a

390-LC PL0390-0601 refractive index detector. The entire SEC-HPLC system was thermostated at 35°C. PMMA standards were used for the calibration. The typical sample concentration was 10 mg/mL.

Fourier Transform Infrared

FTIR analyses were performed using a PerkinElmer Spectrum 1000 in ATR mode, with an accuracy of ± 2 cm^{-1}.

Dynamic Light Scattering

Dynamic Light Scattering (DLS) experiments were performed at 25 °C on a Malvern instrument Nano-ZS equipped with a He-Ne laser as the light source (λ = 633 nm). The scattered light was detected at the scattering angle of ν = 173°. Samples of water solutions of blocks copolymers (3 mg mL^{-1}) were introduced into cells (pathway, 10 mm) without filtration.

Cryogenic-temperature transmission electron microscopy(Cryo TEM).

Vitrified specimens were prepared in a controlled environment vitrification system (CEVS)35 at 25 °C and 100% relative humidity. A drop (~3 µL) of the sample was placed ona perforated carbon film-coated copper grid, blotted with filterpaper, and plunged into liquid ethane at its freezing point. The vitrified specimens were transferred to a 626 Gatan cryoholderand observed at 120 kV acceleration voltage in an FEITecnai T12 G2 transmission electron microscope at about -175 °C in the low-dose imaging mode to minimize electron beam radiation damage. Images were digitally recorded with a Gatan US1000 high-resolution CCD camera.

Autoclave

Polymerizations of VDF were performed in a 100 mL Hastelloy Parr autoclave systems (HC 276), equipped with a mechanical Hastelloy stirring system, a rupture disk (3000 PSI), inlet and outlet valves, and a Parr electronic controller to regulate the stirring speed and the heating. Prior to reaction, the autoclave was pressurized with 30 bars of nitrogen to check for leaks. The autoclave was then put under vacuum ($20 \cdot 10^{-3}$ bar) for 30 minutes to remove any trace of oxygen. A degassed solution of initiator and CTAXA was introduced via a funnel under vacuum. The reactor was then cooled using a liquid nitrogen bath and VDF was transferred by double weighing (*i.e.* mass difference before and after filling the autoclave

with VDF). After warming to ambient temperature, the autoclave was heated to the target temperature under mechanical stirring.

VII.1.3 Syntheses

RAFT Homopolymerization of VDF

Using the experimental setup described above, the polymerization of VDF was performed as follows: A solution of Trigonox 121 (158 mg, 6.87 10^{-4} mol) and CTAXA (1.30 g, 6.25 10^{-3} mol) in DMC (60 mL), was degassed by N_2 bubbling during 30 min. This homogenous solution was introduced into the autoclave using a funnel, VDF gas (21.0 g, 2.97 10^{-1} mol) was transferred in the autoclave at low temperature, and the reactor was gradually heated to 73 °C. The reaction was stopped after 18 h. During the reaction, the pressure increased to a maximum of 25 bars and then decreased to 10 bars after 18 h. The autoclave was cooled down to room temperature (ca. 20 °C), purged from the residual monomers and DMC was removed under vacuum. The crude product was dissolved in 30 mL of warm THF (ca. 40 °C), and left under vigorous stirring for 30 minutes. This polymer solution was then precipitated from 400 mL of chilled hexane. The precipitated polymer (white powder) was filtered through a filter funnel and dried under vacuum ($15 \cdot 10^{-3}$ bar) for two hours at 50 °C. The polymerization yield (65 %) was determined gravimetrically (mass of dried precipitated polymers / mass of monomer introduced in the pressure reactor). Yields were used as conversion, since conversion is very difficult to measure accurately for VDF or other gaseous monomers.

DP and $M_{n(NMR)}$ calculations:

The degree of polymerization (DP) of PVDF can be calculated according to equations SI-Equation V-1 and SI-Equation V-2:

$$\textit{SI-Equation V-1 } DP = \frac{\int_{2.70}^{3.19} CH_2(HT) + \int_{2.28}^{2.43} CH_2(TT) + \int_{4.02}^{4.17} CH_2(End-group)}{2/3 \times \int_{1.19}^{1.24} CH_3(R-CTAXA)}$$

$$\textit{SI-Equation V-2 } M_{n,NMR}(R) = M_{n,CTA} + (DP \times M_{n,VDF})$$

Where $M_{n\,CTA}$ = 208.3 g.mol^{-1} and $M_{n\,VDF}$= 64.04 g.mol^{-1}

^{1}H NMR (400 MHz $(CD_3)_2CO$, δ (ppm), SI-Figure V-4) : 1.19-1.24 (d, -CH(**CH_3**)(C=O)-, $^3J_{HH}$ = 7.1 Hz), 1.40-1.46 (t, -S(C=S)O-CH_2-**CH_3**, $^3J_{HH}$ = 7.2 Hz), 2.28-2.43 (m,-CF_2-**CH_2**-**CH_2**-CF_2-, VDF-VDF TT reverse addition), 2.70-3.19 (t, -CF_2-**CH_2**-CF_2-, VDF-VDF HT regular addition), 3.60-3.69 (s, -(C=O)-O-**CH_3**), 4.02-4.17 (t, -CF_2-**CH_2**-S(C=S)OEt, $^3J_{HF}$ =

18 Hz), 4.67-4.77 (q, (-S(C=S)O-**CH$_2$**-CH$_3$, $^3J_{HH}$ = 7.2 Hz), 6.05-6.45 (tt, $^2J_{HF}$ = 55 Hz , $^3J_{HH}$ = 4.6 Hz -CH$_2$-CF$_2$-**H**).

^{19}F NMR (376 MHz $(CD_3)_2CO$, δ (ppm), SI-Figure V-5) : -115.63 (-CH$_2$-CF$_2$-**CF$_2$**-CH$_2$-CH$_2$-, VDF-VDF HH reverse addition), -114.29 ($^2J_{HF}$ = 55 Hz, -CH$_2$-**CF$_2$**-H), -113.34 (-CH$_2$-**CF$_2$**-CF$_2$-CH$_2$-CH$_2$-, HH reverse addition), -113.09 (CH$_2$-CF$_2$-**CF$_2$**-CH$_2$-S-), -112.69 (-CH$_2$-**CF$_2$**-CF$_2$-CH$_2$-S-), -94.79 (-CH$_2$-CH$_2$-**CF$_2$**-CH$_2$-, TT reverse addition), -93.50 (-CH$_2$-**CF$_2$**-CH$_2$-CH(CH$_3$)(C=O)-), -92.12 (-CH$_2$-**CF$_2$**-CH$_2$-CF$_2$H), -91.44 (-CH$_2$-CH$_2$-CF$_2$-CH$_2$-**CF$_2$**-CH$_2$-CF$_2$-, regular VDF-VDF HT addition), -91.00 (-CH$_2$-**CF$_2$**-CH$_2$-, regular VDF-VDF HT addition)

Synthesis of PVDF-*b*-PVAc block copolymers using PVDF-XA as MacroCTA

The synthesis of a PVDF-*b*-PVAc block copolymer was performed as follows (SI-Scheme V-2): PVDF-XA macroCTA (0.500 g, $1.364 \cdot 10^{-4}$ mol) and AIBN (4.5 mg, $2.728 \cdot 10^{-5}$ mol) were dissolved in 5 mL of DMF. The solution was stirred and bubbled with N_2 for 20 min, and a degassed solution of VAc (1.76 g, $2.05 \cdot 10^{-2}$ mol) was injected. The septum was carefully replaced by a glass stopper and firmly closed with a keck joint clip.

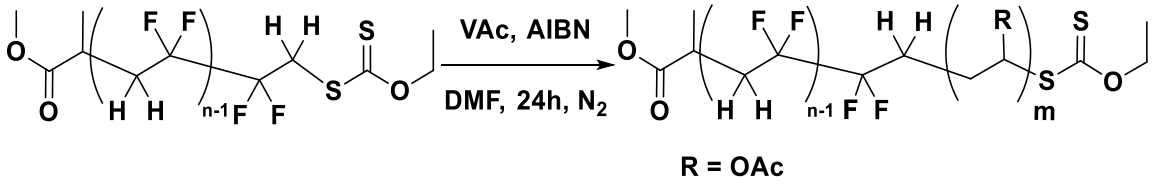

SI-Scheme V-2: Schematic synthetic procedure for the PVDF-b-PVAc block copolymer.

The solution was then stirred and heated at 70 °C for 24 h. The viscous reaction was diluted with 5 mL of acetone and precipitated in a large excess of hexane. The resulting solid was dried until constant weight under vacuum at 40 °C (Yield = 88 %)

DP and $M_{n(NMR)}$ calculations:

The degree of polymerization (DP) can be calculated from ^{1}H NMR using the integrals of the signals corresponding to: the methyl group of the CTA R-group (1.19-1.24 ppm), the CH of PVAc backbone (4.76-5.14 ppm) and the CH$_2$ group end capped with xanthate moieties of the reverse VAc additions (HH, 3.22-3.46 ppm). However, as reported in a previous work, the PVDF-XA chains initiated by R-radicals from the CTA were not all terminated by a CTA Z-group. Transfer to the DMC occurred in the course of the polymerization, leading to around 14 % of dead chains terminated by a -CF$_2$H group. Therefore, a correction factor (α= 0.86)

was introduced in equation SI-Equation V-3 to calculate a more accurate DP and molar mass for the PVAc block.

$$SI\text{-}Equation\ V\text{-}3\ DP = \frac{\int_{4.76}^{5.14} CH + 1/2 \int_{3.22}^{3.46} CH_2(HH\ End-group)}{\frac{\alpha}{3} \times \int_{1.19}^{1.24} CH_3(R-CTAXA)}$$

The molar mass was then calculated using equation SI-Equation V-4:

$$SI\text{-}Equation\ V\text{-}4\ \ M_{n,NMR}(R) = M_{n,PVDF51-XA} + (DP \times M_{n,VAc})$$

where $M_{n\ PVDF51\text{-}XA}$ = 3400 g.mol^{-1}, and $M_{n\ VAc}$= 86.09 g.mol^{-1}.

^{1}H NMR (400 MHz $(CD_3)_2CO$, δ (ppm), SI-Figure V-6) : 1.19-1.24 (d, -CH(**CH_3**)(C=O)-, $^{3}J_{HH}$ = 7.1 Hz), 1.40-1.46 (t, (-S(C=S)O-CH_2-**CH_3**), 1.63-1.92 (m, -CH(OAc)-**CH_2**-CH(OAc)-, VAc), 1.92-2.03 (m, -CH(O**Ac**)-, VAc), 2.28-2.43 (m,-CF_2-**CH_2-CH_2**-CF_2-, VDF-VDF TT reverse addition), 2.70-3.19 (t, -CF_2-**CH_2**-CF_2-, regular VDF-VDF HT addition), 3.21-3.42 (m, -CH(OAc)-**CH_2**-S(C=S)OEt, VAc HH reverse addition), 3.60-3.69 (s, -(C=O)-O-**CH_3**), 3.95-4.13 (-CH_2-**CH_2**(OAc), VAc), 4.63-4.72 (q, (-S(C=S)O-**CH_2**-CH_3, $^{3}J_{HH}$ = 7.2 Hz), 4.76-5.14 (-CH_2-**C**H(OAc)-CH_2-), 6.05-6.45 (tt, $^{2}J_{HF}$ = 55 Hz , $^{3}J_{HH}$ = 4.6 Hz -CH_2-CF_2-**H**).

^{19}F NMR (376 MHz $(CD_3)_2CO$, δ (ppm), SI-Figure V-7) : -115.63 (-CH_2-CF_2-**CF_2**-CH_2-CH_2-, VDF-VDF HH reverse addition), -115.43 (-CH_2-CF_2-**CF_2**-CH_2-CH_2-CH(OAc)-), -114.29 ($^{2}J_{HF}$ = 55 Hz, -CH_2-**CF_2**-H), -113.34 (-CH_2-**CF_2**-CF_2-CH_2-CH_2-, HH reverse addition), -94.79 (-CH_2-CH_2-**CF_2**-CH_2-, TT reverse addition), -93.50 (-CH_2-**CF_2**-CH_2-CH(CH_3)(C=O)-), -92.12 (-CH_2-**CF_2**-CH_2-CF_2H), -91.44 (-CH_2-CH_2-CF_2-CH_2-**CF_2**-CH_2-CF_2-, regular VDF-VDF HT addition), -91.00 (-CH_2-**CF_2**-CH_2-, regular VDF-VDF HT addition).

Saponification of PVDF-*b*-PVAc precursor

PVDF$_{51}$-*b*-PVA$_{172}$ (300 mg, 2.8·10^{-3} eq/mol of ester function) block copolymer was dissolved in 1 g of DMF, then 4 mL of an alcoholic-water mixture (75:25) solution of K_2CO_3 at 0.723 mol/ was added and left under stirring at 60 °C for 3 days. The precipitated PVDF-*b*-PVA amphiphilic polymer was recovered by filtration and dried until constant weight. Exactly same conditions were used for the PVDF treatment necessary to the quantification of deshydrofluoration reactions.

Typical procedure for the preparation of self-assembled objects

$PVDF_{51}$-*b*-PVA_{172} (20 mg) block copolymer was dissolved in 10 g of DMSO for 16 hours at 80 °C. The solution was then filtered on 0.45 µm filter, transferred into dialysis tubing (MWCO = 1000 Da) and dialyzed against deionized nanopure water for 4 days, leading to 17.30 g of solution with a polymer concentration of 1.16 g/L.

SI-Table V-1: Molar mass, dispersity, weight and molar fractions of the PVDF-XA, PVDF-b-PVAc and PVDF-b-PVA BCPs.

Run	$M_{n,NMR}$ (g/mol)	$M_{n,GPC}$ (g/mol)	Đ	wt % VDF/VAc/VA	mol % VDF/VAc/VA
$PVDF_{51}$-*XA*	3,400	8,300	1.40	100/0/0	100/0/0
$PVDF_{51}$-*b*-$PVAc_{172}$	18,300	17,500	1.34	18/82/0	23/77/0
***$PVDF_{51}$-*b*-PVA_{172}**	*11,000	n.a.	n.a.	30/0/70	23//77

Note: * The composition of the PVDF-*b*-PVA diblock copolymer has been determined on the parent copolymer PVDF-*b*-PVAc, because after hydrolysis the resulting copolymer is not sufficiently soluble in any solvents to provide sufficiently accurate spectra. Thus, the corresponding NMR molar mass was calculated using SI-Equation V-5:

SI-Equation V-5 $$M_{n,NMR} = M_{n,PVDF51-XA} + (DP_{PVA} \times M_{n,VA})$$

Where $M_{n\ PVDF51\text{-}XA}$ = 3,400 g.mol^{-1}, M_{nVA} = 44.05 g.mol^{-1}, DP_{PVA} = 172.

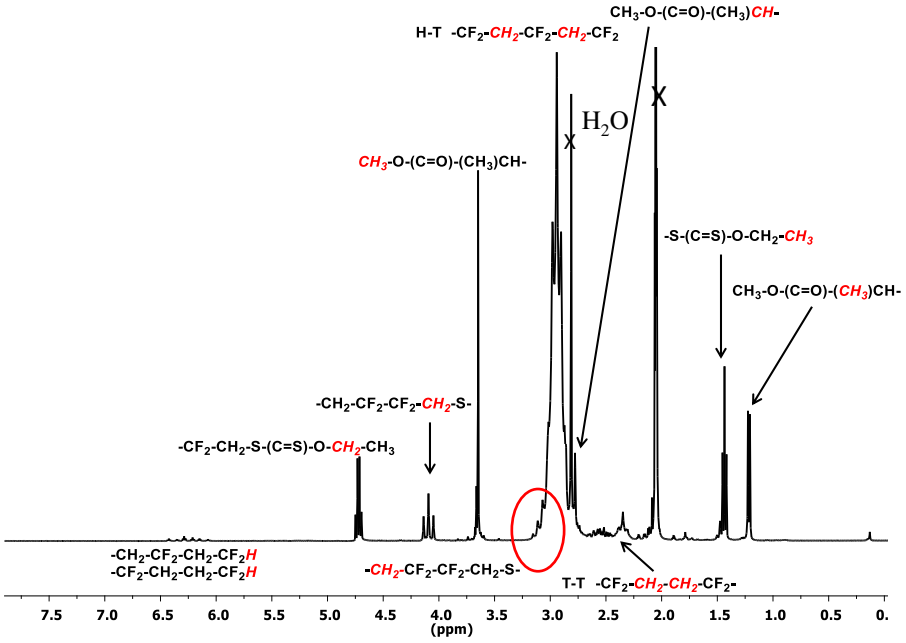

SI-Figure V-4: Expansion region from 0 to 7.8 ppm of ^{1}H NMR spectrum of PVDF$_{51}$-XA in $(CD_3)_2CO$.

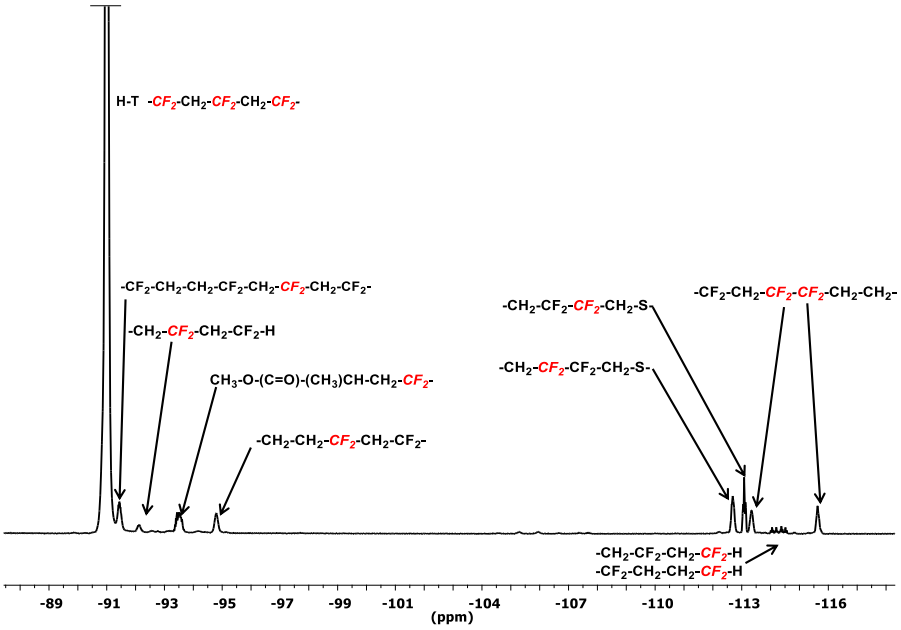

SI-Figure V-5: Expansion region from -87.5 to -118 ppm of ^{19}F NMR spectrum of PVDF$_{51}$-XA in (CD3)2CO.

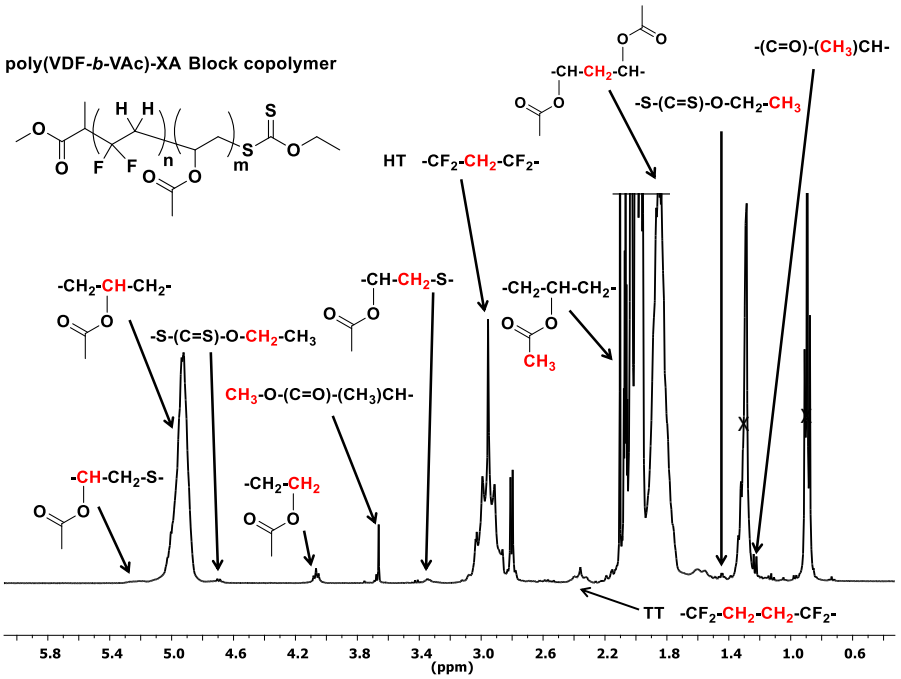

SI-Figure V-6: Expansion region from 0 to 6.1 ppm of ^{1}H NMR spectrum of $PVDF_{51}$-b-$PVAc_{172}$ in $(CD_3)_2CO$.

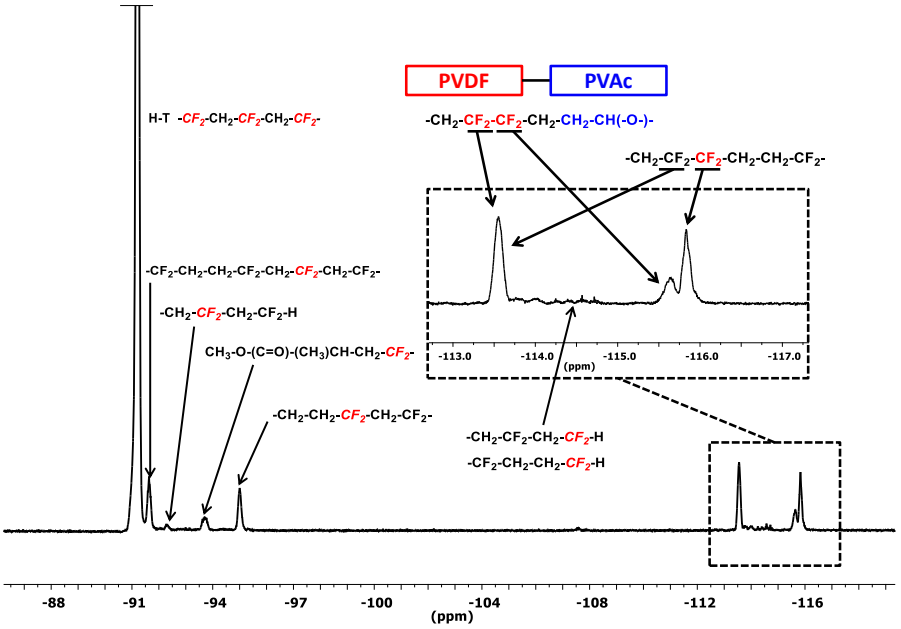

SI-Figure V-7: Expansion region from -87 to -120 ppm of ^{19}F NMR spectrum of $PVDF_{51}$-b-$PVAc_{172}$ in $(CD_3)_2CO$.

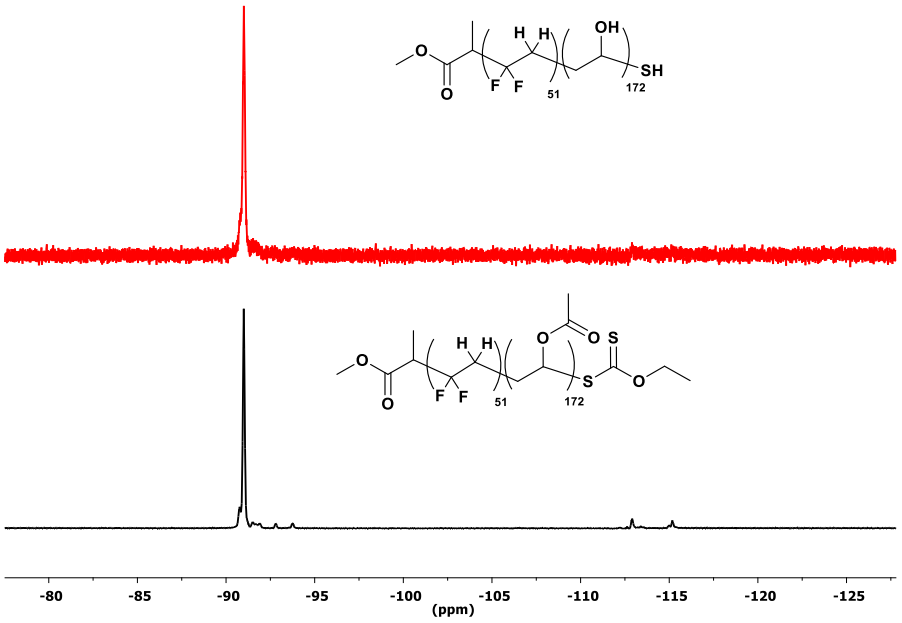

SI-Figure V-8: Expansion region from -78 to -127.5 ppm of ^{19}F NMR spectrum of $PVDF_{51}$-b-$PVAc_{172}$ (bottom) and $PVDF_{51}$-b-PVA_{172} (top) in DMSO-d_6

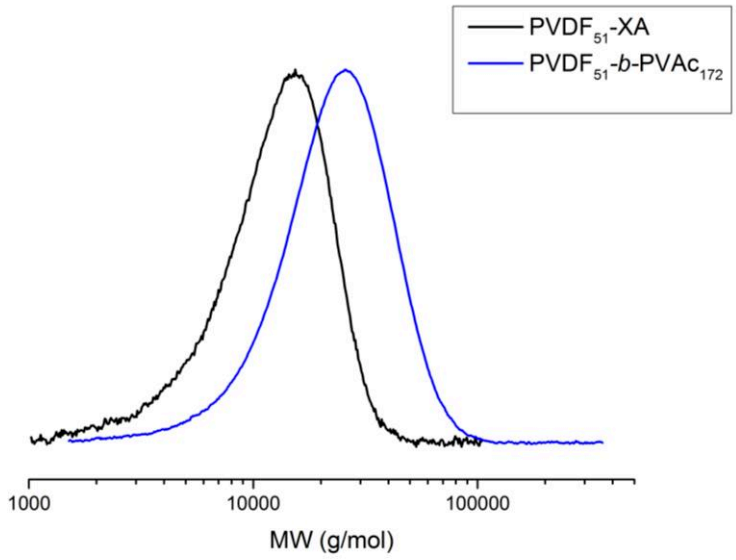

SI-Figure V-9: SEC chromatogram of $PVDF_{51}$ and $PVDF_{51}$-b-$PVAc_{172}$ block copolymer before hydrolysis.

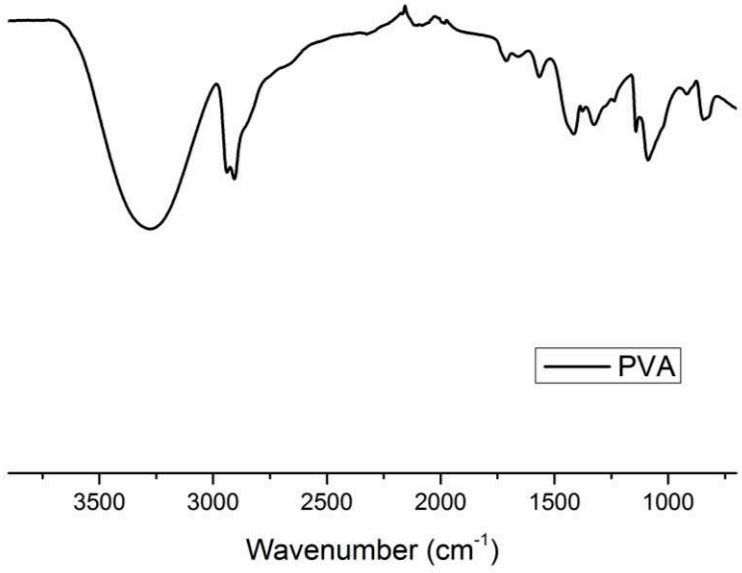

SI-Figure V-10: FTIR spectrum of commercial poly(vinyl alcohol) (>99 % of acetate hydrolysis).

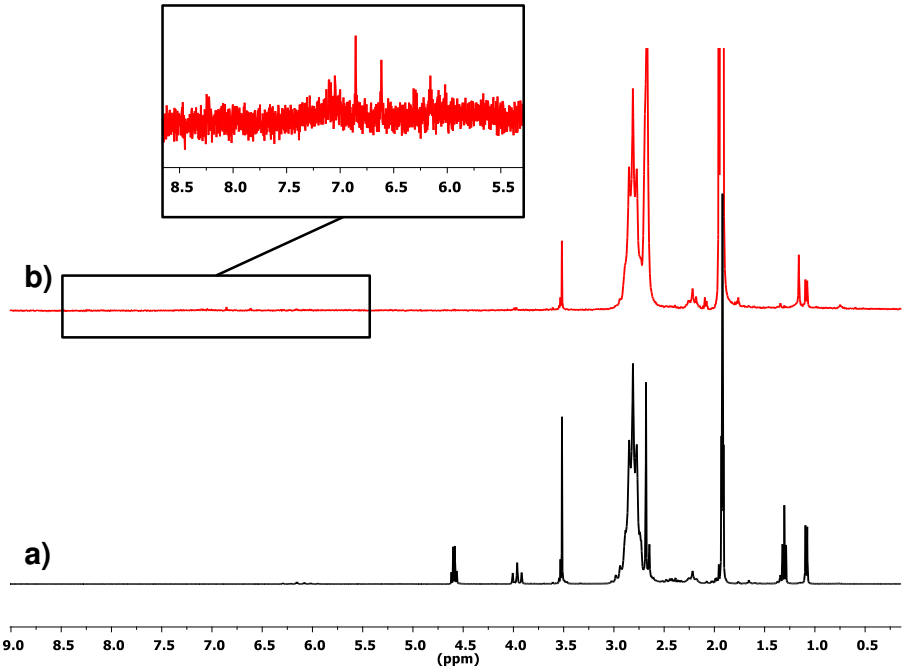

SI-Figure V-11: ^{1}H NMR spectrum of a) PVDF-XA and b) PVDF after treatment with a water/alcoholic solution of K_2CO_3 in $(CD_3)_2CO$.

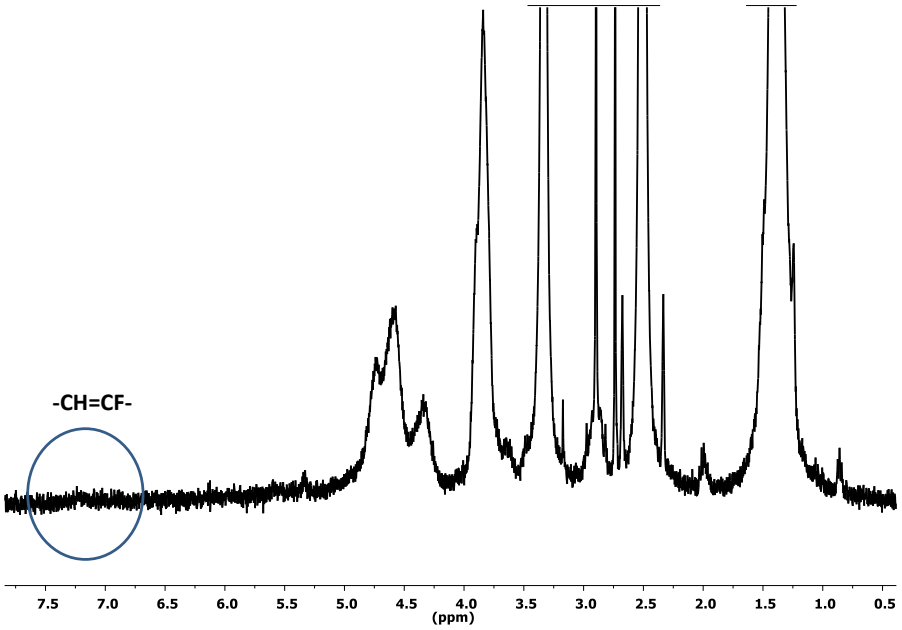

SI-Figure V-12: ^{1}H NMR spectrum of PVDF-b-PVA block copolymer in d_6-DMSO. Circled zone shows the potential –CH=CF- double bonds assigned to the dehydrofluorination reactions.

Conclusion Chapitre V

Ce chapitre décrit l'auto-assemblage en solution du premier copolymère dibloc amphiphile PVDF-*b*-PVA synthétisé par saponification en milieu basique des unités acétate de vinyle du copolymère PVDF-*b*-PVA. Une attention particulière a été consacrée aux réactions de deshydrofluorations occasionnées par la solution de K_2CO_3. En effet, une coloration de la solution (virant du jaune au noir) est immédiatement observée après addition de la solution basique. Cette coloration est exclusivement due à la formation de liaisons C=C sur les chaînes hydrocarbonés du PVDF par attaque basique et élimination d'acide fluorhydrique. Cependant, la coloration noire n'est pas directement reliée à la proportion de réactions de déhydrofluoration, 0.1 % de déhydrofluoration peut colorer entièrement la solution. Les doubles liaisons C=C ont été identifiées de manière très difficile par spectroscopie FTIR et RMN.

Le copolymère amphiphile a ensuite été auto-assemblé et a donné lieu à des micelles sphériques de diamètre moyen de 150 nm, observées par cryo-TEM et par diffusion dynamique de la lumière (DDL). Cependant, cette étude a été particulièrement difficile à exécuter à cause de la faible solubilité du PVA due à sa haute cristallinité. Cette très faible solubilité a très probablement joué un rôle crucial dans les morphologies finales observées.

L'ultime partie de ce mémoire rapporte l'auto-assemblage induit par la polymérisation de copolymère à blocs PVAc-*b*-PVDF synthétisés par polymérisation en dispersion du VDF dans le dimethyl carbonate.

Chapitre VI. Auto-Assemblage Induit par la Polymérisation de Copolymères PVAc-*b*-PVDF

Table des Matières

Introduction Chapitre VI

Comme il a été décrit dans le chapitre précédent, la haute cristallinité et la faible solubilité du PVA a rendu difficile l'étude de l'auto-assemblage en solution des copolymères à blocs PVDF-*b*-PVA. Un moyen de surmonter ce problème consiste donc à améliorer la solubilité du second bloc. Plusieurs voies permettent d'atteindre cet objectif: la première consiste en la modification de la nature chimique du second bloc en sélectionnant un bloc présentant une meilleure solubilité dans l'eau. La seconde, est de choisir un premier bloc organo-soluble puis d'effectuer l'auto-assemblage dans un solvant organique. Cette seconde voie a été choisie, et pour plusieurs raisons. En outre, la chimie RAFT utilisant les xanthates est exclusivement adaptée aux monomères moins activées (LAMs : Less Activated Monomers) tels que l'acétate de vinyle, la *N*-vinylpyrrolidone, la *N*-vinylcaprolactame, pour n'en nommer que quelques-uns. Ayant étudié en partie la polymérisation RAFT de l'acétate de vinyle dans le Chapitre IV de ce mémoire, il était donc logique de s'orienter sur la synthèse RAFT bien connue de ce polymère, qui de plus, présente une très bonne solubilité dans le DMC, solvant de polymérisation du VDF.

Par ailleurs, un des enjeux de ce chapitre est également d'augmenter la concentration en nano-objets dans le milieu dispersé, chose qui ne peut être réalisé par auto-assemblage conventionnel. Un des moyens permettant d'atteindre cet objectif consiste donc à utiliser l'auto-assemblage induit par la polymérisation (Polymerization-induced Self-Assembly, PISA) en dispersion ou en émulsion. De manière générale, la formation d'un second bloc insoluble à partir d'un premier bloc soluble provoque l'auto-assemblage des polymères en agrégat supramoléculaire à haute concentration et directement dans le milieu réactionnel de la polymérisation. Les morphologies les plus communes, qui dépendent du taux de solide et la longueur du bloc hydrophobe, sont de type micelles cylindriques, vers ou vésicules.

L'auto-assemblage induit par la polymérisation de blocs PVAc-*b*-PVDF fait l'objet de ce dernier Chapitre. Le VDF a ainsi été polymérisé par dispersion dans le DMC en présence d'agents RAFT macromoléculaires PVAc. Ce travail rapporte la première PISA du VDF et a fait l'objet d'un article scientifique publié dans *Polymer Chemistry*.[8]

Polymerization-induced self-assembly of PVAc-*b*-PVDF block copolymers *via* RAFT dispersion polymerization of vinylidene fluoride in dimethyl carbonate

Marc Guerre,[a] Mona Semsarilar,[b] Franck Godiard,[c] Bruno Ameduri,[a] Vincent Ladmiral[a]*

[1]Institut Charles Gerhardt, Ingénierie et Architectures Macromoléculaires, UMR 5253 – CNRS, Université Montpellier, ENSCM - 8, Rue Ecole Normale, 34296 Montpellier-France.
[2]Institut Européen des Membranes, IEM, UMR-5635, Université de Montpellier, ENSCM, CNRS, Place Eugène Bataillon, 34095 Montpellier cedex 5, France.
[3]Service de Microscopie Electronique, Universite Montpellier 2, Place Eugene Bataillon, 34095 Montpellier Cedex 5, France
*Corresponding author: vincent.ladmiral@enscm.fr

I. Abstract

Polymerization-induced self-assembly of PVAc-*b*-PVDF block copolymers (BCPs) in dimethyl carbonate (DMC) was performed and studied using vinylidene fluoride (VDF) RAFT dispersion polymerization protocols in DMC in the presence of PVAc macromolecular chain transfer agents (macro-CTAs). The polymerizations were conducted at 73 °C in DMC using three PVAc macro-CTAs of different molar masses and targeting various DP_{PVDF}. The relatively high frequency of head-to-head (HH) additions in VAc polymerization and the much lower reactivity of the resulting PVAc chains terminated with a -CH(OAc)-CH_2-SC(S)OCH_2CH_3 group ($PVAc_T$–XA, where XA stands for the xanthate end-group) compared to their regularly terminated analogs ($PVAc_H$–XA) leads to an accumulation of $PVAc_T$–XA chains during polymerization. These $PVAc_T$–XA reactivate slower than $PVAc_H$–XA in the presence of PVDF• radicals. In addition, RAFT polymerization of VDF is prone to the same chain defect problem and to non-negligible transfer to DMC. In consequence, RAFT dispersion polymerization of VDF in the presence of PVAc macro-CTAs afforded PVAc-*b*-PVDF BCPs (contaminated with starting unreacted PVAc and PVDF homopolymers formed via transfer to DMC). These phenomena were studied using ^{1}H and ^{19}F NMR spectroscopy and size exclusion chromatography. Nevertheless, the VDF RAFT dispersion polymerization in DMC experiments resulted in self-assembled BCP morphologies in the form of crystalline (1–5 μm) ovoidal flakes. These flakes stack on top of each other and form star-like structures. The structures are thought to form by epitaxial growth of the PVDF crystals and interparticle interpenetration crystallization. Although they are formed under polymerization-induced self-

assembly conditions, the morphologies of these BCP structures are governed by the crystallization of PVDF.

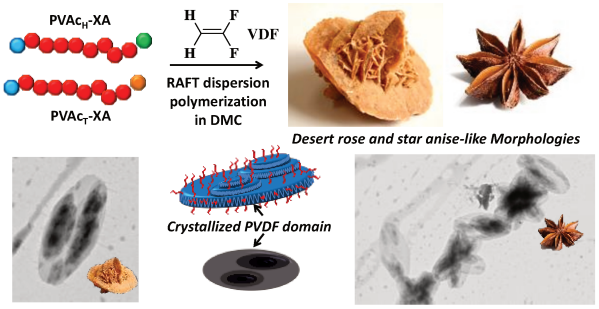

II. Introduction

Polyvinylidene fluoride (PVDF) and its copolymers are very valuable materials for their excellent weatherability, chemical and thermal stability, and outstanding electroactive properties.[1-3] While conventional radical polymerization of VDF is relatively well-known, reversible deactivation radical polymerization (RDRP) of VDF has been scarcely reported.[3,4] The RDRP of VDF was pioneered by Tatemoto[5,6] in 1979 who used and developed Iodine Transfer Polymerization (ITP)[7] to produce PVDF-based thermoplastic elastomers industrially. Since then, numerous articles dealing with the ITP of VDF have been reported.[7-11] Recently, RAFT polymerization has been shown to be a very efficient RDRP technique to control the polymerization of VDF.[12-14] However, the preparation of well-defined narrow-dispersity PVDF with high end-group fidelity remains difficult due to VDF reverse (head-to-head) additions (occurring when a $-CF_2\cdot$ (head) radical adds onto the head of a VDF monomer and forms a $-CH_2-CF_2-CF_2-CH_2\cdot$ radical). These $-CH_2\cdot$ radicals readily form, by transfer to the chain transfer agent, much less reactive chain-ends.[8,9,12,14] The accumulation of these less reactive end-groups was shown to slow down the degenerative chain transfer process, and to lead to significant broadening of the molar mass distribution and to loss of chain-end functionality.[8,12-14] In spite of these difficulties, RAFT polymerization is arguably the most efficient RDRP technique to synthesize well-defined PVDF. It was indeed shown that functionality could be preserved and that PVDF of relatively high molar mass could be prepared albeit at the cost of monomer conversion.[14]

In addition, RAFT polymerization was also used to prepare new PVDF-based architectures such as macromonomers,[15] dendrimers[16] and well-defined block copolymers[17] (including

amphiphilic block copolymers).[18] Indeed, interest in PVDF-based block copolymers[19] (BCP) has surged in the last decade. Several synthetic methods using telomerisation,[20–25] the combination of conventional radical polymerization of VDF from functionalized initiators[26–29] and atom transfer radical polymerization, or click chemistry[30] have been proposed. However, for all their merits, telomerisation only affords oligomers, and functional initiators lead to broad dispersity.

Recently, our research group achieved the RAFT synthesis of well-defined poly(vinylidene fluoride)-*block*-poly(vinyl acetate) (PVDF-*b*-PVAc) BCP by sequential addition of monomers.[17] This study showed that both the regular PVDF chains (terminated with a -CH_2-CF_2-XA group and denoted as $PVDF_H$-XA where XA represents the -$SC(S)OCH_2CH_3$ xanthate motif) and the head-to-head-terminated PVDF chains (chains terminated with a -CF_2-CH_2-XA group and denoted as $PVDF_T$-XA) were reactivated by VAc radicals. This achievement opens the way to the synthesis of new BCPs and exploration of their self-assembly behaviour.[31–33]

Among the various self-assembly techniques, the recently developed Polymerization-Induced Self-Assembly (PISA)[34–37] strategy has emerged as a very powerful and simple method to prepare self-assembled polymer nano-objects. Typically, under PISA conditions, a solvophilic polymer precursor dissolved in a solvent is extended with a solvophobic polymer. The chain extension leads to an “amphiphilic” block copolymer that self-assembles into self-stabilized nano-objects, in the absence of an additional surfactant, as the polymerization progresses. The main advantage of PISA is that it allows the preparation of self-assembled copolymer particles at very high solids content (up to 50 wt%) with high reproducibility. In addition when combined with RDRP techniques, it allows the formation of non-spherical self-assembled morphologies such as worm-like micelles and vesicles.[38–41] So far, most PISA protocols have used RAFT polymerization in dispersion[35,37] or in emulsion[42–45] using thermal initiation. Recently, photo-PISA was reported as a means to carry out PISA at lower temperatures.[46] PISA was mostly performed using water as a continuous phase,[38,39,42-45,47] but organic solvents have also been successfully employed.[40,41,48–50]

The present study is the first report of the PISA of PVDF-containing BCP. Using RAFT dispersion polymerization conditions and PVAc macro-CTAs, PVAc-*b*-PVDF BCPs were self-assembled in dimethyl carbonate (DMC). The first section of this article examines in detail the synthesis of PVAc-*b*-PVDF BCPs, and the structural characteristics of these new

copolymers. The second one deals with the BCP self-assembled structures formed during the RAFT dispersion polymerization of VDF in DMC. Since PVDF is a semicrystalline polymer, the self-assembly of PVDF-based BCPs may be governed by crystallization,[51–53] although it is triggered by the polymerization of VDF.

III. Experimental Section

Materials and methods

All reagents were used as received unless stated otherwise. 1,1- Difluoroethylene (vinylidene fluoride, VDF) was kindly supplied by Arkema (Pierre-Bénite, France). *O*-Ethyl-*S*-(1-methoxycarbonyl)ethyldithiocarbonate (CTA_{XA}) was synthesized according to the method described by Liu et al.[54] tert-Amyl peroxy-2- ethylhexanoate (Trigonox 121, purity 95%) was purchased from AkzoNobel (Chalons-sur-Marne, France). Nonafluoro-tert-butyl alcohol (99%) was purchased from Apollo Scientific. ReagentPlus grade (purity > 99%). 2,2-Azobis (4-methoxy-2,4-dimethyl valeronitrile) (V70, 96%) was purchased from Wako. 2,2-Azobisisobutyronitrile (AIBN), vinyl acetate (VAc), dimethyl carbonate (DMC), tetrahydrofuran, (THF), acetone ($(CH_3)_2CO$), methanol (CH_3OH), and laboratory reagent grade hexane (purity > 95%) were purchased from Sigma Aldrich and used as received. AIBN was purified by recrystallization from methanol twice before use.

Nuclear magnetic resonance (NMR)

Nuclear Magnetic Resonance (NMR) spectra were recorded on a Bruker AC 400 instrument. Deuterated acetone was used as the solvent. Coupling constants and chemical shifts are given in hertz (Hz) and parts per million (ppm), respectively. The experimental conditions for recording ^{1}H and ^{19}F spectra were as follows: flip angle 90° (or 30°), acquisition time 4.5 s (or 0.7 s), pulse delay 2 s (or 2 s), number of scans 128 (or 512), and a pulse width of 5 μs for $_{19}F$ NMR.

Size Exclusion chromatography (SEC)

Size exclusion chromatograms were recorded using a triple detection GPC from Agilent Technologies with its corresponding Agilent software, dedicated to multi-detector GPC calculation. The system used two PL1113-6300 ResiPore 300 × 7.5 mm columns (all range of M_w) with DMF as the eluent with a flow rate of 0.8 mL min^{-1} and toluene as the flow rate marker. The detector suite comprised a PL0390-0605390 LC light scattering detector with 2

scattering angles (15° and 90°), a PL0390-06034 capillary viscometer, and a 390-LC PL0390-0601 refractive index detector. The entire SEC-HPLC system was thermostated at 35 °C. Low dispersity PMMA standards were used for the calibration. The typical sample concentration was 10 mg mL^{-1}.

Dynamic light scattering

Dynamic Light Scattering (DLS) experiments were performed at 25 °C on a Malvern instrument Nano-ZS equipped with a He‑Ne laser as the light source (λ = 633 nm). The scattered light was detected at a scattering angle θ = 173°. Dilute aqueous dispersions of block copolymers (1 mg mL^{-1}) were introduced into cells (path length, 10 mm) without filtration.

Differential scanning calorimetry (DSC)

DSC measurements were performed on 10‑15 mg samples on a Netzsch DSC 200 F3 instrument using the following heating/ cooling cycle: cooling from room temperature (ca. 20 °C) to -50 °C at 20 °C min^{-1}, isotherm plateau at -50 °C for 5 min, first heating ramp from -50 to 200 °C at 10 °C min-1, cooling stage from 200 to -50 °C at 10 °C min^{-1}, isotherm plateau at -50 °C for 3 min, second heating ramp from -50 °C to 200 °C at 10 °C min^{-1} and last cooling stage from 200 °C to room temperature (ca. 20 °C). The instrument was calibrated with noble metals and standards (bismuth, indium, mercury, octadecane, octane and tin) and the accuracy of the measurements were checked before analysis with an indium sample. Melting points were determined at the maximum of the enthalpy peaks.

Transmission electron microscopy

A drop (7 µL) of the sample was placed on a perforated carbon film-coated copper grid for 50 s, blotted with filter paper and dried with a vacuum pump. The sample was transferred in a

single axis tilt sample holder and observed at 100 kV acceleration voltage in a JEOL 1200 EXII transmission electron microscopy at 25 °C.

Autoclave

The radical polymerizations of VDF were performed in a 100 mL Hastelloy Parr autoclave system (HC 276), equipped with a mechanical Hastelloy stirring system, a rupture disk (3000 PSI), inlet and outlet valves, and a Parr electronic controller to regulate the stirring speed and the heating. Prior to the reaction, the autoclave was pressurized with 30 bars of nitrogen to

check for leaks. The autoclave was then put under vacuum (20 10^{-3} mbar) for 30 minutes to remove any trace of oxygen. A degassed solution of the solvent, initiator and xanthate CTA was introduced via a funnel. The reactor was then cooled down in liquid nitrogen to about -80 °C, and the desired quantity of VDF was transferred by determining the difference of weight before and after filling the autoclave with VDF. After warming up to ambient temperature (ca. 20 °C), the autoclave was heated to the targeted temperature under mechanical stirring.

Synthetic procedure

RAFT polymerization of VAc. A typical RAFT polymerization of VAc (run 1, Table VI-1) was carried out as follows: In a 100 mL round bottom flask, *O*-ethyl-*S*-*(*1-methoxycarbonyl)ethyldithiocarbonate (1.613 g, 7.744 10^{-3} mol) and AIBN (0.254 g, 1.55 10^{-3} mol) were degassed by bubbling N_2 for 15 min. Degassed VAc (20.0 g, 2.32 10^{-1} mol) was then introduced in the reaction vessel. The reaction vessel was then placed into an oil bath thermostated at 60 °C. The reaction was carried out under vigorous stirring for 14 hours. The viscous residue was then dissolved in 20 mL of acetone and precipitated from chilled hexane. The resulting filtered polymer was dried until constant weight under vacuum (20 10^{-3} mbar) at 50 °C to remove traces of the solvent. The PVAc was isolated as a yellowish powder in high yield (yield = 70%).

^{1}H NMR (400 MHz, $(CD_3)_2CO$, δ (ppm)) (Figure VI-1): 1.06-1.17 (-CH(C**H$_3$**)(C=O)-), 1.37-1.46 (-S(C=S)O-CH_2-C**H$_3$**), 1.68-1.91 (-CH(OAc)-C**H$_2$**-CH(OAc)-), 1.91-2.04 (-CH(O**Ac)**-), 2.16-2.35 (-C**H$_2$**-CH(OAc)-S(C=S)OEt), 2.38-2.62 (-C**H**(CH_3)(C=O)-O-CH_3), 3.18-3.51 (-CH(OAc)-C**H$_2$**-S(C=S)OEt), 3.56-3.67 (-CH(CH_3)-(C=O)-O-C**H$_3$**), 3.95-4.13 (-CH_2-(OAc)C**H$_2$**), 4.57-4.75 (-S(C=S)O-C**H$_2$**-CH_3), 4.76-5.14 (-CH_2-C**H(**OAc)-CH_2-), 5.13-5.24 (-C**H(**OAc)-CH_2-S(C=S)OEt), 6.50-6.70 (-CH_2-C**H(**OAc)-S(C=S)OEt).

RAFT polymerization of vinylidene fluoride (VDF) using PVAc-XA as a macro-CTA.

Using the autoclave experimental setup described above, a typical dispersion polymerization of VDF (run 4, Table VI-1) was performed as follows: a solution of tert-amyl peroxy-2-ethylhexanoate (143 mg, 6.25 10^{-4} mol) and PVAc-XA (macro-CTA, 18.77 g, 3.12 10^{-3} mol) in dimethyl carbonate DMC (60 mL) was degassed by bubbling N_2 for 30 min. This homogeneous solution was introduced into the autoclave using a funnel, VDF gas (20.0 g, 3.12 10^{-1} mol) was transferred in the autoclave at low temperature, and the reactor was gradually heated to 73 °C. The reaction was stopped after 20 h. During the reaction, the

pressure increased to a maximum of 25 bars and then decreased to 8 bars over 20 h. The autoclave was cooled down to room temperature (ca. 20 °C) and purged from the residual monomer. The resulting dispersion was then transferred into a glass vial. For analysis and microstructure characterization, 2 mL of PVAc-*b*-PVDF dispersion were dried under vacuum, and the crude product was dissolved in 5 mL of warm THF (ca. 40 °C) under vigorous stirring for 5 minutes. This polymer solution was then precipitated in 100 mL of chilled methanol (bad solvent for PVDF but good solvent for PVAc) and isolated as a white powder. It is important to note that to the best of our knowledge, the solubility of PVDF in VDF is unknown. Although this solubility may decrease for high PVDF molar mass, it is possible that a range of temperatures and pressures within which VDF dissolves PVDF exist. Since both emulsion and dispersion polymerizations are used to produce PVDF, VDF is probably capable of, at least, swelling PVDF. Under the PISA conditions used here, VDF is believed to be able to diffuse from the DMC solution into the self-assembled nano-objects.

^{1}H NMR (400 MHz, $(CD_3)_2CO$, δ (ppm)) (Figure VI-3): 1.06-1.17 (m, -CH(C**H$_3$**)(C=O)-, $^{3}J_{HH}$ = 7.1 Hz), 1.40-1.46 (t, (-S(C=S)O-CH_2-C**H$_3$**), 1.63-1.92 (m, -CH(OAc)-C**H$_2$**-CH(OAc)-, VAc), 1.92-2.03 (m, -CH(O**Ac)**-, VAc), 2.28-2.43 (m,-CF_2-C**H$_2$**-C**H$_2$**-CF_2-, VDF-VDF TT reverse addition), 2.70-3.19 (t, -CF_2-C**H$_2$**-CF_2-, regular VDF-VDF HT addition), 3.60-3.69 (s, -(C=O)-O-C**H$_3$**), 4.02-4.17 (-CF_2-C**H$_2$**-S(C=S)OEt, VDF), 4.63-4.72 (q, (-S(C=S)O-C**H$_2$**-CH_3, $^{3}J_{HH}$ = 7.2 Hz), 4.76-5.14 (-CH_2-C**H(**OAc)-CH_2-), 5.18-5.42 (PVAc-C**H**(OAc)-PVDF), 6.05-6.45 (tt, $^{2}J_{HF}$ = 55 Hz , $^{3}J_{HH}$ = 4.6 Hz -CH_2-CF_2-**H**).

^{19}F NMR (376 MHz, $(CD_3)_2CO$, δ (ppm)) (SI-Figure VI-10): -115.63 (-CH_2-CF_2-C**F$_2$**-CH_2-CH_2-, VDF-VDF HH (head-to-head) reverse addition), -113.34 (-CH_2-C**F$_2$**-CF_2-CH_2-CH_2-, HH reverse addition), −113.09 (CH_2-CF_2-C**F$_2$**-CH_2-S-), −112.69 (-CH_2-C**F$_2$**-CF_2-CH_2-S-), -94.79 (-CH_2-CH_2-C**F$_2$**-CH_2-, TT (tail-to-tail) reverse addition), -92.62 (PVAc-CH_2-CH(OAc)-CH_2-C**F$_2$**-PVDF), -92.12 (-CH_2-C**F$_2$**-CH_2-CF_2H), -91.44 (-CH_2-CH_2-CF_2-CH_2-**CF$_2$**-CH_2-CF_2-, regular VDF-VDF HT (head-to-tail) addition), -91.00 (-CH_2-C**F$_2$**-CH_2-, regular VDF-VDF HT addition).

DP and $M_{n(NMR)}$ Calculations

The DP calculation of the PVAc macro-CTA is described in supporting information (SI-Equation VI-5and SI-Equation VI-6).

The degree of polymerization (DP) of the PVDF block can be calculated from the ^{1}H NMR spectrum of the purified BCP using the integrals centered at 1.45 ppm of the signals corresponding to the methyl group (CH_3) of the R-group of the CTA (connected to the PVAc block), the integral of the signals of the CH_2 group of the normal (HT) VDF additions (2.70−3.19 ppm), that of the CH_2 group of the reverse (TT) VDF additions (2.28−2.43 ppm), and that of the terminal VDF units (4.02−4.17 ppm), according to Equation VI-1. The DP of the PVDF block can also be calculated from the ^{1}H NMR spectrum of the crude BCP using Equation VI-2 which uses a correction factor (α) corresponding to the proportion of $PVAc_H$-XA chains (fastly reactivatable chains terminated by a -CH_2CH(OAc)-XA motif where XA represents the ethyl xanthate group) in the PVAc prepared (α = 0.60 for run 1 and α =0.25 for run 8, Table VI-1, for example). Indeed, only $PVAc_H$-XA chains can be quickly reactivated by -$CF_2^{\bullet}$ radicals (vide infra). The $PVAc_T$-XA chains (terminated by a -CH(OAc)CH_2-XA motif) reactivate very slowly (vide infra) and the $PVAc_H$-H chains (terminated by a -CH_2CH_2(OAc) motif generated by transfer reactions) are dead. The $PVAc_T$-H chains (terminated by a -CH_3 end group also generated by transfer reactions), are also dead, and if present, cannot be identified. The NMR signals corresponding to these chains overlap with the -CH_2- and -CH_3 signals of the PVAc chains. Furthermore, the proportion of reverse additions in VAc polymerization has been estimated to represent 1 % of the total number of additions (see above). Therefore, the amount of $PVAc_T$-H chains was neglected in this work.

DP calculation using ^{1}H NMR spectrum of the purified BCP:

$$\textit{Equation VI-1} \quad \boldsymbol{DP} = \frac{\int_{2.70}^{3.19} \boldsymbol{CH_2(HT)} + \int_{2.28}^{2.43} \boldsymbol{CH_2(TT)} + \int_{4.02}^{4.17} \boldsymbol{CH_2(End-group)}}{\boldsymbol{2/3 \times \int_{1.19}^{1.24} CH_3(R_{PVAc-XA})}}$$

DP calculation using ^{1}H NMR spectrum of the crude BCP:

$$\textit{Equation VI-2} \quad \boldsymbol{DP} = \frac{\int_{2.70}^{3.19} \boldsymbol{CH_2(HT)} + \int_{2.28}^{2.43} \boldsymbol{CH_2(TT)} + \int_{4.02}^{4.17} \boldsymbol{CH_2(End-group)}}{\boldsymbol{2/3 \times \alpha \times \int_{1.19}^{1.24} CH_3(R_{PVAc-XA})}}$$

Molar masses were then calculated using Equation VI-3 (with $M_{n,PVAc\text{-}XA}$ calculated using SI-Equation VI-5and SI-Equation VI-6):

$$\textit{Equation VI-3} \quad M_{n,NMR} = M_{n,PVAc-XA} + DP \times M_{n,VDF}$$

Theoretical molar masses were calculated using Equation VI-4 with yield = conversion and the $[VDF]_0/[PVAc\text{-}XA]_0$ ratios listed in Table VI-1.

Equation VI-4 $$M_{n,theo} = \frac{[VDF]_0}{[PVAc-XA]_0} \times Yield \times \frac{1}{\alpha} \times M_{n,VDF} + M_{n,\,PVAc-XA}$$

With $M_{n,VDF}$ = 64.03 g/mol.

IV. Results and Discussion

IV.1 Functionality and Reactivation

Our previous investigations[17] showed that relatively well-defined PVDF-*b*-PVAc block copolymers can be prepared by solution polymerization of VAc in the presence of a PVDF macro-CTA. The question that followed was: "Can similarly well-defined BCPs be prepared by the reverse method (polymerization of VDF in DMC in the presence of a PVAc macro-CTA)?" Since PVAc and VDF are both soluble in DMC, while PVDF is not, the question can be reformulated into "Can RAFT dispersion polymerization of VDF in DMC be efficiently performed using a PVAc macro-CTA?" Scheme VI-1 illustrates this formulation.

PVAc is, like PVDF, prone to chain defects; the proportion of head-to-head (HH) and tail-to-tail (TT) additions in PVAc is temperature dependent and has been estimated at 1.23 % at 25°C and 1.95% at 110 °C.[55-59] These reverse additions were reported to have a detrimental effect on the RAFT polymerization of VAc.[55,59] PVAc chains resulting from a terminal head-to-head VDF addition immediately followed by a xanthate exchange reaction and thus terminated by a $CH(OAc)CH_2$-XA group, (noted -$CH(OAc)$-CH_2-XA or $PVAc_T$-XA for brevity, where XA is the xanthate motif)are very likely to be reactivated much more slowly than their regularly terminated analogues (PVAc-$CH_2CH(OAc)$-XA or $PVAc_H$-XA), to accumulate in the reaction medium as the RAFT polymerization proceeds, to lead to a broadening of the dispersity and to impair the synthesis of well-defined BCP from PVAc macro-CTAs.[59] Consequently, a detailed ^{1}H NMR analysis of the chain ends of a PVAc macro-CTA prepared by RAFT polymerization was carried out. The results of this study are in agreement with those reported previously by Kamigaito's research group.[58-59] Figure VI-1 displays the ^{1}H NMR spectrum of a $PVAc_{18}$-XA synthesized by RAFT polymerization (run 1, Table VI-1). The COSY ^{1}H-^{1}H NMR spectrum of this polymer is shown in SI-Figure VI-6.

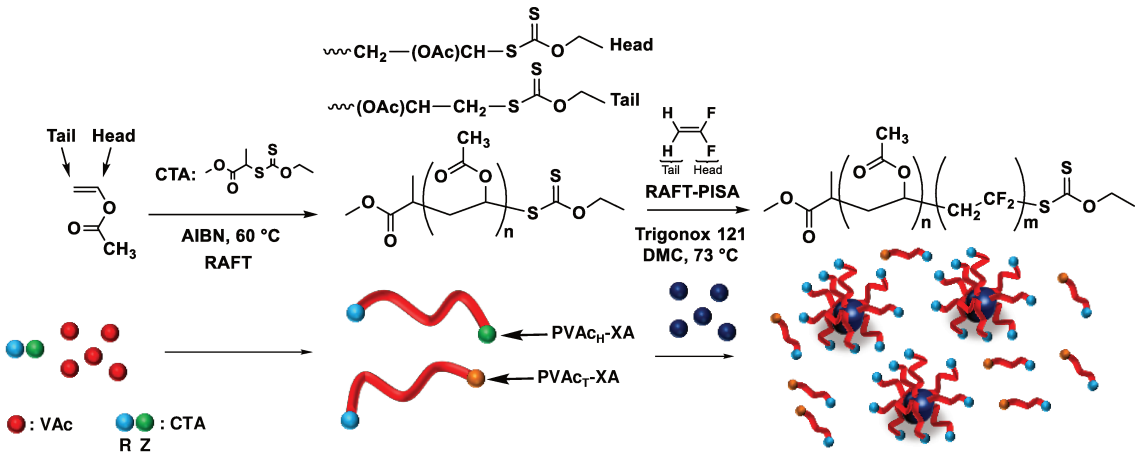

Scheme VI-1: Synthesis and self-assembly of PVAc-b-PVDF block copolymers by RAFT dispersion polymerization of VDF in DMC using PVAc macro-CTA.

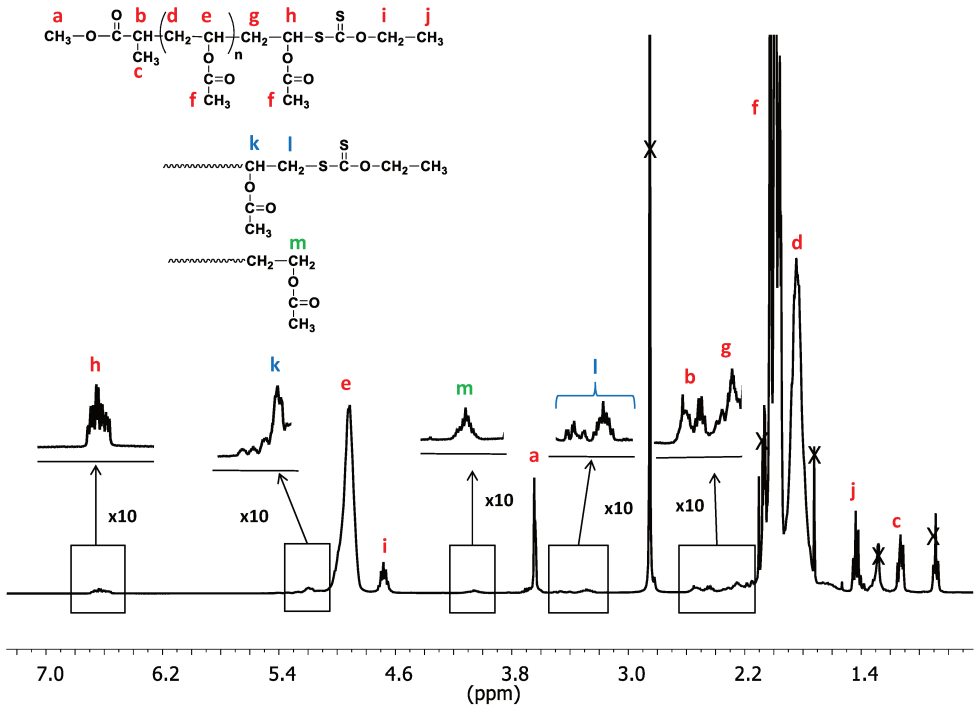

Figure VI-1: Expansion of the 0.6–7.3 ppm region of the ^{1}H NMR spectrum in $(CD_3)_2CO$ of a $PVAc_{18}$–XA macro-CTA synthesized by RAFT polymerization (run 1, Table VI-1); crossed-out peaks correspond to residual hexane, acetone and water.

The characteristic signals of the PVAc backbone and of the xanthate end-groups were clearly identified: *(i)* broad peaks centered at 1.75, 2.00 and 4.92 ppm assigned to the -CH_2-, -CH_3 and -CH- of PVAc, respectively; *(ii)* a multiplet centered at 1.11 ppm, a broad signal ranging from 2.37 to 2.60 ppm, and a singlet at 3.63 ppm corresponding to the CTA R-group; *(iii)* the signals of the CTA Z-group at 1.42 ppm (triplet) and 4.67 ppm (multiplet); *(iv)* a small peak at 2.24 ppm and a complex signal centered at 6.60 ppm assigned to the -CH_2- and –CH- of the terminal VAc unit in $PVAc_H$-XA chains, respectively; *(v)* a broad signal ranging from 3.18 to

3.51 ppm and a peak at 5.18 ppm corresponding to the -CH_2- and the -CH- of the terminal VAc unit in $PVAc_T$-XA chains, respectively; and *(vi)* a multiplet at 4.08 ppm assigned to -CH_2(OAc) chain-ends ($PVAc_H$-H) produced by transfer reactions (to the monomer or the polymer). This NMR end-group analysis was used to calculate the proportions (shown in Table VI-1) of the different types of PVAc chains ($PVAc_H$-XA, $PVAC_T$-XA and $PVAc_H$-H) for the three PVAc macro-CTAs (SI-Figure VI-7) prepared here (run 1, 6, and 8, Table VI-1).

A short $PVAc_{18}$ macro-CTA was prepared (run 1, Table VI-1), and was shown to be composed of 60 mol % of $PVAc_H$-XA, 28 mol % of $PVAc_T$-XA and 12 mol % of PVAc-H. A second PVAc macro-CTA targeting a DP of 150 was also prepared. The synthesis conditions used here (RAFT polymerization in bulk) yielded a PVAc macro-CTA with an average DP of 115 (run 6, Table VI-1) and composed of 90 mol% of $PVAc_T$-XA and 10 mol% of PVAc-H. A third PVAc macro-CTA was synthesized by RAFT polymerization in nonafluoro-tertbutyl alcohol. The use of fluorinated solvents[60,61] had been shown by Koumura et al.[58] to reduce the quantity of reverse addition and improve the syndiotacticity of PVAc synthesized using ITP. Here, this protocol resulted in a PVAc of average DP = 96 with the following composition: $PVAc_H$-XA/$PVAc_T$-XA/ $PVAc_H$-H = 25/67/8 mol % (run 8, Table VI-1).

These PVAc macro- CTAs were then used in VDF dispersion polymerizations in DMC targeting different DP (Table VI-1). DMC was chosen as the VDF polymerization solvent because it has been shown to promote relatively fast polymerization of VDF. Moreover, while VDF is highly soluble in DMC (5.2 mol L^{-1} at P = 33 bar and T = 73 °C),[14] PVDF is only soluble in DMC at high T (90 °C), and its solubility in DMC also probably decreases with increasing molar mass.

Table VI-1: Synthesis and characterization of the PVAc macro-CTAs, and of the PVAc-b-PVDF BCPs prepared by RAFT dispersion polymerization of VDF in DMC

Run	CTA	[M]	$\frac{[M]_0}{[CTA]_0}$	Yield[d] (%)	DP[e] (PM)	$M_{n,theo}$[f] (g/mol)	$M_{n,NMR}$[g] (g/mol) (Purified)	$M_{n,NMR}$[h] (g/mol) (Crude)	$M_{p,SEC}$[i] (g/mol)	Đ[i]	Solids content[d] (%)	$P(M)_H$-XA[j] (mol %)	$P(M)_T$-XA[k] (mol %)	P(M)-H[l] (mol %)
1[b]	CTA_{XA}	VAc	30	70	18	2,000	1,840	n.a.	3,700	1.28	n.a.	60	28	12
2[a]	1	VDF	20	36	18	4,000	3,000	3,100	11,000	1.10	11	0	89	11
3[a]	1	VDF	50	56	78	4,800	6,800	6,900	14,100	1.24	16	0	58	42
4[a]	1	VDF	100	65	145	8,600	11,100	12,000	19,900	1.27	15	0	45	55
5[a]	1	VDF	200	73	257	17,100	18,300	18,400	22,500	1.29	14	0	20	80
6[b]	CTA_{xa}	VAc	150	68	115	9,000	10,100	n.a.	22,300	1.25	n.a.	0	90	10
7[a]	6	VDF	200	45	502	n.a.	42,300	n.a.	30,300	1.30	8	0	17	83
8[c]	CTA_{XA}	VAc	150	76	96	13,100	8,500	n.a.	18,300	1.20	n.a.	25	67	8
9[a]	8	VDF	100	47	205	20,500	19,700	21,600	21,200	1.17	5	0	28	72
10[a]	8	VDF	200	51	303	34,600	29,500	27,900	26,200	1.35	7	0	30	70
11[a]	8	VDF	400	59	442	68,900	39,400	36,800	22,800	1.22	9	0	33	67

Reactions conditions: CTA_{XA} = *O*-ethyl-*S*-(1- methoxycarbonyl)ethyldithiocarbonate, initiator (I) = *Tert*-Amyl peroxy-2-ethylhexanoate and azoisobutyronitrile for VDF and VAc polymerization, respectively. $[I]_0/[CTA]_0$ = 0.1, T = 73 °C and 60°C for VDF and VAc polymerization, respectively. Solvent: Dimethylcarbonate[a] for VDF polymerization and bulk[b] or nonafluoro-*tert*-butyl alcohol[c] for VAc polymerization. [d]Measured by gravimetry. [e] DP determined using Equation VI-1 and SI-Equation VI-5for PVDF and PVAc block, respectively. [f]Determined using: Equation VI-4 for runs 2-5 and 9-11, and SI-Equation VI-6 for runs 1, 6, 8. [g]Determined using Equation VI-3 and SI-Equation VI-7 for PVDF and PVAc block, respectively. [h]Determined using Equation VI-2 and Equation VI-3. [i]Determined using PMMA narrow standard calibration on purified BCP. [j,k,l] $P(M)_H$-XA, $P(M)_T$-XA and P(M)-H stand for $PVAc_H$-XA, $PVAc_T$-XA and PVAc-H for entries (1, 6, 8) corresponding to the synthesis of PVAc macro-CTA, and for $PVDF_H$-XA, $PVDF_T$-XA, PVDF-H for entries (2, 3, 4, 5, 7, 9, 10, 11) corresponding to VDF polymerization. End-group mol % was calculated using SI-Equation VI-8 to SI-Equation VI-13on purified BCP. n.a. stands for not applicable. *Note*: The determination of the molar masses and dispersities of the diblock copolymers using SEC was not possible because it requires a concentration detector such as a RI detector which in the case of PVDF-*b*-PVAc BCPs cannot be used because of the negative response of PVDF and the positive response of PVAc in DMF. Consequently, the SEC molar mass values given in Table VI-1, column 10, are only valid for comparison. Mp values were preferred to M_w or M_n value, as they are more representative of the chain extension and shift towards high molar masses.

The resulting block copolymers were analysed by size exclusion chromatography and ^{1}H NMR spectroscopy. The viscometric SEC traces of the starting macro CTAs and of the resulting PVAc-*b*-PVDF diblock copolymers before and after precipitation in methanol (bad solvent for PVDF but good solvent for PVAc) are shown in Figure VI-2 (for $PVAc_{18}$-XA) and in SI-Figure VI-8 ($PVAc_{115}$-XA and $PVAc_{96}$-XA).

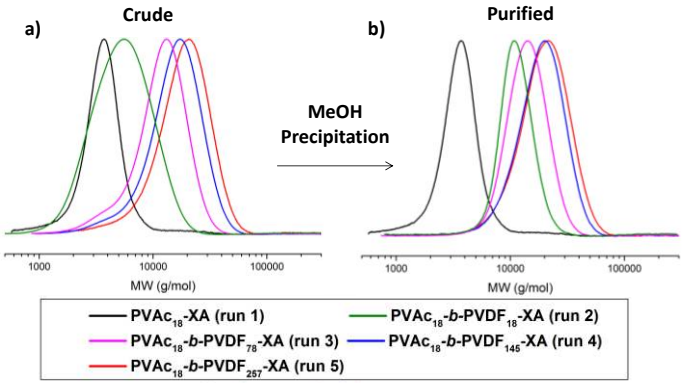

Figure VI-2: Normalized SEC traces (viscometric detector) of: (a) $PVAc_{18}$-XA macro-CTA (black trace), and of crude $PVAc_{18}$-b-PVDFx (X = 18, 78, 145 and 257) BCPs; and of (b) the same polymers purified by precipitation in methanol.

The chromatograms displayed in Figure VI-2 demonstrate that reinitiation occurred and that the formation of $PVAc_{18}$-*b*-PVDF BCPs was successful (shift of the SEC traces to higher molar masses and relatively monomodal distribution). However, SEC chromatograms of the copolymers resulting from the chain extension of the $PVAc_{115}$-XA macro-CTA indicate poor reactivation (SI-Figure VI-8a): broadening of the SEC trace rather than a clear shift toward a higher molar mass. The SEC traces corresponding to the chain extension of the $PVAc_{96}$-XA macro-CTA suggest a suboptimal reinitiation (SI-Figure VI-8c) but better than in the case of $PVAc_{115}$-XA. For all the PVAc macro-CTAs tested, a non-negligible fraction of the starting PVAc macro-CTA did not take part in the VDF polymerization. This is easily seen by comparing the SEC traces of the BCPs before and after precipitation (Figure VI-2, green trace, and SI-Figure VI-8), where the precipitation removes the unreacted PVAc (and probably also very short PVDF block BCPs). These non-reactivated chains are likely the dead chains resulting from transfer reactions (PVAc-H). The methanol soluble fraction collected after the precipitation of the diblock copolymer in cold methanol was carefully analysed by ^{1}H NMR.

Figure VI-3 and SI-Figure VI-13 show the ^{1}H NMR spectra of $PVAc_{18}$-XA (Figure VI-3a), of the crude $PVAc_{18}$-*b*-$PVDF_{78}$ BCP (Figure VI-3b), of the purified $PVAc_{18}$-*b*-$PVDF_{78}$ BCP isolated by precipitation in cold methanol (non-solvent for PVDF, but good solvent for PVAc, Figure VI-3c), and of the methanol-soluble fraction resulting from this precipitation (Figure VI-3d). During the VDF polymerization, all the $PVAc_{H}$-XA chains (terminated with a regularly added VAc unit) were reactivated as can be seen from the total disappearance of the signal at 6.6 ppm (corresponding to the -CH(OAc)-XA terminus) and the apparition of a signal at 5.25 ppm assigned to the $PVAc_{H}$-PVDF linkage (Figure VI-3b). This linkage can also be seen very clearly in the 19F NMR spectrum of the $PVAc_{18}$-*b*-$PVDF_{78}$ BCP (run 3, Table VI-1) at -92.62 ppm (SI-Figure VI-10). The broad triplet at 4.08 ppm assigned to the PVAcH-H dead chains arising from undesirable transfer reactions was clearly visible in the ^{1}H NMR spectra of the PVAc macro-CTA (Figure VI-3a), of the crude BCP (Figure VI-3b), and of the methanol-soluble fraction (Figure VI-3d) but did not appear in the ^{1}H NMR spectrum of the precipitated BCP (Figure VI-3c). The $PVAc_{H}$-H chains were thus removed from the polymer during precipitation. However, the two quartets at 4.7 ppm in the $_{1}$H NMR spectrum of the crude polymer before precipitation (Figure VI-3b) assigned to the -CH_2- of the *O*-ethyl xanthate mark the presence of two populations of xanthate end-groups. In contrast, the $_{1}$H NMR spectrum of the polymer precipitated in cold methanol shows only one

well- defined quartet at 4.7 ppm (Figure VI-3c) indicating that a fraction of xanthate-terminated PVAc did not take part in the polymerization of VDF. The signals at 3.3 and 5.2 ppm, assigned to the VAc terminal unit of the $PVAc_T$-XA chains, are present in the ^1H NMR spectra of the PVAc-XA macro-CTA (Figure VI-1 and Figure VI-3a), of the crude polymer (Figure VI-3b), and of the methanol soluble fraction (Figure VI-3d), but are absent from the ^1H NMR spectrum of the polymer precipitated in cold methanol (Figure VI-3c). These observations suggest that only the $PVAc_H$-XA chains were readily reactivated during the VDF polymerization. Two hypotheses can be considered: *(i)* the $PVAc_T$-XA chains did not take part in the polymerization of VDF, *(ii)* only a fraction of the $PVAc_T$-XA chains was reactivated, in other words, these chains are reactivated by PVDF· radicals, but at a much slower rate than the $PVAc_T$-XA chains. If the first hypothesis *(i)* was true, the polymer resulting from the VDF chain extension of the $PVAc_{115}$-XA ($PVAc_H$-XA/$PVAc_T$-XA/$PVAc_H$-H = 0/90/10 mol%, run 7) should be a mixture of the initial unreacted $PVAc_{115}$ and PVDF homopolymers synthesized under conventional radical polymerization.

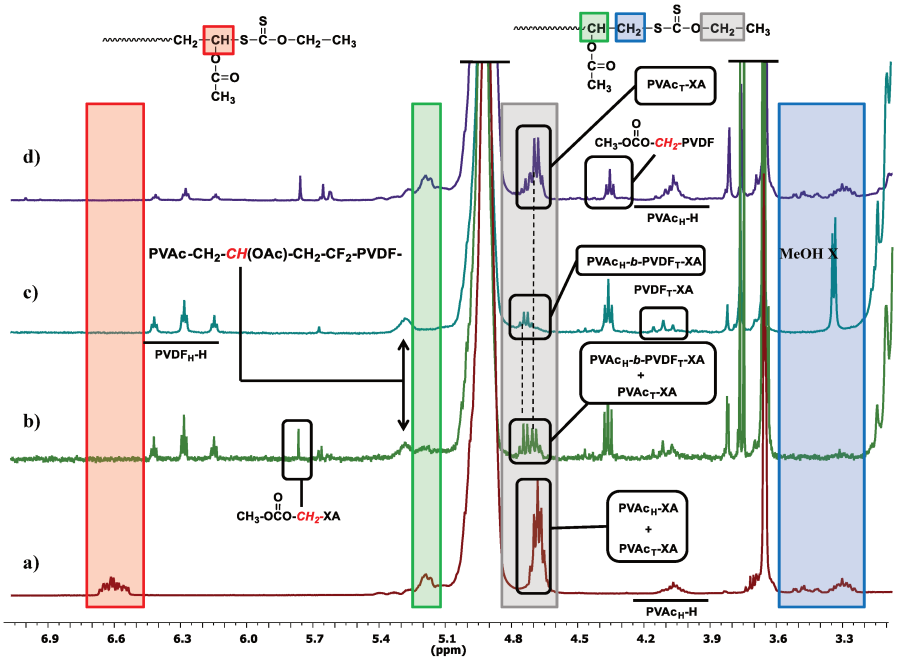

Figure VI-3: Expansion of the 3.15 to 7.1 ppm region of the ^1H NMR spectra recorded in $(CD_3)_2CO$ of: a) $PVAc_{18}$-XA (run 1, Table VI-1), b) crude $PVAc_{18}$-b-$PVDF_{78}$ (run 3, Table VI-1) c) purified $PVAc_{18}$-b-$PVDF_{78}$ (run 3, Table VI-1, precipitated in methanol), (d) the methanol soluble fraction resulting from the precipitation of $PVAc_{18}$-b-$PVDF_{78}$ (run 3, Table VI-1), in cold methanol.

Three observations contradict this hypothesis. The SEC trace of the precipitated $PVAc_{115}$-based BCP (SI-Figure VI-8a), which thus does not contain any unreacted PVAc, is monomodal and the dispersity of the polymer is rather low (1.30). In addition, the ^{1}H NMR spectrum of this precipitated polymer displays signals of PVAc, PVDF and $PVDF_T$-XA (SI-Figure VI-11). These observations suggest the validity of the second hypothesis of a slow reactivation of $PVAc_T$-XA chains. This hypothesis is further supported by the results of the ^{1}H NMR DOSY experiments carried out on the purified BCP (SI-Figure VI-12) which show the presence of only one polymer containing signals of both PVAc and PVDF with a diffusion coefficient of 3.57 10^{-10} m^2 s^{-1} (the $PVAc_{115}$-XA macro-CTA has a diffusion coefficient of 6.53 10^{-10} m^2 s^{-1}). These observations thus indicate that the residual low molar mass peaks observed in Figure VI-2a, SI-Figure VI-8a and c are likely constituted by the slow reactivating $PVAc_T$-XA chains and the PVAc-H dead chains.

In addition to this end-group-dependent reactivation, the formation of the PVDF block was accompanied by a large amount of transfer to DMC.[12-14] The characteristic signals of this transfer reaction can be observed in Figure VI-3 and SI-Figure VI-13: the triplet of triplets at 6.3 ppm corresponding to the $-CF_2H$ chain-end ($PVDF_H$-H), the singlet at 5.8 ppm assigned to the $CH_3OC(O)O-CH_2$-XA (DMC–xanthate adduct),[12] the well-defined triplet at 4.3 ppm and the singlet at 3.73 ppm assigned to the $-CH_2-$ and $-CH_3$ groups of the DMC moieties of DMC-initiated PVDF chains respectively.[14] A new signal (triplet of triplets) at 2.45 ppm was identified, for the first time, and assigned to the $-CH_2-$ of the first added VDF unit in these DMC-initiated PVDF chains ($CH_3OC(O)O-CH_2-CH_2-CF_2-$, SI-Figure VI-14). This very large amount of transfer (up to 80%, run 5, Table VI-1) is caused by the reaction conditions used. For the RAFT polymerization of VDF, when high molar masses are targeted, it is necessary to stop the polymerization at relatively low conversion to avoid the slowdown of the DT mechanism and a significant increase of the transfer reactions.[14]

To summarize, the VDF RAFT dispersion polymerization in DMC using PVAc macro-CTAs afforded relatively well-defined BCPs. The quality of the BCPs was directly dependent on the chain-ends of the PVAc macro-CTAs with a fast reactivation ofthe $PVAc_H$-XA chains, and a much slower reactivation of the $PVAc_T$-XA chains.

IV.2 Polymerization-induced self-assembly

In spite of the less reactivatable $PVAc_T$-XA and non-reactive PVAc-H fractions which remained in the reaction mixture, the VDF RAFT dispersion polymerization in DMC using PVAc macro-CTAs afforded colloidally stable PVAc-*b*-PVDF BCP nanoobjects. Figure VI-4 shows the photograph of the BCP dispersions resulting from the PISA experiments carried out in DMC.

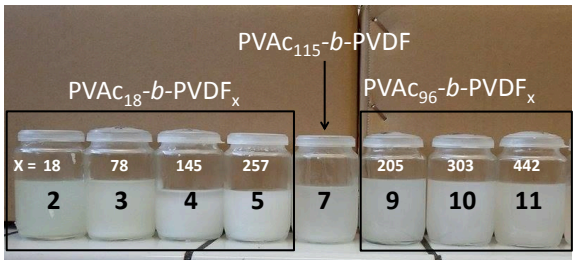

Figure VI-4: Macroscopic appearances of the PVAc-b-PVDF BCP dispersions in DMC.

Surprisingly, the BCP dispersions obtained using $PVAc_{18}$ as the stabilizing block and with DP_{PVDF} ranging from 78 to 257 sedimented within 16 hours, but, could be easily redispersed by simple manual shaking (SI-Figure VI-15). This behavior can be explained by the higher density of PVDF (ρ_{PVDF} = 1.78 g cm^{-3}) compared to that of dimethyl carbonate (ρ_{DMC} = 1.07 g cm^{-3}) and the rather large size of the nano-objects (Figure VI-5a-d) which reduce their buoyancy.

BCP nano-object dispersions prepared from the $PVAc_{115}$ macro-CTA also sedimented. This is probably due to the very poor quality of the BCP in this case (and contamination by the PVDF homopolymer). When $PVAc_{96}$ macro-CTA was used, the sedimentation of the BCP dispersion was much less pronounced (runs 9, 10, and 11, Table VI-1, and Figure VI-4). Figure VI-5 displays the TEM images of the PVAc-*b*-PVDF BCP nano-objects obtained from $PVAc_{18}$-XA (Figure VI-5a-d) and $PVAc_{96}$-XA (Figure VI-5e-g) macro-CTAs.

$PVAc_{18}$-*b*-$PVDF_{18}$ BCP nano-objects appeared as *ca.* 5 µm bundles of crystalline needles (smaller objects are also visible) on the transmission electron micrographs (Figure VI-5a). These well-defined crystalline structures, probably representative of the actual colloidal self-assembled objects present in the DMC dispersion, are quite similar to the spherulitic structures observed by Wang et al.[62] for poly(3-hexylselenophene) solutions. BCP with longer PVDF blocks also self-assembled into very crystalline structures (Figure VI-5b-d).

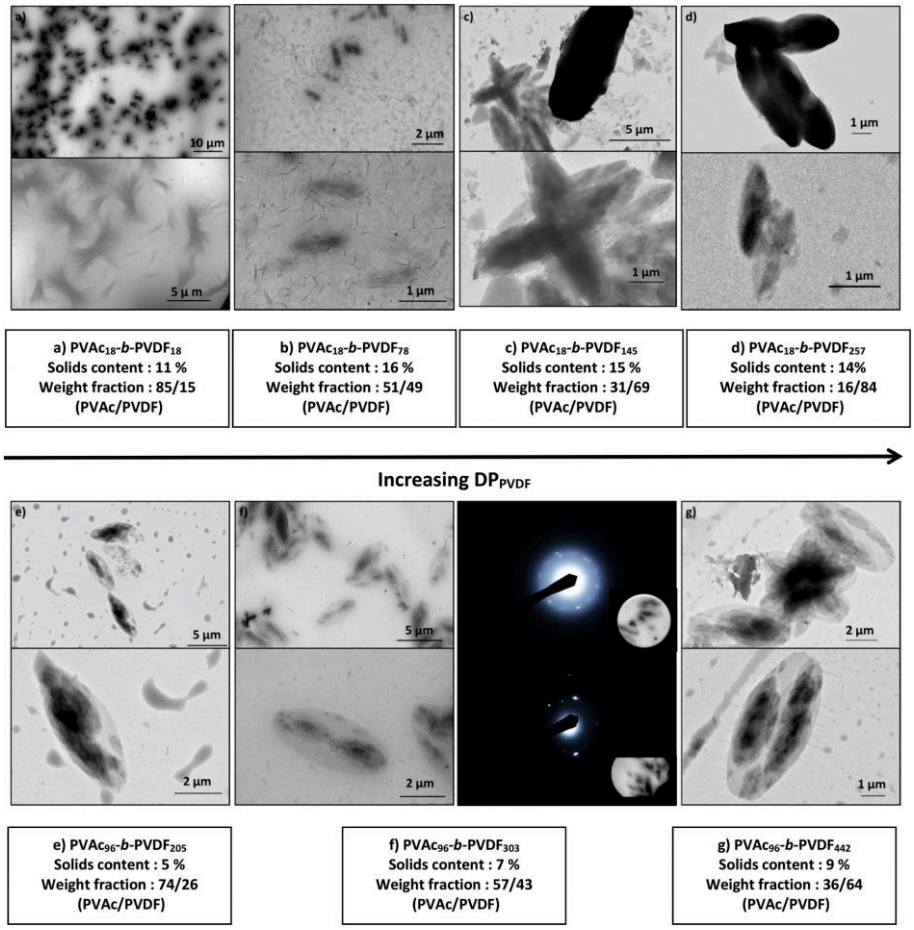

Figure VI-5: Representative TEM images of self-assembled nano-objects prepared by VDF RAFT dispersion polymerization in DMC using $PVAc_{18}$ macro-CTA: a) to d); and $PVAc_{96}$ macro-CTA: e) to g). Weight fractions were determined on the crude PVAc-b-PVDF BCPs dispersions using the following equations: $wt_{PVAc} = wt_{PVAc}/(wt_{PVAc+} wt_{PVDF})$ and $wt_{PVDF} = wt_{PVDF}/(wt_{PVAc+} wt_{PVDF})$ Note: f) shows the TEM images of the $PVAc_{96}$-b-$PVDF_{303}$ BCP dispersion and the corresponding electron diffraction pattern recorded during TEM analysis.

The $PVAc_{18}$-based BCP yielded a mixture of very large (several µm) crystalline structures. Two types of structures were observed: very large aggregates (5-15 µm) and smaller (2-5 µm) ovoidal flake-like structures. $PVAc_{18}$-*b*-$PVDF_{78}$ also presented smaller rod-like or shard-like structures (Figure VI-5b). The ovoidal flake-like structures were also observed in the TEM images of the $PVAc_{96}$-*b*-$PVDF_{205}$ (Figure VI-5e), $PVAc_{96}$-b-$PVDF_{303}$ (Figure VI-5f) and $PVAc_{96}$-*b*-$PVDF_{442}$ (Figure VI-5g) BCP dispersions (in these cases, ill-defined aggregates likely formed by the PVAc homopolymer are also seen). The ovoid flake-like structures observed in Figure VI-5b-g looked very similar to those reported by Wang et al. for the self-assembly of PEG-*b*-PPDO (PPDO = poly(p-dioxanone)) crystalline-coil diblock copolymers.[63] The crystallinity of these self-assembled structures was confirmed by DSC of the dried and ground BCP dispersion samples. SI-Figure VI-17 and SI-Figure VI-18 display the first heating and first cooling of these DSC analyses respectively. The first heating

thermograms clearly reveal PVDF melting transitions ranging from 120 °C to 170 °C (depending on the PVDF molar mass) for all the BCP dispersions. The crystallinity of the PVDF fraction of the self-assembled structures is given in SI-Table VI-2. As expected, this crystallinity tends to increase with increasing PVDF wt % in the dispersion. Interestingly, during the first cooling (SI-Figure VI-18), $PVAc_{18}$-*b*-$PVDF_{18}$ and $PVAc_{96}$-*b*-$PVDF_{205}$ BCPs did not show any PVDF recrystallization exothermic peak. This is in agreement with a previous study on the PVDF-*b*- PVAc BCP[17] and indicates the miscibility of PVDF and PVAc.

The ovoidal structures seemed to be composed of several flakes of different sizes stacked on top of each other. They also formed larger assemblies looking like desert rose or star anise branched structures (Figure VI-5c and g).

This hypothesis of a layered ordering was strengthened by the electron diffraction pattern displayed in Figure VI-5f which shows the characteristic reflection spots of oriented and crystalline PVDF lamellar structures.[64] These stacked and branched structures are thought to be formed through crystallization-driven self-assembly (CDSA) via epitaxial crystallization for the stacked structures and via interpenetration crystallization for the branched structures as described by Wang et al.[63] for the self-assembly of PEG-*b*-PPDO. These coil-crystalline BCP selfassembled morphologies are thus formed under polymerization-induced self-assembly conditions, but their structures are likely governed by the crystallization of the PVDF block.

V. Conclusions

The polymerization of VDF using PVAc-XA as a macro-CTA afforded relatively well-defined PVAc-*b*-PVDF block copolymers (BCPs) albeit with low chain-end functionality due to transfer reactions. Only the PVAc chains terminated with regularly added (HT) VAc units ($PVAc_H$-XA) were reactivated efficiently by PVDF· radicals to yield well-defined BCPs. In contrast, $PVAc_T$-XA (chains terminated by a head-to-head VAc addition) were reactivated at a much slower rate and were responsible for the formation of BCPs of poorer quality (higher than expected DP_{PVDF}, higher dispersity and non-negligible quantities of the PVDF homopolymer). In addition, RAFT polymerization of VAc is prone to transfer reactions and produces a minor fraction of dead chains through H-abstraction. In consequence, PISA protocols such as VDF RAFT dispersion polymerization in DMC using PVAc-XA macro-CTAs led to the formation of block copolymers containing significant quantities of PVAc and

PVDF homopolymers. The PISA of these BCPs afforded new flake-like crystalline structures that were able to further assemble into desert rose-like branched micrometer-sized objects. The morphologies of these structures are thought to be governed by the crystallization of the PVDF block. Further characterization of these self-assembled structures is underway in our laboratory and will be published in due course. This article presents the first examples of the PISA of PVDF-based BCPs.

VI. Acknowledgements

The authors thank Arkema S. A. (Pierre Bénite, France) for providing VDF, the Ministère de l Education Nationale, de l’ Enseignement Supérieur et de la Recherche for the Ph.D grant attributed to MG, and the Common Service of Electronic and Analytical Microscopy of the University of Montpellier for TEM.

VII. References

[1] B. Améduri, B. Boutevin, In *Well-Architectured Fluoropolymers: Synthesis, Properties and Applications*, Elsevier: Amsterdam, 2004.

[2](a) D. A. Seiler, In *Modern Fluoropolymers*, J. Scheirs, Ed.; Wiley: New York, 1997; Chapter 25, 487-506. (b) J; S. Humphrey, R. Amin-Sanayei, In *Encyclopedia of Polymer Science and Technology*, 3rd ed.: H. F. Mark, Ed.: Wiley; New York, 2004; Vol. 4, 510-533.

[3] B. Améduri*, Chem. Rev*., 2009, **109**, 6632-6686.

[4] B. Améduri, *Macromolecules*, 2010, **43**, 10163-10184.

[5] M. Tatemoto, In The First Regular Meeting of Soviet-Japanese Fluorine Chemists, Tokyo, 1979.

[6] M. Tatemoto, T. Nakagawa, US Patent 4,158,678 (assigned to Daikin) 19-06-1979.

[7] G. David, C. Boyer, J. Tonnar, B. Améduri, P. Lacroix-Desmazes, B. Boutevin, *Chem. Rev.*, 2006, **106**, 3936-3962.

[8] C. Boyer, D. Valade, L. Sauguet, B. Améduri, B. Boutevin, *Macromolecules*, 2005, **38**, 10353-10362.

[9] A. D. Asandei, O. I. Adebolu and C. P. Simpson, *J. Am. Chem. Soc*., 2012, **134**, 6080–6083.

[10] A. D. Asandei, O. I. Adebolu, C. P. Simpson and J.-S. Kim, *Angew. Chem., Int. Ed*., 2013, **52**, 10027–10030.

[11] A. D. Asandei, *Chem. Rev*., 2016, **116,** 2244-2274.

[12] M. Guerre, B. Campagne, O. Gimello, K. Parra, B. Améduri, V. Ladmiral, *Macromolecules,* 2015, **48**, 7810-7822.

[13] M. Guerre, T. Soulestin, G. Lopez, C. Totée, B. Améduri, G. Silly, V. Ladmiral, *Macromol. Chem. Phys*., 2016, **217**,2275-2285

[14] M. Guerre, S. M. W. Rahaman, B. Améduri, R. Poli, V. Ladmiral, *Macromolecules*, 2016, **49**, 5386-5396.

[15] M. Guerre, B. Améduri, V. Ladmiral, *Polym. Chem*. 2016, **7**, 441-450.

[16] E. Folgado, M. Guerre, C. Bijani, V. Ladmiral, A-M. Caminade, B. Améduri, A. Ouali, *Polym. Chem*., 2016, **7**, 5625-5629.

[17] M. Guerre, S. M. W. Rahaman, B. Améduri, R. Poli, V. Ladmiral, *Polym. Chem*., 2016**,** **7**, 6918-6933.

[18] M. Guerre, J. Schmidt, Y. Talmon, B. Améduri, V. Ladmiral, *Polym. Chem*., 2017, 8, 1125-1128.

[19] V. S. D. Voet, G. ten Brinke, K. J. Loos, *Polym. Sci.: Part A: Polym. Chem*., 2014, **52**, 2861-2877.

[20] Z. B. Zhang, S. K. Ying, Z. Q. Shi, *Polymer*, 1999, **40,** 1341–1345.

[21] S. M. Jol, W. S. Lee, B. S. Ahn, K. Y. Park, K. A. Kim, I. S. Rhee Paeng, *Polym. Bull*., 2000, **44**, 1–8.

[22] M. Destarac, K. Matyjaszewski, E. Silverman, B. Améduri, B. Boutevin, *Macromolecules*, 2000, **33**, 4613–4615.

[23] Z. Q. Shi, S. Holdcroft, *Macromolecules*, 2004, **37**, 2084–2089.

[24] Z. Q. Shi, S. Holdcroft, *Macromolecules*, 2005, **38**, 4193–4201.

[25] G. Laruelle, E. Nicol, B. Améduri, J. F. Tassin; N. J. Ajellal, *J. Polym. Sci.: Part A: Polym. Chem.,* 2011, **49**, 3960-3969.

[26] K. Xu, K. Li, P. Khanchaitit, Q. Wang, *Chem. Mater*.**,** 2007, **19**, 5937–5945.

[27] C. Chanthad, K. A. Masser, K. Xu, J. Runt, Q. J. Wang, *Mater. Chem.,* 2012, **22**, 341–344.

[28] V. S. D. Voet, M. Tichelaar, S. Tanase, M. C. Mittelmeijer-Hazeleger, G. ten. Brinke, K. Loos, *Nanoscale*, 2013, **5**, 184–192.

[29] V. S. D. Voet, D. Hermida-Merino, G. ten. Brinke, K. Loos, *RSC Adv.,* 2013, **3**, 7938–7946.

[30] R. Vukicevic, U. Schwadtke, S.; Schmucker, P. Schafer, D. Kuckling, S. Beuermann, *Polym. Chem*., 2012, **3**, 409-414.

[31] G. Riess, *Prog. Polym. Sci*., 2003, **28**, 1107-1170.

[32] Y. Mai, A. Eisenberg, *Chem. Soc. Rev*., 2012, **41**, 5969-5985.

[33] T. H. Epps, III, R. K. O'Reilly, *Chem. Sci*, 2016, **7**, 1674-1689.

[34] B. Charleux, G. Delaittre, J. Rieger, F. D'Agosto, *Macromolecules*, 2012, **45**, 6753-6765.

[35] N. J. Warren, S. P. Armes, *J. Am. Chem. Soc*., 2014, **136**, 10174-10185.

[36] J. Rieger, *Macromol. Rapid. Commun*. 2015, **36**, 1458-1471.

[37] S. L. Canning, G. N. Smith, S. P. Armes, *Macromolecules,* 2016, **49**, 1985-2001.

[38] Y. Li, S. P. Armes, *Angew. Chem., Int. Ed.*, 2010, **49**, 4042−4046.

[39] A. Blanazs, A. J. Ryan, S. P. Armes, *Macromolecules,* 2012, **45**, 5099−5107.

[40] D. Zehm, L. P. D. Ratcliffe, S. P. Armes, *Macromolecules,* 2013, **46**, 128−139.

[41] L. A. Fielding, M. J. Derry, V. Ladmiral, J. Rosselgong, A. M. Rodrigues, L. P. D. Ratcliffe, S. Sugihara, S. P. Armes, *Chem. Sci*., 2013, **4**, 2081−2087.

[42] V. J. Cunningham, A. M. Alswieleh, K. L. Thompson, M. Williams, G. J. Leggett, S. P. Armes, O. M. Musa, *Macromolecules*, 2014, **47**, 5613−5623.

[43] X. Zhang, S. Boisse, W. Zhang, P. Beaunier, F. D'Agosto, J. Rieger, B. Charleux, *Macromolecules*, 2011, **44**, 4149-4158.

[44] W. Zhang, F. D'Agosto, O. Boyron, J. Rieger, B. Charleux, *Macromolecules*, 2011, **44**, 7584-7593.

[45] S. Binauld, L. Delafresnaye, B. Charleux, F. D'Agosto, M. Lansalot, *Macromolecules*, 2014, **47**, 3461−3472.

[46] J. Tan, H. Sun, M. Yu, B. S. Sumerlin, L. Zhang, *ACS Macro Lett*., 2015, **4**, 1249−1253.

[47] S. Boissé, J. Rieger, K. Belal, A. Di-Cicco, P. Beaunier, M.-H Li, B. Charleux, *Chem. Commun.,* 2010, **46**, 1950−1952.

[48] M. J. Derry, L. A. Fielding, S. P. Armes, *Prog. Polym. Sci*., 2016, **52**, 1−18.

[59] M. Semsarilar, E. R. Jones, A. Blanazs, S. P. Armes, *Adv. Mater*., 2012, **24**, 3378−3382.

[50] L. P. D. Ratcliffe, B. E. McKenzie, G. M. D. Lilliams, S. L. Brown, S. P. Armes, *Macromolecules*, 2015, **48**, 8594-8607.

[51] J. J. Crassous, P. Schurtenberger, M. Ballauff, A. M. Mihut, *Polymer*, 2015, **62**, 1-148.

[52] J. B. Gilroy, T. Gädt, G. R. Whittell, L. Chabanne, J. M. Mitchels, R. M. Richardson, M. A. Winnik, I. Manners, *Nature Chemistry*, 2010, **2**, 566–570.

[53] Z. M. Hudson, C. E. Boott, M. E. Robinson, P. A. Rupar, M. A. Winnik , I. Manners, *Nature Chemistry*, 2014, **6**,893–898.

[54] X. Liu, O. Coutelier, S. Harrisson, T. Tassaing, J-D. Marty, M. Destarac, *ACS Macro* Lett., 2015, **4**, 89-93.

[55] S. Harrisson, X. Liu, J.-N. Ollagnier, O. Coutelier, J.-D. Marty and M. Destarac, *Polymers*, 2014, **6**, 1437‑1488.

[56] Y. Kwak, A. Goto, T. Fukuda, Y. Kobayashi and S. Yamago, *Macromolecules*, 2006, **39**, 4671‑4679; (b) A. N. Morin,

[57] C. Detrembleur, C. Jérôme, P. D. Tullio, R. Poli and A. Debuigne, *Macromolecules*, 2013, **46**, 4303‑4312.

[58] K. Koumura, K. Satoh, M. Kamigaito, Y. Okamoto, *Macromolecules*, 2006, **39**, 4054-4061

[59] K. Koumura, K. Satoh, M. Kamigaito, *Polymer Journal*, 2009, **41**, 595-603.

[60] K. Koumura, K. Satoh, M. Kamigaito, *Macromolecules*, 2009, **42**, 2497-2504.

[61] D. Wan, K. Satoh, M. Kamigaito, Y. Okamoto, *Macromolecules*, 2005, **38**, 10397-10405.

[62] Y. Wang, X. Liu, J. Peng, F. Qiu, *RSC Adv*., 2015, **5**, 107970–107976.

[63]H. Wang, C-L. Liu, G. Wu, S-C. Chen, F. Song, Y-Z. Wang, Soft Matter, 2013, **9**, 8712-8722

[64]J. Wang, H. Liu, Y. Duan, S. Jiang, S. Yan, J. Am. Chem. Soc., 2003, **125**, 1496-1497.

[65]K. Nakagawa, Y. Ishida, *J. Polym. Sci. Part B*, 1973, **11**, 2153.

[66]J. N. Martins, T. S. Bassano, R. V. B. Oliveira, *Materials Science and Engineering C*, 2012, **32**, 146-151

VIII. Supporting Informations

Equations used to determine the degree of polymerization and molar masses of PVAc macro-CTAs

SI-Equation VI-5

$$DP = \frac{\int_{4.76}^{5.14} CH(OAc) + \frac{1}{2}\int_{3.18}^{3.51} -CH_2-XA + \frac{1}{2}\int_{3.95}^{4.13} -CH(OAc)-H + \int_{6.50}^{6.70} -CH(OAc)-XA}{\frac{1}{3}\int_{1.37}^{1.46} -CH_3\ (R-CTA)}$$

SI-Equation VI-6

$$M_{n,theo} = \frac{[VAc]_0}{[CTA]_0} \times Yield \times M_{n,VAc} + M_{n,CTAXA}$$

SI-Equation VI-7

$$\boldsymbol{M_{n,PVAc-XA} = M_{n,CTAXA} + DP \times M_{n,VAc}}$$

With $M_{n,VAc}$ = 86.09 g/mol, and $M_{n,\ CTAXA}$ = 208.29 g/mol.

Equations used to determine the proportions of the polymers chain ends:

1) PVDF

SI-Equation VI-8

$$(\%)\ PVDF_T - XA = \frac{\frac{1}{2}\int_{4.02}^{4.17} -CF_2-CH_2-XA}{\frac{1}{2}\int_{3.26}^{3.52} -CH_2-CF_2-XA + \int_{6.01}^{6.48} -CH_2-CF_2H + \frac{1}{2}\int_{4.02}^{4.17} -CF_2-CH_2-XA + \frac{1}{3}\int_{1.71}^{1.87} -CF_2-CH_3}$$

SI-Equation VI-9

$$(\%)\ PVDF_H - XA\ = \frac{\frac{1}{2}\int_{3.26}^{3.52} -CH_2-CF_2-XA}{\frac{1}{2}\int_{3.26}^{3.52} -CH_2-CF_2-XA + \int_{6.01}^{6.48} -CH_2-CF_2H + \frac{1}{2}\int_{4.02}^{4.17} -CF_2-CH_2-XA + \frac{1}{3}\int_{1.71}^{1.87} -CF_2-CH_3}$$

SI-Equation VI-10

$$(\%)\ PVDF_{H+T} - H\ = \frac{\int_{6.01}^{6.48} -CH_2-CF_2H + \frac{1}{3}\int_{1.71}^{1.87} -CF_2-CH_3}{\frac{1}{2}\int_{3.26}^{3.52} -CH_2-CF_2-XA + \int_{6.01}^{6.48} -CH_2-CF_2H + \frac{1}{2}\int_{4.02}^{4.17} -CF_2-CH_2-XA + \frac{1}{3}\int_{1.71}^{1.87} -CF_2-CH_3}$$

2) PVAc

SI-Equation VI-11

$$(\%) - CH(OAc) - CH_2 - XA\ = \frac{\frac{1}{2}\int_{3.18}^{3.51} -CH(OAc)-CH_2-XA}{\frac{1}{2}\int_{3.18}^{3.51} -CH(OAc)-CH_2-XA + \frac{1}{2}\int_{3.95}^{4.13} -CH_2-(OAc)CH_2 + \int_{6.50}^{6.70} -CH_2-CH(OAc)-XA}$$

SI-Equation VI-12

$$(\%) - CH_2 - CH(OAc) - XA \;=\; \frac{\int_{6.50}^{6.70} -CH_2-CH(OAc)-XA}{\frac{1}{2}\int_{3.18}^{3.51} -CH(OAc)-CH_2-XA+\frac{1}{2}\int_{3.95}^{4.13} -CH_2-(OAc)CH_2+\int_{6.50}^{6.70} -CH_2-CH(OAc)-XA}$$

SI-Equation VI-13

$$(\%) - CH_2 - (OAc)CH_2 \;=\; \frac{\frac{1}{2}\int_{3.95}^{4.13} -CH_2-(OAc)CH_2}{\frac{1}{2}\int_{3.18}^{3.51} -CH(OAc)-CH_2-XA+\frac{1}{2}\int_{3.95}^{4.13} -CH_2-(OAc)CH_2+\int_{6.50}^{6.70} -CH_2-CH(OAc)-XA}$$

SI-Table VI-2: Weight and molar fractions of crude and precipitated representative PVAc-b-PVDF BCPs.

Run	$PVAc_x$-*b*-$PVDF_y$ X/Y (precipitated BCP)	wt % (PVAc/PVDF) crude	mol % (PVAc/PVDF) crude	wt % (PVAc/PVDF) precipitated
2	18/18	85/15	79/21	57/43
3	18/78	51/49	59/41	24/76
4	18/145	31/69	23/77	14/86
5	18/257	16/84	12/88	9/91
7	115/502	55/45	52/48	24/86
9	96/205	74/26	67/33	39/61
10	96/303	57/43	48/52	30/70
11	96/442	36/64	29/71	22/78

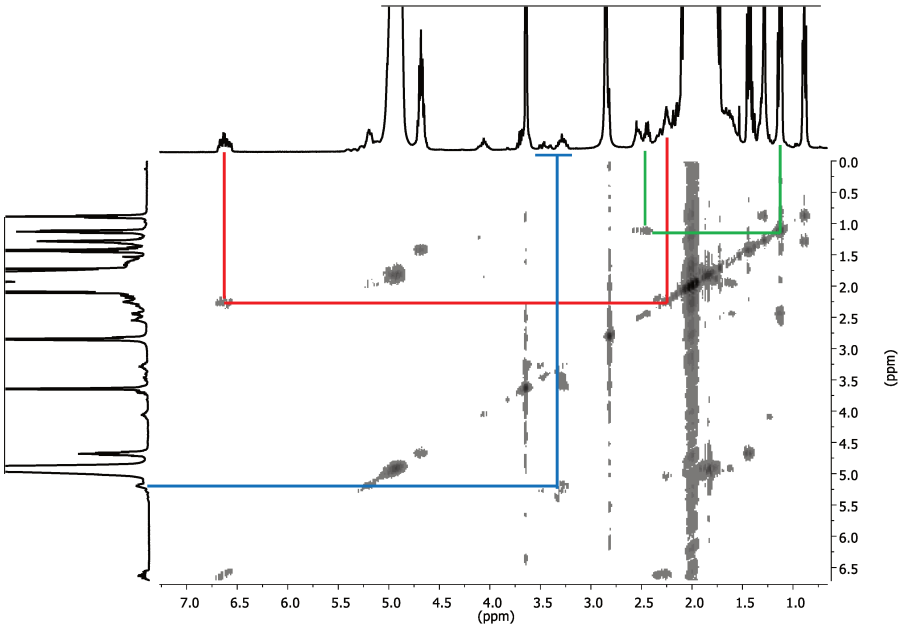

*SI-Figure VI-6: COSY ^1H-^1H NMR spectrum in $(CD_3)_2CO$ of $PVAc_{18}$-XA synthesized by RAFT polymerization (Run 1 Table VI-1). The red line shows the -**CH_2**-$(CH_3(C=O)O$**CH**-XA correlation ($PVAc_H$-XA); the blue line shows the -**CH**$(O(C=O)CH_3)$-**CH_2**-XA correlation ($PVAc_T$-XA); the green line shows the $CH_3O(C=O)($**CH_3**$)$**CH**- correlation (α chain end).*

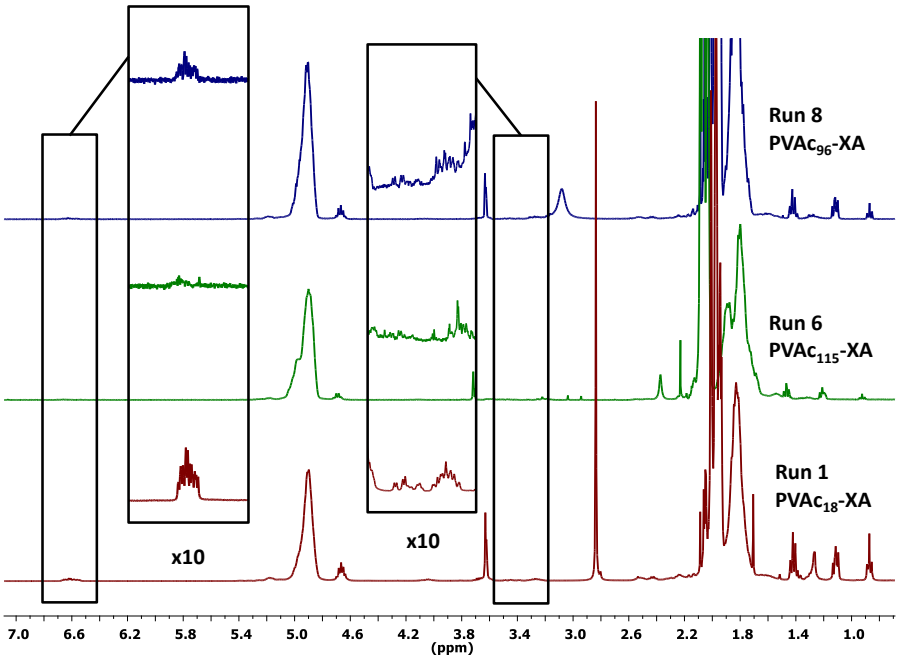

SI-Figure VI-7: ^{1}H NMR spectrum in $(CD_3)_2CO$ of $PVAc_{18}$-XA (red, bottom, run 1 SI-Table VI-2), $PVAc_{115}$-XA (green, middle, run 6 Table VI-1), $PVAc_{96}$-XA (blue, top, run 8 Table VI-1), synthesized by RAFT polymerization.

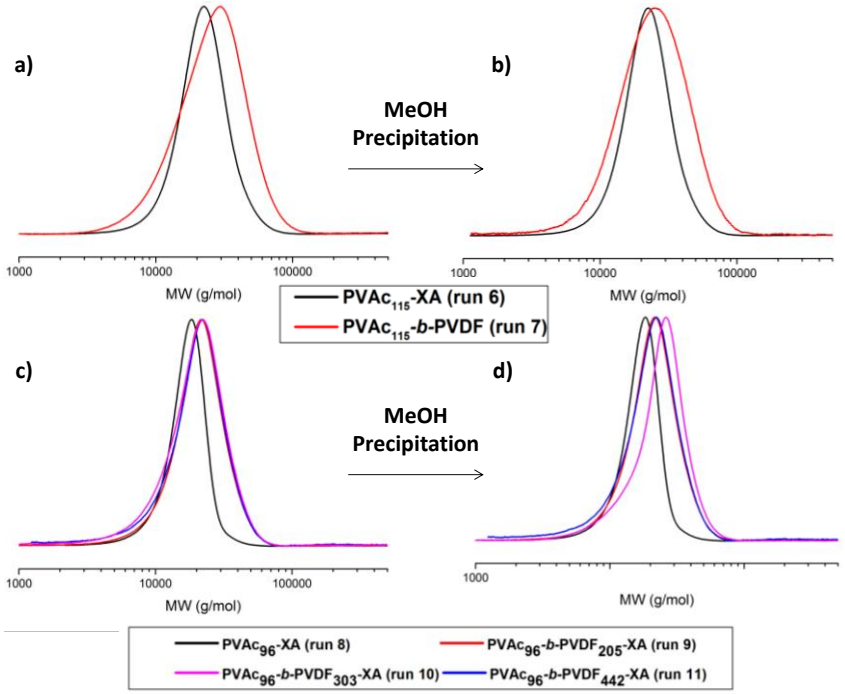

SI-Figure VI-8: Normalized SEC traces (viscosimetric detector) of: a) $PVAc_{115}$-XA and crude $PVAc_{115}$-b-PVDF BCP; b) $PVAc_{115}$-XA and $PVAc_{115}$-b-PVDF BCP precipitated in methanol; c) $PVAc_{96}$-XA and crude $PVAc_{96}$-b-PVDF BCP; and d) $PVAc_{96}$-XA and $PVAc_{96}$-b-PVDF BCP precipitated in methanol.

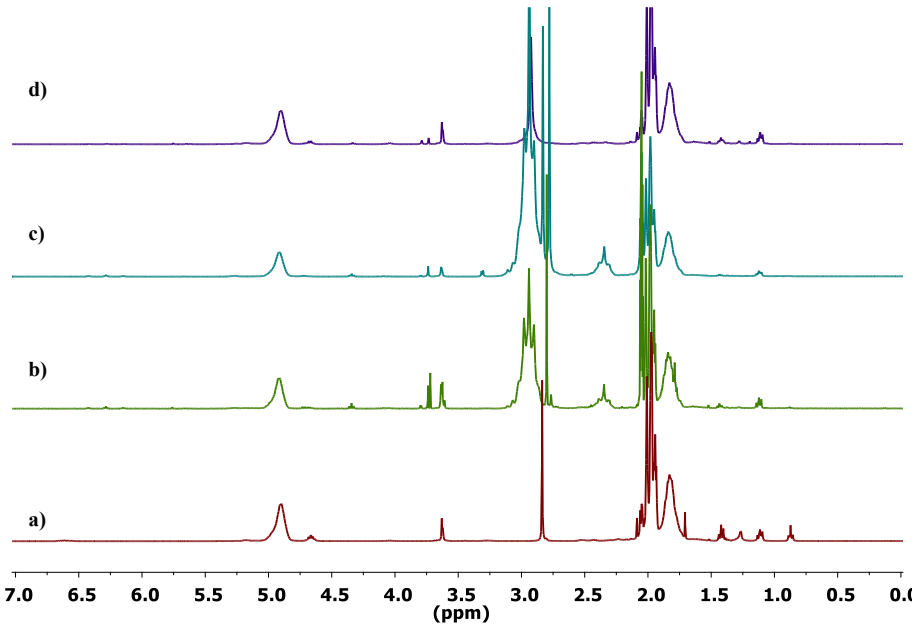

SI-Figure VI-9: Full ^{1}H NMR spectra in $(CD_3)_2CO$ of a) $PVAc_{18}$-XA (Run 1, Table VI-1), b) $PVAc_{18}$-b-$PVDF_{78}$ crude c) $PVAc_{18}$-b-$PVDF_{78}$ precipitated in methanol (d) the methanol soluble fraction resulting from the precipitation of $PVAc_{18}$-b-$PVDF_{78}$ in cold methanol.

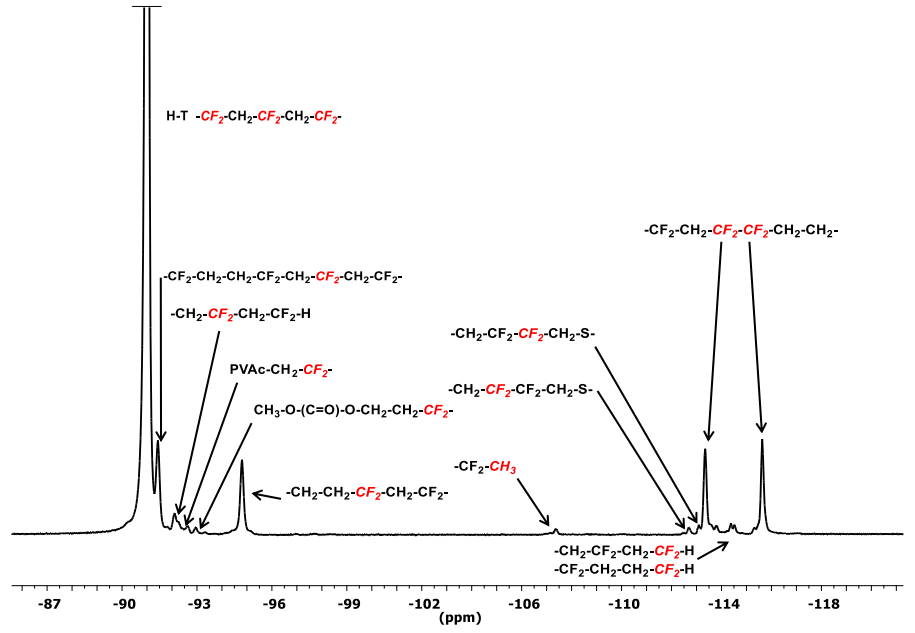

SI-Figure VI-10: ^{19}F NMR spectrum in $(CD_3)_2CO$ of precipitated $PVAc_{18}$-b-$PVDF_{78}$ BCP (Run 3, Table VI-1).

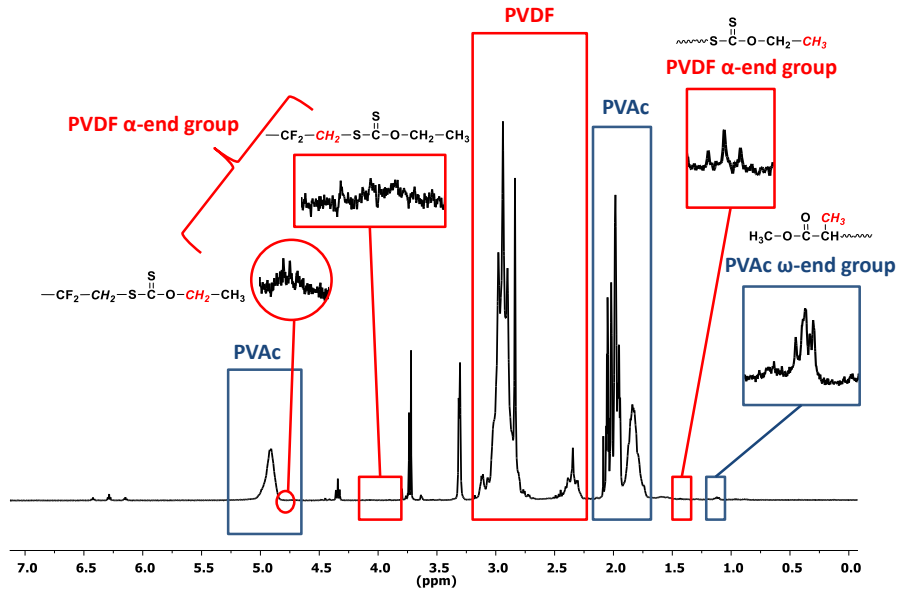

SI-Figure VI-11: ^{1}H NMR spectrum in $(CD_3)_2CO$ of precipitated $PVAc_{115}$-b-$PVDF_{502}$ BCP (Run 7, Table VI-1)

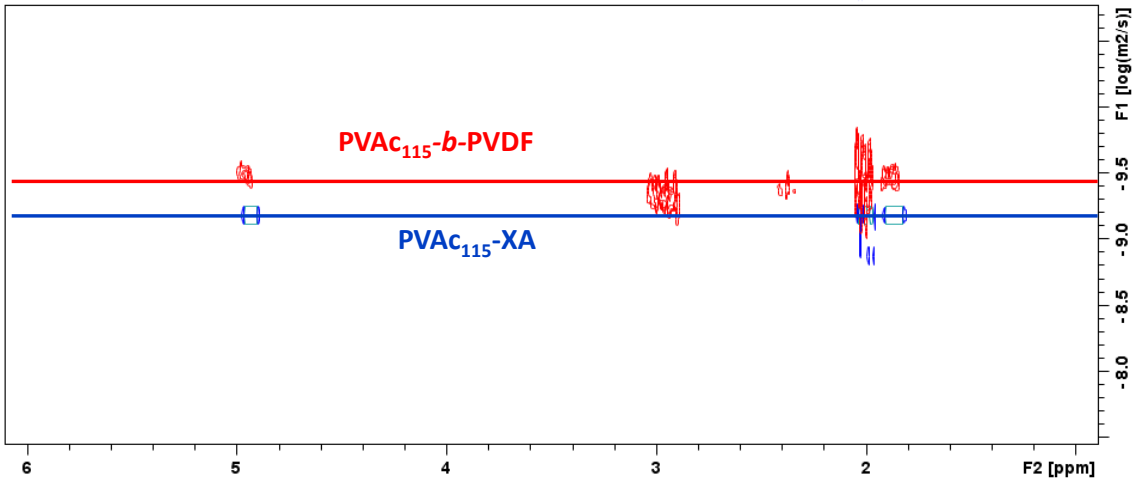

SI-Figure VI-12: Superposed ^{1}H NMR DOSY spectra in $(CD_3)_2CO$ of $PVAc_{115}$-XA (Run 6, Table VI-1, blue signal) and $PVAc_{115}$-b-$PVDF_{502}$ BCP (Run 7, Table VI-1, red signal).

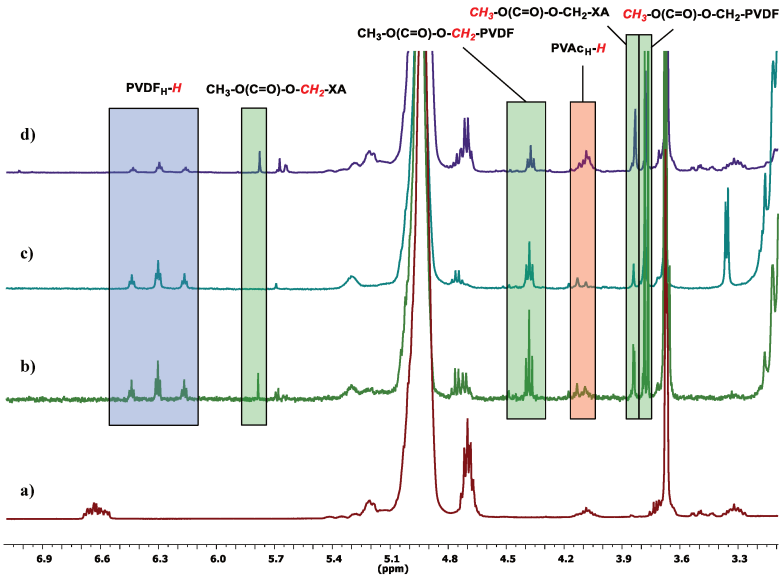

SI-Figure VI-13: Expansion of the 3.05 to 7.1 ppm region of the ^{1}H NMR spectra in $(CD_3)_2CO$ of a) $PVAc_{18}$-XA (run 1, Table VI-1), b) Crude $PVAc_{18}$-b-$PVDF_{78}$ (run 3, Table VI-1) c) $PVAc_{18}$-b-$PVDF_{78}$ (run 3, Table VI-1) precipitated in methanol (d) the methanol soluble fraction resulting from the precipitation of $PVAc_{18}$-b-$PVDF_{78}$ (run 3, Table VI-1) in cold methanol.

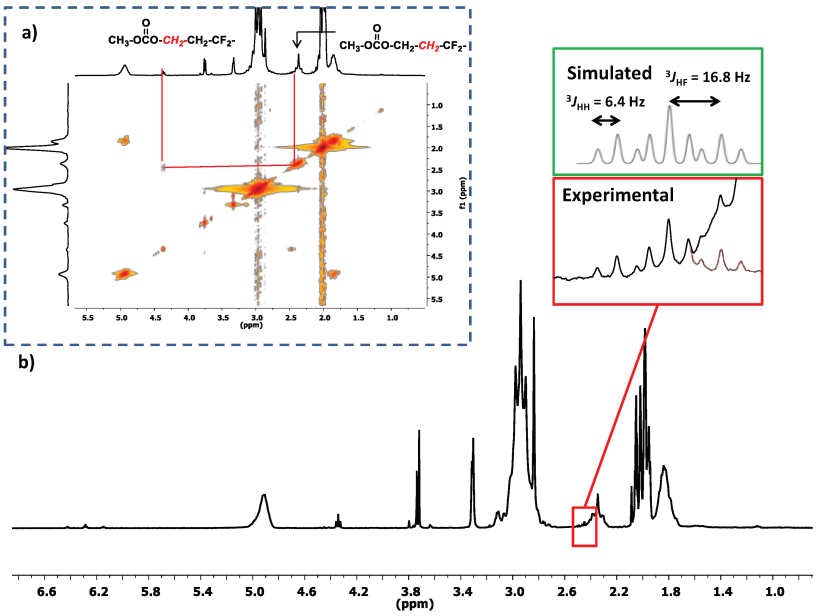

*SI-Figure VI-14: a) COSY ^{1}H-^{1}H NMR spectrum in $(CD_3)_2CO$ of precipitated $PVAc_{115}$-b-$PVDF_{502}$ BCP (Run 7, Table VI-1). The red lines highlight the correlation between the -CH_2- group of DMC and the CH_2 of the first added VDF unit in PVDF chains initiated by DMC b) ^{1}H NMR spectrum in $(CD_3)_2CO$ of precipitated $PVAc_{115}$-b-PVDF BCP (Run 7, Table VI-1). The expansion of thesignals at 2.35-2.55 ppm (red box) shows the experimental pattern (with the expected symmetry drawn in red) of ($CH_3OC(O)$-O-CH_2-**CH_2**-CF_2-protons and the associated simulated pattern.*

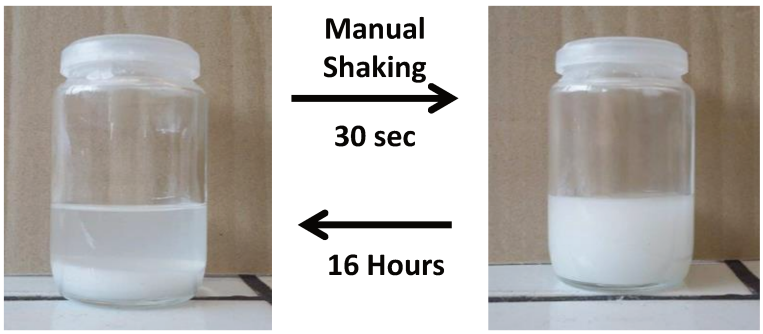

SI-Figure VI-15: Macroscopic aspect of $PVAc_{18}$-b-$PVDF_{257}$ dispersion in DMC (run 5) before and after shaking.

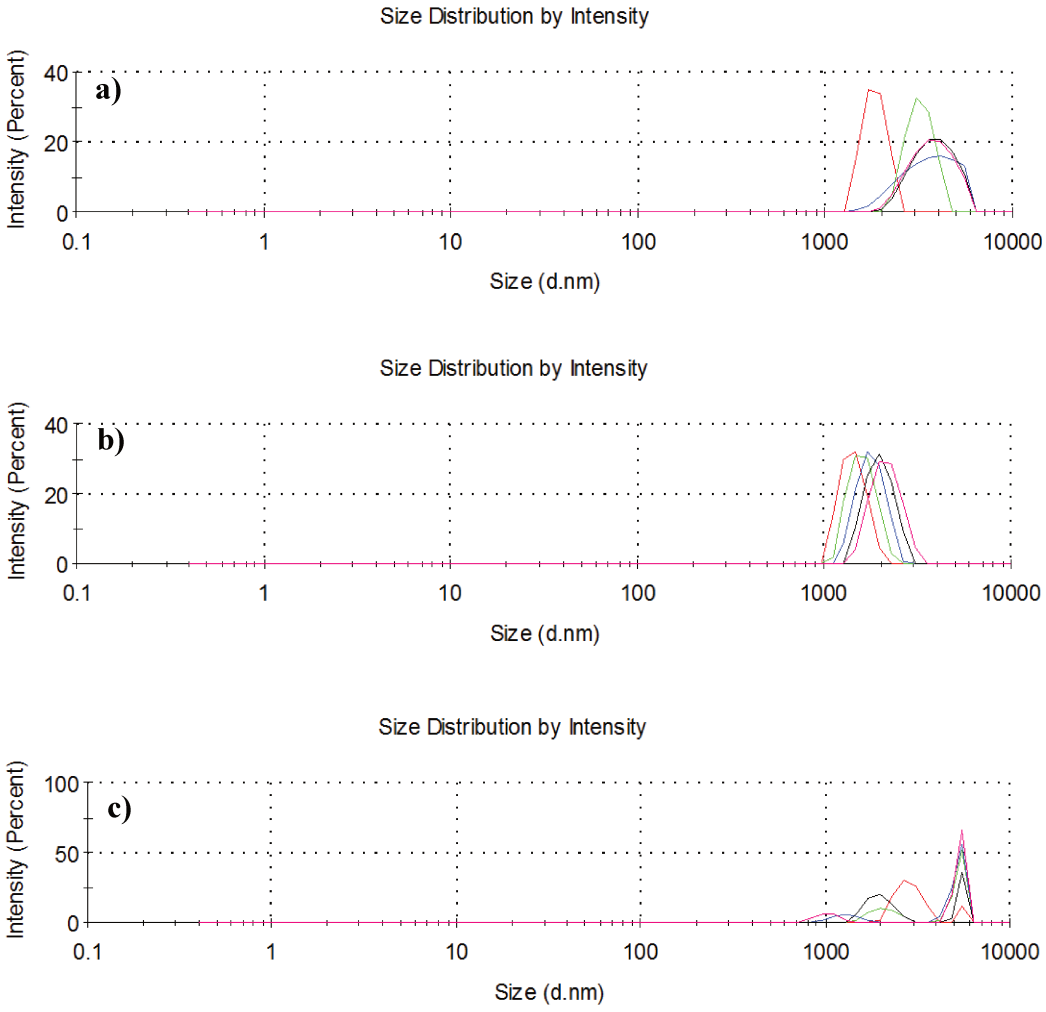

SI-Figure VI-16: Intensity-average diameter distribution and correlation curve of: a) $PVAc_{18}$-b-$PVDF_{18}$ (run 2, Table VI-1), b) $PVAc_{18}$-b-$PVDF_{257}$ (run 5, Table VI-1) and c) $PVAc_{96}$-b-$PVDF_{205}$ (run 9, Table VI-1) BCPs dispersed in dimethylcarbonate at 1 wt%.

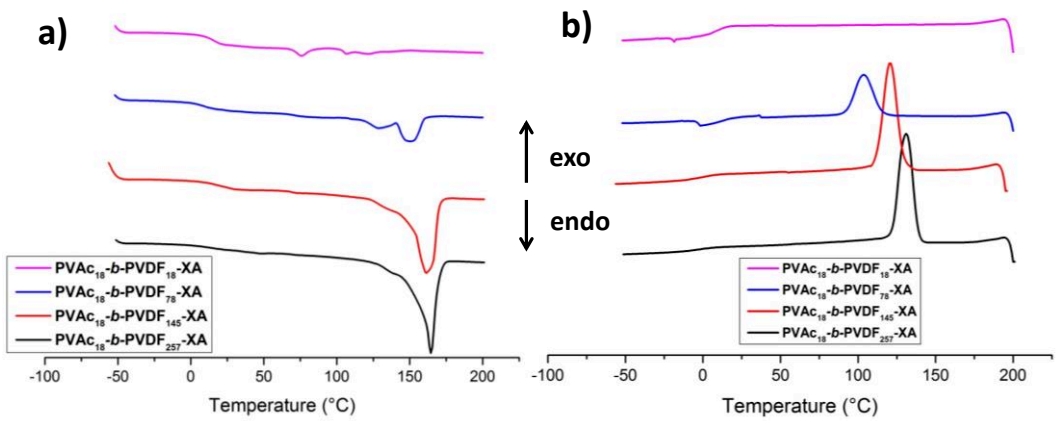

SI-Figure VI-17: DSC thermograms first heating a) followed by cooling b) of PVAc-b-PVDF dried dispersions: $PVAc_{18}$-b-$PVDF_{257}$ (black), $PVAc_{18}$-b-$PVDF_{145}$ (red) $PVAc_{18}$-b-$PVDF_{78}$ (blue) and $PVAc_{18}$-b-$PVDF_{18}$ (pink).

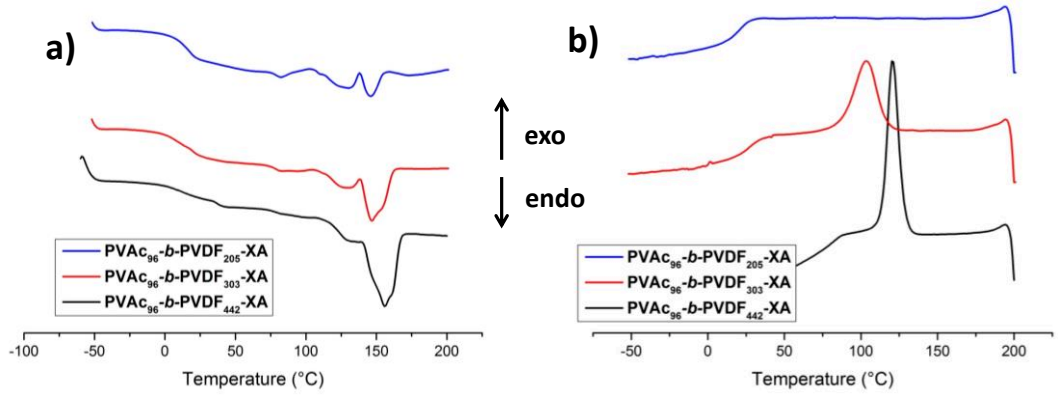

SI-Figure VI-18: DSC thermograms first heating a) followed by cooling b) of PVAc-b-PVDF dried dispersion: $PVAc_{96}$-b-$PVDF_{442}$ (black), $PVAc_{96}$-b-$PVDF_{303}$ (red) and $PVAc_{18}$-b-$PVDF_{205}$ (blue).

SI-Table VI-3:Degree of crystallinity (X_c) of the PVDF fraction in the BCPs dispersions determined using equation S9:

Run	X_c (%)	$PVAc_x$-*b*-$PVDF_y$ X/Y	wt % (PVAc/PVDF) crude
2	33	18/18	85/15
3	45	18/78	51/49
4	81	18/145	31/69
5	64	18/257	16/84
9	42	96/205	74/26
10	51	96/303	57/43
11	52	96/442	36/64

SI-Equation VI-14 $$X_c(\%) = \frac{\Delta H_f}{\Delta H_f^0 \Phi_m} \times 100$$

With $\Delta H_f^0 \Phi_m$ is a heat of fusion of 100 % crystalline PVDF (104.6 $J.g^{-1}$) and Φ_m is the weight fraction of PVDF.[65,66]

Conclusion Chapitre VI

Ce dernier Chapitre décrit l'auto-assemblage induit par la polymérisation en dispersion du VDF, à partir d'agents RAFT macromoléculaires de PVAc. Cette étude a mis en évidence la faible réactivité des extrémités $PVAc_T$-XA (contrairement aux extrémités $PVAc_H$-XA beaucoup plus réactives). Cette faible réactivation est responsable d'une « pollution » non négligeable du milieu réactionnel avec la présence résiduelle d'homopolymères $PVAc_T$-XA dans les dispersions de PVAc-*b*-PVDF. En dépit de ces difficultés, des copolymères diblocs PVAc-*b*-PVDF bien définis avec des dispersités inférieures à 1.4 ont pu être synthétisés avec succès. De plus, le procédé d'auto-assemblage induit par la polymérisation a permis la formation de structures nanométriques auto-assemblées. Néanmoins, ces dispersions ont tendance à sédimenter dans les temps mais sont facilement redispersables par agitation manuelle. Ces structures cristallines de quelques microns, présentent des morphologies de rose des sables et sont composées de plusieurs couches superposées les unes sur les autres avec également certains points de branchement. Bien que l'auto-assemblage ait été provoqué par la polymérisation, il ne fait aucun doute que les morphologies de ces structures sont gouvernées par la cristallisation du bloc PVDF. Cette même cristallisation a été révélé par une étude DSC avec une température de fusion typique du VDF observée à 170 °C et des clichés de diffractions électroniques présentant des tâches de diffractions signifiant une organisation lamellaire.

Conclusion Générale et Perspectives

Conclusion Générale

De part leurs remarquables propriétés, les polymères fluorés constituent une classe de polymères unique conduisant à de nombreuses applications de haute valeur ajoutée. A pression atmosphérique et à température ambiante, la plupart des oléfines fluorés sont gazeux. Leur polymérisation nécessite donc des équipements spécifiques (autoclaves sous pression…). Ils présentent de plus une réactivité singulière qui résulte directement de la présence d'atomes de fluor très électronégatifs sur la double liaison polymérisable. Ces facteurs sont la raison pour laquelle, en dépit de leurs propriétés uniques, les polymères fluorés n'ont pas encore reçu toute l'attention qu'ils méritent de la part de la communauté scientifique. Cependant maintenant qu'il apparaît clairement que les polymères fluorés peuvent permettre des avancées notables dans les domaines de l'énergie pour développer des alternatives aux carburants fossiles (membranes de piles à combustible, séparateurs et électrolytes polymères de batteries lithium, supercondensateurs, dispositifs piézoélectriques), et de l'électronique pour la fabrication de mémoires, la chimie des polymères fluorés connait un regain d'intérêt. La structuration à l'échelle nanométrique de polymères fluorés est aussi un des enjeux majeurs si l'on veut obtenir des avancées significatives dans ces domaines de pointe.

Le premier chapitre de cette thèse est consacré à l'étude de la bibliographie existante, et expose de manière exhaustive les travaux relatifs à l'autoassemblage en solution de copolymère fluorés. Il en ressort une très nette majorité d'articles rapportant l'auto-assemblage de copoly(méthacrylates) fluorés. Leurs accessibilités commerciales ainsi que leurs propriétés très versatiles, qui dépendent fortement de la nature de la chaîne fluorée pendante, en font des monomères de choix pour la synthèse d'architectures fluorées originales. De plus, les techniques de polymérisation radicalaire contrôlée de monomères méthacrylates, très étudiées ces 20 dernières années, offrent une large gamme de choix. Parallèlement, les monomères styréniques, les perfluoropolyéthers ainsi que les perfluoro-cyclobutane éthers ont également suscité beaucoup d'attention. Cependant, un vaste champ en lien avec les copolymères synthétisés à partir d'oléfines fluorées reste totalement inexploré à ce jour.

Ce projet de thèse s'inscrit directement dans ce contexte et a pour objectifs : 1) le développement d'une nouvelle méthode de polymérisation radicalaire contrôlée adaptée au VDF, et 2) l'étude de l'auto-assemblage en solution de copolymères de PVDF. Le prérequis

commun à ces deux objectifs est donc la préparation de polymères à architectures bien contrôlée.

Le deuxième chapitre s'est logiquement orienté dans l'établissement d'une voie de synthèse efficace et adaptée au contrôle de la polymérisation du VDF. La première partie de ce chapitre décrit à l'aide d'une étude cinétique et par spectroscopie RMN, l'efficacité des agents de transfert xanthates dans le contrôle de la polymérisation RAFT du VDF. Bien que les PVDF synthétisés présentent d'excellentes fonctionnalités (85 %) et des distributions de masse molaire relativement étroites (< 1.4), la polymérisation RAFT du VDF est confrontée à de dommageables réactions secondaires. Les réactions de transfert au solvant (DMC) formant des chaînes « mortes » porteuses d'extrémités -CF_2H, et générant des radicaux DMC sont tout particulièrement préjudiciables, et sont responsables de la diminution de la fonctionnalité. Les additions inverses tête-tête sont quant à elle à l'origine de l'élargissement de la distribution des masses molaires causées par la disparition progressive des chaînes réactives $PVDF_H$-XA (bouts de chaînes -CH_2-CF_2-XA) au profit de chaînes moins réactives $PVDF_T$-XA (bout de chaîne -CF_2-CH_2-XA). Enfin, une dernière réaction parasite consomme 30 % d'agent de transfert, qui n'intervient plus dans le mécanisme de polymérisation, mais engendre un dépassement des masses molaires visées.

La deuxième partie de ce Chapitre a permis de conforter l'ensemble des attributions RMN déterminées dans la première partie et a prouvé par RMN la microstructure exacte R-CH_2-CF_2- des extrémités α- du PVDF.

Enfin, la dernière partie de ce chapitre démontre la synthèse de PVDF bien définie et de masses molaires >10.000 $g.mol^{-1}$. Cependant, afin de maintenir un bon contrôle et une bonne fonctionnalité, il est crucial de stopper la réaction à de faibles conversions, avant que la totalité des chaînes n'ait été transformée en $PVDF_T$-XA. Auquel cas, une accélération importante de la conversion, une diminution de la fonctionnalité et un élargissement des masses molaires sont observés. Cette accélération et cette perte de contrôle ont pu être rationalisées par des calculs DFT. En résumé, lorsque toutes les chaînes ont été transformées en $PVDF_T$-XA, le transfert dégénératif, qui est essentiel pour établir un bon contrôle de la polymérisation, est considérablement ralenti. Un deuxième transfert dégénératif se met en fait en place au travers des radicaux $PVDF_T^{\cdot}$ en large minorité. En effet, les radicaux $CH_2^{\bullet}$ intervenant dans le deuxième transfert dégénératif ne sont formés qu'en cas d'addition tête-tête du VDF (4 % du nombre total d'additions) Ainsi, les chaînes actives propagent par des

additions normales tête-queue jusqu'à ce qu'une addition tête-tête ait lieu, et seulement dans ce cas un transfert dégénéré peu avoir lieu avec un autre $PVDF_T$-XA. Le mécanisme de polymérisation n'est alors ni de type conventionnel, ni de type contrôlé, mais se rapproche d'une polymérisation RAFT utilisant un agent RAFT avec une faible constante de transfert C_{Tr}.

Cette meilleure compréhension de la polymérisation RAFT du VDF ouvre de nombreuses voies pour la préparation d'architectures contrôlées à base de PVDF. L'une d'elle par exemple, consiste à effectuer des modifications chimiques sur les fonctions xanthates de bouts de chaînes.

Le troisième chapitre est ainsi consacré à la préparation de macromonomère de PVDF. Un procédé en une étape a été utilisé combinant attaque nucléophile sur l'agent RAFT et addition de Michael. Deux méthodes ont été comparées. L'une utilisant un agent nucléophile de type NaN_3, l'autre une amine primaire, qui est l'agent la plus couramment utilisé. Cette étude a révélé une bien meilleure fonctionnalisation du PVDF lors de la réaction d'aminolyse, utilisant l'hexylamine, avec une transformation des extrémités xanthates en méthacrylate proches de 99%. Dû à cette longue chaîne de PVDF qui restreint considérablement sa mobilité, le macromonomère de PVDF n'a pu être homopolymérisé quantitativement. Il a donc été copolymerisé avec succés en présence de MMA pour donner de nouveaux copolymères de PVDFet PMMA : poly[(PVDF-MA-*co*-MMA)-*b*-PMMA].

Le quatrième chapitre détaille les deux méthodes utilisées dans ce mémoire pour préparer des copolymères diblocs de PVDF. La première méthode consiste à synthétiser un deuxième bloc à partir d'un macro-CTA de PVDF. Cette méthode a permis la synthèse de copolymères PVDF-*b*-PVAc bien définis et présentant des dispersités inférieures à 1,4. Cependant, les extrémités xanthates n'ont pu être réactivées qu'en présence d'Acétate de vinyle (contrairement à la *N*-vinyl pyrollidone, *N*,*N*-dimethylacrylamide ou l'Acrylate de butyle). Cette différence de comportement a pu être rationalisée par des calculs DFT, ainsi que les différences de réactivités observées entre les $PVDF_T$-XA et les $PVDF_H$-XA. La deuxième méthode utilisée associe polymérisation RAFT cationique des éthers vinyliques, et polymérisation RAFT radicalaire du VDF. Cette deuxième génération de blocs a été synthétisée par extension de chaînes de macro CTA de poly(éther vinylique) et a couduit à des blocs PEVE-*b*-PVDF bien définis. Cependant, la polymérisation cationique des éthers vinyliques est idéalement contrôlée en présence d'agents RAFT de type dithiocarbamate. Une

étude cinétique parallèle et similaire à celle des xanthates a dû être achevée. Elle a montré une réelle efficacité de sagents dithiocarbamates pour contrôler la polymérisation du VDF, bien que celle-ci soit beaucoup plus lente qu'en présence de xanthate.

Ces trois premiers chapitres ont permis de synthétiser les tout premiers blocs de PVDF bien définis et présentant des dispersités inférieures à 1,4. Les deux derniers chapitres de ce mémoire traitent de l'auto-assemblage en solution de copolymères à blocs.

Le cinquième chapitre décrit la synthèse et l'auto-assemblage en solution aqueuse de copolymère amphiphile PVDF-*b*-PVA. Ce copolymère dibloc amphiphile a préalablement été obtenu par saponifiation des unités acétate de vinyle en milieu basique. Due à la forte crystallinité des blocs PVDF et PVA, l'auto-assemblage en solution aqueuse a été particulièrement difficile à éffectuer. Néanmoins, le copolymère amphiphile auto-assemblé a donné lieu à des micelles sphériques cœur-(PVDF)-coquille-(PVA) de diamètre moyen de 150 nm, observées par cryo-TEM et par diffusion dynamique de la lumière (DDL).

Enfin le dernier chapitre expose le premier système auto-assemblé induit par la polymérisation de copolymère PVAc-*b*-PVDF. Cette étude a montré l'importance des bouts de chaînes et a fait ressortir la faible réactivité des chaînes $PVAc_T$-XA . En effet, les chaînes $PVAc_T$-XA ont montré une réactivité bien plus lente vis à vis du VDF en comparaison de leurs homologues $PVAc_H$-XA. Cette polymérisation a néanmoins provoqué l'auto-assemblage *in situ* de nano-objets, et a donné lieu à des dispersions colloidablement stables. Les images TEM ont également révélé des morphologies totalement inédites faisait référence à des objets cristallins en forme de rose des sables. Cette cristallinité a été révélée par des analyses DSC et de diffractions par microscopie électroniques (TEM). Cette étude tend à montrer que si la polymérisation a provoqué l'auto-assemblage du copolymère dibloc, celui-ci semble en grande partie gouverné par la cristallisation du PVDF.

Enfin, outre la démonstration de l'efficacité de la technique RAFT pour contrôler la polymérisation du VDF, ce travail a permis la synthèse de nouvelles architectures originales bien définies, qui n'étaient pas possible de préparer auparavant. De plus, la méthodologie décrite dans le chapitre 3 représente un excellent outil pour développer des PVDF fonctionnels à la demande. Ce travail présente les résultats préliminaires de l'auto-assemblage de copolymères à bloc à base de PVDF, qui nécessiteraient d'être approfondis, notamment en ce qui concerne la compréhension du mécanisme de formation des morphologies décrites dans le chapitre VI.

Perspectives-

Les perspectives qui découlent de ces travaux sont nombreuses. Tout d'abord, l'une d'elle est de résoudre l'un des problèmes majeurs de cette étude qui est le contrôle imparfait de la polymérisation du VDF. En effet, les inversions tête-tête du VDF, qui représentent 4 - 4.5 % du nombre total d'additions (à 73°C) sont responsables de l'augmentation de la polymolécularité au cours de la polymérisation. La proportion de ces additions inverses est linéairement reliée à la température de polymérisation (Figure 0-1). L'une des voies possibles pour réduire ces additions est donc de conduire ces polymérisations à basses températures, en utilisant des amorceurs thermiques possédant une faible température de demi-vie, des photo-amorceurs (photo-RAFT) ou des amorceurs redox. Cependant, cette diminution de température ne pourra éliminer en totalité les additions tête-tête (3 % d'additions tête-tête à 20 °C).

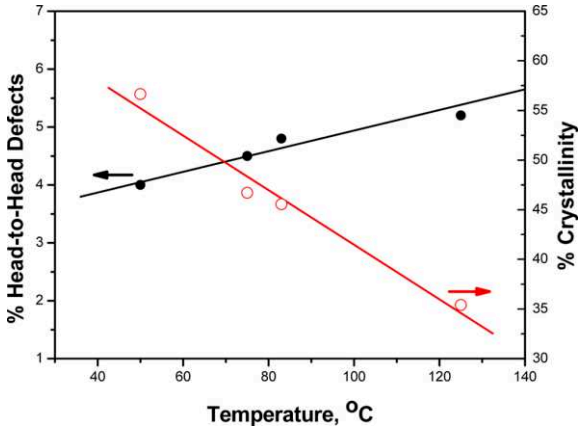

Figure 0-1: Effect of polymerization temperature on the percent head-to-head structural chain defects and percent PVDF crystallinity.[1]

Une autre voie consiste à utiliser un solvant fluoré, qui comme dans le cas de l'acétate de vinyle, pourrait permettre de réduire le taux d'inversion de plusieurs pourcents.[2,3] L'utilisation d'acide de Lewis, qui entrainerait une modification de la réactivité de la double liaison du VDF, pourrait peut-être améliorer de manière significative le contrôle de la polymérisation. Enfin, d'autres méthodes de polymérisations radicalaires contrôlées peuvent aboutir à un meilleur contrôle de la polymérisation. L'étude de l'OMRP (Organomettallic mediated radical polymerization) du VDF qui est en cours d'investigation au sein de notre laboratoire, en collaboration avec le Laboratoire de chimie de coordination de Toulouse et le Centre d'Etude et de Recherche sur les Macromolécules de Liège, pourrait ne pas souffrir de ces additions inverses. Toujours concernant la polymérisation RAFT du VDF, un autre défi

est la réduction des réactions de transfert au solvant qui diminuent de manière non négligeable la fonctionnalité. Une des voies potentielles pour réduire ce problème est la polymérisation en dispersion ou en émulsion dans l'eau, telle qu'elle est utilisée dans l'industrie en polymérisation conventionnelle. Cependant, la polymérisation RAFT n'est pas directement transposable aux conditions utilisées en industrie. Une approche pourrait être, dans la continuité de ce mémoire, de développer la PISA du VDF (de manière similaire au Chapitre VI de ce mémoire) en milieu aqueux.

Une autre perspective est de développer de nouvelles architectures de PVDF basée sur la chimie RAFT. Une des voies envisageable pour diversifier les natures des blocs de PVDF, est l'utilisation des réactions d'aminolyse et d'addition de Michael décrites dans le chapitre II. En utilisant cette méthode, il est possible de coupler n'importe quel bloc possédant une fonction acrylate terminale. Enfin, une autre perspective consiste à synthétiser des agents RAFT fonctionnels. Nous avons par exemple, dans le cadre de travaux annexes, synthétisé un PVDF fonctionnalisé azoture ainsi qu'un PVDF en étoile. Grâce à la chimie RAFT, il est maintenant possible par le biais de différentes réactions de couplage, de préparer une grande variété de copolymère à blocs qu'il était impossible de synthétiser auparavant.

En outre, la très haute cristallinité du PVDF ainsi que sa haute température de fusion (≈ 170 °C) rendent très difficile l'auto-assemblage en solution. C'est d'ailleurs pour faciliter sa mise en forme que le VDF est souvent copolymérisé avec différents monomères fluorés tels que l'HFP ou le TrFE. Cette stratégie permet de diminuer la cristallinité et la température de fusion. Une étude à part entière pourrait ainsi être menée sur le contrôle de la polymérisation RAFT de copolymère VDF/HFP ou VDF/TrFE.

Enfin, cette étude s'est focalisée sur la méthode d'auto-assemblage par dialyse, et en milieux aqueux (chapitre V). D'autres méthodes d'auto-assemblages ainsi que des solvants organiques ou des mélanges de solvants comme milieu dispersant pourraient être envisagés.

Référence :

[1] P. Pladis, A. H. Alexopoulos, C. Kiparissides, *Ind. Eng. Chem. Res*., 2014, **53**, 7352-7364.

[2] K. Koumura, K. Satoh, M. Kamigaito, Y. Okamoto, *Macromolecules*, 2006, **39**, 4054-4061

[3] K. Koumura, K. Satoh, M. Kamigaito, *Polymer Journal*, 2009, **41**, 595-603.

Production Scientifique

Publications

- [1]M. Guerre, B. Campagne, O. Gimello, K. Parra, B. Ameduri, V. Ladmiral, **Deeper Insight into the MADIX Polymerization of Vinylidene Fluoride**, *Macromolecules* (IF : 5. 554) , **2015***,* 48*,* 7810-7822.

- [2]M. Guerre, G. Lopez, T. Soulestin, C. Totée, B. Ameduri, G. Silly, V. Ladmiral, **A journey into the microstructure of PVDF made by RAFT**, *Macrom. Chem. Phys.* (IF : 2.616), **2016**, 217, 2275-2285.

- [3]M. Guerre, S. M. W. Rahaman, B. Ameduri, R. Poli, V. Ladmiral, **The Limits of Vinylidene Fluoride RAFT Polymerization**, *Macromolecules* (IF : 5.554), **2016**, 49, 5386-5396

- [4]M. Guerre, B. Ameduri, V. Ladmiral, **One-pot synthesis of Poly(Vinylidene Fluoride) methacrylate macromonomers via thia-Michael addition**, *Polymer Chemistry* (IF : 5. 687), **2016**, 7, 441-450

- [5]M. Guerre, S. M. W. Rahaman, B. Ameduri, R. Poli, V. Ladmiral, **RAFT synthesis of well-defined PVDF-*b*-PVAc Block Copolymers,** *Polymer Chemistry* (IF : 5.687), **2016***,* 7, 6918-6933.

- [6]M. Guerre, M. Uchiyama, E. Folgado, B. Ameduri, K. Satoh, M. Kamigaito, V. Ladmiral, **Cationic and radical RAFT polymerization combination: A versatile route to well-defined poly(vinylidene fluoride)-based block copolymers**, *ACS Macro Letters* (IF : 5,766), **2017***,* 6, 393-398.

- [7]M. Guerre, J. Schmidt, Y. Talmon, B. Ameduri, V. Ladmiral, **Amphiphilic poly(vinylidene fluoride)-*b*-poly(vinyl alcohol) block copolymer: Synthesis and Self-assembly in water**, *Polymer Chemistry*, (IF : 5.687), **2017**, 8, 1125-1128.

- [8]M. Guerre, M. Semsarilar, B. Ameduri, V. Ladmiral, **Polymerization-induced Self Assembly of PVAc-*b*-PVDF block copolymers via RAFT dispersion polymerization in Dimethylcarbonate**, *Polymer Chemistry,* (IF : 5.687), **2017**, 8, 1477-1487.

- [9]M. Guerre, M. Semsarilar, C. Totée, B. Ameduri, V. Ladmiral, **Self-assembly of poly(vinylidene fluoride)-*block*-poly(2-(dimethylamino)ethylmethacrylate) block copolymers prepared by CuAAC click coupling,** *Polymer Chemistry* (IF : 5.687), **2017**, DOI: 10.1039/C7PY00346C.

- [10]E. Folgado, M. Guerre, C. Bijani, V. Ladmiral, A-M Caminade, B. Améduri, A. Oouali, **Well-defined poly(vinylidene fluoride) (PVDF) based-dendrimers synthesized by click chemistry : enhanced crystallinity of PVDF and increased hydrophobicity of PVDF films**, *Polymer Chemistry* (IF : 5.687), **2016**, 7, 5625-5629.

- [11]G. Lopez, M. Guerre, J. Schmidt, Y. Talmon, V. Ladmiral, J.-P. Habas, B. Améduri, **An Amphiphilic PEG-*b*-PFPE-*b*-PEG triblock copolymer : Synthesis by CuAAC click chemistry and self assembly in water,** *Polymer Chemistry* (IF : 5. 687), **2016**, 7, 402-409.

- [12]G. Lopez, M. Guerre, B. Ameduri, J-P. Habas, V. Ladmiral, **Photocrosslinked PVDF-based star polymer: An all-in-one alternative to PVDF-PMMA blends for outdoor coating application**, *Polymer Chemistry* (IF : 5. 687), **2017**, 8, 3045-3049.

- [13]S. Banerjee, M. Guerre, B. Ameduri, V. Ladmiral, **Towards a Library of Fluorinated Block Copolymers on Demand via Sequential RAFT Polymerization**, *Macromolecules* (IF : 5.554), *in preparation*

- [14]M. Guerre, G. Lopez, B. Ameduri, V. Ladmiral, **Recent advances in the Synthesis and Self-Assembly of Fluorinated Copolymers**, *in preparation*

Communications

- **JIP-JEPO 2015,** Donostia-San Sebastian, University of the Basque Country, Spain

Deeper Insight into the MADIX polymerization of Vinylidene Fluoride, Oral communication in English

- **JPL 2016,** Montpellier, *Faculté de Pharmacie, France*

Deeper Insight into the MADIX polymerization of Vinylidene Fluoride, Oral communication in French

- ***JSPS Summer Program 2016**, University of Nagoya, Japan.*

RAFT/MADIX polymerization of Fluoroolefins, a story of Transfer, Oral communication in English

- ***EPF Lyon 2017**, Lyon convention center, France.*

Designing PVDF-based architectures by reversible addition-fragmentation transfer (RAFT) process, Oral communication in English

Synthèse et Auto-Assemblage de Copolymères Fluorés Amphiphiles

Résumé

Les polymères fluorés constituent une classe de polymères à part, aux propriétés remarquables (résistance chimique et thermique, ferroélectricité et piézoélectricité lorsqu'ils sont semicristallins pour en citer quelques-unes). Les polymères fluorés ont trouvé de nombreuses applications industrielles. Toutefois, ils n'ont pas encore attiré tout l'intérêt qui leur est dû de la part de la communauté scientifique. Il reste en effet difficile de préparer des architectures polymères fluorées bien définies. Les techniques de synthèse développées et utilisées jusqu'à présent permettent la synthèse d'architectures polymères intéressantes, mais elles souffrent de deux inconvénients majeurs : 1) Elles ne permettent pas d'accéder à de hautes masses molaires, et 2) les architectures obtenues ne sont pas bien définies. En conséquence, les études physiques de ségrégation de phases en films ou en masse, et ou bien celles qui portent sur la cristallisation des polymères fluorés ont été limitées aux homopolymères et aux mélanges. De même, il existe très peu de travaux sur l'auto-assemblage d'architectures polymères fluorées en solution. A travers une étude cinétique approfondie, des caractérisations détaillées en spectroscopie (NMR) ainsi que des calculs DFT, cette étude a révélé la remarquable éfficacité de la polymérisation RAFT pour synthétiser des architectures de PVDF bien définies. L'auto-assemblage de copolymères à blocs PVDF-*b*-PVA ainsi que l'autoassemblage induit par la polymérisation de copolymères PVAc-*b*-PVDF ont dévoilé les premières nanostructures de type cœur/coquille et rose des sables à base de PVDF.

Mots-clés: Poly(Fluorure de vinylidène), PVDF, RAFT, Bloc, RMN, Auto-Assemblage

Synthesis and Self-Assembly of Amphiphilic Fluorinated Copolymers

Abstract

Fluoropolymers constitute a specific class of polymers, with remarkable properties (high resistance to chemicals and heat, ferroelectricity and piezoelectricity for semi-crystalline polymers, to name a few). Fluoropolymers have found many industrial applications. However, fluoropolymers have not yet attracted all the interest they deserve from the scientific community. It is indeed difficult to prepare well-defined fluorinated polymeric architectures. The synthesis techniques developed and used so far allow the preparation of interesting architectures, but they suffer from two major drawbacks: 1) They do not allow access to high molar mass, and 2) The resulting architectures are ill-defined. As a result, physical chemistry studies of the phase segregation phenomena in films or in the bulk, or of the crystallization of fluorinated polymers were for the most part limited to homopolymers and blends. Similarly, very few studies of the self-assembly in solution of fluorinated polymeric architectures have been reported. From a deeper kinetic study, NMR characterizations and DFT calculations, this study reveals the remarkable efficiency of the RAFT polymerization to synthesize well-defined PVDF–based architectures. Self-assembly of PVDF-*b*-PVA block copolymers as well as polymerization-induced self-assembly of PVAc-*b*-PVDF block copolymers led to the first crystalline core/shell and desert-rose PVDF-based nanostructures.

Key words: Poly(Vinylidene Fluoride), PVDF, RAFT, Block, NMR, Self-Assembly,